



## THE HYDROFORMYLATION REACTION: FROM COVALENT TO SUPRAMOLECULAR APPROACHES AND OPERANDO KINETIC STUDIES

Alicia Martínez Carrión

**ADVERTIMENT.** L'accés als continguts d'aquesta tesi doctoral i la seva utilització ha de respectar els drets de la persona autora. Pot ser utilitzada per a consulta o estudi personal, així com en activitats o materials d'investigació i docència en els termes establerts a l'art. 32 del Text Refós de la Llei de Propietat Intel·lectual (RDL 1/1996). Per altres utilitzacions es requereix l'autorització prèvia i expressa de la persona autora. En qualsevol cas, en la utilització dels seus continguts caldrà indicar de forma clara el nom i cognoms de la persona autora i el títol de la tesi doctoral. No s'autoritza la seva reproducció o altres formes d'explotació efectuades amb finalitats de lucre ni la seva comunicació pública des d'un lloc aliè al servei TDX. Tampoc s'autoritza la presentació del seu contingut en una finestra o marc aliè a TDX (framing). Aquesta reserva de drets afecta tant als continguts de la tesi com als seus resums i índexs.

**ADVERTENCIA.** El acceso a los contenidos de esta tesis doctoral y su utilización debe respetar los derechos de la persona autora. Puede ser utilizada para consulta o estudio personal, así como en actividades o materiales de investigación y docencia en los términos establecidos en el art. 32 del Texto Refundido de la Ley de Propiedad Intelectual (RDL 1/1996). Para otros usos se requiere la autorización previa y expresa de la persona autora. En cualquier caso, en la utilización de sus contenidos se deberá indicar de forma clara el nombre y apellidos de la persona autora y el título de la tesis doctoral. No se autoriza su reproducción u otras formas de explotación efectuadas con fines lucrativos ni su comunicación pública desde un sitio ajeno al servicio TDR. Tampoco se autoriza la presentación de su contenido en una ventana o marco ajeno a TDR (framing). Esta reserva de derechos afecta tanto al contenido de la tesis como a sus resúmenes e índices.

**WARNING.** Access to the contents of this doctoral thesis and its use must respect the rights of the author. It can be used for reference or private study, as well as research and learning activities or materials in the terms established by the 32nd article of the Spanish Consolidated Copyright Act (RDL 1/1996). Express and previous authorization of the author is required for any other uses. In any case, when using its content, full name of the author and title of the thesis must be clearly indicated. Reproduction or other forms of for profit use or public communication from outside TDX service is not allowed. Presentation of its content in a window or frame external to TDX (framing) is not authorized either. These rights affect both the content of the thesis and its abstracts and indexes.



UNIVERSITAT  
ROVIRA I VIRGILI

# The Hydroformylation Reaction: from Covalent to Supramolecular Approaches and *Operando* Kinetic Studies

---

Alicia Martínez Carrión



DOCTORAL THESIS  
2020

UNIVERSITAT ROVIRA I VIRGILI

THE HYDROFORMYLATION REACTION: FROM COVALENT TO SUPRAMOLECULAR APPROACHES AND OPERANDO KINETIC STUDIES

Alicia Martínez Carrión

UNIVERSITAT ROVIRA I VIRGILI

THE HYDROFORMYLATION REACTION: FROM COVALENT TO SUPRAMOLECULAR APPROACHES AND OPERANDO KINETIC STUDIES

Alicia Martínez Carrión

UNIVERSITAT ROVIRA I VIRGILI

THE HYDROFORMYLATION REACTION: FROM COVALENT TO SUPRAMOLECULAR APPROACHES AND OPERANDO KINETIC STUDIES

Alicia Martínez Carrión

Alicia Martínez Carrión

# The Hydroformylation Reaction: from Covalent to Supramolecular Approaches and *Operando* Kinetic Studies

Doctoral Thesis

Supervised by Prof. Dr. Anton Vidal i Ferran

Institute of Chemical Research of Catalonia (ICIQ)



UNIVERSITAT ROVIRA i VIRGILI

Tarragona 2020

UNIVERSITAT ROVIRA I VIRGILI

THE HYDROFORMYLATION REACTION: FROM COVALENT TO SUPRAMOLECULAR APPROACHES AND OPERANDO KINETIC STUDIES

Alicia Martínez Carrión



UNIVERSITAT  
ROVIRA I VIRGILI

DEPARTAMENT DE QUÍMICA  
ANALÍTICA

I QUÍMICA ORGÀNICA

C/ Marcel·lí Domingo s/n

Campus Sescelades

43007 Tarragona

Prof. Dr. Anton Vidal i Ferran, Group Leader of the Institute of Chemical Research of Catalonia (ICIQ) and Research Professor of the Catalan Institution for Research and Advance Studies (ICREA),

I STATE that the present Doctoral Thesis entitled “**The Hydroformylation Reaction: from Covalent to Supramolecular Approaches and *Operando* Kinetic Studies**” that Alicia Martínez Carrión presents to obtain the PhD degree in chemistry, has been carried out under my supervision, in the corresponding research group at the Institute of Chemical Research of Catalonia (ICIQ).

Tarragona, 8<sup>th</sup> June 2020

PhD Thesis Supervisor

Prof. Dr. Anton Vidal i Ferran



UNIVERSITAT ROVIRA I VIRGILI

THE HYDROFORMYLATION REACTION: FROM COVALENT TO SUPRAMOLECULAR APPROACHES AND OPERANDO KINETIC STUDIES

Alicia Martínez Carrión

## ACKNOWLEDGEMENTS

Como es de bien nacido el ser agradecido, os quiero dedicar estas palabras a todas las personas que habéis contribuido al desarrollo de esta tesis, tanto a nivel científico como personal.

En primer lugar, me gustaría agradecer a mi director de tesis, el **Prof. Dr. Anton Vidal i Ferran**, por darme la oportunidad de llevar a cabo la tesis en su grupo de investigación y de poder trabajar en un centro como el ICIQ. Gracias por tu supervisión y tu dedicación a lo largo de estos años.

A las unidades de soporte del ICIQ, porque vuestro trabajo día a día hace nuestra investigación más llevadera. Quería agradecerle a **Simona** y **Marta** de ChromTAE, por estar siempre dispuestas a ayudar y enseñarme cada vez que se presentaba la ocasión. También a **Xavi** y **José Luis León**, por crear todo lo que necesitamos siempre con una sonrisa. De una manera más especial, quería agradecer a **Marta** y **Cris** de CRTU, por ayudarme a zambullirme en el mundillo de las reacciones a presión. Marta, gracias por tu ayuda y soporte en el diseño del sistema en flujo y por enseñarme tanto durante estos años.

También quiero agradecer al **Prof. Dr. Jordi Burés**, por permitirme realizar una estancia en su grupo en la Universidad de Manchester. Gracias por darme la oportunidad de jugar con el FlowNMR y por no tirar la toalla cuando las cosas no salían. I also would also to thank **Dr. Ralph Adams**, for his daily support and troubleshooting with the NMR spectroscopy, even on a Friday night from an English pub.

Durante estos años de doctorado, me di cuenta de cómo el grupo de investigación se convirtió en mi familia y el laboratorio 1.4 en mi segunda casa. Son muchas las horas que hemos pasado, con muchas risas, algún que otro llanto y, sobre todo, mucha música. Todo empezó contigo **Mónica**, fuiste la primera toma de contacto que tuve a nivel científico, pero también a nivel personal. Porque me enseñaste mucho de química, pero nadie puede quitarte el mérito de ser quien me descubrió el vermut y las fiestas de Santa Tecla. Gracias por hacer que el comienzo fueran tan fácil. **Héctor**, las horas en la vitrina no hubieran sido lo mismo si no hubieras estado en la vitrina de al lado. Porque muchas veces con una sola mirada podíamos estallar de la risa y con otras sabías que necesitaba de tu ayuda o tus consejos. Ay **José Luis**, que cariño se te coge con los años. Gracias por esa forma de ser, altruista, con picor de cerebro ante cualquier novedad y dispuesto a una buena conversación mientras presurizo el reactor. Las noches de San Juan han cobrado otro sentido desde que te conocí. **Rajesh**, thank you for the crazy nights dancing, discovering Tarragona and talking in the rambla about life. **Bala**, you have been such an example of resilience, strength, a master of dancing and the kindest smile of the group. **Joan**, capaz de sacarnos carcajadas con pocas palabras. Y **Laura**, de la que guardo muy buen recuerdo de las horas

que pasamos fuera y dentro del laboratorio. Luego está **Luquitas**, esa enciclopedia con patas al que a veces no hay quien le entendiera. Porque vales mucho, pero te lo digo poco, que se te sube a la cabeza. **Dominik**, although your stay in the group was short, you left a good bunch of sweet memories and anecdotes **Nuria**, una de las personas con las que más he compartido horas de laboratorio. Gracias por no dejarme pasar ni una cuando tenía la cabeza en las nubes y por estar ahí cada día durante estos cuatro años. **Ester**, el terremoto de energía y alegría. Gracias por sentarte a mi lado cuando no le encontraba solución a un problema. **Andrés**, siempre dispuesto a echarme una mano, sobre todo en el final de la tesis. Gracias por darme ánimos en los malos momentos. Y a **Juanjo**, con el que reírse con solo mirar una foto. Hasta que no apareció **Alba**, no deje de ser “la niña” del grupo. Nos has dado los mejores momentos en el laboratorio. Por último, agradecer a **Paula**, por toda su ayuda durante estos estos años de tesis.

I would like to express my gratitude to all the Indian crew. Bala and Rajesh, thank you for inviting me to be part of your gatherings and teach me so much about your cultures. ಧನ್ಯವಾದುలు. **Asmaul**, we started a few years ago wondering how this experience would be. Now, I'm very grateful for having shared with you every badminton match, tea time and spicy Indian dishes over those years. ধন্যবাদ.

La escritura de tesis a veces se hace tan dura como subir una cuesta con piedras en los bolsillos. Pero eso puede mejorar si compartes la sala de tesis con personas como **Ángel**. Muchas gracias por todos los momentos de risas y de comer chocolate con sésamo.

Durante la tesis aparece gente, que empiezan siendo “conocidos de”, y les acabas cogiendo mucho cariño. Muchas gracias **Mónica**, por escucharme y aportar tu granito de arena en los malos momentos. A ti **Alfonso**, aunque te debo muchos dolores por cervezas a traición, estoy inmensamente agradecida de haber compartido tantas charlas de bar y alguna que otra noche de fiesta. Durante estos años me habían hablado de lo maravillosa que eras **Sara**, y he tenido la suerte de poder comprobarlo por mí misma. Y a ti **Ángel**, que decirte del cariño que te tengo, si nos hemos autodenominado cuñados. Siempre nos quedará pendiente un concierto de La Pegatina. Estar en el grupo Vidal, me ha permitido conocer a tres personas maravillosas. **M<sup>a</sup> Ángeles**, gracias por tu apoyo y consejos, sobre todo cuando no veía fin a la escritura de la tesis. **Gema**, gracias por las charlas durante la noche de San Juan, las rutas y escapadas y por estar ahí, aunque no nos viéramos a menudo. **Sofi**, me alegro del día que decidiste empezar a comer con nosotras. Porque de no haber sido así, no habría podido comprobar lo brillante, paciente, buena persona y mejor cocinera que eres.

Toda experiencia sabe mejor si es compartida. Mis compañeros durante esta aventura fuera y dentro del ICIQ han sido los Pavipollos. También me gusta llamarlos, por lo que se han convertido, mi segunda familia. Nuestra historia comenzó gracias a ti, **Nuria**. Desde el principio fuiste el punto de unión y también la persona que más empeño ha puesto en sacar las cosas adelante, ya sea una escapada o conseguir una mesa en el Tastum. Me gusta pensar que, en este tiempo, has sido mi cabeza, esa parte que me ha ayudado a ser objetiva, a racionalizar todo o a recordar hasta la última fecha. Señorita donde las haya, también has sido la mejor compañera gastronómica en busca de las mejores bravas y de experiencias descubriendo Cataluña. Conocerte mientras hacías el máster me llevó a **Andreu**. Has sido parte de esta historia desde el principio, en la que, ha sido un orgullo verte evolucionar de los coloretos por cualquier chiste, a que no se te pueda llevar la contraria por tener más información que Google. La persona a quién abrazar cuando los días se hacían cuesta arriba y el mejor compañero de siestas. Los días pasaban y las horas de la comida significaban pasar un ratito al día con **Cris**. Gracias por enseñarme que no hay edad para cerrar los bares, por ser un ejemplo de mujer fuerte que se come el mundo a cada paso que da y estar siempre disponible para un buen abrazo. Cogerte la mano en uno de los días más importantes de tu vida ha sido el mejor regalo que me has podido hacer. Pasaron los meses, llego la primavera y con ella mi pequeña gran revolución: **Ester**. Tu llegada supuso un punto de inflexión, no sabíamos todo lo que nos habíamos perdido hasta que te conocimos. Durante estos años, has sido el corazón, la locura y el cariño hecho persona. Compañera de llantos y anhelos, gracias por darme tantos momentos bonitos. Una de las cosas por las que más agradecida te puedo estar es por llevarnos de cervezas para conocer a Jesús y a Miguel. Ese día le diste la vuelta a mi mundo. Y apareció **Miguel**, al que tuve que aprender a entender cuando hablaba (traductor Nuria®). Si algo he aprendido algo estos años, es que la vida hay que tomársela con calma y que tú eres el mejor ejemplo a seguir. Panchu, ho! como filosofía de vida. Gracias por ser ese amigo que siempre está ahí, lo mismo para comer un cacho de queso, para dejarte la sudadera o para dormirte en su hombro. Junto con Miguel, siempre estaba Jesús, ese pack inseparable que te hace ver lo que es una amistad de verdad. El primer año de tesis se terminaba, y llegaron las nuevas incorporaciones del piso patera. Así conocimos a ese amigo con el que todos nos metemos, pero del que notamos su ausencia y al que se le quiere mucho, pero no se le dice por si se pone pesao. **Kike**, esa persona que tiene el culo y la mente inquieta, que me gana a pedir agua en los bares y con el que tener largas conversaciones en el portal cuando nos volvíamos a casa por ser los abuelos del grupo. Gracias por darme fuerza y ánimos cuando estaba estancada. Entonces es cuando **Chuchi** apareció en escena. Porque si algo ha caracterizado estos años, es tu risa de fondo cuando se hacían los silencios y tus pies arrastrándose por el ICIQ. Gran compañero de festivales, de cervezas en verano mientras escribíamos la tesis y mejor chef. Entonces llegaron las nuevas incorporaciones. Y apareció mi tocaya, **Alicia**.

Siempre dispuesta a ayudarnos con los problemas que se nos presentaban. Y como en todo grupo, está el bromista, el que se entera del último video de moda y te lo repite hasta que no puedes sacártelo de la cabeza. Así es **Raúl**, genio de hacer tonterías y de sacarnos sonrisas. Cuando pensábamos que estábamos todos, apareció mi otra mitad manchega: **Alba**. Porque esa naturalidad que te caracteriza ha hecho que hayas traído un poquito de nuestra tierra a esta experiencia. Gracias por acompañarme en la búsqueda del animal más adorable y por esa capacidad para entendernos tan solo con una mirada. Para rematar, conocimos a la niña de nuestros ojos, que consigue sacar el niño que todos llevamos dentro. A mi pequeña **Victoria**, gracias por regalarnos tu sonrisa, esa inocencia al ir descubriendo el mundo y que todo es posible, por pequeñas que sean las probabilidades. Aunque en tiempo de descuento, apareció **Ana**. Gracias por estar tan perdida como yo en las partidas de Trivial y por haber formado parte de las últimas cervezas de esta etapa.

Cada decisión en la vida me lleva cada vez un poquito más lejos de Albacete. Y ahí está mi familia, aguantando mis ausencias en cada paso del camino y queriéndome más cerca por mucho que me aleje. A mi padre y a mi madre, por enseñarme el valor del esfuerzo y del trabajo sin esperar ninguna recompensa a cambio. A mis tíos por escucharme cuando he tenido algún problema, o para disfrutar con ellos de una cañita o vermú en una terraza en cada reencuentro. A mis tíos de Barcelona, (Jesús y M<sup>a</sup> Ángeles), porque esta tesis me ha dado la oportunidad de estar más cerca de vosotros y disfrutar de vuestra compañía. A mi abuela, por ser un ejemplo de lucha y de fuerza personal ante las adversidades. Y, por último, a mi hermano. Porque he crecido creyendo que éramos polos opuestos y durante estos años he podido comprobar que somos como dos gotas de agua. Gracias por tus visitas, por ser parte de esta experiencia y por haberte convertido en mi mejor amigo a lo largo de estos años.

También quiero dar las gracias a todas esas personas que llevan años a mi lado y que han seguido con su apoyo y cariño durante esta etapa. A todos los que me acompañan desde el colegio y el instituto, a mis viejóvenes, los de la carrera, mis chicas de la residencia o los amigos del máster. A **Paula, María y Rocío**, por ser el punto de apoyo en los días malos. A **Natalia**, porque a pesar de los kilómetros de distancia, hemos hecho la tesis juntas.

Mis últimas palabras son para ti, **Jesús**. Gracias por aparecer, quedarte y convertirme en el mejor compañero con el que compartir esta experiencia. Por tu paciencia y cariño, por hacerme ser la mejor versión de mí misma y ser los hombros en los que resguardarme cuando afuera solo había nubes negras. Mi juez más crítico y quien vio todo de lo que era capaz, aun cuando yo no creía en mí misma. Después de superar esta tesis, no habrá obstáculo imposible de vencer a tu lado. Porque si la verdadera felicidad consiste en hacer felices a los demás, la mía estos años ha sido hacerte sonreír cada día. T'estimo.

The research work developed in the present PhD thesis has been possible thanks to the ICIQ Foundation for the predoctoral fellowship (ICIQ-02/15C-1) and the financial support provided by the ICIQ Foundation and MINECO (CTQ2014-60256-P and CTQ201789814-P). A 3-month stay abroad at the University of Manchester was funded by the Dial-a-Molecule Interdisciplinary Mobility funding and the Royal Society of Chemistry Research Mobility Grant.



UNIVERSITAT  
ROVIRA I VIRGILI



UNIVERSITAT ROVIRA I VIRGLI

THE HYDROFORMYLATION REACTION: FROM COVALENT TO SUPRAMOLECULAR APPROACHES AND OPERANDO KINETIC STUDIE

Alicia Martínez Carrión

*A mi padre,  
porque en cada caída,  
tu recuerdo me ha dado la fuerza para levantarme*



UNIVERSITAT ROVIRA I VIRGILI

THE HYDROFORMYLATION REACTION: FROM COVALENT TO SUPRAMOLECULAR APPROACHES AND OPERANDO KINETIC STUDIES

Alicia Martínez Carrión

*“Lo que me llevará al final serán mis pasos, no el camino”*

Fito & Fitipaldis

*“Antes se cansará la razón de imaginar  
que el Universo de maravillarnos”*

Blaise Pascal

UNIVERSITAT ROVIRA I VIRGILI

THE HYDROFORMYLATION REACTION: FROM COVALENT TO SUPRAMOLECULAR APPROACHES AND OPERANDO KINETIC STUDIES

Alicia Martínez Carrión

## LIST OF PUBLICATIONS

When this dissertation was submitted, the results contained herein have so far resulted in the following publications:

- “Kinetic Treatments for Catalyst Activation and Deactivation Processes Based on Variable Time Normalization Analysis” Martínez-Carrión, A.; Howlett, M. G.; Alamillo-Ferrer, C.; Clayton, A. D.; Bourne, R. A.; Codina, A.; Vidal-Ferran, A.; Adams, R. W.; Burés, J. *Angew. Chem. Int. Ed.* **2019**, *58*, 10189-10193.

Other publications related to the topic covered in the present dissertation in a general way are presented below:

- “Efficient Modular Phosphorus-containing Ligands for Stereoselective Catalysis” (general overview on the research activities of the group) Llorente, N.; Fernández-Pérez, H.; Núñez-Rico, J. L.; Carreras, L.; Martínez-Carrión, A.; Iniesta, E.; Romero-Navarro, A.; Martínez-Bascuñana, A. Vidal-Ferran, A. *Pure Appl. Chem.* **2019**, *91*, 3-15.

UNIVERSITAT ROVIRA I VIRGILI

THE HYDROFORMYLATION REACTION: FROM COVALENT TO SUPRAMOLECULAR APPROACHES AND OPERANDO KINETIC STUDIES

Alicia Martínez Carrión

# TABLE OF CONTENTS

LIST OF ACRONYMS AND ABBREVIATIONS.....	XIX
PROLOGUE.....	XXIII
<b>INTRODUCTION.....</b>	<b>1</b>
I.1. The hydroformylation reaction.....	1
I.1.1. Cobalt-catalyzed hydroformylation.....	3
I.1.2. Rhodium-catalyzed hydroformylation.....	6
I.1.3. Enantioselective rhodium-catalyzed hydroformylation.....	9
I.1.4. The hydroformylation reaction mechanism.....	13
I.2. Supramolecular approaches in rhodium-catalyzed hydroformylation.....	15
I.2.1. Rhodium-catalyzed hydroformylations in confined spaces.....	17
I.2.2. Supramolecular assembled bidentate ligands in rhodium- catalyzed hydroformylation.....	22
I.2.3. Substrate preorganization in rhodium-catalyzed hydroformylation.....	25
I.2.4. Distal regulation in rhodium-catalyzed hydroformylation.....	28
I.3. Mechanistic and kinetic studies in hydroformylation reactions.....	31
I.3.1. <i>Operando</i> spectroscopy in hydroformylation reactions.....	33
I.3.2. FlowNMR for <i>online</i> reaction monitoring.....	34
I.3.3. Visual kinetic analysis for reaction kinetics elucidation.....	36
<b>OBJECTIVES.....</b>	<b>39</b>
<b>CHAPTER I.....</b>	<b>43</b>
1.1 ABSTRACT.....	43
1.2 INTRODUCTION.....	43
1.3 RESULTS AND DISCUSSION.....	46
1.4 CONCLUSIONS.....	57
1.5 EXPERIMENTAL SECTION.....	58
1.5.1 General considerations.....	58
1.5.2 Synthesis of ligands <b>L1-L4</b> .....	58
1.5.2.1 General procedure for the synthesis of supramolecular bisphosphite ligands.....	60
1.5.3 Substrate synthesis.....	64

1.5.4	General procedure for Rh-catalyzed hydroformylation of 7-vinylidenetriecane <b>7</b> .....	66
1.5.5	Complete set of results for the Rh-catalyzed hydroformylation of 7-vinylidenetriecane <b>7</b> .....	67
1.5.5.1	Catalytic results for ligand <b>L1</b> .....	67
1.5.5.2	Catalytic results for ligand <b>L2</b> .....	68
1.5.5.3	Catalytic results for ligand <b>L3</b> .....	68
1.5.5.4	Catalytic results for ligand <b>L4</b> .....	69
1.5.6	Collection of spectra.....	70
<b>CHAPTER II</b>	.....	<b>87</b>
2.1	ABSTRACT.....	87
2.2	INTRODUCTION.....	88
2.3	RESULTS AND DISCUSSION.....	90
2.3.1	Cobalt-catalyzed hydroformylation of styrene <b>5</b> .....	95
2.3.2	Cobalt-catalyzed hydroformylation of oct-1-ene and internal octenes.....	100
2.4	CONCLUSIONS.....	113
2.5	EXPERIMENTAL SECTION.....	114
2.5.1	General considerations.....	114
2.5.2	General structural comments on X-ray crystal of <b>2</b> .....	114
2.5.3	Synthesis of [Co(H)(CO) <sub>2</sub> (Xantphos)] <b>2</b> .....	129
2.5.4	General procedure for the cobalt-catalyzed hydroformylation of styrene <b>5</b> and octenes <b>12, 16-20</b> .....	130
2.5.5	Determination of the conversion, chemoselectivity and regioselectivity in hydroformylation reaction mixtures.....	130
2.5.6	Selected GC chromatograms.....	132
2.5.7	Complete set of results for the cobalt-catalyzed hydroformylation.....	133
2.5.7.1	Cobalt-catalyzed hydroformylation of styrene <b>5</b> .....	133
2.5.7.2	Cobalt -catalyzed hydroformylation of oct-1-ene <b>12</b> .....	134
2.5.7.3	Cobalt -catalyzed hydroformylation of internal octenes <b>16-20</b> .....	135
2.5.8	Collection of spectra.....	136

<b>CHAPTER III</b>	<b>141</b>
3.1 ABSTRACT	141
3.2 INTRODUCTION	142
3.3 RESULTS AND DISCUSSION	144
3.3.1 Optimization of the hydroformylation reaction conditions	146
3.3.2 Expansion of the substrate scope of the supramolecularly regulated Rh(I)-catalyzed enantioselective hydroformylation	152
3.3.3 Studies in the <i>in situ</i> formation of supramolecular Rh(I)-complexes derived from ligand (R)- <b>L6</b> and mechanistic studies	156
3.3.3.1 Complexation studies	156
3.3.3.2 Mechanistic studies	167
3.3.4 Rationalization of the stereochemical outcome of the hydroformylation reaction	169
3.4 CONCLUSIONS	176
3.5 EXPERIMENTAL SECTION	177
3.5.1 General considerations	177
3.5.2 Synthesis of ligands	178
3.5.2.1 General procedure for the synthesis of supramolecular bisphosphite ligands	179
3.5.3 Synthesis of regulation agents: alkali BArF salts	185
3.5.4 Substrate synthesis	185
3.5.4.1 General procedure for the synthesis of aryl vinyl ethers	185
3.5.5 General procedure for Rh-catalyzed enantioselective hydroformylation of aryl vinyl ethers	190
3.5.6 General procedure for oxidation of 2-aryloxypropanal to 2-aryloxypropanoic acid derivatives	191
3.5.7 Determination of the enantiomeric ratio and absolute configuration of the hydroformylation products	194
3.5.8 Selected GC and HPLC chromatograms	196
3.5.9 Complete set of results for the Rh-catalyzed enantioselective hydroformylation of aryl vinyl ethers	208
3.5.9.1 Study of the influence of the ligand, RA, rhodium to RA ratio and reaction conditions	208
3.5.9.2 Substrate scope	209
3.5.10 Coordination studies	211
3.5.10.1 Experimental procedure for the complexation experiments	211



3.5.10.1.1 General procedure for the complexation experiments under inert atmosphere.....	211
3.5.10.1.2 General procedure for the complexation experiments under syngas (H <sub>2</sub> /CO) atmosphere.....	212
3.5.10.2 NMR spectral data for the complexes obtained in the complexation experiments.....	214
3.5.10.3 Spectra of the complexation experiments.....	215
3.5.11 Deuteroformylation results.....	232
3.5.12 Computational methods.....	233
3.5.13 Collection of spectra.....	255
<b>CHAPTER IV.....</b>	<b>295</b>
4.1 ABSTRACT.....	296
4.2 INTRODUCTION.....	296
4.3 RESULTS AND DISCUSSION.....	298
4.4 CONCLUSIONS.....	309
4.5 EXPERIMENTAL SECTION.....	310
4.5.1 General considerations.....	310
4.5.2 Experimental setup.....	310
4.5.3 Preparation of the catalyst precursors in flow experiments.....	311
4.5.4 General procedure for the Rh-catalyzed enantioselective hydroformylation of vinyl acetate <b>1</b> with variable partial pressures.....	312
4.5.5 Determination of the regioselectivity and enantiomeric excess of <b>2</b> .....	313
4.5.6 Selected GC chromatograms.....	313
4.5.7 Complete set of results for the Rh-catalyzed enantioselective hydroformylation of vinyl acetate <b>1</b> .....	314
4.5.8 Selected spectra.....	315
4.5.9 Kinetic data.....	320
<b>CONCLUSIONS.....</b>	<b>335</b>
<b>SUMMARY /RESUMEN/RESUM.....</b>	<b>339</b>
Summary in english.....	339
Resumen en castellano.....	345
Resum en català.....	351

## LIST OF ACRONYMS AND ABBREVIATIONS

The acronyms and abbreviations used in this manuscript have been used following the recommendations given by the American Chemical Society in the ACS guidelines for authors (accessed June 2020 (<https://pubs.acs.org/doi/10.1021/bk-2006-STYG.ch010>)). Additional abbreviations and acronyms used in this manuscript are referenced in the list below:

<b>[<math>\alpha</math>]</b>	specific rotation [expressed without units; the units, (deg·mL)/(g·dm), are understood]
<b>°</b>	angle
<b>Å</b>	angstrom(s)
<b>Ac</b>	acetyl
<b>acac</b>	acetylacetonate
<b>AcO</b>	acetate
<b>AHF</b>	asymmetric hydroformylation
<b>API</b>	Active Pharmaceutical Ingredient
<b>aq.</b>	aqueous
<b>Ar</b>	aryl, argon
<b>atm</b>	atmosphere(s)
<b>BArF</b>	tetrakis[3,5-bis(trifluoromethyl)phenyl]borate]
<b>br</b>	broad (spectral)
<b>Bu, <sup>n</sup>Bu</b>	<i>normal</i> butyl
<b><sup>t</sup>Bu</b>	<i>tert</i> -butyl
<b>°C</b>	degrees, Celsius
<b>ca.</b>	<i>circa</i> (about)
<b>calcd</b>	calculated
<b>CD</b>	cyclodextrin
<b>cat.</b>	catalyst
<b>cm</b>	centimeter(s)

<b>cm<sup>-1</sup></b>	wavenumber(s)
<b>COD</b>	1,5-cyclooctadiene
<b>conv.</b>	conversion
<b>Cy</b>	cyclohexane (solvent)
<b>δ</b>	chemical shift in ppm
<b>d</b>	doublet (spectral)
<b>DCM</b>	dichloromethane
<b>DFT</b>	density-functional theory
<b>DMA</b>	dimethylacetamide
<b>DMF</b>	dimethylformamide
<b>ea</b>	equatorial-axial (coordination)
<b>EDG</b>	electron-donating groups
<b>ee</b>	equatorial-equatorial (coordination)
<b>ee</b>	enantiomeric excess
<b>e.g.</b>	<i>exempli gratia</i> (for example)
<b>eq.</b>	equation(s)
<b>equiv.</b>	equivalent(s)
<b>er</b>	enantiomeric ratio
<b>ESI</b>	electrospray ionization
<b>et al.</b>	<i>et alii</i> (and co-workers)
<b>Et</b>	ethyl
<b>EWG</b>	electron-withdrawing groups
<b>FID</b>	flame ionization detector
<b>FMoc</b>	9-fluorenylmethoxycarbonyl
<b>g</b>	gram(s)
<b>GC</b>	gas chromatography
<b>h</b>	hour(s)
<b>HF</b>	hydroformylation
<b>HMBC</b>	heteronuclear multiple-bond correlation spectroscopy

<b>HPLC</b>	high-performance liquid chromatography
<b>HRMS</b>	high resolution mass spectrometry
<b>Hz</b>	hertz
<i>i.e.</i>	<i>id est</i> (in other words)
<b>IS</b>	internal standard
<b>IR</b>	infrared
<i>J</i>	coupling constant (expressed in Hz)
<b>L</b>	liter(s)
<b>L<sub>n</sub></b>	undetermined ligand(s)
<b>LDA</b>	lithium diisopropylamide
<b>μ</b>	micro- (prefix)
<b>m</b>	multiplet (spectral); milli- (prefix)
<b>M</b>	molar (moles per liter)
<b>M<sup>+</sup></b>	parent molecular ion
<b>MALDI</b>	matrix-assisted laser desorption ionization
<b>Me</b>	methyl
<b>MHz</b>	megahertz
<b>min.</b>	minute(s)
<b>mM</b>	milimolar (milimoles per liter)
<b>mol</b>	mole(s), molecular
<b>mp</b>	melting point
<b>MS</b>	mass spectrometry
<b>MTBE</b>	methyl <i>tert</i> -butyl ether
<i>m/z</i>	mass-to-charge ratio
<b>n.d.</b>	not detected
<b>nm</b>	nanometer(s)
<b>NMR</b>	nuclear magnetic resonance
<b>OPiv</b>	pivalate
<b>ORTEP</b>	oak ridge thermal ellipsoid plot program

<b>P</b>	phosphorus
<b>Ph</b>	phenyl
<b>ppm</b>	part(s) per million
<b><i>i</i>Pr</b>	<i>iso</i> -propyl
<b>q</b>	quartet (spectral)
<b><i>rac</i></b>	racemic
<b>ref</b>	reference
<b>rpm</b>	revolution per minute
<b>RA</b>	regulation agent
<b>RPKA</b>	reaction progress kinetic analysis
<b>s</b>	singlet (spectral); second(s)
<b>t</b>	triplet (spectral); time
<b>T</b>	temperature
<b>tbp</b>	trigonal bipyramid (geometry)
<b>THF</b>	tetrahydrofuran
<b>TMS</b>	tetramethylsilyl; tetramethylsilane
<b>TOF</b>	time-of-flight; turnover frequency
<b>TON</b>	turnover number
<b>TPP</b>	tetra phenyl porphyrin
<b><i>t<sub>R</sub></i></b>	retention time (in chromatography)
<b>Ts</b>	<i>p</i> -toluenesulfonyl (tosyl)
<b>vol</b>	volume
<b>v/v</b>	volume per unit volume
<b>VTNA</b>	variable time normalization analysis

## PROLOGUE

The present doctoral thesis has been divided in five main parts: a general introduction divided in three main parts and four chapters on the research activities of this thesis. Each chapter has been divided in the following parts: (i) abstract, (ii) introduction, (iii) results and discussion, (iv) conclusions and (v) experimental sections. Compounds have been numbered independently in each chapter. References have been included as footnotes and numbered independently in each chapter.

The introduction has been distributed in three main sections. In the first place, a general overview of the hydroformylation reaction, with the most relevant metals and ligands employed in this transformation over the years. Secondly, a summary of the recent advances in the hydroformylation transformation with supramolecular catalysts. The last section covers a general overview of *operando* techniques and instrumentation applied in hydroformylation reactions and the types of visual kinetic analysis for the extraction of mechanistic and/or kinetic information in a rapid and simple way.

Chapter I discloses the rhodium-catalyzed hydroformylation of a representative 1,1'-disubstituted allene employing a supramolecularly regulated catalytic system.

Chapter II presents the cobalt-catalyzed hydroformylation of terminal aryl and alkyl alkenes and internal aliphatic alkenes in presence of Xantphos as ligand. A comparison of the catalytic performance of the isolated and *in situ* formed catalyst is studied.

Chapter III comprises the supramolecularly regulated rhodium-catalyzed enantioselective hydroformylation of aryl vinyl ethers. The use of the matching regulation agent resulted in an improvement of the catalytic activity and the enantiomeric ratio.

Chapter IV includes the development of an experimental setup for the high-pressure reaction monitoring. The application of a kinetic analysis enables the simplification of the reaction profiles and present some insights into the reaction kinetics. This work has been published in *Angew. Chem. Int. Ed.* **2019**, *58*, 10189-10193.

UNIVERSITAT ROVIRA I VIRGILI

THE HYDROFORMYLATION REACTION: FROM COVALENT TO SUPRAMOLECULAR APPROACHES AND OPERANDO KINETIC STUDIES

Alicia Martínez Carrión

# Introduction



UNIVERSITAT ROVIRA I VIRGILI

THE HYDROFORMYLATION REACTION: FROM COVALENT TO SUPRAMOLECULAR APPROACHES AND OPERANDO KINETIC STUDIES

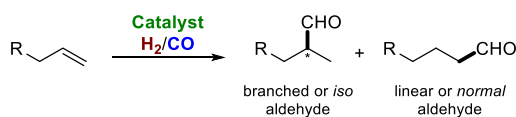
Alicia Martínez Carrión

# INTRODUCTION

## I.1 The hydroformylation reaction

In 1938, Otto Roelen discovered by serendipity the *oxo*-process, while studying the Fisher-Tropsch process.<sup>1</sup> The use of a cobalt catalyst doped with thorium in the reaction between ethylene and syngas<sup>2</sup> led to a mixture of propionaldehyde and other high boiling point compounds that were named as *oxo*-products.<sup>3</sup> This was the first report for what is known as the hydroformylation reaction.<sup>4</sup>

The hydroformylation reaction entails the formal addition of CO and H<sub>2</sub> to an olefin in presence of a catalyst to generate aldehydes as final products (Scheme 1). The use of an unsymmetrical alkene leads to the formation of two different isomers depending on the position of the formal addition of the CHO and H groups: branched isomers (also known as *iso*-aldehydes) with a stereogenic center and linear isomers (*n*-aldehydes).



**Scheme 1.** General scheme of the hydroformylation reaction

Initial development of hydroformylation reactions was closely related with industrial activity, but in the 1990s chemists found hydroformylation reactions of great interest and applicability in academic research (Figure 1). This transformation is a catalytic process that can be considered the most important example of application of homogeneous catalysis at the industrial scale.<sup>5,6,7</sup> In

<sup>1</sup> Chakrabarti, D.; Prasad, V.; de Klerk, A. *Chem. Ind.* **2016**, *142*, 184-222.

<sup>2</sup> Syngas is an acronym that refers to synthesis gas, a mixture of CO and H<sub>2</sub> in a 1:1 ratio.

<sup>3</sup> Roelen, O., DE849548, **1938/1951**.

<sup>4</sup> The term “hydroformylation” was more generally used since 1949 after the publication of the work of Adkins and Krsek (Adkins, H.; Krsek, G. *J. Am. Chem. Soc.* **1949**, *71*, 3051-3055). The term “*oxo*-process” is still used in industry.

<sup>5</sup> Wiese, K.-D.; Obst, D. *Top. Organomet. Chem.* **2006**, *18*, 1-33.

<sup>6</sup> de Vries, J. G.; *Hydroformylation of Alkenes: Industrial Applications*. In *Science of Synthesis, C-1 Building Blocks in Organic Synthesis*; Van Leeuwen, P. W. N. M., Eds.; Georg Thieme Verlag, Stuttgart, **2014**.

<sup>7</sup> Börner, A.; Franke, R.; *Hydroformylation: Fundamentals, Processes, and Applications in Organic Synthesis*; Wiley-VCH, Weinheim, **2016**.

2008, the production of 10.4 million metric tons per year of *oxo*-products, comprising bulk and fine chemicals, was reported.<sup>8</sup>

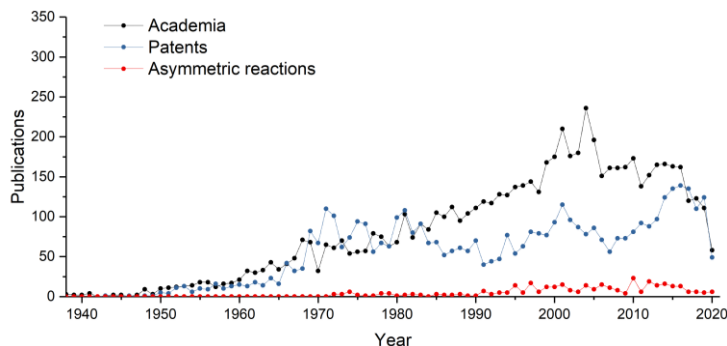


**Figure 1.** Publications and patents issued over the last 80 years<sup>9</sup>

Linear aldehydes are key intermediates in the fabrication of detergents and plasticizers and branched aldehydes are relevant intermediates in the production of fine chemicals and drugs. From the synthetic point of view, aldehydes have a huge number of applications due to: (i) the versatility of the formyl group (CHO) for being transformed into different functionalities;<sup>10</sup> (ii) the tolerance of a wide range of functional groups to hydroformylation reaction conditions;<sup>6,11</sup> and (iii) the potential formation of a new stereogenic center throughout the process.

Early studies revealed the difficult task of selectivity control in the hydroformylation reaction (Scheme 2). The first challenge is intrinsic to the alkene reactivity, which may lead to two isomers depending on the position of the formal addition of the CHO and H groups (Scheme 2a). The structure of the final products depends on the nature of the alkene and the catalytic system, the metal center and the characteristics of the ligand. Catalyst design has been a useful tool for controlling the regioselectivity of the reaction. The second challenge is the double bond isomerization of the alkene (Scheme 2b). This process can take place through different reaction pathways under hydroformylation reaction conditions to form the thermodynamically favored internal alkenes.<sup>12</sup> The isomerized alkene can undergo subsequent

<sup>8</sup> Naqui, S.; *Oxo Alcohols. Process Economics Programm Report 21E*; SRI Consulting, Menlo Park, CA, **2010**.

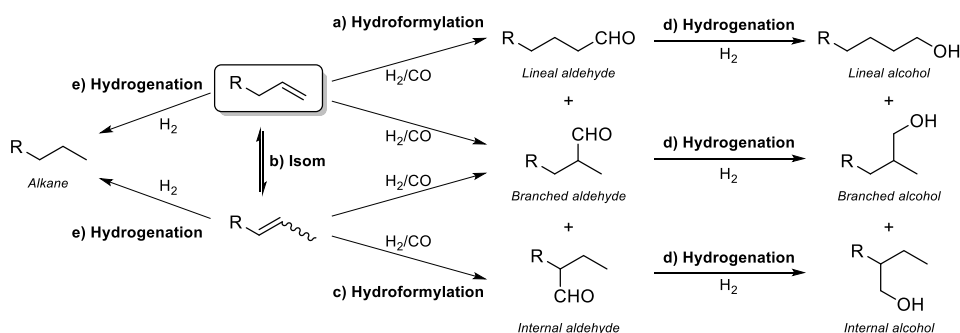
<sup>9</sup> Source: Scifinder. Keywords: Hydroformylation, *oxo*-reaction, asymmetric hydroformylation, enantioselective hydroformylation. Date: 2<sup>nd</sup> June 2020.

<sup>10</sup> Beller, M., Eds.; *Catalytic Carbonylation Reactions*; Springer-Verlag, Berlin Heidelberg, **2006**.

<sup>11</sup> Breit, B.; Seiche, W. *Synthesis* **2001**, 1-36.

<sup>12</sup> Vilches-Herrera, M.; Domke, L.; Börner, A. *ACS Catal.* **2014**, *4*, 1706-1724.

hydroformylation reaction (Scheme 2c), yielding mixtures of internal aldehydes in addition to the branched and linear aldehydes. It was observed that higher CO partial pressures reduced isomerization processes.<sup>13</sup> In addition, chemoselectivity issues should be overcome. The presence of H<sub>2</sub> as a reactant made feasible the hydrogenation of the CHO and C=C groups as side reactions competing with the hydroformylation process (Scheme 2d and 2e, respectively). It was observed that strong  $\sigma$ -donor ligands and metal centers with high electron density favor the formation of alcohols (Scheme 2d).



**Scheme 2.** Chemo- and regioselectivity of the hydroformylation reaction

### I.1.1 Cobalt-catalyzed hydroformylation

The first reports in hydroformylation reactions were described using cobalt-based catalysts in the absence of organic ligands (unmodified catalysts). Initial investigations pointed to the hydrido carbonyl complexes [Co(H)(CO)<sub>4</sub>] as the active species.<sup>14</sup> The formation of the active catalyst was achieved, either from cobalt(II) salts or from [Co<sub>2</sub>(CO)<sub>8</sub>].<sup>15</sup> Using unmodified cobalt catalysts, harsh reaction conditions (100-180 °C and 100-300 bar) were needed to afford the corresponding mixture of aldehydes. Moreover, the above mentioned side-reaction products were also formed.<sup>16</sup>

<sup>13</sup> van Leeuwen, P. W. N. M.; Claver, C., Eds.; *Rhodium Catalyzed Hydroformylation*; Kluwer Academic Publishers, Dordrecht, **2002**.

<sup>14</sup> (a) Wender, I.; Sternberg, H. W.; Orchin, M. *J. Am. Chem. Soc.* **1953**, *75*, 3041-3042. (b) Chadwick, J. C.; Duchateau, R.; Freixa, Z.; van Leeuwen, P. W. N. M., Eds.; *Homogeneous Catalysts: Activity-Stability-Deactivation*; Wiley-VCH, Weinheim, **2011**.

<sup>15</sup> Hebrard, F.; Kalck, P. *Chem. Rev.* **2009**, *109*, 4272-4282.

<sup>16</sup> (a) Adkins, H.; Krsek, G. *J. Am. Chem. Soc.* **1949**, *71*, 3051-3055. (b) Lai, R.; Ucciani, E. *J. Mol. Catal.* **1978**, *4*, 401-410. (c) Ungvary, F.; Marko, L. *Organometallics* **1982**, *1*, 1120-1125.

The introduction of phosphorus(III)-containing ligands,<sup>17</sup> such as phosphines, for the stabilization of the cobalt-based catalytic species enabled the use of lower pressures (< 100 bar), although higher temperatures were needed (160-200 °C) to overcome the intrinsically lower catalytic activity. Initial studies with P(<sup>t</sup>Bu)<sub>3</sub> **1** showed an improvement in the formation of linear aldehydes and reduction of isomerization processes.<sup>18</sup>

A few years later, structurally diverse arrays of cyclic tertiary phosphines were developed (Figure 2). Bicyclic limonene-based ligands Lim **2**,<sup>19</sup> with variable lengths in the alkyl chain R, and a set of ligands derived from 4-vinyl-1-cyclohexene **3** (VCH ligands)<sup>20</sup> were developed by Sasol and applied to the cobalt-catalyzed hydroformylation of alkenes. The Shell Oil Company developed the Phoban ligands **4**, a new type of phosphines derived from 1,5-cyclooctadiene.<sup>20,21</sup> There are scarce reports of monophosphites in cobalt-catalyzed hydroformylations.<sup>22</sup> Poor activity was observed when P(OPh)<sub>3</sub> **5** was used as ligand,<sup>22a</sup> and the use of more sterically hindered phosphites, such as **6** (Figure 2), did not improve the catalytic activity of the cobalt-based catalysts.<sup>22b</sup>

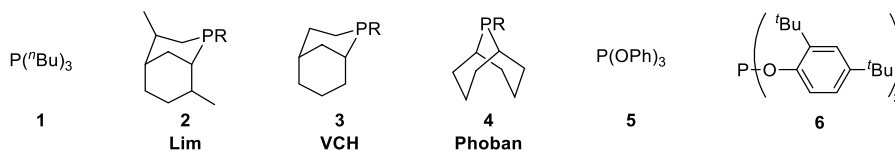


**Figure 2.** Monodentate ligands used in cobalt-catalyzed hydroformylation

In 1980s, reports employing bischelating phosphine ligands **7-10** showed suppression of isomerizations, but also lower catalytic activity compared to [Co(H)(CO)<sub>4</sub>] (Figure 3).<sup>23</sup> In the recent years, the interest in cobalt-catalyzed hydroformylation reactions employing bidentate ligands has re-emerged. In 2016,

<sup>17</sup> Kamer, P. C. J.; van Leeuwen, P. W. N. M., Eds.; *Phosphorus(III) Ligands in Homogeneous Catalysis: Design and Synthesis*; John Wiley & Sons Ltd., Chichester, **2012**.

<sup>18</sup> (a) Tucci, E. R. *Ind. Eng. Chem. Prod. Res. Dev.* **1968**, *7*, 32-38. (b) Slaugh, L. H.; Mullineaux, R. D. *J. Organometal. Chem.* **1968**, *13*, 469-477.

<sup>19</sup> (a) Crause, C.; Bennie, L.; Damoense, L.; Dwyer, C. L.; Grove, C.; Grimmer, N.; van Rensburg, W. J.; Kirk, M. M.; Mokheseng, K. M.; Otto, S.; Steynberg, P. *J. Dalton Trans.* **2003**, 2036-2042. (b) Polas, A.; Wilton-Ely, J. D. E. T.; Slawin, A. M. Z.; Foster, D. F.; Steynberg, P. J.; Green, M. J.; Cole-Hamilton, D. *J. Dalton Trans.* **2003**, 4669-4677.

<sup>20</sup> Bungu, P. N.; Otto, S. *Dalton Trans.* **2011**, *40*, 9238-9249.

<sup>21</sup> Bungu, P. N.; Otto, S. *Dalton Trans.* **2007**, 2876-2884.

<sup>22</sup> (a) Haumann, M.; Meijboom, R.; Moss, J. R.; Roodt, A. *Dalton Trans.* **2004**, 1679-1686. (b) Meijboom, R.; Haumann, M.; Roodt, A.; Damoense, L. *Helv. Chim. Acta* **2005**, *88*, 676-693.

<sup>23</sup> (a) Cornely, W.; Fell, B. *J. Mol. Catal.* **1982**, *16*, 89-94. (b) Murata, K.; Matsuda, A.; Masuda, T. *J. Mol. Catal.* **1984**, *23*, 121-132.

Kluwer *et al.* reported that the use of a ferrocene-based bisphosphine ligand **11** provided an efficient cobalt catalyst for the hydroformylation of oct-1-ene. The efficiency was attributed to the presence of a well-defined molecular framework with a stable and rigid coordination sphere and the direct use of the active catalyst rather than *in situ* prepared species.<sup>24</sup>

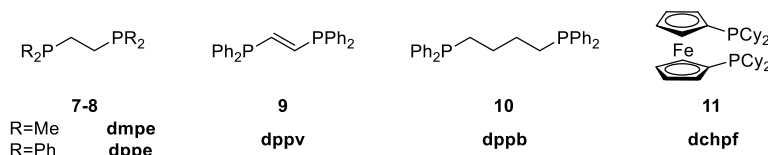
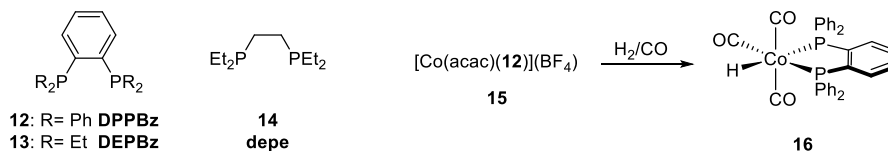


**Figure 3.** Bidentate ligands used in cobalt-catalyzed hydroformylations

In 2020, Stanley *et al.* reported the hydroformylation reaction based on cobalt(II) cationic complexes (Scheme 3).<sup>25</sup> The use of electron donating bisphosphine ligands **8**, **12-14** provided an unusual catalytic activity for both terminal and internal alkyl alkenes, similar as for  $[\text{Co}(\text{H})(\text{CO})_4]$ , but employing a lower pressure (30 bar). The  $19 e^-$  complex **16** was proposed as the active catalytic species. The results obtained by cobalt(II) complexes could suppose a breakthrough in cobalt-catalyzed hydroformylation in academia and industry.



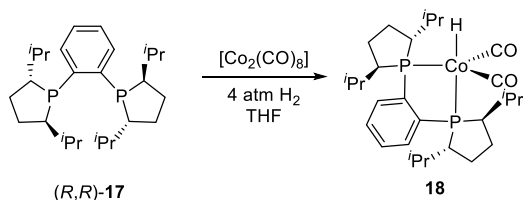
**Scheme 3.** Cationic cobalt-catalyzed hydroformylation with electron donating bisphosphine ligands

Chirik *et al.* have reported the synthesis and reactivity of relevant intermediates in cobalt-catalyzed hydroformylation reactions derived from ligand (*R,R*)-(*i*<sup>Pr</sup>DuPhos) **17** (Scheme 4).<sup>26</sup> Hydrido cobalt complex **18** was applied in the hydroformylation of styrene and the hydrogenation product was the only product observed.

<sup>24</sup> Kluwer, A. M.; Krafft, M. J.; Hartenbach, I.; de Bruin, B.; Kaim, W. *Top. Catal.* **2016**, *59*, 1787-1792.

<sup>25</sup> Hood, D. M.; Johnson, R. A.; Carpenter, A. E.; Younker, J. M.; Vinyard, D. J.; Stanley, G. G. *Science* **2020**, *367*, 542-548.

<sup>26</sup> MacNeil, C.; Mendelsohn, L.; Zhong, H.; Pabst, T.; Chirik, P. J. *Angew. Chem. Int. Ed.* **2020**, *59*, 8912-8916.



**Scheme 4.** Cobalt-catalyzed hydroformylation of styrene employing hydrido cobalt complex **18**

### I.1.2 Rhodium-catalyzed hydroformylation

First reports of Rh-catalyzed hydroformylations with unmodified Rh-catalysts provided an attractive alternative to cobalt-catalyzed processes, due to the mild reaction conditions and the high chemoselectivities towards aldehydes. Even though other metals have been of interest in the hydroformylation reaction,<sup>6,27</sup> cobalt and rhodium catalysts have prevailed, both in the academic and industrial sectors.

In contrast with cobalt-catalyzed hydroformylations, the use of  $\sigma$ -donor ligands in Rh-based hydroformylations, not only improved selectivity, but also increased the reaction rates. The development of the Wilkinson catalyst  $[\text{RhCl}(\text{PPh}_3)_3]$  for the hydrogenation of alkenes put monophosphines under scrutiny in Rh-catalyzed hydroformylations.<sup>28</sup> Early studies revealed the close dependence between selectivity and ligand concentration, observing higher linear aldehyde formation when the ligand concentration was increased. Wilkinson<sup>28,29</sup> and Andreetta<sup>30</sup> suggested that, amongst the different catalytically active species in equilibrium, the intermediates with two coordinated phosphines led to higher amounts of linear product.

The introduction of bidentate bisphosphine ligands in Rh-catalyzed hydroformylations reduced the number of active metal complexes, due to the chelate effect. Depending on the coordination site to which the ligating groups are bonded in the pentacoordinate trigonal bipyramidal (tbp) geometry, two

<sup>27</sup> Pospech, J.; Fleischer, I.; Franke, R.; Buchholz, S.; Beller, M. *Angew. Chem. Int. Ed.* **2013**, *52*, 2852-2872.

<sup>28</sup> Evans, D.; Osborn, J. A.; Wilkinson, G. *J. Chem. Soc. A* **1968**, 3133-3142.

<sup>29</sup> (a) Evans, D.; Yagupsky, G.; Wilkinson, G. *J. Chem. Soc. A* **1968**, 2660-2665. (b) Wilkinson, G.; Brown, C. K. *J. Chem. Soc. A* **1970**, 2753-2764.

<sup>30</sup> Gregorio, G.; Montrasi, G.; Tampieri, M.; Cavalieri d'Oro, P.; Pagani, G.; Andreetta, A. *Chim. Ind. (Milan)* **1980**, *62*, 389-394.

different coordination geometries can be observed (Figure 4): (a) coordination of both ligating groups to the equatorial plane of the metal complex (denoted as eq-eq) or, (b) one ligating group coordinates to the equatorial position and the other occupies the axial position (denoted as eq-ax).

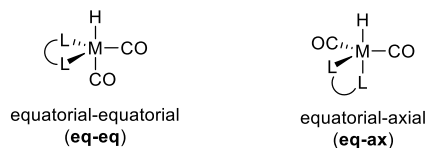


**Figure 4.** Representative coordination modes of bidentate ligands in the hydroformylation catalyst

Initial studies with small bite angle ligands (for instance compounds **8** and **19**) showed a preferred coordination in the eq-ax fashion at the *tbp* rhodium center and led to a decrease of the regioselectivity.<sup>13</sup> The use of bisphosphine ligands with a wide bite angle allowed for the formation of intermediates with different coordination modes. Amongst the bisphosphine ligands, BISBI ligand **20** provided a high regioselectivity towards the linear aldehyde in the hydroformylation of hex-1-ene, with l/b ratios up to 67:1.<sup>31</sup> The X-ray structure of [Rh(H)(**20**)(PPh<sub>3</sub>)(CO)] revealed the eq-eq coordination of the two phosphorus atoms to the rhodium center.<sup>32</sup>

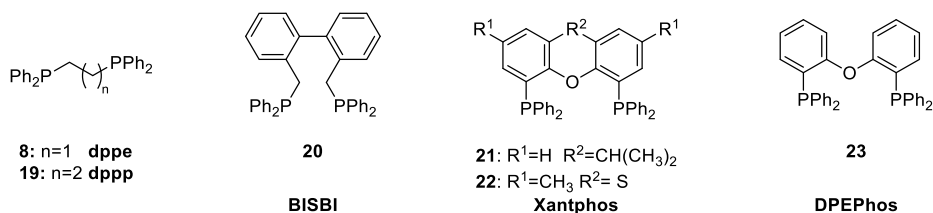


**Figure 5.** Bidentate phosphine ligands for Rh-catalyzed hydroformylations

A few years later, Xantphos-type ligands (for instance **21** and **22**) were developed to study the effect of the bite angle in the outcome of the hydroformylation reaction. As previously observed for **20**, wide bite angle ligands led to higher amounts of the linear product in the hydroformylation of

<sup>31</sup> (a) Devon, T. J.; Phillips, G. W.; Puckette, T. A.; Stavinoha, J. L.; Vanderbilt, J. J. US4694109A, **1987**. (b) Devon, T. J.; Phillips, G. W.; Puckette, T. A.; Stavinoha, J. L.; Vanderbilt, J. J. US5332846A, **1994**.

<sup>32</sup> Casey, C. P.; Whiteker, G. T.; Melville, M. G.; Petrovich, L. M.; Gavney, J. A. Jr.; Powell, D. R. *J. Am. Chem. Soc.* **1992**, *114*, 5535-5543.



oct-1-ene.<sup>33</sup> *In situ* IR and NMR spectroscopy studies of  $[\text{Rh}(\text{H})(\text{CO})_2(\mathbf{22})]$  revealed a dynamic equilibrium of the eq-ax and eq-eq complexes.<sup>34</sup> The comparison of the catalytic performance employing Xantphos-derived catalytic systems and the analogous acyclic ligand DPEPhos **23**, with a lower bite angle, indicated that the xanthene backbone provides high linear regioselectivities.<sup>33</sup>

The use of phosphite ligands in hydroformylation constituted a breakthrough in the field, due to the higher reactivity compared to monophosphine-based catalysts. This behavior was rationalized as a result of the higher  $\pi$ -acceptor character of phosphite ligands with respect to phosphines, making the Rh–CO bond weaker and favoring the CO dissociation and subsequent alkene coordination. The use of substituents at the *ortho* position of the phosphite group led to ligands **24–25** (Figure 6), which provided high reaction rates for internal alkenes and also moderate regioselectivities for terminal alkenes.<sup>35</sup> Bryant and co-workers reported the advantages of Biphephos ligand **26**, a bidentate ligand with encumbered phosphite groups and substituents at the 3,3' positions of a [1,1'-biphenyl]-2,2'-diol (Figure 6).<sup>36</sup> Initial studies showed the efficiency of ligand **26** in the formation of linear aldehydes and the role of bulky substituents for the high selectivities achieved.<sup>37</sup>

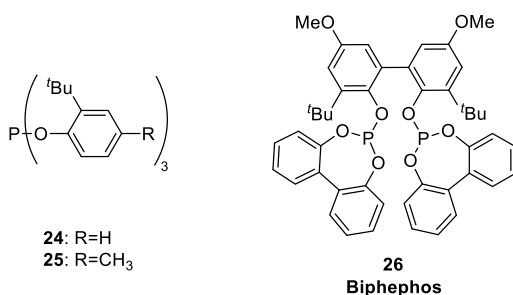


**Figure 6.** Mono- and bidentate phosphite ligands for Rh-catalyzed hydroformylations

<sup>33</sup> Kranenburg, M.; van der Burgt, Y. E. M.; Kamer, P. C. J.; van Leeuwen, P. W. N. M.; Goubitz, K.; Fraanje, J. *Organometallics* **1995**, *14*, 3081-3089.

<sup>34</sup> van der Veen, L. A.; Boele, M. D. K.; Bregman, F. R.; Kamer, P. C. J.; van Leeuwen, P. W. N. M.; Goubitz, K.; Fraanje, J.; Schenk, H.; Bo, C. J. *Am. Chem. Soc.* **1998**, *120*, 11616-11626.

<sup>35</sup> (a) van Leeuwen, P. W. N. M.; Roobeek, C. F. J. *Organomet. Chem.* **1983**, *258*, 343-350. (b) van Rooy, A.; Orij, E. N.; Kamer, P. C. J.; van Leeuwen, P. W. N. M. *Organometallics* **1995**, *14*, 34-43.

<sup>36</sup> (a) Billig, E.; Abatjoglou, A. G.; Bryant, D. R. US4668651A, **1987**. (b) Billig, E.; Abatjoglou, A. G.; Bryant, D. R. US4769498A, **1988**.

<sup>37</sup> Cuny, G. D.; Buchwald, S. L. J. *Am. Chem. Soc.* **1993**, *115*, 2066-2068.

### I.1.3 Enantioselective rhodium-catalyzed hydroformylation

*Chirality* is the geometric property of an arrangement of atoms in a molecule of being non-superimposable to its mirror image (Figure 7).<sup>38</sup> The two mirror images of an arrangement of atoms in a molecule are called *enantiomers*, which differ in the optical and biological properties. Chirality is found in Nature in many forms: biological systems, like human beings, are made of biomolecules such as L-aminoacids or D-carbohydrates and limonene enantiomers possess different olfactory properties (Figure 7). The demand for high optical purity in the pharmaceutical industry increased after the Thalidomide case, with tough requirements from the U.S. Food and Drug Administration (FDA) for high chemical and optical purity in active pharmaceutical ingredients.<sup>39</sup>

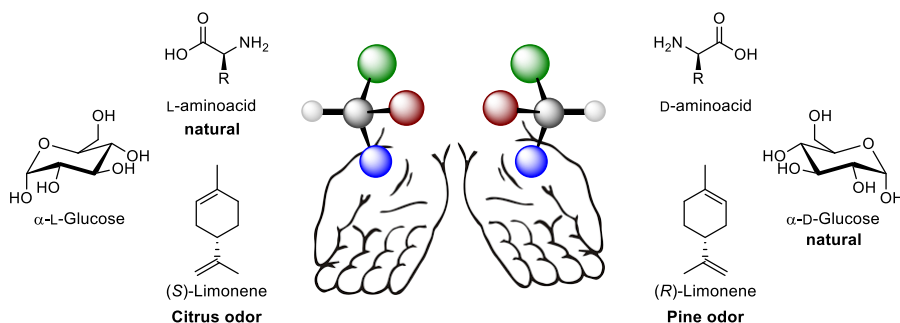


**Figure 7.** Schematic representation of chiral molecules with representative examples of amino acids, carbohydrates and terpenes<sup>40</sup>

Among the different strategies to obtain optically (or enantiomerically) pure molecules, enantioselective or asymmetric catalytic synthesis is a highly interesting option for the preparation of optically active compounds, as this method only requires catalytic amounts of an enantiomerically pure compound (*i.e.*, the enantioselective catalytic system). Moreover, this approach generates a reduced number of side-products and improves the product isolation. These reasons have inspired the scientific community to design and develop organo-,<sup>41</sup>

<sup>38</sup> IUPAC. *Compendium of Chemical Terminology*, 2<sup>nd</sup> Ed. (the "Gold Book"). Blackwell Scientific Publications, Oxford, 1997.

<sup>39</sup> (a) Kim, J. H.; Scialli, A. R. *Toxicol. Sci.* **2011**, *122*, 1-6. (b) Kim, J. H.; Scialli, A. R. *Toxicol. Sci.* **2012**, *125*, 613.

<sup>40</sup> Image borrowed from <https://in.pinterest.com/pin/334533078567985090/> and modified.

<sup>41</sup> Berkessel, A.; Gröger, H.; *Asymmetric Organocatalysis: From Biomimetic Concepts to Applications in Asymmetric Synthesis*; Wiley-VCH, Weinheim, 2005.

bio-<sup>42</sup> or metal-based enantioselective catalysts for pivotal transformations in organic synthesis, including hydroformylation.<sup>43</sup> The hydroformylation process towards branched products may generate a stereogenic center. Thus, this chemistry provides a useful synthetic methodology to obtain valuable synthetic intermediates (*i.e.*, optically enriched or enantiopure aldehydes) with relevance in the life-science and fine-chemical sectors.

The use of enantiopure bisphosphines as ligands (Figure 8) expanded the scope of alkenes to be enantioselectively hydroformylated. Ligands with small bite angles, such as (*R,R*)-Chiraphos **27**, led to moderate enantioselectivities in the Rh-catalyzed hydroformylation of styrene (51% *ee*).<sup>44</sup> The use of a ligand with a wide bite angle, such as (*S,S*)-DIOP **28** and related ligands, did not bring substantial advantages in the enantioselectivities for a wide variety of alkenes (*e.g.*, alkyl-substituted alkenes, *N*-acetamidoacrylate) (30-59% *ee*).<sup>45</sup> (*R*)-BINAP **29**, which can be considered a privileged structure in enantioselective catalysis, led to low conversions and moderate enantioselectivities (*e.g.*, up to 60% *ee* for vinyl acetate).<sup>46</sup> The design of bisphospholane ligands **30-31** for enantioselective hydroformylations translated into high levels of enantioinduction. Among different phospholane-based designs, (*R,R*)-Ph-BPE **30** exhibited one of the best catalytic results in the enantioselective hydroformylation of styrene, allyl cyanide and vinyl acetate, with moderate to excellent reaction rates, regio- and enantioselectivities (82 to 94% *ee*).<sup>47</sup> The bisdiazaphospholane ligands, such as (*S,S*)-BDP **31**, have been applied to a broad array of substrates with enantioselectivities surpassing 90% *ee* in all cases.<sup>48</sup>

---

<sup>42</sup> Hilterhaus, L.; Liese, A.; Ketting, U.; Antranikian, G., Eds.; *Applied Biocatalysis: From Fundamental Science to Industrial Applications*; Wiley-VCH, Weinheim, **2016**.

<sup>43</sup> Sandoval, C. A.; Noyori, R.; *An Overview of Recent Developments in Metal-Catalyzed Asymmetric Transformations*, p 335-362. In *Organic Chemistry - Breakthroughs and Perspectives*; Ding, K.; Dai, L-X., Eds.; Wiley-VCH, Weinheim, **2012**.

<sup>44</sup> Diéguez, M.; Pereira, M. M.; Masdeu-Bultó, A. M.; Claver, C.; Bayón, J. C. *J. Mol. Catal. A: Chem.* **1999**, *143*, 111-122.

<sup>45</sup> Agbossou, F.; Carpentier, J.-F.; Mortreux, A. *Chem. Rev.* **1995**, *95*, 2485-2506.

<sup>46</sup> (a) Lee, C. W.; Alper, H. *J. Org. Chem.* **1995**, *60*, 499-503. (b) Sakai, N.; Nozaki, K.; Mashima, K.; Takaya, H. *Tetrahedron: Asymmetry* **1992**, *3*, 583-586. (c) Hoegaerts, D.; Jacobs, P. A. *Tetrahedron: Asymmetry* **1999**, *10*, 3039-3043.

<sup>47</sup> Klosin, J.; Landis, C. R. *Acc. Chem. Res.* **2007**, *40*, 1251-1259.

<sup>48</sup> Wong, G. W.; Landis, C. R. *Aldrichimica Acta* **2014**, *47*, 29-38.

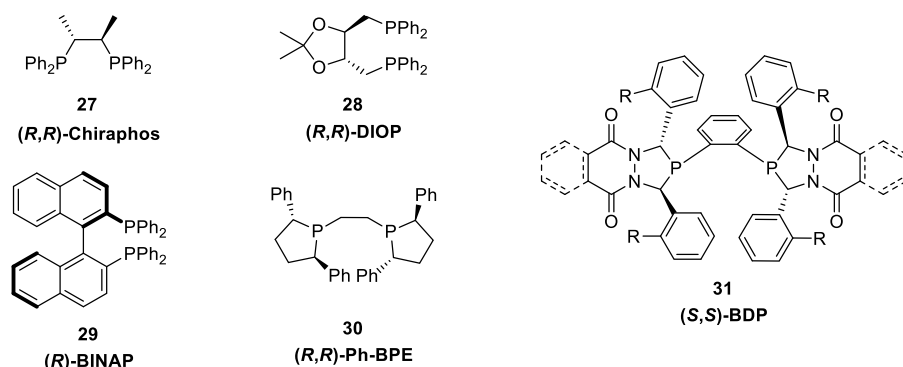


**Figure 8.** Bisphosphine ligands for Rh-catalyzed enantioselective hydroformylations

Takaya *et al.* reported the enantioselective hydroformylation of vinyl acetate with a 50% *ee* employing bisphosphite ligand **32**.<sup>46b</sup> It was not until Babin *et al.* reported the excellent performance of (R,R)-Chiraphite ligand **33** (Figure 9) in enantioselective hydroformylations, when the real potential of bisphosphite ligands was recognized.<sup>49</sup> Buisman *et al.* performed an extensive study of these ligands and analyzed the influence of the size and nature of the bridging moiety between the two phosphite groups.<sup>50</sup> Best results were obtained when pentane-2,4-diol was used to link the two phosphite groups (see substructure in blue in Figure 9), due to the formation of a 8-membered ring rhodium chelate, in which the bisphosphite groups coordinated in an eq-eq fashion to the *tbp* rhodium center.<sup>51</sup> The same authors demonstrated the chiral cooperativity among the bridging unit and the biaryl moieties in catalytic species derived from **34** and **35**. Attachment of trimethylsilyl groups at the 3 and 3' positions of the BINOL moiety as in ligand **35** translated into high stereoselectivities (up to 86% *ee* for styrene).<sup>52</sup>

<sup>49</sup> Babin, J. E.; Whiteker, G. T. WO9303839A1, **1993**.

<sup>50</sup> Buisman, G. J. H.; Vos, E. J.; Kamer, P. C. J.; van Leeuwen, P. W. N. M. *J. Chem. Soc. Dalton Trans.* **1995**, 409-417.

<sup>51</sup> Buisman, G. J. H.; van der Veen, L. A.; Kamer, P. C. J.; van Leeuwen, P. W. N. M. *Organometallics* **1997**, *16*, 5681-5687.

<sup>52</sup> Buisman, G. J. H.; van der Veen, L. A.; Klootwijk, A.; de Lange, W. G. J.; Kamer, P. C. J.; van Leeuwen, P. W. N. M.; Vogt, D. *Organometallics* **1997**, *16*, 2929-2939.

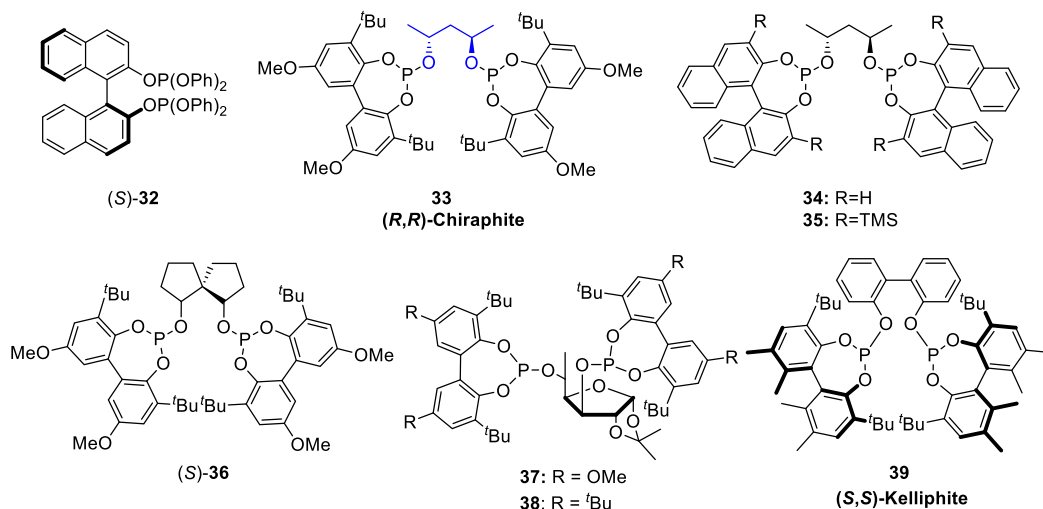


**Figure 9.** Enantiopure bisphosphite ligands for Rh-catalyzed enantioselective hydroformylations

The good results obtained with bulky bisphosphite ligands encouraged the design and synthesis of new structures with different backbones (Figure 9). The use of a spirocyclic backbone bridging unit in ligand **36** led to moderate enantioselectivities in the hydroformylation of styrene (69% *ee*).<sup>53</sup> The use of ligands based on 1,2-*O*-isopropylidene- $\alpha$ -D-xylofuranose backbones **37–38** provided moderate to excellent enantioselectivities for vinyl acetate (73% *ee*), and styrene (93% *ee*) (Figure 9).<sup>54</sup> Dow Pharma introduced (*S,S*)-Kelliphite **39**, which contains two stereogenic axes at the bulky phosphite groups (Figure 9). Despite the low enantioselectivity obtained for styrene, the catalytic system derived from **39** gave good enantioselectivities for the enantioselective hydroformylation of vinyl acetate and allyl cyanide.<sup>55</sup>

Simultaneously to the development of chiral bisphosphites, a new type of ligand was discovered by Takaya and Nozaki in 1993. By the combination of a BINAP-related phosphine motif and a phosphite with axial stereogenic elements, an enantiopure hybrid phosphine-phosphite (P–OP) ligand was developed.<sup>56</sup> (*R,S*)-

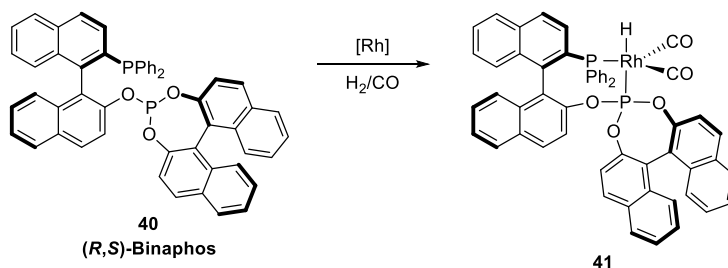
<sup>53</sup> Jiang, Y.; Xue, S.; Li, Z.; Deng, J.; Mi, A.; Chan, A. S. C. *Tetrahedron: Asymmetry* **1998**, *9*, 3185–3189.

<sup>54</sup> (a) Gual, A.; Godard, C.; Castellón, S.; Claver, C. *Adv. Synth. Catal.* **2010**, *352*, 463–477. (b) Diéguez, M.; Pàmies, O.; Ruiz, A.; Claver, C.; Castellón, S. *Chem. Commun.* **2000**, 1607–1608.

<sup>55</sup> (a) Cogley, C. J.; Gardner, K.; Klosin, J.; Praquin, C.; Hill, C.; Whiteker, G. T.; Zanotti-Gerosa, A.; Petersen, J. L.; Abboud, K. A. *J. Org. Chem.* **2004**, *69*, 4031–4040. (b) Cogley, C. J.; Klosin, J.; Qin, C.; Whiteker, G. T. *Org. Lett.* **2004**, *6*, 3277–3280.

<sup>56</sup> Sakai, N.; Mano, S.; Nozaki, K.; Takaya, H. *J. Am. Chem. Soc.* **1993**, *115*, 7033–7034.

Binaphos **40** has been one of the most versatile and highly enantioselective ligands in enantioselective hydroformylation for a broad array of substrates.<sup>57</sup> Structural and spectroscopic studies revealed a highly preferred eq-ax coordination mode in the rhodium complex **41**, with the hydrido and the phosphite ligands being in axial positions, and the phosphine and two CO groups in the equatorial plane (Scheme 5).<sup>58</sup> This coordination mode was demonstrated to be an exception of (*R,S*)-Binaphos **40** rather than a principle in hydroformylation complexes with P–OP ligands.



**Scheme 5.** Coordination mode of (*R,S*)-Binaphos **40** in the hydrido dicarbonyl rhodium complex

#### 1.1.4 The hydroformylation reaction mechanism

The first mechanistic proposal for the hydroformylation reaction was reported in 1961 by Heck and Breslow for the unmodified cobalt-catalyzed transformation.<sup>59</sup> So far, the scientific community has used this seminal mechanistic proposal to rationalize the Rh-catalyzed reaction in presence or absence of organic ligands. The vast structural diversity of organic ligands provides a high number of potential coordination geometries for the resulting metal centers. For the sake of simplicity, the whole catalytic cycle in the discussion that follows for metal-catalyzed hydroformylations will be depicted for bidentate phosphorus ligands that are coordinated to the metal center in a bis-equatorial fashion (eq-eq).

The mechanism depicted in Scheme 6 corresponds to the dissociative mechanism proposed by Wilkinson *et al.*<sup>28</sup> The first step is the formation of the hydrido dicarbonyl metal complex **42**, which is generally generated *in situ* under

<sup>57</sup> Pizzano, A. *Chem. Rec.* **2016**, *16*, 2595-2618.

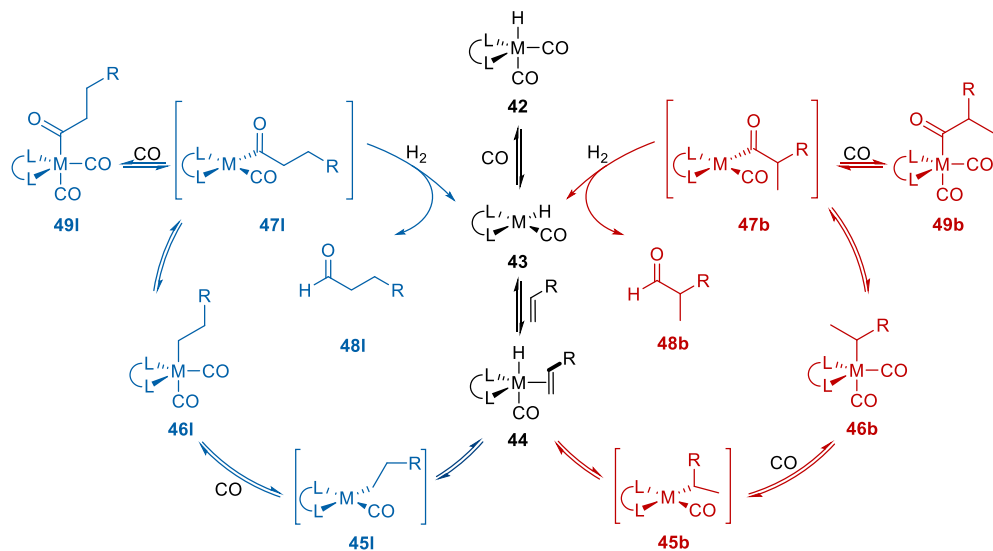
<sup>58</sup> Nozaki, K.; Sakai, N.; Nanno, T.; Higashijima, T.; Mano, S.; Horiuchi, T.; Takaya, H. *J. Am. Chem. Soc.* **1997**, *119*, 4413-4423.

<sup>59</sup> Heck, R. F.; Breslow, D. S. *J. Am. Chem. Soc.* **1961**, *83*, 4022-4027.

H<sub>2</sub>/CO atmosphere, either in the presence or absence of the substrate. The complex **42** is an off-cycle species with a pentacoordinate trigonal bipyramidal (tbp) geometry. It has been commonly accepted that the hydrido ligand occupies the axial position.<sup>13</sup> The formation of catalytically active species starts with the dissociation of one CO ligand, usually from an equatorial position, and the unsaturated square planar complex **43** is formed. Complexes **42** and **43** are in fast equilibrium and the equilibrium is shifted to complex **42** upon increasing the CO concentration in the reaction mixture. The reaction proceeds by coordination of the alkene to the metal center to form complex **44** followed by the subsequent *cis* insertion of the C=C group into the Rh–H, which has been proposed as the regio-determining step.<sup>34</sup> In the case of enantioselective hydroformylations, the coordination of the alkene to the metal center can take place with differentiation of the two enantiotopic faces of the alkene. It is well established that the stereodetermining step depends on the nature of the catalytic system: whilst some authors have proposed the alkene coordination as the stereodetermining-step for their catalytic systems,<sup>34</sup> other authors claim that the alkene insertion in the Rh–H bond is the regio- and enantio-determining step in their case.<sup>60</sup> Two different isomeric alkyl complexes can be formed after the insertion of the C=C group into the Rh–H bond. If the insertion process leads to the linear alkyl complex **45i**, the linear aldehyde is formed *via* the reaction pathway indicated in blue in Scheme 6. Alternatively, the branched aldehyde is formed from the branched alkyl complex **45b** by following the reaction pathway indicated in red in Scheme 6. Depending on the catalytic system, the insertion reaction can be reversible, thus affecting the overall regioselectivity of the process. The unsaturated square planar alkyl complexes **45** evolve to the saturated complexes **46** upon coordination of CO. Migratory insertion of the CO group into the alkyl–Rh bond leads to square-planar acyl complexes **47**. These complexes can undergo two possible reaction pathways (in addition to reverting to alkyl complex **46**). First, hydrogenolysis can take place by reaction of complex **47** with H<sub>2</sub> to form aldehydes **48b** or **48i**, with the active rhodium complex **43** being recovered. Second, CO can coordinate to complex **47** leading to the saturated acyl complex **49**, a common resting state in the hydroformylation reaction, which can be usually observed by spectroscopic techniques.

---

<sup>60</sup> (a) Carbó, J. J.; Maseras, F.; Bo, C.; van Leeuwen, P. W. N. M. *J. Am. Chem. Soc.* **2001**, *123*, 7630-7637. (b) Carbó, J. J.; Lledós, A.; Vogt, D.; Bo, C. *Chem. - Eur. J.* **2006**, *12*, 1457-1467. (c) Aguado-Ullate, S.; Saureu, S.; Guasch, L.; Carbó, J. J. *Chem. - Eur. J.* **2012**, *18*, 995-1005.



**Scheme 6.** Hydroformylation mechanism for cobalt- and rhodium-catalyzed processes in presence of bidentate ligands

## I.2 Supramolecular approaches in rhodium-catalyzed hydroformylation

The critical step in most organometallic catalytic enantioselective processes is the assembly of a supramolecular system around a metal center. It involves the substrate, the metal precursor and the enantiopure ligand, which is generally bound to the metal through several functional groups. In this complex system, the metal center provides a low-energy reaction pathway that enables catalysis, whereas the enantiomerically pure ligand activates and creates an asymmetric environment around the metal ultimately enabling preferential recognition of one of the enantiotopic elements of the substrate. When high enantioselectivities in the overall process are obtained, the enantioselective catalyst provides a perfect three-dimensional template for the substrate(s) and reagent(s). Structural changes to the substrate(s) and/or reagent(s) often translate to a loss of enantioselectivity.

In some cases, supramolecular interactions have been exploited to construct the skeletons of the desired (enantio)selective catalysts. This is done by attaching two (or more) building blocks that contain the functional groups desired for catalysis as well as the motifs needed for the supramolecular assembly. These methodologies have enabled synthesis of libraries of structurally diverse supramolecular catalysts with greater ease than by standard covalent chemistry. In other examples, supramolecular interactions have been exploited to facilitate a good three-dimensional match for the substrate(s), reagent(s) and catalytic



system, thus enhancing the (stereo)selectivity of the corresponding transformation. The term supramolecular chemistry has been defined as the chemistry beyond the molecules encompassing the formation of higher order molecular complexes by reversible interactions.<sup>61</sup> Taking nature as an inspiration source, chemists have taken advantage of supramolecular interactions as a toolbox to implement in catalysis, giving rise to a new field of research known as “*supramolecular catalysis*”.<sup>62</sup> Supramolecular interactions (or non-covalent bonding interactions) have been categorized according to their nature and strength (Figure 10).<sup>63</sup> These reversible interactions have been widely studied by the supramolecular scientific community and applied within supramolecular chemistry studies. Metal-ligand interactions have also been widely employed in supramolecular chemistry, though they cannot be considered non-covalent.

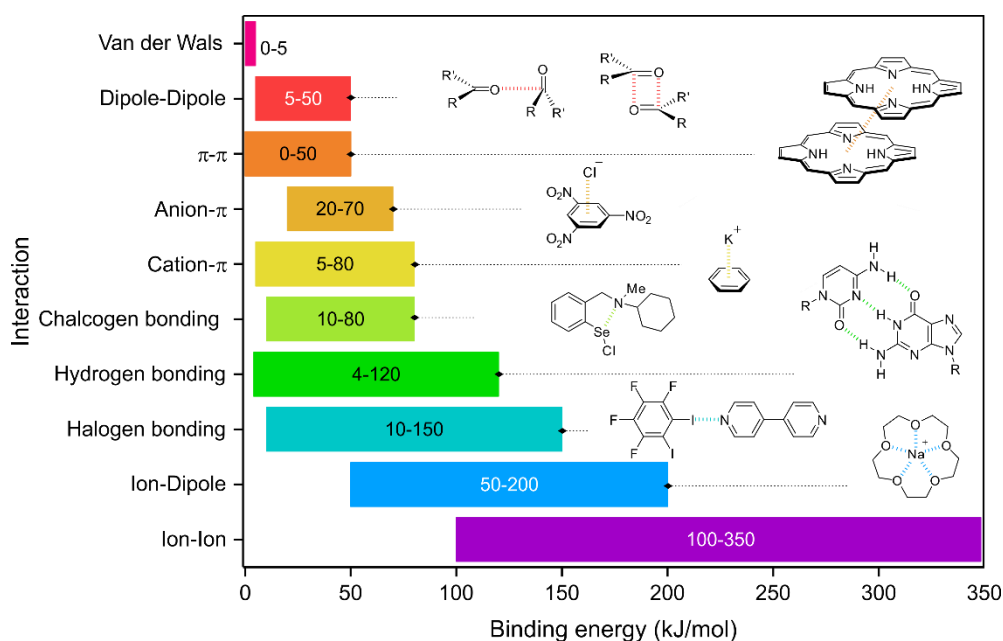


**Figure 10.** Schematic representation of supramolecular interactions

<sup>61</sup> Steed, J. W.; Atwood, J. L., Eds.; *Supramolecular Chemistry*, 2<sup>nd</sup> Ed.; John Wiley & Sons Ltd., Chichester, **2009**.

<sup>62</sup> To avoid confusion, the name *supramolecular catalysis* is reserved to processes, which involve supramolecular interactions and do not take part of the basic catalytic reaction.

<sup>63</sup> For halogen bonding interactions, see: Cavallo, G.; Metrangolo, P.; Milani, R.; Pilati, T.; Priimagi, A.; Resnati, G.; Terraneo, G. *Chem. Rev.* **2016**, *116*, 2478-2601. For chalcogen bonding interactions, see: Breugst, M.; von der Heiden, D.; Schmauck, J. *Synthesis* **2017**, *49*, 3224-3236. For anion- $\pi$  interaction, see: Chifotides, H. T.; Dunbar, K. R. *Acc. Chem. Res.* **2013**, *46*, 894-906. For the rest of interactions, see ref 61.

Initial developments of supramolecular catalysts were deeply inspired by biological systems, such as enzymes, as catalysts. Their unique properties (*e.g.*, enhancement of the reaction rates under mild conditions, chiral recognition, high turnover numbers and competitive inhibition processes) have served as a source of inspiration for the practitioners of supramolecular catalysts. In addition to these features, the possibility to introduce stereogenic elements in the non-natural supramolecular catalysts and to enhance the robustness towards high temperatures and new reaction media, has boosted the applicability of supramolecular catalysis.<sup>61</sup> An ample array of catalytic transformations has been of interest for supramolecular catalytic practitioners.<sup>64</sup> In the field of the hydroformylation transformation, a numerous approaches and supramolecular interactions have been studied.<sup>64d,65</sup> In the following pages, an overview of representative examples of supramolecular approaches for hydroformylation reactions will be discussed.

### 1.2.1 Rhodium-catalyzed hydroformylations in confined spaces

Initial designs for supramolecular hydroformylation catalysts mimicking enzyme catalysis focused on the *host-guest approach*. The pioneering work by Monflier *et al.* introduced chemically modified  $\beta$ -cyclodextrin ( $\beta$ -CD) **50** as inverse phase-transfer catalyst for biphasic hydroformylations of terminal alkenes with water-soluble phosphine ligands (Scheme 7, left).<sup>66</sup> The hydrophobic cavity was optimal for binding unfunctionalized olefins and moderate regioselectivities for the linear aldehydes were achieved. A different approach was developed by Reetz *et al.*<sup>67</sup> and Hapiot and co-workers,<sup>68</sup> in which the  $\beta$ -CD was modified to incorporate the coordinating groups (ligands **51** and **52** in Scheme 7, middle). These catalytic systems were more efficient than the analogous  $\beta$ -CD and ligand combination. Matt and co-workers reported the covalent confinement of

---

<sup>64</sup> For comprehensive reviews, see: (a) van Leeuwen, P. W. N. M., Eds.; *Supramolecular Catalysis*; Wiley-VCH, Weinheim, **2008**. (b) Raynal, M.; Ballester, P.; Vidal-Ferran, A.; van Leeuwen, P. W. N. M. *Chem. Soc. Rev.* **2014**, *43*, 1660-1673. (c) Raynal, M.; Ballester, P.; Vidal-Ferran, A.; van Leeuwen, P. W. N. M. *Chem. Soc. Rev.* **2014**, *43*, 1734-1787. (d) Vaquero, M.; Rovira, L.; Vidal-Ferran, A. *Chem. Commun.* **2016**, *52*, 11038-11051.

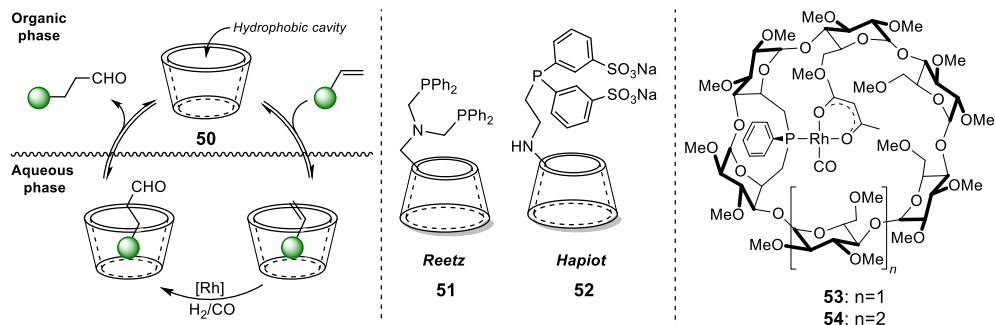
<sup>65</sup> For a comprehensive review, see: Nurttala, S. S.; Linnebank, P. R.; Krachko, T.; Reek, J. N. H. *ACS Catal.* **2018**, *8*, 3469-3488.

<sup>66</sup> (a) Hapiot, F.; Bricout, H.; Tilloy, S.; Monflier, E. *Top. Curr. Chem.* **2013**, *342*, 49-78. (b) Hapiot, F.; Manuel, S.; Bricout, H.; Tilloy, S.; Monflier, E. *Appl. Organomet. Chem.* **2015**, *29*, 580-587.

<sup>67</sup> Reetz, M. T.; Waldvogel, S. R. *Angew. Chem. Int. Ed. Engl.* **1997**, *36*, 865-867.

<sup>68</sup> Leblond, J.; Potier, J.; Manuel, S.; Bricout, H.; Machut-Binkowski, C.; Landy, D.; Tilloy, S.; Monflier, E.; Hapiot, F. *Catal. Sci. Technol.* **2017**, *7*, 3823-3830.

rhodium complexes **53-54** within the cyclodextrin cavity (Scheme 7, right). The high enantioselectivity (up to 95% *ee*) achieved in the enantioselective hydroformylation of styrene was an elegant example of selectivity control by the second coordination sphere of the catalytically active rhodium center.<sup>69</sup>



**Scheme 7.** Schematic representation of  $\beta$ -CD as inverse phase transfer catalyst (*left*). Chemically modified  $\beta$ -CD with phosphine groups (*middle*).  $\alpha$ - and  $\beta$ -CD ( $n=1, 2$ ) with a confined phosphorus ligand inside the cavity (*right*)

Another host-guest approach in hydroformylation reactions is the use of calix[4]arene scaffolds (Figure 11).<sup>70</sup> Calix[4]arenes are organic macrocycles based on phenolic moieties linked by methylene groups. Upper rim-functionalized calix[4]arenes such as **55** have been less studied than lower rim-functionalized calix[4]arenes (Figure 11a).<sup>71</sup> In the case of lower rim-functionalized calix[4]arenes, bulky phosphite coordinating groups, such as in ligand **56** (Figure 11b) provided high selectivity for the linear aldehyde.<sup>72</sup>

<sup>69</sup> Jouffroy, M.; Gramage-Doria, R.; Armspach, D.; Sémeril, D.; Oberhauser, W.; Matt, D.; Toupet, L. *Angew. Chem. Int. Ed.* **2014**, *53*, 3937-3940.

<sup>70</sup> Sémeril, D.; Matt, D. *Coord. Chem. Rev.* **2014**, *279*, 58-95.

<sup>71</sup> Natarajan, N.; Pierrevelcin, M.-C.; Sémeril, D.; Bauder, C.; Matt, D.; Ramesh, R. *Catal. Commun.* **2019**, *118*, 70-75.

<sup>72</sup> Sémeril, D.; Jeunesse, C.; Matt, D.; Toupet, L. *Angew. Chem. Int. Ed.* **2006**, *45*, 5810-5814.

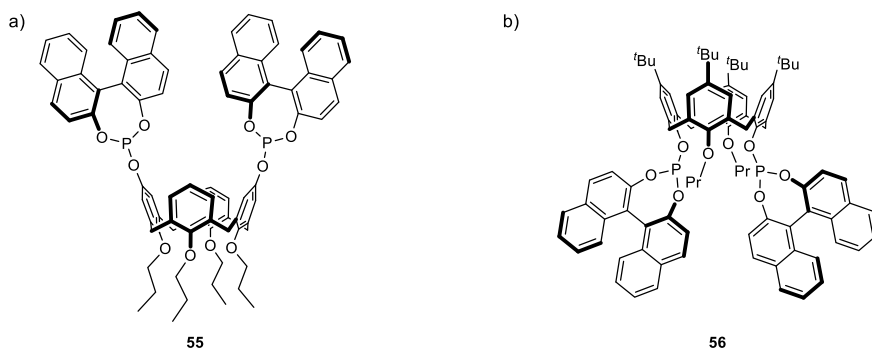


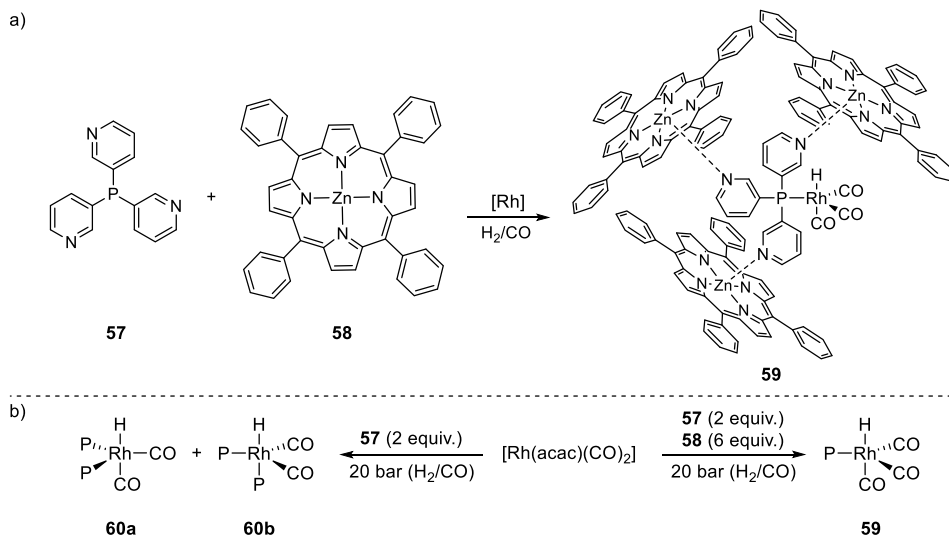
**Figure 11.** Calix[4]arenes with a) upper rim and b) lower rim functionalization

Over the past decades, different designs beyond the conventional *host-guest approach* have arisen as suitable strategies to develop supramolecular catalysts in confined spaces. Reek *et al.* introduced the *ligand template approach* for preparing hydroformylation catalysts.<sup>73</sup> Taking advantage of the strong binding between pyridine moieties and zinc porphyrins, tri(pyridin-3-yl)phosphine **57** was used as template for porphyrin **58** (Zn-TPP) binding, thus creating hemispherical assemblies and allowing for the preparation of an sterically encumbered hydrido tricarbonyl monophosphine Rh-catalysts **59** (Scheme 8a).<sup>74</sup> In the absence of porphyrin **58**, the active rhodium-catalysts derived from **57** incorporated two phosphine units in equilibrium between **60a** (eq-eq) and **60b** (eq-ax) (Scheme 8b). Rhodium catalysts derived from **59** provided higher activity and lower selectivity towards the linear aldehydes (TOF = 400 h<sup>-1</sup>, 1/b ratio = 37.5:62.5) than those derived from **60** (TOF = 43 h<sup>-1</sup>, 1/b ratio = 73.7:26.3) in the hydroformylation of oct-1-ene.<sup>74</sup> The use of catalysts derived from **59** in the hydroformylation of *trans*-oct-2-ene and *trans*-oct-3-ene enhanced the regioselectivity towards the corresponding internal aldehyde (selectivity up to 88% and 75%, respectively), although a low conversion were obtained (32% and 45% conv. respectively).<sup>75</sup>

<sup>73</sup> For comprehensive reviews of the ligand template approach for confined catalysts, see: (a) Leenders, S. H. A. M.; Gramage-Doria, R.; de Bruin, B.; Reek, J. N. H. *Chem. Soc. Rev.* **2015**, *44*, 433-448. (b) Jongkind, L. J.; Caumes, X.; Hartendorp, A. P. T.; Reek, J. N. H. *Acc. Chem. Res.* **2018**, *51*, 2115-2128. (c) Mouarrawis, V.; Plessius, R.; van der Vlugt, J. I.; Reek, J. N. H. *Front. Chem.* **2018**, *6*, 623-643.

<sup>74</sup> (a) Slagt, V. F.; Reek, J. N. H.; Kamer, P. C. J.; van Leeuwen, P. W. N. M. *Angew. Chem. Int. Ed.* **2001**, *40*, 4271-4274. (b) Besset, T.; Norman, D. W.; Reek, J. N. H. *Adv. Synth. Catal.* **2013**, *355*, 348-352.

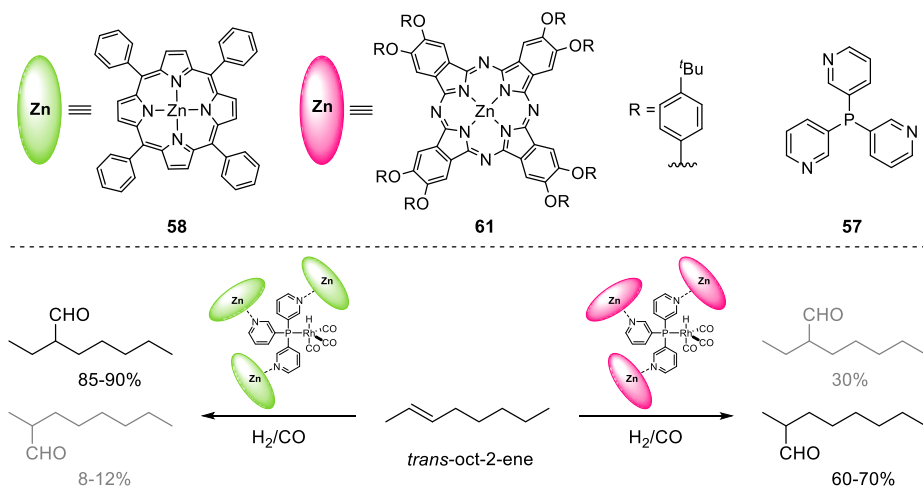
<sup>75</sup> Kuil, M.; Soltner, T.; van Leeuwen, P. W. N. M.; Reek, J. N. H. *J. Am. Chem. Soc.* **2006**, *128*, 11344-11345.



**Scheme 8.** a) Representation of the supramolecular assembly based on Zn-porphyrin **58** and tri(pyridin-3-yl) phosphine **57**. b) Coordination studies of  $[\text{Rh}(\text{acac})(\text{CO})_2]$  with phosphines **57** and  $\mathbf{57} \cdot (\mathbf{58})_3$

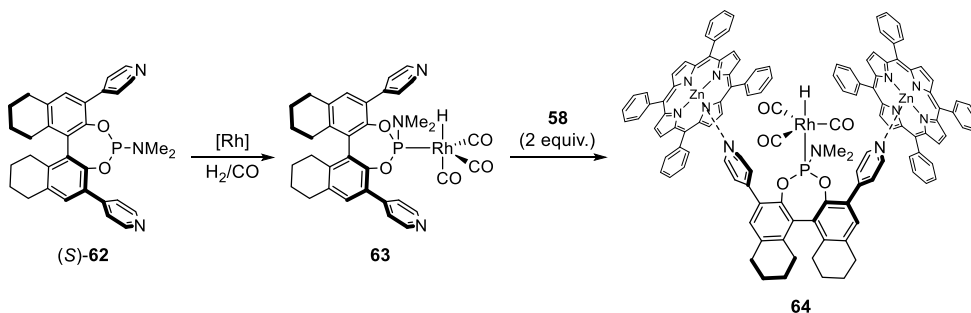
Steric and electronic modifications in heterocyclic counterpart have been able to control the regioselectivity, which constitutes an elegant example of selectivity control by the second coordination sphere.<sup>76</sup> Hydroformylations of internal alkenes such as *trans/cis*-oct-2-ene have been regiocontrolled by fine-tuning the structure of the heterocyclic counterpart (Scheme 9). Rhodium catalysts derived from **57** and Zn-phthalocyanine **61** led to the formation of 2-methyloctanal, whilst catalysts derived from **57** and porphyrin Zn-TPP **58** preferably led to 2-ethylheptanal.

<sup>76</sup> Bocokić, V.; Kalkan, A.; Lutz, M.; Spek, A. L.; Gryko, D. T.; Reek, J. N. H. *Nat. Commun.* **2013**, 4, 2670/1-2670/9.



**Scheme 9.** Regioselective hydroformylation of *trans*-oct-2-ene with supramolecular phosphine-derived rhodium catalysts

The introduction of ligand (*S*)-**62** led to an elegant example of supramolecular control of the coordination geometry (Scheme 10).<sup>77</sup> The addition of porphyrin **58** shifts the coordination mode of the phosphoramidite from an equatorial position in Rh-complex **63** to an axial one in complex **64**. This approach enhanced the enantioselectivity (from 25% *ee* in absence and 45% *ee* in presence of Zn-TPP **58**).



**Scheme 10.** Change in the coordination mode of rhodium complex **63** upon addition of Zn-TPP **58**

<sup>77</sup> (a) Bellini, R.; Chikkali, S. H.; Berthon-Gelloz, G.; Reek, J. N. H. *Angew. Chem. Int. Ed.* **2011**, *50*, 7342-7345. (b) Bellini, R.; Reek, J. N. H. *Chem. - Eur. J.* **2012**, *18*, 7091-7099.

## 1.2.2 Supramolecular assembled bidentate ligands in rhodium-catalyzed hydroformylation

The great utility of bidentate ligands in Rh-catalyzed hydroformylation reactions<sup>13</sup> has led to the practitioners of this chemistry to apply supramolecular interactions for the construction of the skeleton of bidentate supramolecular rhodium-catalysts.<sup>78</sup> This approach has enabled the generation of large libraries of bidentate ligands by assembling two complementary phosphorus-monodentate building blocks in the presence of a rhodium precursor as template using high-throughput synthetic protocols.

The *metal-template approach* was introduced by Reek and co-workers and consisted of the use of a Zn-porphyrin-based structure **65** that allowed for the binding of two pyridyl phosphines **66** (Figure 12). With this strategy, the *in situ* generation of the supramolecular bidentate ligand **65•(66)<sub>2</sub>**, in combination with the complexation of the resulting supramolecular complex to the rhodium center in a bidentate fashion led to hydroformylation catalyst **67** with unprecedented ease and in an efficient manner.<sup>79</sup> The generated supramolecular catalyst **67** behaved as other phosphorus-bidentate complexes in the hydroformylation of oct-1-ene, with low catalytic activity and high linear to branched ratios (33% conv., l/b ratio = 75:25).

---

<sup>78</sup> For comprehensive reviews, see: (a) Wilkinson, M. J.; van Leeuwen, P. W. N. M.; Reek, J. N. H. *Org. Biomol. Chem.* **2005**, *3*, 2371-2383. (b) Goudriaan, P. E.; van Leeuwen, P. W. N. M.; Birkholz, M.-N.; Reek, J. N. H. *Eur. J. Inorg. Chem.* **2008**, 2939-2958. (c) Bellini, R.; van der Vlugt, J. I.; Reek, J. N. H. *Isr. J. Chem.* **2012**, *52*, 613-629.

<sup>79</sup> (a) Slagt, V. F.; van Leeuwen, P. W. N. M.; Reek, J. N. H. *Chem. Commun.* **2003**, 2474-2475. (b) Kuil, M.; Goudriaan, P. E.; Kleij, A. W.; Tooke, D. M.; Spek, A. L.; van Leeuwen, P. W. N. M.; Reek, J. N. H. *Dalton Trans.* **2007**, 2311-2320.

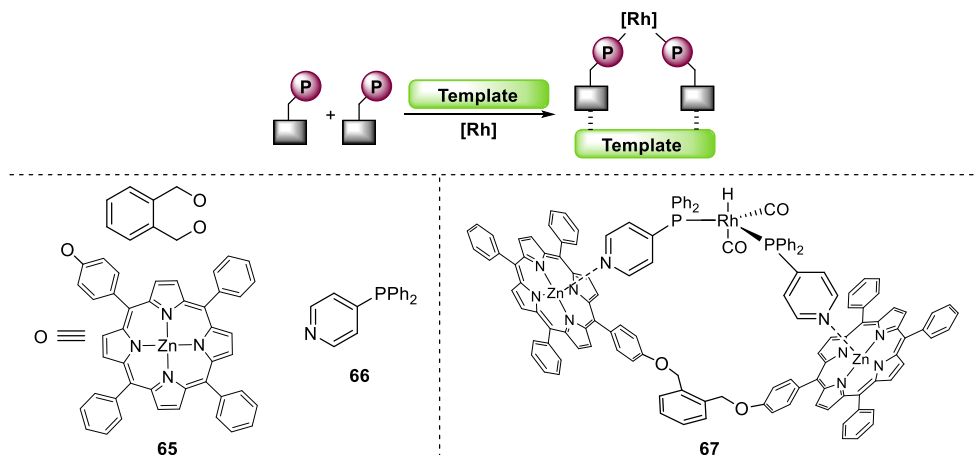


**Figure 12.** Schematic representation of metal-templated formation of bidentate supramolecular bisphosphine complexes

A different supramolecular approach was proposed by Reek *et al.* to form bidentate ligands that involve the interaction of structurally diverse phosphorus(III)-based ligands functionalized with a Zn-TPP templates (**68-70**) and a broad array of pyridyl-containing phosphorus-based ligands (Figure 13). This type of bidentate ligands, known as SUPRAPHos, allowed for the formation of large libraries of bidentate ligands by combinatorial chemistry. In the hydroformylation of styrene, the catalytic system derived from **68** and **71** improved the selectivity for the branched aldehyde (b/l ratio = 91.2:8.8), compared to the monodentate ligand **68**.<sup>80</sup> In the enantioselective hydroformylation of styrene, the role of the different ligating groups in the catalytic outcome was unveiled. The use of rhodium catalytic systems derived from phosphite ligands, such as **69-71**, led to high catalytic activity and low enantioselectivity (89% conv. and <2% *ee*). On the other hand, catalytic systems based on phosphoramidite ligands, such as **69-73**, provided high enantioselectivity but low catalytic activity (1% conv., 76% *ee*).<sup>81</sup> This combinatorial screening also revealed the unusual regioselectivity observed in the hydroformylation of styrene using the rhodium catalytic system derived from

<sup>80</sup> Reek, J. N. H.; Roeder, M.; Goudriaan, P. E.; Kamer, P. C. J.; van Leeuwen, P. W. N. M.; Slagt, V. F. J. *Organomet. Chem.* **2005**, *690*, 4505-4516.

<sup>81</sup> Goudriaan, P. E.; Jang, X.-B.; Kuil, M.; Lemmens, R.; van Leeuwen, P. W. N. M.; Reek, J. N. H. *Eur. J. Org. Chem.* **2008**, 6079-6092.



phosphoramidite porphyrin (*S*)-**70** and pyridyl phosphine **72**, providing a selectivity for the linear aldehyde up to 72%.<sup>82</sup>

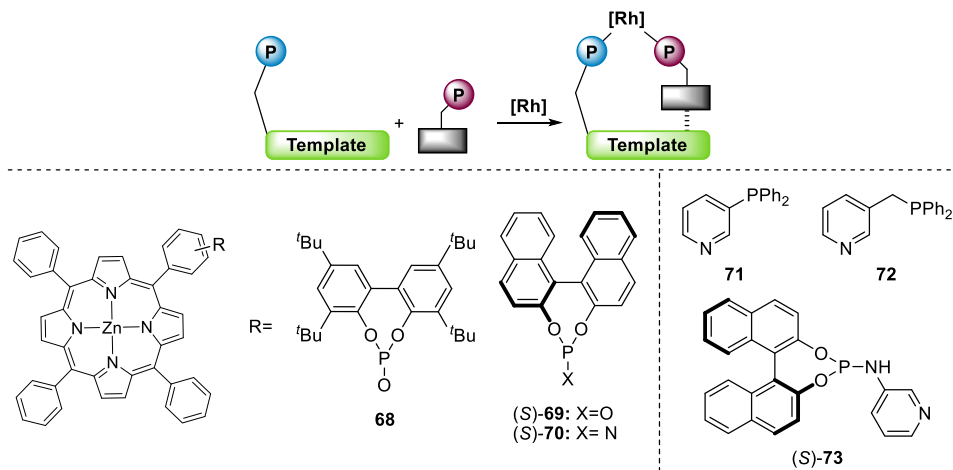


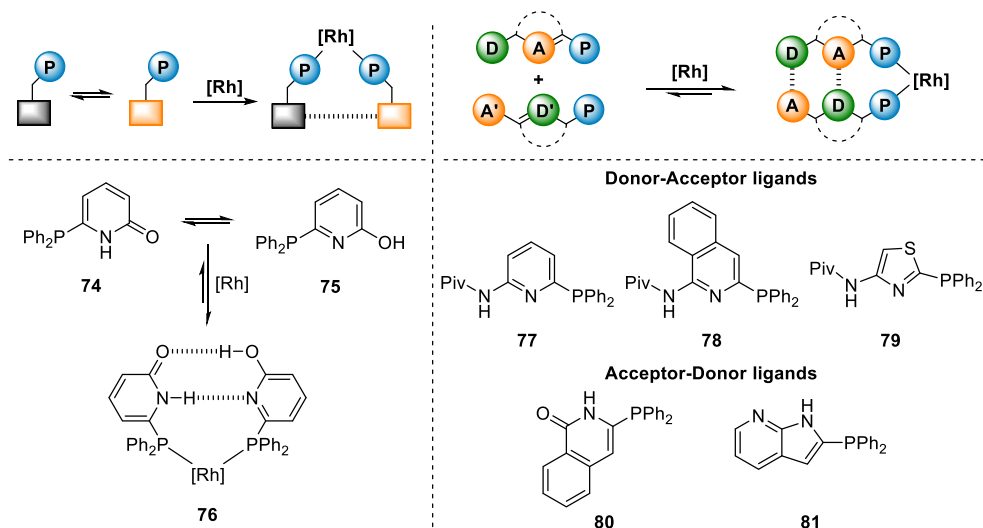
**Figure 13.** Schematic representation of metal-template approach using SUPRAPHos-type ligands for styrene hydroformylation

Breit *et al.* exploited an elegant strategy to construct the skeleton of highly interesting supramolecular catalysts. This was done by attaching two building blocks that contained the functional groups desired for catalysis as well as the motifs needed for the hydrogen bonding interactions. This concept was introduced in hydroformylation reactions with the ligand 6DPPon **74**.<sup>83</sup> It was envisaged that the tautomeric system 2-pyridone **74**/2-hydroxypyridine **75**, which is in equilibrium in organic solvents, could form a hydrogen-bonded heterodimer complex in presence of a rhodium precursor to form complex **76** (Scheme 11, left). The hydroformylation of oct-1-ene with supramolecular catalyst **76** revealed a high selectivity towards the linear aldehyde (l/b ratio = 97:3) at the expense of a low catalytic activity (56% conv. after 4 h), even at high temperatures up to 100 °C.<sup>83</sup> Moderate conversions and high regioselectivities are common features of bidentate phosphines in hydroformylation reactions, which ultimately demonstrate the bidentate nature of the hydrogen bond-assembled ligand. The high catalytic activity exhibited by 6DPPon **74** allowed for the reaction to take place at room temperature and ambient pressure (RTAP). High selectivities were obtained for the hydroformylation of oct-1-ene (l/b ratios up

<sup>82</sup> Goudriaan, P. E.; Kuil, M.; Jiang, X.-B.; van Leeuwen, P. W. N. M.; Reek, J. N. H. *Dalton Trans.* **2009**, 1801-1805.

<sup>83</sup> Breit, B.; Seiche, W. J. *Am. Chem. Soc.* **2003**, *125*, 6608-6609.

to 99:1),<sup>84</sup> even also when water was employed as solvent (l/b ratio up to 99:1).<sup>85</sup>



**Scheme 11.** Schematic representation of Breit's self-assembly approaches towards a library of hydrogen-bonded bidentate supramolecular rhodium catalysts

Inspired in the AT base-pair model, Breit *et al.* designed different ligands with complementary donor-acceptor hydrogen bonding motifs (Scheme 11, right).<sup>86</sup> This strategy allowed for the straightforward generation of bidentate supramolecular rhodium complexes by combination of a donor-acceptor ligand **77-79** with an acceptor-donor ligand **80-81** employing combinatorial chemistry protocols. It is interesting to note that supramolecular complex  $[Rh(\mathbf{79}\cdot\mathbf{80})]$  catalyzed the hydroformylation of oct-1-ene in MeOH with a l/b ratio = 97:3, which was close to the obtained when toluene was used as solvent (l/b ratio = 98:2).

### 1.2.3 Substrate preorganization in rhodium-catalyzed hydroformylation

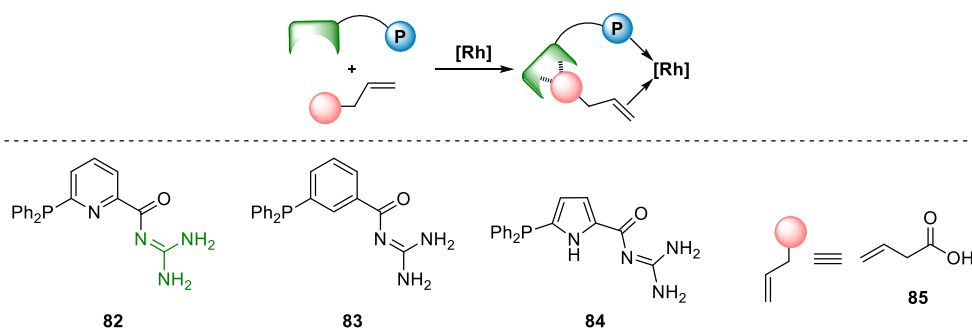
A different approach based on exploiting supramolecular interactions relied on substrate preorganization with respect to the catalytic center. This supramolecular strategy relied on the simultaneous interaction of the substrate to the metal center and to a specific recognition site in the catalytic system for the

<sup>84</sup> Seiche, W.; Schuschkowski, A.; Breit, B. *Adv. Synth. Catal.* **2005**, *347*, 1488-1494.

<sup>85</sup> Straub, A. T.; Otto, M.; Usui, I.; Breit, B. *Adv. Synth. Catal.* **2013**, *355*, 2071-2075.

<sup>86</sup> (a) Breit, B.; Seiche, W. *Angew. Chem. Int. Ed.* **2005**, *44*, 1640-1643. (b) Waloch, C.; Wieland, J.; Keller, M.; Breit, B. *Angew. Chem. Int. Ed.* **2007**, *46*, 3037-3039.

substrate.<sup>87</sup> For instance, Breit *et al.* envisioned that the presence of a phosphine group to coordinate selectively to the metal center, and a recognition site (guanidinium moiety indicated in green in Scheme 12) to selectively interact with functionalized substrates, could lead to selective and efficient catalytic systems (Scheme 12).<sup>88</sup> For high activity and selectivity, the recognition and catalytic units must be integrated in the same molecule. In the rhodium-catalyzed hydroformylation of but-3-enoic acid **85**, the designed catalyst [Rh(**82**)] outperformed standard ligands, such as PPh<sub>3</sub> and Xantphos (TOF = 250 h<sup>-1</sup>, 1/b = 23:1). The use of phenyl- or pyrrol-based acyl guanidinium ligands **83** and **84** revealed to be active in the hydrogenation of terminal aldehydes, yielding terminal alcohols with excellent catalytic activity (up to 98% yield). Due to this reactivity, ligand **83** was applied in the tandem hydroformylation-hydrogenation of terminal alkenes, yielding terminal aliphatic alcohols with good regioselectivity (1/b ratios up to 92:8).<sup>89</sup> On the other hand, the combination of **82** and **84** allowed the tandem decarboxylative hydroformylation-hydrogenation of  $\alpha,\beta$ -unsaturated carboxylic acids to terminal alcohols.<sup>90</sup>



**Scheme 12.** Schematic representation of substrate preorganization in hydroformylation reactions with acyl guanidinium phosphine ligands

A different design was proposed by Reek and co-workers, in which the bisphosphine ligand bore the DIM scaffold (see fragment indicated in green in Figure 14) for the recognition of carboxylate motifs (Figure 14).<sup>91</sup> Coordination

<sup>87</sup> For comprehensive reviews, see: (a) Dydio, P.; Reek, J. N. H. *Chem. Sci.* **2014**, *5*, 2135-2145. (b) Davis, H. J.; Phipps, R. J. *Chem. Sci.* **2017**, *8*, 864-877.

<sup>88</sup> (a) Smejkal, T.; Breit, B. *Angew. Chem. Int. Ed.* **2008**, *47*, 311-315. (b) Smejkal, T.; Gribkov, D.; Geier, J.; Keller, M.; Breit, B. *Chem. Eur. J.* **2010**, *16*, 2470-2478.

<sup>89</sup> Diab, L.; Smejkal, T.; Geier, J.; Breit, B. *Angew. Chem. Int. Ed.* **2009**, *48*, 8022-8026.

<sup>90</sup> Diab, L.; Gellrich, U.; Breit, B. *Chem. Commun.* **2013**, *49*, 9737-9739.

<sup>91</sup> (a) Dydio, P.; Dzik, W. I.; Lutz, M.; de Bruin, B.; Reek, J. N. H. *Angew. Chem. Int. Ed.* **2011**, *50*, 396-400. (b) Dydio, P.; Detz, R. J.; Reek, J. N. H. *J. Am. Chem. Soc.* **2013**, *135*, 10817-10828.

studies under hydroformylation conditions revealed the formation of the bidentate hydrido dicarbonyl rhodium complex with a pentacoordinate *tbp* geometry, with the *eq-eq* and *eq-ax* coordination modes in fast equilibrium. The hydroformylation of  $\omega$ -unsaturated carboxylic acids **85**, **89-95**, in the presence of *para*DIMPhos **86**,<sup>92</sup> revealed the high selectivity for pent-4-enoic acid **89** (l/b ratio = 97.6:2.4), whose chain length allowed for a perfect match with the DIM pocket and the metal center.<sup>91a</sup> The use of *ortho*DIMPhos **87** allowed for the hydroformylation of but-3-enoic acid **85** with high regioselectivities (l/b ratio = 84:1).<sup>93</sup> This supramolecular catalyst also showed high catalytic activity in the hydroformylation of internal alkenes, such as pent-3-enoic acid **96** with a outer/inner ratio = 91.6:8.3.<sup>93</sup> The incorporation of the BINOL-based phosphite fragment to the DIM scaffold to prepare ligand **88** allowed for the hydroformylation of internal unsaturated carboxylic acids **96-98** (outer/inner ratio up to 78:1),<sup>91b</sup> and 2-vinyl- **99** and 2-allyl- benzoic acids **100**<sup>94</sup> with perfect regioselectivities towards linear aldehydes (Figure 14). The high selectivity towards the linear aldehydes was rationalized on the basis of restrictions in the alkene to form the branched alkyl rhodium complex with the carboxylate being bound to the DIM pocket.<sup>91b,94b</sup>

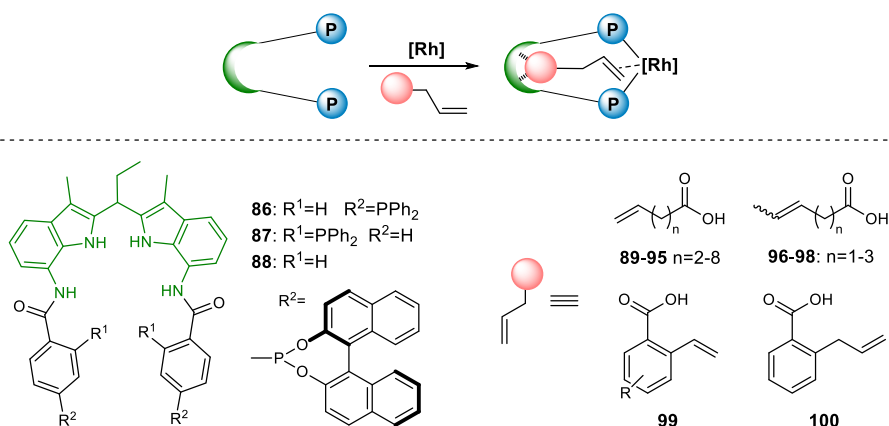


**Figure 14.** Substrate preorganization in hydroformylation reactions using DIM pockets

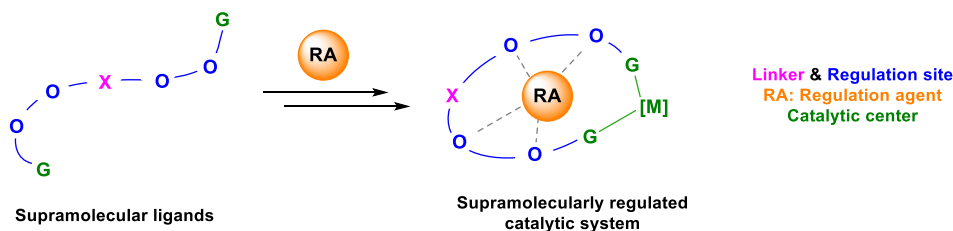
<sup>92</sup> The addition of a base was needed for the *in situ* generation of the carboxylates.

<sup>93</sup> Bai, S.-T.; Sinha, V.; Kluwer, A. M.; Linnebank, P. R.; Abiri, Z.; de Bruin, B.; Reek, J. N. H. *ChemCatChem* **2019**, *11*, 5322-5329.

<sup>94</sup> (a) Dydio, P.; Reek, J. N. H. *Angew. Chem. Int. Ed.* **2013**, *52*, 3878-3882. (b) Dydio, P.; Detz, R. J.; de Bruin, B.; Reek, J. N. H. *J. Am. Chem. Soc.* **2014**, *136*, 8418-8429.

## I.2.4 Distal regulation in rhodium-catalyzed hydroformylation

Inspired by the process of allosteric regulation in Nature, new types of catalytic systems have emerged in the field of supramolecular hydroformylation in recent years. Our research group has contributed to this area of research by reporting supramolecularly regulated catalysts that contain polyethyleneoxy chains as regulation sites and phosphorus- or nitrogen-ligating groups for catalysis. Our regulation mechanism is triggered by the addition of a regulation agent (RA) capable of interacting with the regulation site *via* supramolecular interactions. The choice of RA determines the rigidity and conformational flexibility of the whole catalytic system, which translates into a modulation of the (stereo)selectivity in the transformation of interest. Our group has exploited this regulation strategy in enantioselective hydroformylation reactions, with the modular ligand design indicated in Scheme 13.<sup>95</sup>



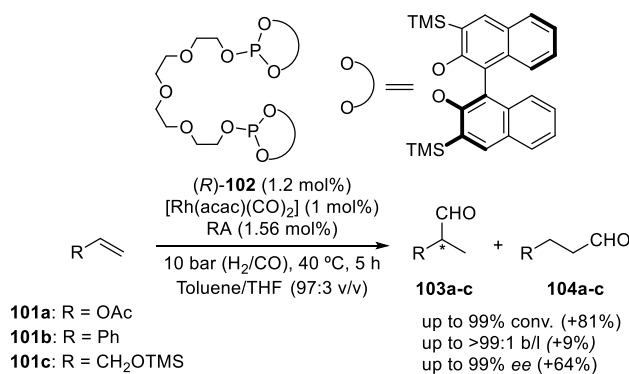
**Scheme 13.** Schematic representation of the regulation strategy in our research group

As regards the regulation site, its design was based on linear polyethyleneoxy chains, which had a flexible structure and were placed in a distal position to the catalytic site. An array of structurally diverse regulation agents (RA) triggered the regulation mechanism by binding to the regulation site. The range of RA tested encompassed alkali metal, alkali earth metal, lanthanide and ammonium salts. As regards the catalytic site, we initially focused on phosphorus(III) ligating groups containing stereogenic elements. More recently, our group has also used oxazoline moieties as ligating groups for transition metal-based catalysis.<sup>96</sup> Regarding the metal center, rhodium(I)-, palladium(II)-, gold(I)- and copper(I)-catalyzed transformations have been explored.

<sup>95</sup> Llorente, N.; Fernández-Pérez, H.; Núñez-Rico, J. L.; Carreras, L.; Martínez-Carrión, A.; Iniesta, E.; Romero-Navarro, A.; Martínez-Bascuñana, A.; Vidal-Ferran, A. *Pure Appl. Chem.* **2019**, *91*, 3-15.

<sup>96</sup> Iniesta, E.; Vidal-Ferran, A. *Chem. Commun.* **2020**, *56*, 6364-6367.

This supramolecular approach has been applied to enantioselective hydrogenations,<sup>97</sup> enantioselective allylic substitutions,<sup>98</sup> enantioselective hydroformylations and the achiral insertion of metal carbenoids into O–H bonds<sup>96</sup> and C–H bonds.<sup>99</sup> In the field of enantioselective hydroformylation, this strategy was employed for model substrates such as vinyl esters, styrene, protected allyl alcohols, as well as heterocyclic alkenes.<sup>100</sup> For vinyl esters, such as vinyl acetate **101a**, a remarkable increase of the enantioselectivity was observed when RbBArF was used as RA in presence of rhodium-catalysts derived from ligand **102** (increase of a 81% in the conv., 9% in the amounts of branched aldehydes and 64% *ee* in the AHF of vinyl acetate) (Scheme 14). Regulation effects for styrene **101b** and allyloxytrimethylsilane **101c** were not as pronounced as for vinyl esters.



**Scheme 14.** Supramolecular enantioselective hydroformylation of olefins with rhodium(I) complexes derived from ligand **102** (up to >99% conv. >99:1 b/l ratio and 99% *ee* for **101a**)

A second generation of supramolecular bisphosphite ligands with a stereogenic element in the regulation site was designed.<sup>100c</sup> Ligand (*R,S*)-**108** was synthesized and applied to the enantioselective hydroformylation of heterocyclic alkenes, which are challenging substrates in hydroformylations due to chemo- and regiocontrol issues. In the hydroformylation of five-membered heterocyclic alkenes, such as 2,3- and 2,5-dihydrofurans **105-106**, the use of KBarF improved

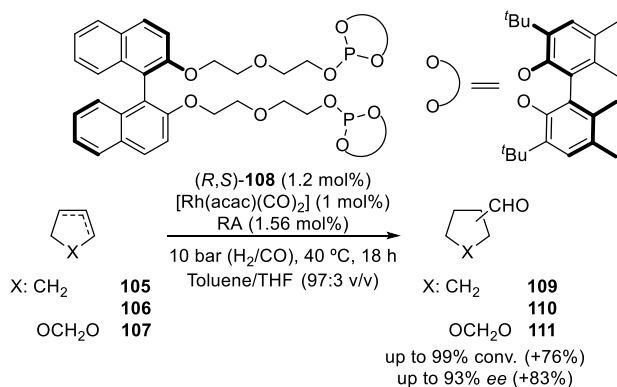
<sup>97</sup> Fernández-Pérez, H.; Mon, I.; Frontera, A.; Vidal-Ferran, A. *Tetrahedron* **2015**, *71*, 4490-4494.

<sup>98</sup> Rovira, L.; Fernández-Pérez, H.; Vidal-Ferran, A. *Organometallics* **2016**, *35*, 528-533.

<sup>99</sup> Carreras, L.; Franconetti, A.; Grabulosa, A.; Frontera, A.; Vidal-Ferran, A. *Org. Chem. Front.* **2020**, DOI: 10.1039/d0qo00416b.

<sup>100</sup> (a) Mon, I.; Jose, D. A.; Vidal-Ferran, A. *Chem. - Eur. J.* **2013**, *19*, 2720-2725. (b) Vidal-Ferran, A.; Mon, I.; Bauzá, A.; Frontera, A.; Rovira, L. *Chem. - Eur. J.* **2015**, *21*, 11417-11426. (c) Rovira, L.; Vaquero, M.; Vidal-Ferran, A. *J. Org. Chem.* **2015**, *80*, 10397-10403.

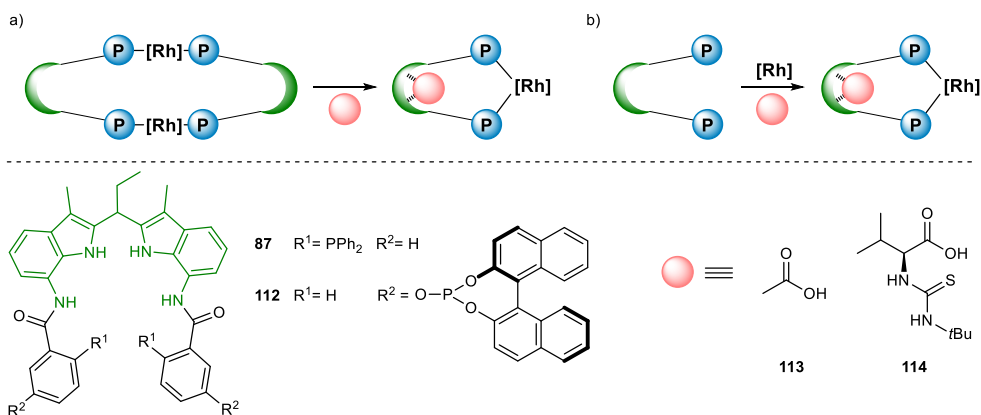
the enantioselectivity (enhancement of 64% and 71% *ee* in the enantioselective hydroformylation of 2,3-dihydrofuran **105** and 2,5-dihydrofuran **106**, respectively). The hydroformylation of 7-membered heterocyclic alkenes such as dioxepin **107** with rhodium-catalytic complexes derived from **108** led to an enhancement of the catalytic activity by 76% and to high enantioselectivity (93% *ee*), with the results of our group being the highest enantioselectivity reported in the literature for this substrate.



**Scheme 15.** Supramolecular enantioselective hydroformylation of heterocyclic olefins with rhodium(I) complexes derived from ligand **108**

In 2019, the group of Reek and co-workers took advantage of substrate-preorganization in DIM-type ligands (see pages 26-27 in this section) and expanded the approach to non-functionalized substrates in the presence of carboxylic acids **113-114** as DIM binders (Scheme 16).<sup>101</sup> The preferred formation of the dimeric complex derived from *ortho*DIMPhos **87** was shifted towards the corresponding monomeric complex by binding of the carboxylic acid **113** (Scheme 16a), which is referred to as the “effector” by the authors. As a result of this process, *ortho*DIMPhos **87** was transformed into a more regioselective catalyst for the hydroformylation of oct-1-ene (the effector addition enhanced the branched aldehyde formation from 19% up to 37%).<sup>101a</sup> For *meta*DIMPhosphite **112**, moderate catalytic activity and enantioselectivity were obtained in the presence of **114** as effector (up to 72% *ee* in the hydroformylation of vinyl acetate) (Scheme 16b).<sup>101b</sup>

<sup>101</sup> (a) Bai, S.-T.; Sinha, V.; Kluwer, A. M.; Linnebank, P. R.; Abiri, Z.; Dydio, P.; Lutz, M.; de Bruin, B.; Reek, J. N. H. *Chem. Sci.* **2019**, *10*, 7389-7398. (b) Bai, S.-T.; Kluwer, A. M.; Reek, J. N. H. *Chem. Commun.* **2019**, *55*, 14151-14154.



**Scheme 16.** Schematic representation of the formation of monomeric rhodium complexes by addition of an effector

### I.3 Mechanistic and kinetic studies in hydroformylation reactions

Mechanistic studies are a useful tool for elucidating the factors that affect a chemical transformation. Classic approaches in kinetic studies, such as the determination of initial rates or pseudo-first order analysis, have been commonly applied. Unfortunately, the information that they provide lacks detail on the overall reaction process. On the other hand, the monitoring of the reaction progress under real catalytic conditions provides an accurate information on relevant intermediates, catalyst resting states and rate limiting steps. The huge progress in the development of techniques for the reaction monitoring has not been concurrent with progress for the treatment of vast amounts of kinetic data generated during the monitoring of the transformation.

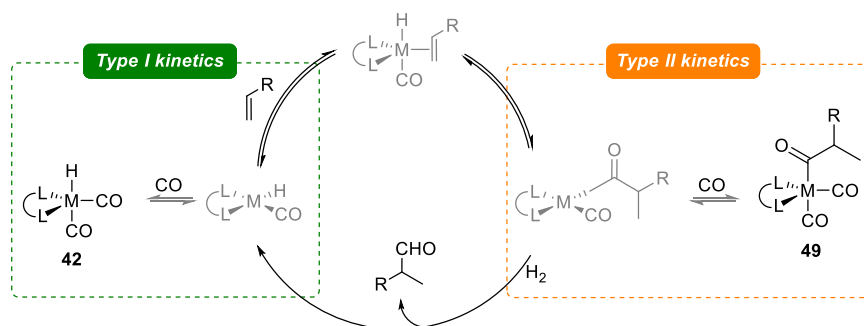
Hydroformylation is a reaction with a severe dependence on the reaction conditions. Therefore, slight modifications on the reaction conditions may affect the kinetic behavior and make the comparison of kinetic data of different experiments very complex. Kinetic studies on hydroformylation reactions are numerous and have led to the classification of the kinetics in two main groups (Scheme 17):<sup>13</sup>

- *Type I kinetics* are characterized by a positive-order dependence on alkene and catalyst concentration, a negative-order dependence on CO concentration and no rate dependence for the  $\text{H}_2$  concentration. These reaction orders imply that the alkene coordination and/or insertion into the Rh–H bond are the rate-determining steps. In this case, complex **42** is generally considered the



catalyst's resting state. Type I kinetics is the most commonly observed profile for mono and bidentate phosphorus ligands.

- Type II kinetics are characterized by a positive-order dependence in catalyst and H<sub>2</sub> concentration, a negative-order dependence on CO concentration and no rate dependence for the alkene concentration. The reaction rate dependence on H<sub>2</sub> suggests hydrogenolysis as the rate determining step.<sup>102</sup> In this case, the acyl rhodium complex **49** is generally considered the catalyst's resting state. Rhodium catalysts derived from bulky phosphite ligands have shown to follow this kinetic behavior but type II kinetics are an exception rather than a rule.



**Scheme 17.** Types of kinetics in hydroformylation reactions

As for all homogeneous catalytic systems, the elucidation of hydroformylation active species is crucial for a better understanding of the reaction mechanism. However, the use of harsh reaction conditions in hydroformylation reactions (*i.e.*, high temperatures and pressures) makes the characterization of reaction intermediates difficult. Therefore, the design and development of high-pressure setups for studying hydroformylation reactions is needed for gaining fundamental knowledge of the hydroformylation reaction mechanism. High-pressure infrared (HP-IR) and high-pressure nuclear magnetic resonance (HP-NMR) have been the most widely used spectroscopic techniques for hydroformylation studies. In this regard, tailor-made cells were developed with the limitation that operational conditions had to adapt to the materials used for the construction of the monitoring window.<sup>103</sup> The use of HP-IR and HP-NMR

<sup>102</sup> Hydrogenolysis comprises two elementary steps: oxidative addition of H<sub>2</sub> to the Rh center and reductive elimination to form the aldehyde and regenerate the active catalyst. However, in hydroformylation reaction mechanisms, the two steps are depicted as a single irreversible step.

<sup>103</sup> Kamer, P. C. J.; van Rooy, A.; Schoemaker, G. C.; van Leeuwen, P. W. N. M. *Coord. Chem. Rev.* **2004**, *248*, 2409-2424.

devices have allowed the *in situ* determination of hydroformylation reaction intermediates and provided a more complete picture of the overall parameters affecting the catalytic reaction.<sup>104,105</sup>

### 1.3.1 *Operando* spectroscopy in hydroformylation reactions

In the initial spectroscopic studies, the term *in situ* was widely used for any experiment that allowed the monitoring of catalytic species under catalytic conditions. More recently, the scientific community has introduced the term *operando* spectroscopy to settle the difference between studies with or without real-time analysis.<sup>106</sup> Therefore, *in situ* spectroscopy encompasses the study of the catalytic intermediates under catalytic conditions, meanwhile *operando* spectroscopy implies the study of the catalytic intermediates under catalytic conditions and the simultaneous measurement of activity and selectivity parameters. Thus, *operando* spectroscopy is a *in situ* spectroscopy over time that allows kinetic measurements.

The implication of real-time analysis in *operando* spectroscopy for high-pressure reactions makes mass transfer limitation an issue, which obliges the design of the high-pressure instrument to ensure an active gas-liquid mixing. In this case, the period of time for equilibrating and achieving an equal composition of the reaction mixture in the sensor and the reactor (recycle period  $\tau$ ) is an important parameter. *Operando* HP-IR spectroscopy has been widely used to study a variety of carbonylation reactions, including hydroformylations, and unravel mechanistic and kinetic intricacies of different catalytic systems.<sup>105,107</sup> On the other hand, NMR spectroscopy is slower in the time scale than IR spectroscopy and higher catalyst concentrations than in IR studies are needed to improve the signal-to-noise ratio. Examples in the literature have reported the development of HP-NMR cells that fit in commercially available probes or tailor-made high-pressure

---

<sup>104</sup> Damoense, L.; Datt, M.; Green, M.; Steenkamp, C. *Coord. Chem. Rev.* **2004**, *248*, 2393-2407.

<sup>105</sup> Diebolt, O.; van Leeuwen, P. W. N. M.; Kamer, P. C. J. *ACS Catal.* **2012**, *2*, 2357-2370.

<sup>106</sup> Ryczkowski, J. *Ann. Univ. Mariae Curie-Skłodowska, Sect. AA: Chem.* **2005**, *60*, 145-150.

<sup>107</sup> (a) Diebolt, O.; Tricas, H.; Freixa, Z.; van Leeuwen, P. W. N. M. *ACS Catal.* **2013**, *3*, 128-137. (b) Gueven, S.; Nieuwenhuizen, M. M. L.; Hamers, B.; Franke, R.; Priske, M.; Becker, M.; Vogt, D. *ChemCatChem* **2014**, *6*, 603-610. (c) Kubis, C.; Sawall, M.; Block, A.; Neymeyr, K.; Ludwig, R.; Börner, A.; Selent, D. *Chem. - Eur. J.* **2014**, *20*, 11921-11931. (d) Joerke, A.; Seidel-Morgenstern, A.; Hamel, C. *J. Mol. Catal. A: Chem.* **2017**, *426*, 10-14. (e) Dreimann, J. M.; Kohls, E.; Warmeling, H. F. W.; Stein, M.; Guo, L. F.; Garland, M.; Dinh, T. N.; Vorholt, A. J. *ACS Catal.* **2019**, *9*, 4308-4319.

probes.<sup>108</sup> In many cases, the slow gas-liquid mixing entailed a limitation and hampered the measurement of reproducible kinetic data. Iggo<sup>109</sup> and Selent<sup>110</sup> developed a NMR flow cell with a constant stream of gas bubbling through the reaction liquid to overcome mass-transfer limitations. Landis *et al.* designed a reactor for high-throughput high-pressure NMR spectroscopy, the so-called Wisconsin High-Pressure NMR Reactor (WiHP-NMRR).<sup>111</sup> The WiHP-NMRR comprises the reactor and several modules for gas delivery, for the injection of sample under ambient or for the cleaning of the system. This design enables keeping the gas concentration in solution constant and is compatible with commercial NMR probes, allowing mechanistic investigations and development of microkinetic models for hydroformylation reactions under operating conditions.<sup>112</sup>

### 1.3.2 FlowNMR for *online* reaction monitoring

A different approach for reaction monitoring under reaction conditions consisted of continuously pumping an aliquot of the reaction mixture into the NMR probe in the spectrometer for the analysis.<sup>113</sup> This technique is known as flowNMR and allows for the real-time monitoring of the reaction mixture, avoiding disturbances to the reaction mixture that could alter the composition. Moreover, this monitoring method lacks mass transfer limitations.<sup>114</sup> The system can operate in an open circuit, for the recovery or disposal of the reaction mixture, or in a close loop, which maintains the reaction conditions intact. The absence of an external influence in the reaction sampling and the minimal delay in the mixing and spectra acquisition make flowNMR a suitable technique for obtaining reproducible and reliable kinetic data.

As previously observed, the requirement of special NMR probes and tubes precludes the application of this technique in academia and industry. The

---

<sup>108</sup> (a) Horvath, I. T.; Millar, J. M. *Chem. Rev.* **1991**, *91*, 1339-1351. (b) Laurenczy, G.; Helm, L.; *High Pressure NMR Cells*, p 81-106. In *Mechanisms in Homogeneous Catalysis: A Spectroscopic Approach*; Heaton, B., Eds.; Wiley-VCH: Weinheim, **2005**.

<sup>109</sup> Iggo, J. A.; Shirley, D.; Tong, N. C. *New J. Chem.* **1998**, *22*, 1043-1045.

<sup>110</sup> Selent, D.; Baumann, W.; Börner, A. DE10333143A1, **2005**.

<sup>111</sup> Beach, N. J.; Knapp, S. M. M.; Landis, C. R. *Rev. Sci. Instrum.* **2015**, *86*, 104101-104109.

<sup>112</sup> (a) Brezny, A. C.; Landis, C. R. *Acc. Chem. Res.* **2018**, *51*, 2344-2354. (b) Brezny, A. C.; Landis, C. R. *ACS Catal.* **2019**, *9*, 2501-2513.

<sup>113</sup> (a) Fyfe, C. A.; Cocivera, M.; Damji, S. W. H. *Acc. Chem. Res.* **1978**, *11*, 277-282. (b) Keifer, P. A. *Curr. Opin. Chem. Biol.* **2003**, *7*, 388-394. (c) Keifer, P. A. *Annu. Rep. NMR Spectrosc.* **2007**, *62*, 1-47.

<sup>114</sup> Foley, D. A.; Dunn, A. L.; Zell, M. T. *Magn. Reson. Chem.* **2016**, *54*, 451-456.

development and commercialization of NMR Flow probes (Figure 15),<sup>115</sup> compatible with standard spectrometers, have facilitated the implementation of this technique and the development of this area of research.<sup>116</sup>

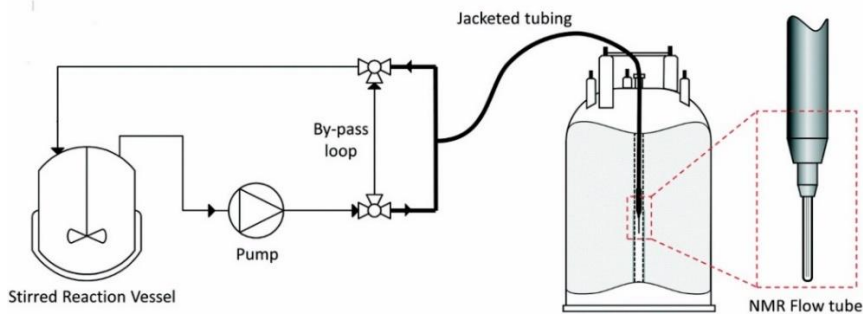


**Figure 15.** Schematic representation of a NMR Flow probe<sup>117</sup>

FlowNMR practitioners have recently highlighted some important aspects to bear in mind for the quantification of compounds with flowNMR techniques.<sup>118</sup> As aliquots of the bulk mix circulate separately into the spectrometer, the circulating mix has to be representative of the reaction vessel composition. Due to the short period of time in which the sample is inside the magnetic field of the spectrometer, only partial magnetization of the nuclear spins takes place with an overall decrease of the intensity of the signals. This, the so-called in-flow effect, can be overcome by the application of a correction factor. On the other hand, off-flow effects encounter the constant replacement of nuclei during the acquisition with magnetized nuclei in the detector. This effect translates into a fast decay of the signal. At high flow rates, the in-flow effects dominate the data acquisition process. As a drawback, the inherent delay between reactor and spectrometer makes this technique not feasible for the detection of compounds with a short life. The growth of this area of research has led to Hasse *et al.* to

<sup>115</sup> Foley, D. A.; Bez, E.; Codina, A.; Colson, K. L.; Fey, M.; Krull, R.; Piroli, D.; Zell, M. T.; Marquez, B. L. *Anal. Chem.* **2014**, *86*, 12008-12013.

<sup>116</sup> (a) Foley, D. A.; Doecke, C. W.; Buser, J. Y.; Merritt, J. M.; Murphy, L.; Kissane, M.; Collins, S. G.; Maguire, A. R.; Kaerner, A. *J. Org. Chem.* **2011**, *76*, 9630-9640. (b) Foley, D. A.; Wang, J.; Maranzano, B.; Zell, M. T.; Marquez, B. L.; Xiang, Y.; Reid, G. L. *Anal. Chem.* **2013**, *85*, 8928-8932. (c) Merritt, J. M.; Buser, J. Y.; Campbell, A. N.; Fennell, J. W.; Kallman, N. J.; Koenig, T. M.; Moursy, H.; Pietz, M. A.; Scully, N.; Singh, U. K. *Org. Process Res. Dev.* **2014**, *18*, 246-256. (d) Goldbach, M.; Danieli, E.; Perlo, J.; Kaptein, B.; Litvinov, V. M.; Bluemich, B.; Casanova, F.; Duchateau, A. L. L. *Tetrahedron Lett.* **2016**, *57*, 122-125.

<sup>117</sup> This image was borrowed from Hall, A. M. R.; Chouler, J. C.; Codina, A.; Gierth, P. T.; Lowe, J. P.; Hintermair, U. *Catal. Sci. Technol.* **2016**, *6*, 8406-8417.

<sup>118</sup> Hall, A. M. R.; Chouler, J. C.; Codina, A.; Gierth, P. T.; Lowe, J. P.; Hintermair, U. *Catal. Sci. Technol.* **2016**, *6*, 8406-8417.

develop prediction methods for the real magnetization in flow experiments for any reaction mixture and to design flow systems that overcome the herein described intrinsic limitations.<sup>119</sup>

Hintermaier *et al.* have demonstrated the application of flowNMR to other complex transformations, such as the Eosin Y-mediated photo-oxidation of *N*-allyl benzylamine.<sup>120</sup> Deeper insight into the photocatalyst mode of action was obtained by the variation of reaction conditions during the NMR data acquisition in flow. In the field of high-pressure reactions, Buser *et al.* reported the monitoring and quantification of H<sub>2</sub> dissolved in organic solvents *via* high-pressure flowNMR.<sup>121</sup> In 2020, Hintermaier *et al.* have reported the use of flowNMR in the kinetic studies of PPh<sub>3</sub>-assisted rhodium-catalyzed hydroformylation of hex-1-ene, which has enabled the characterization of previously elusive catalytic intermediates.<sup>122</sup>

### 1.3.3 Visual kinetic analysis for reaction kinetics elucidation

The different experimental methods for data acquisition can be depicted in two main groups: (i) differential measurements, in which the transformation rate is measured over time and/or conversion and concentration is calculated from these data; (ii) integral measurements, where the concentration is measured over time and reaction rates are calculated *a posteriori*. Visual kinetic analysis based on graphical methods has emerged as a suitable approach for obtaining kinetic information in an easy and rapid manner, with a minimum number of experiments (Figure 16).<sup>123</sup> The development of the Reaction Progress Kinetic Analysis (RPKA) by Blackmond entails a breakthrough in the visual kinetic analysis.<sup>124</sup> Graphical representation of reaction rates *vs.* concentrations allows for the identification of catalyst deactivation, product inhibition and elucidation of the reaction order of any reaction component. This analytic method, in spite

---

<sup>119</sup> Friebel, A.; Specht, T.; von Harbou, E.; Münnemann, K.; Hasse, H. *J. Magn. Reson.* **2020**, *312*, 106683-106691.

<sup>120</sup> Hall, A. M. R.; Broomfield-Tagg, R.; Camilleri, M.; Carbery, D. R.; Codina, A.; Whittaker, D. T. E.; Coombes, S.; Lowe, J. P.; Hintermaier, U. *Chem. Commun.* **2018**, *54*, 30-33.

<sup>121</sup> (a) Buser, J. Y.; McFarland, A. D. *Chem. Commun.* **2014**, *50*, 4234-4237. (b) Buser, J. Y.; Luciani, C. V. *React. Chem. Eng.* **2018**, *3*, 442-446.

<sup>122</sup> Bara-Estaun, A.; Lyall, C.; Lowe, J. P.; Pringle, P. G.; Kamer, P.; Franke, R.; Hintermaier, U. *Faraday Discuss.* **2020**, 10.1039/c9fd00145j.

<sup>123</sup> (a) Blackmond, D. G. *J. Am. Chem. Soc.* **2015**, *137*, 10852-10866. (b) Nielsen, C. D. T.; Burés, J. *Chem. Sci.* **2019**, *10*, 348-353.

<sup>124</sup> Blackmond, D. G. *Angew. Chem. Int. Ed.* **2005**, *44*, 4302-4320.

of providing quick understanding of complex reaction mechanisms, is designed for the use of differential data acquisition. Reek *et al.* used this method in the kinetic studies of the hydroformylation reaction pent-4-enoic acid **89** and *ortho*-vinyl benzoic acid **99** employing the supramolecular catalyst derived from **86** (Figure 14). The analyses revealed product inhibition, due to the competitive binding of the substrates and products for the DIM pocket.<sup>94b</sup>

In the case of integral measurement techniques, data manipulation is required. The development of Variable Time Normalization Analysis (VTNA) by Burés allows for the use of concentration profiles over time from extensive monitoring techniques without complex mathematical treatments of the data.<sup>125</sup> Both kinetic analysis methods are powerful due to the simplicity of the visual comparison of data, the reduced number of required experiments and completeness of the provided information. As a caveat of these methods, the reliability on merely visual analysis makes these methods inadequate for obtaining high precision data. Nevertheless, the rigor of these methods is enough for the elucidation of reaction orders.

### Visual kinetic analysis

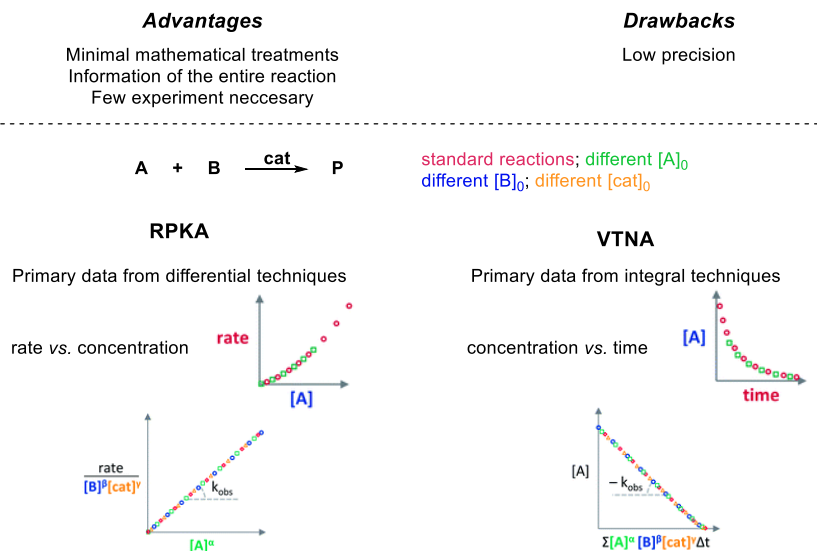


**Figure 16.** General representation of visual kinetic analysis

<sup>125</sup> (a) Burés, J. *Angew. Chem. Int. Ed.* **2016**, *55*, 16084-16087. (b) Burés, J. *Angew. Chem. Int. Ed.* **2016**, *55*, 2028-2031.

UNIVERSITAT ROVIRA I VIRGILI

THE HYDROFORMYLATION REACTION: FROM COVALENT TO SUPRAMOLECULAR APPROACHES AND OPERANDO KINETIC STUDIES

Alicia Martínez Carrión

## OBJECTIVES

As previously summarized in this section, different approaches have been applied in (enantioselective) hydroformylation reactions. In cobalt-catalyzed hydroformylations, the use of phosphine-type ligands has facilitated the development of highly stable catalysts that have allowed the use of mild reaction conditions. Rhodium-catalyzed hydroformylations have prevailed over the rest of catalytic metals, due to the high reactivity and selectivity of rhodium catalysts under mild reaction conditions. The combination of rhodium metal precursors with an array of structurally diverse  $C_{1-}$  or  $C_{2-}$ -symmetric bidentate trivalent phosphorus ligands has allowed for the hydroformylation of an ample range of olefins with superb chemo-, regio- and enantioselectivities.

The use of supramolecular chemistry in catalysis has enabled the development of catalytic systems that can be constructed or fine-tuned by using reversible interactions. It has been demonstrated by our group, that supramolecularly regulated  $\alpha,\omega$ -substituted bisphosphites are suitable ligands in enantioselective hydroformylation reactions of vinyl arenes, vinyl esters and heterocyclic alkenes. No examples of supramolecular catalytic systems in the enantioselective hydroformylation of aryl vinyl ethers have been reported. Supramolecular approaches have been used in the hydroformylation of 1,1'-disubstituted allenes, but no examples have been reported with a supramolecularly regulated catalytic system.

Visual kinetic analysis is a useful tool to obtain mechanistic information in a simple way about the entire reaction. The development of *operando* instrumentation for NMR spectroscopy under high-pressure conditions is underdeveloped. FlowNMR is a suitable alternative for its implementation in the monitoring of the progress of hydroformylation reactions.

Therefore, the objectives of the present thesis are as follows:

- To design and develop supramolecularly regulated bisphosphine and bisphosphite ligands. Evaluation of the catalytic properties of these supramolecular ligands in the rhodium-catalyzed hydroformylation of 1,1'-disubstituted allenes.
- To expand the scope of bisphosphine ligands in cobalt-catalyzed hydroformylations by evaluating the catalytic properties of Xantphos in



the cobalt-catalyzed hydroformylation of alkyl- and aryl-substituted alkenes.

- To evaluate the catalytic properties of supramolecularly regulated bisphosphite ligands in the rhodium-catalyzed enantioselective hydroformylation of aryl vinyl ethers.
- To design and develop a high-pressure experimental setup for FlowNMR measurements. Application of visual kinetic analysis to the study of catalytic systems with catalyst activation.

# Chapter I

## Rhodium-catalyzed Hydroformylation of 1,1'-Disubstituted Allenes by Supramolecularly Regulated Ligands

UNIVERSITAT ROVIRA I VIRGILI

THE HYDROFORMYLATION REACTION: FROM COVALENT TO SUPRAMOLECULAR APPROACHES AND OPERANDO KINETIC STUDIES

Alicia Martínez Carrión

# Rhodium-catalyzed Hydroformylation of 1,1'-Disubstituted Allenes by Supramolecularly Regulated Ligands

(Unpublished results)

Alicia Martínez-Carrión<sup>a,b</sup>, Anton Vidal-Ferran<sup>b,c\*</sup>

- a Universitat Rovira i Virgili, Departament de Química Analítica i Química Orgànica, C. Marcel·lí Domingo 1, 43007, Tarragona, Spain.
- b Institut Català d'Investigació Química (ICIQ) & Barcelona Institute of Science and Technology (BIST), Av. Països Catalans 16, 43007, Tarragona, Spain.
- c Institució Catalana de Recerca i Estudis Avançats (ICREA), Pg. Lluís Companys 23, 08010, Barcelona, Spain.

## 1.1 ABSTRACT

Modular bisphosphine and bisphosphite supramolecularly regulated ligands containing a polyethyleneoxy chain as regulation site have been synthesized. The ligands have been successfully tested in the Rh-catalyzed hydroformylation of 1,1'-disubstituted allenes. Rhodium complexes derived from the combination of supramolecular bisphosphine and bisphosphite ligands with alkali metal BARF salts as regulation agents (RA) led to an enhancement of the catalytic activity (up to 60% increase in the yield).

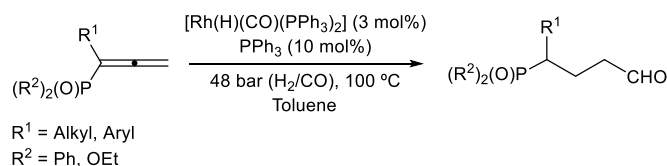
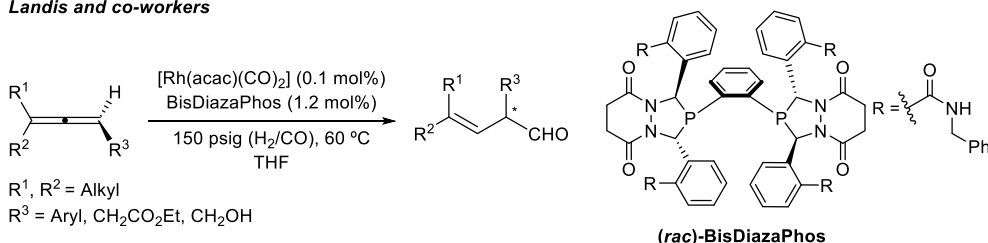
## 1.2 INTRODUCTION

The hydroformylation reaction is a powerful synthetic methodology that allows the transformation of unsaturated hydrocarbons into aldehydes by C–C bond formation. This reaction has been widely studied since its discovery in 1938 with a shift from cobalt to rhodium as catalytic metal center.<sup>1</sup> While alkene and alkyne hydroformylation has been studied for a broad array of substrates with a set of

---

<sup>1</sup> Börner, A. Franke, R.; *Hydroformylation: Fundamentals, Processes, and Applications in Organic Synthesis*; Wiley-VCH, Weinheim, 2016.

catalytic systems, the literature on hydroformylation of allenes remains scarce.<sup>2</sup> Hydroformylation of allenes has to address regioselectivity as well as chemoselectivity issues, as a consequence of the multiple reaction pathways leading to undesired side-products. Fell and co-workers reported for the first time the hydroformylation of allenes.<sup>2a</sup> The use of PPh<sub>3</sub> in the rhodium-catalyzed hydroformylation 1,2-butadiene, led to the formation of complex mixtures of products with mono- and dihydroformylation products. Guo and co-workers reported the tandem hydroformylation-hydrogenation of 1,2-allenyl phosphine oxides and phosphonates with a total regioselectivity towards the linear aldehyde, employing PPh<sub>3</sub> as ligand (Scheme 18).<sup>2c</sup> Landis and co-workers have employed the phospholane-based bisdiazaphos ligands in the hydroformylation of 1,1',3-trisubstituted allenes yielding  $\beta,\gamma$ -unsaturated aldehydes with low catalyst loadings (up to 0.1 mol%) (Scheme 18).<sup>2c</sup>

**Guo and co-workers****Landis and co-workers**

**Scheme 18.** Hydroformylation of 1,2-allenyl phosphine oxides/phosphonates and 1,1',3-trisubstituted allenes

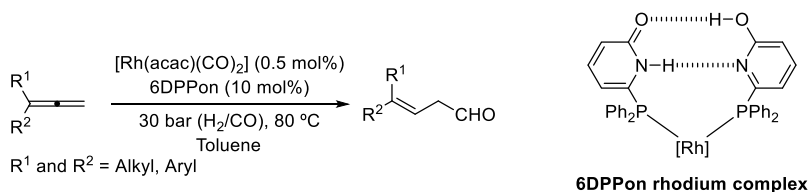
Ligand design in hydroformylation reactions plays an important role. Among the diverse coordinating groups, phosphorus(III)-containing ligands have proved to be suitable for this transformation.<sup>3</sup> Structurally diverse libraries of ligands

<sup>2</sup> (a) Fell, B.; Beutler, M. *Erdöl & Kohle, Erdgas, Petrochem.* **1976**, *29*, 149-153. (b) Huo, C.-F.; Li, Y.-W.; Beller, M.; Jiao, H. *Chem. - Eur. J.* **2005**, *11*, 889-902. (c) Guo, H.; Ma, S. *Adv. Synth. Catal.* **2008**, *350*, 1213-1217. (d) Köpfer, A.; Breit, B. *Angew. Chem., Int. Ed.* **2015**, *54*, 6913-6917. (e) Eshon, J.; Landis, C. R.; Schomaker, J. M. *J. Org. Chem.* **2017**, *82*, 9270-9278.

<sup>3</sup> Kamer, P. C. J.; van Leeuwen, P. W. N. M., Eds.; *Phosphorus(III) Ligands in Homogeneous Catalysis: Design and Synthesis*; John Wiley & Sons Ltd., Chichester, **2012**.

have been reported over the last decades, at the expense in many cases of high synthetic efforts to introduce structural variations in the catalytic system. Supramolecular chemistry has emerged as a useful tool to construct and develop new catalysts employing supramolecular interactions.<sup>4</sup> In the field of hydroformylation chemistry,<sup>5</sup> different approaches have been employed for the design of supramolecular catalysts: (i) ligand-substrate preorganization,<sup>6</sup> (ii) construction of bidentate ligand by self-assembly processes,<sup>7</sup> (iii) confinement of the metal-based catalyst<sup>8</sup> and (iv) distal regulation with regulation agents.<sup>9</sup>

A supramolecular approach has been applied in the hydroformylation of allenes. Breit *et al.* employed the self-assembled 6-DPPon system in the hydroformylation of 1,1'-disubstituted allenes, obtaining  $\beta,\gamma$ -unsaturated aldehydes of symmetrical and unsymmetrical allenes with an excellent regiocontrol and stereoselectivity (Scheme 19).<sup>2d</sup>



**Scheme 19.** Hydroformylation of 1,1'-disubstituted allenes with supramolecular self-assembled 6DPPon system

The use of supramolecular bisphosphite ligands regulated with an external agent has been previously developed and applied by our group for the asymmetric hydroformylation of vinyl esters and other alkenes<sup>10</sup> and heterocyclic olefins,<sup>11</sup> proving to be highly efficient and enantioselective catalysts (Scheme 20). Herein

<sup>4</sup> For selected reviews, see: (a) Meeuwissen, J.; Reek, J. N. H. *Nat. Chem.* **2010**, *2*, 615-621. (b) Raynal, M.; Ballester, P.; Vidal-Ferran, A.; van Leeuwen, P. W. N. M. *Chem. Soc. Rev.* **2014**, *43*, 1660-1733. (c) Raynal, M.; Ballester, P.; Vidal-Ferran, A.; van Leeuwen, P. W. N. M. *Chem. Soc. Rev.* **2014**, *43*, 1734-1787.

<sup>5</sup> For a selected review of supramolecular hydroformylation, see: Nurttala, S. S.; Linnebank, P. R.; Krachko, T.; Reek, J. N. H. *ACS Catal.* **2018**, *8*, 3469-3488.

<sup>6</sup> Dydio, P.; Reek, J. N. H. *Chem. Sci.* **2014**, *5*, 2135-2145.

<sup>7</sup> Bellini, R.; van der Vlugt, J. I.; Reek, J. N. H. *Isr. J. Chem.* **2012**, *52*, 613-629.

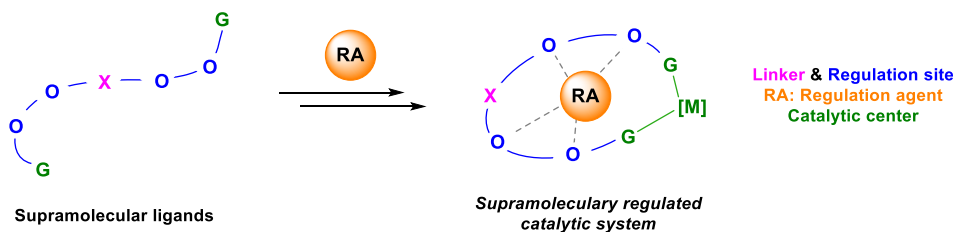
<sup>8</sup> (a) Leenders, S. H. A. M.; Gramage-Doria, R.; de Bruin, B.; Reek, J. N. H. *Chem. Soc. Rev.* **2015**, *44*, 433-448. (b) Mouarrawis, V.; Plessius, R.; van der Vlugt, J. I.; Reek, J. N. H. *Front. Chem.* **2018**, *6*, 623-643.

<sup>9</sup> Vaquero, M.; Rovira, L.; Vidal-Ferran, A. *Chem. Commun.* **2016**, *52*, 11038-11051.

<sup>10</sup> (a) Mon, I.; Jose, D. A.; Vidal-Ferran, A. *Chem. - Eur. J.* **2013**, *19*, 2720-2725. (b) Vidal-Ferran, A.; Mon, I.; Bauzá, A.; Frontera, A.; Rovira, L. *Chem. - Eur. J.* **2015**, *21*, 11417-11426.

<sup>11</sup> Rovira, L.; Vaquero, M.; Vidal-Ferran, A. *J. Org. Chem.* **2015**, *80*, 10397-10403.

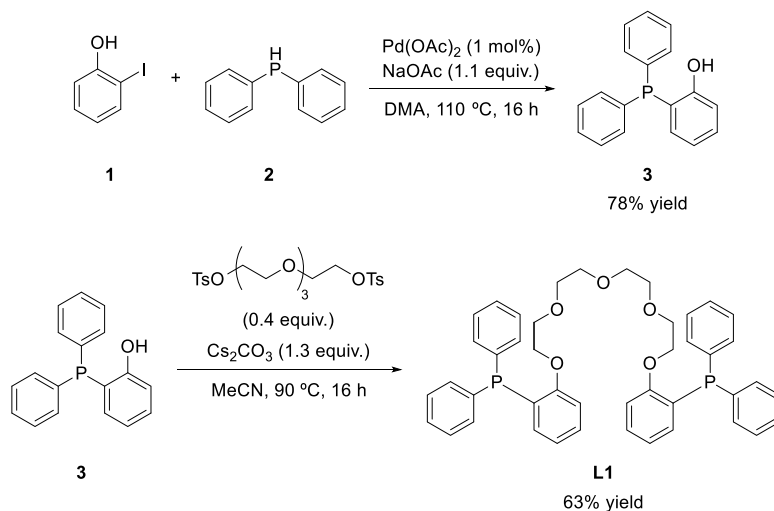
we describe the design and synthesis of new supramolecularly regulated phosphorus(III)-containing ligands and their application in the hydroformylation of 1,1'-disubstituted allenes.



**Scheme 20.** Design principle of the supramolecularly regulated ligands developed in our research group

### 1.3 RESULTS AND DISCUSSION

With the aim of testing our regulation strategy in challenging substrates, we developed a new supramolecular catalyst for the rhodium catalyzed hydroformylation of symmetrically 1,1'-disubstituted allenes. The new supramolecular ligand **L1** incorporated phosphine moieties as coordinating groups (Scheme 21). The first step in the synthesis of the ligand was the preparation of 2-(diphenylphosphino)phenol **3** by palladium-catalyzed arylation of diphenyl phosphine **2** with 2-iodophenol **1**, with the target product **3** being obtained in 78% yield.

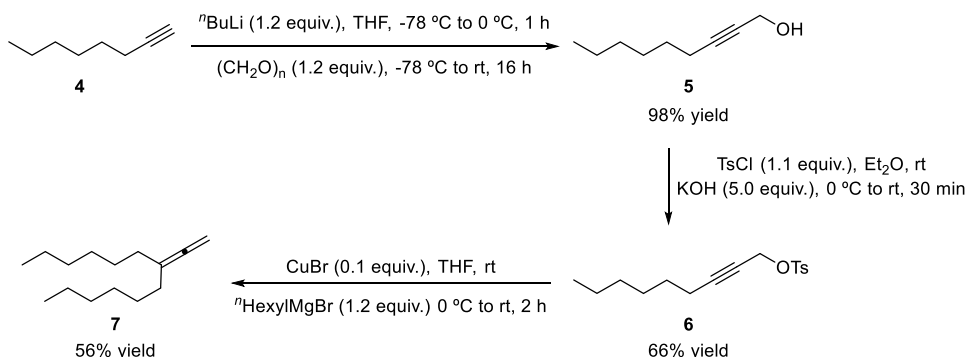


**Scheme 21.** Synthesis of supramolecular ligand **L1**

The last step was the nucleophilic attack of the alkoxide group in phosphine **3** to the ditosylated tetraethyleneglycol, obtaining the desired ligand **L1** in 63%

yield. As regulation site, we chose a tetraethyleneglycol moiety due to its favorable binding properties towards cationic species through ion-dipole interactions<sup>12</sup> that should allow us introducing subtle geometrical modifications in the supramolecular catalyst by changing the size of the cation. The regulation agents selected for this metal-catalyzed transformation were the alkali metal BArF salts (BArF = [B(3,5-(CF<sub>3</sub>)<sub>2</sub>C<sub>6</sub>H<sub>3</sub>)<sub>4</sub>]<sup>-</sup>), due to the non-coordinating nature of the BArF anion and availability through well-established synthetic procedures.<sup>13</sup>

To test the activity of our supramolecularly regulated catalysts in the hydroformylation of allenes, 7-vinylidenetridecane **7** was selected as model substrate. Substrate **7** was synthesized following a reported procedure (Scheme 22).<sup>2c</sup> Non-2-yl-1-ol **5** was synthesized from commercially available oct-1-yne **4** by deprotonation with *n*-BuLi and subsequent reaction with paraformaldehyde obtaining **5** in almost quantitative yield (98% yield). Subsequent tosylation of **5** led to the formation of **6** in 66% yield. The final product **7** was synthesized in 56% yield by copper-catalyzed nucleophilic addition of *n*-hexyl magnesium bromide to tosylated product **6**.



**Scheme 22.** Synthesis of vinylidenetridecane **7**

Preliminary hydroformylation studies were performed with catalytic amounts of [Rh( $\kappa^2$ O,O'-acac)(CO)<sub>2</sub>] as metal precursor (1 mol%), supramolecular ligand **L1** (1.2 mol%) and NaBArF as RA (1.56 mol%) under 10 bar syngas (H<sub>2</sub>/CO 1:1 ratio) and 5 h reaction time. For the sake of the solubilization of the RA, the minimum amount of THF was used (3 vol% with respect to toluene). The

<sup>12</sup> Steed, J. W.; Atwood, J. L., Eds.; *Supramolecular Chemistry*, 2<sup>nd</sup> Ed.; John Wiley & Sons Ltd., Chichester, 2009.

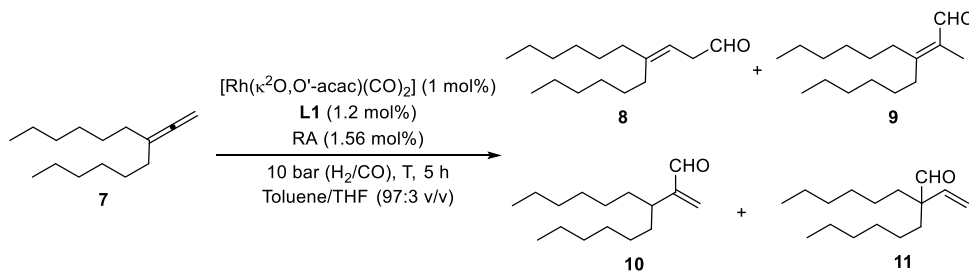
<sup>13</sup> Carreras, L.; Rovira, L.; Vaquero, M.; Mon, I.; Martin, E.; Benet-Buchholz, J.; Vidal-Ferran, A. *RSC Adv.* 2017, 7, 32833-32841.



L1/RA ratio used ensured the quantitative formation of the supramolecular complex.<sup>9</sup>

Allenes are well known for their higher reactivity with respect to alkenes in transition metal catalysis.<sup>14</sup> For this reason, a temperature screening was initially carried out in presence and absence of regulation agent (Table 1, entries 1-6).

**Table 1.** Temperature screening in the Rh-catalyzed hydroformylation of **7** using **L1**



Entry	Temperature (°C)	RA	Conv. (%) <sup>[a]</sup>	Yield (%) of <b>8</b> <sup>[a]</sup>	Ratio <b>8:9:10:11</b>
1	0	None	67	n.d.	0:0:0:0
2	0	NaBArF	20	n.d.	0:0:0:0
3	25	None	>99	n.d.	0:0:0:0
4	25	NaBArF	>99	n.d.	0:0:0:0
5	40	None	>99	3	3:0:0:0
6	40	NaBArF	>99	6	6:0:0:0

The hydroformylations were performed in a parallel autoclave. Reaction conditions: [alkene] = 0.26 M; stirring rate = 800 rpm; H<sub>2</sub>/CO in a 1:1 ratio, unless otherwise cited. [a] Conversion, yield and product ratio were determined by using <sup>1</sup>H NMR spectroscopy with 1,3,5-trimethoxybenzene as internal standard.

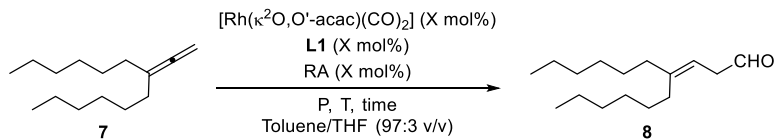
Despite the high reactivity of allenes in hydroformylations, low catalytic activity was observed when low temperatures were employed. Unreacted starting material **7** was detected, and no hydroformylation products **8-11** were detected either by NMR or GC analysis techniques (Table 1, entries 1-2). The presence of NaBArF as regulation agent (Table 1, entry 2) reduced the amount of consumed allene. When the reaction temperature was increased up to 25 °C (Table 1, entries 3-4), full conversion of allene **7** was observed, however no hydroformylation products **8-11** were observed in the presence or absence of RA. Only at 40 °C in the presence or absence of NaBArF as regulation agent, the formation of

<sup>14</sup> Krause, N.; Hashmi, A. S. K., Eds.; *Modern Allene Chemistry*; Wiley-VCH, Weinheim, 2004.

aldehyde **8** was observed. In terms of regioselectivity, among all the possible aldehyde products, only product **8** was formed in low yield (Table 1, entries 5-6). Regioselectivity was confirmed by  $^1\text{H}$  NMR, as the only signal observed in the aldehyde region had a triplet multiplicity, which is only in agreement with regioisomer **8**. Computational calculations at the DFT level, could account for the observed regioselectivity towards the linear aldehyde **8**, as this compound is the kinetic and thermodynamically favored regioisomer.<sup>2b</sup> The formation of this isomer is in agreement with previous examples in the literature, in which only regioisomer **8** was observed.<sup>2</sup>

After screening the temperature of the reaction, the influence of the total pressure on the hydroformylation of allene **7** was considered, as well as other rhodium metal precursors. When the total pressure of syngas (1:1  $\text{H}_2/\text{CO}$  ratio) was increased up to 30 bar at 25 °C (Table 2, entries 1-2), traces of **8** were detected in the presence of NaBArF (Table 2, entry 2), proving that a higher total pressure of syngas was slightly beneficial for the hydroformylation reaction.

**Table 2.** Screening of the reaction conditions in the Rh-catalyzed hydroformylation of **7** using **L1**



Entry	Temperature (°C)	Pressure (bar)	Time (h)	Cat. loading (mol%) <sup>[c]</sup>	RA	Conv. (%) <sup>[a]</sup>	Yield (%) of <b>8</b> <sup>[a]</sup>
1					None	>99	n.d.
2	25	30	5	1	NaBArF	>99	2
3 <sup>[b]</sup>	40	10	5	1	NaBArF	>99	1
4	40	10	5	2	NaBArF	>99	11
5					None	>99	14
6	80	30	1	1	NaBArF	>99	16
7					None	>99	1
8	40	10	18	1	NaBArF	>99	22

The hydroformylation reactions were performed in a parallel autoclave. Reaction conditions: [alkene] = 0.26 M; stirring rate = 800 rpm;  $\text{H}_2/\text{CO}$  in a 1:1 ratio, unless otherwise cited. [a] Conversion and yield were determined by using  $^1\text{H}$  NMR spectroscopy with 1,3,5-trimethoxybenzene as internal standard. [b]  $[\text{Rh}(\text{OMe})_2(\text{COD})]_2$  was used as catalyst precursor. [c] 1 mol% of catalyst was prepared with 1 mol% of Rh precursor, 1.2 mol% of **L1** and 1.56 mol% of RA. 2 mol% of catalyst was prepared by a two-fold increase in the amounts of all components.

Despite  $[\text{Rh}(\kappa^2\text{O},\text{O}'\text{-acac})(\text{CO})_2]$  is a common metal precursor for hydroformylation reactions, due to the lability of the acetylacetonato ligand under hydroformylation reactions conditions, another metal precursor was used in order to study the influence in the catalytic outcome. The reaction was carried out employing  $[\text{Rh}(\text{OMe})_2(\text{COD})]_2$  as metal precursor (Table 2, entry 3) in the presence of NaBARF. Hydroformylation products were only formed in trace amounts and, for this reason, further optimization studies were done with  $[\text{Rh}(\kappa^2\text{O},\text{O}'\text{-acac})(\text{CO})_2]$  as the metal precursor.

In order to make the supramolecular catalytic system more active towards the hydroformylation reaction, the optimal amount of catalyst was investigated. Under similar catalytic conditions, higher amounts of catalyst were used (Table 2, entry 4) in presence of NaBARF. The use of a 2 mol% of catalyst, led to a moderate increase of the yield for the hydroformylation product **8** (up to 11% yield). Nevertheless we decided to continue studying the reaction conditions to improve the catalytic system activity, rather than using higher catalyst loadings.

The low activity observed led us to suggest that the catalytic active species in hydroformylation chemistry (*i.e.*, hydrido dicarbonyl rhodium complexes) were not formed under the catalyst screening conditions. To maximize the formation of the hydroformylation product, and taking into account the effect of temperature and pressure, reactions were performed at 80 °C and 30 bar of syngas (Table 2, entries 5-6). Under these conditions, product **8** was formed in a 14% yield in the absence of RA and 16% yield in the presence of NaBARF. Despite higher amounts of the hydroformylation product **8** were formed under these conditions, poor regulation effects were observed.

It has been reported in the literature, that high temperatures and/or low pressures increase the isomerization of alkenes due to equilibrium processes in the catalytic cycle.<sup>15</sup> For this reason, and with the aim of increasing the formation of aldehydes, milder reaction conditions and longer reaction times were used (Table 2, entries 7-8). With these conditions, traces of aldehyde **8** were observed in the absence of RA. However, when NaBARF was used, product **8** was obtained in a 22% yield. These results show that, despite hydroformylation product **8** can be formed using harsh reaction conditions (high temperature and pressure of syngas), milder reaction conditions can also be used due to the presence of a

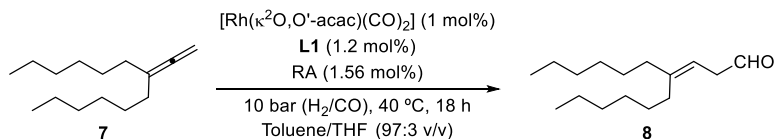
---

<sup>15</sup> Van Leeuwen, P. W. N. M.; Claver, C. Eds.; *Rhodium Catalyzed Hydroformylation*; Kluwer Academic Publishers, Dordrecht, **2002**.

regulation agent that accelerates the formation of the active catalytic species with respect to experiments in the absence of regulation agent.

Our research group has reported supramolecularly regulated catalysts that contain polyethyleneoxy chains as regulation sites and phosphorus ligating groups for catalysis. Our regulation mechanism is triggered by the addition of a regulation agent (RA) capable of interacting with the regulation site *via* supramolecular interactions. The choice of RA determines the rigidity and conformational flexibility of the whole catalytic system, which translates into a modulation of the selectivity in the transformation of interest. To study the effect of the regulation agents in the outcome of the reaction, a set of alkali metal BArF salts was tested using the best catalytic conditions: 10 bar syngas, 40 °C, 18 h (Table 3).

**Table 3.** Screening of regulation agents in the Rh-catalyzed hydroformylation of **7** using **L1**

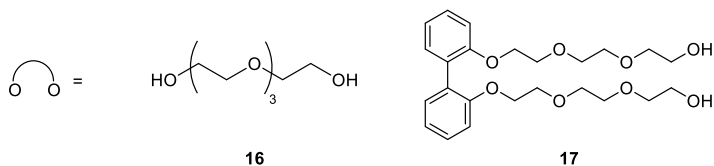
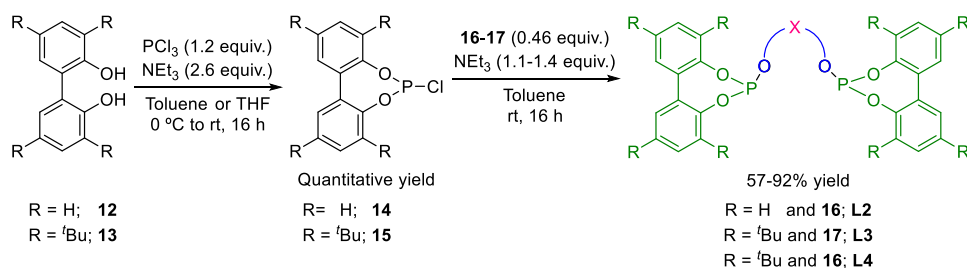


Entry	RA	Conversion (%) <sup>[a]</sup>	Yield (%) of <b>8</b> <sup>[a]</sup>
1	None	>99	1
2	LiBArF	>99	3
3	NaBArF	>99	22
4	KBArF	>99	3
5	RbBArF	>99	3
6	CsBArF	>99	2

The hydroformylations were performed in a parallel autoclave. Reaction conditions: [alkene] = 0.26 M; stirring rate = 800 rpm;  $\text{H}_2/\text{CO}$  in a 1:1 ratio, unless otherwise cited. [a] Conversion and yield were determined by using  $^1\text{H}$  NMR spectroscopy with 1,3,5-trimethoxybenzene as internal standard.

The use of a set of alkali metal BArF salts with differently sized cationic components did not improve the catalytic outcome to an important extent, with NaBArF being the RA that promoted a higher yield of **8**. Although the hydroformylated product **8** was formed under catalytic conditions, low yields were obtained. As previously observed, aldehydes **9-11** were not detected. Accounting on the results obtained, we decided to explore other parameters that could influence the catalytic activity. Organic ligands are a crucial component in the catalytic systems in homogeneous catalysis, allowing modifications of the

steric and electronic properties of the catalyst.<sup>1</sup> Fine tuning of the  $\sigma$ -donor and  $\pi$ -acceptor properties of the ligands can accelerate the reaction rate and increase the selectivity by disfavoring side reactions. With the purpose of assessing the influence of other coordinating groups in the outcome of the Rh-catalyzed hydroformylation of 1,1'-disubstituted allenes, phosphite ligating groups were chosen. Bisphosphite-based ligands are common motifs employed for hydroformylation reactions. In general terms, the use of phosphite ligands increases the reaction rate if compared with phosphine-based systems.<sup>15</sup> Thus, an analogous ligand to **L1** bearing phosphite moieties was synthesized (Scheme 23). **L2** was synthesized by *O*-phosphorylation of the corresponding chlorophosphite derivative **14** with tetraethyleneglycol **16** in 57% yield.



**Scheme 23.** Synthesis of supramolecular ligands **L2-L4**

The modular design of our bisphosphite supramolecular ligands allows changing any element (binding site and coordinating group) following the same synthetic procedure. It has been reported in the literature that 3,3'-disubstituted [1,1'-biaryl]-2,2'-diols have higher stability if compared with 3,3'-unsubstituted analogues.<sup>16</sup> Besides, better catalytic activity and regioselectivity have been observed in hydroformylation chemistry when bulky substituents are located at the 3 and 3' positions of the [1,1'-biphenyl]-2,2'-diol motif.<sup>17</sup> For this reason 3,3',5,5'-tetra-*tert*-butyl-[1,1'-biphenyl]-2,2'-diol **13** was selected for the synthesis of new supramolecular ligands. For the regulation site, polyether groups such as

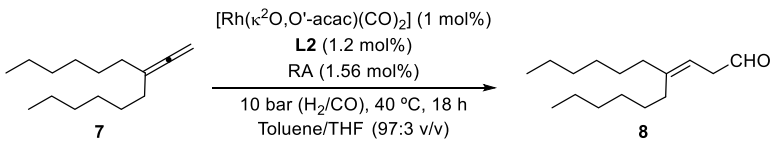
<sup>16</sup> Gual, A.; Godard, C.; de la Fuente, V.; Castellón, S.; *Design and synthesis of phosphite ligands for homogeneous catalysis*, p. 81-131. In *Phosphorus(III) Ligands in Homogeneous Catalysis: Design and Synthesis*; Kamer, P. C. J.; van Leeuwen, P. W. N. M., Eds.; John Wiley & Sons Ltd., Chichester, **2012**.

<sup>17</sup> Franke, R.; Selent, D.; Börner, A. *Chem. Rev.* **2012**, *112*, 5675-5732.

those derived from compounds **16** or **17** were selected. We considered that introducing changes in the size and number of oxygens would provide a wider range of binding possibilities and could influence the outcome of the hydroformylation reactions. Consequently, ligands **L3** and **L4** were synthesized in moderate to high yields (89-92% yield), following the same synthetic methodology as for **L2** (Scheme 23).

For initial catalytic studies involving phosphite-based ligands **L2-L4**, we chose 10 bar of syngas, 40 °C and 18 h, as these reaction conditions provided the best results for **L1**. Initial evaluation of the effects of the regulation agents on **L2** revealed a different trend compared to **L1** (Table 4). The modification of the coordinating group did not affect the regioselectivity observed with phosphine ligand **L1**. As previously observed, aldehydes **9-11** were not detected. When no RA was used, aldehyde **8** was formed with the highest yield (12% yield; Table 4, entry 1). Although the absence of regulation agent led to the formation of higher amounts of linear aldehyde **8**, the yield of the hydroformylation product **8** increased with the radius of the alkali cation in the RA (Table 4, entries 2-6).

**Table 4.** Screening of RAs in the Rh-catalyzed hydroformylation of **7** using **L2**



Entry	RA	Conversion (%) <sup>[a]</sup>	Yield (%) of <b>8</b> <sup>[a]</sup>
1	None	>99	12
2	LiBArF	>99	3
3	NaBArF	>99	3
4	KBArF	>99	5
5	RbBArF	>99	8
6	CsBArF	>99	10

The hydroformylations were performed in a parallel autoclave. Reaction conditions: [alkene] = 0.26 M; stirring rate = 800 rpm; H<sub>2</sub>/CO in a 1:1 ratio, unless otherwise cited. [a] Conversion and yield were determined by <sup>1</sup>H NMR spectroscopy with 1,3,5-trimethoxybenzene as internal standard.

Studies on the regulation effects of an array of RAs for ligand **L3** with bulky substituents in *ortho* position and 1,1'-biphenyl moiety as linker in the binding site were performed. Hydroformylation of **7** was carried out under identical catalytic conditions as for **L2**. When no RA was used, poor yield was obtained (Table 5,

entry 1). Surprisingly, all RAs led to similar results without having been able to identify a RA that provoked important enhancements in the yield (Table 5, entries 2-6).

**Table 5.** Screening of regulation agents in the Rh-catalyzed hydroformylation of **7** using **L3**

Entry	RA	Conversion (%) <sup>[a]</sup>	Yield (%) of <b>8</b> <sup>[a]</sup>
1	None	>99	5
2	LiBArF	>99	7
3	NaBArF	>99	7
4	KBArF	>99	6
5	RbBArF	>99	7
6	CsBArF	>99	7

The hydroformylations were performed in a parallel autoclave. Reaction conditions: [alkene] = 0.26 M; stirring rate = 800 rpm; H<sub>2</sub>/CO in a 1:1 ratio, unless otherwise cited. [a] Conversion and yield were determined by <sup>1</sup>H NMR spectroscopy with 1,3,5-trimethoxybenzene as internal standard.

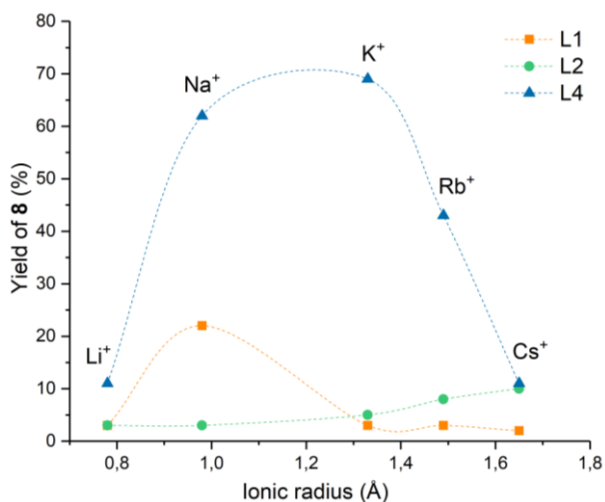
The effects of the binding site were also studied by comparing **L3** and **L4**, which have the same phosphite moiety but differ in the structure of the linker. Studies on the regulation effects of an array of RAs for ligand **L4** provided better catalytic results (Table 6). In absence of RA, aldehyde **8** was formed with a 9% yield (Table 6, entry 1), as previously observed for **L3**. When KBArF was used as RA, a remarkable improvement in the yield was observed, obtaining aldehyde **8** with a 69% yield (Table 6, entry 4). The yield in the formation of **8** with NaBArF is quite similar to that for KBArF (Table 6, compare entries 3 and 4). Regulation effects of larger RAs, like RbBArF and CsBArF, led to lower yield in the formation of **8** (43 and 11% yield, respectively; Table 6, entries 5-6).

**Table 6.** Screening of regulation agents in the Rh-catalyzed hydroformylation of **7** using **L4**

Entry	RA	Conversion (%) <sup>[a]</sup>	Yield (%) of <b>8</b> <sup>[a]</sup>
1	None	>99	9
2	LiBArF	>99	11
3	NaBArF	>99	62
4	KBArF	>99	69
5	RbBArF	>99	43
6	CsBArF	>99	11

The hydroformylations were performed in a parallel autoclave. Reaction conditions: [alkene] = 0.26 M; stirring rate = 800 rpm; H<sub>2</sub>/CO in a 1:1 ratio, unless otherwise cited. [a] Conversion and yield were determined by <sup>1</sup>H NMR spectroscopy with 1,3,5-trimethoxybenzene as internal standard.

The supramolecular regulation of the catalytic reaction is closely related with the size of the regulation agent used, but also with the coordinating group employed. In Graph 1, the yield of product **8** and the ionic radius of the regulation agents are compared for ligands **L1**, **L2** and **L4**, which contain the same regulation site.



**Graph 1.** Correlation between catalytic activity of ligands **L1**, **L2** and **L4** and RA ionic radius



In case of ligand **L1**, the use of phosphine moieties as coordinating groups shows a better regulation with NaBArF. Ligand **L2**, which bears 3 and 3' unsubstituted [1,1'-biaryl]-2,2'-diol-based phosphite groups, has a slight preference for cations with large ionic radius, as CsBArF. Finally, ligand **L4**, with ligating groups containing bulky substituents at the 3 and 3' positions of the [1,1'-biaryl]-2,2'-diol-based phosphite group shows the highest catalytic activity and the highest regulation effect (increase in a 60% of the yield of **8**) with KBArF as regulation agent. These results also confirm the beneficial effects of the substituents at the 3 and 3' positions of the [1,1'-biaryl]-2,2'-diol-based phosphite group in the ligand.

These results support the design principle of our supramolecular regulation approach: screening a set of regulation agents to obtain the highest yield for the substrate of interest. The rapid tailoring of the catalyst system for a substrate of interest has been demonstrated.

## 1.4 CONCLUSIONS

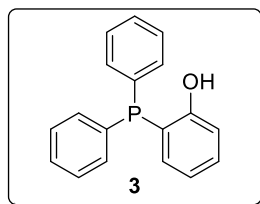
In summary, an array of phosphine- and phosphite-containing supramolecular ligands incorporating a polyethyleneoxy chain as regulation site has been synthesized. Supramolecular ligands have been successfully used in the Rh-catalyzed hydroformylation of a representative example of a 1,1'-disubstituted allene. The use of a ligand with phosphine moieties as coordinating groups was not active in the hydroformylation reaction, but led to the formation of the  $\beta,\gamma$ -unsaturated aldehyde in 22% in the presence of an external regulation agent (21% increase in the yield with NaBARF as the regulation agent). The use of 3,3'-disubstituted [1,1'-biphenyl]-2,2'-diol phosphite motifs in the supramolecular ligands improved the catalytic activity with respect to that observed for the bisphosphine ligands. For the supramolecularly regulated bisphosphite ligand **L4**, the use of an external regulation agent provided a remarkable enhancement in the yield of the corresponding  $\beta,\gamma$ -unsaturated aldehyde (up to 60% increase). The benefits of our regulation approach have been demonstrated, as the presence of alkali metal BARF salts increase the catalytic activity. These studies have demonstrated that the modular design of the supramolecular ligands and the right combination of coordinating group, binding site and regulation agent is crucial for the catalytic outcome in the hydroformylation of allenes, with the formation of side-products being suppressed.

## 1.5 EXPERIMENTAL SECTION

### 1.5.1 General considerations

All syntheses were carried out using chemicals purchased from commercial sources unless otherwise cited. Air- and moisture-sensitive manipulations and hydroformylation reactions were performed under inert atmosphere, either in a N<sub>2</sub>-filled glove box or with standard Schlenk techniques. Glassware was dried *in vacuo* before use with a hot air gun. All solvents were dried and deoxygenated by using a Solvent Purification system (SPS). Silica gel 60 (230-400 mesh) or C18-SiO<sub>2</sub> (200-400 mesh) was used for column chromatography. NMR spectra were recorded at room temperature, otherwise cited, in a 300 MHz, 400 MHz or 500 MHz spectrometers in CDCl<sub>3</sub> unless otherwise cited. <sup>1</sup>H NMR, <sup>13</sup>C{<sup>1</sup>H} and <sup>13</sup>C{<sup>1</sup>H,<sup>31</sup>P} NMR chemical shifts were quoted in ppm relative to the residual solvent peaks. <sup>31</sup>P{<sup>1</sup>H} NMR chemical shifts were quoted in ppm relative to 85% phosphoric acid in water. IR spectra were recorded using Attenuate Total Reflection (ATR) techniques unless otherwise cited. High-resolution mass spectra (HRMS) were recorded by using electrospray ionization (ESI) method in positive mode. Melting points were determined in open capillaries and are uncorrected.

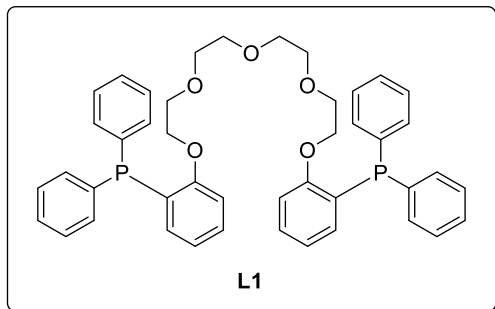
### 1.5.2 Synthesis of ligands L1-L4



**Compound 3:** The preparation of **3** was performed following a reported procedure.<sup>18</sup> A mixture of *ortho*-iodo phenol **1** (3.1 g, 13.70 mmol), diphenylphosphine **2** (2.4 ml, 13.70 mmol), palladium (II) acetate (30.7 mg, 0.14 mmol) and sodium acetate (1.2 g, 15.0 mmol) in anhydrous DMA (43 mL) was stirred under N<sub>2</sub> atmosphere at 110 °C for 16 h. The reaction mixture was filtered through a pad of Celite<sup>®</sup>. The filtrate was concentrated *in vacuo*. After purification by column chromatography over SiO<sub>2</sub> using DCM, 2-(diphenylphosphino)phenol **3** was obtained as a colorless solid (3 g, 78% yield). Spectroscopic data for this compound were in agreement with the reported ones.<sup>18</sup> <sup>1</sup>H NMR (400 MHz, CDCl<sub>3</sub>) δ 7.38–7.29 (m, 11H), 7.01–6.98 (m, 1H), 6.96–6.92 (m, 1H), 6.91–6.88 (m, 1H), 6.20 (s, 1H) ppm. <sup>13</sup>C{<sup>1</sup>H,<sup>31</sup>P} NMR (126 MHz, CDCl<sub>3</sub>) δ 159.3 (1 C,

<sup>18</sup> Kapadnis, P. B.; Hall, E.; Ramstedt, M.; Galloway, W. R. J. D.; Welch, M.; Spring, D. R. *Chem. Commun.* **2009**, 538-540.

*Carom*O<sup>H</sup>), 135.1 (2 C, *Carom*P), 134.9 (1 C, *Carom*H), 133.5 (4 C, *Carom*H), 131.7 (1 C, *Carom*H), 129.1 (2 C, *Carom*H), 128.8 (4 C, *Carom*H), 121.3 (1 C, *Carom*H), 121.1 (1 C, *Carom*P), 115.7 (1 C, *Carom*H) ppm. <sup>31</sup>P{<sup>1</sup>H} NMR (162 MHz, CDCl<sub>3</sub>) δ -26.0 ppm.



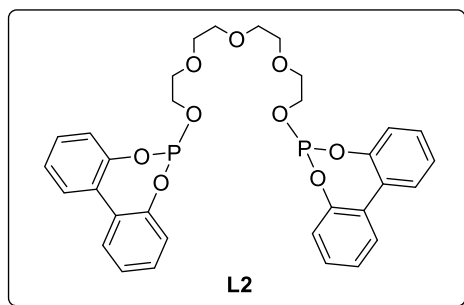
**Compound L1:** The preparation of **L1** was performed by modifying a reported procedure.<sup>19</sup> Under N<sub>2</sub> atmosphere, Cs<sub>2</sub>CO<sub>3</sub> (2.3 g, 6.40 mmol) was added in one portion to a solution of 2-(diphenylphosphino)phenol **3** (1.5 g, 5.24 mmol) and ditosylate

tetraethyleneglycol (1.2 g, 2.32 mmol) in deoxygenated acetonitrile (66 mL). The resulting mixture was refluxed overnight. The reaction mixture was concentrated under reduced pressure and dissolved with AcOEt (34 mL). The combined organic phases were washed with brine (68 mL), dried over MgSO<sub>4</sub> and the solvent was evaporated under reduced pressure. After purification by column chromatography over SiO<sub>2</sub> using Cy/AcOEt 70:30, product **L1** was obtained as a white solid (1 g, 63% yield). Mp: 116–117 °C. IR (neat, cm<sup>-1</sup>)  $\bar{\nu}$  3519, 3056, 2869, 1904, 1582, 1472, 1433, 1272, 1243, 1128, 1067, 1040, 1025, 999, 917, 857, 747, 695, 610, 551, 498. <sup>1</sup>H NMR (500 MHz, CD<sub>2</sub>Cl<sub>2</sub>) δ 7.34–7.28 (m, 22H), 6.91 (dd, *J* = 7.9, 4.4 Hz, 2H), 6.86 (t, *J* = 7.4 Hz, 2H), 6.69–6.66 (m, 2H), 4.03–4.01 (m, 4H), 3.50–3.48 (m, 2H), 3.46–3.41 (m, 8H) ppm. <sup>13</sup>C{<sup>1</sup>H,<sup>31</sup>P} NMR (126 MHz, CD<sub>2</sub>Cl<sub>2</sub>) δ 160.7 (2 C, *Carom*O), 137.4 (4 C, *Carom*P), 134.3 (8 C, *Carom*H), 133.8 (2 C, *Carom*H), 130.6 (2 C, *Carom*H), 129.0 (4 C, *Carom*H), 128.7 (8 C, *Carom*H), 126.7 (2 C, *Carom*P), 121.5 (2 C, *Carom*H), 111.9 (2 C, *Carom*H), 71.1 (2 C, COCH<sub>2</sub>CH<sub>2</sub>CO), 70.8 (4 C, COCH<sub>2</sub>CH<sub>2</sub>CO), 69.7 (2 C, COCH<sub>2</sub>CH<sub>2</sub>CO), 69.0 (2 C, POCH<sub>2</sub>) ppm. <sup>31</sup>P{<sup>1</sup>H} NMR (202 MHz, CD<sub>2</sub>Cl<sub>2</sub>) δ -12.4 ppm. HRMS (ESI) *m/z* [M+H] calcd for C<sub>44</sub>H<sub>45</sub>O<sub>5</sub>P<sub>2</sub> 715.2737, found 715.2726.

<sup>19</sup> Song, F.-T.; Ouyang, G.-H.; Li, Y.; He, Y.-M.; Fan, Q.-H. *Eur. J. Org. Chem.* **2014**, 2014, 6713–6719.

### 1.5.2.1 General procedure for the synthesis of supramolecular bisphosphite ligands

Under argon atmosphere, compound **12** or **13** (0.75 mmol) was azeotropically dried with anhydrous toluene (3 x 5 mL), dissolved in anhydrous toluene (5 mL) and added dropwise to a solution of  $\text{PCl}_3$  (0.90 mmol) and  $\text{NEt}_3$  (1.95 mmol) in anhydrous toluene (5 mL) at  $0^\circ\text{C}$ . The solution was allowed to reach room temperature and was stirred overnight. The turbid reaction mixture was filtered through a pad of Celite<sup>®</sup> and the solvent evaporated under reduced pressure. The resulting residue was dissolved in anhydrous toluene (9 mL) and  $\text{NEt}_3$  (1.80-2.25 mmol). A solution of diol **16** or **17** (0.35 mmol) in anhydrous toluene (9 mL) was added dropwise to the previous solution and allowed to react overnight at room temperature. The reaction mixture was filtered through a pad of Celite<sup>®</sup> and the solvent was evaporated under vacuum. The resulting mixture was purified by filtration through a pad of basic alumina with DCM (16 mL) to afford the desired product.

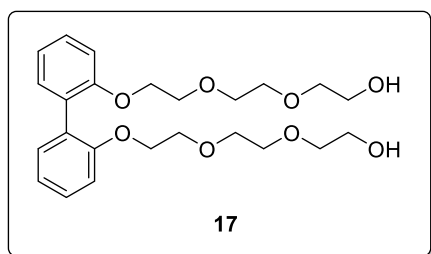


**Compound L2:** The preparation of **L2** was performed modifying the general procedure for the synthesis of supramolecular bisphosphite ligands from a reported procedure.<sup>20</sup> Under argon atmosphere, [1,1'-biphenyl]-2,2'-diol **12** (1.1 g, 6.07 mmol) was azeotropically dried with anhydrous

toluene (3 x 5 mL), dissolved in anhydrous THF (18.2 mL) and the reaction mixture was cooled to  $0^\circ\text{C}$ . This solution was added dropwise *via* cannula to a solution mixture of  $\text{PCl}_3$  (584  $\mu\text{L}$ , 6.67 mmol) and  $\text{NEt}_3$  (2.2 mL, 15.80 mmol) in anhydrous THF (6 mL) at  $0^\circ\text{C}$ . The reaction mixture was allowed to reach room temperature and was stirred overnight. The turbid reaction mixture was filtered through a pad of Celite<sup>®</sup> and the solvent evaporated under vacuum. The resulting residue was dissolved in anhydrous toluene (11.3 mL) and  $\text{NEt}_3$  (2.4 mL, 17.30 mmol). A solution of tetraethyleneglycol **16** (542 mg, 2.79 mmol) in anhydrous toluene (11.3 mL) was added dropwise to the previous solution and allowed to react overnight at room temperature. The reaction mixture was filtered through a pad of Celite<sup>®</sup> and the solvent evaporated under reduced pressure. The resulting mixture was purified by filtration through a pad of basic alumina with DCM (16

<sup>20</sup> Frank, D. J.; Franzke, A.; Pfaltz, A. *Chem. - Eur. J.* **2013**, *19*, 2405-2415.

mL) and the solvent was evaporated under vacuum. Product **L2** was obtained as a colorless oil (988 mg, 57% yield). IR (neat,  $\text{cm}^{-1}$ )  $\bar{\nu}$  3063, 2871, 1600, 1567, 1498, 1475, 1434, 1350, 1272, 1247, 1208, 1184, 1097, 1032, 957, 890, 851, 763, 749, 733, 701, 603, 550, 518, 438.  $^1\text{H}$  NMR (500 MHz,  $\text{CD}_2\text{Cl}_2$ )  $\delta$  7.49 (dd,  $J = 7.6$ , 1.7 Hz, 4H), 7.37 (td,  $J = 7.7$ , 1.7 Hz, 4H), 7.29 (t,  $J = 7.5$  Hz, 4H), 7.21 (d,  $J = 8.0$  Hz, 4H), 4.10–4.07 (m, 4H), 3.65–3.61 (m, 12H) ppm.  $^{13}\text{C}\{^1\text{H},^{31}\text{P}\}$  NMR (126 MHz,  $\text{CD}_2\text{Cl}_2$ )  $\delta$  150.2 (4 C, *CaromOP*), 131.4 (4 C, *Carom*), 130.3 (4 C, *CaromH*), 129.7 (4 C, *CaromH*), 125.5 (4 C, *CaromH*), 122.4 (4 C, *CaromH*), 71.1 (2 C,  $\text{COCH}_2\text{CH}_2\text{CO}$ ), 71.06 (2 C,  $\text{COCH}_2\text{CH}_2\text{CO}$ ), 71.02 (2 C,  $\text{COCH}_2\text{CH}_2\text{CO}$ ), 70.9 (2 C,  $\text{POCH}_2$ ), 64.4 (2 C,  $\text{POCH}_2$ ) ppm.  $^{31}\text{P}\{^1\text{H}\}$  NMR (202 MHz,  $\text{CD}_2\text{Cl}_2$ )  $\delta$  145.2 ppm. HRMS (ESI)  $m/z$   $[M+\text{Na}]$  calcd for  $\text{C}_{32}\text{H}_{32}\text{NaO}_9\text{P}_2$  645.1414, found 645.1391.

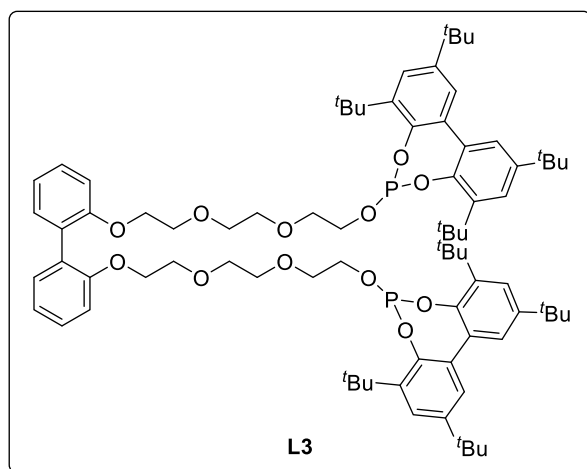


**Compound 17:** The preparation of compound **17** was performed following a reported procedure.<sup>21</sup> A mixture of 8-tosyloxy-3,6-dioxaoctanol (4 g, 13.10 mmol) and  $\text{K}_2\text{CO}_3$  (3.9 g, 28.30 mmol) were added to [1,1'-biphenyl]-2,2'-diol **12** (1.2 g, 6.57 mmol) in anhydrous

acetonitrile (59.7 mL) under Ar atmosphere and the resulting mixture was refluxed for 60 h. The reaction mixture was filtered and concentrated under reduced pressure. After purification by column chromatography over  $\text{SiO}_2$  using  $\text{AcOEt}/\text{MeOH}$  95:5, 2,2'-bis[2-[2-(2-hydroxyethoxy)ethoxy]ethoxy]-biphenyl **17** was obtained as a colorless oil (2.1 g, 70% yield). Spectroscopic data for this compound were in agreement with the reported ones.<sup>22</sup>  $^1\text{H}$  NMR (400 MHz,  $\text{CDCl}_3$ )  $\delta$  7.30–7.23 (m, 4H), 6.98 (td,  $J = 11.1$  Hz,  $J = 1.0$  Hz, 2H), 6.94 (dd,  $J = 8.2$  Hz,  $J = 1.0$  Hz, 2H), 4.09–4.06 (m, 4H), 3.71–3.67 (m, 8H), 3.54–3.48 (m, 12H) ppm.  $^{13}\text{C}\{^1\text{H}\}$  NMR (101 MHz,  $\text{CDCl}_3$ )  $\delta$  156.5 (2 C, *CaromO*), 131.6 (2 C, *Carom*), 128.6 (4 C, *CaromH*), 120.8 (2 C, *CaromH*), 112.6 (2 C, *CaromH*), 72.7 (2 C,  $\text{COCH}_2\text{CH}_2\text{CO}$ ), 71.0 (2 C,  $\text{COCH}_2\text{CH}_2\text{CO}$ ), 70.6 (2 C,  $\text{COCH}_2\text{CH}_2\text{OH}$ ), 69.8 (2 C,  $\text{COCH}_2\text{CH}_2$ ), 68.7 (2 C, *CaromOCH}\_2\text{CH}\_2*), 61.8 (2 C,  $\text{CH}_2\text{CH}_2\text{OH}$ ) ppm.

<sup>21</sup> Jose, D. A.; Mon, I.; Fernández-Pérez, H.; Escudero-Adán, E. C.; Benet-Buchholz, J.; Vidal-Ferran, A. *Org. Lett.* **2011**, *13*, 3632-3635.

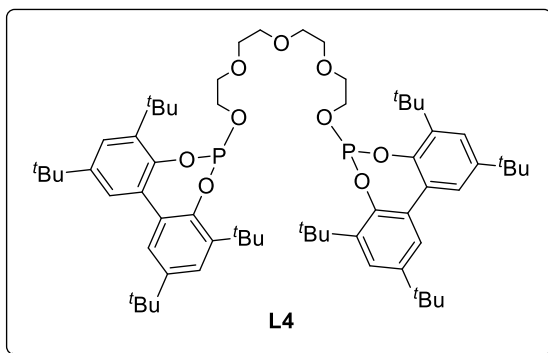
<sup>22</sup> Czech, B.; Czech, A.; Bartsch, R. A. J. *Heterocycl. Chem.* **1984**, *21*, 341-343.



**Compound L3:** The preparation of **L3** was performed following the general procedure for the synthesis of supramolecular bisphosphite ligands. Under argon atmosphere, 3,3',5,5'-tetra-*tert*-butyl-2,2'-dihydroxybiphenyl **13** (2 g, 4.80 mmol) was azeotropically dried with anhydrous toluene (3 x 10 mL), dissolved in anhydrous

toluene (30 mL) and the reaction mixture was cooled to 0 °C. This solution was added dropwise *via* cannula to a mixture of PCl<sub>3</sub> (502 μL, 5.82 mmol) and NEt<sub>3</sub> (1.7 mL, 12.60 mmol) in anhydrous toluene (30 mL) at 0° C. The reaction mixture was allowed to reach room temperature and was stirred overnight. The turbid reaction mixture was filtered through a pad of Celite® and the solvent evaporated under vacuum. The resulting residue was dissolved in anhydrous toluene (35 mL) and NEt<sub>3</sub> (635 μL, 4.52 mmol). A solution of 2,2'-bis[2-[2-(2-hydroxyethoxy)ethoxy]ethoxy]biphenyl **17** (1.1 g, 2.49 mmol) in anhydrous toluene (35 mL) was added dropwise to the previous solution and allowed to react overnight at room temperature. The reaction mixture was filtered through a pad of Celite® and the solvent evaporated under reduced pressure. The resulting mixture was purified by filtration through a pad of basic alumina with DCM (16 mL) and the solvent was evaporated under vacuum. Product **L3** was obtained as a white solid (2.9 g, 89% yield). Mp: 80–82 °C. IR (neat, cm<sup>-1</sup>)  $\bar{\nu}$  2955, 2905, 2868, 1594, 1504, 1437, 1394, 1361, 1281, 1261, 1228, 1124, 1090, 1034, 928, 868, 850, 777, 750, 696, 650, 614. <sup>1</sup>H NMR (500 MHz, CD<sub>2</sub>Cl<sub>2</sub>)  $\delta$  7.49 (d, *J* = 2.5 Hz, 4H), 7.30–7.25 (m, 4H), 7.22 (d, *J* = 2.5 Hz, 4H), 7.01–6.97 (m, 4H), 4.10–4.08 (m, 4H), 3.97–3.94 (m, 4H), 3.69–3.67 (m, 4H), 3.54–3.52 (m, 4H), 3.50 (s, 8H), 1.51 (s, 36H), 1.39 (s, 36H) ppm. <sup>13</sup>C {<sup>1</sup>H, <sup>31</sup>P} NMR (126 MHz, CD<sub>2</sub>Cl<sub>2</sub>)  $\delta$  156.8 (2 C, *Carom*O), 147.1 (4 C, *Carom*OP), 146.4 (4 C, *Carom*C(CH<sub>3</sub>)<sub>3</sub>), 140.5 (4 C, *Carom*C(CH<sub>3</sub>)<sub>3</sub>), 133.1 (4 C, *Carom*), 132.0 (2 C, *Carom*), 128.9 (4 C, *Carom*H), 128.6 (4 C, *Carom*H), 126.8 (4 C, *Carom*H), 124.8 (4 C, *Carom*H), 120.9 (2 C, *Carom*H), 112.8 (2 C, *Carom*H), 71.13 (2 C, COCH<sub>2</sub>CH<sub>2</sub>CO), 71.10 (2 C, COCH<sub>2</sub>CH<sub>2</sub>CO), 71.0 (2 C, COCH<sub>2</sub>CH<sub>2</sub>CO), 70.1 (2 C, COCH<sub>2</sub>CH<sub>2</sub>CO), 68.8 (2 C, *Carom*OCH<sub>2</sub>CH<sub>2</sub>), 64.4 (2 C, POCH<sub>2</sub>), 35.8 (4 C, C(CH<sub>3</sub>)<sub>3</sub>), 35.0 (4 C, C(CH<sub>3</sub>)<sub>3</sub>),

31.7 (12 C, C(CH<sub>3</sub>)<sub>3</sub>), 31.3 (12 C, C(CH<sub>3</sub>)<sub>3</sub>) ppm. <sup>31</sup>P{<sup>1</sup>H} NMR (202 MHz, CD<sub>2</sub>Cl<sub>2</sub>) δ 142.1 ppm. HRMS (ESI) *m/z* [M+Na] calcd for C<sub>80</sub>H<sub>112</sub>NaO<sub>12</sub>P<sub>2</sub> 1349.7521, found 1349.7527.

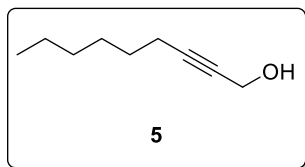


**Compound L4:** The preparation of **L4** was performed following the general procedure for the synthesis of supramolecular bisphosphite ligands. Under argon atmosphere, 3,3',5,5'-tetra-*tert*-butyl-2,2'-dihydroxybiphenyl **13** (2 g, 4.80 mmol) was

azeotropically dried with anhydrous toluene (3 x 10 mL), dissolved in anhydrous toluene (30 mL) and the reaction mixture was cooled to 0 °C. This solution was added dropwise *via* cannula to a solution mixture of PCl<sub>3</sub> (502 μL, 5.82 mmol) and NEt<sub>3</sub> (1.7 mL, 12.60 mmol) in anhydrous toluene (30 mL) at 0° C. The reaction mixture was allowed to reach room temperature and was stirred overnight. The turbid reaction mixture was filtered through a pad of Celite® and the solvent evaporated under vacuum. The resulting residue was dissolved in anhydrous toluene (60 mL) and NEt<sub>3</sub> (635 μL, 4.52 mmol). A solution of tetraethyleneglycol **16** (331 mg, 1.89 mmol) in anhydrous toluene (60 mL) was added dropwise to the previous solution and allowed to react overnight at room temperature. The reaction mixture was filtered through a pad of Celite® and the solvent evaporated under reduced pressure. The resulting mixture was purified by filtration through a pad of basic alumina with DCM (16 mL) and the solvent was evaporated under vacuum. Product **L4** was obtained as a white solid (1.9 g, 92% yield). Mp: 91–93 °C. IR (neat, cm<sup>-1</sup>)  $\bar{\nu}$  2955, 2905, 2868, 1595, 1437, 1394, 1361, 1281, 1229, 1201, 1173, 1124, 1090, 1034, 941, 914, 869, 851, 803, 777, 764, 697, 650, 616. 549. <sup>1</sup>H NMR (500 MHz, CD<sub>2</sub>Cl<sub>2</sub>) δ 7.47 (d, *J* = 2.4 Hz, 4H), 7.19 (d, *J* = 2.4 Hz, 4H), 3.98–3.94 (m, 4H), 3.58 (s, 12H), 1.49 (s, 36H), 1.37 (s, 36H) ppm. <sup>13</sup>C{<sup>1</sup>H, <sup>31</sup>P} NMR (126 MHz, CD<sub>2</sub>Cl<sub>2</sub>) δ 147.1 (4 C, *Carom*OP), 146.4 (4 C, *Carom*C(CH<sub>3</sub>)<sub>3</sub>), 140.5 (4 C, *Carom*C(CH<sub>3</sub>)<sub>3</sub>), 133.1 (4 C, *Carom*), 126.8 (4 C, *Carom*H), 124.8 (4 C, *Carom*H), 71.2 (2 C, COCH<sub>2</sub>CH<sub>2</sub>CO), 71.0 (2 C, COCH<sub>2</sub>CH<sub>2</sub>CO), 70.9 (2 C, POCH<sub>2</sub>), 64.4 (2 C, POCH<sub>2</sub>), 35.7 (4 C, C(CH<sub>3</sub>)<sub>3</sub>), 35.0 (4 C, C(CH<sub>3</sub>)<sub>3</sub>), 31.7 (12 C, C(CH<sub>3</sub>)<sub>3</sub>), 31.3 (12 C, C(CH<sub>3</sub>)<sub>3</sub>) ppm. <sup>31</sup>P{<sup>1</sup>H} NMR (202 MHz, CD<sub>2</sub>Cl<sub>2</sub>) δ 142.1 ppm. HRMS (ESI) *m/z* [M+H] calcd for C<sub>64</sub>H<sub>97</sub>O<sub>9</sub>P<sub>2</sub> 1071.6597, found 1071.6602.

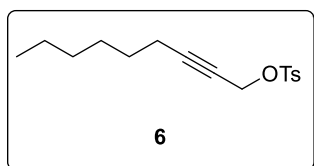


### 1.5.3 Substrate synthesis



**Compound 5:** The preparation of **5** was performed following a reported procedure.<sup>2c</sup> A mixture of oct-1-yne **4** (4.5 mL, 30.50 mmol) and THF (24.4 mL) was stirred and cooled to  $-78\text{ }^{\circ}\text{C}$ . To the stirred solution, *n*-BuLi (1.6 M in hexane, 23.3 mL, 37.20 mmol) was

added dropwise. The reaction mixture was allowed to warm up to  $0\text{ }^{\circ}\text{C}$  and was stirred for 1 h. The reaction mixture was cooled down again to  $-78\text{ }^{\circ}\text{C}$  and added *via* cannula over paraformaldehyde (1.1 g, 36.60 mmol). The reaction mixture was allowed to reach room temperature and stirred for 16 h, quenched by adding a saturated aqueous solution of  $\text{NH}_4\text{Cl}$  (18.3 mL) and extracted with  $\text{Et}_2\text{O}$  (3 x 16 mL). The combined organic phases were washed with brine (16 mL), dried over  $\text{MgSO}_4$  and the solvent was evaporated under reduced pressure. After purification by column chromatography over  $\text{SiO}_2$  using DCM, non-2-yl-1-ol **5** was obtained as a colorless oil (4.2 g, 98% yield). Spectroscopic data for this compound were in agreement with the reported ones.<sup>23</sup>  $^1\text{H}$  NMR (500 MHz,  $\text{CDCl}_3$ )  $\delta$  4.24 (bs, 2H), 2.19 (tt,  $J = 10.7, 2.2$  Hz, 2H), 1.73 (bs, 1H), 1.52–1.46 (m, 2H), 1.40–1.23 (m, 6H), 0.88 (t,  $J = 7.0$  Hz, 3H) ppm.  $^{13}\text{C}\{^1\text{H}\}$  NMR (126 MHz,  $\text{CDCl}_3$ )  $\delta$  86.8 (1 C,  $\text{C}\equiv\text{C}$ ), 78.4 (1 C,  $\text{C}\equiv\text{C}$ ), 51.5 (1 C,  $\text{HO}-\text{CH}_2-\text{C}\equiv\text{C}$ ), 31.5 (1 C,  $\text{CH}_2$ ), 28.70 (1 C,  $\text{CH}_2$ ), 28.67 (1 C,  $\text{CH}_2$ ), 22.7 (1 C,  $\text{CH}_2$ ), 18.9 (1 C,  $\text{C}\equiv\text{C}-\text{CH}_2$ ), 14.2 (1 C,  $\text{CH}_3$ ) ppm.

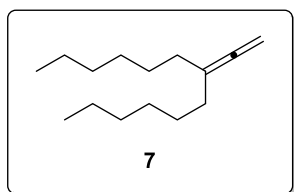


**Compound 6:** The preparation of **6** was performed following a reported procedure.<sup>2c</sup> To a stirred solution of non-2-yl-1-ol **5** (4.4 g, 31.40 mmol) in  $\text{Et}_2\text{O}$  (50.2 mL) *p*-toluenesulfonyl chloride (6.6 g, 34.50 mmol) was added and the reaction

mixture was cooled down to  $0\text{ }^{\circ}\text{C}$ . Then, freshly ground KOH (8.8 g, 158.00 mmol) was added in small portions over ten minutes. The resulting mixture was allowed to reach room temperature and stirred for 30 minutes, quenched by pouring the crude mixture into iced  $\text{H}_2\text{O}$  (8 mL). The aqueous phase was extracted with  $\text{Et}_2\text{O}$  (3 x 20 mL) and the combined organic phases were washed with brine (30 mL), dried over  $\text{MgSO}_4$  and solvent was evaporated under reduced pressure. After purification by column chromatography over  $\text{SiO}_2$  using Cy/AcOEt 97:3, 1-(4-methylbenzenesulfonate)-2-nonyn-1-ol **6** was obtained as

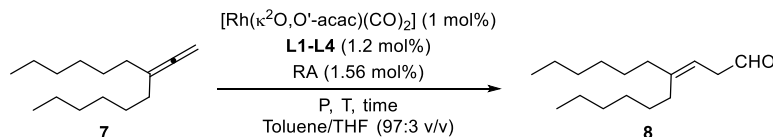
<sup>23</sup> Yamamoto, H.; Nishiyama, M.; Imagawa, H.; Nishizawa, M. *Tetrahedron Lett.* **2006**, *47*, 8369-8373.

a yellowish oil (6.1 g, 66% yield). Spectroscopic data for this compound were in agreement with the reported ones.<sup>2c</sup>  $^1\text{H}$  NMR (400 MHz  $\text{CDCl}_3$ )  $\delta$  7.81 (d,  $J = 8.3$  Hz, 2H), 7.33 (d,  $J = 8.0$  Hz, 2H), 4.70 (t,  $J = 2.2$  Hz, 2H), 2.44 (s, 3H), 2.05 (tt,  $J = 7.1, 2.2$  Hz, 2H), 1.39–1.21 (m, 8H), 0.88 (t,  $J = 7.0$  Hz, 3H) ppm.  $^{13}\text{C}\{^1\text{H}\}$  NMR (101 MHz,  $\text{CDCl}_3$ )  $\delta$  144.9 (1 C, *Carom*), 133.6 (1 C, *CaromCH}\_3*), 129.8 (2 C, *CaromH*), 128.3 (2 C, *CaromH*), 90.8 (1 C,  $\text{C}\equiv\text{C}$ ), 71.9 (1 C,  $\text{C}\equiv\text{C}$ ), 58.9 (1 C,  $\text{O}-\text{CH}_2-\text{C}\equiv\text{C}$ ), 31.4 (1 C,  $\text{CH}_2$ ), 28.6 (1 C,  $\text{CH}_2$ ), 28.2 (1 C,  $\text{CH}_2$ ), 22.6 (1 C,  $\text{CH}_2$ ), 21.8 (1 C, *CaromCH}\_3*), 18.8 (1 C,  $\text{C}\equiv\text{C}-\text{CH}_2$ ), 14.2 (1 C,  $\text{CH}_3$ ) ppm.



**Compound 7:** The preparation of **7** was performed following the reported procedure.<sup>2c</sup> A mixture of  $\text{CuBr}$  (129 mg, 0.90 mmol), 1-(4-methylbenzenesulfonate)-2-nonyn-1-ol **6** (2.6 g, 9.00 mol) in THF (18 mL) was cooled down to 0 °C. *n*-Hexylmagnesium bromide (11.3 mL, 1 M in THF, 11.30 mmol) was added dropwise. The reaction mixture was allowed to reach room temperature and stirred for 2 h, quenched by adding a sat. solution of  $\text{NH}_4\text{Cl}$  (9.5 mL) and the aqueous layer was extracted with  $\text{Et}_2\text{O}$  (3 x 6 mL). The combined organic phases were washed with brine (30 mL), dried over  $\text{MgSO}_4$  and the solvent was evaporated under reduced pressure. After purification by column chromatography over  $\text{SiO}_2$  using pentane, 7-vinylideneundecane, **7** was obtained as a colorless oil (1.1 g, 56% yield). Spectroscopic data for this compound were in agreement with the reported ones.<sup>2c</sup>  $^1\text{H}$  NMR (400 MHz,  $\text{CDCl}_3$ )  $\delta$  4.62 (q,  $J = 3.2$  Hz, 2H), 1.94–1.89 (m, 4H), 1.43–1.38 (m, 4H), 1.31–1.26 (m, 12H), 0.90–0.87 (m, 6H) ppm.  $^{13}\text{C}\{^1\text{H}\}$  NMR (101 MHz,  $\text{CDCl}_3$ )  $\delta$  205.9 (1 C,  $\text{C}=\text{C}=\text{CH}_2$ ), 103.5 (1 C,  $\text{C}=\text{C}=\text{CH}_2$ ), 75.3 (1 C,  $\text{C}=\text{C}=\text{CH}_2$ ), 32.3 (2 C,  $\text{CH}_2\text{C}=\text{C}$ ), 31.9 (2 C,  $\text{CH}_2$ ), 29.2 (2 C,  $\text{CH}_2$ ), 27.7 (2 C,  $\text{CH}_2$ ), 22.8 (2 C,  $\text{CH}_2$ ), 14.2 (2 C,  $\text{CH}_3$ ) ppm.

### 1.5.4 General procedure for Rh-catalyzed hydroformylation of 7-vinylidenetriecane **7**



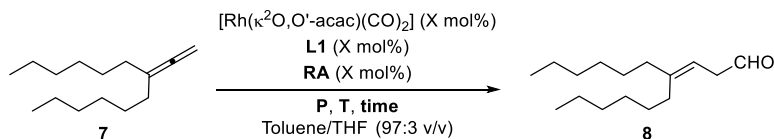
**Scheme 24.** General procedure for the Rh-catalyzed hydroformylation of **7** with supramolecular ligands **L1-L4**

In a glove box filled with nitrogen, ligands **L1-L4** (*ca.* 2.07  $\mu\text{mol}$  in 360  $\mu\text{L}$  of toluene), BArF salt (*ca.* 2.69  $\mu\text{mol}$  in 19.9  $\mu\text{L}$  of THF) and  $[\text{Rh}(\kappa^2\text{O},\text{O}'\text{-acac})(\text{CO})_2]$  (*ca.* 1.72  $\mu\text{mol}$  in 65  $\mu\text{L}$  of toluene) were added to a 2 mL vial equipped with a magnetic stirrer. Substrate (*ca.* 172.7  $\mu\text{mol}$ ), dodecane (*ca.* 51.8  $\mu\text{mol}$ ) and additional toluene were charged to provide the desired final solution of toluene/THF (97:3 v/v). The vial was transferred into an autoclave and taken out of the glove box. The autoclave was purged three times with syngas (1:1  $\text{H}_2/\text{CO}$  at a pressure not higher than 10 bar) and finally, the autoclave was pressurized with syngas to the desired pressure. The reaction mixture was stirred at the selected temperature (metallic block) for the selected reaction time. The reaction was cooled if needed and the pressure was carefully released in a well-ventilated hood. Conversion and regioselectivity for the hydroformylation products were determined by  $^1\text{H}$  NMR analysis from the reaction mixture using 1,3,5-trimethoxybenzene as internal standard.

## 1.5.5 Complete set of results for the Rh-catalyzed hydroformylation of 7-vinylidenetriecane 7

### 1.5.5.1 Catalytic results for ligand L1

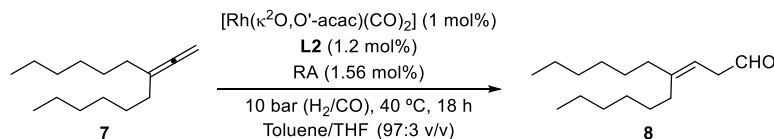
**Table 7.** Complete set of results in the Rh-catalyzed hydroformylation of 7 using L1



Entry	Temperature (°C)	Pressure (bar)	Time (h)	Cat. loading (mol%) <sup>[b]</sup>	RA	Conv. (%) <sup>[a]</sup>	Yield (%) of 8 <sup>[a]</sup>
1	25	30	5	1	None	>99	n.d.
2					NaBArF	>99	2
3 <sup>[a]</sup>	40	10	5	1	NaBArF	>99	1
4	40	10	5	2	NaBArF	>99	11
5	80	30	1	1	None	>99	14
6					NaBArF	>99	16
7	40	10	18	1	None	>99	1
8					NaBArF	>99	22
9	40	10	18	1	None	>99	1
10	40	10	18	1	LiBArF	>99	3
11	40	10	18	1	NaBArF	>99	22
12	40	10	18	1	KBArF	>99	3
13	40	10	18	1	RbBArF	>99	3
14	40	10	18	1	CsBArF	>99	2

The hydroformylations were performed in a parallel autoclave. Reaction conditions: [alkene] = 0.26 M; stirring rate = 800 rpm; H<sub>2</sub>/CO in a 1:1 ratio, unless otherwise cited. [a] Conversion and yield were determined by using <sup>1</sup>H NMR spectroscopy with 1,3,5-trimethoxybenzene as internal standard. [a] [Rh(OMe)<sub>2</sub>(COD)]<sub>2</sub> was used as catalyst precursor. [b] 1 mol% of catalyst was prepared with 1 mol% of Rh precursor, 1.2 mol% of L1 and 1.56 mol% of RA. 2 mol% of catalyst was prepared by a two-fold increase in the amounts of all components.

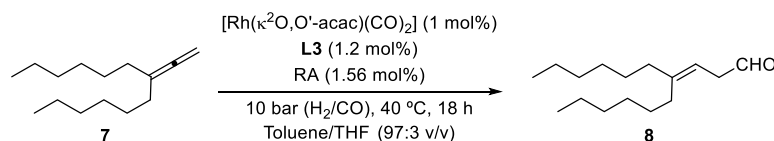
## 1.5.5.2 Catalytic results for ligand L2

**Table 8.** Complete set of results in the Rh-catalyzed hydroformylation of **7** using **L2**

Entry	RA	Conversion (%) <sup>[a]</sup>	Yield (%) of <b>8</b> <sup>[a]</sup>
1	None	>99	12
2	LiBArF	>99	3
3	NaBArF	>99	3
4	KBArF	>99	5
5	RbBArF	>99	8
6	CsBArF	>99	10

The hydroformylations were performed in a parallel autoclave. Reaction conditions: [alkene] = 0.26 M; stirring rate = 800 rpm;  $\text{H}_2/\text{CO}$  in a 1:1 ratio, unless otherwise cited. [a] Conversion and yield were determined by  $^1\text{H}$  NMR spectroscopy with 1,3,5-trimethoxybenzene as internal standard.

## 1.5.5.3 Catalytic results for ligand L3

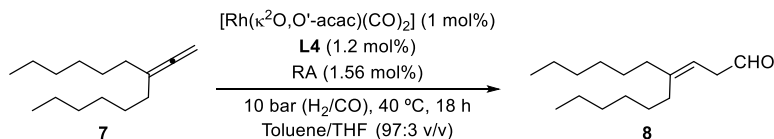
**Table 9.** Complete set of results in the Rh-catalyzed hydroformylation of **7** using **L3**

Entry	RA	Conversion (%) <sup>[a]</sup>	Yield (%) of <b>8</b> <sup>[a]</sup>
1	None	>99	5
2	LiBArF	>99	7
3	NaBArF	>99	7
4	KBArF	>99	6
5	RbBArF	>99	7
6	CsBArF	>99	7

The hydroformylations were performed in a parallel autoclave. Reaction conditions: [alkene] = 0.26 M; stirring rate = 800 rpm;  $\text{H}_2/\text{CO}$  in a 1:1 ratio, unless otherwise cited. [a] Conversion and yield were determined by  $^1\text{H}$  NMR spectroscopy with 1,3,5-trimethoxybenzene as internal standard.

### 1.5.5.4 Catalytic results for ligand L4

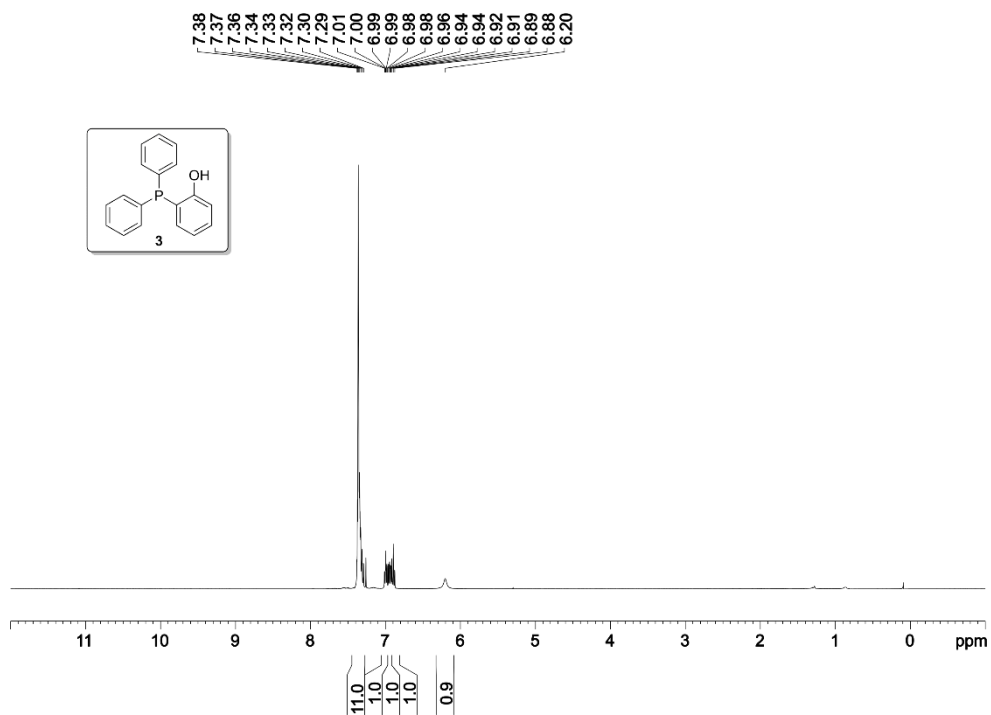
**Table 10.** Complete set of results in the Rh-catalyzed hydroformylation of **7** using **L4**



Entry	RA	Conversion (%) <sup>[a]</sup>	Yield (%) of <b>8</b> <sup>[a]</sup>
1	None	>99	9
2	LiBArF	>99	11
3	NaBArF	>99	62
4	KBArF	>99	69
5	RbBArF	>99	43
6	CsBArF	>99	11

The hydroformylations were performed in a parallel autoclave. Reaction conditions: [alkene] = 0.26 M; stirring rate = 800 rpm;  $\text{H}_2/\text{CO}$  in a 1:1 ratio, unless otherwise cited. [a] Conversion and yield were determined by  $^1\text{H}$  NMR spectroscopy with 1,3,5-trimethoxybenzene as internal standard.

## 1.5.6 Collection of spectra

Figure 17.  $^1\text{H}$  NMR spectrum (400 MHz,  $\text{CDCl}_3$ ) of **3**

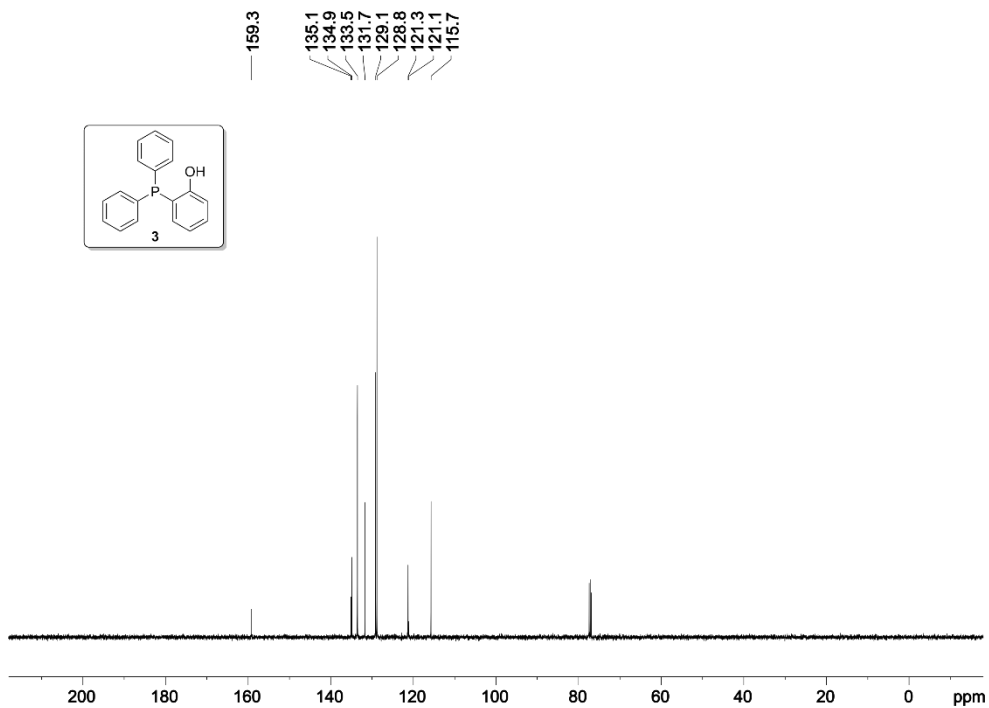


Figure 18.  $^{13}\text{C}\{^1\text{H},^{31}\text{P}\}$  NMR spectrum (126 MHz,  $\text{CDCl}_3$ ) of **3**

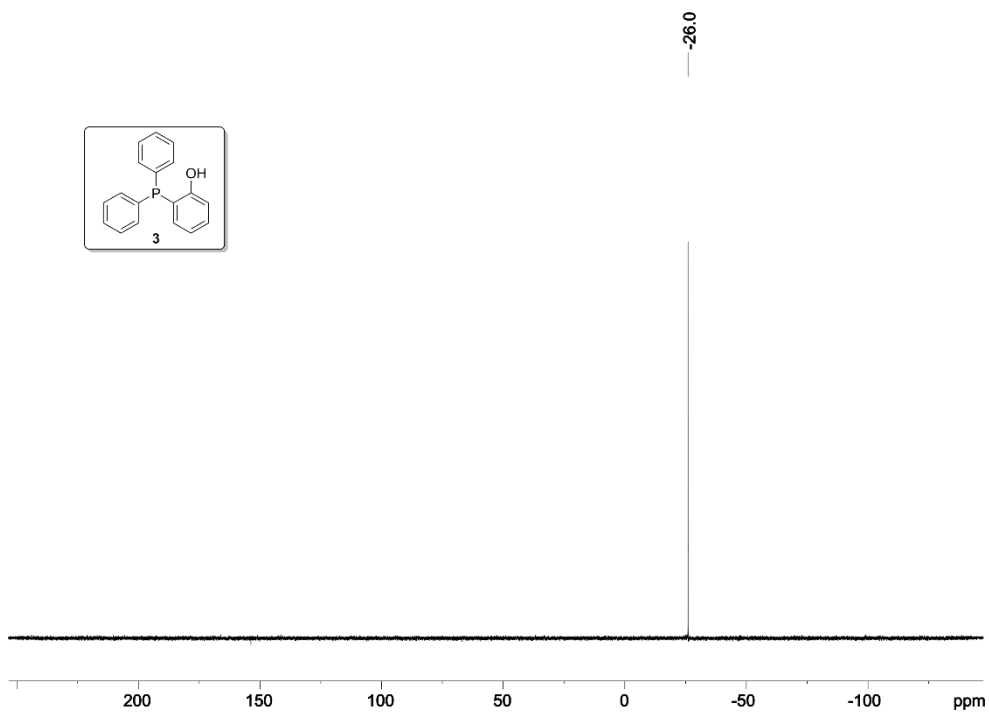


Figure 19.  $^{31}\text{P}\{^1\text{H}\}$  NMR spectrum (162 MHz,  $\text{CDCl}_3$ ) of **3**



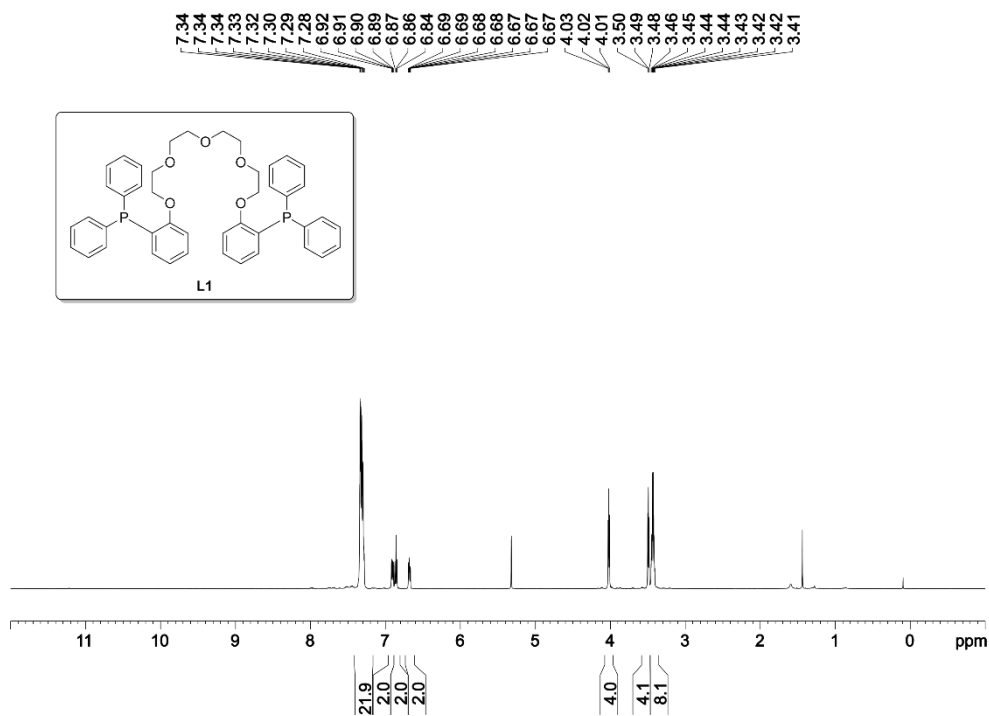


Figure 20.  $^1\text{H}$  NMR spectrum (500 MHz,  $\text{CD}_2\text{Cl}_2$ ) of L1

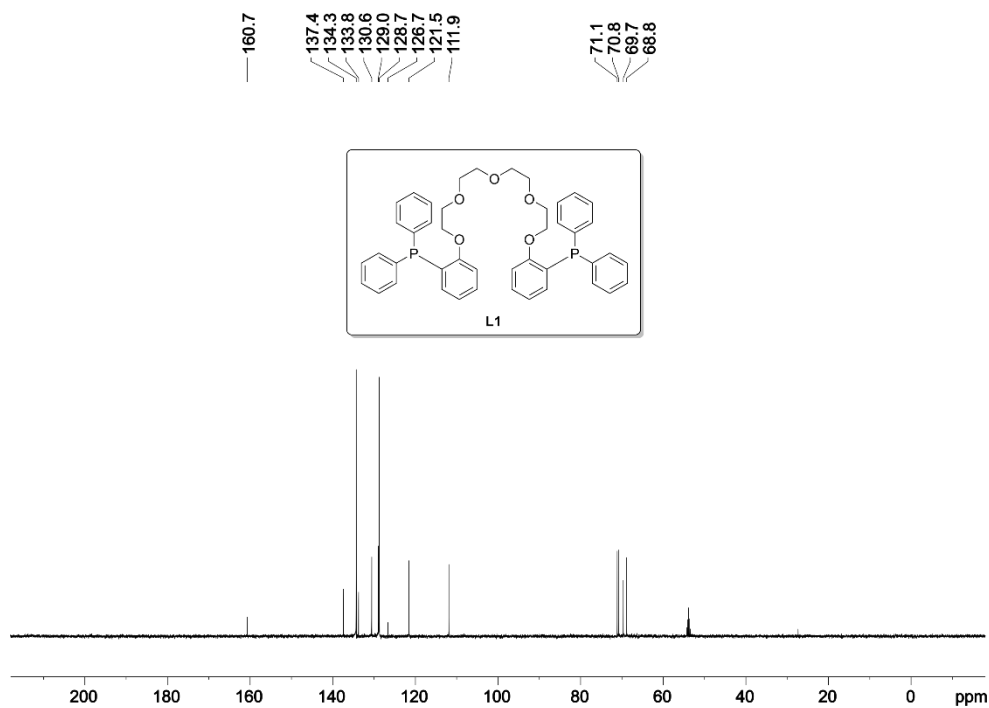


Figure 21.  $^{13}\text{C}\{^1\text{H}, ^{31}\text{P}\}$  NMR spectrum (126 MHz,  $\text{CD}_2\text{Cl}_2$ ) of L1

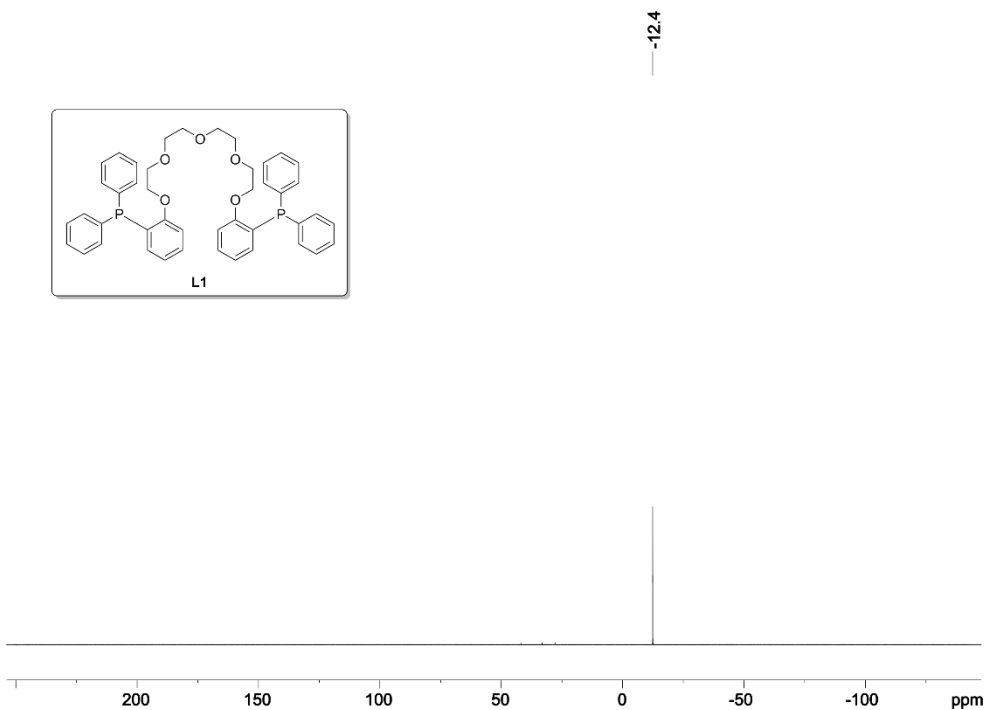


Figure 22.  $^{31}\text{P}\{^1\text{H}\}$  NMR spectrum (202 MHz,  $\text{CD}_2\text{Cl}_2$ ) of L1

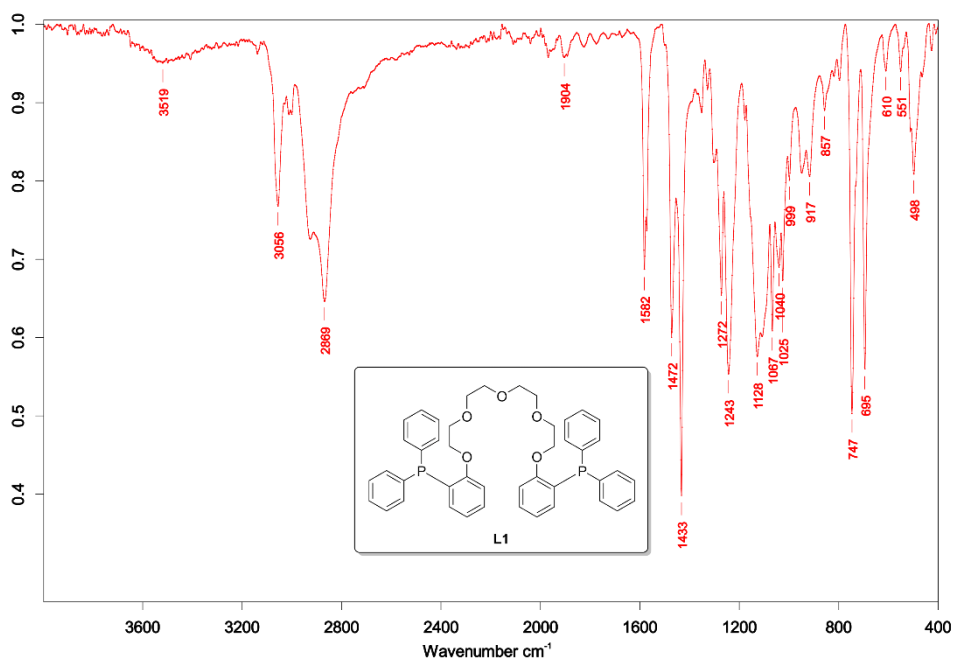


Figure 23. IR spectrum of L1

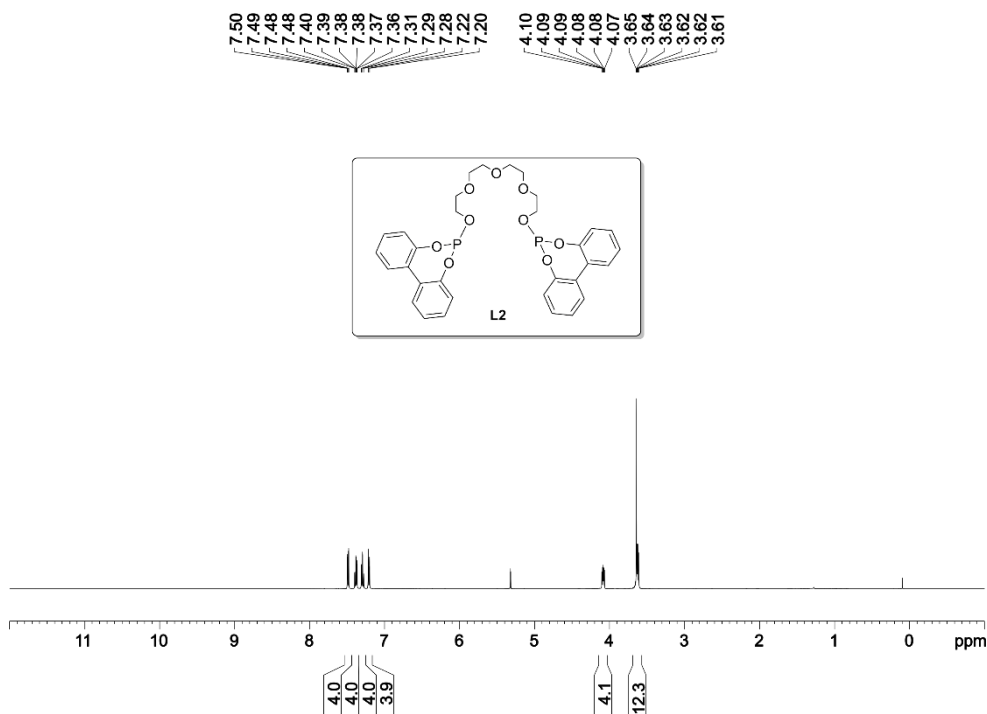


Figure 24.  $^1\text{H}$  NMR spectrum (500 MHz,  $\text{CD}_2\text{Cl}_2$ ) of L2

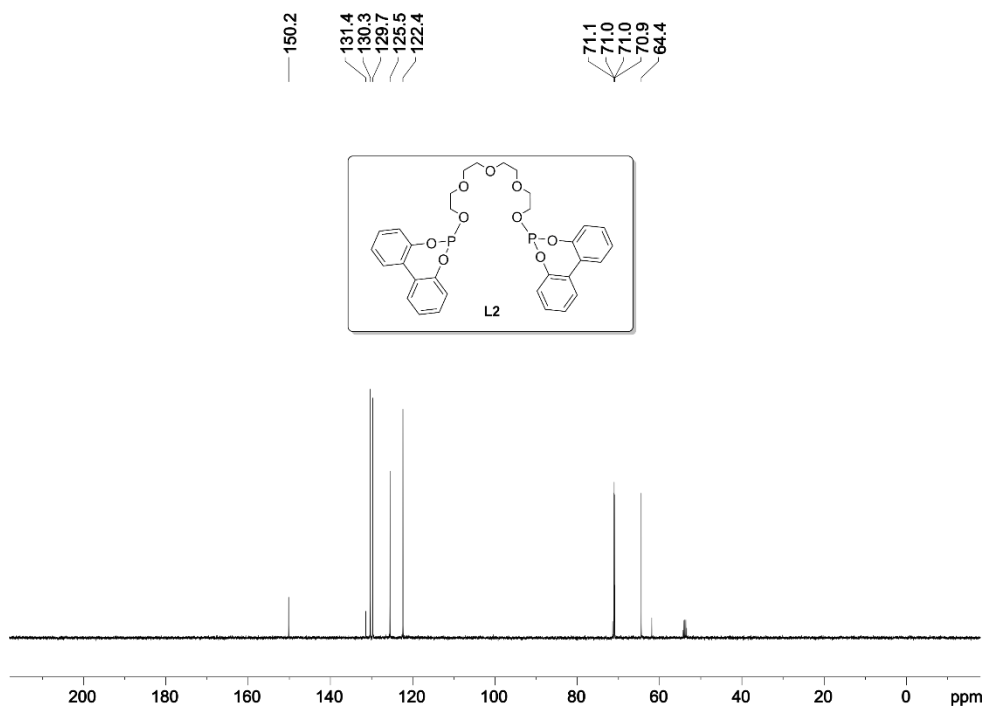


Figure 25.  $^{13}\text{C}\{^1\text{H}, ^{31}\text{P}\}$  NMR spectrum (126 MHz,  $\text{CD}_2\text{Cl}_2$ ) of L2

145.2

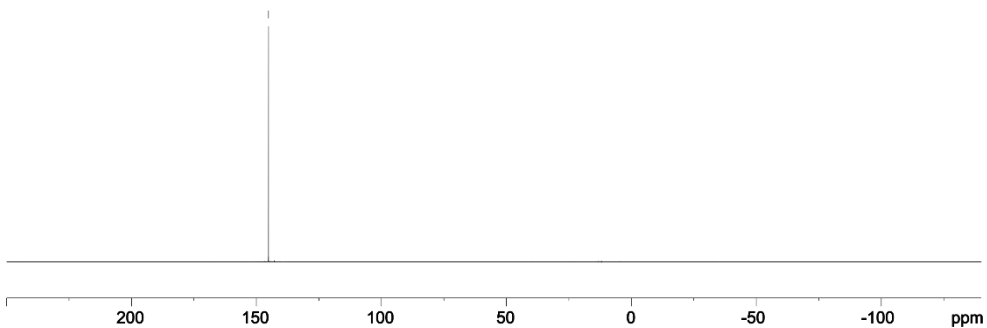
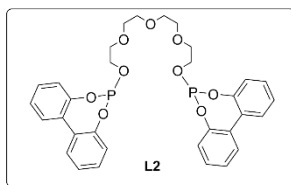


Figure 26.  $^{31}\text{P}\{^1\text{H}\}$  NMR spectrum (202 MHz,  $\text{CD}_2\text{Cl}_2$ ) of L2

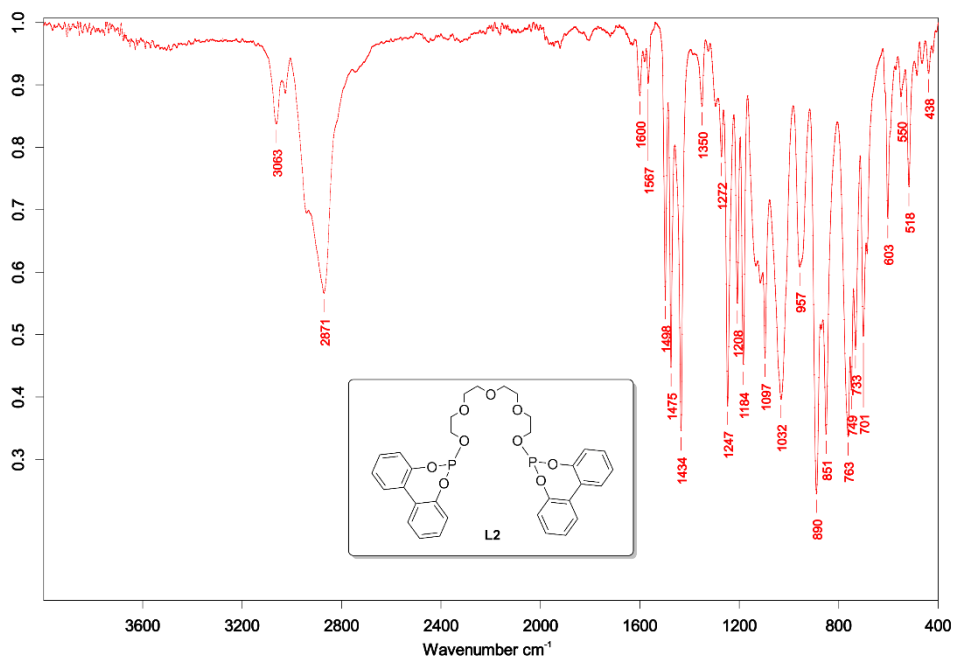
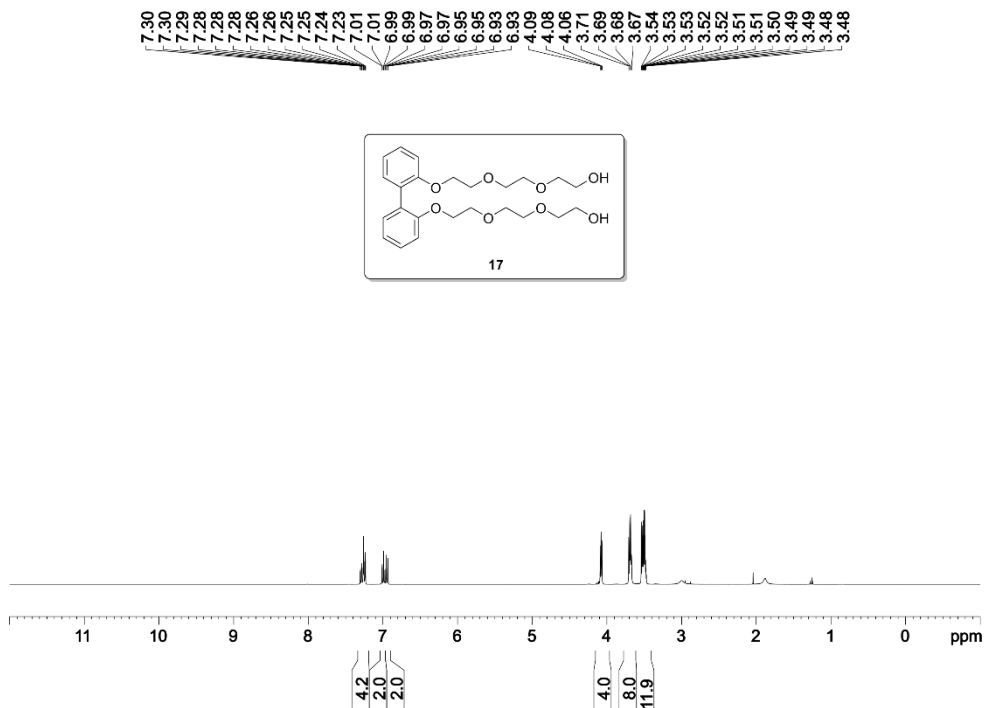
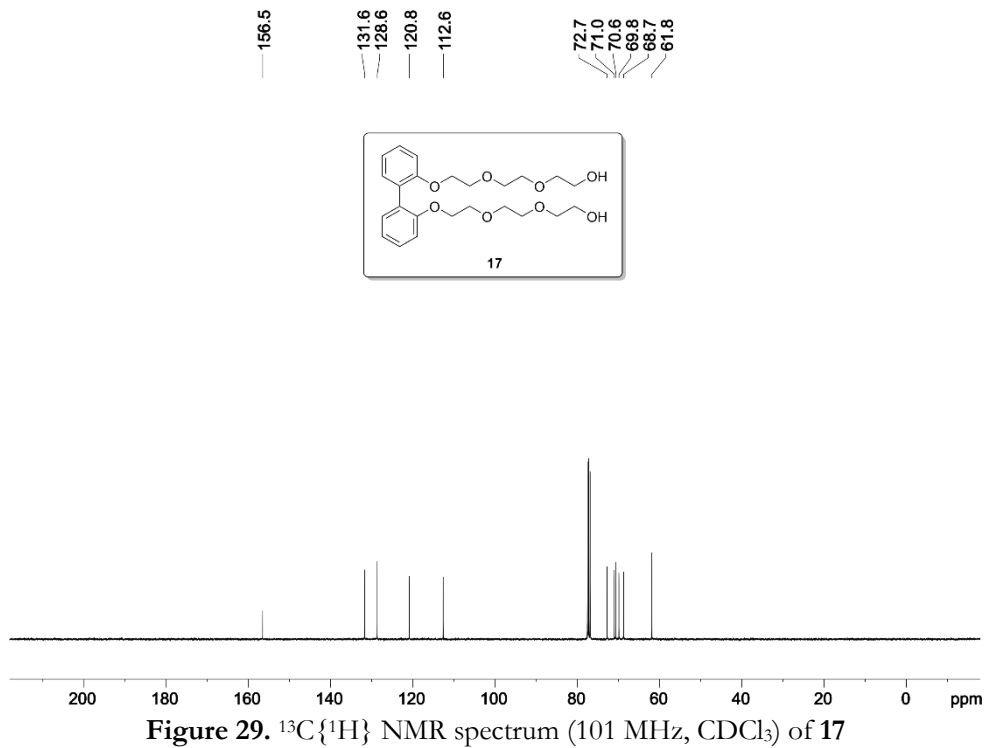


Figure 27. IR spectrum of L2

Figure 28.  $^1\text{H}$  NMR spectrum (400 MHz,  $\text{CDCl}_3$ ) of 17Figure 29.  $^{13}\text{C}\{^1\text{H}\}$  NMR spectrum (101 MHz,  $\text{CDCl}_3$ ) of 17

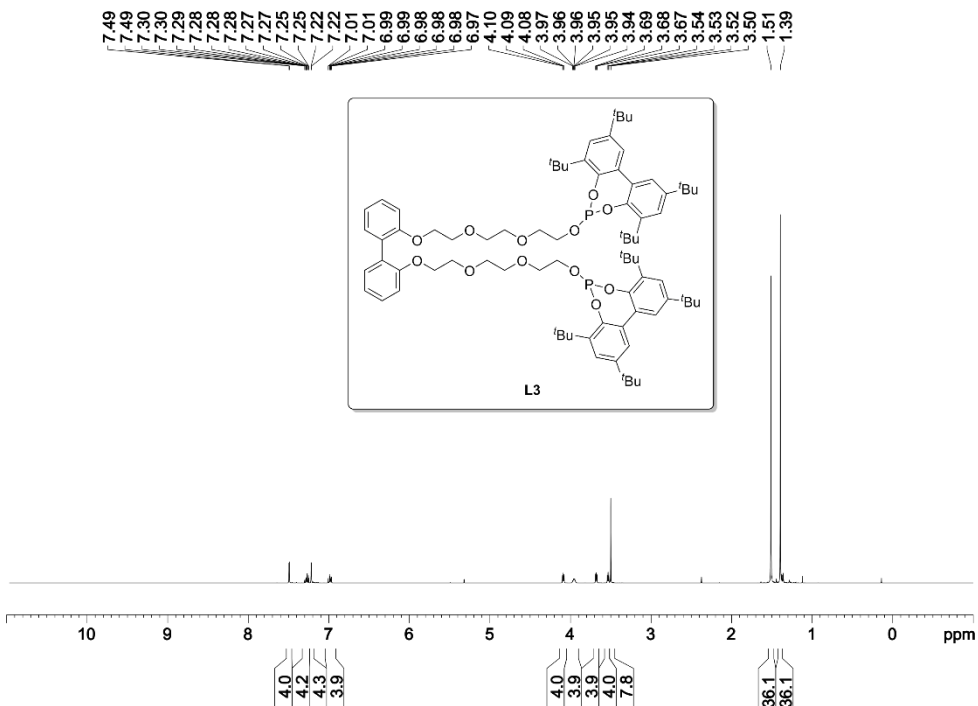


Figure 30.  $^1\text{H}$  NMR spectrum (500 MHz,  $\text{CD}_2\text{Cl}_2$ ) of L3

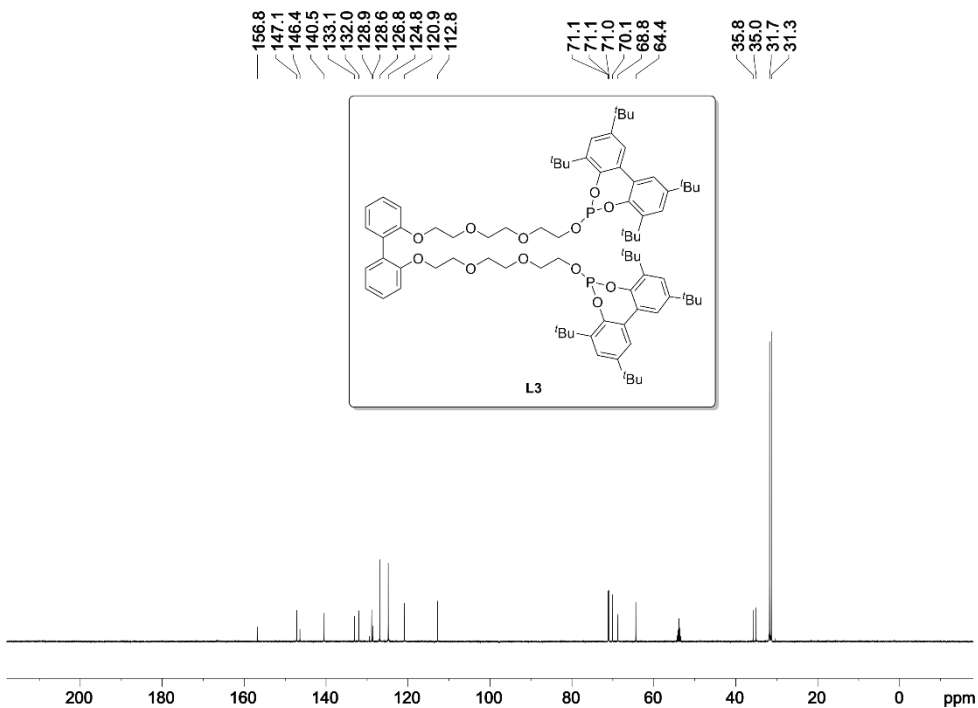


Figure 31.  $^{13}\text{C}\{^1\text{H},^{31}\text{P}\}$  NMR spectrum (126 MHz,  $\text{CD}_2\text{Cl}_2$ ) of L3

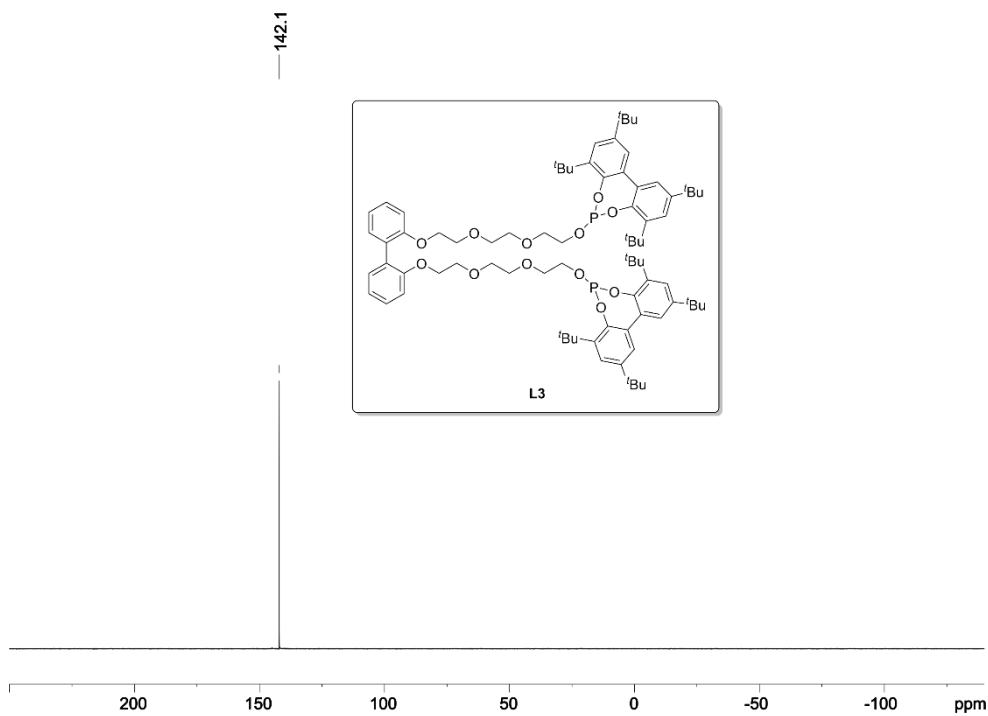


Figure 32.  $^{31}\text{P}\{^1\text{H}\}$  NMR spectrum (202 MHz,  $\text{CD}_2\text{Cl}_2$ ) of L3

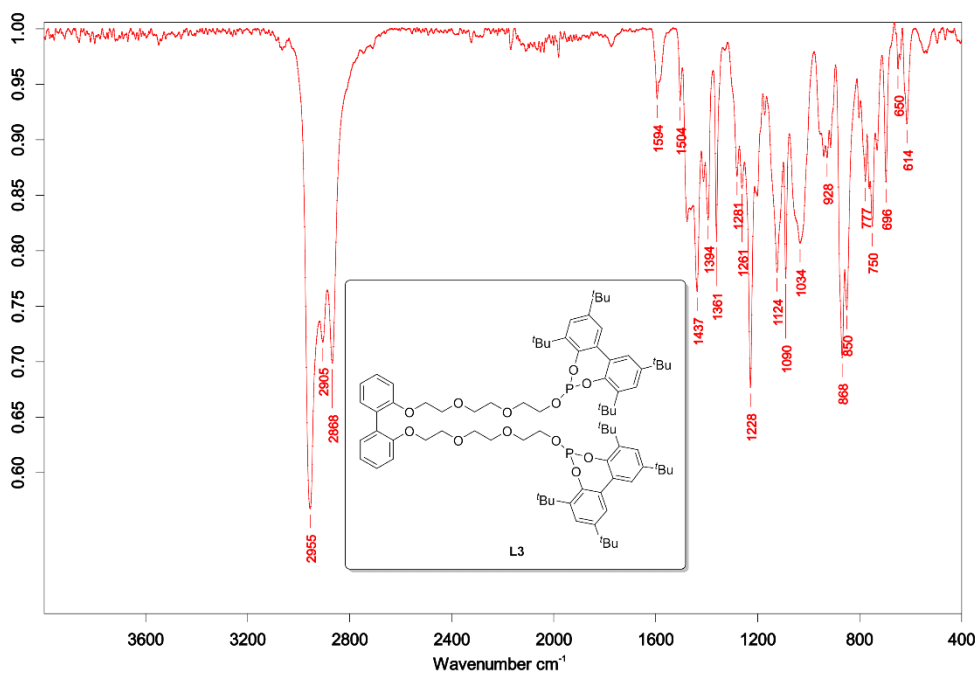


Figure 33. IR spectrum of L3

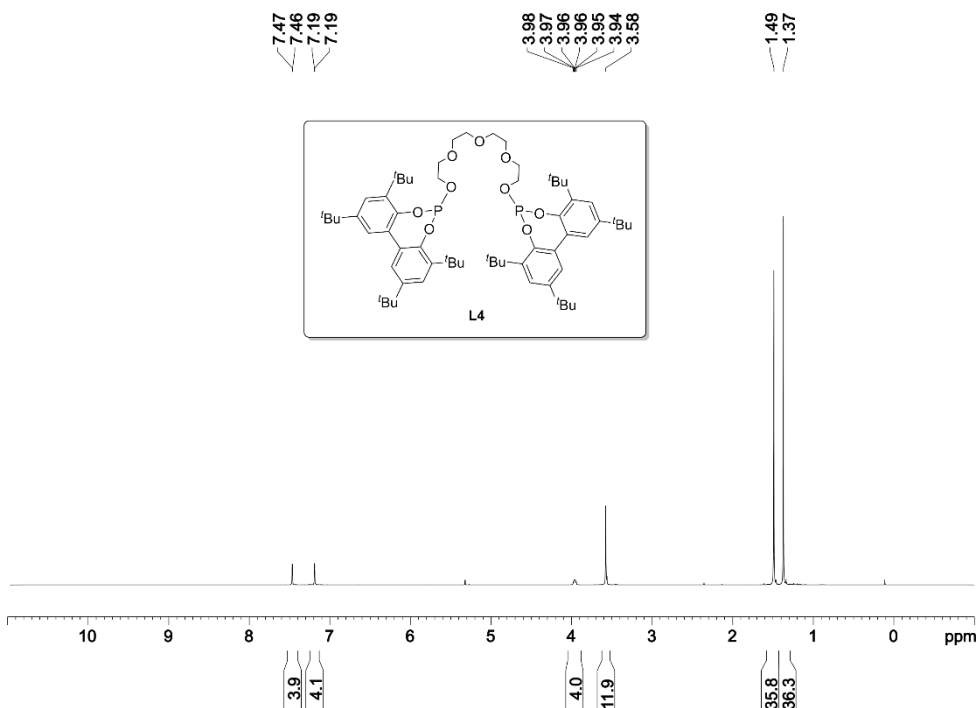


Figure 34. <sup>1</sup>H NMR spectrum (500 MHz, CD<sub>2</sub>Cl<sub>2</sub>) of L4

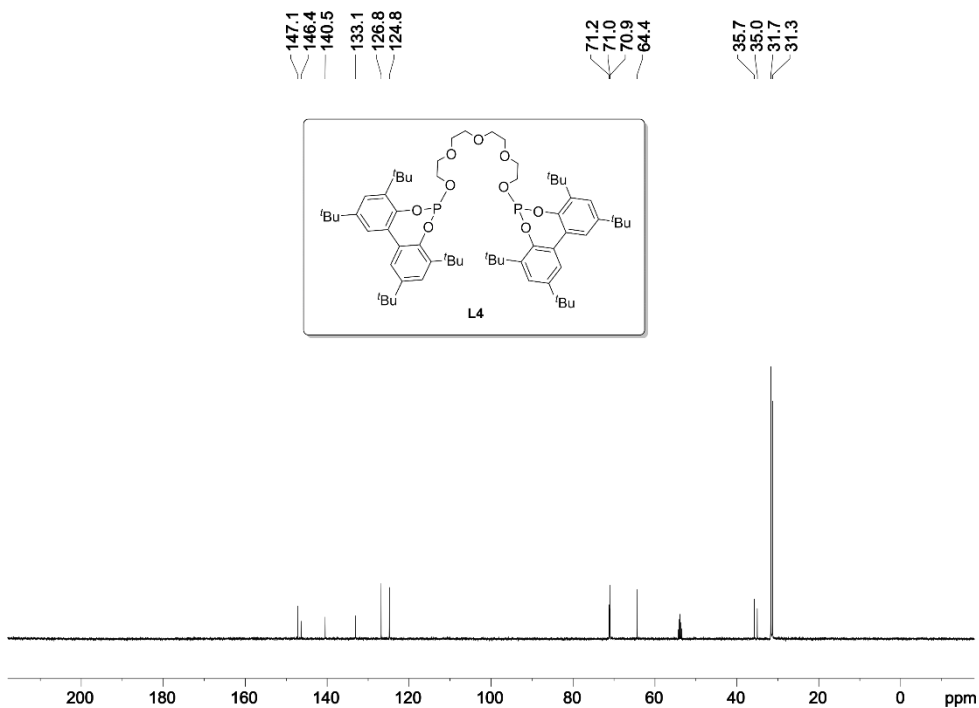


Figure 35. <sup>13</sup>C{<sup>1</sup>H,<sup>31</sup>P} NMR spectrum (126 MHz, CD<sub>2</sub>Cl<sub>2</sub>) of L4



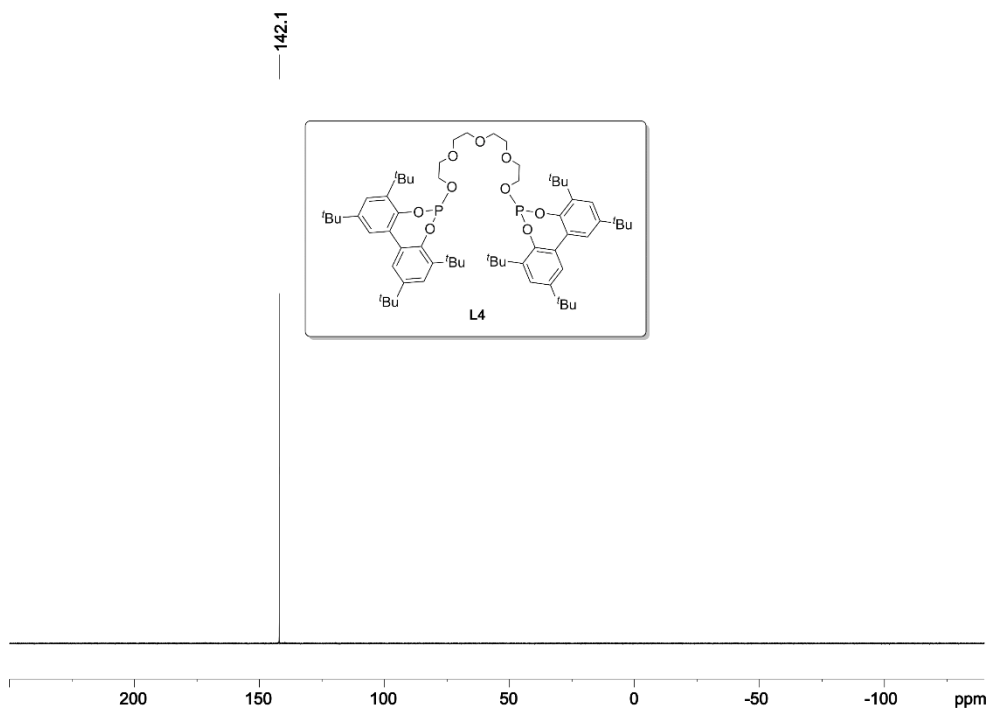


Figure 36.  $^{31}\text{P}\{^1\text{H}\}$  NMR spectrum (202 MHz,  $\text{CD}_2\text{Cl}_2$ ) of L4

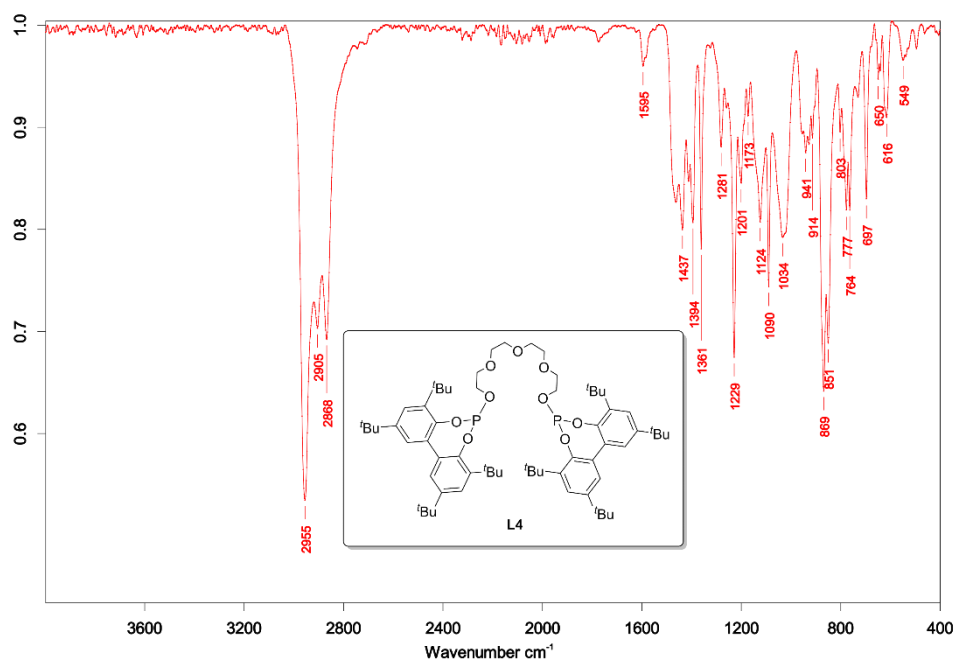
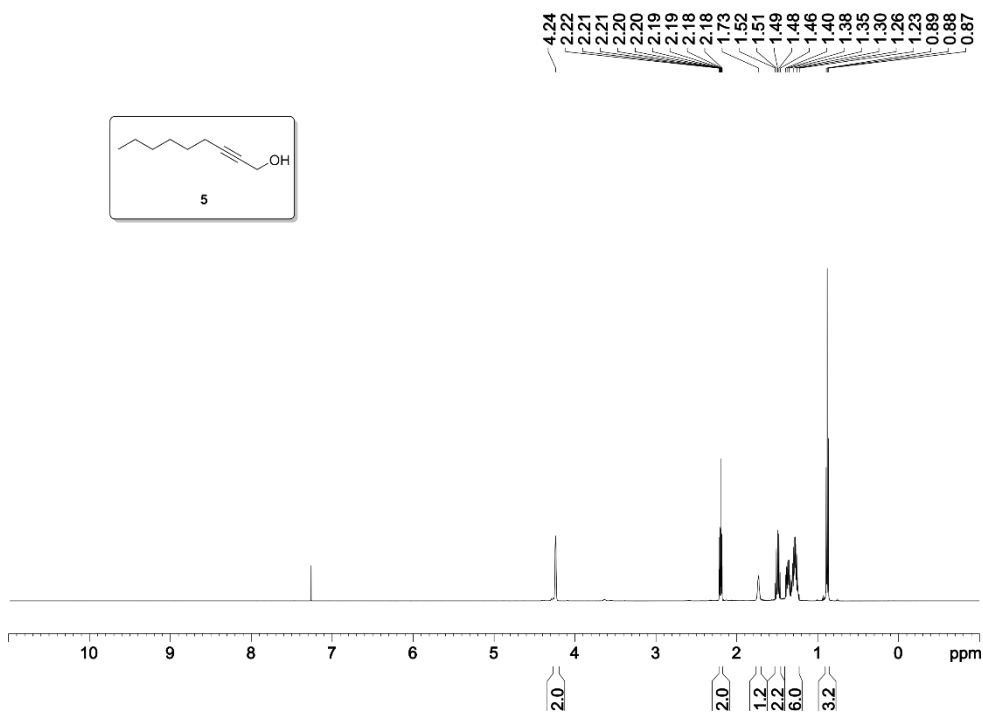
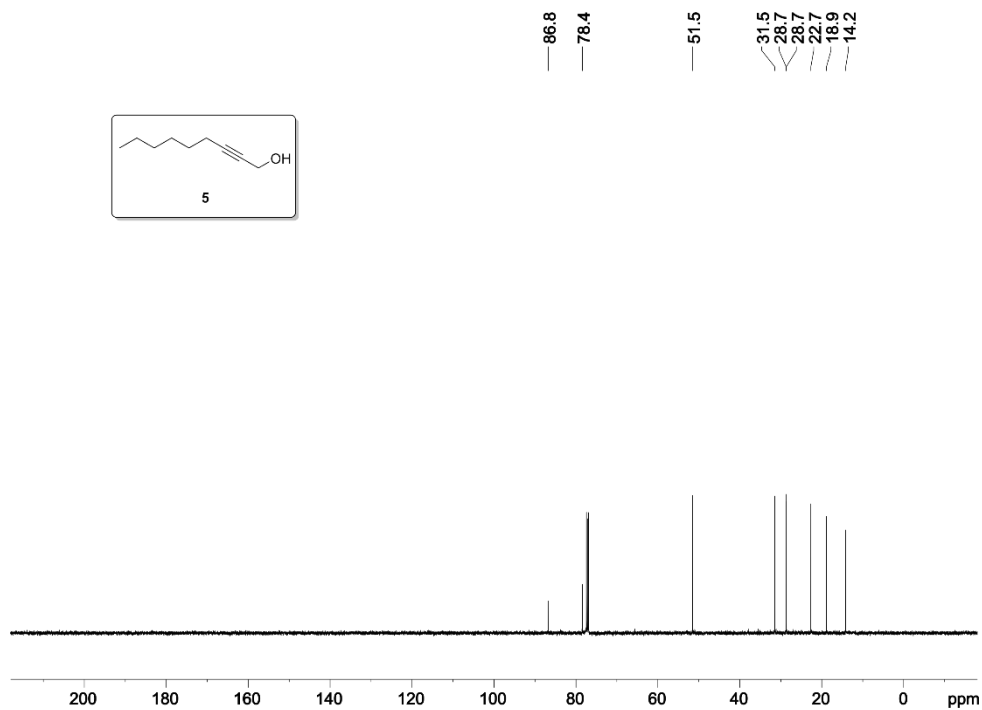
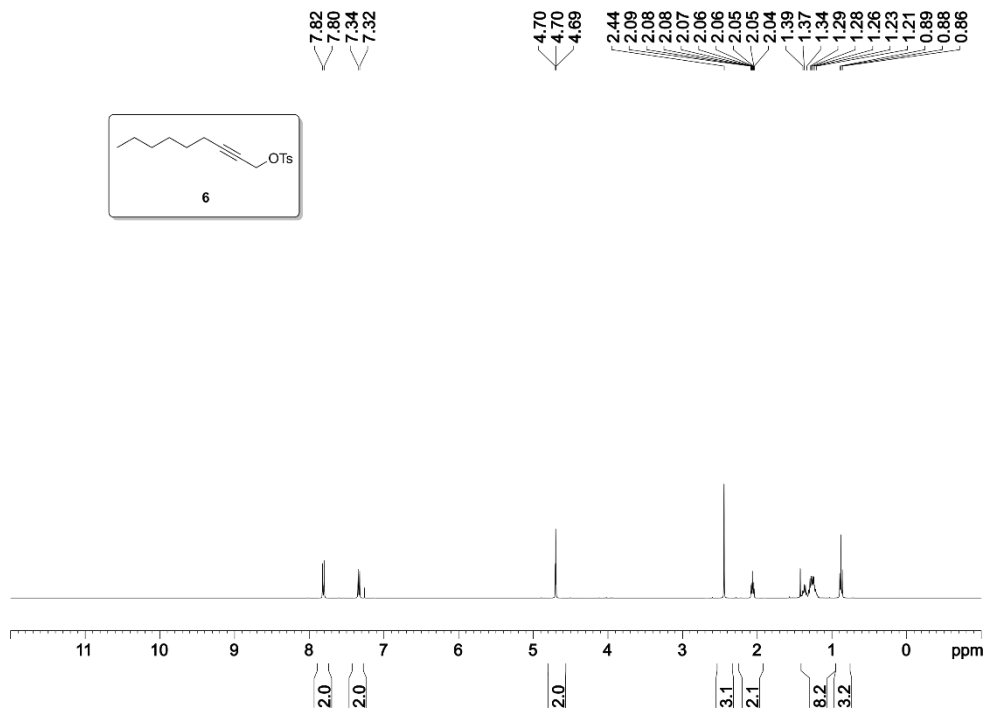
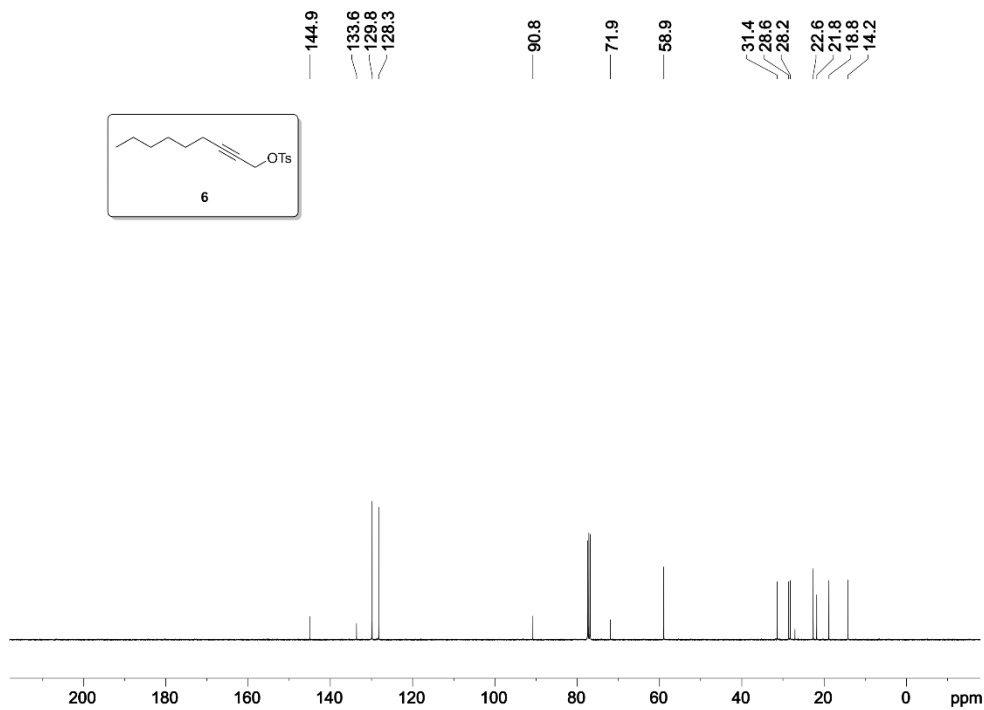


Figure 37. IR spectrum of L4

Figure 38.  $^1\text{H}$  NMR spectrum (400 MHz,  $\text{CDCl}_3$ ) of 5Figure 39.  $^{13}\text{C}\{^1\text{H}\}$  NMR spectrum (101 MHz,  $\text{CDCl}_3$ ) of 5

Figure 40.  $^1\text{H}$  NMR spectrum (400 MHz,  $\text{CDCl}_3$ ) of 6Figure 41.  $^{13}\text{C}\{^1\text{H}\}$  NMR spectrum (101 MHz,  $\text{CDCl}_3$ ) of 6

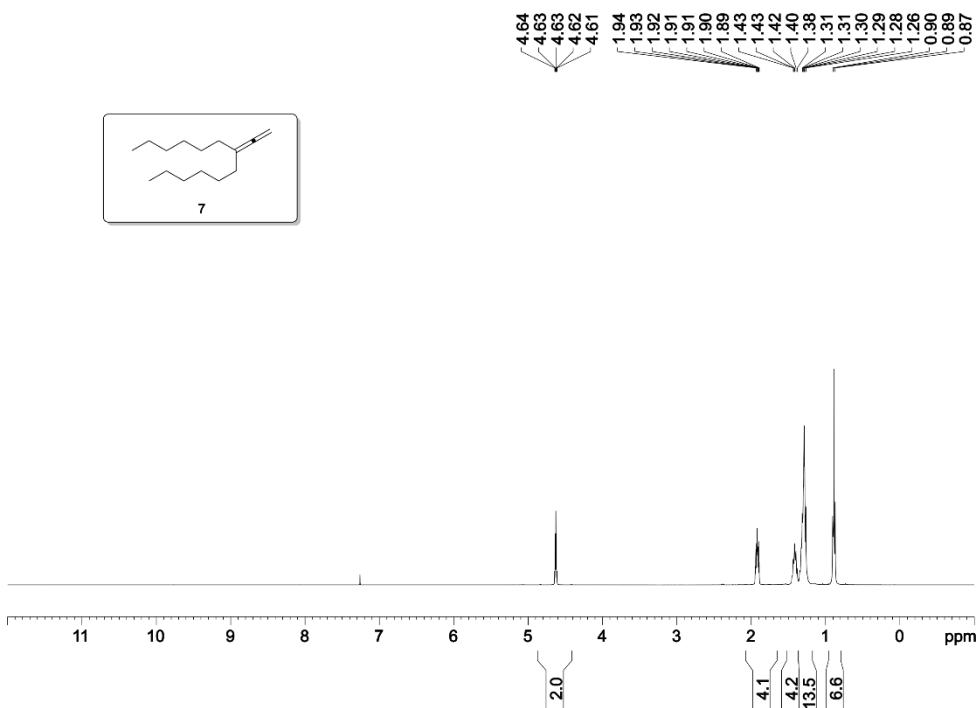


Figure 42.  $^1\text{H}$  NMR spectrum (400 MHz,  $\text{CDCl}_3$ ) of 7

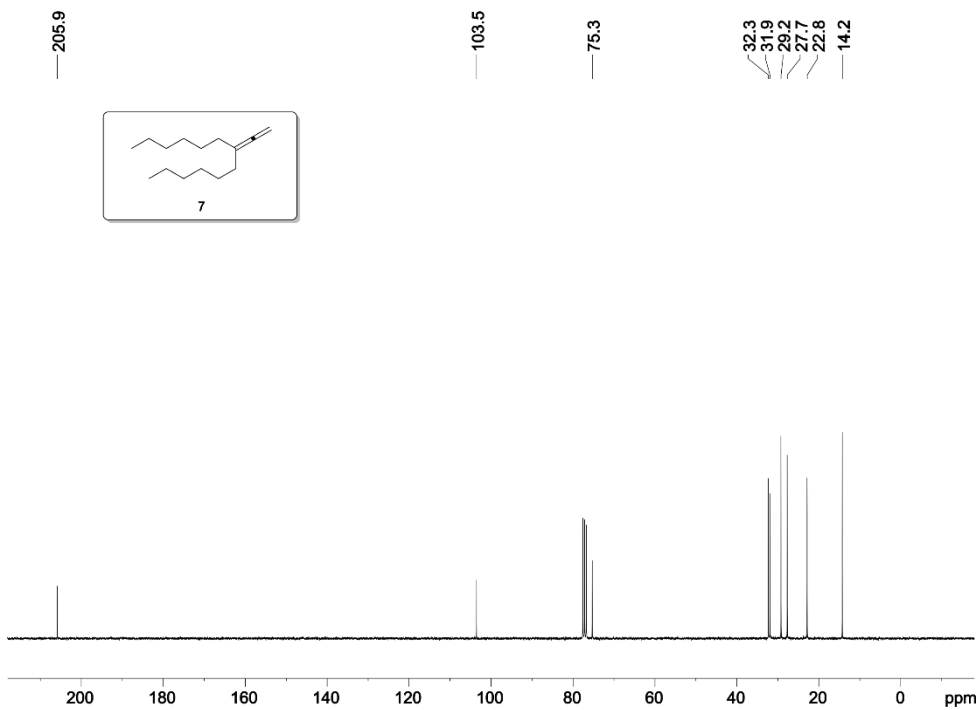
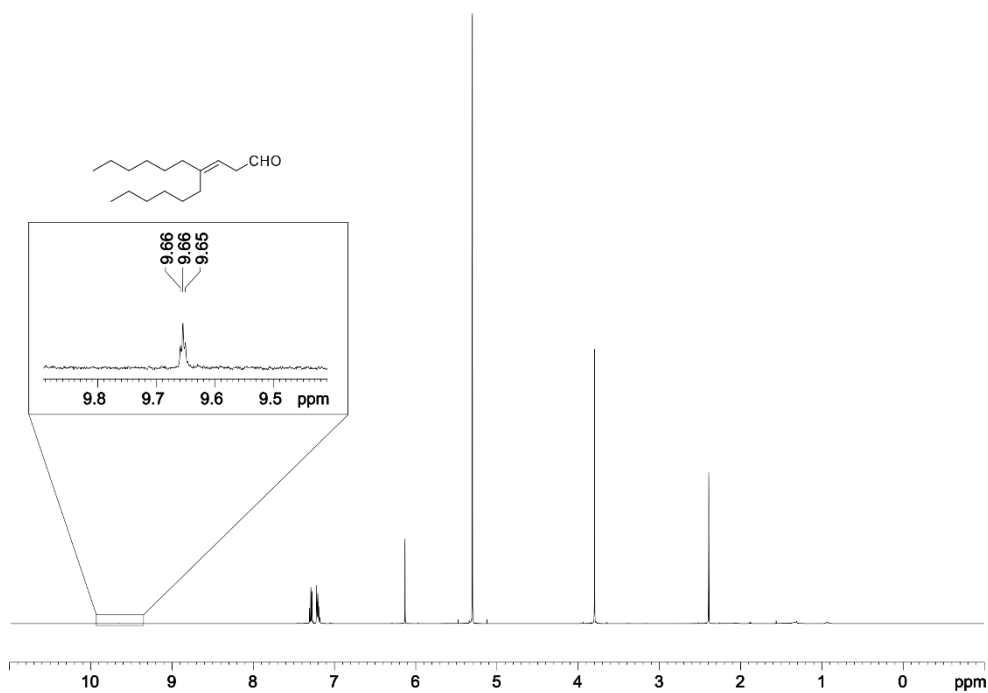


Figure 43.  $^{13}\text{C}\{^1\text{H}\}$  NMR spectrum (101 MHz,  $\text{CDCl}_3$ ) of 7



**Figure 44.**  $^1\text{H}$  NMR spectrum (500 MHz,  $\text{CDCl}_3$ ) of the reaction mixture of the Rh-catalyzed hydroformylation of **7** using supramolecularly regulated ligands **L1-L4**

## **Chapter II**

### **Cobalt-Catalyzed Hydroformylation of Alkyl- and Aryl-substituted Alkenes using Xantphos as Ligand**

UNIVERSITAT ROVIRA I VIRGILI

THE HYDROFORMYLATION REACTION: FROM COVALENT TO SUPRAMOLECULAR APPROACHES AND OPERANDO KINETIC STUDIES

Alicia Martínez Carrión

# Cobalt-Catalyzed Hydroformylation of Alkyl- and Aryl-substituted Alkenes using Xantphos as Ligand

(Unpublished results)

Alicia Martínez-Carrión<sup>a,b</sup>, Anton Vidal-Ferran<sup>b,c\*</sup>

- a Universitat Rovira i Virgili, Departament de Química Analítica i Química Orgànica, C. Marcel·lí Domingo 1, 43007, Tarragona, Spain.
- b Institut Català d'Investigació Química (ICIQ) & Barcelona Institute of Science and Technology (BIST), Av. Països Catalans 16, 43007, Tarragona, Spain.
- c Institució Catalana de Recerca i Estudis Avançats (ICREA), Pg. Lluís Companys 23, 08010, Barcelona, Spain.

## 2.1 ABSTRACT

Active hydroformylation catalysts derived from cobalt and Xantphos as ligand have been synthesized and tested in the hydroformylation of styrene and several linear octene isomers. The preformed complex  $[\text{Co}(\text{H})(\text{CO})_2(\text{Xantphos})]$  has shown lower selectivity towards aldehydes than the active catalyst formed *in situ* from  $[\text{Co}_2(\text{CO})_8]$  and the Xantphos ligand. For styrene, the catalytic system has shown a preferred selectivity towards ethylbenzene (*i.e.*, the hydrogenation product of styrene). In the case of oct-1-ene, the linear aldehyde was obtained with a good regioselectivity and moderate chemoselectivity, with respect to the different products arising from the side-reactions. In the case of internal octenes, a tandem isomerization-hydroformylation process occurs. Linear to branched ratios for all studied octene isomers remained practically constant, independently of the position or geometry of the C=C double bond in the starting material. Moreover, side-products were formed in similar amounts for all octene isomers. This tandem reaction may be a valuable tool for the valorization of petroleum feedstocks.



## 2.2 INTRODUCTION

Cobalt-catalyzed hydroformylations are directly connected with the discovery of the hydroformylation reaction (also called the *oxo*-reaction) by Otto Roelen in 1938.<sup>1</sup> First reports of cobalt-catalyzed hydroformylations avoided the use of ligands and operated at high temperatures and pressures. The introduction of phosphine ligands stabilized the active catalyst and improved regioselectivity towards lineal aldehydes. Under these conditions, the syngas pressure could be decreased, although high temperatures were still required to overcome the low intrinsic catalytic activity of phosphine-modified cobalt catalysts.<sup>2</sup>

Alkenes, under cobalt-catalyzed hydroformylation reaction conditions, can undergo several side-reactions. The isomerization of terminal and internal alkenes in presence of unmodified cobalt-catalysts has been observed. The formation of hydrogenated products is enhanced when phosphine ligands are used. In the presence of these ligands, the hydrogenation of aldehydes has also been reported, leading to the formation of the corresponding alcohols. Therefore, chemo- and regio-selectivity control in cobalt-catalyzed hydroformylations remains a challenge.

Tertiary heterocyclic trialkyl phosphines<sup>3</sup> have been exploited as stable and selective ligands in cobalt-catalyzed hydroformylations, with the good catalytic results being attributed to their steric hindrance.<sup>2</sup> The use of bisphosphine ligands was studied in the past and these ligands showed low catalytic activity. Nevertheless, suppression of isomerization processes in linear alkenes was observed.<sup>4</sup> Recently, the use of bisphosphine ligands with a well-defined rigid backbone has improved the catalytic results in the hydroformylation of terminal linear alkenes in terms of the yield of aldehydes.<sup>5</sup> Synthesis and reactivity assessment of relevant intermediates in cobalt-catalyzed hydroformylation employing enantiopure bisphosphine ligands have also been studied.<sup>6</sup>

---

<sup>1</sup> Roelen, O., DE849548, **1938/1951**.

<sup>2</sup> Börner, A. F., Robert.; *Hydroformylation: Fundamentals, Processes, and Applications in Organic Synthesis*; Wiley-VCH, Weinheim, **2016**.

<sup>3</sup> For examples, see Figure 2 in the Introduction.

<sup>4</sup> Cornely, W.; Fell, B. *J. Mol. Catal.* **1982**, *16*, 89-94.

<sup>5</sup> Kluwer, A. M.; Krafft, M. J.; Hartenbach, I.; de Bruin, B.; Kaim, W. *Top. Catal.* **2016**, *59*, 1787-1792.

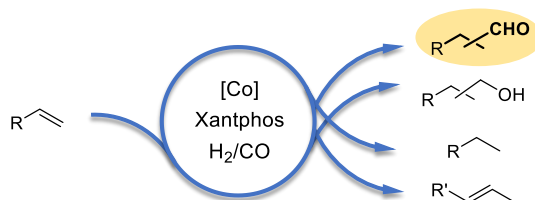
<sup>6</sup> MacNeil, C.; Mendelsohn, L.; Zhong, H.; Pabst, T.; Chirik, P. J. *Angew. Chem. Int. Ed.* **2020**, *59*, 8912-8916.

Lately, the use of cationic cobalt(II) complexes with bisphosphine ligands has enabled the hydroformylation of terminal and branched internal alkenes with high catalytic activity.<sup>7</sup> In case of terminal alkenes, such as hex-1-ene, low linear to branched ratios were observed. Moreover, side-reactions, such as C=C isomerization, CHO reduction and C=C hydrogenation took place to a great extent.

9,9-Dimethyl-4,5-bis(diphenylphosphino)xanthene, which is commonly referred to as Xantphos, has found wide application in homogeneous catalysis since it was reported in 1995.<sup>8</sup> While rhodium-catalyzed hydroformylations using Xantphos-type ligands have been widely studied for a broad variety of substrates with a preferred selectivity towards the linear aldehydes, the use of Xantphos-type ligands in cobalt-catalyzed hydroformylation remains unexplored.

Mechanistic studies of cobalt-catalyzed hydroformylation reactions over the last decades pointed out to the  $[\text{Co}(\text{H})(\text{CO})_{4-x}\text{L}_x]$  complexes as the active catalytic species in the catalytic cycle. Nevertheless, the number of potentially active cobalt species formed under hydroformylation reaction conditions led us to consider whether a similar catalytic outcome would be observed with the preformed or the *in situ* generated catalysts.

Herein, we describe the cobalt-catalyzed hydroformylation of styrene and several octene isomers employing *in situ* generated or preformed cobalt-Xantphos-derived complex as catalysts.



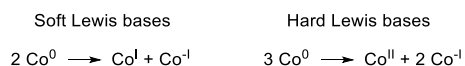
**Scheme 25.** Cobalt-catalyzed hydroformylation of structurally diverse alkenes with Xantphos

<sup>7</sup> Hood, D. M.; Johnson, R. A.; Carpenter, A. E.; Younker, J. M.; Vinyard, D. J.; Stanley, G. G. *Science* **2020**, *367*, 542-548.

<sup>8</sup> van Leeuwen, P. W. N. M.; Kamer, P. C. J. *Catal. Sci. Technol.* **2018**, *8*, 26-113.

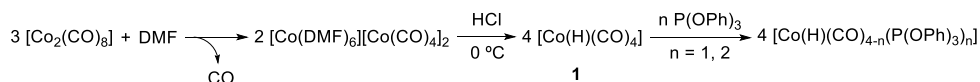
## 2.3 RESULTS AND DISCUSSION

With the aim of expanding the scope of bisphosphine-catalyzed hydroformylation reactions using cobalt complexes, and corroborating the role of the cobalt-Xantphos-derived complexes as active catalysts in hydroformylation reactions, the hydrido dicarbonyl complex  $[\text{Co}(\text{H})(\text{CO})_2(\text{Xantphos})]$  was prepared. Diverse synthetic methodologies have been employed in the synthesis of hydrido cobalt complexes, starting from different cobalt precursors. Many alternatives have been used for the synthesis of  $[\text{Co}(\text{H})(\text{CO})_4]$  **1**, the intermediate in the synthesis of  $[\text{Co}(\text{H})(\text{CO})_2(\text{Xantphos})]$  and also an active catalytic species in hydroformylation.<sup>9</sup> One approach is the reaction of  $[\text{Co}_2(\text{CO})_8]$  with a Lewis base, which leads to a disproportionation reaction. Depending on the Lewis base used,  $\text{Co}^{\text{I}}/\text{Co}^{-\text{I}}$  or  $\text{Co}^{\text{II}}/\text{Co}^{-\text{I}}$  ionic pairs are obtained (Scheme 26).



**Scheme 26.** General scheme of cobalt carbonyl complexes disproportionation

Roodt and co-workers reported a methodology where DMF was used to promote the disproportionation of  $[\text{Co}_2(\text{CO})_8]$  into  $[\text{Co}(\text{DMF})_6]^{2+}$  and  $[\text{Co}(\text{CO})_4]^{-}$  species. Complex  $[\text{Co}(\text{H})(\text{CO})_4]$  **1** was obtained after acidification of the reaction mixture with HCl (Scheme 27).<sup>10</sup> This methodology was used for the synthesis of mono- and bidentate ligand-modified cobalt catalysts  $[\text{Co}(\text{H})(\text{CO})_{4-n}(\text{P}(\text{OPh})_3)_n]$ , by direct addition of stoichiometric amounts of  $\text{P}(\text{OPh})_3$  to  $[\text{Co}(\text{H})(\text{CO})_4]$ .



**Scheme 27.** Synthesis of  $[\text{Co}(\text{H})(\text{CO})_4]$  **1** and/or ligand-modified hydrido carbonyl cobalt complexes

This methodology has been recently applied by Kluwer *et al.*<sup>5</sup> in the synthesis of  $[\text{Co}(\text{H})(\text{CO})_2(\text{dchpf})]$ .<sup>11</sup> The reaction of the bisphosphine dchpf ligand with  $[\text{Co}_2(\text{CO})_8]$ , through the formation of complex  $[\text{Co}(\text{H})(\text{CO})_4]$  **1**, led to the

<sup>9</sup> Hebrard, F.; Kalck, P. *Chem. Rev.* **2009**, *109*, 4272-4282.

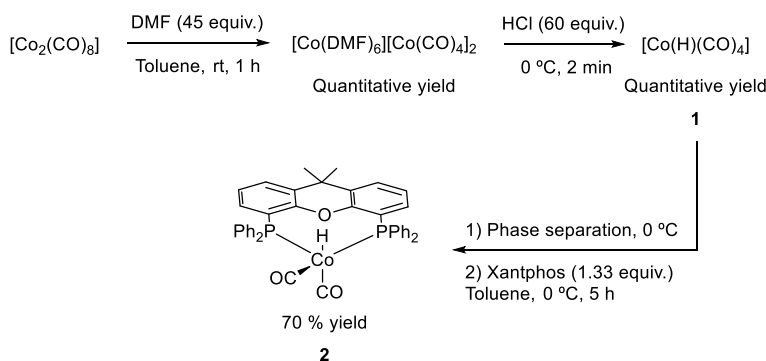
<sup>10</sup> Haumann, M.; Meijboom, R.; Moss, J. R.; Roodt, A. *Dalton Trans.* **2004**, 1679-1686.

<sup>11</sup> The ligand with the abbreviation dchpf corresponds to 1,1'-bis(dicyclohexylphosphino)ferrocene.

displacement of two molecules of CO and formation of the  $[\text{Co}(\text{H})(\text{CO})_2(\text{dchpf})]$  complex.

Although there were previous examples of hydrido dicarbonyl bisphosphine cobalt complexes,<sup>5</sup> this is the first report in the literature in which a hydrido dicarbonyl bisphosphine cobalt complex was isolated and directly tested in hydroformylation reactions. During the writing of this thesis, Chirik and co-workers have reported synthetic protocols for preparing the hydrido bisphosphine cobalt complex  $[\text{Co}(\text{H})(\text{CO})_2((\text{R},\text{R})\text{-}(\text{Pr-DuPhos}))]$  using  $[\text{Co}_2(\text{CO})_8]$ ,  $[\text{Co}(\mu\text{-Cl})((\text{R},\text{R})\text{-}(\text{Pr-DuPhos}))_2]$  or  $\text{Co}(\text{OPiv})_2$  as metal precursors.<sup>6</sup>

Following the synthetic methodology represented in Scheme 27, the complex  $[\text{Co}(\text{H})(\text{CO})_2(\text{Xantphos})]$  **2** was efficiently synthesized.<sup>5</sup> The structure of complex **2** was established by standard spectroscopic techniques, such as  $^1\text{H}$  NMR spectroscopy (*i.e.*, presence of a triplet signal at  $-11.23$  ppm, corresponding to the hydrido ligand coupled with two equivalent phosphorus nuclei from the Xantphos ligand;  $^2J_{\text{P-H}}=23.3$  Hz). This result suggested that both phosphine groups were coordinated in an equatorial position and the hydrido ligand in an axial position in a cobalt trigonal bipyramidal complex. Optimization studies of the reaction conditions for synthesizing **2**, led us to identify that, for the total complexation of the cobalt in the reaction, an excess of 1.33 equiv. of ligand were required (whilst for the formation of  $[\text{Co}(\text{H})(\text{CO})_2(\text{dchpf})]$  the use of only 1.03 equiv. was described). Further optimization of the reaction conditions led us to obtain complex **2** in a 70% isolated yield (Scheme 28).



**Scheme 28.** Synthesis of  $[\text{Co}(\text{H})(\text{CO})_2(\text{Xantphos})]$  complex **2**

The IR spectra of complex **2** presented two strong bands at 1971 and 1910  $\text{cm}^{-1}$  (Table 11, entry 2). These values were in agreement with the reported

vibration wavenumbers of terminal CO groups coordinated to a metal complex.<sup>12</sup> Moreover, the presence of two bands confirmed the presence of one single stereoisomer of complex **2**. Vogt *et al.* correlated the CO stretching band ( $\bar{\nu}_{\text{CO}}$ ) with the electronic nature of the ligand and the selectivity towards linear aldehydes in hydroformylation reactions.<sup>13</sup> For Rh-catalyzed hydroformylations, Vogt *et al.* observed that ligands with higher  $\pi$ -acceptor character presented higher  $\bar{\nu}_{\text{CO}}$  wavenumbers and were more selective towards the formation of linear aldehydes. Though the relationship between the ligand donating character of bisphosphine ligands and the outcome of rhodium-catalyzed hydroformylations has been established,<sup>14</sup> prediction of results with cobalt-based catalysts should be made more judiciously. Tucci and co-workers studied the correlation between ligand donicity and catalytic outcome for phosphines in cobalt-catalyzed hydroformylation of hex-1-ene.<sup>15</sup> Higher reaction rates were observed with phosphines with low donicity. On the other hand, phosphines with a higher donor character enhanced the regioselectivity for the linear aldehyde and favored the formation of alcohols as side-reaction products. No effect was observed in the alkene hydrogenation.

**Table 11.** Selected bond distances (Å), angles (°) and carbonyl stretching band wavenumbers ( $\text{cm}^{-1}$ ) of  $[\text{Co}(\text{H})(\text{CO})_2(\text{dchpf})]$  and complex **2**

Entry	Complex	Co–P1	Co–P2	Co–H	Co–C40	Co–C41	P1–Co–P2	$\bar{\nu}_{\text{CO}}$
1 <sup>[a]</sup>	$[\text{Co}(\text{H})(\text{CO})_2(\text{dchpf})]$	2.19(1)	2.18(1)	-	1.76(1)	1.76(1)	108.7(1)	1960 1891
2 <sup>[b]</sup>	<b>2</b>	2.1927(5)	2.1899(5)	1.50(2)	1.726(2)	1.750(2)	110.196(18)	1971 1910

[a]See ref 5. [b]X-ray values. IR spectroscopy of the sample measured neat.

The structure of complex **2** was confirmed by single crystal X-ray diffraction analysis, which allowed establishing, unequivocally, the geometry of complex **2** (Figure 45). X-ray analysis confirmed the position of the hydrido ligand in an axial coordination fashion in a distorted cobalt trigonal bipyramidal center. The position of the two phosphine groups in the equatorial coordination sites of the

<sup>12</sup> (a) van Boven, M.; Alemdaroglu, N.; Penninger, J. M. L. *J. Organomet. Chem.* **1975**, *84*, 65-74. (b) van Boven, M.; Alemdaroglu, N. H.; Penninger, J. M. L. *Ind. Eng. Chem., Prod. Res. Dev.* **1975**, *14*, 259-264.

<sup>13</sup> Boymans, E.; Janssen, M.; Mueller, C.; Lutz, M.; Vogt, D. *Dalton Trans.* **2013**, *42*, 137-142.

<sup>14</sup> Jiao, Y.; Torne, M. S.; Gracia, J.; Niemantsverdriet, J. W.; van Leeuwen, P. W. N. M. *Catal. Sci. Technol.* **2017**, *7*, 1404-1414.

<sup>15</sup> Tucci, E. R. *Ind. Eng. Chem., Prod. Res. Develop.* **1970**, *9*, 516-521.

trigonal bipyramidal geometry was also demonstrated. The P–Co–P bond angle observed (110.2°) (Table 11, entry 2) was slightly higher than that observed for complex [Co(H)(CO)<sub>2</sub>(dchpf)] (108.7°) (Table 11, entry 1),<sup>5</sup> and was in agreement with that theoretically calculated (111.4°).<sup>16</sup> Fluxional equilibria between the equatorial-equatorial (eq-eq) and equatorial-axial (eq-ax) geometries in [Rh(H)(CO)<sub>2</sub>(Xantphos)] complexes have been observed.<sup>17</sup> However, complex **2** appeared to be configurationally stable in the NMR studies that we performed.

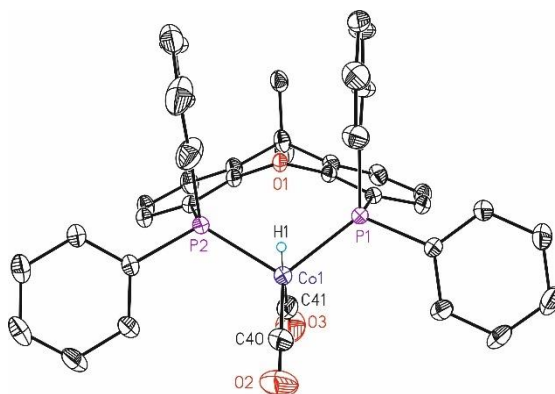


**Figure 45.** ORTEP drawing (thermal ellipsoids drawn at a 50% probability level) showing the structure of complex **2**. Hydrogen atoms have been omitted for the sake of clarity except for the hydrido ligand. Color scheme: C: black, H: blue, Co: purple, O: red, P: pink

For the sake of comparison, the catalytic performance of the cobalt complexes generated *in situ* and the isolated complex **2** was compared. The *in situ* catalyst was generated by mixing the Xantphos ligand and [Co<sub>2</sub>(CO)<sub>8</sub>] under hydroformylation reaction conditions. The use of bisphosphine ligands as soft Lewis bases leads to the disproportionation reaction of [Co<sub>2</sub>(CO)<sub>8</sub>] into a Co<sup>I</sup>/Co<sup>-I</sup> system (Scheme 29). Hanson and co-workers observed a correlation between the ligand nature and the stabilization of the ionic complex.<sup>18</sup> The use of bisphosphine ligands with higher donicity or longer chain,<sup>19</sup> led to the stabilization of the ionic derivatives (**3a-c**), which evolved to dimeric cobalt complex **4** over time and/or by heating. Dimeric complexes **4d** were employed

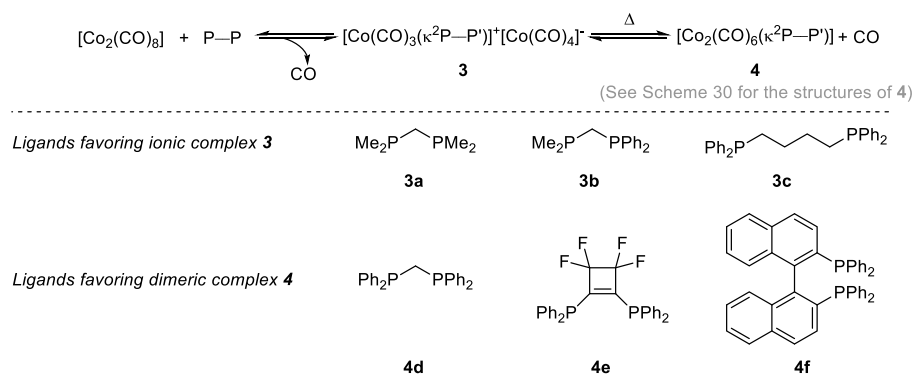
<sup>16</sup> van der Veen, L. A.; Keeven, P. H.; Schoemaker, G. C.; Reek, J. N. H.; Kamer, P. C. J.; van Leeuwen, P. W. N. M.; Lutz, M.; Spek, A. L. *Organometallics* **2000**, *19*, 872-883.

<sup>17</sup> van der Veen, L. A.; Kamer, P. C. J.; van Leeuwen, P. W. N. M. *Organometallics* **1999**, *18*, 4765-4777.

<sup>18</sup> Lisic, E. C.; Hanson, B. E. *Inorg. Chem.* **1986**, *25*, 812-815.

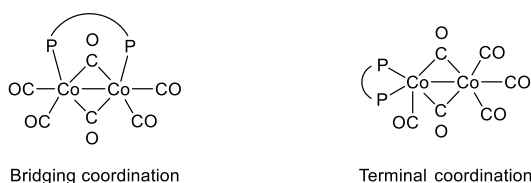
<sup>19</sup> Thornhill, D. J.; Manning, A. R. *J. Chem. Soc., Dalton Trans.* **1973**, 2086-2090.

in the cobalt-catalyzed hydroformylation of hex-1-ene, showing activity in this chemistry.<sup>20</sup>



**Scheme 29.** Reactivity of  $[\text{Co}_2(\text{CO})_8]$  with bisphosphine ligands

Initial studies of the dimeric complexes **4** with diverse bisphosphine ligands revealed a bridging coordination of the ligand to the two cobalt atoms (Scheme 30).<sup>21</sup> Hanson and co-workers observed that in the NMR time scale for the bridging coordination structure indicated in Scheme 30, a single resonance for all the CO ligands was observed due to fast ligand exchange processes taking place.<sup>18</sup> As an exception, when BINAP was used as ligand, the dimeric complex exhibited a different coordination mode.<sup>22</sup> In this case, the bisphosphine ligand was coordinated in a terminal position to a single cobalt atom (Scheme 30).



**Scheme 30.** Coordination mode of bisphosphine ligands in  $[\text{Co}_2(\text{CO})_6(\text{P-P})]$  complexes

To test the activity of cobalt-catalysts derived from Xantphos as ligand in hydroformylation reactions, we chose styrene and oct-1-ene as model substrates.

<sup>20</sup> Hanson, B. E.; Fanwick, P. E.; Mancinila, J. S. *Inorg. Chem.* **1982**, *21*, 3811-3815.

<sup>21</sup> (a) Cullen, W. R.; Crow, J. P.; Harrison, W.; Trotter, J. *J. Am. Chem. Soc.* **1970**, *92*, 6339-6341.

(b) Fukumoto, T.; Matsumura, Y.; Okawara, R. *J. Organometal. Chem.* **1974**, *39*, 437-444.

<sup>22</sup> (a) Gibson, S. E.; Lewis, S. E.; Loch, J. A.; Steed, J. W.; Tozer, M. J. *Organometallics* **2003**, *22*, 5382-5384. (b) Gibson, S. E.; Kaufmann, K. A. C.; Haycock, P. R.; White, A. J. P.; Hardick, D. J.; Tozer, M. J. *Organometallics* **2007**, *26*, 1578-1580. (c) Amezquita-Valencia, M.; Cabrera, A. J. *Mol. Catal. A: Chem.* **2013**, *366*, 17-21.

Their different nature allowed us to assess the behavior of the catalytic system with structurally diverse alkenes.

### 2.3.1 Cobalt-catalyzed hydroformylation of styrene 5

Despite the fact that the hydroformylation of styrene has been widely studied with rhodium-based catalysts, only a few reports on the hydroformylation of styrene with unmodified complex  $[\text{Co}(\text{H})(\text{CO})_4]$  as catalyst, have been published.<sup>23</sup> Moderate selectivities toward the formation of aldehydes were observed at high temperatures. Ucciani and co-workers observed at full substrate conversion, a 75% chemoselectivity and a low regioselectivity (58:42 b/l ratio) for the aldehydes employing harsh conditions (160 bar  $\text{H}_2/\text{CO}$ , 105 °C).<sup>23a</sup> Botteghi *et al.* used lower pressures (80 atm) and observed temperature effects in the catalytic activity and chemoselectivity.<sup>23b</sup> As expected, conversion increased with the temperature (*i.e.*, 87.3% conv. at 110 °C and 57.4% conv. at 60 °C), but selectivity towards aldehydes worsened with increasing temperatures (*i.e.*, 61% sel. at 60 °C and 35% sel. at 110 °C). The regioselectivity was not dependent with the reaction temperature. The authors used pyridine as reaction promoter. Higher catalytic activity was observed, although lower selectivities towards aldehydes were achieved. It is worth noting that the hydroformylation of styrene employing Rh-based catalysts leads predominantly to the formation of the branched aldehyde, due to the higher stability of the branched alkyl-metal intermediate.<sup>17</sup> As an exception, some examples reported high regioselectivities (beyond 80%) for the linear aldehyde in the rhodium-catalyzed hydroformylation of styrene.<sup>13,24</sup>

We envisioned that the combination of a metal center such as cobalt with a bisphosphine ligand showing a preference for linear aldehydes, such as Xantphos, would be suitable to increase the regioselectivity towards the linear aldehyde. Initial studies focused on the optimization of the reaction conditions, initially with the catalyst formed *in situ*, and subsequently with the isolated complex **2**. The effect of the temperature in the cobalt-hydroformylation of styrene in the presence of Xantphos was studied (Table 12). As previously reported in the literature, high reaction temperatures were needed to obtain full conversion.<sup>23a</sup> When low temperatures were used (90 and 110 °C; Table 12,

---

<sup>23</sup> (a) Lai, R.; Ucciani, E. *J. Mol. Catal.* **1978**, *4*, 401-410. (b) Botteghi, C.; Branca, M.; Marchetti, M.; Saba, A. *J. Organomet. Chem.* **1978**, *161*, 197-205.

<sup>24</sup> (a) Klein, H.; Jackstell, R.; Beller, M. *Chem. Commun.* **2005**, 2283-2285. (b) Yu, S.; Chie, Y.-m.; Guan, Z.-h.; Zou, Y.; Li, W.; Zhang, X. *Org. Lett.* **2009**, *11*, 241-244.



entries 1-2), hydroformylation products (3-phenylpropanal **6** and 2-phenylpropanal **7**) and hydrogenations products (ethylbenzene **8**) were formed in similar amounts. The formation of **11**, which derives from the reductive dimerization of two styrene units, was also observed.<sup>25</sup> When the reaction temperature was increased up to 140 °C, a dramatic change in the product distribution was observed (Table 12, entry 3). While only 7% of a mixture of aldehydes **6** and **7** was formed, hydrogenation product **8** was obtained as the main product with a 60% selectivity. The preferred formation of the hydrogenation product **6** has been reported by Chirik and co-workers during the writing of the present thesis with  $[\text{Co}(\text{H})(\text{CO})_2((R,R)\text{-}i\text{-Pr-DuPhos})]$  as catalyst.<sup>6</sup> Reaction temperature also favored the reductive dimerization towards **11** (28% selectivity). A clear trend in the regioselectivity as a function of the temperature could be established, with the preferential formation of linear aldehyde **6** being observed when high temperatures were employed.

**Table 12.** Temperature effects in the cobalt-catalyzed hydroformylation of styrene **5** with Xantphos

Entry	T (°C)	Conv. (%) <sup>[a]</sup>	Selectivity <sup>[a]</sup>				6/7 or 1/b ratio <sup>[a]</sup>
			6 + 7 (%)	8 (%)	9 + 10 (%)	11 (%)	
1	90	12	13	13	0	8	35:65
2	110	27	19	30	0	19	45:55
3	140	>99	7	60	1	28	53:47

The hydroformylations were performed in a parallel autoclave. Reaction conditions: [alkene] = 0.26 M; reaction time = 21 h, stirring rate = 800 rpm; H<sub>2</sub>/CO in a 1:1 ratio, unless otherwise cited. [a] Conversion, 1/b ratio and product distribution were determined by GC analysis on an achiral stationary phase (HP-5). Selectivities were calculated as mol of compound/mol of converted substrate.

<sup>25</sup> Reductive dimerization product **11** has also been observed as a side-product in the hydrogenation of styrene with phosphide zirconocene cation-based frustrated Lewis pair catalysts; see: Normand, A. T.; Daniliuc, C. G.; Wibbeling, B.; Kehr, G.; Le Gendre, P.; Erker, G. *J. Am. Chem. Soc.* **2015**, *137*, 10796-10808.

Under these conditions, the effect of the partial pressure of each gas (*i.e.*, the relative molar ratio CO and H<sub>2</sub>) in the reaction outcome is unknown. It was observed that, as in the case of unmodified rhodium catalysts<sup>26</sup> or with bisdiazaphospholane ligands,<sup>27,28</sup> an excess of CO with respect to H<sub>2</sub> affects the outcome of the reaction by increasing the selectivity towards the hydroformylation products. We turned our attention towards the effect of varying the relative molar amounts of each gas in the cobalt-Xantphos-catalyzed hydroformylation of styrene (Table 13).

**Table 13.** Pressure effects in the cobalt-catalyzed hydroformylation of styrene **5** with Xantphos

Entry	H <sub>2</sub> /CO ratio	Conv. (%) <sup>[a]</sup>	Selectivity <sup>[a]</sup>				6/7 or 1/b ratio <sup>[a]</sup>
			6 + 7 (%)	8 (%)	9 + 10 (%)	11 (%)	
1 <sup>[b]</sup>	1:1	>99	7	60	1	28	53:47
2	1:3	26	8	15	0	8	53:47

The hydroformylations were performed in a parallel autoclave. Reaction conditions: Pressure: 40 bar, [alkene] = 0.26 M; reaction time = 21 h, stirring rate = 800 rpm; H<sub>2</sub>/CO in a 1:1 ratio, unless otherwise cited. [a] Conversion, 1/b ratio and product distribution were determined by GC analysis on an achiral stationary phase (HP-5). Selectivities were calculated as mol of compound/mol of converted substrate. [b] These results have been already shown in Table 12 but are included here for comparison.

Equal molar amounts of CO and H<sub>2</sub> at 40 bar led to hydrogenated product **8** in a 60% selectivity and to the styrene dimerization product **11** in 28% selectivity (Table 13, entry 1). Interestingly, a 1:3 ratio of H<sub>2</sub>/CO led to a reduction in the formation of both hydrogenated **9** and dimerized product **11** (15% and 8% selectivity, respectively) at the expense of a much lower conversion (Table 13, entry 2), if compared with the reaction with a 1:1 H<sub>2</sub>/CO ratio (Table 13, entry

<sup>26</sup> Lazzaroni, R.; Raffaelli, A.; Settambolo, R.; Bertozzi, S.; Vitulli, G. *J. Mol. Catal.* **1989**, *50*, 1-9.

<sup>27</sup> Watkins, A. L.; Landis, C. R. *J. Am. Chem. Soc.* **2010**, *132*, 10306-10317.

<sup>28</sup> Bisdiazaphospholane ligands entail a structurally diverse type of ligands, with a common diazaphospholane backbone. For the structure, see Introduction, figure 8.

1). The low catalytic activity observed with high partial pressure of CO could be explained due to a lower formation of active catalyst.<sup>29</sup> An influence of the H<sub>2</sub>/CO ratio in the reaction regioselectivity was not observed, which differs with previous studies for the hydroformylation of styrene employing rhodium complexes as catalysts.<sup>26,27</sup>

It is well known that changes in the L/Co molar ratio can lead to the formation of different catalytic species that could influence the activity and selectivity in the cobalt-catalyzed hydroformylation. In case of bisphosphine ligands, Murata and co-workers reported the hydroformylation of structurally diverse alkenes with a variable ratio of 1,2-bis(diphenylphosphino)ethane (dppe) and [Co<sub>2</sub>(CO)<sub>8</sub>].<sup>30</sup> The most active catalyst was obtained when a *ca.* 1:1 ratio of dppe and Co<sub>2</sub>(CO)<sub>8</sub> (L/Co ratio) was used. With higher L/Co ratios, lower catalytic activity was observed.

Besides studying the effects of temperature and H<sub>2</sub>/CO relative molar ratio, we also studied the effects of Xantphos/[Co<sub>2</sub>(CO)<sub>8</sub>] ratio (L/Co ratio) in the outcome of the hydroformylation reaction. The results of this study have been summarized in Table 14. In the absence of ligand, and under hydroformylation reaction conditions, the complex [Co<sub>2</sub>(CO)<sub>8</sub>] is transformed into complex **1** [Co(H)(CO)<sub>4</sub>], which is an active complex in hydroformylation chemistry.<sup>9</sup> The reaction in the absence of ligand, with [Co(H)(CO)<sub>4</sub>] as catalyst generated *in situ* was performed. Full conversion of styrene **5** was observed and small amounts of aldehydes **6** and **7** were obtained (14% selectivity) (Table 14, entry 1). Regioselectivity towards the linear aldehyde **6** was moderate with a 59:41 l/b ratio. The absence of ligand did not prevent the formation of side-reaction products, such as the hydrogenated one **8** (73% selectivity), alcohols **9-10** arising from hydrogenation of the aldehydes **6-7** and dimerized product **11** (4% and 5% selectivity, respectively). In presence of different ratios of Xantphos and [Co<sub>2</sub>(CO)<sub>8</sub>] under hydroformylation conditions, the active catalyst was generated *in situ* (Table 14, entries 2-4). When a 1:1 L/Co ratio was used (Table 14, entry 2) similar conversion and regioselectivity was observed as in the absence of ligand (Table 14, entry 1). The presence of Xantphos led to a lower selectivity (63%) in the formation of the hydrogenation product **8** and a higher selectivity for the

---

<sup>29</sup> Dissociation of one molecule of CO is necessary to obtain electronically unsaturated cobalt complexes, and this dissociation process becomes more difficult by increasing the CO amounts in the reaction mixture. For the catalytic cycle, see the Introduction, scheme 6.

<sup>30</sup> (a) Murata, K.; Matsuda, A.; Bando, K.; Sugi, Y. *J. Chem. Soc., Chem. Commun.* **1979**, 785-786. (b) Murata, K.; Matsuda, A.; Masuda, T. *J. Mol. Catal.* **1984**, *23*, 121-132.

formation of product **11**. Under this catalytic conditions, it was likely that  $[\text{Co}(\text{H})(\text{CO})_2(\text{Xantphos})]$  and  $[\text{Co}(\text{H})(\text{CO})_4]$  were formed simultaneously by reaction of  $\text{H}_2$  with the ionic or dimeric complex derived from the reaction of  $[\text{Co}_2(\text{CO})_8]$  and Xantphos. Higher L/Co ratios (from 2:1 to 4:1) showed similar behavior of the corresponding catalytic species in terms of conversion and regioselectivity (Table 14, entries 3-4). In the case of a 2:1 L/Co ratio (Table 14, entry 3), the formation of hydrogenation product **8** decreased down to a 60% selectivity, with full conversion, and the amounts of dimerization product **11** increased up to a 28% selectivity. Cabrera *et al.* observed the formation of  $[\text{Co}(\text{H})(\text{CO})_2(\text{BINAP})]$  when BINAP and  $[\text{Co}_2(\text{CO})_8]$  were mixed in a 2:1 ratio under hydrogenation conditions.<sup>22c</sup> When a 4:1 L/Co ratio was used (Table 14, entry 4), the formation of the hydrogenation product **8** was further reduced (down to a 52% selectivity) and formation of alcohols **9-10** was suppressed. Unfortunately, important amounts of reductive dimerization products of two **11** or more styrene units were observed (*ca.* 26% selectivity) (Table 14, entry 4).

**Table 14.** L/Co ratio effects in the cobalt-catalyzed hydroformylation of styrene **5** with Xantphos as ligand

Entry	L/Co ratio	Conv. (%) <sup>[a]</sup>	Selectivity <sup>[a]</sup>				6/7 or 1/b ratio <sup>[a]</sup>
			6 + 7 (%)	8 (%)	9 + 10 (%)	11 (%)	
1	0:1	>99	14	73	4	5	59:41
2	1:1	>99	11	63	2	21	54:46
3 <sup>[c]</sup>	2:1	>99	7	60	1	28	53:47
4	4:1	98	9	52	0	19 <sup>[b]</sup>	53:47
5	Complex 2	93	15	50	0	16	53:47

The hydroformylations were performed in a parallel autoclave. Reaction conditions: [alkene] = 0.26 M; reaction time = 21 h, stirring rate = 800 rpm;  $\text{H}_2/\text{CO}$  in a 1:1 ratio, unless otherwise cited. [a] Conversion, 1/b ratio and product distribution were determined by GC analysis on an achiral stationary phase (HP-5). Selectivities were calculated as mol of compound/mol of converted substrate. [b] In addition to the observation of the reductive dimerization product of two styrene units **11**, a reductive trimerization was also observed (7% selectivity). [c] These results have been already shown in Table 12 but are included here for comparison.

With the aim of elucidating the behavior of complex **2** in the outcome of the cobalt-catalyzed hydroformylation of styrene, the hydroformylation reaction was carried out using pre-formed complex **2** as catalyst (Table 14, entry 5). Full conversion was observed and aldehydes **6-7** were formed in a 15% selectivity, which is similar to the results obtained with the unmodified cobalt catalyst (Table 14, entry 1) and better than the results obtained with *in situ* prepared catalyst (Table 14, entry 3). Regioselectivity was maintained with a 53:47 l/b ratio and, despite hydrogenated product **8** being again the major product, side-reactions such as hydrogenation and styrene dimerization were reduced (down to a 50% and 16% selectivity, respectively), if compared with the *in situ* formed complex.

In conclusion, variation of the L/Co ratio had an effect in the product distribution employing bisphosphine ligands, as previously reported in the literature. The absence of ligand enhanced the formation of aldehydes **6-7** and reduced the formation of the dimerization product **11** (the formation of **11** increased when higher L/Co ratios were used). Unfortunately, the absence of ligand also favored the formation of C=C and CHO hydrogenation products. The progressive increase of the L/Co ratio translated into a decrease in the hydroformylation selectivity. The selectivity towards the hydrogenated product **8** also decreased with high L/Co ratios, though this process remained as the major reaction pathway in all cases. Despite the fact that the cobalt-based catalytic system is more selective towards hydrogenation than hydroformylation reactions, the use of the preformed catalyst (*i.e.*, complex **2**) reduced the amounts of hydrogenation and styrene dimerization products.

### 2.3.2 Cobalt-catalyzed hydroformylation of oct-1-ene and internal octenes

The cobalt-catalyzed hydroformylation of oct-1-ene **12** has been widely studied using different approaches, as for instance the biphasic hydroformylation with  $[\text{Co}_2(\text{CO})_8]$  as catalyst and  $\text{P}(\text{tBu})_3$ <sup>31</sup> or  $\text{Ph}_2\text{PBU}$ <sup>32</sup> as ligands, or in presence of cyclodextrines, Co(II)-precursors and sulphonated phosphine ligands.<sup>33</sup> In all cases, alkene hydrogenation and reduction of the target aldehydes to the

<sup>31</sup> Bartik, T.; Bartik, B.; Hanson, B. E. *J. Mol. Catal.* **1993**, *85*, 121-129.

<sup>32</sup> Wu, D.; Zhang, J.; Wang, Y.; Jiang, J.; Jin, Z. *Appl. Organomet. Chem.* **2012**, *26*, 718-721.

<sup>33</sup> (a) Dabbawala, A. A.; Parmar, D. U.; Bajaj, H. C.; Jasra, R. V. *J. Mol. Catal. A: Chem.* **2008**, *282*, 99-106. (b) Dabbawala, A. A.; Parmar, J. N.; Jasra, R. V.; Bajaj, H. C.; Monflier, E. *Catal. Commun.* **2009**, *10*, 1808-1812. (c) Dabbawala, A. A.; Bajaj, H. C.; Bricout, H.; Monflier, E. *Appl. Catal., A* **2012**, *413-414*, 273-279.

corresponding alcohols were the major transformations taking place. In general, changes in the ligand/metal ratios had a strong influence in the outcome of the reaction. *N*-heterocyclic carbenes (NHC) as ligands have been employed in the cobalt-catalyzed hydroformylation of this substrate, with an atypical regioselectivity towards the branched aldehyde (*i.e.*, 2-methyloctanal) under mild conditions being observed.<sup>34</sup> This reaction has also been studied under photocatalytic conditions proving that the formation of active species is faster than under thermal conditions.<sup>35</sup> Moreover, the reaction has been performed in butane expanded liquids (BXLs) with the aim of increasing the gas pressure in the media and, consequently, the catalytic activity.<sup>36</sup> The hydroformylation of oct-1-ene **12** catalyzed by  $[\text{Co}(\text{H})(\text{CO})_4]$  in the absence of ligand showed similar reaction rates for the isomerization and hydroformylation processes.<sup>37</sup> Interestingly, the use of tertiary alkyl phosphines as ligands translated into the selective formation of aldehydes. In particular cases, the major products obtained were the corresponding alcohols obtained by hydrogenation of the aldehydes.<sup>38</sup> During the writing of the present thesis, Chirik and co-workers reported the application of  $[\text{Co}(\text{H})(\text{CO})_2((R,R)\text{-}(\text{Pr-DuPhos}))]$  in the asymmetric hydroformylation of oct-1-ene, however no conversion was observed under catalytic conditions.<sup>6</sup> The hydroformylation of oct-1-ene **12** can potentially lead to a mixture of different products. The main aldehydes nonanal **13a** and 2-methyloctanal **13b** are obtained by direct hydroformylation, meanwhile 2-ethylheptanal **13c** and 2-propylhexanal **13d**, derive from the tandem-isomerization-hydroformylation reaction. The corresponding alcohols nonan-1-ol **14a**, 2-methyloctan-1-ol **14b**, 2-ethylheptan-1-ol **14c** and 2-propylhexan-1-ol **14d**, are obtained as a consecutive hydrogenation of the corresponding aldehydes **13a-d**. Other side products are the hydrogenation product octane **15** and unreacted internal octenes, derived from the isomerization reaction of oct-1-ene **12**.

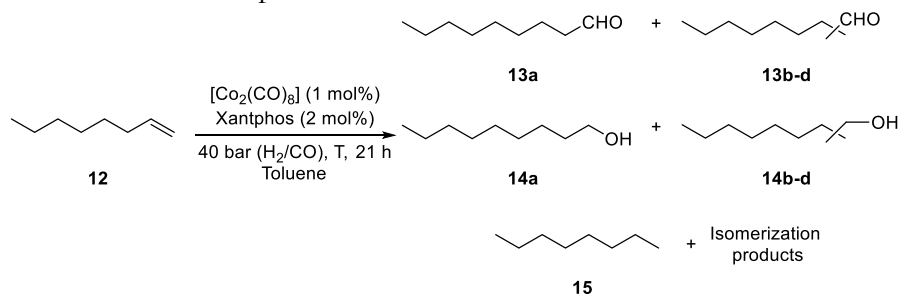
<sup>34</sup> Llewellyn, S. A.; Green, M. L. H.; Cowley, A. R. *Dalton Trans.* **2006**, 4164-4168.

<sup>35</sup> Mirbach, M. J.; Topalsavoglou, N.; Nhu, P. T.; Mirbach, M. F.; Saus, A. *Chem. Ber.* **1983**, *116*, 1422-1440.

<sup>36</sup> Liu, D.; Xie, Z.; Snavely, W. K.; Chaudhari, R.; Subramaniam, B. *React. Chem. Eng.* **2018**, *3*, 344-352.

<sup>37</sup> Haymore, B. L.; van Asselt, A.; Beck, G. R. *Ann. N. Y. Acad. Sci.* **1983**, *415*, 159-175.

<sup>38</sup> (a) Polas, A.; Wilton-Ely, J. D. E. T.; Slawin, A. M. Z.; Foster, D. F.; Steynberg, P. J.; Green, M. J.; Cole-Hamilton, D. J. *Dalton Trans.* **2003**, 4669-4677. (b) Bungu, P. N.; Otto, S. *Dalton Trans.* **2011**, *40*, 9238-9249.

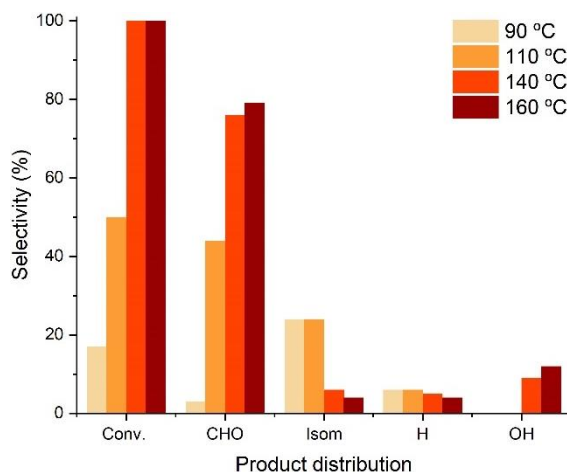
**Table 15.** Temperature effects in the cobalt-catalyzed hydroformylation of oct-1-ene **12** with Xantphos

Entry	T (°C)	Conv. (%) <sup>[a]</sup>	Selectivity <sup>[a]</sup>				Regioselectivity <sup>[a]</sup>
			13a-d (%)	14a-d (%)	15 (%)	Isom (%)	13a/13b (13a/13b/13c/13d)
1	90	17	3	0	6	24	81:19 (75:18:4:3)
2	110	50	44	0	6	24	80:20 (73:18:5:4)
3	140	>99	76	9	5	6	73:27 (62:23:8:7)
4	160	>99	79	12	4	4	70:30 (56:24:11:9)

The hydroformylations were performed in a parallel autoclave. Reaction conditions: [alkene] = 0.26 M; stirring rate = 800 rpm; H<sub>2</sub>/CO in a 1:1 ratio, unless otherwise cited. [a] Conversion, l/b ratio and product distribution were determined by GC analysis on an achiral stationary phase (HP-5). Selectivities were calculated as mol of compound/mol of converted substrate.

As previously indicated, hydroformylation is a chemical transformation highly influenced by the reaction conditions. For that reason, initial catalytic studies were performed to optimize the reaction temperature (Table 15), whilst other reaction variables remained constant. Temperature screening (90-160 °C) revealed a correlation between temperature and catalytic activity in terms of conversion. At 90 °C (Table 15, entry 1), low conversion was achieved. Increasing the reaction temperature up to 110 °C (Table 15, entry 2) favored the formation of aldehyde products **13a-d** (44% selectivity) with a high regioselectivity towards the linear aldehyde (80:20 l/b ratio), although side-products such unreacted isomerized starting alkene (24% selectivity) and hydrogenated product (6% selectivity for **15**) were observed. When the reaction was carried out at 140 °C (Table 15, entry 3), full conversion was observed, with the mixture of aldehydes being obtained with higher selectivity (76%) than at 110 °C (44%). Temperature has a positive effect in the selectivity towards the aldehydes **13a-d** and also towards the alcohols **14a-d**, but at a lower extent. Increasing the temperature

translates into high rates for the hydroformylation of internal alkenes with an overall increase in the amounts of aldehydes. High temperatures mediate C=C isomerization processes in the presence of the cobalt catalyst and the overall process can be referred to as a tandem-isomerization-hydroformylation reaction.<sup>39</sup> In this regard, regioselectivity for the linear aldehyde decreases with the temperature. Thus, high temperatures had a positive influence in the conversion and selectivity towards the formation of all possible aldehydes **13a-d**, but it also favored hydrogenation side-reactions (Graph 2), with which the complexity of the reaction mixture increased with the temperature.



**Graph 2.** Temperature effects in the cobalt catalyzed hydroformylation of oct-1-ene

Previous examples in the literature for oct-1-ene **12** correlated the total pressure of syngas with the formation of oxygen-containing products (aldehydes **13a-d** and alcohols **14a-d**), observing a higher amount of these products by increasing the total pressure of the system.<sup>5</sup> With the aim of understanding the effects of the pressure in the hydroformylation of oct-1-ene **12**, we decided to explore the influence of relative molar ratios of CO and H<sub>2</sub> in syngas. It is well known in the literature that high partial pressures of CO disfavor the isomerization processes and can diminish the hydrogenation of C=C and CHO groups.<sup>17</sup> In addition, reported examples in the literature employing a higher ratio of H<sub>2</sub> than CO (for instance a 2:1 ratio) in the hydroformylation of oct-1-ene **12** with cobalt-modified catalysts showed the preferred formation of alcohols **14a-d** with respect to the aldehydes **13a-d**.<sup>38</sup> Along this line of reasoning, we hypothesized that 40 bar of pressure with a 1:3 H<sub>2</sub>/CO ratio could be suitable for our studies (Table 16, entry

<sup>39</sup> Vilches-Herrera, M.; Domke, L.; Börner, A. *ACS Catal.* **2014**, *4*, 1706-1724.



2). These conditions led to a decrease in the conversion (52% conv.) and aldehyde selectivity (31% selectivity in this case compared to a 76% selectivity with a 1:1 H<sub>2</sub>/CO ratio). Unexpectedly, an excess of CO led to higher amounts of unreacted isomerized starting material (13% selectivity), similar hydrogenation product **15** (4% selectivity) with alcohols **14a-d** not being formed (0% selectivity). Consequently, further studies for optimizing the reaction conditions were carried out at 140 °C and 40 bar of 1:1 H<sub>2</sub>/CO.

**Table 16.** Effects of the H<sub>2</sub>/CO ratio in the cobalt-catalyzed hydroformylation of oct-1-ene **12** with Xantphos

Entry	H <sub>2</sub> /CO ratio	Conv. (%) <sup>[a]</sup>	Selectivity <sup>[a]</sup>				Regioselectivity <sup>[a]</sup>
			13a-d (%)	14a-d (%)	15 (%)	Isom. (%)	13a/13b (13a/13b/13c/13d)
1 <sup>[b]</sup>	1:1	>99	76	9	5	6	73:27 (62:23:8:7)
2	1:3	52	31	0	4	13	76:24 (68:21:6:5)

The hydroformylations were performed in a parallel autoclave. Reaction conditions: Pressure: 40 bar, [alkene] = 0.26 M; reaction time = 21 h, stirring rate = 800 rpm. [a] Conversion, 1/b ratio and product distribution were determined by GC analysis on an achiral stationary phase (HP-5). Selectivities were calculated as mol of compound/mol of converted substrate. [b] These results have been already shown in Table 15 but are included here for comparison.

As previously discussed for the cobalt-catalyzed hydroformylation of styrene, the L/Co ratio played an important role in the outcome of the reaction. Consequently, effects in the product distribution due to changes in the Xantphos/[Co<sub>2</sub>(CO)<sub>8</sub>] ratios were studied for the cobalt-catalyzed hydroformylation of oct-1-ene **12**. In the first place, we studied the reaction in absence of ligand, to assess the catalytic behavior of unmodified [Co(H)(CO)<sub>4</sub>] complex. Under standard catalytic conditions (140 °C, 40 bar of 1:1 H<sub>2</sub>/CO) (Table 17, entry 1) total conversion was observed. Aldehydes **13a-d** were obtained in good selectivity (70%) and moderate regioselectivity towards linear

aldehyde nonanal **13a** (66%) were observed. The absence of ligand led to the formation of alcohols **14a-d** in considerable amounts (26% selectivity).

**Table 17.** L/Co ratio effects in the cobalt-catalyzed hydroformylation of oct-1-ene **12** with Xantphos and comparison with complex **2**

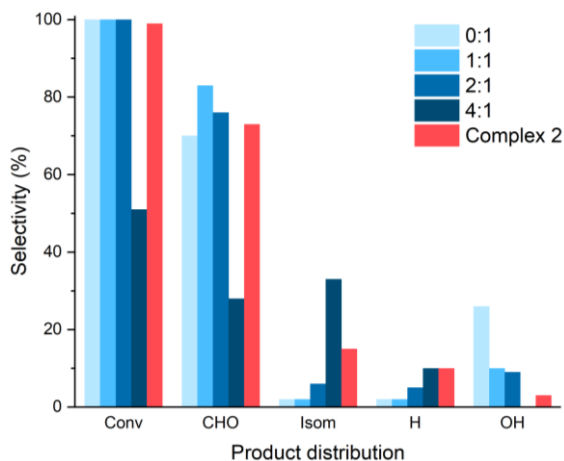
Entry	L/Co ratio	Conv. (%) <sup>[a]</sup>	Selectivity <sup>[a]</sup>				Regioselectivity <sup>[a]</sup> 13a/13b (13a/13b/13c/13d)
			13a-d (%)	14a-d (%)	15 (%)	Isom. (%)	
1	0:1	>99	70	26	2	2	77:23 (66:19:8:7)
2	1:1	>99	83	10	2	2	76:24 (65:21:8:6)
3 <sup>[b]</sup>	2:1	>99	76	9	5	6	73:27 (62:23:8:7)
4	4:1	51	28	0	10	33	72:28 (64:26:6:4)
5	Complex <b>2</b>	99	73	3	10	15	74:26 (64:22:8:6)

<sup>a</sup>The hydroformylations were performed in a parallel autoclave. Reaction conditions: [alkene] = 0.26 M; reaction time = 21 h, stirring rate = 800 rpm; H<sub>2</sub>/CO in a 1:1 ratio, unless otherwise cited. [a] Conversion, l/b ratio and product distribution were determined by GC analysis on an achiral stationary phase (HP-5). Selectivities were calculated as mol of compound/mol of converted substrate. [b] These results have been already shown in Table 15 but are included here for comparison.

In the presence of different ratios of Xantphos and [Co<sub>2</sub>(CO)<sub>8</sub>] under hydroformylation conditions, the active catalyst was generated *in situ* under hydroformylation conditions (Table 17, entries 2-4). The addition of ligand in a 1:1 ratio with respect to [Co<sub>2</sub>(CO)<sub>8</sub>] had a great impact in the catalytic outcome (Table 17, entry 2). Interestingly, the selectivity in the formation of aldehydes **13a-d** increased up to 83% in the presence of ligand and the formation of alcohols **14a-d** was reduced (reduction in the selectivity from 26% to 10%). The regioselectivity towards linear aldehyde nonanal **13a**, the amounts of isomerized starting material and hydrogenated product **15** were not affected by the addition of ligand. Under these catalytic conditions, it was likely that both [Co(H)(CO)<sub>2</sub>(Xantphos)] and [Co(H)(CO)<sub>4</sub>] were formed in the

hydroformylation reaction mixture (Scheme 29). When the hydroformylation reaction was carried out with a 2:1 L/Co ratio (Table 17, entry 3), a decrease in the selectivity towards aldehydes (down to 76%) was observed, together with a slight increase in the amounts of unreacted isomerized alkenes (up to 6%) and hydrogenation product **15** (up to 5%). The effect of increasing the amount of ligand with respect to the cobalt precursor has an almost negligible effect in the linear to branched ratio (from l/b ratio = 77:23 with no ligand, to a l/b ratio = 73:27 with a 2:1 L/Co ratio). These results indicated that, with our catalytic conditions, regioselectivity was mainly controlled by the temperature rather than by the presence of ligand. Further ligand addition up to a 4:1 L/Co ratio (Table 17, entry 4) showed a decrease in the conversion down to 51%. In presence of an excess of ligand, isomerization of oct-1-ene **12** to internal alkenes was the most favorable process (33% selectivity). Aldehydes **13** were only obtained with a selectivity of 28%, together with hydrogenation product **15** (10%). Interestingly, no alcohols **14a-d** were observed. The lower selectivity towards aldehydes with higher L/Co ratio could be justified by assuming the coordination of more than one ligand unit to the metal center, which prevents alkene coordination.

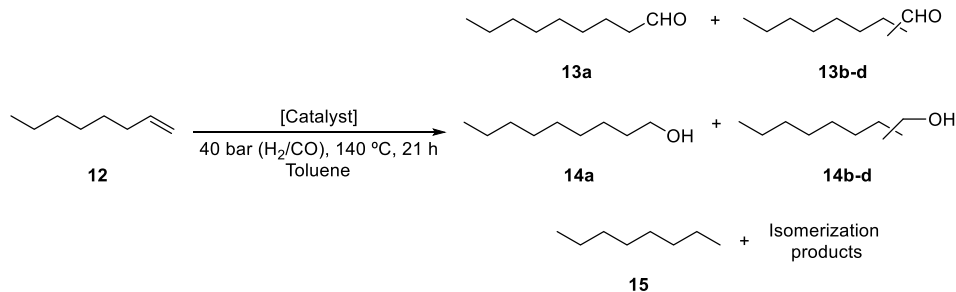
For the sake of comparison, the hydroformylation reaction of oct-1-ene **12** was carried out using complex **2** as catalyst under analogous reaction conditions (Table 17, entry 5). As in entries 1-3 in Table 17, full conversion was observed when complex **2** was employed. The selectivity towards aldehydes **13a-d** decreased to 73% using complex **2** with respect to the results obtained with *in situ* generated complex **2** (Table 17, entry 2). The generation of the catalyst *in situ* by employing a 1:1 L/Co ratio, rather than using preformed catalyst **2**, has an overall beneficial effect, as regioselectivity is not affected and the amounts of unreacted isomerized starting material are reduced in a 13%, despite the selectivity towards alcohols **14a-d** increased slightly (7%). Overall, the *in situ* generation of the catalyst by employing a 1:1 L/Co ratio can be considered the most advantageous option for hydroformylating oct-1-ene **12**. A rationale for this interesting observation is missing, as results seem to point to the presence of more than one cobalt complex when the catalyst is generated *in situ*.



**Graph 3.** Ligand/Co ratio effect in the cobalt catalyzed hydroformylation of oct-1-ene

To test the influence of the ligand in the outcome of the reaction, a comparative study between the catalytic data reported for  $[\text{Co}(\text{H})(\text{CO})_2(\text{dchpf})]^5$  and experimental data within this thesis for complex **2**  $[\text{Co}(\text{H})(\text{CO})_2(\text{Xantphos})]$  (Table 18) was done. Under similar reaction conditions (pressure, temperature, time and solvent), both cobalt complexes displayed conversions higher than 95%. Complex **2** showed a greater selectivity than  $[\text{Co}(\text{H})(\text{CO})_2(\text{dchpf})]$  (28%) towards hydroformylation products. Regioselectivity was slightly improved when Xantphos was used as ligand (amounts of nonanal **13a** were 7% higher for **2** than for  $[\text{Co}(\text{H})(\text{CO})_2(\text{dchpf})]$ ). As for rhodium hydroformylation catalysts, these results demonstrate that linear to branched ratios with cobalt catalysts increase with the magnitude of the bite angle.<sup>40</sup> When  $[\text{Co}(\text{H})(\text{CO})_2(\text{dchpf})]$  was used as catalyst, high amounts of unreacted isomerized alkenes were observed, whilst, the use of complex **2** as catalyst reduced this process by *ca.* 30%. Overall, complex **2** shows a more attractive catalytic behavior towards hydroformylation products than  $[\text{Co}(\text{H})(\text{CO})_2(\text{dchpf})]$ .

<sup>40</sup> See reference 11 for calculated natural bite angles for a range of Xantphos-type ligands and how these values correlate to product distribution in the rhodium-catalyzed hydroformylation of oct-1-ene **12**.

**Table 18.** Comparative study of [Co(H)(CO)<sub>2</sub>(dchpf)] and complex **2** as catalysts in the hydroformylation of oct-1-ene **12**

Entry	Catalyst	Conv. (%)	Selectivity				Regioselectivity 13a/13b (13a/13b/13c/13d)
			13a-d (%)	14a-d (%)	15 (%)	Isom. (%)	
1 <sup>[a]</sup>	[Co(H)(CO) <sub>2</sub> (dchpf)]	95.1	44.3	1.3	6.6	42.9	67:33 (56.7:27.7:7.3:5.4)
2 <sup>[b]</sup>	Complex <b>2</b>	>99	73	3	10	15	74:26 (64:22:8:6)

[a] Reaction conditions: The hydroformylation was performed in an AMTEC SPR16 parallel autoclave. Reaction conditions: [catalyst]= 0.99 mM; [alkene] = 1 M; stirring rate= 1000 rpm; H<sub>2</sub>/CO in a 1:1 ratio, unless otherwise cited. Conversion, l/b ratio and product distribution were determined by GC analysis on an achiral stationary phase (ChirasilDex CB). [b] Reaction conditions: The hydroformylation was performed in a HEL parallel autoclave. Reaction conditions: catalyst= 1 mol%; [alkene] = 0.26 M; stirring rate= 800 rpm; H<sub>2</sub>/CO in a 1:1 ratio, unless otherwise cited. Conversion, l/b ratio and product distribution were determined by GC analysis on an achiral stationary phase (HP-5). Selectivities were calculated as mol of compound/mol of converted substrate.

Having demonstrated that Xantphos-based cobalt catalysts are active and selective in the hydroformylation of oct-1-ene **12**, we then attempted to broaden the substrate scope to internal aliphatic alkenes with the C=C double bond at different positions and with different geometries for the double bond. These type of substrates are inherently less reactive than the analogous terminal alkenes and studies of their cobalt-catalyzed hydroformylation are scarce.<sup>4,37,41</sup> The results of this study have been summarized in Table 19.

<sup>41</sup> (a) Fell, B.; Rupilius, W.; Asinger, F. *Tetrahedron Lett.* **1968**, *9*, 3261-3266. (b) Asinger, F.; Fell, B.; Rupilius, W. *Ind. Eng. Chem., Prod. Res. Develop.* **1969**, *8*, 214. (c) Kniese, W.; Nienburg, H. J.; Fischer, R. *J. Organometal. Chem.* **1969**, *17*, 133-141. (d) Beller, M.; Krauter, J. G. E. *J. Mol. Catal. A: Chem.* **1999**, *143*, 31-39.

**Table 19.** Substrate scope of internal aliphatic alkenes **16-20** in the cobalt-catalyzed hydroformylation with Xantphos

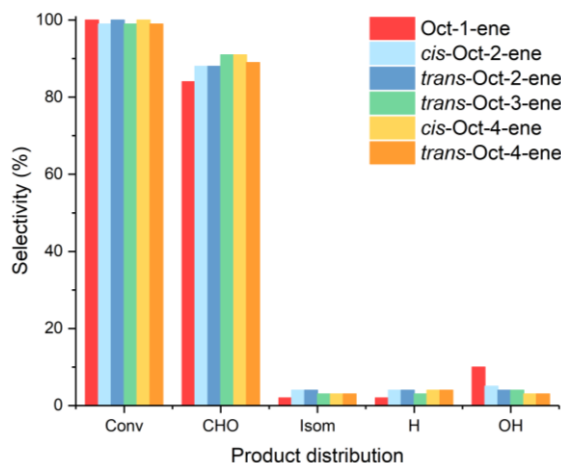
Entry	Substrate	Conv. (%) <sup>[a]</sup>	Selectivity <sup>[a]</sup>				Regioselectivity <sup>[a]</sup> 13a/13b (13a/13b/13c/13d)
			13a-d (%)	14a-d (%)	15 (%)	Isom. (%)	
1 <sup>[b]</sup>	Oct-1-ene	>99	83	10	2	2	76:24 (65:21:8:6)
2	<i>cis</i> -Oct-2-ene	99	88	5	4	4	74:26 (62:22:9:7)
3	<i>trans</i> -Oct-2-ene	>99	88	4	4	4	75:25 (62:22:9:7)
4	<i>trans</i> -Oct-3-ene	99	91	4	3	3	74:26 (60:21:10:9)
5	<i>cis</i> -Oct-4-ene	>99	91	3	4	3	74:26 (59:21:10:10)
6	<i>trans</i> -Oct-4-ene	99	89	3	4	3	75:25 (60:21:9:10)

The hydroformylations were performed in a parallel autoclave. Reaction conditions: [alkene] = 0.26 M; reaction time = 21 h, stirring rate = 800 rpm; H<sub>2</sub>/CO in a 1:1 ratio, unless otherwise cited. [a] Conversion, l/b ratio and product distribution were determined by GC analysis on an achiral stationary phase (HP-5). Selectivities were calculated as mol of compound/mol of converted substrate. [b] These results have been already shown in Table 17 but are included here for comparison.

Hydroformylation of structurally diverse octene isomers was performed under optimized catalytic conditions forming *in situ* the active catalyst (Table 19). In all cases, full conversion and high selectivities towards the aldehydes **13a-d** were observed, obtaining improved results with respect to those for terminal oct-1-ene **12**. For *cis*-oct-2-ene **16** and *trans*-oct-2-ene **17**, aldehydes **13a-d** were formed in a 88% selectivity. Side-products, such as unreacted isomerized starting material, hydrogenated product **15**, alcohol **14a** and alcohols **14b-d**, were obtained in low amounts (selectivities of 4%, 4%, 5% and 4%, respectively) (Table 19, entries 2-3). In the case of *trans*-oct-3-ene **18**, the corresponding aldehydes were obtained with a 91% selectivity, whilst the sum of all side-reactions amounted to 7% (*i.e.*, 3% selectivity towards unreacted isomerized

starting material and hydrogenated product **15** and 4% selectivity towards formation of alcohols **14a-d**). For *cis*-oct-4-ene **19** and *trans*-oct-4-ene **20** (Table 19, entry 5-6) the results were similar, with a slightly higher aldehyde selectivity for the *cis*-oct-4-ene (91%) compared to *trans*-oct-4-ene (89%). For all the octene isomers **12**, **16-20** studied, a similar product distribution of aldehydes **13a-d** was observed, being the hydroformylation of oct-1-ene **12** more regioselective toward linear aldehyde **13a** with a 76:24 l/b ratio, a 65% selectivity for **13a**, 21% selectivity for **13b**, 8% selectivity for **13c** and 6% selectivity for **13d**. It is worth mentioning that, despite the position and geometry of the unsaturation, similar regioselectivities were obtained for all studied octene isomers (linear to branched ratios ranged from 73:27 to 74:26; compare results in the regioselectivity column for all entries in Table 19).

In general terms, very high aldehyde selectivities were observed (from 83% to 91%) and low selectivities towards side-reactions (Graph 4), whose side-products were formed in similar amounts for all octene isomers, independently of the position or geometry of the C=C double bond. The selectivity towards aldehydes **13a-d** increased slightly for internal alkenes, with the highest selectivity being obtained for *trans*-oct-3-ene **18** and *cis*-oct-4-ene **19**.



**Graph 4.** Cobalt-catalyzed hydroformylation of terminal and internal octenes with Xantphos as ligand

As we previously described for oct-1-ene **12**, the use of preformed complex **2** [Co(H)(CO)<sub>2</sub>(Xantphos)] led to lower selectivities towards the aldehydes **13a-d** (selectivities ranging from 54% to 72%). The selectivity towards the formation of aldehydes was eroded due to the formation of important amounts of

hydrogenated products (up to 17% selectivity) and isomerized starting material (up to 34%). For the complete set of results, see Section 2.5.7.3.

It is interesting to point out that linear to branched ratios for all studied octene isomers remained practically constant, independently of the position or geometry of the C=C double bond in the starting material. These results led us to hypothesize that under the effects of our Xantphos-cobalt based catalyst, a tandem isomerization-hydroformylation reaction could be taking place. It is well established in the literature, that isomerization processes are favored at high temperatures. Moreover, it cannot be ruled out that alkene isomerization takes place as result of alkene coordination to the metal center following two potential isomerization pathways: (i) through alkyl complex formation and subsequent  $\beta$ -hydride elimination; or (ii) through the formation of a  $\pi$ -allyl complexes.<sup>42</sup> The rather constant linear to branched ratios observed amongst the different positional isomers and the preservation of this ratio even if the relative amounts of CO and H<sub>2</sub> in syngas were modified, led us to suggest a thermal isomerization process. In this scenario, the regioselectivity observed would directly correspond to the product distribution obtained after the isomerization processes.

In the recent years, the valorization of petrochemical feedstocks has emerged as a driving force in fundamental research with the aim of producing higher value-added products derived from petrochemicals. Researchers have found in the hydroformylation reaction a useful platform to transform unsaturated hydrocarbons into value-added products, such as aldehydes. Whilst the valorization of Raffinate II (*i.e.*, a mixture of isomeric butenes derived from Crack-C4 from naphtha steam cracking) into the corresponding aldehydes by hydroformylation is a well-established process,<sup>43</sup> the hydroformylation of C<sub>8</sub>-olefins has received less attention at the industrial scale, despite its huge economic importance.<sup>44</sup> Taking into account the similar regioselectivities observed in the hydroformylation of terminal and internal octenes with our catalyst, we envisaged using a mixture of octenes in the cobalt-catalyzed hydroformylation. For practical reasons, we prepared an equimolar mixture of all octene isomers (**12** and **16-20**) and this mixture was subjected to our optimized

---

<sup>42</sup> Molloy, J. J.; Morack, T.; Gilmour, R. *Angew. Chem., Int. Ed.* **2019**, *58*, 13654-13664.

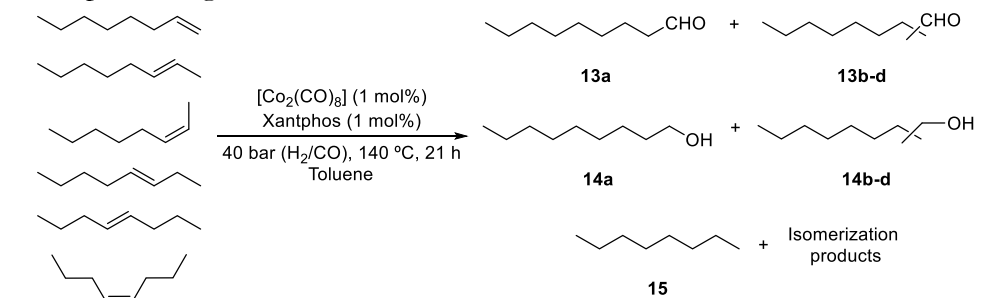
<sup>43</sup> Jones, D. S. J.; Pujadó, P. R.; *Handbook of Petroleum Processing*; Springer, Dordrecht, **2006**.

<sup>44</sup> Franke, R.; Selent, D.; Börner, A. *Chem. Rev.* **2012**, *112*, 5675-5732.



hydroformylation conditions with *in situ* formed cobalt-catalyst (140 °C, 40 bar H<sub>2</sub>/CO in 1:1 ratio, 1:1 ratio Xantphos/[Co<sub>2</sub>(CO)<sub>8</sub>], 0.26 M).

**Table 20.** Cobalt-catalyzed hydroformylation of an octene mixture using Xantphos as ligand



Entry	Substrate	Conv. <sup>[a]</sup> (%)	Selectivity <sup>[a]</sup>				Regioselectivity <sup>[a]</sup>
			13a-d (%)	14a-d (%)	15 (%)	Isom. (%)	13a/13b (13a/13b/13c/13d)
1	Octene mixture <sup>[b]</sup>	99	90	3	3	2	74:26 (61:21:9:8)

The hydroformylations were performed in a parallel autoclave. Reaction conditions: [alkene] = 0.26 M; reaction time = 21 h, stirring rate = 800 rpm; H<sub>2</sub>/CO in a 1:1 ratio, unless otherwise cited. [a] Conversion, 1/b ratio and product distribution were determined by GC analysis on an achiral stationary phase (HP-5). Selectivities were calculated as mol of compound/mol of converted substrate. [b] The mixture of octenes contained equimolecular amounts of each substrate (38.62 μmol).

The mixture of octenes was successfully hydroformylated with a high selectivity towards the formation of aldehydes **13a-d** (90%), with low final amounts of isomerized starting materials (2%), hydrogenated product **15** (3%) and alcohol derivatives **14a-d** (3%). These results are promising and could be very advantageous as a valorization tool for hydrocarbon feedstocks in the petrochemical industry.

## 2.4 CONCLUSIONS

In summary, the complex  $[\text{Co}(\text{H})(\text{CO})_2(\text{Xantphos})]$  has been efficiently synthesized and characterized for its application in the hydroformylation of styrene, oct-1-ene and a set of octene isomers. Comparative studies employing preformed catalyst  $[\text{Co}(\text{H})(\text{CO})_2(\text{Xantphos})]$  or the catalyst formed *in situ* from Xantphos and  $[\text{Co}_2(\text{CO})_8]$  indicated that higher selectivities towards the desired aldehydes were obtained with the *in situ* prepared catalyst.

For styrene, the cobalt-catalyzed hydroformylation took place with poor selectivities towards the formation of aldehydes, with the corresponding hydrogenated product being the major product being formed. Moderate linear to branched product ratios were observed (up to 59:41), taking into consideration the inherent preference of styrene to yield branched aldehydes. The regioselectivity was majorly influenced by the temperature, observing higher ratios of the linear aldehyde by increasing the temperature.

The cobalt-catalyzed hydroformylation of oct-1-ene employing Xantphos as ligand was highly selective towards aldehydes under the optimized catalytic reaction conditions (140 °C, 40 bar  $\text{H}_2/\text{CO}$  in 1:1 ratio, 1/1 ratio Xantphos/ $[\text{Co}_2(\text{CO})_8]$ , 0.26 M), with formation of side-reaction products such as hydrogenated products, unreacted isomerized starting material, and alcohol derivatives being minimized. Hydroformylation of internal octene isomers have been successfully carried out. High aldehyde selectivities were observed in all the cases, independently of the position or geometry of the C=C double bond in the starting material. Linear to branched ratios for all studied octene isomers also remained practically constant, independently of the substrate being hydroformylated. These results led us to hypothesize that under the effects of our Xantphos-cobalt based catalyst, a tandem isomerization-hydroformylation process could be taking place. Cobalt-catalyzed hydroformylation of a mixture of octenes with Xantphos as ligand, has proven to be an interesting strategy in the valorization of petroleum feedstocks with potential application at the industrial scale.

## 2.5 EXPERIMENTAL SECTION

### 2.5.1 General considerations

All syntheses were carried out using chemicals purchased from commercial sources unless otherwise cited. Air- and moisture-sensitive manipulations and hydroformylation reactions were performed under inert atmosphere, either in a N<sub>2</sub>-filled glove box or with standard Schlenk techniques. Glassware was dried *in vacuo* before use with a hot air gun. All solvents were dried and deoxygenated by using a Solvent Purification system (SPS). All solvents and reagents (liquids) have been degassed using freeze-pump-thaw cycles and stored at low temperature with activated molecular sieves (4 Å) under N<sub>2</sub> atmosphere. NMR spectra were recorded at room temperature, unless otherwise cited, in a 300 MHz, 400 MHz or 500 MHz spectrometers in CDCl<sub>3</sub>, unless otherwise noted. <sup>1</sup>H, <sup>13</sup>C{<sup>1</sup>H} and <sup>13</sup>C{<sup>1</sup>H,<sup>31</sup>P} NMR chemical shifts were quoted in ppm relative to the residual solvent peaks. <sup>31</sup>P{<sup>1</sup>H} NMR chemical shifts were quoted in ppm relative to 85% phosphoric acid in water. IR spectra were recorded using Attenuate Total Reflection (ATR) techniques unless otherwise cited. High-resolution mass spectra (HRMS) were recorded by matrix-assisted laser desorption/ionization (MALDI) method.

### 2.5.2 General structural comments on X-ray crystal of **2**

Crystals of **2** were grown by solvent diffusion, using toluene and *n*-pentane at -20 °C under inert atmosphere. The measured crystals were prepared under inert conditions and immersed in perfluoropolyether as protecting oil for manipulation.

Crystal structure determination for complex **2** was carried out using a Rigaku diffractometer equipped with a Pilatus 200K area detector, a Rigaku MicroMax-007HF microfocus rotating anode with MoK $\alpha$  radiation, confocal Max Flux optics and an Oxford Cryosystems low temperature device Cryostream 700 plus ( $T = -173$  °C). Full-sphere data collection was used with  $\omega$  and  $\varphi$  scans. *Programs used:* Data collection and reduction with CrysAlisPro<sup>45</sup> V/60A and absorption correction with Scale3 Abspack scaling algorithm.<sup>46</sup> Crystal structure solution was

<sup>45</sup> Data collection and reduction with CrysAlisPro 1.171.39.12b (Rigaku OD, 2015).

<sup>46</sup> Empirical absorption correction using spherical harmonics as implemented in Scale3 Abspack scaling algorithm, CrysAlisPro 1.171.39.12b (Rigaku OD, 2015).

achieved using the computer program SHELXT.<sup>47</sup> Visualization was performed with the program SHELXle.<sup>48</sup> Missing atoms were subsequently located from difference Fourier synthesis and added to the atom list. Least-squares refinement on  $F^2$  using all measured intensities was carried out using the program SHELXL 2015.<sup>49</sup> All non-hydrogen atoms were refined including anisotropic displacement parameters.

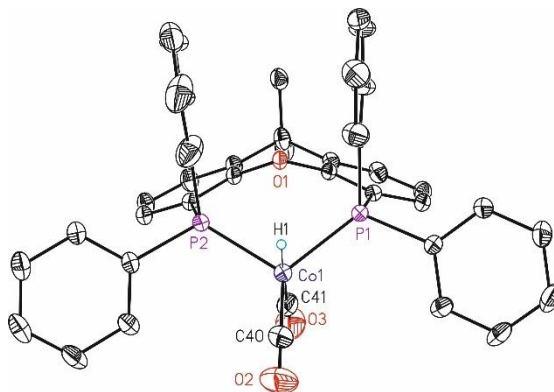


**Figure 46.** ORTEP drawing (thermal ellipsoids drawn at a 50% probability level) showing the structure of **2**. Color Scheme: C: black, H: white, Co: yellow, O: red, P: dark red. (To be deposited at the Cambridge Crystallographic Data Center, CCDC)

Comments to complex **2**: The asymmetric unit contains one molecule of the metal complex, one molecule of toluene and 0.5 molecules of pentane. The toluene molecule is disordered in three orientations with a ratio of 65:25:10. The half pentane molecule is disordered in two orientations and shared with the neighboring asymmetric unit. The hydrogen atom attached to the cobalt atom was localized from the residual electron density and refined free on its position. The Co–H distance is of 1.50(2) Å, which is in the range for the expected distance for this type of bonds (a search in the CCDC for similar structures gave distances in the range 1.39–1.58 Å).

<sup>47</sup> SHELXT; Sheldrick, G.M. *Acta Cryst.* **2015**, *A71*, 3–8.

<sup>48</sup> SHELXle; Hübschle, C.B.; Sheldrick, G.M.; Dittrich, B. *J. Appl. Cryst.* **2011**, *44*, 1281–1284.

<sup>49</sup> SHELXL; Sheldrick, G.M. *Acta Cryst.* **2015**, *C71*, 3–8.

**Table 21.** Crystal data and structural parameters for complex **2**

Compound	<b>2</b>
<b>Formula</b>	C <sub>50,50</sub> H <sub>47</sub> CoO <sub>3</sub> P <sub>2</sub>
<b>Solvent</b>	Toluene/Pentane
<b>Formula weight</b>	822.75
<b>Temperature (K)</b>	293(2)
<b>Crystal system</b>	Monoclinic
<b>Space group</b>	P2(1)/n
<b>a (Å)</b>	9.9652(3)
<b>b (Å)</b>	18.3490(5)
<b>c (Å)</b>	23.3602(9)
<b>α (°)</b>	90
<b>β (°)</b>	96.462(3)
<b>γ (°)</b>	90
<b>Volume (Å<sup>3</sup>)</b>	4244.3(2)
<b>Z</b>	4
<b>ρ (g·cm<sup>-3</sup>)</b>	1.288
<b>μ (mm<sup>-1</sup>)</b>	0.522
<b>θ<sub>max</sub> (°)</b>	34.798
<b>Reflect. collected</b>	76515
<b>Unique reflect.</b>	17442 [R(int) = 0.0548]
<b>Absorpt. correction</b>	Multi-scan
<b>Parameters/restrains</b>	678/739
<b>R1/wR2 [I&gt;2σ(I)]</b>	0.0512/0.1233
<b>R1/wR2 (all data)</b>	0.1079/0.1468
<b>Goodnes-of-fit (F<sup>2</sup>)</b>	1.009
<b>Peak/hole (e/Å<sup>-3</sup>)</b>	0.986/−0.643

**Table 22.** Bond lengths (Å) for complex **2**

Entry	Atoms	Length (Å)
1	Co1 C40	1.726(2)
2	Co1 C41	1.750(2)
3	Co1 P2	2.1899(5)
4	Co1 P1	2.1927(5)
5	P1 C16	1.8307(16)
6	P1 C22	1.8311(16)
7	P1 C2	1.8341(17)
8	P2 C28	1.8287(18)
9	P2 C12	1.8337(18)
10	P2 C34	1.8343(17)
11	O1 C13	1.3818(19)
12	O1 C1	1.3848(19)
13	O2 C40	1.156(3)
14	O3 C41	1.151(3)
15	C1 C6	1.384(2)
16	C1 C2	1.396(2)
17	C2 C3	1.399(2)
18	C3 C4	1.389(3)
19	C4 C5	1.394(3)
20	C5 C6	1.394(2)
21	C6 C7	1.532(2)
22	C7 C14	1.524(3)
23	C7 C8	1.531(2)
24	C7 C15	1.545(3)
25	C8 C13	1.386(2)
26	C8 C9	1.401(2)
27	C9 C10	1.396(3)
28	C10 C11	1.387(3)
29	C11 C12	1.401(2)
30	C12 C13	1.398(2)
31	C16 C17	1.386(2)
32	C16 C21	1.394(2)

Table 22. cont.

---

33	C17 C18	1.390(3)
34	C18 C19	1.382(3)
35	C19 C20	1.383(3)
36	C20 C21	1.388(3)
37	C22 C27	1.392(2)
38	C22 C23	1.393(3)
39	C23 C24	1.389(3)
40	C24 C25	1.384(3)
41	C25 C26	1.377(3)
42	C26 C27	1.390(3)
43	C28 C29	1.382(3)
44	C28 C33	1.398(3)
45	C29 C30	1.395(3)
46	C30 C31	1.372(4)
47	C31 C32	1.376(4)
48	C32 C33	1.382(3)
49	C34 C39	1.389(3)
50	C34 C35	1.392(2)
51	C35 C36	1.393(3)
52	C36 C37	1.380(3)
53	C37 C38	1.384(3)
54	C38 C39	1.394(3)
55	C1S C2S	1.324(7)
56	C1S C6S	1.475(7)
57	C1S C7S	1.475(7)
58	C2S C3S	1.380(7)
59	C3S C4S	1.375(6)
60	C3S C7S'	1.483(8)
61	C4S C5S	1.379(7)
62	C5S C6S	1.338(7)
63	C1S'' C2S''	1.318(8)
64	C1S'' C6S''	1.471(8)
65	C1S'' C7S''	1.484(8)

---

Table 22. cont.

---

66	C2S''	C3S''	1.382(8)
67	C3S''	C4S''	1.372(7)
68	C4S''	C5S''	1.381(8)
69	C5S''	C6S''	1.339(8)
70	C1X	C2X	1.321(8)
71	C1X	C6X	1.472(8)
72	C1X	C7X	1.480(8)
73	C2X	C3X	1.382(8)
74	C3X	C4X	1.377(8)
75	C4X	C5X	1.381(8)
76	C5X	C6X	1.339(8)
77	C1T	C2T	1.523(7)
78	C2T	C3T	1.534(7)
79	C3T	C4T	1.509(7)
80	C4T	C5T	1.559(8)

---



**Table 23** Bond angles (°) for **2**

Entry	Atoms	Angle (°)
1	C40 Co1 C41	102.41(11)
2	C40 Co1 P2	117.45(7)
3	C41 Co1 P2	99.19(7)
4	C40 Co1 P1	123.08(7)
5	C41 Co1 P1	98.77(7)
6	P2 Co1 P1	110.196(18)
7	C16 P1 C22	102.52(8)
8	C16 P1 C2	101.45(7)
9	C22 P1 C2	102.16(7)
10	C16 P1 Co1	115.24(6)
11	C22 P1 Co1	118.25(5)
12	C2 P1 Co1	114.90(5)
13	C28 P2 C12	103.60(8)
14	C28 P2 C34	101.68(8)
15	C12 P2 C34	101.04(8)
16	C28 P2 Co1	116.87(6)
17	C12 P2 Co1	115.80(6)
18	C34 P2 Co1	115.58(6)
19	C13 O1 C1	113.41(12)
20	C6 C1 O1	119.65(14)
21	C6 C1 C2	124.70(15)
22	O1 C1 C2	115.65(14)
23	C1 C2 C3	116.74(15)
24	C1 C2 P1	117.04(12)
25	C3 C2 P1	126.04(13)
26	C4 C3 C2	120.22(16)
27	C3 C4 C5	120.96(16)
28	C6 C5 C4	120.49(17)
29	C1 C6 C5	116.85(16)
30	C1 C6 C7	117.00(15)
31	C5 C6 C7	126.11(16)

Table 23. cont.

---

32	C14 C7 C8	112.24(15)
33	C14 C7 C6	111.74(16)
34	C8 C7 C6	106.34(14)
35	C14 C7 C15	109.58(16)
36	C8 C7 C15	108.22(15)
37	C6 C7 C15	108.56(14)
38	C13 C8 C9	116.85(16)
39	C13 C8 C7	117.29(15)
40	C9 C8 C7	125.82(16)
41	C10 C9 C8	120.14(17)
42	C11 C10 C9	121.23(17)
43	C10 C11 C12	120.36(16)
44	C13 C12 C11	116.58(16)
45	C13 C12 P2	117.40(12)
46	C11 C12 P2	125.74(13)
47	O1 C13 C8	119.30(14)
48	O1 C13 C12	115.91(15)
49	C8 C13 C12	124.78(15)
50	C17 C16 C21	118.54(16)
51	C17 C16 P1	119.36(13)
52	C21 C16 P1	122.10(13)
53	C16 C17 C18	120.78(18)
54	C19 C18 C17	120.45(19)
55	C18 C19 C20	119.14(17)
56	C19 C20 C21	120.60(19)
57	C20 C21 C16	120.46(17)
58	C27 C22 C23	118.19(16)
59	C27 C22 P1	123.51(14)
60	C23 C22 P1	118.30(13)
61	C24 C23 C22	120.84(18)
62	C25 C24 C23	120.23(19)
63	C26 C25 C24	119.45(18)

---

Table 23. cont.

64	C25	C26	C27	120.52(18)
65	C26	C27	C22	120.74(18)
66	C29	C28	C33	118.59(19)
67	C29	C28	P2	123.69(16)
68	C33	C28	P2	117.72(15)
69	C28	C29	C30	119.9(2)
70	C31	C30	C29	121.1(3)
71	C30	C31	C32	119.3(2)
72	C31	C32	C33	120.4(3)
73	C32	C33	C28	120.7(2)
74	C39	C34	C35	118.74(16)
75	C39	C34	P2	118.86(13)
76	C35	C34	P2	122.37(13)
77	C34	C35	C36	120.50(18)
78	C37	C36	C35	120.28(18)
79	C36	C37	C38	119.71(18)
80	C37	C38	C39	120.14(19)
81	C34	C39	C38	120.61(19)
82	O2	C40	Co1	176.6(2)
83	O3	C41	Co1	179.5(2)
84	C2S	C1S	C6S	118.9(5)
85	C2S	C1S	C7S	124.1(5)
86	C6S	C1S	C7S	117.1(5)
87	C1S	C2S	C3S	119.2(5)
88	C4S	C3S	C2S	122.8(5)
89	C4S	C3S	C7S'	116.9(7)
90	C2S	C3S	C7S'	120.3(6)
91	C3S	C4S	C5S	118.9(5)
92	C6S	C5S	C4S	119.9(5)
93	C5S	C6S	C1S	120.3(5)
94	C2S''	C1S''	C6S''	118.7(7)
95	C2S''	C1S''	C7S''	122.5(7)

Table 23. cont.

96	C6S"	C1S"	C7S"	118.5(8)
97	C1S"	C2S"	C3S"	119.9(7)
98	C4S"	C3S"	C2S"	122.3(7)
99	C3S"	C4S"	C5S"	118.5(7)
100	C6S"	C5S"	C4S"	120.5(7)
101	C5S"	C6S"	C1S"	119.9(7)
102	C2X	C1X	C6X	118.3(7)
103	C2X	C1X	C7X	123.7(9)
104	C6X	C1X	C7X	117.2(9)
105	C1X	C2X	C3X	119.8(8)
106	C4X	C3X	C2X	122.5(8)
107	C3X	C4X	C5X	118.3(8)
108	C6X	C5X	C4X	120.3(9)
109	C5X	C6X	C1X	120.3(8)
110	C1T	C2T	C3T	109.3(5)
111	C4T	C3T	C2T	111.6(6)
112	C3T	C4T	C5T	108.3(6)

**Table 24.** Torsion angles (°) for complex 2

Entry	Atoms	T. angle (°)
1	C13 O1 C1 C6	40.8(2)
2	C13 O1 C1 C2	-139.04(15)
3	C6 C1 C2 C3	2.3(3)
4	O1 C1 C2 C3	-177.83(14)
5	C6 C1 C2 P1	-173.00(13)
6	O1 C1 C2 P1	6.84(19)
7	C16 P1 C2 C1	177.58(13)
8	C22 P1 C2 C1	-76.76(14)
9	Co1 P1 C2 C1	52.58(14)
10	C16 P1 C2 C3	2.74(16)
11	C22 P1 C2 C3	108.40(15)
12	Co1 P1 C2 C3	-122.27(14)
13	C1 C2 C3 C4	-1.9(2)
14	P1 C2 C3 C4	172.96(13)
15	C2 C3 C4 C5	0.1(3)
16	C3 C4 C5 C6	1.5(3)
17	O1 C1 C6 C5	179.32(15)
18	C2 C1 C6 C5	-0.8(3)
19	O1 C1 C6 C7	1.3(2)
20	C2 C1 C6 C7	-178.85(16)
21	C4 C5 C6 C1	-1.1(3)
22	C4 C5 C6 C7	176.71(17)
23	C1 C6 C7 C14	-161.75(16)
24	C5 C6 C7 C14	20.4(3)
25	C1 C6 C7 C8	-39.0(2)
26	C5 C6 C7 C8	143.24(18)
27	C1 C6 C7 C15	77.29(19)
28	C5 C6 C7 C15	-100.5(2)
29	C14 C7 C8 C13	161.22(17)
30	C6 C7 C8 C13	38.7(2)
31	C15 C7 C8 C13	-77.73(19)
32	C14 C7 C8 C9	-20.9(3)

Table 24. cont.

33	C6 C7 C8 C9	-143.38(18)
34	C15 C7 C8 C9	100.1(2)
35	C13 C8 C9 C10	-0.2(3)
36	C7 C8 C9 C10	-178.11(18)
37	C8 C9 C10 C11	-0.9(3)
38	C9 C10 C11 C12	0.3(3)
39	C10 C11 C12 C13	1.3(3)
40	C10 C11 C12 P2	-172.46(14)
41	C28 P2 C12 C13	79.03(14)
42	C34 P2 C12 C13	-175.94(13)
43	Co1 P2 C12 C13	-50.28(14)
44	C28 P2 C12 C11	-107.23(16)
45	C34 P2 C12 C11	-2.20(17)
46	Co1 P2 C12 C11	123.46(14)
47	C1 O1 C13 C8	-41.0(2)
48	C1 O1 C13 C12	138.22(15)
49	C9 C8 C13 O1	-178.79(16)
50	C7 C8 C13 O1	-0.7(2)
51	C9 C8 C13 C12	2.0(3)
52	C7 C8 C13 C12	-179.90(16)
53	C11 C12 C13 O1	178.22(14)
54	P2 C12 C13 O1	-7.5(2)
55	C11 C12 C13 C8	-2.6(3)
56	P2 C12 C13 C8	171.73(14)
57	C22 P1 C16 C17	156.42(15)
58	C2 P1 C16 C17	-98.21(16)
59	Co1 P1 C16 C17	26.57(17)
60	C22 P1 C16 C21	-24.18(17)
61	C2 P1 C16 C21	81.20(17)
62	Co1 P1 C16 C21	-154.03(14)
63	C21 C16 C17 C18	-1.6(3)
64	P1 C16 C17 C18	177.81(17)
65	C16 C17 C18 C19	1.0(3)

Table 24. cont.

66	C17	C18	C19	C20	0.5(3)
67	C18	C19	C20	C21	-1.4(3)
68	C19	C20	C21	C16	0.7(3)
69	C17	C16	C21	C20	0.8(3)
70	P1	C16	C21	C20	-178.63(16)
71	C16	P1	C22	C27	111.06(15)
72	C2	P1	C22	C27	6.23(16)
73	Co1	P1	C22	C27	-120.98(14)
74	C16	P1	C22	C23	-68.44(15)
75	C2	P1	C22	C23	-173.27(14)
76	Co1	P1	C22	C23	59.53(15)
77	C27	C22	C23	C24	-0.4(3)
78	P1	C22	C23	C24	179.17(15)
79	C22	C23	C24	C25	1.4(3)
80	C23	C24	C25	C26	-1.2(3)
81	C24	C25	C26	C27	0.0(3)
82	C25	C26	C27	C22	1.0(3)
83	C23	C22	C27	C26	-0.8(3)
84	P1	C22	C27	C26	179.66(15)
85	C12	P2	C28	C29	-6.40(18)
86	C34	P2	C28	C29	-110.95(17)
87	Co1	P2	C28	C29	122.25(15)
88	C12	P2	C28	C33	173.95(15)
89	C34	P2	C28	C33	69.40(16)
90	Co1	P2	C28	C33	-57.40(16)
91	C33	C28	C29	C30	0.2(3)
92	P2	C28	C29	C30	-179.45(16)
93	C28	C29	C30	C31	-1.5(3)
94	C29	C30	C31	C32	1.0(4)
95	C30	C31	C32	C33	0.8(4)
96	C31	C32	C33	C28	-2.2(4)
97	C29	C28	C33	C32	1.6(3)
98	P2	C28	C33	C32	-178.69(17)

Table 24. cont.

99	C28	P2	C34	C39	-160.42(16)
100	C12	P2	C34	C39	93.02(17)
101	Co1	P2	C34	C39	-32.79(18)
102	C28	P2	C34	C35	21.36(18)
103	C12	P2	C34	C35	-85.19(16)
104	Co1	P2	C34	C35	149.00(14)
105	C39	C34	C35	C36	-0.1(3)
106	P2	C34	C35	C36	178.15(15)
107	C34	C35	C36	C37	-0.8(3)
108	C35	C36	C37	C38	0.9(3)
109	C36	C37	C38	C39	-0.2(3)
110	C35	C34	C39	C38	0.8(3)
111	P2	C34	C39	C38	-177.48(17)
112	C37	C38	C39	C34	-0.7(4)
113	C6S	C1S	C2S	C3S	1.9(11)
114	C7S	C1S	C2S	C3S	-176.4(6)
115	C1S	C2S	C3S	C4S	0.5(9)
116	C1S	C2S	C3S	C7S'	178.7(8)
117	C2S	C3S	C4S	C5S	-3.1(8)
118	C7S'	C3S	C4S	C5S	178.7(7)
119	C3S	C4S	C5S	C6S	3.0(11)
120	C4S	C5S	C6S	C1S	-0.7(17)
121	C2S	C1S	C6S	C5S	-1.8(17)
122	C7S	C1S	C6S	C5S	176.5(10)
123	C6S''	C1S''	C2S''	C3S''	-5(2)
124	C7S''	C1S''	C2S''	C3S''	168.7(15)
125	C1S''	C2S''	C3S''	C4S''	5(2)
126	C2S''	C3S''	C4S''	C5S''	-2(2)
127	C3S''	C4S''	C5S''	C6S''	-1.6(19)
128	C4S''	C5S''	C6S''	C1S''	2(2)
129	C2S''	C1S''	C6S''	C5S''	1(2)
130	C7S''	C1S''	C6S''	C5S''	-172.6(14)
131	C6X	C1X	C2X	C3X	6(6)



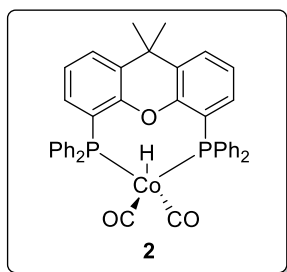
**Table 24. cont.**

---

132	C7X	C1X	C2X	C3X	176(3)
133	C1X	C2X	C3X	C4X	-7(6)
134	C2X	C3X	C4X	C5X	7(7)
135	C3X	C4X	C5X	C6X	-6(11)
136	C4X	C5X	C6X	C1X	5(12)
137	C2X	C1X	C6X	C5X	-5(7)
138	C7X	C1X	C6X	C5X	-176(6)
139	C1T	C2T	C3T	C4T	176.8(7)
140	C2T	C3T	C4T	C5T	-179.6(8)

---

### 2.5.3 Synthesis of [Co(H)(CO)<sub>2</sub>(Xantphos)] **2**



**Compound 2:** The preparation of complex **2** was performed by modifying a reported procedure in the literature.<sup>5</sup> Under argon atmosphere, [Co<sub>2</sub>(CO)<sub>8</sub>] (94.8 mg, 0.25 mmol) was dissolved in anhydrous toluene (1.7 mL) in a 2 mL vial with stirring and anhydrous DMF (869  $\mu$ L, 11.20 mmol) was added to the previous solution. After formation of a pink precipitate (*ca.* 1 h), the reaction mixture was cooled down to 0 °C and aqueous HCl (2.5 mL, 6 M, 15.00 mmol) was added at once. After stirring for 2 minutes, two phases were formed: the aqueous phase (pink) and the organic phase (yellow). The organic phase was separated under argon atmosphere at 0 °C and a solution of Xantphos (202 mg, 0.33 mmol) in anhydrous toluene (3.7 mL) was added. The reaction proceeded by CO releasing, which led to the formation of a yellow precipitate. After 5 h stirring at 0 °C, the crude mixture was stored in the freezer under N<sub>2</sub> for 2 h. The liquid and precipitate were separated, the precipitate was washed with anhydrous *n*-pentane (5 mL) and solid was dried under vacuum. Product **2** was obtained as a yellow solid (161 mg, 70% yield). IR (neat, cm<sup>-1</sup>)  $\bar{\nu}$  3057, 2956, 2928, 2861, 1917 ( $\bar{\nu}_{\text{CO}}$ ), 1910 ( $\bar{\nu}_{\text{CO}}$ ), 1586, 1479, 1433, 1404, 1358, 1307, 1227, 1180, 1154, 1118, 1091, 1068, 1026, 999, 794, 779, 748, 689, 655, 536, 509, 469, 441. <sup>1</sup>H NMR (500 MHz, CD<sub>2</sub>Cl<sub>2</sub>)  $\delta$  7.48 (dd, *J* = 7.9, 1.2 Hz, 2H), 7.36 (bs, 8H), 7.28–7.25 (m, 4H), 7.18 (t, *J* = 7.4 Hz, 8H), 7.02 (t, *J* = 7.7 Hz, 2H), 6.36–6.33 (m, 2H), 1.69 (s, 6H), –11.23 (t, *J* = 23.3 Hz, 1H) ppm. <sup>13</sup>C{<sup>1</sup>H,<sup>31</sup>P} NMR (126 MHz, CD<sub>2</sub>Cl<sub>2</sub>)  $\delta$  209.3 (2 C, CO), 155.9 (2 C, *Carom*O), 136.3 (4 C, *Carom*P), 135.5 (2 C, *Carom*C(CH<sub>3</sub>)<sub>2</sub>), 133.6 (8 C, *Carom*H), 129.7 (2 C, *Carom*H), 129.5 (4 C, *Carom*H), 128.3 (8 C, *Carom*H), 127.5 (2 C, *Carom*P), 126.2 (2 C, *Carom*H), 124.0 (2 C, *Carom*H), 37.0 (2 C, CH<sub>3</sub>), 27.1 (1 C, C(CH<sub>3</sub>)<sub>2</sub>) ppm. <sup>31</sup>P{<sup>1</sup>H} NMR (202 MHz, CD<sub>2</sub>Cl<sub>2</sub>)  $\delta$  43.4 ppm. HRMS (MALDI) *m/z* [M–2CO–H] calcd for C<sub>39</sub>H<sub>32</sub>OP<sub>2</sub> 637.1255, found 637.1270.

## 2.5.4 General procedure for the cobalt-catalyzed hydroformylation of styrene **5** and octenes **12**, **16-20**

In a glove box filled with nitrogen, Xantphos (*ca.* 2.7  $\mu\text{mol}$  in 360  $\mu\text{L}$  of toluene) and  $[\text{Co}_2(\text{CO})_8]$  (*ca.* 2.7  $\mu\text{mol}$  in 360  $\mu\text{L}$  of toluene) or  $[\text{Co}(\text{H})(\text{CO})_2(\text{Xantphos})]$  (*ca.* 2.3  $\mu\text{mol}$  in 65  $\mu\text{L}$  of toluene) were added into a 2 mL vial equipped with a magnetic stirrer. Substrate (*ca.* 230  $\mu\text{mol}$ ), dodecane (*ca.* 69  $\mu\text{mol}$ ) and additional toluene were charged to provide the desired final solution having a 0.26 M concentration of substrate. The vial was transferred into an autoclave and taken out of the glove box. The autoclave was purged three times with syngas (1:1  $\text{H}_2/\text{CO}$  ratio, at a pressure not higher than 10 bar) and, finally, the autoclave was pressurized with syngas to the desired pressure. The reaction mixture was stirred at the selected temperature (metallic block) for the selected reaction time. The reaction was cooled down to room temperature (ice bath) and the pressure was carefully released in a well-ventilated hood. Conversion, chemo- and regioselectivity of the products arising from hydroformylation reaction conditions were determined by GC analysis on an achiral stationary phase (HP-5) using dodecane as internal standard.

## 2.5.5 Determination of the conversion, chemoselectivity and regioselectivity in hydroformylation reaction mixtures

The conversion and product distribution were determined by GC analysis of the reaction mixtures.

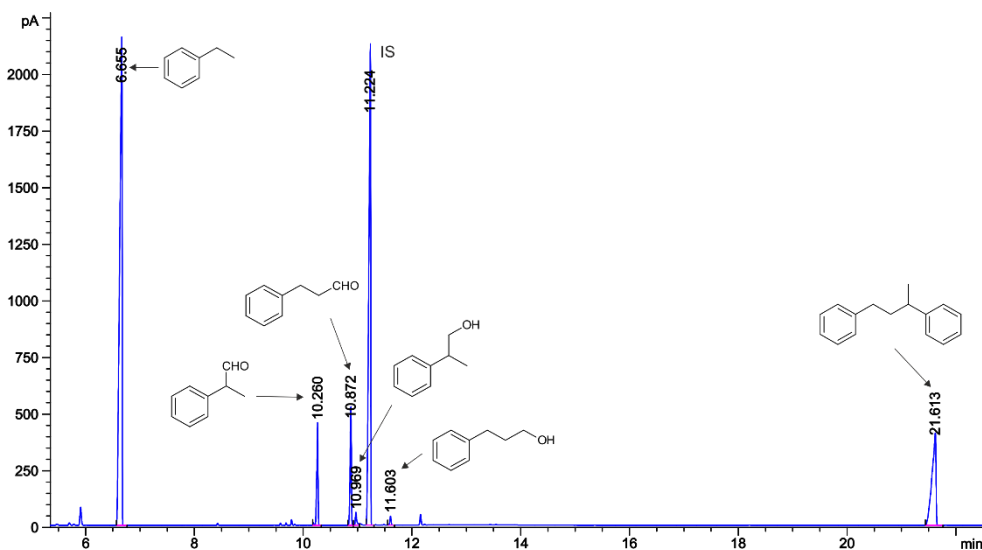
GC analysis conditions for hydroformylation reaction mixtures of styrene (**5**): Conversion, chemo- and regio-selectivity in the mixtures arising from hydroformylation reaction conditions were determined by GC-FID analysis with a HP-5 column (5% phenyl methyl siloxane; 30 m x 320  $\mu\text{m}$  x 0.25  $\mu\text{m}$ ). Flow rate: 2.3 mL/min. Temperature program: 35  $^\circ\text{C}$  for 5 min, then up to 150  $^\circ\text{C}$  at 20  $^\circ\text{C}/\text{min}$  and 10 min at 150  $^\circ\text{C}$ , then up to 320  $^\circ\text{C}$  at 20  $^\circ\text{C}/\text{min}$ . Retention times: 6.6 min for **8** (ethylbenzene), 10.3 min for **7** (2-phenylpropanal), 10.9 min for **6** (3-phenylpropanal), 10.9 min for **10** (2-phenyl-propan-1-ol), 11.2 min for IS (dodecane), 11.6 min for **9** (3-phenyl-propan-1-ol), 21.6 min for **11** (1,3-diphenylbutane).

GC analysis conditions for hydroformylation reaction mixtures of oct-1-ene (**12**), *cis*-oct-2-ene (**16**), *trans*-oct-2-ene (**17**), *trans*-oct-3-ene (**18**), *cis*-oct-4-ene (**19**) and *trans*-oct-4-ene (**20**): Conversion, chemo- and regio-selectivity in the mixtures

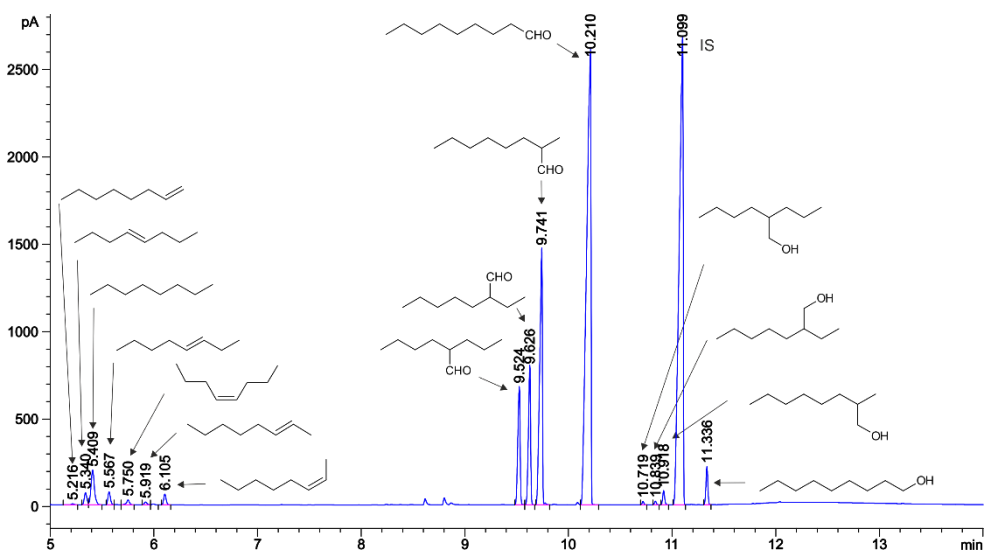
arising from hydroformylation reaction conditions were determined by GC-FID analysis with a HP-5 column (5% phenyl methyl siloxane; 30 m x 320  $\mu\text{m}$  x 0.25  $\mu\text{m}$ ). Flow rate: 2.3 mL/min. Temperature program: 35  $^{\circ}\text{C}$  for 5 min, then up to 150  $^{\circ}\text{C}$  at 20  $^{\circ}\text{C}/\text{min}$  and 10 min at 150  $^{\circ}\text{C}$ , then up to 320  $^{\circ}\text{C}$  at 20  $^{\circ}\text{C}/\text{min}$ . Retention times: 5.2 min for **5** (oct-1-ene), 5.3 min for **20** (*trans*-oct-4-ene), 5.4 min for **15** (octane), 5.6 min for **18** (*trans*-oct-3-ene), 5.7 min for **19** (*cis*-oct-4-ene), 5.9 min for **17** (*trans*-oct-2-ene), 6.1 min for **16** (*cis*-oct-2-ene), 9.5 min for **13d** (2-propylhexanal), 9.6 min for **13c** (2-ethylheptanal), 9.7 min for **13b** (2-methyloctanal), 10.2 min for **13a** (nonanal), 10.7 min for **14d** (2-propyl-hexan-1-ol), 10.8 min for **14c** (2-ethyl-heptan-1-ol), 10.9 min for **14b** (2-methyl-octan-1-ol), 11.1 min for IS (dodecane), 11.3 min for **14a** (nonan-1-ol).

## 2.5.6 Selected GC chromatograms

Representative example of a GC chromatogram of the mixtures derived from styrene **5** under cobalt-catalyzed hydroformylation reaction conditions



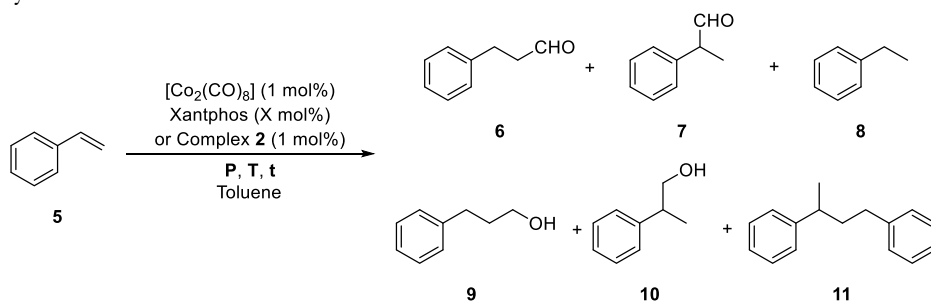
Representative example of a GC chromatogram of the mixtures derived from oct-1-ene **12** and internal octenes **16-20** under cobalt-catalyzed hydroformylation reaction conditions



## 2.5.7 Complete set of results for cobalt-catalyzed hydroformylation

### 2.5.7.1 Cobalt-catalyzed hydroformylation of styrene 5

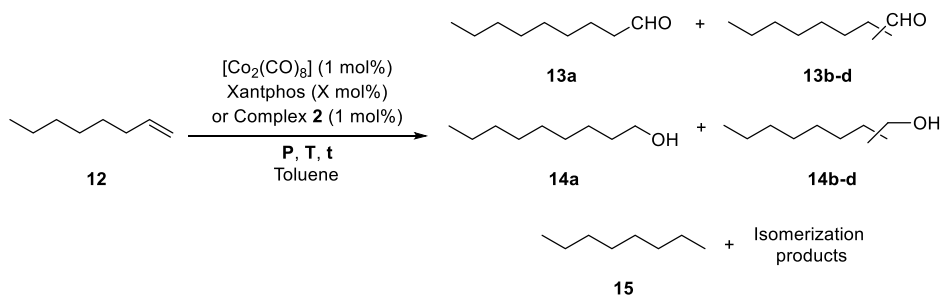
**Table 25.** Complete set of results of cobalt-catalyzed hydroformylation of styrene 5



Entry	T (°C)	Pressure (H <sub>2</sub> /CO) (bar)	L/Co ratio or Complex 2	Conv. (%) <sup>[a]</sup>	Selectivity <sup>[a]</sup>				6/7 or 1/b ratio <sup>[a]</sup>
					6 + 7 (%)	8 (%)	9 + 10 (%)	11 (%)	
1	90	40 (1:1)	2:1	12	13	13	0	8	35:65
2	110	40 (1:1)	2:1	27	19	30	0	19	45:55
3	140	40 (1:1)	2:1	>99	7	60	1	28	53:47
4	140	40 (1:3)	2:1	26	8	15	0	8	53:47
5	140	40 (1:1)	0:1	>99	14	73	4	5	59:41
6	140	40 (1:1)	1:1	>99	11	63	2	21	54:46
7	140	40 (1:1)	4:1	98	9	52	0	19 <sup>[b]</sup>	53:47
8	140	40 (1:1)	Complex 2	93	15	50	0	16	53:47

The hydroformylations were performed in a parallel autoclave. Reaction conditions: [alkene] = 0.26 M; reaction time = 21 h; stirring rate = 800 rpm. [a] Conversion, 1/b ratio and product distribution were determined by GC analysis on an achiral stationary phase (HP-5). Selectivities were calculated as mol of compound/mol of converted substrate. [b] In addition to the observation of the reductive dimerization product of two styrene units, a reductive trimerization was also observed (7% selectivity)

## 2.5.7.2 Cobalt-catalyzed hydroformylation of oct-1-ene 12

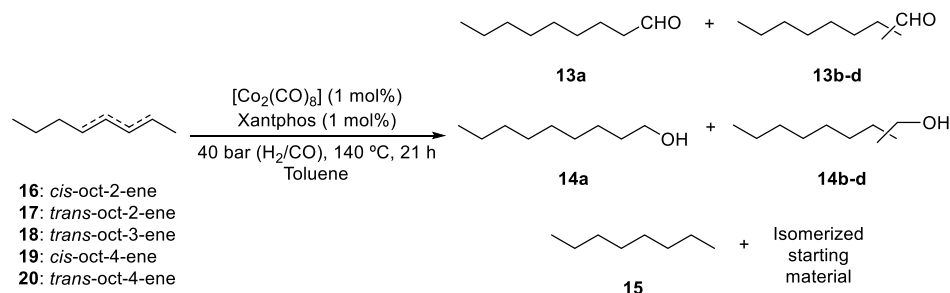
**Table 26.** Complete set of results of cobalt-catalyzed hydroformylation of oct-1-ene 12

Entry	T (°C)	Pressure (H <sub>2</sub> /CO) (bar)	L/Co ratio or Complex 2	[ ] (M)	Conv. (%) <sup>[a]</sup>	Selectivity <sup>[a]</sup>				Regioselectivity <sup>[a]</sup>
						13a-d (%)	14a-d (%)	15 (%)	Isom. (%)	13a/13b (13a/13b/13c/13d)
1	90	40 (1:1)	2:1	0.26	17	3	0	6	24	81:19 (75:18:4:3)
2	110	40 (1:1)	2:1	0.26	50	44	0	6	24	80:20 (73:18:5:4)
3	140	40 (1:1)	2:1	0.26	>99	76	9	5	6	73:27 (62:23:8:7)
4	160	40 (1:1)	2:1	0.26	>99	79	12	4	4	70:30 (56:24:11:9)
5	140	40 (1:3)	2:1	0.26	52	31	0	4	13	76:24 (68:21:6:5)
6	140	40 (1:1)	0:1	0.26	>99	70	26	2	2	77:23 (66:19:8:7)
7	140	40 (1:1)	1:1	0.26	>99	83	10	2	2	76:24 (65:21:8:6)
8	140	40 (1:1)	4:1	0.26	51	28	0	10	33	72:28 (64:26:6:4)
9	140	40 (1:1)	Complex 2	0.26	99	73	3	10	15	74:26 (64:22:8:6)
10	140	40 (1:1)	1:1	0.1	>99	84	5	3	7	75:25 (63:21:9:7)
11	140	40 (1:1)	1:1	0.5	>99	80	16	3	2	74:26 (61:21:10:8)
12	140	40 (1:1)	1:1	1	>99	67	31	0	1	69:31 (52:23:14:12)

The hydroformylations were performed in a parallel autoclave. Reaction conditions: [alkene] = 0.26 M; reaction time = 21 h; stirring rate = 800 rpm; H<sub>2</sub>/CO in a 1:1 ratio, unless otherwise cited. [a] Conversion, l/b ratio and product distribution were determined by GC analysis on an achiral stationary phase (HP-5). Selectivities were calculated as mol of compound/mol of converted substrate.

### 2.5.7.3 Cobalt-catalyzed hydroformylation of internal octenes 16-20

**Table 27.** Complete set of results of cobalt-catalyzed hydroformylation of internal alkenes 16-20

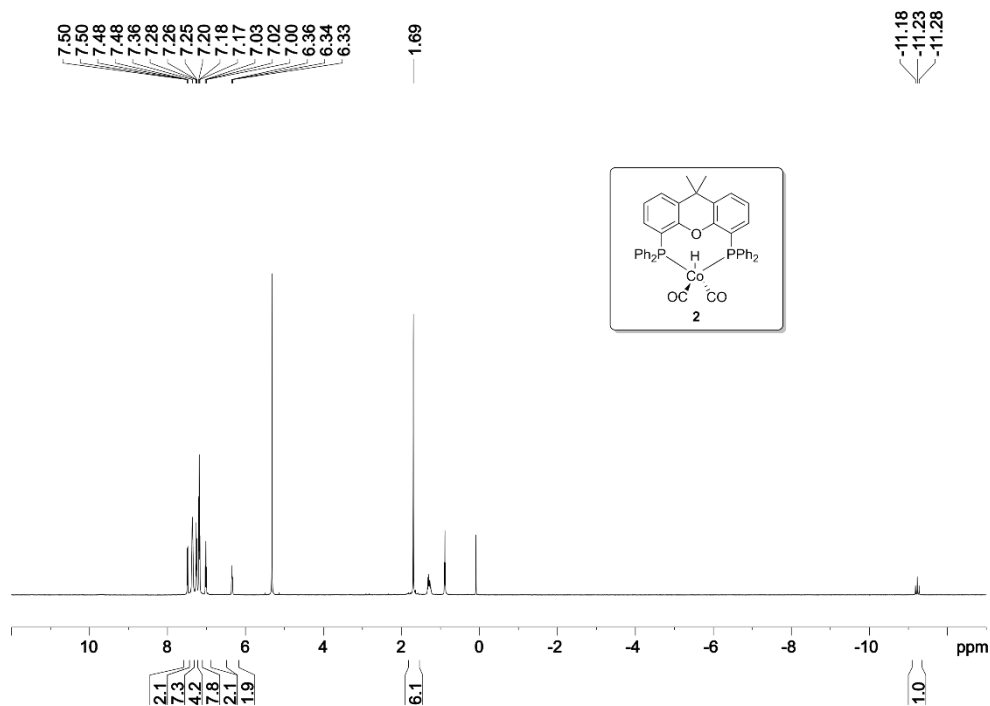


Entry	Substrate	T (°C)	Pressure (H <sub>2</sub> /CO) (bar)	L/Co ratio or Complex 2	Conv. (%) <sup>[a]</sup>	Selectivity <sup>[a]</sup>				Regioselectivity <sup>[a]</sup> 13a/13b (13a/13b/13c/13d)
						13a-d (%)	14a-d (%)	15 (%)	Isom. (%)	
1	<i>cis</i> -Oct-2-ene	140	40 (1:1)	1:1	99	89	5	4	4	74:26 (62:22:9:8)
2		140	40 (1:1)	Complex 2	99	55	1	11	34	74:26 (63:22:8:7)
3	<i>trans</i> -Oct-2-ene	140	40 (1:1)	1:1	>99	88	4	4	4	75:25 (62:22:9:8)
4		140	40 (1:1)	Complex 2	>99	58	1	11	31	74:26 (63:22:8:7)
5	<i>trans</i> -Oct-3-ene	140	40 (1:1)	1:1	99	92	4	3	3	74:26 (61:22:10:9)
6		140	40 (1:1)	Complex 2	94	72	1	18	10	73:27 (60:22:9:9)
7	<i>cis</i> -4-Oct-ene	140	40 (1:1)	1:1	>99	91	3	4	3	74:26 (59:21:10:9)
8		140	40 (1:1)	Complex 2	98	62	1	15	22	74:26 (61:21:9:9)
9	<i>trans</i> -4-Oct-ene	140	40 (1:1)	1:1	99	90	3	4	3	75:25 (60:21:10:10)
10		140	40 (1:1)	Complex 2	79	68	0	19	13	74:26 (60:21:9:10)
11	Octene mixture	140	40 (1:1)	1:1	99	91	3	3	2	74:26 (61:21:9:8)
12		140	40 (1:1)	Complex 2	93	65	1	15	17	74:26 (62:21:9:8)

The hydroformylations were performed in a parallel autoclave. Reaction conditions: [alkene] = 0.26 M; reaction time = 21 h; stirring rate = 800 rpm; H<sub>2</sub>/CO in a 1:1 ratio, unless otherwise cited. [a] Conversion, l/b ratio and product distribution were determined by GC analysis on an achiral stationary phase (HP-5). Selectivities were calculated as mol of compound/mol of converted substrate.



## 2.5.8 Collection of spectra



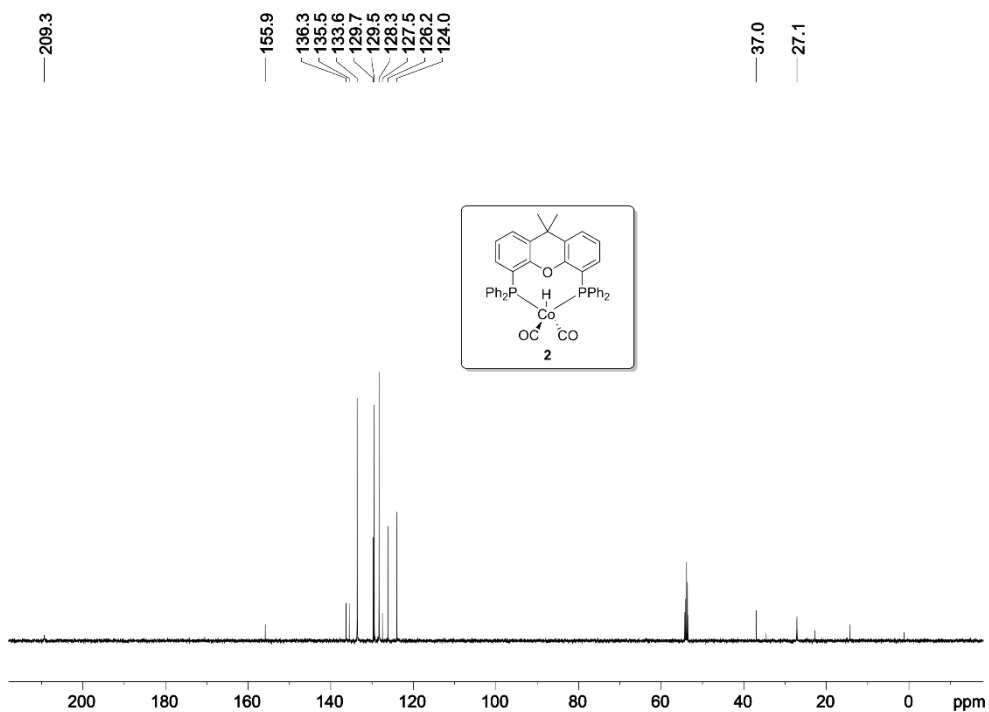


Figure 48.  $^{13}\text{C}\{^1\text{H},^{31}\text{P}\}$  NMR spectrum (126 MHz,  $\text{CD}_2\text{Cl}_2$ ) of **2**

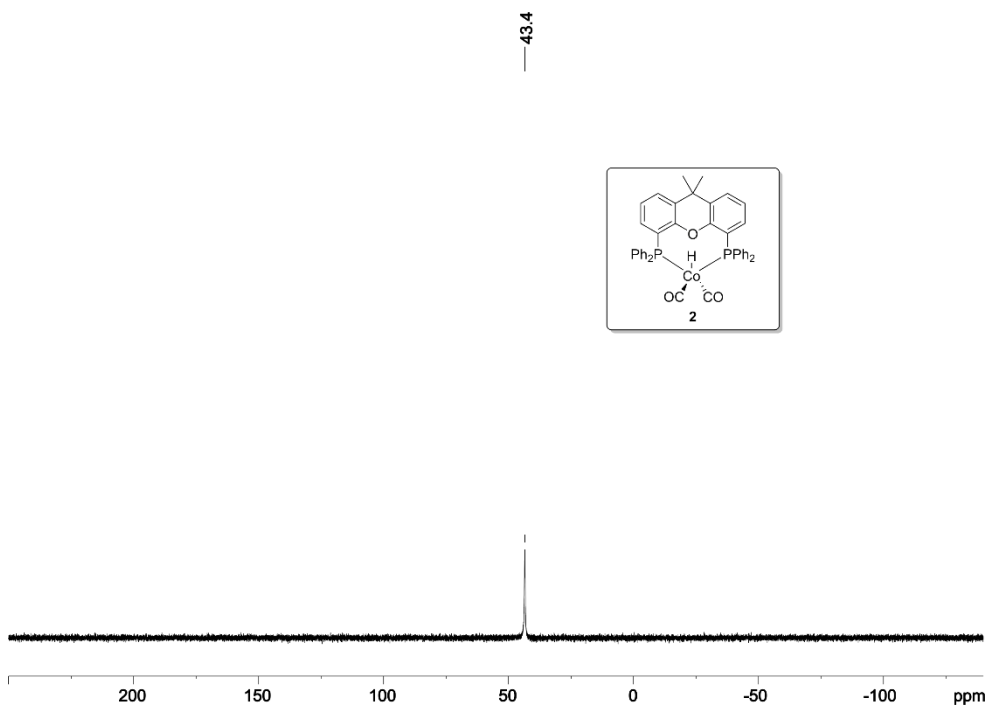


Figure 49.  $^{31}\text{P}\{^1\text{H}\}$  NMR spectrum (202 MHz,  $\text{CD}_2\text{Cl}_2$ ) of **2**

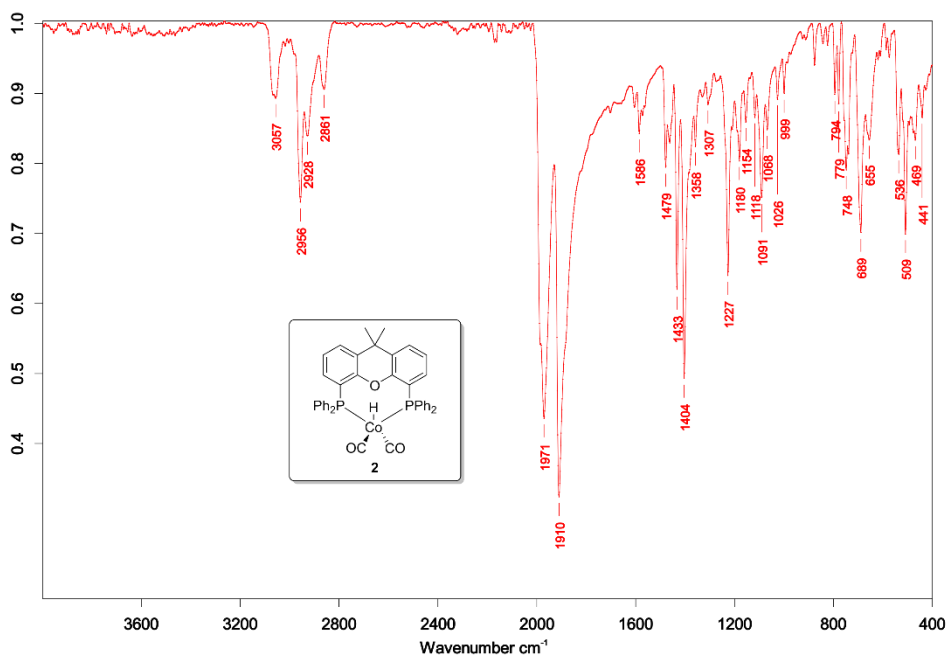


Figure 50. IR spectrum of 2

## **Chapter III**

# Enantioselective Hydroformylation of Aryl Vinyl Ethers Catalyzed by Supramolecularly Regulated Rhodium- Bisphosphite Complexes

UNIVERSITAT ROVIRA I VIRGILI

THE HYDROFORMYLATION REACTION: FROM COVALENT TO SUPRAMOLECULAR APPROACHES AND OPERANDO KINETIC STUDIES

Alicia Martínez Carrión

# Enantioselective Hydroformylation of Aryl Vinyl Ethers Catalyzed by Supramolecularly Regulated Rhodium-Bisphosphite Complexes

*(Unpublished results)*

Alicia Martínez-Carrión<sup>a,b</sup>, Antoni Frontera<sup>c</sup>, Anton Vidal-Ferran<sup>b,d\*</sup>

- a Universitat Rovira i Virgili, Departament de Química Analítica i Química Orgànica, C. Marcel·lí Domingo 1, 43007, Tarragona, Spain.
- b Institut Català d'Investigació Química (ICIQ) & Barcelona Institute of Science and Technology (BIST), Av. Països Catalans 16, 43007, Tarragona, Spain.
- c Departament de Química, Universitat de les Illes Balears, Crta. de Valldemossa km 7.5, 07122 Palma de Mallorca, Spain.
- d Institució Catalana de Recerca i Estudis Avançats (ICREA), Pg. Lluís Companys 23, 08010, Barcelona, Spain.

## 3.1 ABSTRACT

Supramolecular  $\alpha,\omega$ -bisphosphite ligands in combination with appropriate regulation agents (RA) provide conformationally adaptable rhodium complexes for the enantioselective hydroformylation of aryl vinyl ethers. Catalytic activity in terms of conversion, regio- and enantioselectivity can be optimized by the choice of the matched RA for each substrate, providing high regioselectivities and enantiomeric ratios in the final 2-aryloxypropanals. These products have found application as building blocks for the production of agrochemicals. A tentative rationalization of the stereochemical outcome of the reaction from relevant intermediates in the rhodium-based hydroformylation catalytic cycle is also provided.

## 3.2 INTRODUCTION

Enantioselective hydroformylation is an atom-economical transformation for the synthesis of valuable building blocks in an optically pure (or enantioenriched) form. The resulting aldehydes have found application in the pharmaceutical, agrochemical and fragrance industrial sectors.<sup>1</sup> Since the application of (*R,S*)-Binaphos in enantioselective hydroformylations in the early nineties (see p. 12 of the introduction),<sup>2</sup> rhodium-catalyzed enantioselective hydroformylations have been widely investigated with a set of structurally diverse phosphorus-based enantiopure ligands having been developed and employed in the hydroformylation of almost all types of olefins.

Despite numerous studies in the enantioselective hydroformylation of functionalized alkenes, there are few examples of rhodium-catalyzed hydroformylation of aryl vinyl ethers.<sup>3</sup> Studies on the use of these starting materials were mainly a side stream in the highly scrutinized hydroformylation of vinyl arenes. Optically pure 2-aryloxypropanals derived from aryl vinyl ethers are direct precursors of the corresponding 2-aryloxypropanoic acids, which are valuable agrochemicals.<sup>4</sup> First reports of enantioselective rhodium-catalyzed hydroformylation of aryl vinyl ethers employing enantiopure neomenthyl-diphenyl phosphine,<sup>5</sup> pyridyl-containing phosphine and phosphine oxide ligands,<sup>6</sup> bisphosphites or ferrocenyl-based diphosphines lacked of enantioselectivity.<sup>7</sup> Further studies employing (*S,R*)-Binaphos reported moderate catalytic activity, regio- and enantio-selectivities.<sup>8</sup>

---

<sup>1</sup> Whiteker, G. T.; Copley, C. J.; *Applications of Rhodium-Catalyzed Hydroformylation in the Pharmaceutical, Agrochemical, and Fragrance Industries*, p 35-46. In *Organometallics as Catalysts in the Fine Chemical Industry*; Beller, M.; Blaser, H.-U., Eds.; Springer-Verlag, Berlin Heidelberg, **2012**.

<sup>2</sup> Sakai, N.; Mano, S.; Nozaki, K.; Takaya, H. *J. Am. Chem. Soc.* **1993**, *115*, 7033-7034.

<sup>3</sup> (a) Lazzaroni, R.; Bertozzi, S.; Poci, P.; Troiani, F.; Salvadori, P. *J. Organomet. Chem.* **1985**, *295*, 371-376. (b) Amer, I.; Alper, H. *J. Am. Chem. Soc.* **1990**, *112*, 3674-3676. (c) Abu-Gnim, C.; Amer, I. *J. Organomet. Chem.* **1996**, *516*, 235-243. (d) Ajjou, A. N.; Alper, H. *J. Am. Chem. Soc.* **1998**, *120*, 1466-1468. (e) Marchetti, M.; Mangano, G.; Paganelli, S.; Botteghi, C. *Tetrahedron Lett.* **2000**, *41*, 3717-3720. (f) Paganelli, S.; Zanchet, M.; Marchetti, M.; Mangano, G. *J. Mol. Catal. A: Chem.* **2000**, *157*, 1-8. (g) Clark, H. J.; Wang, R.; Alper, H. *J. Org. Chem.* **2002**, *67*, 6224-6225.

<sup>4</sup> Ariëns, E. J.; van Rensen, J. J. S.; Welling, W., Eds.; *Chemicals in Agriculture, Vol. 1: Stereoselectivity of Pesticides: Biological and Chemical Problems*; Elsevier, Amsterdam, **1988**.

<sup>5</sup> Tanaka, M.; Watanabe, Y.; Yamamoto, K.; Takegami, Y. *Chem. Lett.* **1972**, 483-485.

<sup>6</sup> Basoli, C.; Botteghi, C.; Cabras, M. A.; Chelucci, G.; Marchetti, M. *J. Organomet. Chem.* **1995**, *488*, C20-C22.

<sup>7</sup> Botteghi, C.; Delogu, G.; Marchetti, M.; Paganelli, S.; Sechi, B. *J. Mol. Catal. A: Chem.* **1999**, *143*, 311-323.

<sup>8</sup> Solinas, M.; Gladiali, S.; Marchetti, M. *J. Mol. Catal. A: Chem.* **2005**, *226*, 141-147.

Among the different approaches to create libraries of enantioselective catalysts for hydroformylations,<sup>9</sup> the use of supramolecular interactions had attracted the attention of the research community in this chemistry and in other transformations of interest.<sup>10</sup> Our group has taken advantage of the supramolecular approach to catalysis and reported the enantioselective hydroformylation of vinyl esters<sup>11</sup> and heterocyclic olefins<sup>12</sup> by supramolecularly regulating the geometry of the active site of the catalyst with minimal synthetic effort. The group developed hydroformylation catalysts possessing two different structural features: a catalytic site consisting of two identical phosphorus-ligating groups and a distal regulation site containing a polyether chain. Ion-dipole interactions between the polyether chain and the regulation agent (RA; *e.g.*, alkali metal salts)<sup>13</sup> bring the ligating groups together at the metal center. Furthermore, the library of catalysts arising upon the binding of an array of RAs to the regulation site not only preserves most of the structural characteristics but also incorporates structural peculiarities that depend on the size and shape of the RA employed. The possibility to modify the geometry of the active site by addition of an external regulation agent (RA), allowed for subtle geometric changes in the catalytic site (*i.e.*, in the magnitude of the P–Rh–P bond angle), which translated into remarkable increases in the regio- and enantio-selectivity of the hydroformylation reactions under study.

Herein, we report the enantioselective hydroformylation of aryl vinyl ethers by supramolecularly regulated rhodium-catalysts to afford optically enriched 2-aryloxypropanals (Scheme 31). We also provide a tentative rationalization of the stereochemical outcome of the reaction from relevant intermediates in the rhodium-based hydroformylation catalytic cycle.

---

<sup>9</sup> For selected reviews, see: (a) Klosin, J.; Landis, C. R. *Acc. Chem. Res.* **2007**, *40*, 1251-1259. (b) Gual, A.; Godard, C.; Castellón, S.; Claver, C. *Tetrahedron: Asymmetry* **2010**, *21*, 1135-1146. (c) Fernández-Pérez, H.; Etayo, P.; Panossian, A.; Vidal-Ferran, A. *Chem. Rev.* **2011**, *111*, 2119-2176. (d) van Leeuwen, P. W. N. M.; Kamer, P. C. J.; Claver, C.; Pàmies, O.; Diéguez, M. *Chem. Rev.* **2011**, *111*, 2077-2118.

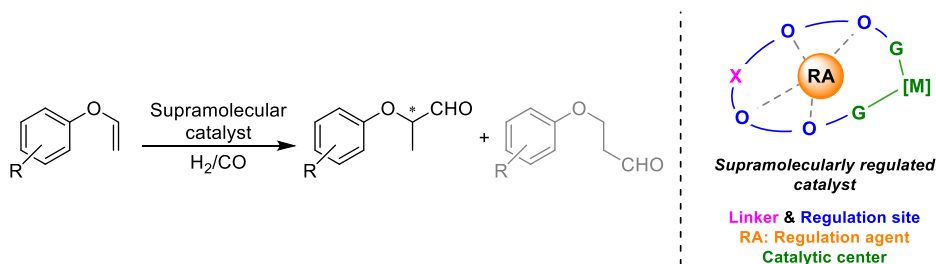
<sup>10</sup> (a) Raynal, M.; Ballester, P.; Vidal-Ferran, A.; van Leeuwen, P. W. N. M. *Chem. Soc. Rev.* **2014**, *43*, 1660-1733. (b) Vaquero, M.; Rovira, L.; Vidal-Ferran, A. *Chem. Commun.* **2016**, *52*, 11038-11051. (c) Nurttala, S. S.; Linnebank, P. R.; Krachko, T.; Reek, J. N. H. *ACS Catal.* **2018**, *8*, 3469-3488.

<sup>11</sup> (a) Mon, I.; Jose, D. A.; Vidal-Ferran, A. *Chem. - Eur. J.* **2013**, *19*, 2720-2725. (b) Vidal-Ferran, A.; Mon, I.; Bauzá, A.; Frontera, A.; Rovira, L. *Chem. - Eur. J.* **2015**, *21*, 11417-11426.

<sup>12</sup> Rovira, L.; Vaquero, M.; Vidal-Ferran, A. *J. Org. Chem.* **2015**, *80*, 10397-10403.

<sup>13</sup> Steed, J. W.; Atwood, J. L., Eds.; *Supramolecular Chemistry*, 2<sup>nd</sup> Ed.; John Wiley & Sons Ltd., Chichester, **2009**.



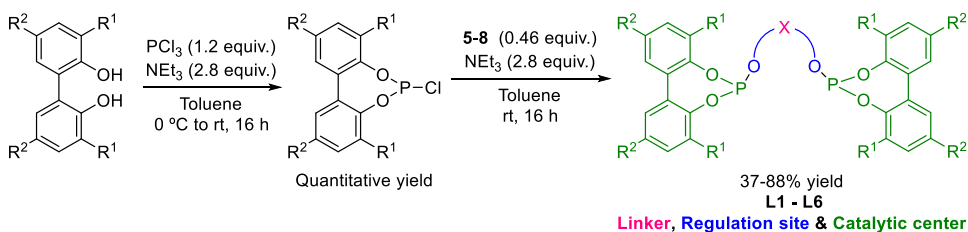


**Scheme 31.** Supramolecularly regulated enantioselective hydroformylation of aryl vinyl ethers

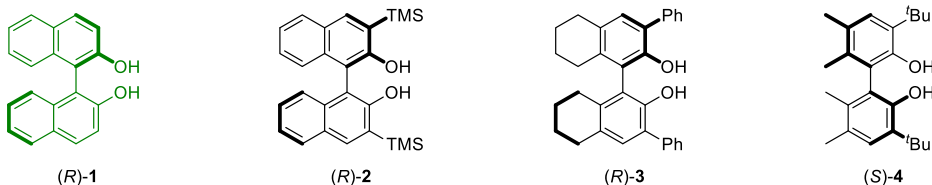
### 3.3 RESULTS AND DISCUSSION

With the aim of developing efficient supramolecularly regulated catalysts for the enantioselective hydroformylation of aryl vinyl ethers, we designed and prepared an array of diverse bisphosphite ligands. Our design was inspired in previous work of our research group, who developed supramolecularly regulated bisphosphite ligands possessing a catalytic site consisting of two identical phosphite fragments and a distal regulation site containing a polyether chain.

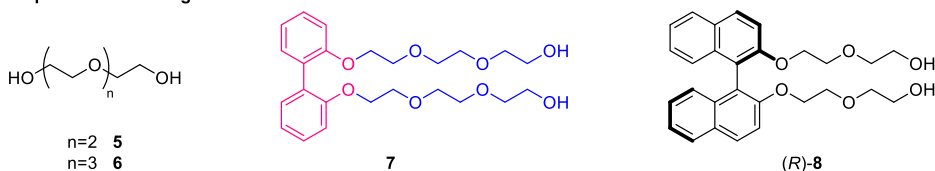
Our design aimed at combining (i) structurally diverse linkers (comprising conformationally labile or stable [1,1'-biaryl]-2,2'-diol fragments as in compounds **7** or (*R*)-**8**, respectively; Scheme 32) with polyethyleneoxy chains of different lengths for the regulation site; and (ii) phosphorus-coordinating groups in the active site derived from enantiopure bisphosphites containing [1,1'-biaryl]-2,2'-diol motifs. It is interesting to note that our ligand design encompassed the modification of the structure of the [1,1'-biaryl]-2,2'-diol-based phosphite groups by introducing substituents at the positions more prone to affecting the steric environment of the metal center (hydrogen, trimethylsilyl, phenyl and *tert*-butyl substituents at the 3 and 3' positions of the biaryl motif; Scheme 32). The presence or absence of a linker fragment in the regulation site of the target ligands was also considered to aid comparison (whilst polyethyleneoxy chains derived from **5** and **6** do not incorporate any [1,1'-biaryl]-2,2'-diol linker group, those derived from **7** and (*R*)-**8** do).



**Stereogenic [1,1'-biaryl]-2,2'-diol motifs**



**Components of the regulation site**



**Scheme 32.** General procedure for the synthesis of supramolecular bisphosphite ligands **L1-L6**

The synthesis of the required bisphosphite ligands could be straightforwardly achieved by following well-established synthetic protocols from our group or from others. For instance, whilst compounds (R)-1, (S)-4, 5 and 6 are commercially available, the synthesis of (R)-2, (R)-3 and polyethyleneoxy-containing compounds 7 and (R)-8 had already been reported in the literature.<sup>14</sup> The corresponding chlorophosphites derived from diols (R)-1, (R)-2, (R)-3 and (S)-4 were prepared following well established synthetic procedures optimized by the group.<sup>11b,12</sup> Supramolecular ligands **L1-L6** were synthesized in 37-88% yield following the general procedure indicated in Scheme 32 by *O*-phosphorylation of diols 5-7 and (R)-8 with the corresponding chlorophosphites in the presence of triethylamine as the base (Figure 51). The complete set of bisphosphite ligands synthesized within the present Thesis is shown in Figure 51.

<sup>14</sup> For details in their preparation and the corresponding references, see section 3.5.2 in the experimental section.

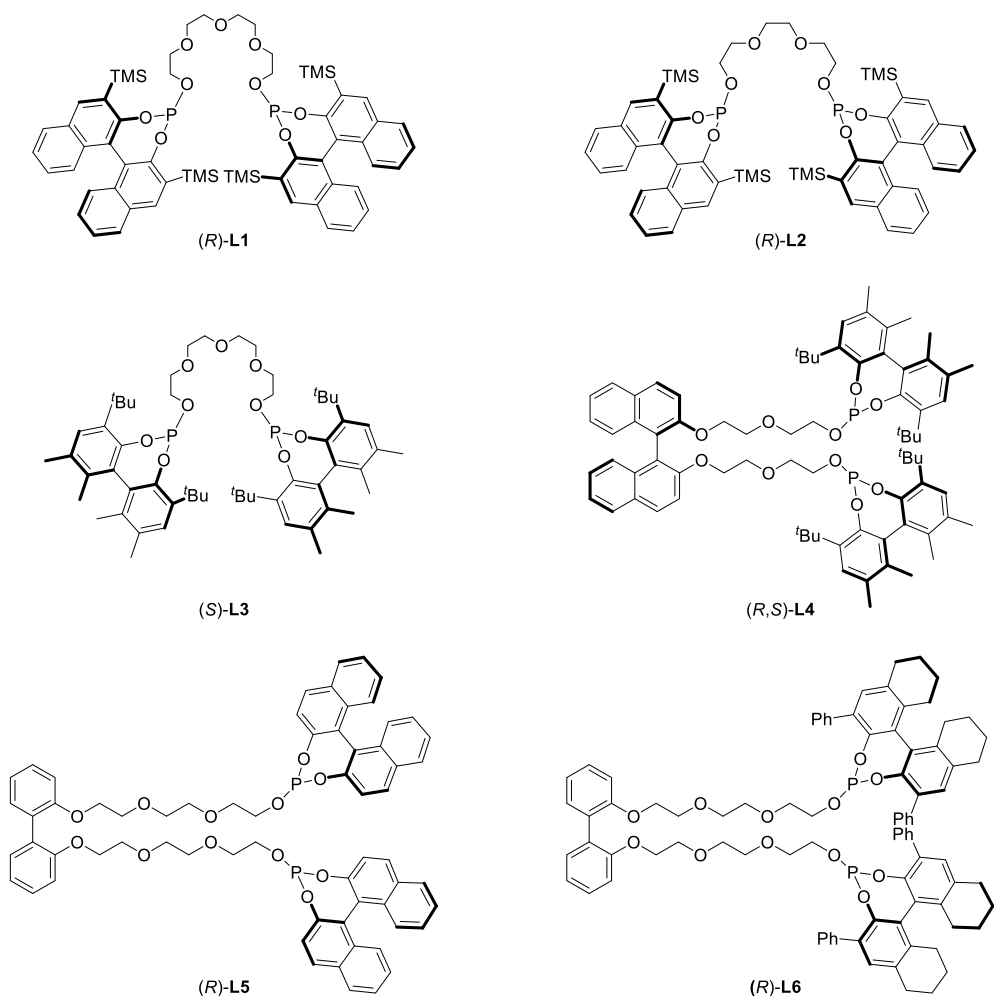


**Figure 51.** Supramolecularly regulated ligands **L1-L6** with a distal regulation site synthesized for the enantioselective hydroformylation of aryl vinyl ethers

### 3.3.1 Optimization of the hydroformylation reaction conditions

At the outset of our studies, we planned to assess the catalytic activity of the supramolecular ligands **L1-L6** with an array of RAs in the enantioselective hydroformylation of aryl vinyl ethers. For the initial studies, we chose (vinyloxy)benzene **9a** as model substrate. Our first studies focused on determining the influence of the ligand in the outcome of the reaction in terms of catalytic activity, regio- and enantio-selectivity. The substrate to catalyst ratio (S/C) was set to 100:1 (1 mol% of catalyst). The required amounts of catalyst were prepared *in situ* by mixing 1 mol% of  $[\text{Rh}(\kappa^2\text{O},\text{O}'\text{-acac})(\text{CO})_2]$  as metal precursor, a slight excess of ligand **L1-L6** (1.2 mol%) to ensure full complexation of rhodium, and a slight excess of NaBARF with respect to ligand (1.3 mol%) to

ensure quantitative formation of the supramolecular complex  $[\text{Rh}\{(\text{L1-L6})\cdot\text{NaBARf}\}]^+$ , at 10 bar syngas ( $\text{H}_2/\text{CO}$  in a 1:1 ratio), 40 °C, for 18 h and in the presence of substrate **9a** (Table 28).

Initial investigations focused on determining the influence of the length of the regulation site (Table 28, entries 1-2). To this purpose, the catalytic performance of (R)-**L1** and (R)-**L2**, which differed only in the length of the polyethyleneoxy chain, was compared. Even though a better catalytic activity in terms of conversion was observed for the ligand (R)-**L2** (70% conv., Table 28, entry 2) than for its analogue (R)-**L1** incorporating a shorter polyethyleneoxy chain (25% conv., Table 28, entry 1), similar branched to linear (b/l) ratios were observed. The enantioselectivity was the most pronounced difference between both ligands, with the longest regulation site (*i.e.*, in ligand (R)-**L1**) providing a high enantiomeric ratio (84:16 *er*).

**Table 28.** Ligand screening for the Rh-catalyzed enantioselective hydroformylation of (viniloxyl)benzene **9a**

Entry	Ligand	Conversion (%) <sup>[a]</sup>	b/l ratio <sup>[b]</sup>	<i>er</i> ( <i>S</i> : <i>R</i> ) <sup>[b]</sup>
1	(R)- <b>L1</b>	25	91:9	84:16
2	(R)- <b>L2</b>	70	89:11	61:39
3	( <i>S</i> )- <b>L3</b>	57	89:11	19:81
4 <sup>[c]</sup>	( <i>R,S</i> )- <b>L4</b>	36	> 99:1	76:24
5	(R)- <b>L5</b>	20	76:24	50:50
6	(R)- <b>L6</b>	96	99:1	88:12

The enantioselective hydroformylations were performed in a parallel autoclave. Reaction conditions: [alkene] = 0.26 M; stirring rate = 800 rpm;  $\text{H}_2/\text{CO}$  in a 1:1 ratio, unless otherwise cited. [a] Conversion was determined by using  $^1\text{H}$  NMR spectroscopy. [b] b/l ratio and *er* values were determined by GC analysis on a chiral stationary phase ( $\beta$ -Dex<sup>TM</sup> 225). [c] 6.5% of phenol was present in the reaction mixture.

Aiming to compare the effect of the bisphosphite motif, ligands with the same regulation site and different bisphosphite motifs were tested (Table 28, entries 1 and 3). The use of the 3,3'-*di-tert*-butyl-1,1'-biphenyl-2,2'-diol-containing ligand (*S*)-**L3** (Table 28, entry 3) enhanced the catalytic activity (57% conv.) when compared to that with ligand (R)-**L1** (25% conv.). The main difference was in the catalytic activity, as regioselectivities and enantiomeric ratios were similar for

both ligands (compare entries 1 and 3 in Table 28). Though the phosphite groups in ligands (*S*)-**L3** and (*R*)-**L1** are quite similar (both of them incorporate substituents at the 3 and 3' positions of the [1,1'-biaryl]-2,2'-diol-derived phosphite groups), their catalytic activities are different. These results highlight the importance of combining adequately the structures of the phosphite groups and regulation sites in the outcome of the hydroformylation reactions and led us to continue our investigations with ligands incorporating new structural motifs. First, a conformationally stable BINOL group as linker in a six oxygen-containing regulation site and the same phosphite groups as in ligand (*S*)-**L3** was considered (see the structure for the new ligand (*R,S*)-**L4** in Figure 51 and the results in catalysis in Table 28, entry 4). The modified regulation site did not improve the catalytic activity (36% conv.) or the enantiomeric ratio (76:24 *er*), but led to a perfect selectivity towards the branched aldehyde (>99:1 b/l ratio). Second, a conformationally labile [1,1'-biphenyl]-2,2'-diol group as linker in an eight oxygen-containing regulation site and phosphite groups derived from (*R*)-BINOL were considered (see the structure for the new ligand (*R*)-**L5** in Figure 51 and the results in catalysis in Table 28, entry 5). In this case, low catalytic activity (20% conv.), moderate regioselectivity (76:24 b/l ratio) and no enantioselectivity in the hydroformylation of **9a** were observed. As reported in the literature, these results confirm that substituents at the 3 and 3' positions of the [1,1'-biaryl]-2,2'-diol-derived phosphite groups have a beneficial effect in the catalytic performance, mainly in the enantioselectivity.<sup>15</sup> Finally, a third structural variation consisting of maintaining the same regulation site as in the last ligand, but incorporating phenyl groups at the 3 and 3' positions of the octahydro-[1,1'-binaphthalene]-2,2'-diol motif was considered (see the structure for the new ligand (*R*)-**L6** in Figure 51 and the results in catalysis in Table 28, entry 6). This ligand provided excellent catalytic activity (96% conv.), regioselectivity (99:1 b/l ratio) and the highest enantiomeric ratio within all ligands studied (88:12 *er*).

The design principle of our supramolecular ligands allowed for the formation of different catalytic systems by the addition of different regulation agents (RAs), with a potential modification of the geometry of the catalytic site without any further synthetic effort. Previous studies of the group showed that these changes in the geometry of the catalytic site may translate into improvements of the catalytic activity and the regio- and enantio-selectivity in the transformation under study. Consequently, we then assessed the influence of different alkali metal BArF salts as regulation agents in the enantioselective hydroformylation of

---

<sup>15</sup> (a) Franke, R.; Selent, D.; Börner, A. *Chem. Rev.* **2012**, *112*, 5675-5732. (b) van Leeuwen, P. W. N. M.; Claver, C., Eds.; *Rhodium Catalyzed Hydroformylation*; Kluwer Academic Publishers, Dordrecht, **2002**.

(vinyloxy)benzene **9a** (Table 29). In the absence of regulation agent (Table 29, entry 1), low reactivity (25% conv.), excellent regioselectivity for the branched aldehyde **10a** and moderate enantiomeric ratios (78:22 *er*) were observed. When RAs were used, the catalytic activity and regioselectivity increased in all cases.

**Table 29.** RA screening in the Rh-catalyzed enantioselective hydroformylation of (vinyloxy)benzene **9a**

Entry	RA	Conversion (%) <sup>[a]</sup>	b/1 ratio <sup>[b]</sup>	<i>er</i> ( <i>S</i> : <i>R</i> ) <sup>[b]</sup>
1	None	25	92:8	78:22
2	LiBArF	95	>99:1	92:8
3	NaBArF	96	99:1	88:12
4	KBArF	>99	98:2	85:15
5	RbBArF	88	98:2	84:16
6	CsBArF	99	98:2	79:21

The enantioselective hydroformylations were performed in a parallel autoclave. Reaction conditions: [alkene] = 0.26 M; stirring rate = 800 rpm; H<sub>2</sub>/CO in a 1:1 ratio, unless otherwise cited. [a] Conversion was determined by using <sup>1</sup>H NMR spectroscopy. [b] b/1 ratio and *er* values were determined by GC analysis on a chiral stationary phase (β-Dex™ 225).

In the case of the enantioselectivity, a strong dependence on the RA used was observed. The use of RAs with small cationic radius like LiBArF provided the highest enantiomeric ratio (92:8 *er*, Table 29, entry 2). As the ionic radius of the cationic component of the RA increased, the catalytic system became less selective and the enantiomeric ratio decreased, from 88:12 *er* with NaBArF (Table 29, entry 3) to 85:15 *er* for KBArF (Table 29, entry 4) and further down to 84:16 *er* with RbBArF (Table 29, entry 5) and 79:21 *er* with CsBArF (Table 29, entry 6). In the case of CsBArF, the catalytic results are quite similar to those observed in absence of RA, which indicates the neutral contribution of CsBArF as RA to the enantioselectivity of the reaction.

We next evaluated the effect of the amount of regulation agent under catalytic conditions. To this purpose, the amount of LiBArF was varied while the amounts of rhodium precursor and (R)-L6 were left constant. In general terms, changes in the amount of the LiBArF as RA did not affect the regioselectivity or the enantiomeric ratio of the reaction. However, these changes affected the activity of the catalytic system, with lower conversions being observed with

substoichiometric amounts of RA with respect to rhodium precursor (0.78 equiv., Table 30, entry 1). This lower reactivity was attributed to a slow rate of formation of catalytically active rhodium species, as previously observed in the absence of RA.<sup>11b</sup> Regarding the results obtained by increasing the amount of LiBARF, no significant changes in the catalytic activity and selectivity were observed employing amounts of LiBARF ranging from 1 to 3 equiv. of LiBARF with respect to rhodium precursor (Table 30, entries 2-5). However, increasing amounts of LiBARF (5 equiv.) provided a lower catalytic activity, which may be ascribed to solubility issues that hamper the homogeneous diffusion of the gas in solution.

**Table 30.** Effect of the amount of regulation agent under catalytic conditions in the Rh-catalyzed enantioselective hydroformylation of (vinylxy)benzene **9a**

Entry	RA ratio	Conversion (%) <sup>[a]</sup>	b/l ratio <sup>[b]</sup>	<i>er</i> ( <i>S</i> : <i>R</i> ) <sup>[b]</sup>
1	0.78	58	>99:1	91:9
2	1	95	>99:1	91:9
3	1.56	95	>99:1	92:8
4	2	95	>99:1	92:8
5 <sup>[c]</sup>	3	92	>99:1	92:8
6 <sup>[c]</sup>	5	82	>99:1	92:8

The enantioselective hydroformylations were performed in a parallel autoclave. Reaction conditions: [alkene] = 0.26 M; stirring rate = 800 rpm; H<sub>2</sub>/CO in a 1:1 ratio, unless otherwise cited. [a] Conversion was determined by using <sup>1</sup>H NMR spectroscopy. [b] b/l ratio and *er* values were determined by GC analysis on a chiral stationary phase (β-Dex<sup>TM</sup> 225). [c] 5% THF was used to dissolve LiBARF.

Subsequent research activities targeted the study of the effects of the reaction conditions (*i.e.*, temperature, overall pressure and H<sub>2</sub>/CO ratio) in the catalytic outcome of the reaction. With the aim of carrying out the reaction under the mildest possible reaction conditions, the effect of the overall reaction pressure was studied. Standard catalytic studies involved using 10 bar of syngas with a H<sub>2</sub>/CO 1:1 ratio (Table 31, entry 1). Lowering the overall pressure to 5 bar led to a slight decrease in the conversion (90% conv. with respect to 95% conv. at 10 bar) without the regioselectivity or the enantiomeric ratio being affected (Table 31, entry 2). It is common in enantioselective catalytic processes that lowering the reaction temperature translate into increased stereoselectivities at

the expense of a lower conversion.<sup>9a</sup> When the hydroformylation reaction of **9a** was carried out at 25 °C (Table 31, entry 3), the regioselectivity remained constant with a slight increase in the enantiomeric ratio (up to 94:6 *er*) but a very low conversion (16%, Table 31, entry 3), which could be further improved by extending the reaction time to 48 h (73% conv.; Table 31, entry 4). Interestingly, it has been reported in the literature that the enantioselectivity in the hydroformylation of (vinyloxy)benzene **9a** with Rh(I)/(*S,R*)-Binaphos-derived catalysts was eroded with increased reaction times, due to the racemization of the final aldehyde.<sup>8</sup> With our catalytic system, extended reaction times did not alter the enantiomeric ratio, which reflects the mildness of our supramolecularly regulated catalytic system.

**Table 31.** Effects of the reaction conditions in the Rh-catalyzed enantioselective hydroformylation of (vinyloxy)benzene **9a**

Entry	Pressure (H <sub>2</sub> /CO bar)	Temperature (°C)	Time (h)	Conversion (%) <sup>[a]</sup>	b/l ratio <sup>[b]</sup>	<i>er</i> ( <i>S</i> : <i>R</i> ) <sup>[b]</sup>
1	10	40	18	95	>99:1	92:8
2	5	40	18	90	>99:1	92:8
3	10	25	18	16	>99:1	94:6
4	10	25	48	73	>99:1	94:6
5 <sup>[c]</sup>	10 (9:1)	25	48	98	>99:1	93:7
6	10 (1:9)	25	48	22	>99:1	93:7

The enantioselective hydroformylations were performed in a parallel autoclave. Reaction conditions: [alkene] = 0.26 M; stirring rate = 800 rpm; H<sub>2</sub>/CO in a 1:1 ratio, unless otherwise cited. [a] Conversion was determined by using <sup>1</sup>H NMR spectroscopy. [b] b/l ratio and *er* values were determined by GC analysis on a chiral stationary phase (β-Dex™ 225). [c] 4% hydrogenated product was observed.

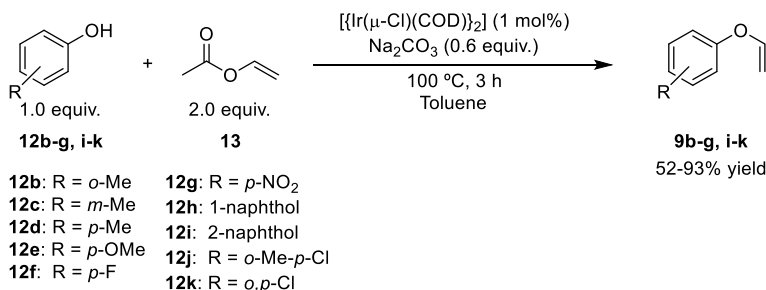
Previous reports from our group have shown that changes in the H<sub>2</sub>/CO ratio in syngas have an effect in the outcome of the hydroformylation reactions.<sup>12</sup> With our catalytic system, we observed that higher ratios of H<sub>2</sub> led to an improvement in the catalytic activity (98% conv.) with no significant changes in the regioselectivity or the enantiomeric ratio. Unfortunately, an increase in the H<sub>2</sub>/CO ratio from 1:1 to 9:1 led to the formation of noticeable amounts of hydrogenated product (4% of ethoxybenzene, Table 31, entry 5). Regarding an increase in the CO amounts, a change in the H<sub>2</sub>/CO ratio from 1:1 to 1:9 only affected the reactivity by decreasing the final conversion down to a 22%, with



the regio- or enantio-selectivity remaining constant (Table 31, entry 6). According to the literature, this behavior is due to the displacement of the phosphorus-coordinating groups by CO at the rhodium center.<sup>16</sup>

### 3.3.2 Expansion of the substrate scope of the supramolecularly regulated Rh(I)-catalyzed enantioselective hydroformylation

Having demonstrated that the highly stereoselective hydroformylation of (vinyloxy)benzene **9a** with our supramolecular regulation approach was feasible, we then attempted to broaden the substrate scope to a set of structurally diverse aryl vinyl ethers. The targeted substrates to be hydroformylated **9b-g,i-k** were synthesized by an iridium-catalyzed coupling reaction of the corresponding phenols and vinyl acetate **13** in the presence of a base (Scheme 33).<sup>17</sup> The corresponding products were isolated with moderate to excellent yields (from 52% to 93% isol. yields). For substrate **9h**, a different methodology for its synthesis was employed. For the detailed information on the synthesis of these substrates, see the section 3.5.4 in the experimental part.



**Scheme 33.** General procedure for the synthesis of aryl vinyl ethers **9b-g, i-k**

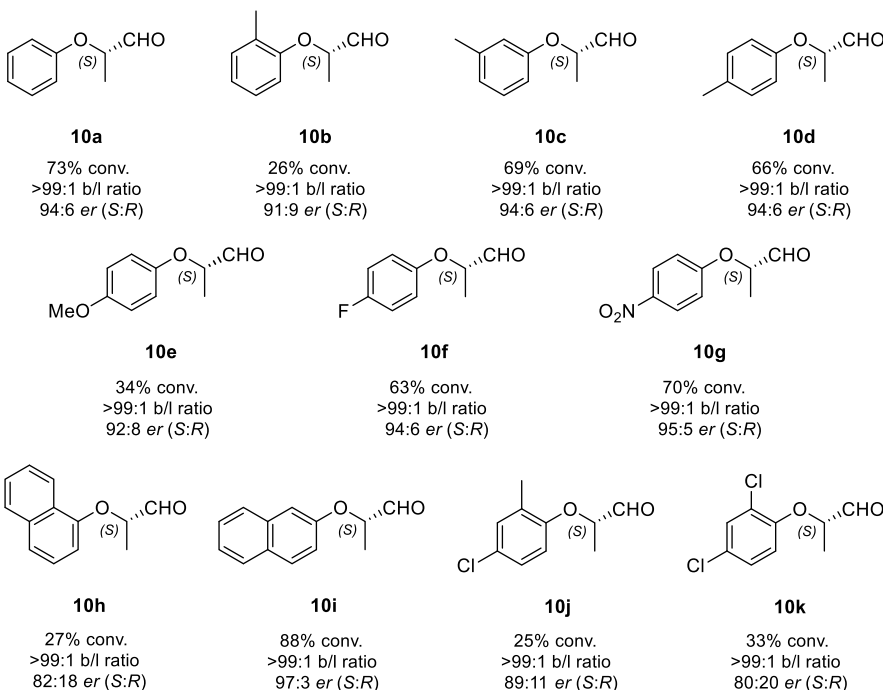
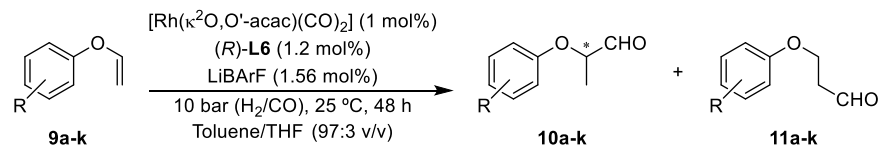
After determining optimal catalytic conditions for the hydroformylation reaction of **9a**, and having demonstrated that the use of a regulation agent remarkably improved the regio- and stereoselectivity of its enantioselective hydroformylation, we then attempted to expand our approach to the previously mentioned set of aryl vinyl ethers (Scheme 34). For each substrate, the complete set of alkali metal BARF salts was tested with the lead ligand discovered for substrate **9a** (bisphosphite (*R*)-**L6**).<sup>18</sup> The best catalytic results for **9b-k** in terms of reactivity and stereoselectivity were obtained when LiBARF was used as the regulation agent (Scheme 34). As for (vinyloxy)benzene (**9a**), the

<sup>16</sup> Börner, A. Franke, R.; *Hydroformylation: Fundamentals, Processes, and Applications in Organic Synthesis*; Wiley-VCH, Weinheim, 2016.

<sup>17</sup> Okimoto, Y.; Sakaguchi, S.; Ishii, Y. *J. Am. Chem. Soc.* **2002**, *124*, 1590-1591.

<sup>18</sup> For all the set of catalytic results, see section 3.5.9.2 in the experimental part.

hydroformylation of aryl vinyl ethers **9b-k** in the absence of a regulation agent provided poor catalytic activities (up to 24% conv. at best), high regioselectivities (from 89:11 to >99:1 b/l ratio) and moderate enantiomeric ratios (from 57:43 *er* to 85:15 *er*).



**Scheme 34.** Expansion of the substrate scope of the supramolecularly regulated Rh-catalyzed enantioselective hydroformylation

The activity of the catalyst towards substrate **9b**, which incorporates a methyl substituent at the *ortho* position, decreased dramatically if compared with the analogous substrates bearing substituents at the *meta* (**9c**) and *para* (**9d**) positions. Thus, clear steric effects in the activity of the catalysts towards the positional isomers of methyl-substituted (vinyloxy)benzenes **9b-d** were observed (conversions for the *ortho*, *meta* and *para*-substituted isomers were 26%, 69% and 66%, respectively). Regioselectivity was not affected by steric factors and the enantiomeric ratio decreased slightly for the *ortho* isomer **9b** (from 94:6 *er* for the *meta* or *para* isomers to 91:9 *er* for the *ortho* isomer **9b**). Electronic effects were assessed by introducing electron donating (ED) or electron withdrawing (EW)

groups at the *para* position of the aromatic ring. Best catalytic results were obtained for the unsubstituted compound **9a**. The presence of strongly donating groups, as in 1-methoxy-4-(vinyl)benzene **9e**, led to a decrease in the reaction reactivity, with a 34% conv. Weakly donating or withdrawing groups, like the *para*-methyl or *para*-fluoro substituents in substrates **9d** or **9f**, respectively, did not affect the reactivity and behaved similarly (66% and 63 % conv., respectively). The presence of strong withdrawing groups, as in 1-nitro-4-(vinyl)benzene **9g**, affected the activity of the catalyst (70% conv. in 24 h, compared to 73% conv. in 48 h for **9a**). As previously observed in positional aryl vinyl ether isomers, the regioselectivity was not affected by the electronic nature of the substituents (*er* ranged from 92:8 to 95:5).

After investigating steric and electronic effects in the supramolecularly regulated hydroformylation of aryl vinyl ethers, we broadened our study to their naphthyl-substituted analogues. Enantioselective hydroformylation of 1-(vinyl)naphthalene **9h** proceeded with low conversion (27% conv.), even in combination with all alkali metal BArF salts as RAs.<sup>18</sup> Excellent regioselectivity and moderate enantiomeric ratio (82:18 *er*) were observed with LiBArF. It is noteworthy to mention that for this substrate a great enhancement in the enantiomeric ratio was observed when LiBArF was used as RA (from an enantiomeric ratio of 57:43 to 82:18). Aldehyde **10h** is a synthetic intermediate of Napropamide, a commercially available herbicide with different bioactivity for each enantiomer (Figure 52).<sup>19</sup> A different behavior was observed for 2-(vinyl)naphthalene **9i**. High catalytic activity (88% conv.), excellent regioselectivity (>99:1 b/l ratio) and enantiomeric ratio (97:3 *er*) were displayed when LiBArF was used as the regulation agent.

Aryloxypropanoic acids are well-known for their herbicide properties.<sup>20</sup> With the aim of expanding this methodology to the synthesis of biologically relevant molecules in agro sciences, the hydroformylation of 4-chloro-2-methyl-1-(vinyl)benzene **9j** and 2,4-dichloro-1-(vinyl)benzene **9k** were studied. The hydroformylation products of these substrates can be considered advanced synthetic intermediates of Mecoprop (*i.e.*, 2-(2-methyl-4-chlorophenoxy)-propanoic acid) and Dichloroprop (*i.e.*, 2-(2,4-dichlorophenoxy)-propanoic acid) (Figure 52), which could be straightforwardly obtained by oxidation of the hydroformylation products.

<sup>19</sup> Qi, Y.; Liu, D.; Zhao, W.; Liu, C.; Zhou, Z.; Wang, P. *Pestic Biochem Physiol* **2015**, *125*, 38-44.

<sup>20</sup> Schmitzer, P.; Epp, J.; Gast, R.; Lo, W.; Nelson, J.; *Herbicidal Carboxylic Acids as Synthetic Auxins*; p 281-292. In *Bioactive Carboxylic Compound Classes Pharmaceuticals and Agrochemicals*; Lamberth, C.; Dinges, J., Eds.; Wiley-VCH, Weinheim, **2016**.

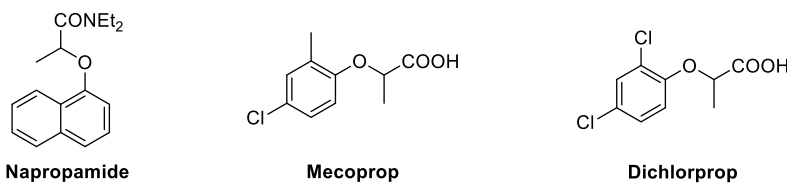
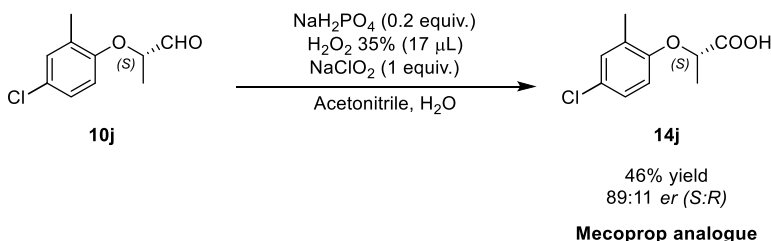


**Figure 52.** Napropamide, Mecoprop and Dichlorprop, an example of herbicides based on aryloxypropanoic acid

The hydroformylation of substrates **9j** and **9k** proceeded with excellent regioselectivities (>99:1 b/l ratio) and moderate enantiomeric ratios (89:11 *er* and 80:20 *er* for **9j** and **9k**, respectively), but low conversions (25% conv. for **9j** and 33% conv. for **9k**) as expected for *ortho*-substituted (vinyl)benzene derivatives. To overcome the low conversion in the hydroformylation of *ortho*-substituted substrates, higher catalyst loadings were used (3 mol%) with considerable enhancements in the conversion: **9j** (60% conv.) and **9k** (65% conv.).<sup>21</sup> No appreciable influence in the regioselectivity and enantioselectivity due to the higher catalyst loadings was observed.<sup>18</sup>

With the aim of completing the total synthesis of Mecoprop's enantiomer, the hydroformylation reaction mixture of **10j** was directly oxidized to the corresponding carboxylic acid in 46% isolated overall yield employing sodium chlorite as oxidizing agent.<sup>22</sup>



**Scheme 35.** General procedure for the oxidation of 2-aryloxypropanal to the corresponding 2-aryloxypropanoic acids derivatives

<sup>21</sup> The use of 3 mol% of catalyst also led to enhancements in the yield of the hydroformylations of all substrates showing moderate reactivity with 1 mol% of catalyst: **9b** (57% conv.), **9e** (70% conv.), **9f** (91% conv.) and **9h** (62% conv.).

<sup>22</sup> For experimental details of the oxidation of 2-aryloxypropanals to 2-aryloxypropanoic acid derivatives, see section 3.5.6 in the experimental part.

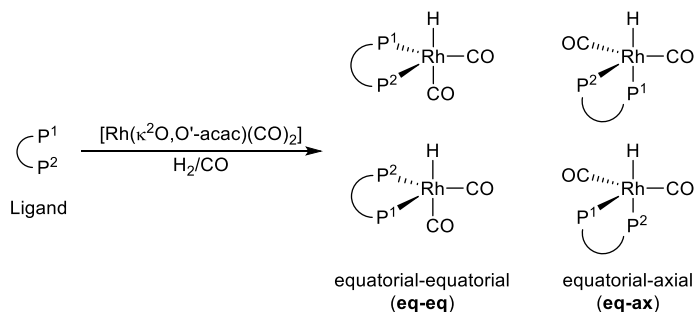
Our supramolecularly regulated hydroformylation catalyst rendered the target products with an excellent regiocontrol towards the formation of branched aldehydes and good stereocontrol towards the *S*-configured derivatives **10a-k**.<sup>23</sup>

### 3.3.3 Studies in the *in situ* formation of supramolecular Rh(I)-complexes derived from ligand (*R*)-L6 and mechanistic studies

#### 3.3.3.1 Complexation studies

After having studied the enantioselective hydroformylation of aryl vinyl ethers with supramolecular ligand (*R*)-L6 and the effects of the regulation agent in the catalytic activity and selectivity, we performed coordination and mechanistic studies in order to gain insights into the catalytic process.

It has been widely studied that phosphorus bidentate ligands under syngas atmosphere react with rhodium complex  $[\text{Rh}(\kappa^2\text{O},\text{O}'\text{-acac})(\text{CO})_2]$  to form the corresponding hydrido dicarbonyl rhodium(I) complexes  $[\text{Rh}(\text{H})(\text{CO})_2(\text{P}^1\text{-P}^2)]$ . These neutral complexes are considered one of the resting states in the hydroformylation mechanism (see page 13 in the introduction).<sup>15b</sup> These complexes display a bipyramidal trigonal geometry around the metal center. The different coordination modes of the bidentate phosphorus ligands within a pentacoordinate geometry may lead to the formation of different stereoisomeric complexes (Scheme 36).



**Scheme 36.** Coordination modes of bidentate phosphorus ligands in hydrido dicarbonyl rhodium(I) complexes

In order to study the formation of catalytically relevant species in our supramolecularly regulated hydroformylation process and elucidate their structure, complexation experiments were carried out between the lead ligand

<sup>23</sup> The majority of this work was developed before elucidating the absolute configuration of the hydroformylation products. For that reason, the results herein presented lead to the (*S*)-configured products, despite the active herbicides being the (*R*) enantiomers.

(R)-**L6** and the standard rhodium precursor for this chemistry ( $[\text{Rh}(\kappa^2\text{O},\text{O}'\text{-acac})(\text{CO})_2]$ ). As an initial complexation experiment, hydroformylation reaction conditions between all components were assayed but in the absence of substrate. To this purpose, stoichiometric amounts of  $[\text{Rh}(\kappa^2\text{O},\text{O}'\text{-acac})(\text{CO})_2]$ , (R)-**L6** and LiBArF were mixed in toluene-*d*<sub>8</sub>/THF-*d*<sub>8</sub> (97:3 v/v) and transferred to a reactor. The reactor was pressurized with 10 bar of syngas (1:1 ratio of H<sub>2</sub>/CO), heated at 40 °C and stirred for 16 h.<sup>24</sup> The solution was then transferred to a high-pressure NMR tube, which was pressurized to 10 bar syngas.

<sup>31</sup>P NMR showed the presence of three set of signals (Figure 53). The upfield signals observed as a doublet at 127.7 ppm ( $^1J_{\text{Rh-P}} = 181.9$  Hz) were assigned to the complex  $[\text{Rh}(\kappa^2\text{O},\text{O}'\text{-acac})(\kappa^2\text{P},\text{P}'\text{-}\{((\text{R})\text{-L6})\cdot\text{LiBArF}\})]$  (Table 32, entry 4). Analogous rhodium complexes, which were formed by displacement of the CO groups in the initial rhodium precursor by the phosphorus groups, had been previously described as intermediates that evolved to the corresponding hydrido dicarbonyl complexes under syngas atmosphere.<sup>25</sup> To confirm the previous assumption, the experiment was repeated under inert atmosphere.<sup>26</sup> In the IR spectrum in solution under N<sub>2</sub>, the two CO stretching bands observed in  $[\text{Rh}(\kappa^2\text{O},\text{O}'\text{-acac})(\text{CO})_2]$  at 2081 and 2011 cm<sup>-1</sup> disappeared due to the displacement of the CO ligands. This observation was in agreement with the proposed structure for this complex as  $[\text{Rh}(\kappa^2\text{O},\text{O}'\text{-acac})(\kappa^2\text{P},\text{P}'\text{-}\{((\text{R})\text{-L6})\cdot\text{LiBArF}\})]$ . Moreover, <sup>31</sup>P NMR analysis showed the same spectral data for the experiment under inert atmosphere and those for the upfield signals in the experiment under syngas atmosphere (Figure 53).

<sup>24</sup> For experimental details, see section 3.5.10.1 in the experimental section.

<sup>25</sup> (a) van Rooy, A.; Kamer, P. C. J.; van Leeuwen, P. W. N. M.; Goubitz, K.; Fraanje, J.; Veldman, N.; Spek, A. L. *Organometallics* **1996**, *15*, 835-847. (b) Kubis, C.; Ludwig, R.; Sawall, M.; Neymeyr, K.; Börner, A.; Wiese, K.-D.; Hess, D.; Franke, R.; Selent, D. *ChemCatChem* **2010**, *2*, 287-295.

<sup>26</sup> For the experimental details and spectra, see section 3.5.10.1 and 3.5.10.3, respectively, in experimental section.

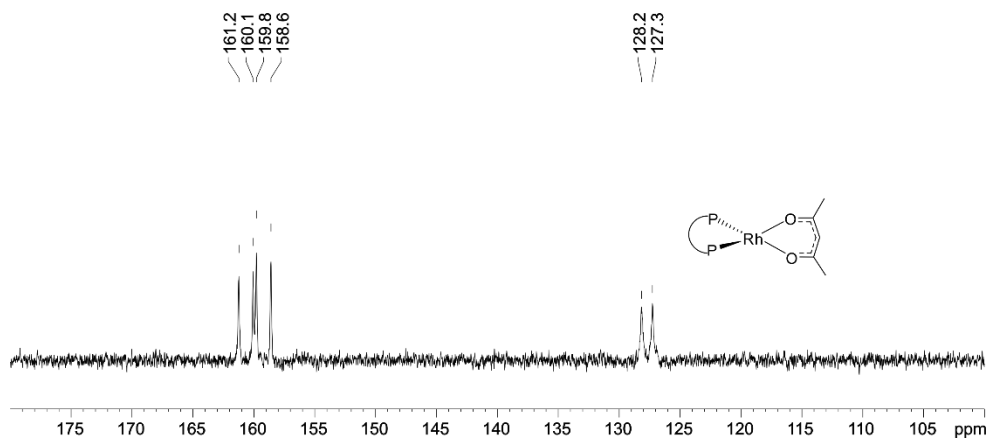


**Figure 53.** High-pressure  $^{31}\text{P}$  NMR spectrum of  $[\text{Rh}(\kappa^2\text{O},\text{O}'\text{-acac})(\text{CO})_2]$ ,  $(R)\text{-L6}$  and  $\text{LiBArF}$  (202 MHz, 10 bar  $\text{H}_2/\text{CO}$ , 25 °C, toluene- $d_8$ /THF- $d_8$  (97:3 v/v))

The second and third group of signals observed in the  $^{31}\text{P}$  NMR of the initial complexation experiment (Figure 53) were observed downfield and were described as a doublet at 160.6 ppm ( $^1J_{\text{Rh-P}} = 234.1$  Hz) and a second doublet at 159.2 ppm ( $^1J_{\text{Rh-P}} = 241.5$  Hz) with similar intensities (Table 32, entries 5 and 6). The analysis of the multinuclear NMR data was in agreement with a bidentate coordination mode for the bisphosphite and formation of hydrido dicarbonyl complexes  $[\text{Rh}(\text{H})(\text{CO})_2(\kappa^2\text{P},\text{P}'\text{-}\{(R)\text{-L6}\}\bullet\text{LiBArF})]$ . The presence of two different doublets made us consider a few options: (i) more than one bidentate coordination mode was present and the observed spectra corresponded to a mixture of different stereoisomers (Scheme 36); (ii) upon coordination to a pentacoordinate metal center, the two non-equivalent P-groups in ligand  $(R)\text{-L6}$  exhibited distinct chemical shifts; (iii) the regulation agent is not simultaneously bound to all oxygen-coordination sites, with molecular movements inside the metallacrown ether motif and  $\text{LiBArF}$  migration being possible; and (iv) the metallacrown derivative existed as a non-equilibrating mixture of conformers and  $\text{LiBArF}$  was bound to both conformers.

The first hypothesis, suggesting the presence of an equilibrium between eq-eq and eq-ax coordination modes (see Scheme 36) was ruled out, on the basis of a comparative analysis between the expected and observed magnitudes of the  $^1\text{H}\text{-}^{31}\text{P}$  and  $^{31}\text{P}\text{-}^{31}\text{P}$  coupling constants for the different stereoisomers. For instance, the coordination of a phosphite moiety in an axial position leads to a large coupling constant with the axial hydrido ligand through two bonds ( $^2J_{\text{P-H}} > 150$  Hz),<sup>27</sup> which was not observed. As indicated in Table 32 (entries 5 and 6), no proper splitting of the corresponding  $^{31}\text{P}$  signals due to their coupling with the

<sup>27</sup> Diebolt, O.; van Leeuwen, P. W. N. M.; Kamer, P. C. J. *ACS Catal.* **2012**, *2*, 2357-2370.

hydrido ligand was observed. This feature points to an equatorial coordination mode for the two P-groups, as for these geometries the coupling process between the phosphorus and hydrido nuclei often translates just into a broadening of the signals.<sup>27</sup>

The second hypothesis, suggesting that the two phosphite groups in ligand (R)-**L6** would have different chemical shifts once coordinated, was also considered to be unlikely after performing variable temperature NMR studies. The NMR spectra at temperatures ranging from 25 °C to –60 °C did not show any major changes, such as signal splitting and only differed in the width of the signals. Scalar P–P coupling between non-equivalent phosphorus nuclei should translate into splitting of the signals in the <sup>31</sup>P NMR spectrum, as previously observed for other bisphosphite ligands (<sup>2</sup>J<sub>P–P</sub> ≈ 247.0–277.6 Hz).<sup>28</sup> Such signal splitting was not the case in our rhodium complexes, which led us to rule out the second hypothesis.

<sup>1</sup>H NMR showed two different hydrido signals, both as broad signals of equal intensity centered at –11.13 and –11.21 ppm with a width at half height ≈ 20.3 and 19.3 Hz, respectively (Table 32, entries 5 and 6). The broadness of the signals, the lack of proper signal splitting and the magnitudes of the expected coupling constants (all <sup>1</sup>J<sub>Rh–H</sub> and <sup>2</sup>J<sub>P–H</sub> should be much lower than *ca.* 20 Hz)<sup>29</sup> seemed to indicate that each signal in the hydride region of the <sup>1</sup>H NMR spectrum could belong to a different rhodium complex undergoing its own fluxional processes.

---

<sup>28</sup> Buisman, G. J. H.; van der Veen, L. A.; Klootwijk, A.; de Lange, W. G. J.; Kamer, P. C. J.; van Leeuwen, P. W. N. M.; Vogt, D. *Organometallics* **1997**, *16*, 2929–2939.

<sup>29</sup> The large Rh–P and small P–H coupling constant point to an equatorial-equatorial coordination of the bisphosphite ligand to a trigonal-bipyramidal rhodium center with the hydrido ligand in the apical position. For reported examples in the literature, see: Chikkali, S. H.; van der Vlugt, J. I.; Reek, J. N. H. *Coord. Chem. Rev.* **2014**, *262*, 1–15.



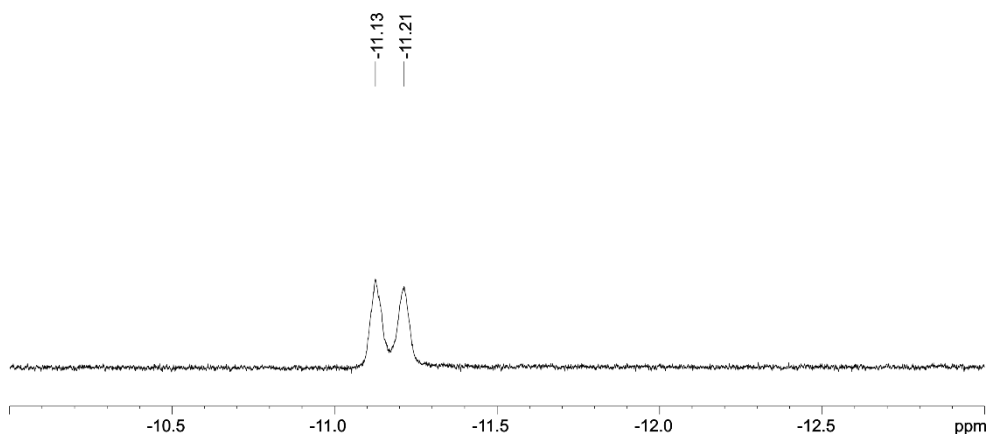


**Figure 54.** High-pressure  $^1\text{H}$  NMR spectrum of  $[\text{Rh}(\kappa^2\text{O},\text{O}'\text{-acac})(\text{CO})_2]$ , (R)-**L6** and LiBArF (202 MHz, 10 bar  $\text{H}_2/\text{CO}$ , 25 °C, toluene- $d_8$ /THF- $d_8$  (97:3 v/v))

$^1\text{H}$ - $^{31}\text{P}$  HMBC spectroscopy confirmed two different P–H couplings, due to the presence of two different cross-peaks (Figure 55).

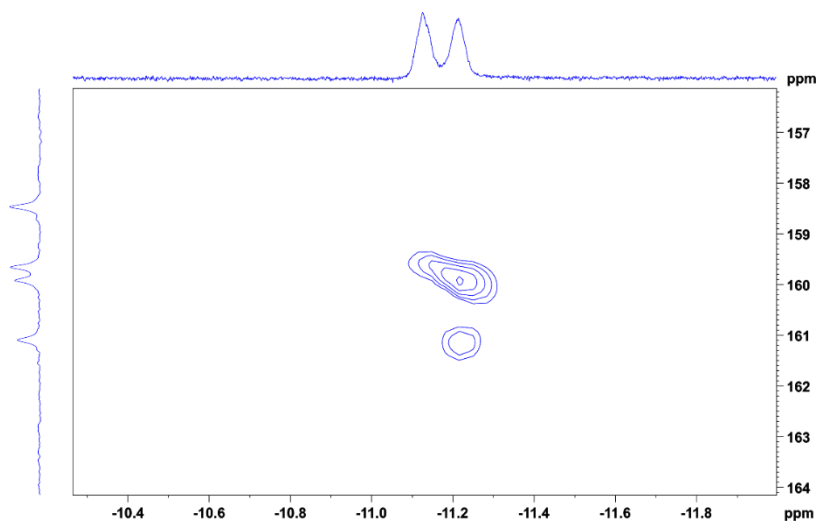
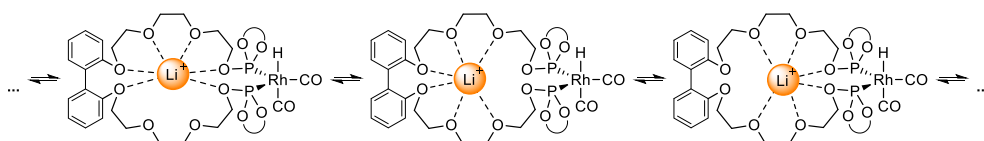


**Figure 55.** High-pressure  $^1\text{H}$ - $^{31}\text{P}$  HMBC spectrum of  $[\text{Rh}(\kappa^2\text{O},\text{O}'\text{-acac})(\text{CO})_2]$ , (R)-**L6** and LiBArF (10 bar  $\text{H}_2/\text{CO}$ , 25 °C, toluene- $d_8$ /THF- $d_8$  (97:3 v/v))

Given the small size of the cationic counterpart of LiBArF and the large size and high number of oxygen coordination sites in the metallacrown ether motif, we proposed as third hypothesis that the two rhodium species could arise from the non-simultaneous coordination of LiBArF to all oxygen sites and migration of LiBArF between sites. Similar migration processes have been reported in the

literature.<sup>30</sup>  $^7\text{Li}$  NMR revealed the presence of two different magnetic environments for  $^7\text{Li}$  nuclei with broad signals centered at 0.60 ppm and  $-1.47$  ppm (see section 3.5.10.3 in the experimental section).<sup>31</sup> Some potential structures for the rhodium complexes are indicated in Scheme 37. It should be noted that the number of potential structures is high. The fact that  $^7\text{Li}$  NMR signals are broad may be indicating that each signal arises from a number of complexes with similar magnetic environments for the  $^7\text{Li}$  nuclei.



**Scheme 37.** Molecular movement of the LiBARf salt in the metallocrown ether of ligand (*R*)-**L6**

The presence of distinct conformations in the metallocrown skeleton with similar energies (the intensities of the two sets of signals in NMR is roughly the same), but also with sufficiently high interconversion energy barriers to be observed as independent chemical species, may also account for the observation of two sets of signals (fourth hypothesis). Along this line of reasoning, the presence of a [1,1'-biphenyl]-2,2'-diol-based moiety in (*R*)-**L6** contributing with an additional stereogenic axis, could facilitate the generation of two distinct conformations by hindered rotation around this stereogenic axis.

To elucidate the role of the RA in the enantioselective hydroformylation process of aryl vinyl ethers, a similar complexation experiment to that previously discussed was carried out in the absence of RA.  $^{31}\text{P}$  NMR analysis revealed the presence of three groups of signals. The major signals, which were observed upfield, corresponded to a doublet at 146.4 ppm ( $^1J_{\text{Rh-P}} = 289.7$  Hz) and a singlet at 142.2 ppm (Table 32, entry 1). This multiplicity was previously observed with our supramolecular ligands when no RA was used and was assigned to complex  $[\text{Rh}(\kappa^2\text{O}, \text{O}'\text{-acac})(\text{CO})(\kappa^1\text{P}-\{(R)\text{-L6}\})]$ .<sup>11</sup> To confirm this assignment, this complex was independently synthesized by addition of (*R*)-**L6** to the metal precursor  $[\text{Rh}(\kappa^2\text{O}, \text{O}'\text{-acac})(\text{CO})_2]$  under inert atmosphere. The  $^{31}\text{P}$  NMR spectrum was in agreement with the previously observed and the IR spectrum showed the presence of only one  $\text{C}\equiv\text{O}$  band at  $2005\text{ cm}^{-1}$  (see section 3.5.10.3 in

<sup>30</sup> (a) Tamburini, S.; Vigato, P. A.; Gatos, M.; Bertolo, L.; Casellato, U. *Inorg. Chim. Acta* **2006**, *359*, 183-196. (b) Peruzzo, V.; Lanza, A.; Nestola, F.; Vigato, P. A.; Tamburini, S. *Inorg. Chim. Acta* **2014**, *416*, 226-234.

<sup>31</sup> Comparison of the  $^7\text{Li}$  NMR signals in the rhodium complex and in LiBARf ruled out the presence of unbound LiBARf in the reaction mixture ( $^7\text{Li}$  chemical shift of LiBARf =  $-0.90$  ppm).

the experimental section). The minor set of signals corresponded to a doublet at 165.4 ppm ( $^1J_{\text{Rh-P}} = 237.8$  Hz) and a second doublet at 160.9 ppm ( $^1J_{\text{Rh-P}} = 235.7$  Hz). These signals were in agreement with complex  $[\text{Rh}(\text{H})(\text{CO})_2(\kappa^2\text{P},\text{P}'\text{-}\{(R)\text{-L6}\})]$  (Table 32, entries 2 and 3).

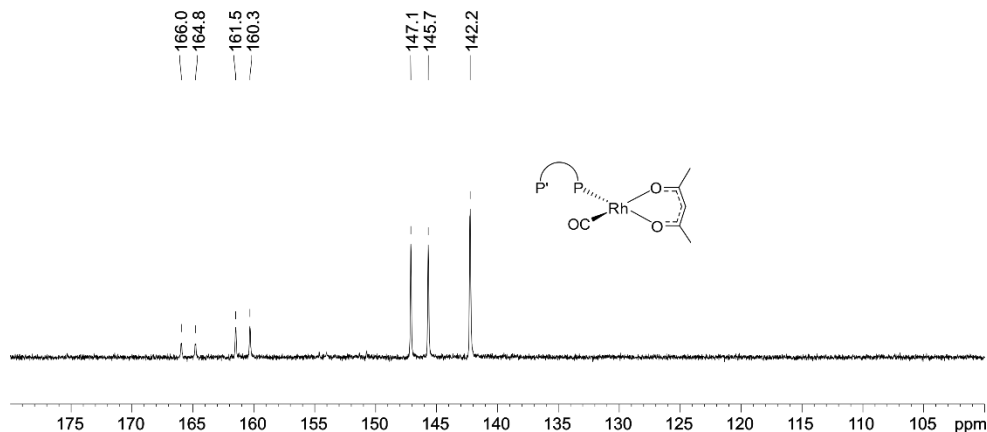


**Figure 56.** High-pressure  $^{31}\text{P}$  NMR spectrum of  $[\text{Rh}(\kappa^2\text{O},\text{O}'\text{-acac})(\text{CO})_2]$  and  $(R)\text{-L6}$  (202 MHz, 10 bar  $\text{H}_2/\text{CO}$ , 25 °C, toluene- $d_8$ /THF- $d_8$  (97:3 v/v))

$^1\text{H}$  NMR confirmed the presence of two hydride signals with different intensities at  $-11.11$  and  $-11.23$  ppm. The H–P coupling was confirmed by running  $^1\text{H}\{^{31}\text{P}\}$  NMR experiments and also by the presence of cross-peak signals in  $^1\text{H}\text{-}^{31}\text{P}$  HMBC spectroscopy between the hydrido and the corresponding phosphite groups (see section 3.5.10.3 in the experimental section). Again, the small  $^2J_{\text{P-H}}$  coupling constants ( $^2J_{\text{P-H}} = 7.8$  and roughly 8.9 Hz; see Table 32, entries 2 and 3) pointed to a bisequatorial coordination of the phosphite groups in a trigonal-bipyramidal metal center with the hydrido ligand in an apical position. The presence of two set of signals for the phosphite groups in  $[\text{Rh}(\text{H})(\text{CO})_2(\kappa^2\text{P},\text{P}'\text{-}\{(R)\text{-L6}\})]$  complexes suggests different chemical species (*i.e.*, third or fourth hypothesis), which are not interconverting at room temperature.

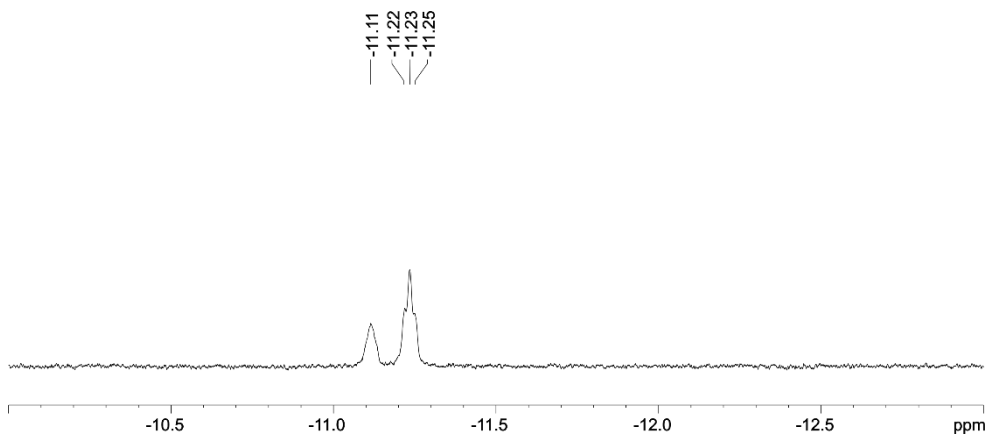


**Figure 57.** High-pressure  $^1\text{H}$  NMR spectrum of  $[\text{Rh}(\kappa^2\text{O},\text{O}'\text{-acac})(\text{CO})_2]$  and  $(R)\text{-L6}$  (202 MHz, 10 bar  $\text{H}_2/\text{CO}$ , 25 °C, toluene- $d_8$ /THF- $d_8$  (97:3 v/v))

To finalize these complexation studies, stoichiometric amounts of  $[\text{Rh}(\kappa^2\text{O},\text{O}'\text{-acac})(\text{CO})_2]$ ,  $(R)\text{-L6}$  and the rest of regulation agents (*i.e.*, NaBArF, KBArF, RbBArF or CsBArF) were mixed in toluene- $d_8$ /THF- $d_8$  (97:3 v/v) and transferred to a reactor. The reactor was pressurized with 10 bar of syngas (1:1 ratio of  $\text{H}_2/\text{CO}$ ), heated at 40 °C and stirred for 16 h. Stacked plots of selected regions of the  $^1\text{H}$ ,  $^1\text{H}\{^{31}\text{P}\}$  and  $^{31}\text{P}$  NMR spectra are shown in Figure 58 and Figure 59, respectively. In the case of NaBArF, KBArF or RbBArF, two sets of signals in each case in agreement with two hydrido dicarbonyl complexes  $[\text{Rh}(\text{H})(\text{CO})_2(\kappa^2\text{P},\text{P}'\text{-}\{(R)\text{-L6}\}\cdot\text{NaBArF or KBArF or RbBArF})]$  were observed (see Table 32, entries 7-12). For NaBArF, KBArF and RbBArF, most of the structural features of the hydrido dicarbonyl complexes coincided with those of LiBArF (*i.e.*, bisequatorial coordination of the supramolecular bisphosphite ligand to the rhodium center). If migration of the BArF salt between sites would be taking place, this process would be disfavored as the size of the cation in the salt increased. It is reasonable to assume that larger cationic components of the BArF salt tend to interact with a higher number of oxygens from the metallacrown ether motif and to occupy most of the internal space of the metallacrown motif, with the migration process between sites been disfavored. As the intensity of the second set of signals decreases as the radius of the alkali metal increases, it may be assumed that migration of the salt between coordination sites may be taking place. However, the presence of two distinct conformations in the metallacrown skeleton, with sufficiently high interconversion energy barriers, cannot be ruled out in the rhodium complexes derived from NaBArF, KBArF or RbBArF.

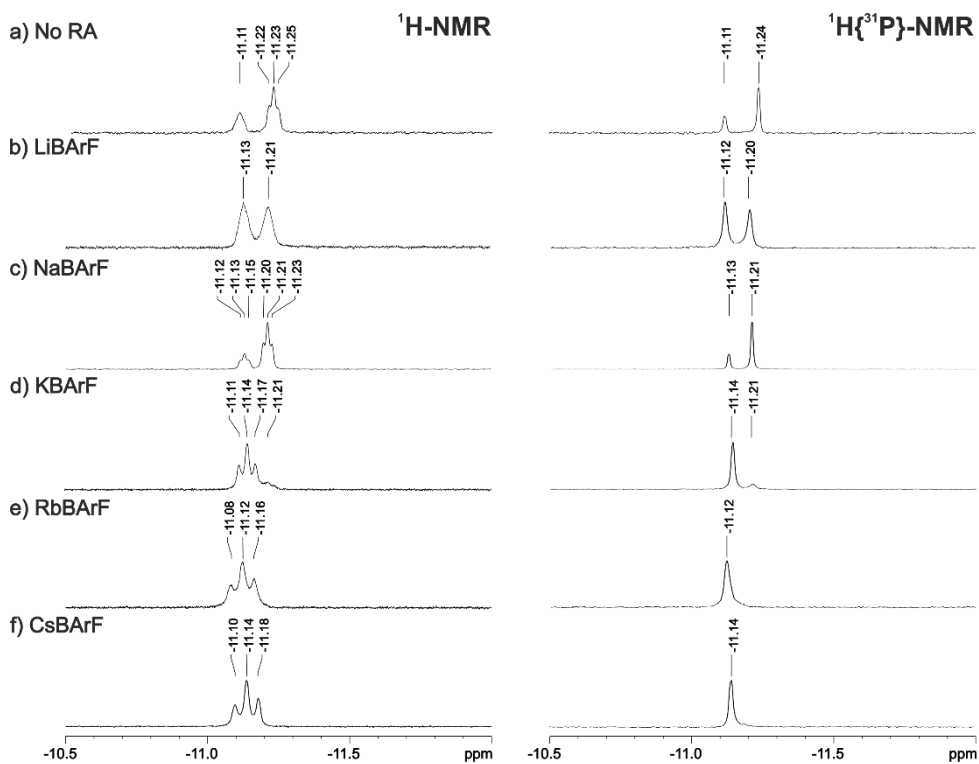


**Figure 58.** Stacked plot of the hydride region in the  $^1\text{H}$  NMR and  $^1\text{H}\{^{31}\text{P}\}$  NMR spectra of the complexation studies between  $[\text{Rh}(\kappa^2\text{O}, \text{O}'\text{-acac})(\text{CO})_2]$  and  $(R)\text{-L6}$  under  $\text{H}_2/\text{CO}$  atmosphere, with: a) No RA, b) LiBArF, c) NaBArF, d) KBArF, e) RbBArF, f) CsBArF

In the case of CsBArF, only one  $[\text{Rh}(\text{H})(\text{CO})_2(\kappa^2\text{P},\text{P}'-\{((R)\text{-L6})\cdot\text{CsBArF}\})]$  complex was observed with an equatorial-equatorial coordination of the bisphosphite ligands to the rhodium center (see Table 32, entry 13).

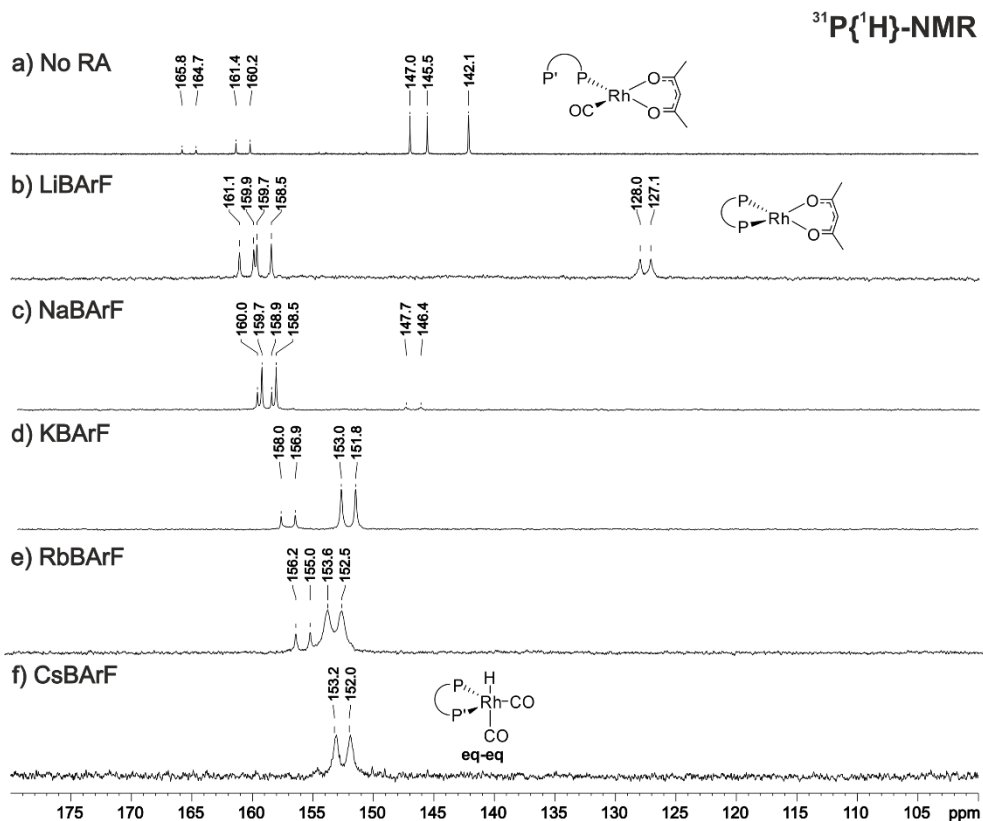


**Figure 59.** Stacked plot of the  $^{31}\text{P}\{^1\text{H}\}$  NMR spectra of the complexation studies between  $[\text{Rh}(\kappa^2\text{O},\text{O}^1\text{-acac})(\text{CO})_2]$  and  $(R)\text{-L6}$  under  $\text{H}_2/\text{CO}$  atmosphere, with: a) No RA, b) LiBArF, c) NaBArF, d) KBArF, e) RbBArF, f) CsBArF

**Table 32.** NMR spectral data for the rhodium complexes derived from alkali metal BArF salts in the presence of  $[\text{Rh}(\kappa^2\text{O},\text{O}'\text{-acac})(\text{CO})_2]$  and (R)-**L6** under  $\text{H}_2/\text{CO}$  atmosphere

Entry	RA	Complex	$\delta^{31\text{P}}$ (ppm)	$^1J_{\text{Rh-P}}$ (Hz)	$\delta^1\text{H}$ (ppm)	$^2J_{\text{P-H}}$ (Hz)
1		$[\text{Rh}(\kappa^2\text{O},\text{O}'\text{-acac})(\text{CO})(\kappa^1\text{P}-\{(R)\text{-L6}\})]$	146.4 142.2	289.7	-	-
2	None	$[\text{Rh}(\text{H})(\text{CO})_2(\kappa^2\text{P},\text{P}'-\{(R)\text{-L6}\})]$	165.4	237.8	-11.11	$\approx 8.9$
3		$[\text{Rh}(\text{H})(\text{CO})_2(\kappa^2\text{P},\text{P}'-\{(R)\text{-L6}\})]^*$	160.9	235.7	-11.23	7.8
4		$[\text{Rh}(\kappa^2\text{O},\text{O}'\text{-acac})(\kappa^2\text{P},\text{P}'-\{(R)\text{-L6}\}\cdot\text{LiBArF})]$	127.7	181.9	-	-
5	LiBArF	$[\text{Rh}(\text{H})(\text{CO})_2(\kappa^2\text{P},\text{P}'-\{(R)\text{-L6}\}\cdot\text{LiBArF})]$	160.6	234.1	-11.21	$\approx 19.3^{[b]}$
6		$[\text{Rh}(\text{H})(\text{CO})_2(\kappa^2\text{P},\text{P}'-\{(R)\text{-L6}\}\cdot\text{LiBArF})]^*$	159.2	241.5	-11.13	$\approx 20.3^{[b]}$
7		$[\text{Rh}(\text{H})(\text{CO})_2(\kappa^2\text{P},\text{P}'-\{(R)\text{-L6}\}\cdot\text{NaBArF})]$	159.6	240.2	-11.13	7.1
8	NaBArF	$[\text{Rh}(\text{H})(\text{CO})_2(\kappa^2\text{P},\text{P}'-\{(R)\text{-L6}\}\cdot\text{NaBArF})]^*$	159.2	238.6	-11.21	7.5
9		$[\text{Rh}(\text{H})(\text{CO})_2(\kappa^2\text{P},\text{P}'-\{(R)\text{-L6}\}\cdot\text{KBArF})]$	157.6	234.3	-11.14	13.8
10	KBArF	$[\text{Rh}(\text{H})(\text{CO})_2(\kappa^2\text{P},\text{P}'-\{(R)\text{-L6}\}\cdot\text{KBArF})]^*$	152.6	243.1	-11.21	n.m.
11		$[\text{Rh}(\text{H})(\text{CO})_2(\kappa^2\text{P},\text{P}'-\{(R)\text{-L6}\}\cdot\text{RbBArF})]$	155.7	241.3	-11.12	19.8
12	RbBArF	$[\text{Rh}(\text{H})(\text{CO})_2(\kappa^2\text{P},\text{P}'-\{(R)\text{-L6}\}\cdot\text{RbBArF})]^*$	153.2	239.5	-11.12	19.8
13	CsBArF	$[\text{Rh}(\text{H})(\text{CO})_2(\kappa^2\text{P},\text{P}'-\{(R)\text{-L6}\}\cdot\text{CsBArF})]$	152.7	244.2	-11.14	20.1

[a] NMR data was acquired under 10 bar syngas ( $\text{H}_2/\text{CO}$  in a 1:1 ratio) at 25 °C in 5 mm sapphire NMR tube in toluene- $d_8$ /THF- $d_6$  (97:3 v/v). [b] The width was measured at half height. The assignment of the signals of these complexes is tentative due to the small intensity of the cross-peak between the hydrido and the phosphite signals in the  $^1\text{H}-^{31}\text{P}$  HMBC spectrum.

All these results led us to conclude that catalytically active rhodium species towards hydroformylation were formed by mixing stoichiometric amounts of  $[\text{Rh}(\kappa^2\text{O},\text{O}'\text{-acac})(\text{CO})_2]$ , (R)-**L6** and the regulation agent under syngas atmosphere. Catalytic species derived from LiBArF were the slowest to be formed, as important amounts of unreactive rhodium species (*i.e.*,  $[\text{Rh}(\kappa^2\text{O},\text{O}'\text{-acac})(\kappa^2\text{P},\text{P}'-\{(R)\text{-L6}\}\cdot\text{LiBArF})]$ ) remained in the reaction mixture and were detected.

Two different  $[\text{Rh}(\text{H})(\text{CO})_2(\kappa^2\text{P},\text{P}'-\{(R)\text{-L6}\}\cdot\text{RA})]$  complexes are formed under hydroformylation reaction conditions, with the exception of CsBArF for which only one complex is formed. All hydrido dicarbonyl complexes presented a bisequatorial coordination of the supramolecular bisphosphite ligand in a trigonal-bipyramidal metal center with the hydrido ligand in the apical position. We postulated that the migration of the regulation agent between coordination sites within the same chemical species could be one of the possible

rationalizations for the formation of two isomeric rhodium complexes. The fact that this potential migration process between sites is disfavored as the size of the cationic component of the regulation agent increases would be in favor of this process being at the origin of the formation of two isomeric  $[\text{Rh}(\text{H})(\text{CO})_2(\kappa^2\text{P},\text{P}^-\{\{(\text{R})\text{-L6}\}\bullet\text{RA}\})]$  complexes.

Alternatively, the presence of two distinct conformations in the metallacrown skeleton, with sufficiently high interconversion energy barriers between them to be individually observed, may also account for the observation of two different complexes. In such scenario, the regulation agent would be distributed between the two conformations. The presence of a [1,1'-biphenyl]-2,2'-diol-based moiety in (R)-L6 contributing with an additional stereogenic element could be at the origin of the generation of two isomeric rhodium complexes by hindered rotation around the stereogenic axis in the regulation site.

Despite extensive spectroscopic studies and theoretical conformational analysis, we did not get sound evidences for the rationalization and understanding of the whole set experimental results and spectroscopic data. It is plausible, that the two phenomena (migration between coordination sites *vs.* existence of non-interconvertible conformers) may be operating simultaneously at a different extent in each particular case due to the different characteristics of the regulation agents.

### 3.3.3.2 Mechanistic studies

Together with the studies to elucidate the role of the regulation agent in the hydroformylation process, we also performed mechanistic studies in order to gain insight into the rhodium-catalyzed transformation. In spite of the fact that hydroformylation reactions have been widely studied since their discovery, and that the general mechanism proposed early in 1961 is still considered valid, the particularities of each catalytic system and the nature of the substrate have shown that mechanistic generalizations should be made cautiously. For instance, for many catalytic systems, alkene insertion to the rhodium center has been assumed to be a reversible step, whilst hydrogenolysis has been assumed to be irreversible. We decided to investigate the nature of these particular steps in the catalytic cycle with our lead supramolecularly regulated catalyst.

Lazzaroni *et al.* reported the use of deuterium NMR as a useful tool to elucidate the characteristics of the catalytic pathway in hydroformylation reactions directly from the crude mixture, without any reaction work-up and/or purification



steps.<sup>32</sup> The required deuterioformylation reaction was carried out under optimized catalytic conditions (10 bar D<sub>2</sub>/CO in a 1:1 ratio, 25 °C, 48 h) with ligand (R)-**L6**, LiBARF as regulation agent and alkene **9a** as substrate. The use of deuterium gas led to a lower reactivity (16% conv.), if compared with H<sub>2</sub> (73% conv.). Interestingly, no effects were observed in the regioselectivity (>99:1 b/l ratio) or the enantiomeric ratio (94:6 *er*) of the reaction. The similarities amongst <sup>1</sup>H and <sup>2</sup>H NMR allowed for a straightforward assignment of the peaks by comparison of the chemical shifts. As expected, major signals in <sup>2</sup>H NMR corresponded to the deuterated hydroformylation product, with a <sup>2</sup>H nucleus at the aldehyde group (9.40 ppm, Figure 60) and another at the α-methyl substituent (1.12 ppm, Figure 60).

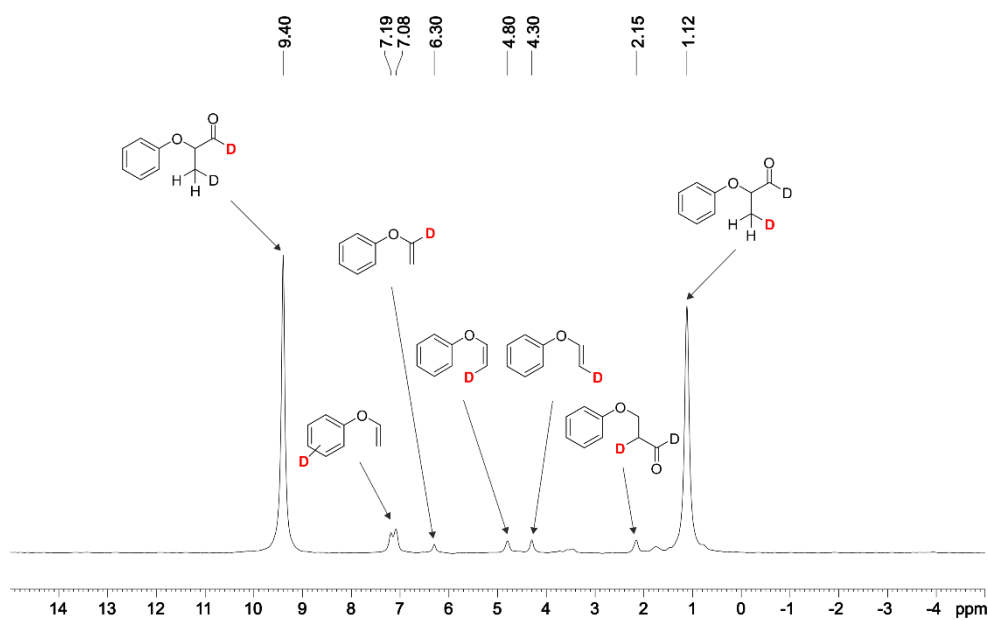
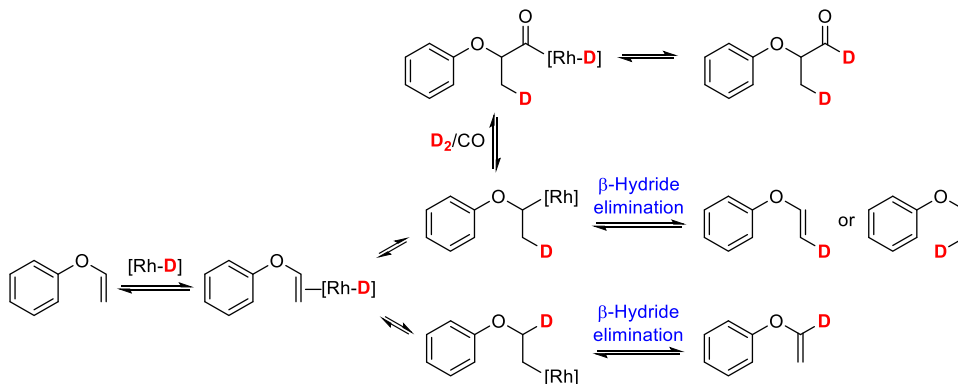


**Figure 60.** <sup>2</sup>H NMR spectrum of the crude deuterioformylation reaction mixture

<sup>2</sup>H NMR also revealed the formation of minor amounts of products containing vinylic <sup>2</sup>H nuclei. The presence of <sup>1</sup>H/<sup>2</sup>H scrambling in the three different vinylic positions, suggested that alkene insertion took place under the reaction conditions, forming both branched and linear alkyl rhodium complexes that underwent β-hydride elimination with recovery of partially deuterated (vinyloxy)benzene (Scheme 38). These results confirmed the reversibility of the

<sup>32</sup> (a) Uccello-Barretta, G.; Lazzaroni, R.; Settambolo, R.; Salvadori, P. *J. Organomet. Chem.* **1991**, *417*, 111-119. (b) Lazzaroni, R.; Settambolo, R.; Uccello-Barretta, G. *Organometallics* **1995**, *14*, 4644-4650.

alkene insertion step with our supramolecularly regulated catalyst, as previously observed for other examples in the literature.<sup>32</sup>

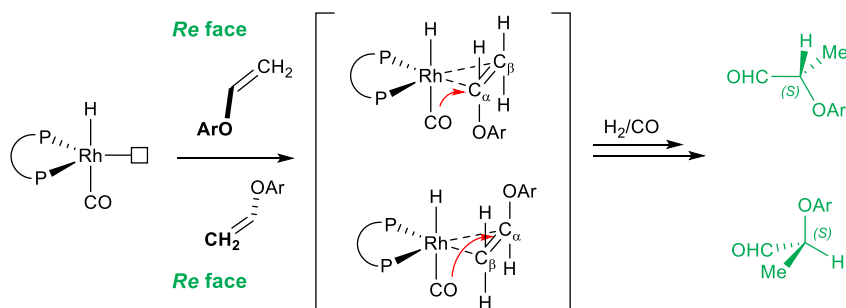


**Scheme 38.** Schematic representation of the deuterioformylation reaction of (vinyloxy)benzene **9a**

Once the reversibility of the alkene insertion was demonstrated, we focused on investigating the hydrogenolysis step. To verify its reversibility, compound *rac*-**10a** was subjected to hydroformylation reaction conditions employing our supramolecularly regulated catalyst. No alkene formation was observed and *rac*-**10a** was fully recovered, suggesting that under catalytic conditions the hydrogenolysis step is, in our case, irreversible.

### 3.3.4 Rationalization of the stereochemical outcome of the hydroformylation reaction

As previously discussed in Section 3.3.2 of this Thesis, supramolecularly regulated catalysts derived from [Rh( $\kappa^2$ O,O'-acac)(CO<sub>2</sub>)], ligand (*R*)-**L6** and LiBARF led to (*S*)-configured 2-aryloxypropanals. The stereofacial control in the approach of the substrate to the rhodium catalytic species indicated in Scheme 39, together with CO delivery to the alpha carbon (C<sub>α</sub>) of the functionalized alkene from the side of the metal (*i.e.*, CO delivery to the *Re* face of the alkene), would justify the formation of the (*S*)-configured aldehydes.



**Scheme 39.** Stereochemical outcome in the Rh-catalyzed hydroformylation of aryl vinyl ethers with (R)-**L6**

Subsequent steps towards the rationalization of the stereochemical outcome of the reaction involved getting an estimate of the three-dimensional structure of the supramolecular catalyst derived from  $[\text{Rh}(\kappa^2\text{O},\text{O}'\text{-acac})(\text{CO})_2]$ , ligand (R)-**L6** and LiBARF. As discussed in Section 3.3.3.1, two different catalytically active complexes  $[\text{Rh}(\text{H})(\text{CO})_2(\kappa^2\text{P},\text{P}'\text{-}\{((\text{R})\text{-}\mathbf{L6})\cdot\text{LiBARF}\})]$  were formed in a similar ratio from the rhodium precursor, the ligand and LiBARF under hydroformylation reaction conditions. Both hydrido dicarbonyl complexes presented a bisequatorial coordination of the supramolecular bisphosphite ligand to a trigonal-bipyramidal metal center with the hydrido ligand in the apical position. Despite extensive spectroscopic studies, the unequivocal assignment of the structures of these two complexes could not be made.

Since a complete conformational search at the computational level for complexes  $[\text{Rh}(\text{H})(\text{CO})_2(\kappa^2\text{P},\text{P}'\text{-}\{((\text{R})\text{-}\mathbf{L6})\cdot\text{Li}^+\})]$  was not possible with the computational tools available to our research group (the cationic supramolecular complex has 197 atoms), a few initial structures for the hydrido dicarbonyl complexes derived from (R)-**L6** and  $\text{Li}^+$  were constructed. All initial geometries incorporated a bisequatorial coordination of the supramolecular bisphosphite ligand in a trigonal-bipyramidal metal center with the hydrido ligand in the apical position. This limited set of initial structures incorporated both the (R)- and (S)-configured [1,1'-biphenyl]-2,2'-diol-based linker and considered all relative positions for the carbonyl and hydrido ligands in apical positions. This set of initial geometries was optimized at the M06-2X-D3/def2-SVP level of theory considering the solvent effects of toluene. These optimization studies led to the structure shown in Figure 61 as the lowest in energy. The most stable structure for the  $[\text{Rh}(\text{H})(\text{CO})_2(\kappa^2\text{P},\text{P}'\text{-}\{((\text{R})\text{-}\mathbf{L6})\cdot\text{Li}^+\})]$  complex contained a (S)-configured [1,1'-biphenyl]-2,2'-diol-based linker and a hexacoordinate lithium cation in the regulation site with the phosphite oxygens not being coordinated to the lithium cation.

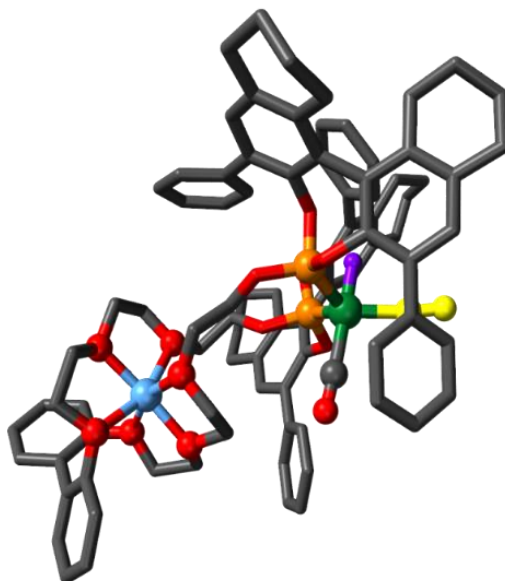


**Figure 61.** Optimized geometry of **B-Li (S)**

The hydroformylation of a given alkene starts by its coordination to the rhodium center with displacement of the equatorial CO ligand (see CO group in yellow in the structure **B-Li (S)**, Figure 61). The alkene can approach the rhodium center with four possible orientations: the aryloxy group at the left pointing up (approach **S1**) and down (approach **S2**) and the aryloxy group at the right pointing up (approach **S3**) and down (approach **S4**) (see Figure 62 with aryloxy being the phenoxy substituent). The four possible rhodium alkene complexes were constructed from structure **B-Li (S)** and (vinyloxy)benzene **9a** as substrate and were optimized at the M06-2X-D3/def2-SVP level of theory considering the solvent effects of toluene. The optimized structures are shown in Figure 62. To aid comparison between structures, the rhodium atom has been placed at the center of an octant diagram with the two phosphorus groups placed at the back of the diagram with a parallel alignment to the y axis.

The hydroformylation reaction proceeds by insertion of the olefinic CH<sub>2</sub> carbon into the Rh–H bond, delivery of the hydrido ligand to the beta alkene carbon C<sub>β</sub> (see Figure 62 with the hydrido ligand marked in purple) and subsequent insertion of the CO ligand into the branched alkyl rhodium complex. Both, H and CO deliveries, take place from the side of the metal, which implies that complexes **S1** and **S4** lead to the minor observed enantiomer of the final 2-phenoxypropanal. Namely, the hydroformylation reaction should proceed from complexes **S2** or **S3** as those lead to the final (*S*)-configured 2-phenoxypropanal, which is the major enantiomer produced during the hydroformylation process.

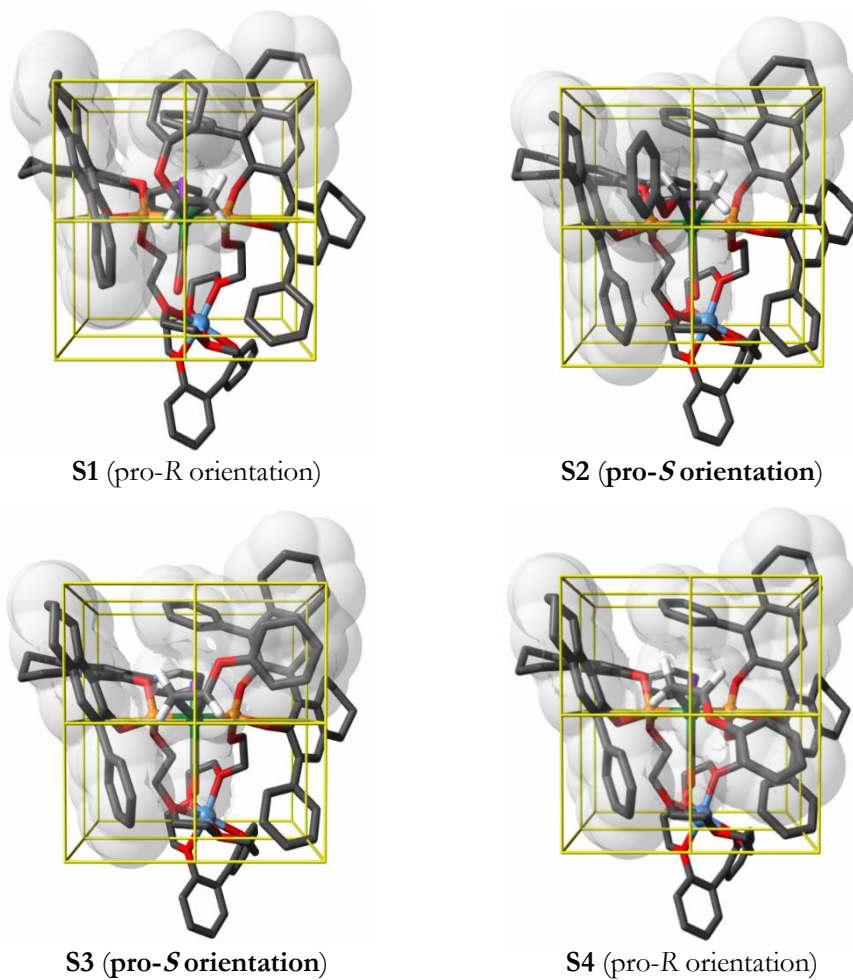


**Figure 62.** Optimized geometry of complex **B-Li (S)** interacting with **9a** in a pro-*R* orientation (complexes **S1** and **S4**) or a pro-*S*-orientation (complexes **S2** and **S3**)

The figure that follows shows a focused view of the catalytic site with the right orientation for structures **S1-S4** (Figure 63).

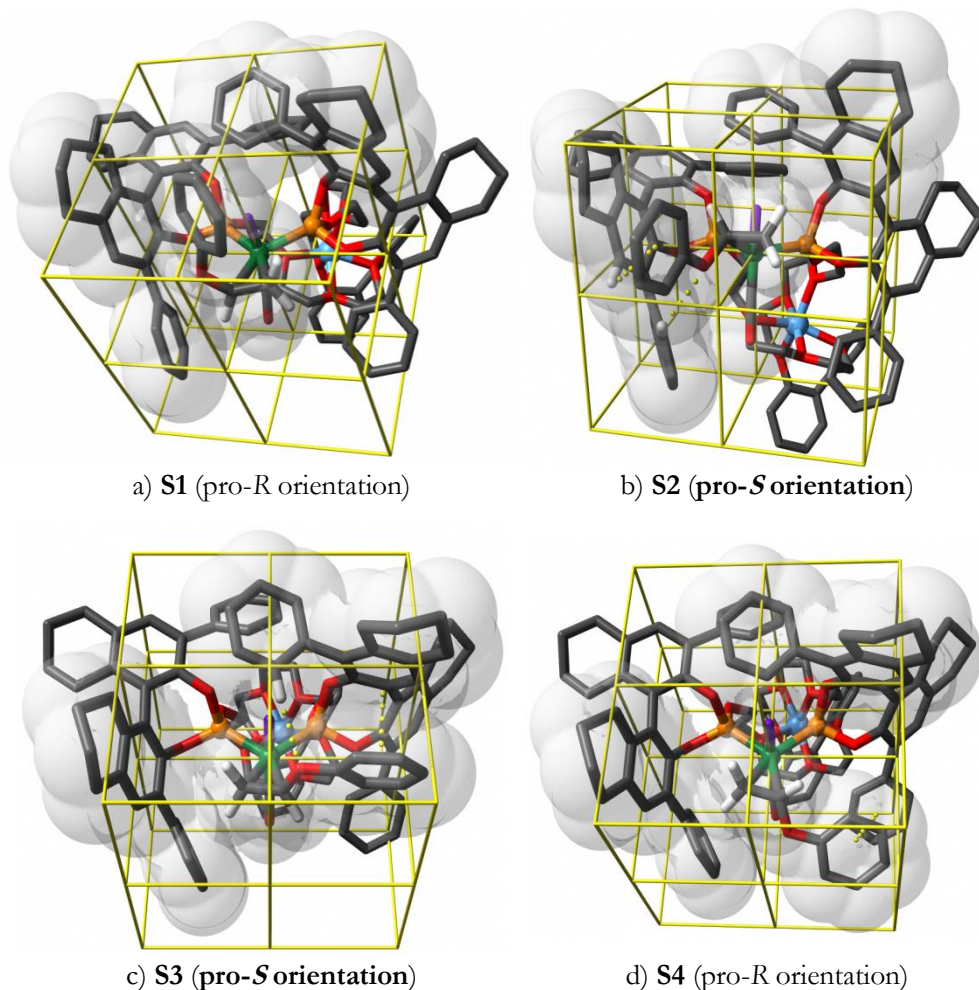
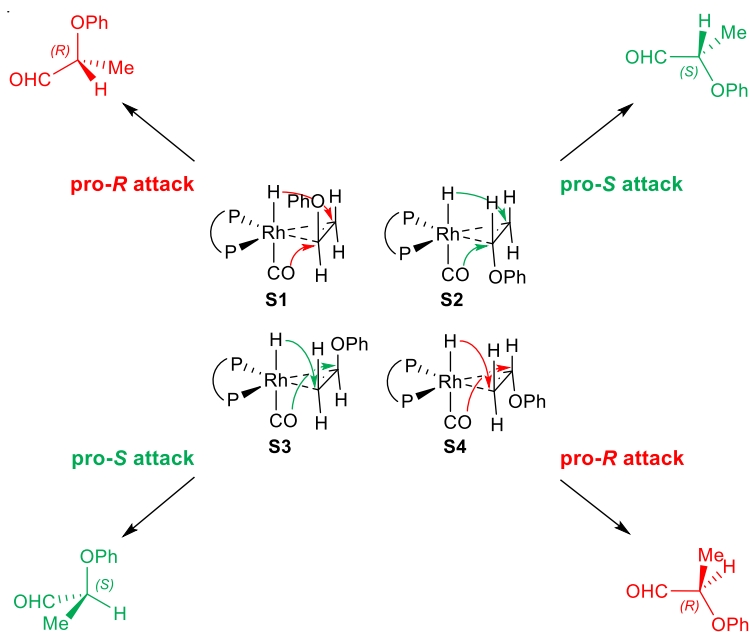


**Figure 63.** Catalytic site of the optimized geometry for complexes **S1-S4**

These complexes constitute starting points of four different hydroformylation reaction manifolds and are not the corresponding transition states for the insertion of the terminal alkene carbon into the Rh–H bond. Thus, statements on the role of these complexes in the hydroformylation reaction should be made cautiously. In all these complexes, the most appropriated orientation for the C=C insertion step was found in complex **S3**, with a H–Rh–C $_{\alpha}$ –C $_{\beta}$  torsion angle equal to 88.7° (the same torsion angles in complexes **S1**, **S2** and **S4** were 88.3°, 84.6° and 100.7°, respectively). Along this line of reasoning, the H–Rh–C $_{\alpha}$  bond angle in **S3** was 87.7°, indicating an almost perpendicular

arrangement of the C=C bond with respect to the Rh–H bond (the same bond angles in complexes **S1**, **S2** and **S4** were 84.7°, 82.4° and 82.4°, respectively). Complex **S3** presents two stabilizing and directional CH–O and  $\pi$ – $\pi$  interactions involving the substrate (see Figure 63c with the supramolecular interactions being marked with yellow balls). A stabilizing and directional CH–O interaction, as well as a CH– $\pi$  interaction (pointing to the center of the aromatic ring in Figure 63b), could be identified in complex **S2**. We postulate that these secondary interactions in complexes **S2** and **S3** could favor the progress of the hydroformylation reaction through them, as both lead to the observed enantiomer of the hydroformylation product (Scheme 40). CH–O interactions are not present in complex **S4** and not directional in **S1**. Moreover, analogous  $\pi$ – $\pi$  and CH– $\pi$  interactions to those in **S2** and **S3** are less favored in complexes **S1** and **S4**. On the basis of the above mentioned arguments, we postulated that progress of the hydroformylation reaction could be disfavored through these complexes.



**Scheme 40.** Rationalization of the stereochemical outcome of the Rh-catalyzed hydroformylation of (vinylxy)benzene **9a** with ligand (*R*)-**L6**

The optimization of the geometry and calculation of the electronic energy of complexes **S1–S4** were made as monocationic species:  $\text{Li}^+$  was included in the regulation site, but the  $\text{BARF}^-$  counterion was not considered. Participation of the  $\text{BARF}^-$  anion in the substrate complexes with the phenoxy group pointing in the same direction than the lithium cation (*i.e.*, **S2** and **S4**) allows for a simultaneous stabilization of the positive charge of the lithium and the positive

electronic density of the oxygen bound to the double bond (See Figure 64). If this would be the case, the reaction manifold starting from **S2** would be the most relevant as it would be the only one leading to the observed enantiomer of the hydroformylation product. As it can be observed in the Figure 64, the match between the rhodium complex and BArF is better in **S2** than in **S4**, as the average distances between the closest  $\text{CF}_3$  group to  $\text{Li}^+$  and the vinylic oxygen are better balanced in **S2** ( $d_{\text{F-Li}} = 4.0 \text{ \AA}$  and  $d_{\text{F-O}} = 3.77 \text{ \AA}$ , respectively) than in **S4** ( $d_{\text{F-Li}} = 3.5 \text{ \AA}$  and  $d_{\text{F-O}} = 4.7 \text{ \AA}$ , respectively). Moreover, complex **S2** presents two stabilizing and directional  $\text{CH-O}$  and  $\text{H-}\pi$  interactions involving the substrate (see Figure 64a with all supramolecular interactions being marked with yellow balls), which could not be identified in complex **S4**. Thus, if the assumption that the BArF anion is simultaneously interacting with the substrate and the lithium cation would be valid, the hydroformylation reaction would progress from complex **S2**, leading the aldehyde with the observed configuration.

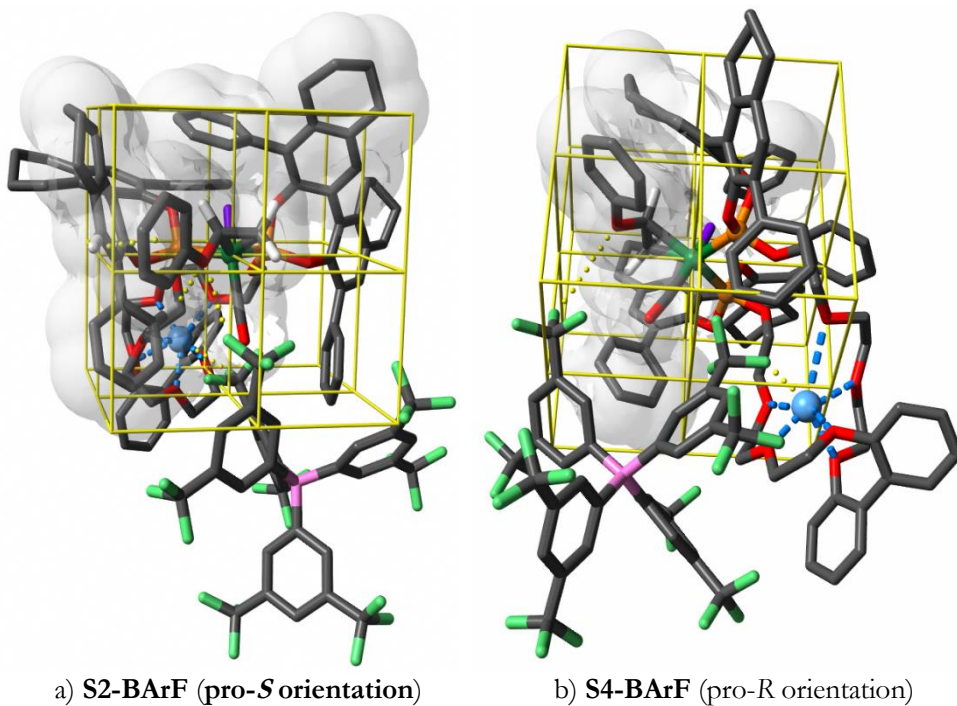


**Figure 64.** Optimized geometry of complex **S2-BArF** (pro-*S*-orientation) and **S4-BArF** (pro-*R*-orientation)



### 3.4 CONCLUSIONS

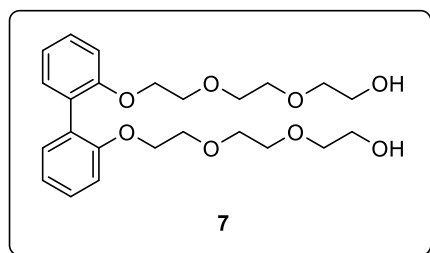
In summary, the rhodium-catalyzed enantioselective hydroformylation of challenging aryl vinyl ethers has been described employing supramolecularly regulated rhodium complexes derived from polyether-containing bisphosphite ligands. The presence of regulation agents had an important influence in the catalytic activity and enantioselectivity, probably by inducing subtle changes in the geometry of the catalytic site. By choosing the matched regulation agent for a given substrate, the catalytic activity (up to 66%) and enantioselectivity (up to 97:3 *er*) were enhanced. The enantioselectivities attained with our supramolecularly regulated catalyst are among the highest reported in the hydroformylation of aryl vinyl ethers. Steric effects induced by *ortho* substituents to the vinyloxy group in the aromatic ring of the substrates, as well as electronic effects induced by strong electron-donating groups to the aryl group of the substrate, decreased the conversion of the hydroformylation reaction. Our synthetic methodology was applied to the preparation of advanced synthetic intermediates of relevant agrochemicals such as Napropamide, Mecoprop and Dichlorprop. Complexation studies demonstrated that the formation of catalytic species under syngas atmosphere in the presence of regulation agents led to the formation of two isomeric hydrido dicarbonyl rhodium complexes, with their ratio depending on the RA used. It was demonstrated that the bisphosphite ligand was coordinated to the equatorial positions of a trigonal bipyramidal rhodium center with the hydrido ligand being coordinated at the apical position. Mechanistic studies revealed the reversibility of the alkene insertion under catalytic conditions and the irreversibility of the hydrogenolysis step. A tentative rationalization of the stereochemical outcome of the reaction from the alkene complexes with catalytic species derived from  $[\text{Rh}(\kappa^2\text{O},\text{O}'\text{-acac})(\text{CO})_2]$ , (*R*)-**L6** and LiBARF as the regulation agent has been made.

## 3.5 EXPERIMENTAL SECTION

### 3.5.1 General considerations

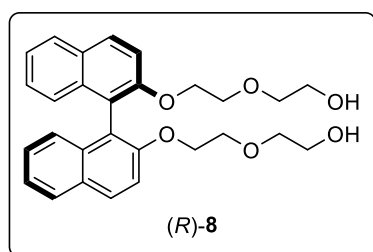
All syntheses were carried out using chemicals purchased from commercial sources unless otherwise cited. Air- and moisture-sensitive manipulations and hydroformylation reactions were performed under inert atmosphere, either in a N<sub>2</sub>-filled glove box or with standard Schlenk techniques. Glassware was dried *in vacuo* before use with a hot air gun. All solvents were dried and deoxygenated by using a Solvent Purification system (SPS). Silica gel 60 (230-400 mesh), C18-SiO<sub>2</sub> (200-400 mesh) or basic Al<sub>2</sub>O<sub>3</sub> was used for column chromatography, as indicated in each case. NMR spectra were recorded at room temperature, in a 300 MHz, 400 MHz or 500 MHz spectrometers in CDCl<sub>3</sub> unless otherwise cited. <sup>1</sup>H NMR, <sup>13</sup>C{<sup>1</sup>H} and <sup>13</sup>C{<sup>1</sup>H,<sup>31</sup>P} NMR chemical shifts were quoted in ppm relative to the residual solvent peaks. <sup>31</sup>P{<sup>1</sup>H} NMR chemical shifts were quoted in ppm relative to 85% phosphoric acid in water. <sup>11</sup>B{<sup>1</sup>H} NMR chemical shifts are quoted in ppm relative to BF<sub>3</sub>·(CH<sub>3</sub>)<sub>2</sub>O in CDCl<sub>3</sub>. <sup>19</sup>F{<sup>1</sup>H} NMR chemical shifts are quoted in ppm relative to CFCl<sub>3</sub> in CDCl<sub>3</sub>. <sup>7</sup>Li NMR chemical shifts are quoted in ppm relative to LiCl in D<sub>2</sub>O. IR spectra were recorded using Attenuate total reflection techniques, unless otherwise cited. High-resolution mass spectra (HRMS) were recorded by using electrospray ionization (ESI) method in positive or negative mode or matrix-assisted laser desorption ionization (MALDI) in positive mode, using *trans*-2-[3-(4-*tert*-butylphenyl)-2-methyl-2-propenylidene]malononitrile (dctb) as matrix. A Time-of-flight (TOF) detector was used in all cases. Melting points were determined in open capillaries and are uncorrected. Enantiomeric excesses were determined by GC or HPLC using chiral stationary phases. GC analysis were performed on an Agilent 6890N chromatograph equipped with a FID detector. HPLC analysis were performed on an Agilent 1200 Series chromatograph equipped with a diode array UV detector. Specific optical rotation measurements were carried out on a Jasco P-1030 model polarimeter equipped with a PMT detector using the Sodium line at 589 nm.

### 3.5.2 Synthesis of ligands



**Compound 7:** The preparation of **7** was performed following the reported procedure.<sup>33</sup> A mixture of 8-tosyloxy-3,6-dioxioctanol (4 g, 13.10 mmol) and K<sub>2</sub>CO<sub>3</sub> (3.9 g, 28.30 mmol) were added to [1,1'-biphenyl]-2,2'-diol (1.2 g, 6.57 mmol) in anhydrous acetonitrile (59.7 mL) under Ar

atmosphere. The resulting mixture was refluxed for 60 h and filtered. The solution was concentrated under reduced pressure. After purification by column chromatography over SiO<sub>2</sub> using AcOEt/MeOH 95:5 as eluents, 2,2'-bis[2-[2-(2-hydroxyethoxy)ethoxy]ethoxy]biphenyl **7** was obtained as a colorless oil (2.1 g, 70% yield). Spectroscopic data for this compound were in agreement with the reported ones.<sup>34</sup> <sup>1</sup>H NMR (400 MHz, CDCl<sub>3</sub>) δ 7.30–7.23 (m, 4H), 6.98 (td, *J* = 11.1 Hz, *J* = 1.0 Hz, 2H), 6.94 (dd, *J* = 8.2 Hz, *J* = 1.0 Hz, 2H), 4.09–4.06 (m, 4H), 3.71–3.67 (m, 8H), 3.54–3.48 (m, 12H) ppm. <sup>13</sup>C {<sup>1</sup>H} NMR (101 MHz, CDCl<sub>3</sub>) δ 156.5 (2 C, *Carom*O), 131.6 (2 C, *Carom*), 128.6 (4 C, *Carom*H), 120.8 (2 C, *Carom*H), 112.6 (2 C, *Carom*H), 72.7 (2 C, COCH<sub>2</sub>CH<sub>2</sub>CO), 71.0 (2 C, COCH<sub>2</sub>CH<sub>2</sub>CO), 70.6 (2 C, COCH<sub>2</sub>CH<sub>2</sub>OH), 69.8 (2 C, COCH<sub>2</sub>CH<sub>2</sub>), 68.7 (2 C, *Carom*OCH<sub>2</sub>CH<sub>2</sub>), 61.8 (2 C, CH<sub>2</sub>CH<sub>2</sub>OH) ppm.



**Compound (R)-8:** A mixture of (R)-[1,1'-binaphthalene]-2,2'-diol (1.7 g, 6.13 mmol), 2-(2-hydroxyethoxy)ethyl-4-methylbenzenesulfonate<sup>35</sup> (3.2 g, 12.30 mmol) and K<sub>2</sub>CO<sub>3</sub> (3.6 g, 26.30 mmol) in anhydrous acetonitrile (53 mL) was refluxed for 72 h. The reaction mixture was filtered and the organic solution concentrated

under reduced pressure. After purification by column chromatography over SiO<sub>2</sub> using AcOEt/MeOH 95:5 as eluents, (R)-2,2'-(((1,1'-binaphthalene)-2,2'-diylbis(oxy))bis(ethane-2,1-diyl))bis(oxy))diethanol (R)-**8** was obtained as a clear brown oil (1.3 g, 46% yield). Spectroscopic data for this compound were in agreement with the reported ones.<sup>12</sup> <sup>1</sup>H NMR (500 MHz, CDCl<sub>3</sub>) δ 7.95 (d, *J* = 8.9 Hz, 2H), 7.87 (d, *J* = 8.2 Hz, 2H), 7.43 (d, *J* = 9.0 Hz, 2H), 7.35–7.32 (m, 2H), 7.24–7.21 (m, 2H), 7.15 (s, 1H), 7.14 (s, 1H), 4.17–4.13 (m, 2H), 4.03–3.99

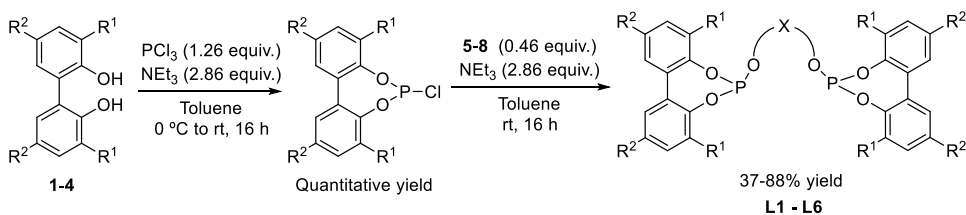
<sup>33</sup> Jose, D. A.; Mon, I.; Fernández-Pérez, H.; Escudero-Adán, E. C.; Benet-Buchholz, J.; Vidal-Ferran, A. *Org. Lett.* **2011**, *13*, 3632-3635.

<sup>34</sup> Czech, B.; Czech, A.; Bartsch, R. A. *J. Heterocycl. Chem.* **1984**, *21*, 341-343.

<sup>35</sup> Li, Y.; Mullen, K. M.; Sardinha, J.; Felix, V.; Beer, P. D. *Dalton Trans.* **2011**, *40*, 12180-12190.

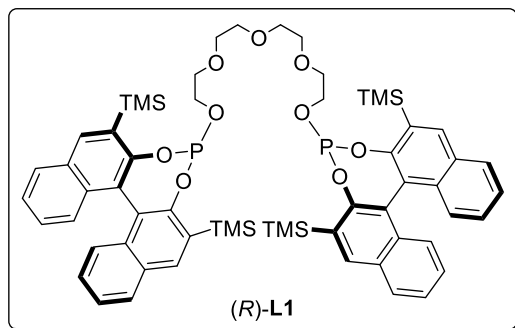
(m, 2H), 3.53–3.49 (m, 2H), 3.45–3.40 (m, 6H), 3.22–3.15 (m, 4H), 2.53 (bs, 2H) ppm.  $^{13}\text{C}\{^1\text{H}\}$  NMR (125 MHz,  $\text{CDCl}_3$ )  $\delta$  154.4 (2 C, *Carom*O), 134.2 (2 C, *Carom*), 129.6 (2 C, *Carom*), 129.5 (2 C, *Carom*H), 128.0 (2 C, *Carom*H), 126.5 (2 C, *Carom*H), 125.6 (2 C, *Carom*H), 123.9 (2 C, *Carom*H), 120.8 (2 C, *Carom*), 116.1 (2 C, *Carom*H), 72.5 (2 C,  $\text{COCH}_2\text{CH}_2$ ), 70.0 (2 C,  $\text{CH}_2\text{CH}_2\text{O}$ ), 69.7 (2 C, *Carom* $\text{OCH}_2\text{CH}_2$ ), 61.7 (2 C,  $\text{CH}_2\text{CH}_2\text{OH}$ ) ppm.

### 3.5.2.1 General procedure for the synthesis of supramolecular bisphosphite ligands



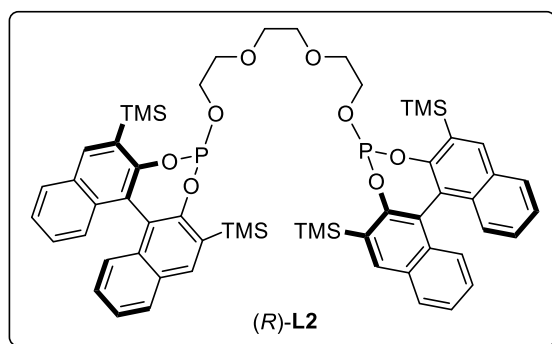
**Scheme 41.** General procedure for the synthesis of supramolecular bisphosphite ligands **L1-L6**

The preparation of supramolecular bisphosphite ligands was performed following a reported procedure.<sup>11b</sup> Under argon atmosphere, diol **1-4** (0.75 mmol) was azeotropically dried with anhydrous toluene (3 x 5 mL), dissolved in anhydrous toluene (11 mL) and added dropwise to a pre-cooled solution of  $\text{PCl}_3$  (0.95 mmol) and  $\text{NEt}_3$  (2.14 mmol) in anhydrous toluene (11 mL) at 0° C. The solution was allowed to reach room temperature and was stirred overnight. The turbid reaction mixture was filtered through a pad of Celite® and the solvent evaporated under reduce pressure. The resulting residue was dissolved in anhydrous toluene (11 mL). A solution of diol **5-8** (0.35 mmol) and  $\text{NEt}_3$  (298  $\mu\text{L}$ , 2.14 mmol) in anhydrous toluene (11 mL) was added dropwise to the chlorophosphite-containing solution. The mixture was allowed to react overnight at room temperature, filtered through a pad of Celite® and concentrated under vacuum. The resulting mixture was purified by filtration through a basic alumina pad eluting with DCM (16 mL) to afford the desired product.



**Compound (R)-L1:** The preparation of (R)-L1 was performed following the general procedure for the synthesis of supramolecular bisphosphite ligands from (R)-3,3'-bis(trimethyl silyl-[1.1'-binaphthalene]-2,2'-diol<sup>36</sup> (R)-2 (2 g, 4.64 mmol), anhydrous toluene (68 mL), PCl<sub>3</sub> (512 μL, 5.85 mmol), NEt<sub>3</sub> (1.9 mL,

13.30 mmol), tetraethyleneglycol **6** (370 μL, 2.14 mmol). Product (R)-L1 was obtained as a white solid (1.8 g, 76% yield). The spectroscopic data were in agreement with those reported in the literature.<sup>11b</sup> <sup>1</sup>H NMR (500 MHz, CD<sub>2</sub>Cl<sub>2</sub>) δ 8.13–8.10 (m, 4H), 7.95–7.92 (m, 4H), 7.43–7.38 (m, 4H), 7.23–7.19 (m, 4H), 7.16–7.14 (m, 2H), 7.08–7.06 (m, 2H), 4.00–3.94 (m, 2H), 3.48–3.42 (m, 14H), 0.48 (s, 18H), 0.47 (s, 18H) ppm. <sup>13</sup>C {<sup>1</sup>H, <sup>31</sup>P} NMR (126 MHz, CD<sub>2</sub>Cl<sub>2</sub>) δ 153.0 (2 C, CaromOP), 152.2 (2 C, CaromOP), 137.6 (2 C, CaromH), 137.5 (2 C, CaromH), 134.3 (2 C, Carom), 134.2 (2 C, Carom), 133.0 (2 C, CaromSi), 132.3 (2 C, CaromSi), 131.4 (2 C, Carom), 131.0 (2 C, Carom), 128.8 (2 C, CaromH), 128.7 (2 C, CaromH), 127.0 (2 C, CaromH), 126.9 (2 C, CaromH), 126.8 (2 C, CaromH), 125.2 (2 C, CaromH), 125.1 (2 C, CaromH), 123.0 (2 C, Carom), 122.2 (2 C, Carom), 70.9 (2 C, COCH<sub>2</sub>CH<sub>2</sub>CO), 70.9 (2 C, COCH<sub>2</sub>CH<sub>2</sub>CO), 70.8 (2 C, COCH<sub>2</sub>CH<sub>2</sub>CO), 64.2 (2 C, POCH<sub>2</sub>), 0.1 (6 C, SiCH<sub>3</sub>), 0.0 (6 C, SiCH<sub>3</sub>) ppm. <sup>31</sup>P {<sup>1</sup>H} NMR (202 MHz, CD<sub>2</sub>Cl<sub>2</sub>) δ 138.7 ppm.

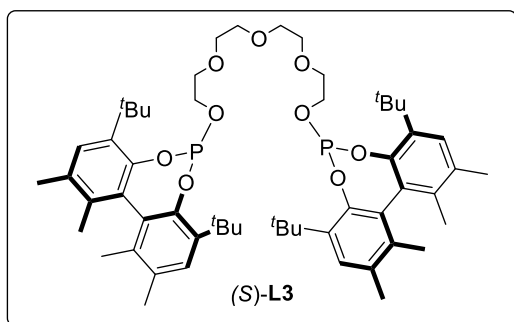


**Compound (R)-L2:** The preparation of (R)-L2 was performed following the general procedure for the synthesis of supramolecular bisphosphite ligands from (R)-3,3'-bis(trimethyl silyl-[1.1'-binaphthalene]-2,2'-diol<sup>36</sup> (R)-2 (323 mg, 0.75 mmol), anhydrous toluene (11 mL), PCl<sub>3</sub> (82.7 μL,

0.95 mmol), NEt<sub>3</sub> (298 μL, 2.14 mmol), triethyleneglycol **5** (370 μL, 0.34 mmol). Product (R)-L2 was obtained as a white solid (135 mg, 37% yield). Mp: 147–149 °C. [ $\alpha$ ]<sub>D</sub><sup>25</sup> = –606.7 (c. 0.1, CH<sub>2</sub>Cl<sub>2</sub>). IR (neat, cm<sup>-1</sup>)  $\bar{\nu}$  3050, 2951, 2895, 1618,

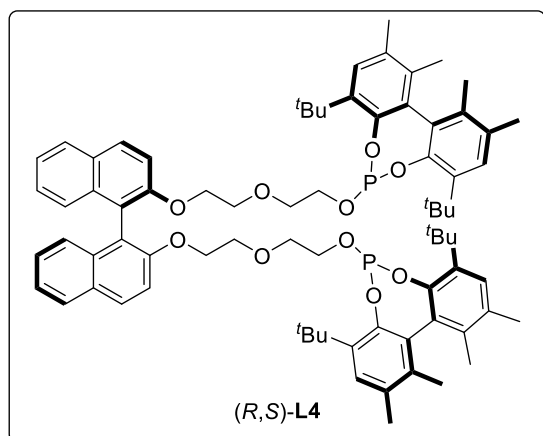
<sup>36</sup> (R)-3,3'-bis(trimethyl silyl-[1.1'-binaphthalene]-2,2'-diol (R)-2 has been synthesized following the reported procedure: Kauch, M.; Snieckus, V.; Hoppe, D. *J. Org. Chem.* **2005**, *70*, 7149-7158.

1577, 1492, 1441, 1383, 1247, 1221, 1193, 1149, 1092, 1024, 975, 946, 826, 796, 744, 673, 631, 589, 510.  $^1\text{H}$  NMR (500 MHz,  $\text{CD}_2\text{Cl}_2$ )  $\delta$  8.12 (d,  $J = 16.9$  Hz, 4H), 7.96–7.91 (m, 4H), 7.43–7.38 (m, 4H), 7.23–7.19 (m, 4H), 7.16–7.15 (m, 2H), 7.09–7.07 (m, 2H), 4.00–3.92 (m, 2H), 3.47–3.41 (m, 10H), 0.48 (s, 18H), 0.47 (s, 18H) ppm.  $^{13}\text{C}\{^1\text{H},^{31}\text{P}\}$  NMR (126 MHz,  $\text{CD}_2\text{Cl}_2$ )  $\delta$  153.0 (2 C, *Carom*OP), 152.3 (2 C, *Carom*OP), 137.6 (2 C, *Carom*H), 137.5 (2 C, *Carom*H), 134.4 (2 C, *Carom*), 134.2 (2 C, *Carom*), 133.0 (2 C, *Carom*Si), 132.3 (2 C, *Carom*Si), 131.5 (2 C, *Carom*), 131.0 (2 C, *Carom*), 128.8 (2 C, *Carom*H), 128.8 (2 C, *Carom*H), 127.0 (2 C, *Carom*H), 126.9 (2 C, *Carom*H), 126.8 (2 C, *Carom*H), 125.2 (2 C, *Carom*H), 125.2 (2 C, *Carom*H), 123.0 (2 C, *Carom*), 122.2 (2 C, *Carom*), 71.0 (2 C,  $\text{COCH}_2\text{CH}_2\text{CO}$ ), 70.8 (2 C,  $\text{COCH}_2\text{CH}_2\text{CO}$ ), 64.2 (2 C,  $\text{POCH}_2$ ), 0.2 (6 C,  $\text{SiCH}_3$ ), 0.0 (6 C,  $\text{SiCH}_3$ ) ppm.  $^{31}\text{P}\{^1\text{H}\}$  NMR (202 MHz,  $\text{CD}_2\text{Cl}_2$ )  $\delta$  138.70 ppm. HRMS (ESI):  $m/z$   $[\text{M}+\text{Na}]^+$  calcd for  $\text{C}_{58}\text{H}_{68}\text{O}_8\text{P}_2\text{Si}_4$  1089.3359, found 1089.3353.



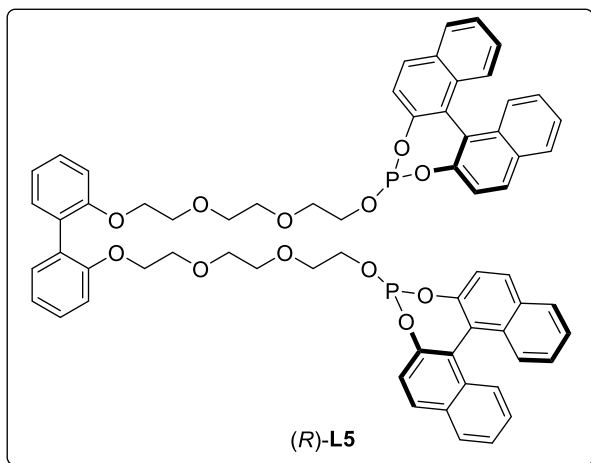
**Compound (S)-L3:** The preparation of (S)-L3 was performed following the general procedure for the synthesis of supra-molecular bisphosphite ligands from (S)-5,5'-6,6'-tetramethyl-3,3'-di-*tert*-butyl-1,1'-biphenyl-2,2'-diol (S)-4 (265 mg, 0.75 mmol), anhydrous toluene (10

mL),  $\text{PCl}_3$  (82.4  $\mu\text{L}$ , 0.94 mmol),  $\text{NEt}_3$  (297  $\mu\text{L}$ , 2.14 mmol), tetraethyleneglycol **6** (66.8 mg, 0.34 mmol). Product (S)-L3 was obtained as a white solid (312 mg, 83% yield). The spectroscopic data were in agreement with those reported in the literature.<sup>12</sup>  $^1\text{H}$  NMR (500 MHz,  $\text{CD}_2\text{Cl}_2$ )  $\delta$  7.19 (s, 2H), 7.17 (s, 2H), 3.96–3.90 (m, 2H), 3.58–3.51 (m, 10H), 3.50–3.48 (m, 4H), 2.27 (s, 12H), 1.85 (s, 6H), 1.78 (s, 6H), 1.45 (s, 18H), 1.42 (s, 18H) ppm.  $^{13}\text{C}\{^1\text{H},^{31}\text{P}\}$  NMR (126 MHz,  $\text{CD}_2\text{Cl}_2$ )  $\delta$  145.7 (2 C, *Carom*OP), 145.6 (2 C, *Carom*OP), 138.5 (2 C, *Carom*C( $\text{CH}_3$ )<sub>3</sub>), 137.4 (2 C, *Carom*C( $\text{CH}_3$ )<sub>3</sub>), 135.4 (2 C, *Carom*CH<sub>3</sub>), 134.8 (2 C, *Carom*CH<sub>3</sub>), 132.9 (2 C, *Carom*CH<sub>3</sub>), 132.2 (2 C, *Carom*CH<sub>3</sub>), 132.0 (2 C, *Carom*), 131.1 (2 C, *Carom*), 128.5 (2 C, *Carom*H), 128.2 (2 C, *Carom*H), 71.2 (2 C,  $\text{COCH}_2\text{CH}_2\text{CO}$ ), 70.9 (2 C,  $\text{COCH}_2\text{CH}_2\text{CO}$ ), 70.9 (2 C,  $\text{COCH}_2\text{CH}_2\text{CO}$ ), 64.1 (2 C,  $\text{POCH}_2$ ), 35.0 (2 C,  $\text{C}(\text{CH}_3)_3$ ), 35.0 (2 C,  $\text{C}(\text{CH}_3)_3$ ), 31.5 (6 C, *Carom*C( $\text{CH}_3$ )<sub>3</sub>), 31.3 (6 C, *Carom*C( $\text{CH}_3$ )<sub>3</sub>), 20.5 (4 C, *Carom*CH<sub>3</sub>), 16.8 (2 C, *Carom*CH<sub>3</sub>), 16.5 (2 C, *Carom*CH<sub>3</sub>) ppm.  $^{31}\text{P}\{^1\text{H}\}$  NMR (202 MHz,  $\text{CD}_2\text{Cl}_2$ )  $\delta$  134.6 ppm.



**Compound (R,S)-L4** : The preparation of (R,S)-L4 was performed following the general procedure for the synthesis of supramolecular bisphosphite ligands from (*S*)-5,5'-6,6'-tetramethyl-3,3'-di-*tert*-butyl-1,1'-biphenyl-2,2'-diol (*S*)-4 (424 mg, 1.20 mmol), anhydrous toluene (20 mL), PCl<sub>3</sub> (132 μL, 1.51 mmol), NEt<sub>3</sub> (476 μL, 3.42 mmol), (R)-2,2'-(((1,1'-binaphthalene]-

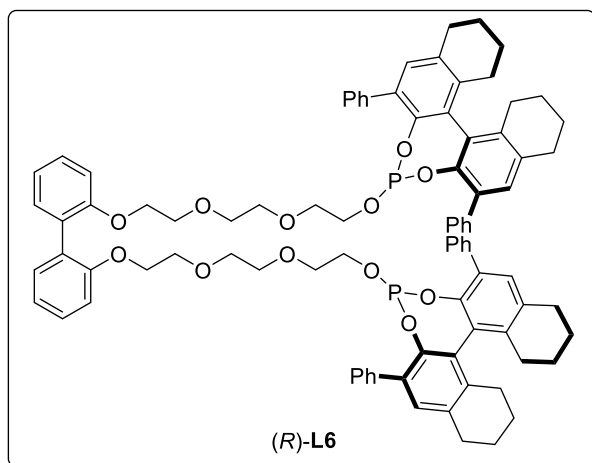
2,2'-diylbis(oxy))bi(ethane-2,1-diyl))bis-(oxy))diethanol (R)-8 (255 mg, 0.55 mmol). Product (R,S)-L4 was obtained as a white solid (554 mg, 82% yield). The spectroscopic data were in agreement with those reported in the literature.<sup>12</sup> <sup>1</sup>H NMR (400 MHz, CDCl<sub>3</sub>) δ 7.82 (s, 1H), 7.80 (s, 1H), 7.75 (s, 1H), 7.73 (s, 1H), 7.31 (s, 1H), 7.29 (s, 1H), 7.24–7.24 (m, 1H), 7.22–7.22 (m, 1H), 7.17–7.09 (m, 8H), 4.01–3.98 (m, 4H), 3.58–3.51 (m, 2H), 3.39–3.36 (m, 4H), 3.21–3.14 (m, 2H), 2.94–2.90 (m, 4H), 2.26 (s, 6H), 2.25 (s, 6H), 1.87 (s, 6H), 1.79 (s, 6H), 1.42 (s, 18H), 1.40 (s, 18H) ppm. <sup>13</sup>C{<sup>1</sup>H, <sup>31</sup>P} NMR (125 MHz, CDCl<sub>3</sub>) δ 154.3 (2 C, *Carom*OCH<sub>2</sub>), 145.6 (4 C, *Carom*OP), 138.2 (4 C, *Carom*C(CH<sub>3</sub>)<sub>3</sub>), 137.1 (2 C, *Carom*C(CH<sub>3</sub>)<sub>3</sub>), 135.1 (2 C, *Carom*C(CH<sub>3</sub>)<sub>3</sub>), 134.4 (1 C, *Carom*CH<sub>3</sub>), 134.2 (2 C, *Carom*H), 132.5 (1 C, *Carom*CH<sub>3</sub>), 131.9 (1 C, *Carom*CH<sub>3</sub>), 131.6 (1 C, *Carom*CH<sub>3</sub>), 130.9 (2 C, *Carom*H), 129.5 (4 C, *Carom*), 129.4 (2 C, *Carom*H), 128.1 (2 C, *Carom*CH<sub>3</sub>), 127.9 (2 C, *Carom*CH<sub>3</sub>), 127.9 (2 C, *Carom*H), 126.4 (2 C, *Carom*H), 125.6 (2 C, *Carom*H), 123.8 (2 C, *Carom*H), 120.7 (2 C, *Carom*), 115.8 (2 C, *Carom*H), 70.9 (2 C, COCH<sub>2</sub>CH<sub>2</sub>CO), 70.1 (2 C, COCH<sub>2</sub>CH<sub>2</sub>CO), 69.5 (2 C, *Carom*OCH<sub>2</sub>), 63.6 (2 C, POCH<sub>2</sub>), 34.8 (2 C, *Carom*C(CH<sub>3</sub>)<sub>3</sub>), 34.8 (2 C, *Carom*C(CH<sub>3</sub>)<sub>3</sub>), 31.4 (6 C, *Carom*C(CH<sub>3</sub>)<sub>3</sub>), 31.3 (6 C, *Carom*C(CH<sub>3</sub>)<sub>3</sub>), 20.6 (2 C, *Carom*CH<sub>3</sub>), 20.6 (2 C, *Carom*CH<sub>3</sub>), 16.9 (2 C, *Carom*CH<sub>3</sub>), 16.7 (2 C, *Carom*CH<sub>3</sub>) ppm. <sup>31</sup>P{<sup>1</sup>H} NMR: (202 MHz, CDCl<sub>3</sub>) δ 133.8 ppm.



**Compound (R)-L5:** The preparation of (R)-L5 was performed following the general procedure for the synthesis of supramolecular bisphosphite ligands from (R)-[1,1'-binaphthalene]-2,2'-diol (R)-1 (304 mg, 1.06 mmol), anhydrous toluene (12 mL),  $\text{PCl}_3$  (118  $\mu\text{L}$ , 1.34 mmol),  $\text{NEt}_3$  (296  $\mu\text{L}$ , 2.13 mmol), 2,2'-bis[2-[2-(2-

hydroxyethoxy)ethoxy]ethoxy]biphenyl **7** (218 mg, 0.48 mmol). Product (R)-L5 was obtained as a white solid (460 mg, 88% yield). The spectroscopic data were in agreement with those reported in the literature.<sup>11a</sup>  $^1\text{H}$  NMR (500 MHz,  $\text{CD}_2\text{Cl}_2$ )  $\delta$  8.00–7.98 (m, 2H), 7.96–7.891 (m, 6H), 7.52–7.50 (m, 2H), 7.46–7.40 (m, 6H), 7.34–7.32 (m, 4H), 7.28–7.22 (m, 8H), 6.97–6.92 (m, 4H), 4.07–4.01 (m, 6H), 3.90–3.84 (m, 2H), 3.66–3.64 (m, 4H), 3.52–3.49 (m, 12H) ppm.  $^{13}\text{C}\{^1\text{H}, ^{31}\text{P}\}$  NMR (126 MHz,  $\text{CD}_2\text{Cl}_2$ )  $\delta$  156.8 (2 C, *CaromO*), 149.0 (2 C, *CaromOP*), 148.0 (2 C, *CaromOP*), 133.2 (2 C, *Carom*), 132.9 (2 C, *Carom*), 132.0 (2 C, *CaromH*), 131.5 (2 C, *Carom*), 130.8 (2 C, *CaromH*), 130.5 (2 C, *CaromH*), 128.8 (2 C, *CaromH*), 128.7 (2 C, *CaromH*), 128.6 (4 C, *Carom*), 127.1 (2 C, *CaromH*), 126.7 (2 C, *CaromH*), 126.6 (2 C, *CaromH*), 125.5 (4 C, *CaromH*), 125.3 (4 C, *CaromH*), 124.4 (2 C, *Carom*), 123.1 (2 C, *Carom*), 122.2 (2 C, *CaromH*), 120.8 (4 C, *CaromH*), 112.7 (2 C, *CaromH*), 71.1 (2 C,  $\text{COCH}_2\text{CH}_2\text{CO}$ ), 71.0 (4 C,  $\text{COCH}_2\text{CH}_2\text{CO}$ ), 70.1 (2 C,  $\text{COCH}_2\text{CH}_2\text{CO}$ ), 68.7 (2 C, *CaromOCH}\_2*), 64.8 (2 C,  $\text{POCH}_2$ ) ppm.  $^{31}\text{P}\{^1\text{H}\}$  NMR (202 MHz,  $\text{CD}_2\text{Cl}_2$ )  $\delta$  146.3 ppm.





**Compound (R)-L6:** The preparation of (R)-L6 was performed following the general procedure for the synthesis of supramolecular bisphosphite ligands from (R)-3,3'-diphenyl-

5,5',6,6',7,7',8,8'-octahydro-[1,1'-binaphthalene]-2,2'-diol (R)-3<sup>37</sup> (612 mg, 1.35 mmol), anhydrous toluene (31 mL), PCl<sub>3</sub> (149 μL, 1.70 mmol), NEt<sub>3</sub> (537 μL, 3.86 mmol), 2,2'-bis[2-(2-(2-hydroxyethoxy)ethoxy)ethoxy]biphenyl **7** (280 mg, 0.62 mmol). Product (R)-L6 was obtained as a white solid (740 mg, 85% yield). The spectroscopic data were in agreement with those reported in the literature.<sup>11b</sup> <sup>1</sup>H NMR (400 MHz, CD<sub>2</sub>Cl<sub>2</sub>) δ 7.60–7.55 (m, 8H), 7.40–7.35 (m, 8H), 7.30–7.19 (m, 12H), 6.97–6.91 (m, 4H), 4.02–3.99 (m, 4H), 3.58–3.56 (m, 4H), 3.36–3.30 (m, 6H), 3.26–3.23 (m, 4H), 3.12–3.01 (m, 4H), 2.96–2.89 (m, 10H), 2.77–2.69 (m, 4H), 2.42–2.35 (m, 4H), 1.90–1.82 (m, 12H), 1.71–1.67 (m, 4H) ppm. <sup>13</sup>C{<sup>1</sup>H, <sup>31</sup>P} NMR (126 MHz, CD<sub>2</sub>Cl<sub>2</sub>) δ 156.8 (2 C, *Carom*O), 143.4 (4 C, *Carom*OP), 138.7 (2 C, *Carom*), 138.2 (2 C, *Carom*), 138.1 (2 C, *Carom*), 137.5 (2 C, *Carom*), 135.2 (2 C, *Carom*H), 134.6 (2 C, *Carom*H), 132.3 (2 C, *Carom*), 132.0 (2 C, *Carom*H), 131.9 (2 C, *Carom*), 130.9 (2 C, *Carom*), 130.5 (4 C, *Carom*H), 130.1 (4 C, *Carom*H), 130.0 (4 C, *Carom*H), 129.7 (2 C, *Carom*), 128.8 (2 C, *Carom*), 128.6 (2 C, *Carom*), 128.5 (4 C, *Carom*H), 127.5 (2 C, *Carom*H), 127.3 (2 C, *Carom*H), 120.8 (2 C, *Carom*H), 112.8 (2 C, *Carom*H), 70.9 (2 C, COCH<sub>2</sub>CH<sub>2</sub>CO), 70.7 (2 C, COCH<sub>2</sub>CH<sub>2</sub>CO), 70.7 (2 C, COCH<sub>2</sub>CH<sub>2</sub>CO), 70.0 (2 C, COCH<sub>2</sub>CH<sub>2</sub>CO), 68.7 (2 C, COCH<sub>2</sub>CH<sub>2</sub>CO), 63.3 (2 C, POCH<sub>2</sub>), 29.7 (2 C, CH<sub>2</sub>Carom), 28.2, (2 C, CH<sub>2</sub>Carom) 28.2 (4 C, CH<sub>2</sub>Carom), 23.2 (2 C, CH<sub>2</sub>CH<sub>2</sub>), 23.2 (2 C, CH<sub>2</sub>CH<sub>2</sub>), 23.1 (4 C, CH<sub>2</sub>CH<sub>2</sub>) ppm. <sup>31</sup>P{<sup>1</sup>H} NMR (162 MHz, CD<sub>2</sub>Cl<sub>2</sub>) δ 142.8 ppm.

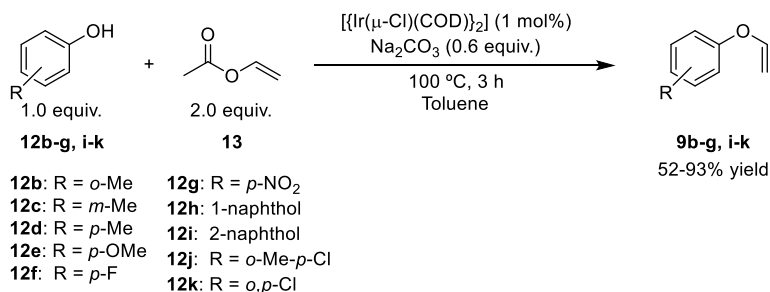
<sup>37</sup> (R)-3,3'-diphenyl-5,5',6,6',7,7',8,8'-octahydro-[1,1'-binaphthalene]-2,2'-diol (R)-3 has been synthesized by following the reported procedure in: Erre, G.; Junge, K.; Enthaler, S.; Addis, D.; Michalik, D.; Spannenberg, A.; Beller, M. *Chem. - Asian J.* **2008**, *3*, 887-894.

### 3.5.3 Synthesis of regulation agents: alkali BArF salts

NABArF was purchased from a commercial supplier, dried under vacuum ( $10^{-2}$  mbar,  $120\text{ }^{\circ}\text{C}$ , 18 h) and used afterwards. LiBArF, KBArF, RbBArF and CsBArF were synthesized following the reported procedure.<sup>38</sup>

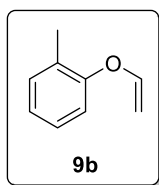
### 3.5.4 Substrate synthesis

#### 3.5.4.1 General procedure for the synthesis of aryl vinyl ethers



**Scheme 42.** General procedure for the synthesis of aryl vinyl ethers **9b-g,i-k**

The synthesis of non-commercially available aryl vinyl ether derivatives (**9b-g,i-k**) was performed adapting a reported procedure.<sup>17</sup> Under an inert atmosphere, a mixture of [ $\{\text{Ir}(\mu\text{-Cl})(\text{COD})\}_2$ ] (0.01 mmol),  $\text{Na}_2\text{CO}_3$  (0.6 mmol) and toluene (1 mL) was prepared. The corresponding phenol **12b-g,i-k** (1 mmol) and vinyl acetate **13** (2 mmol) were added to the previous solution. The reaction mixture was stirred at  $100\text{ }^{\circ}\text{C}$  for 3 h. After quenching with diethyl ether and evaporating the solvent, the desired product was isolated by column chromatography over  $\text{SiO}_2$  using pentane/DCM 80:20 as eluents.

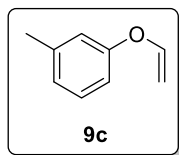


**Compound 9b:** The preparation of **9b** was performed following the general procedure indicated above from 2-methylphenol **12b** (1.8 g, 16.60 mmol), vinyl acetate (3.1 mL, 33.20 mmol), NaOAc (1.6 g, 19.90 mmol) and [ $\{\text{Ir}(\mu\text{-Cl})(\text{COD})\}_2$ ] (112 mg, 0.16 mmol) in anhydrous toluene (16.6 mL). After purification by column chromatography over  $\text{SiO}_2$ , product **9b** was obtained as a colorless oil (2 g, 91% isolated yield). The spectroscopic data were in agreement with those reported in the literature.<sup>39</sup>  $^1\text{H NMR}$  (500 MHz,  $\text{CDCl}_3$ )  $\delta$  7.20–7.15

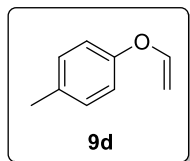
<sup>38</sup> Carreras, L.; Rovira, L.; Vaquero, M.; Mon, I.; Martin, E.; Benet-Buchholz, J.; Vidal-Ferran, A. *RSC Advances* **2017**, 7, 32833-32841.

<sup>39</sup> Trofimov, B. A.; Oparina, L. A.; Kolyvanov, N. A.; Vysotskaya, O. V.; Gusarova, N. K. *Russ. J. Org. Chem.* **2015**, 51, 188-194.

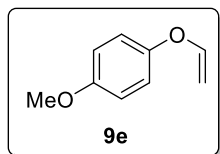
(m, 2H), 7.02–6.99 (m, 1H), 6.91 (d,  $J = 8.0$  Hz, 1H), 6.63 (dd,  $J = 13.8, 6.2$  Hz, 1H), 4.60 (dd,  $J = 13.8, 1.7$  Hz, 1H), 4.36 (dd,  $J = 6.2, 1.7$  Hz, 1H), 2.26 (s, 3H) ppm.  $^{13}\text{C}\{^1\text{H}\}$  NMR (126 MHz,  $\text{CDCl}_3$ )  $\delta$  154.8 (1 C, *Carom*O), 149.2 (1 C, OCH), 131.3 (1 C, *Carom*H), 128.7 (1 C, *Carom*H), 127.1 (1 C, *Carom*), 123.6 (1 C, *Carom*H), 117.2 (1 C, *Carom*H), 93.7 (1 C,  $\text{CH}_2$ ), 16.1 (1 C,  $\text{CH}_3$ ) ppm.



**Compound 9c:** The preparation of **9c** was performed following the general procedure indicated above from 3-methylphenol **12c** (2.2 g, 20.10 mmol), vinyl acetate (3.7 mL, 40.10 mmol),  $\text{Na}_2\text{CO}_3$  (1.3 g, 12.00 mmol) and  $[\{\text{Ir}(\mu\text{-Cl})(\text{COD})\}_2]$  (135 mg, 0.20 mmol) in anhydrous toluene (20.1 mL). After purification by column chromatography over  $\text{SiO}_2$ , product **9c** was obtained as a colorless oil (2 g, 74% isolated yield). The spectroscopic data were in agreement with those reported in the literature.<sup>40</sup>  $^1\text{H}$  NMR (300 MHz,  $\text{CDCl}_3$ )  $\delta$  7.23–7.18 (m, 1H), 6.91–6.89 (m, 1H), 6.83–6.81 (m, 2H), 6.65 (dd,  $J = 13.7, 6.1$  Hz, 1H), 4.76 (dd,  $J = 13.7, 1.7$  Hz, 1H), 4.43 (dd,  $J = 6.1, 1.6$  Hz, 1H), 2.36 (s, 3H) ppm.  $^{13}\text{C}\{^1\text{H}\}$  NMR (75 MHz,  $\text{CDCl}_3$ )  $\delta$  157.0 (1 C, *Carom*O), 148.4 (1 C, OCH), 139.9 (1 C, *Carom*), 129.5 (1 C, *Carom*H), 124.1 (1 C, *Carom*H), 117.9 (1 C, *Carom*H), 114.2 (1 C, *Carom*H), 94.9 (1 C,  $\text{CH}_2$ ), 21.5 (1 C,  $\text{CH}_3$ ) ppm.



**Compound 9d:** The preparation of **9d** was performed following the general procedure indicated above from 4-methylphenol **12d** (2 g, 18.50 mmol), vinyl acetate (3.4 mL, 37.00 mmol),  $\text{NaOAc}$  (1.8 g, 22.20 mmol) and  $[\{\text{Ir}(\mu\text{-Cl})(\text{COD})\}_2]$  (124 mg, 0.18 mmol) in anhydrous toluene (18.5 mL). After purification by column chromatography over  $\text{SiO}_2$ , product **9d** was obtained as a colorless oil (2.3 g, 93% isolated yield). The spectroscopic data were in agreement with those reported in the literature.<sup>39,41</sup>  $^1\text{H}$  NMR (500 MHz,  $\text{CDCl}_3$ )  $\delta$  7.14–7.11 (m, 2H), 6.92–6.89 (m, 2H), 6.62 (dd,  $J = 13.7, 6.1$  Hz, 1H), 4.71 (dd,  $J = 13.8, 1.7$  Hz, 1H), 4.38 (dd,  $J = 6.1, 1.6$  Hz, 1H), 2.32 (s, 3H) ppm.  $^{13}\text{C}\{^1\text{H}\}$  NMR (126 MHz,  $\text{CDCl}_3$ )  $\delta$  154.8 (1 C, *Carom*O), 148.9 (1 C, OCH), 132.8 (1 C, *Carom*), 130.2 (2 C, *Carom*H), 117.3 (2 C, *Carom*H), 94.4 (1 C,  $\text{CH}_2$ ), 20.8 (1 C,  $\text{CH}_3$ ) ppm.

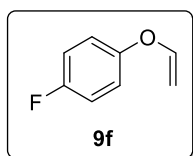


**Compound 9e:** The preparation of **9e** was performed following the general procedure indicated above from 4-methoxyphenol **12e** (662 mg, 5.32 mmol), vinyl acetate (1 mL, 10.70 mmol),  $\text{Na}_2\text{CO}_3$  (339 mg, 3.20 mmol) and

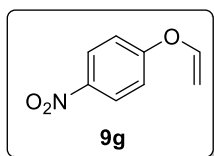
<sup>40</sup> Sheng, S.-R.; Liu, X.-L.; Wang, X.-C.; Xin, Q.; Song, C.-S. *Synthesis* **2004**, 2833-2836.

<sup>41</sup> Yu, L.; Tang, N.; Sheng, S.; Chen, R.; Liu, X.; Cai, M. *Chin. J. Chem.* **2012**, *30*, 1027-1030.

$[\{\text{Ir}(\mu\text{-Cl})(\text{COD})\}_2]$  (35.8 mg, 0.05 mmol) in anhydrous toluene (5.3 mL). After purification by column chromatography over  $\text{SiO}_2$ , product **9e** was obtained as a colorless oil (548.0 mg, 68% isolated yield). The spectroscopic data were in agreement with those reported in the literature.<sup>42</sup>  $^1\text{H}$  NMR (400 MHz,  $\text{CDCl}_3$ )  $\delta$  6.97–6.93 (m, 2H), 6.87–6.83 (m, 2H), 6.59 (dd,  $J = 13.8, 6.2$  Hz, 1H), 4.64 (dd,  $J = 13.8, 1.7$  Hz, 1H), 4.33 (dd,  $J = 6.1, 1.7$  Hz, 1H), 3.78 (s, 3H) ppm.  $^{13}\text{C}\{^1\text{H}\}$  NMR (101 MHz,  $\text{CDCl}_3$ )  $\delta$  155.8 (1 C,  $\text{CH}_3\text{OCarom}$ ), 150.7 (1 C,  $\text{CaromO}$ ), 149.6 (1 C, OCH), 118.8 (2 C,  $\text{CaromH}$ ), 114.8 (2 C,  $\text{CaromH}$ ), 93.7 (1 C,  $\text{CH}_2$ ), 55.8 (1 C,  $\text{OCH}_3$ ) ppm.



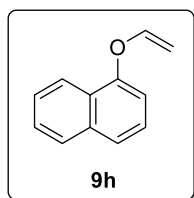
**Compound 9f:** The preparation of **9f** was performed following the general procedure indicated above from 4-fluoro-phenol **12f** (1.9 g, 16.90 mmol), vinyl acetate (3 mL, 33.80 mmol),  $\text{Na}_2\text{CO}_3$  (1.1 g, 10.10 mmol) and  $[\{\text{Ir}(\mu\text{-Cl})(\text{COD})\}_2]$  (114 mg, 0.17 mmol) in anhydrous toluene (16.9 mL). After purification by column chromatography over  $\text{SiO}_2$ , product **9f** was obtained as a colorless oil (1.2 g, 52% isolated yield). The spectroscopic data were in agreement with those reported in the literature.<sup>39</sup>  $^1\text{H}$  NMR (500 MHz,  $\text{CDCl}_3$ )  $\delta$  7.03–6.95 (m, 4H), 6.58 (dd,  $J = 13.7, 6.1$  Hz, 1H), 4.70 (dd,  $J = 13.8, 1.7$  Hz, 1H), 4.41 (dd,  $J = 6.1, 1.8$  Hz, 1H) ppm.  $^{13}\text{C}\{^1\text{H}\}$  NMR (126 MHz,  $\text{CDCl}_3$ )  $\delta$  158.9 (d,  $J = 241.2$  Hz, 1 C,  $\text{CaromF}$ ), 152.8 (d,  $J = 2.6$  Hz, 1 C,  $\text{CaromO}$ ), 148.9 (1 C, OCH), 118.8 (d,  $J = 8.2$  Hz, 2 C,  $\text{CaromH}$ ), 116.2 (d,  $J = 23.5$  Hz, 2 C,  $\text{CaromH}$ ), 94.9 (1 C,  $\text{CH}_2$ ) ppm.  $^{19}\text{F}\{^1\text{H}\}$  NMR (471 MHz,  $\text{CDCl}_3$ )  $\delta$  -120.6 ppm.



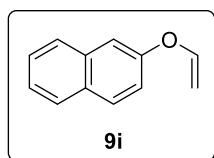
**Compound 9g:** The preparation of **9g** was performed following the general procedure indicated above from 4-nitro-phenol **12g** (1 g, 7.43 mmol), vinyl acetate (1.4 mL, 14.90 mmol),  $\text{Na}_2\text{CO}_3$  (472.4 mg, 4.46 mmol) and  $[\{\text{Ir}(\mu\text{-Cl})(\text{COD})\}_2]$  (49.9 mg, 0.07 mmol) in anhydrous chlorobenzene (7.4 mL). After purification by column chromatography over  $\text{SiO}_2$ , product **9g** was obtained as colorless crystals (836 mg, 68% isolated yield). The spectroscopic data were in agreement with those reported in the literature.<sup>43</sup>  $^1\text{H}$  NMR (500 MHz,  $\text{CDCl}_3$ )  $\delta$  8.25–8.21 (m, 2H), 7.09–7.06 (m, 2H), 6.68 (dd,  $J = 13.6, 6.0$  Hz, 1H), 4.99 (dd,  $J = 13.6, 2.0$  Hz, 1H), 4.69 (dd,  $J = 6.0, 2.0$  Hz, 1H) ppm.  $^{13}\text{C}\{^1\text{H}\}$  NMR (101 MHz,  $\text{CDCl}_3$ )  $\delta$  161.7 (1 C,  $\text{CaromO}$ ), 146.1 (1 C, OCH), 143.2 (1 C,  $\text{CNO}_2$ ), 126.1 (2 C,  $\text{CaromH}$ ), 116.5 (2 C,  $\text{CaromH}$ ), 99.3 (1 C,  $\text{CH}_2$ ) ppm.

<sup>42</sup> Matysiak, S.; Fitznar, H.-P.; Schnell, R.; Pfeleiderer, W. *Helv. Chim. Acta* **1998**, *81*, 1545-1566.

<sup>43</sup> Blouin, M.; Frenette, R. *J. Org. Chem.* **2001**, *66*, 9043-9045.

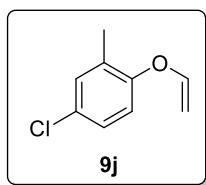


**Compound 9h:** The preparation of **9h** was performed adapting a reported procedure.<sup>44</sup> A mixture of vinyl bromide (3.7 mL, 1 M in THF, 3.70 mmol), 1-naphthol **12h** (800.1 mg, 5.55 mmol, 1.5 equiv.), CuCl (91.6 mg, 0.92 mmol), 2,2,6,6-tetramethyl-3,5-heptanedione (197  $\mu$ L, 0.92 mmol), Cs<sub>2</sub>CO<sub>3</sub> (2.4 g, 7.40 mmol) and toluene (3.7 mL, 5 mL/mmol) were stirred at reflux for 5 h under inert atmosphere. The crude mixture was cooled down, diluted with MTBE (10 mL) and filtered through a pad of Celite<sup>®</sup>. The filtrate was washed with 28% aqueous ammonium hydroxide and dried over K<sub>2</sub>CO<sub>3</sub>. After purification by column chromatography over SiO<sub>2</sub> using pentane/DCM 80:20 as eluents, product **9h** was obtained as a colorless oil (440 mg, 70% isolated yield). The spectroscopic data were in agreement with those reported in the literature.<sup>39</sup> <sup>1</sup>H NMR (400 MHz, CDCl<sub>3</sub>)  $\delta$  8.31–8.27 (m, 1H), 7.90–7.86 (m, 1H), 7.63–7.61 (d, *J* = 8.4 Hz, 1H), 7.57–7.53 (m, 2H), 7.43 (dd, *J* = 7.9 Hz, 1H), 7.05 (dd, *J* = 7.6, 1.0 Hz, 1H), 6.84 (dd, *J* = 13.7, 6.1 Hz, 1H), 4.94 (dd, *J* = 13.7, 1.6 Hz, 1H), 4.57 (dd, *J* = 6.1, 1.7 Hz, 1H) ppm. <sup>13</sup>C{<sup>1</sup>H} NMR (101 MHz, CDCl<sub>3</sub>)  $\delta$  152.8 (1 C, *Carom*O), 148.7 (1 C, OCH), 134.8 (1 C, *Carom*), 127.7 (1 C, *Carom*H), 126.7 (1 C, *Carom*H), 126.0 (1 C, *Carom*), 125.9 (1 C, *Carom*H), 125.7 (1 C, *Carom*H), 123.1 (1 C, *Carom*H), 122.0 (1 C, *Carom*H), 110.6 (1 C, *Carom*H), 95.6 (1 C, CH<sub>2</sub>) ppm.

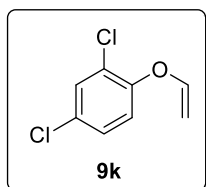


**Compound 9i:** The preparation of **9i** was performed following the general procedure indicated above from 2-naphthol **12i** (652.4 mg, 4.53 mmol), vinyl acetate (838  $\mu$ L, 9.05 mmol), NaOAc (445.5 mg, 5.43 mmol) and [Ir( $\mu$ -Cl)(COD)]<sub>2</sub> (30.4 mg, 0.04 mmol). After purification by column chromatography, product **9i** was obtained as colorless crystals (609 mg, 79% isolated yield). The spectroscopic data were in agreement with those reported in the literature.<sup>39</sup> <sup>1</sup>H NMR (300 MHz, CDCl<sub>3</sub>)  $\delta$  7.84 (d, *J* = 8.7 Hz, 2H), 7.79 (d, *J* = 8.1 Hz, 1H), 7.51 (ddd, *J* = 8.2, 6.8, 1.4 Hz, 1H), 7.43 (ddd, *J* = 8.1, 6.9, 1.4 Hz, 1H), 7.37 (d, *J* = 2.5 Hz, 1H), 7.27 (dd, *J* = 8.9, 2.5 Hz, 1H), 6.82 (dd, *J* = 13.7, 6.1 Hz, 1H), 4.90 (dd, *J* = 13.7, 1.7 Hz, 1H), 4.56 (dd, *J* = 6.1, 1.7 Hz, 1H) ppm. <sup>13</sup>C{<sup>1</sup>H} NMR (75 MHz, CDCl<sub>3</sub>)  $\delta$  154.8 (1 C, *Carom*O), 148.2 (1 C, OCH), 134.4 (1 C, *Carom*), 130.2 (1 C, *Carom*), 129.9 (1 C, *Carom*H), 127.9 (1 C, *Carom*H), 127.2 (1 C, *Carom*H), 126.7 (1 C, *Carom*H), 124.7 (1 C, *Carom*H), 119.0 (1 C, *Carom*H), 111.7 (1 C, *Carom*H), 95.8 (1 C, CH<sub>2</sub>) ppm.

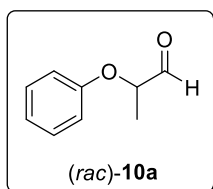
<sup>44</sup> Wan, Z.; Jones, C. D.; Koenig, T. M.; Pu, Y. J.; Mitchell, D. *Tetrahedron Lett.* **2003**, *44*, 8257–8259.



**Compound 9j:** The preparation of **9j** was performed following the general procedure indicated above from **12j** (0.99 mg, 6.79 mmol), vinyl acetate (1.3 mL, 13.60 mmol),  $\text{Na}_2\text{CO}_3$  (431.7 mg, 4.07 mmol) and  $[\{\text{Ir}(\mu\text{-Cl})(\text{COD})\}_2]$  (45.6 mg, 0.07 mmol) in anhydrous toluene (6.8 mL). After purification by column chromatography over  $\text{SiO}_2$ , product **9j** was obtained as a colorless oil (1.1 g, 86% isolated yield). IR (neat,  $\text{cm}^{-1}$ )  $\bar{\nu}$  2924, 1641, 1482, 1384, 1292, 1240, 1186, 1150, 953, 908, 874, 808, 731, 653, 557, 443.  $^1\text{H}$  NMR (300 MHz,  $\text{CDCl}_3$ )  $\delta$  7.18–7.11 (m, 1H), 6.86 (d,  $J = 8.5$  Hz, 1H), 6.58 (dd,  $J = 13.8$ , 6.2 Hz, 1H), 4.61 (dd,  $J = 13.8$ , 1.8 Hz, 1H), 4.39 (dd,  $J = 6.2$ , 1.9 Hz, 1H), 2.23 (d,  $J = 0.8$  Hz, 3H) ppm.  $^{13}\text{C}\{^1\text{H}\}$  NMR (75 MHz,  $\text{CDCl}_3$ )  $\delta$  153.3 (1 C, *Carom*O), 148.8 (1 C, OCH), 131.0 (1 C, *Carom*H), 130.6 (1 C, *Carom*CH<sub>3</sub>), 128.4 (1 C, *Carom*Cl), 126.9 (1 C, *Carom*H), 118.3 (1 C, *Carom*H), 94.3 (1 C, CH<sub>2</sub>), 16.1 (1 C, CH<sub>3</sub>) ppm. HRMS (APCI)  $m/z$   $[\text{M}+\text{H}]^+$  calcd for  $\text{C}_9\text{H}_{10}\text{ClO}$  169.0413, found 169.0415.



**Compound 9k:** The preparation of **9k** was performed following the general procedure indicated above from 2,4-chloro-phenol **12k** (1.1 g, 6.71 mmol), vinyl acetate (1.2 mL, 13.40 mmol),  $\text{Na}_2\text{CO}_3$  (426.9 mg, 4.03 mmol) and  $[\{\text{Ir}(\mu\text{-Cl})(\text{COD})\}_2]$  (45.1 mg, 0.01 mmol) in anhydrous toluene (6.7 mL). After purification by column chromatography over  $\text{SiO}_2$ , product **9k** was obtained as a colorless oil (944 mg, 78% isolated yield). IR (neat,  $\text{cm}^{-1}$ )  $\bar{\nu}$  3071, 1640, 1625, 1583, 1474, 1383, 1311, 1275, 1134, 1101, 1058, 950, 866, 836, 808, 742, 695, 649, 561, 443.  $^1\text{H}$  NMR (300 MHz,  $\text{CDCl}_3$ )  $\delta$  7.41 (d,  $J = 2.5$  Hz, 1H), 7.20 (dd,  $J = 8.7$ , 2.5 Hz, 1H), 6.98 (d,  $J = 8.7$  Hz, 1H), 6.55 (dd,  $J = 13.7$ , 6.1 Hz, 1H), 4.74 (dd,  $J = 13.7$ , 2.2 Hz, 1H), 4.51 (dd,  $J = 6.1$ , 2.2 Hz, 1H) ppm.  $^{13}\text{C}\{^1\text{H}\}$  NMR (101 MHz,  $\text{CDCl}_3$ )  $\delta$  151.1 (1 C, *Carom*O), 148.0 (1 C, OCH), 130.5 (1 C, *Carom*H), 129.0 (1 C, *Carom*Cl), 128.0 (1 C, *Carom*H), 125.5 (1 C, *Carom*Cl), 119.4 (1 C, *Carom*H), 96.2 (1 C, CH<sub>2</sub>) ppm. HRMS (APCI)  $m/z$   $[\text{M}+\text{H}]^+$  calcd for  $\text{C}_8\text{H}_7\text{Cl}_2\text{O}$  188.9868, found 188.9876.



**Compound (rac)-10a:** The preparation of **(rac)-10a** was performed following a reported procedure.<sup>45</sup>  $\text{LiAlH}_4$  (1 M in THF, 21.2 mL, 21.20 mmol) was added to a stirred solution of 2-phenoxypropionic acid (2 g, 11.80 mmol) in  $\text{Et}_2\text{O}$  (29.5 mL) at 0 °C. The mixture was stirred at room temperature for 16 h. The reaction was quenched by the careful sequential addition of  $\text{H}_2\text{O}$  (0.8 mL), 15% aq.  $\text{NaOH}$  (0.8 mL) and  $\text{H}_2\text{O}$  (2.5 mL). The resulting mixture was

<sup>45</sup> Ling, K. B.; Smith, A. D. *Chem. Commun.* **2011**, 47, 373-375.

stirred vigorously for 30 min and then filtered through Celite<sup>®</sup> using MeOH as eluent. The filtrate was concentrated *in vacuo*. The oily residue was dissolved in Et<sub>2</sub>O and then dried, filtered and concentrated *in vacuo*. After purification by column chromatography over SiO<sub>2</sub> using Cy/AcOEt 90:10 as eluents, 2-phenoxypropan-1-ol **15** was obtained as a colorless oil (1.2 g, 66% isolated yield). The spectroscopic data were in agreement with those reported in the literature.<sup>46</sup> <sup>1</sup>H NMR (500 MHz, CDCl<sub>3</sub>) δ 7.31–7.27 (m, 2H), 6.98–6.93 (m, 3H), 4.47–4.53 (m, 1H), 3.77–3.69 (m, 2H), 2.19 (dd, *J* = 7.6, 5.1 Hz, 1H), 1.28 (d, *J* = 6.2 Hz, 3H) ppm. <sup>13</sup>C{<sup>1</sup>H} NMR (101 MHz, CDCl<sub>3</sub>) δ 157.8 (1 C, *CaromO*), 129.7 (2 C, *CaromH*), 121.3 (1 C, *CaromH*), 116.2 (2 C, *CaromH*), 74.8 (1 C, CH), 66.4 (1 C, CH<sub>2</sub>), 15.9 (1 C, CH<sub>3</sub>) ppm. DMSO (565 μL, 7.95 mmol) was added dropwise to a stirred solution of oxalyl chloride (2.4 mL, 4.77 mmol) in CH<sub>2</sub>Cl<sub>2</sub> (31.2 mL) at –78 °C. After 5 min, a solution of 2-phenoxypropan-1-ol **15** (605 mg, 4.0 mmol) in CH<sub>2</sub>Cl<sub>2</sub> (8 mL) was added dropwise via syringe. The solution was stirred at –78 °C for 30 min and NEt<sub>3</sub> (2.2 mL, 15.90 mmol) was subsequently added. The resulting mixture was allowed to reach room temperature (30 min). The reaction was quenched by adding H<sub>2</sub>O (20 mL) and the aqueous layer extracted with CH<sub>2</sub>Cl<sub>2</sub> (3 x 25 mL). The combined organic extracts were washed with 0.1 M aq. HCl (80 mL), H<sub>2</sub>O (80 mL), sat. aq. NaHCO<sub>3</sub> (80 mL) and brine (80 mL), then dried over MgSO<sub>4</sub>, filtered and concentrated *in vacuo*. After purification by column chromatography over SiO<sub>2</sub> using Cy/AcOEt 90:10 as eluents, 2-phenoxypropanal (*rac*)-**10a** was obtained as a colorless oil (408 mg, 68% isolated yield). The spectroscopic data were in agreement with those reported in the literature.<sup>47</sup> <sup>1</sup>H NMR (500 MHz, CDCl<sub>3</sub>) δ 9.73 (d, *J* = 2.0 Hz, 1H), 7.32–7.29 (m, 2H), 7.02–6.99 (m, 1H), 6.90 (dt, *J* = 8.8, 1.0 Hz, 2H), 4.64 (qd, *J* = 6.9, 2.0 Hz, 1H), 1.49 (d, *J* = 7.0 Hz, 3H) ppm. <sup>13</sup>C{<sup>1</sup>H} NMR (126 MHz, CDCl<sub>3</sub>) δ 202.6 (1 C, CO), 157.4 (1 C, *CaromO*), 129.9 (2 C, *CaromH*), 122.0 (1 C, *CaromH*), 115.4 (2 C, *CaromH*), 77.9 (1 C, CH), 15.7 (1 C, CH<sub>3</sub>) ppm.

### 3.5.5 General procedure for the Rh-catalyzed enantioselective hydroformylation of aryl vinyl ethers

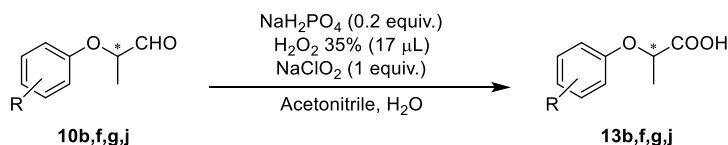
In a glove box filled with nitrogen, ligands **L1-L6** (*ca.* 2.7 μmol in 360 μL of toluene), BARF salt (*ca.* 3.6 μmol in 27 μL of THF) and [Rh(κ<sup>2</sup>O,O'-acac)(CO)<sub>2</sub>] (*ca.* 2.3 μmol in 65 μL of toluene) were placed into a 2 mL vial equipped with a magnetic stirrer. Substrate **9a-k** (*ca.* 230 μmol), dodecane (*ca.* 69 μmol) and

<sup>46</sup> Carocci, A.; Catalano, A.; Lovece, A.; Lentini, G.; Duranti, A.; Lucini, V.; Pannacci, M.; Scaglione, F.; Franchini, C. *Bioorg. Med. Chem.* **2010**, *18*, 6496-6511.

<sup>47</sup> Preti, L.; Attanasi, O. A.; Caselli, E.; Favi, G.; Ori, C.; Davoli, P.; Felluga, F.; Prati, F. *Eur. J. Org. Chem.* **2010**, 4312-4320.

additional toluene were charged to provide the desired final solution of toluene/THF (97:3 v/v). The vial was transferred into an autoclave and taken out of the glove box. The autoclave was purged three times with syngas (1:1 H<sub>2</sub>/CO at a pressure not higher than that planned for the hydroformylation reaction and without stirring) and, finally, the autoclave was pressurized with syngas to the desired pressure. The reaction mixture was stirred at the selected temperature (metallic block) for the selected reaction time. The reaction was cooled if required and the pressure was carefully released in a well-ventilated hood. Conversions of **9a-9k** were determined by <sup>1</sup>H NMR analysis from the reaction mixtures. Branched to linear ratios for products derived from the hydroformylation of **9a-9k** were determined by GC analysis with a Supelco β-Dex<sup>TM</sup> 225 column by using the dodecane present in the reaction mixture as internal standard. Enantiomeric ratios for the products derived from the hydroformylations of **9a**, **9c-e** and **9h-i** were determined by GC analysis with a Supelco β-Dex<sup>TM</sup> 225 column by using the dodecane present in the reaction mixture as internal standard. The enantiomeric ratios for the branched hydroformylation products derived from **9b**, **9f**, **9g** and **9j** were determined by HPLC analysis after derivatization to the corresponding carboxylic acids.

### 3.5.6 General procedure for the oxidation of 2-aryloxypropanals to 2-aryloxypropanoic acid derivatives

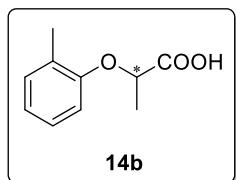


**Scheme 43.** General procedure for the oxidation of 2-aryloxypropanals to 2-aryloxypropanoic acid derivatives

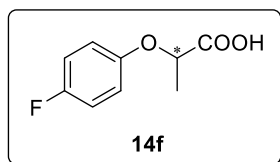
The derivatization of the 2-aryloxypropanals towards the corresponding acid derivatives was performed following a reported procedure.<sup>8</sup> A solution of NaH<sub>2</sub>PO<sub>4</sub> (5 mg, 0.04 mmol) in H<sub>2</sub>O (73 µL) and H<sub>2</sub>O<sub>2</sub> 35% (17 µL) were added to a solution of the 2-aryloxypropanal crude mixture (**10b**, **10f**, **10g** and **10j**) (0.20 mmol) in acetonitrile (186 µL) and was stirred for 5 min. A solution of NaClO<sub>2</sub> (19 mg, 0.2 mmol) in H<sub>2</sub>O (209 µL) were sequentially added at 10 °C to the pre-cooled reaction mixture. The solution was allowed to reach room temperature and was stirred at room temperature for 24 h. The reaction was quenched with a sat. solution of Na<sub>2</sub>SO<sub>3</sub> (2 mL), acidified with HCl 2 M (5 mL) and extracted with AcOEt (3 x 1 mL). The organic phases were combined and dried over Na<sub>2</sub>SO<sub>4</sub>. After solvent evaporation, the product was isolated by



column chromatography over SiO<sub>2</sub> using Cy/AcOEt/formic acid 80:20:1 as eluents to afford the desired product.

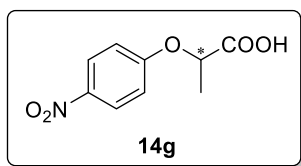


**Compound 14b:** The derivatization of the branched hydroformylation product towards the acid derivative **14b** was performed following the general procedure above indicated. After purification by column chromatography over SiO<sub>2</sub>, product **14b** was obtained as a colorless solid (7.7 mg, 75% isolated yield). Mp: 74–75 °C.  $[\alpha]_D^{25} = -12.6$  (c. 0.26, CHCl<sub>3</sub>) (reported<sup>48</sup>  $[\alpha]_D^{25} = +18.3$  (c. 10, CHCl<sub>3</sub>) for a sample of the (R) enantiomer with a 93% optical purity). IR (neat, cm<sup>-1</sup>)  $\bar{\nu}$  2984, 1703, 1590, 1493, 1457, 1294, 1234, 1192, 1139, 1051, 839, 841, 767, 743, 712, 665, 606, 567, 442. <sup>1</sup>H NMR (400 MHz, CDCl<sub>3</sub>)  $\delta$  7.17–7.09 (m, 2H), 6.90 (td, *J* = 7.4, 1.0 Hz, 1H), 6.72 (d, *J* = 8.2 Hz, 1H), 4.76 (q, *J* = 6.8 Hz, 1H), 2.27 (s, 3H), 1.65 (d, *J* = 6.8 Hz, 3H) ppm. <sup>13</sup>C{<sup>1</sup>H} NMR (101 MHz, CDCl<sub>3</sub>)  $\delta$  177.4 (1 C, COOH), 155.6 (1 C, *Carom*O), 131.3 (1 C, *Carom*H), 127.7 (1 C, *Carom*H), 126.9 (1 C, *Carom*H), 121.8 (1 C, *Carom*H), 112.2 (1 C, *Carom*H), 72.6 (1 C, CH), 18.6 (1 C, CH<sub>3</sub>), 16.4 (1 C, CH<sub>3</sub>) ppm. HRMS (ESI) *m/z* [M–H]<sup>-</sup> calcd for C<sub>10</sub>H<sub>11</sub>O<sub>3</sub> 179.0714, found 179.0718.

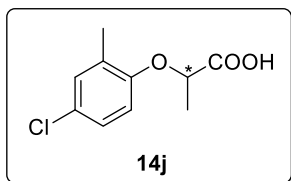


**Compound 14f:** The derivatization of the branched hydroformylation product towards the acid derivative **14f** was performed following the general procedure above indicated. After purification by column chromatography over SiO<sub>2</sub>, product **14f** was obtained as a colorless solid (9.3 mg, 50% isolated yield). Mp: 113–114 °C.  $[\alpha]_D^{25} = -18.5$  (c. 0.65, MeOH). IR (neat, cm<sup>-1</sup>)  $\bar{\nu}$  2998, 1714, 1503, 1448, 1420, 1369, 1333, 1290, 1206, 1137, 1095, 1043, 919, 823, 755, 683, 636, 516, 421. <sup>1</sup>H NMR (400 MHz, CDCl<sub>3</sub>)  $\delta$  7.00–6.95 (m, 2H), 6.87–6.83 (m, 2H), 4.72 (q, *J* = 6.8 Hz, 1H), 1.64 (d, *J* = 6.8 Hz, 3H) ppm. <sup>13</sup>C{<sup>1</sup>H} NMR (101 MHz, CDCl<sub>3</sub>)  $\delta$  177.4 (1 C, COOH), 158.1 (d, *J* = 240.1 Hz, 1 C, *Carom*F), 153.4 (d, *J* = 2.2 Hz, 1 C, *Carom*O), 116.7 (d, *J* = 8.1 Hz, 2 C, *Carom*H), 116.2 (d, *J* = 23.1 Hz, 2 C, *Carom*H), 73.1 (1 C, CH), 18.6 (1 C, CH<sub>3</sub>) ppm. <sup>19</sup>F{<sup>1</sup>H} NMR (376 MHz, CDCl<sub>3</sub>)  $\delta$  -122.2 ppm. HRMS (ESI) *m/z* [M–H]<sup>-</sup> calcd for C<sub>9</sub>H<sub>8</sub>FO<sub>3</sub> 183.0463, found 183.0471.

<sup>48</sup> The absolute configuration was determined to the *S* by comparison of the specific optical rotation with reported data (Eveleens, W.; Spaans, J.; Wissink, H. G., EP0009285, 1980.).



**Compound 14g:** The derivatization of the branched hydroformylation product towards the acid derivative **14g** was performed following the general procedure above indicated. After purification by column chromatography over SiO<sub>2</sub>, product **14g** was obtained as a colorless solid (19.7 mg, 81% isolated yield). Mp: 129–130 °C.  $[\alpha]_D^{26} = -44.3$  (c. 1.2, acetone) (reported<sup>49</sup>  $[\alpha]_D^{20} = -41.2$  (c. 1, abs. EtOH) for a sample of the (*S*) enantiomer with a 80.8% optical purity). IR (neat, cm<sup>-1</sup>)  $\bar{\nu}$  2944, 1727, 1592, 1510, 1496, 1343, 1299, 1246, 1182, 1106, 1044, 904, 845, 750, 688, 655, 506. <sup>1</sup>H NMR (300 MHz, CDCl<sub>3</sub>)  $\delta$  8.23–8.18 (m, 2H), 6.97–6.92 (m, 2H), 4.91 (q, *J* = 6.8 Hz, 1H), 1.72 (d, *J* = 6.9 Hz, 3H) ppm. <sup>13</sup>C{<sup>1</sup>H} NMR (101 MHz, CDCl<sub>3</sub>)  $\delta$  176.4 (1 C, COOH), 162.2 (1 C, *Carom*O), 142.4 (1 C, CNO<sub>2</sub>), 126.1 (2 C, *Carom*H), 115.1 (2 C, *Carom*H), 72.3 (1 C, CH), 18.4 (1 C, CH<sub>3</sub>) ppm. HRMS (ESI)  $m/z$  [M–H]<sup>-</sup> calcd for C<sub>9</sub>H<sub>8</sub>NO<sub>5</sub> 210.0408, found 210.0414.



**Compound 14j:** The derivatization of the branched hydroformylation product towards the acid derivative **14j** was performed following the general procedure above indicated. After purification by column chromatography over SiO<sub>2</sub>, product **14j** was obtained as a colorless solid (3.7 mg, 46% isolated yield). Mp: 94–95 °C.  $[\alpha]_D^{25} = -14.7$  (c. 0.5, acetone) (reported<sup>50</sup>  $[\alpha]_D^{25} = +29.3$  (c. 0.9, acetone) for a sample of the (*R*) enantiomer with a >99% optical purity). IR (neat, cm<sup>-1</sup>)  $\bar{\nu}$  2919, 1700, 1490, 1455, 1292, 1241, 1188, 1141, 1050, 901, 879, 791, 660, 554, 444. <sup>1</sup>H NMR (400 MHz, CDCl<sub>3</sub>)  $\delta$  7.14 (dd, *J* = 2.7, 0.9 Hz, 1H), 7.08–7.05 (m, 1H), 6.63 (d, *J* = 8.7 Hz, 1H), 4.73 (q, *J* = 6.9 Hz, 1H), 2.24 (s, 3H), 1.66 (d, *J* = 6.8 Hz, 3H) ppm. <sup>13</sup>C{<sup>1</sup>H} NMR (101 MHz, CDCl<sub>3</sub>)  $\delta$  177.1 (1 C, COOH), 154.3 (1 C, *Carom*O), 131.1 (1 C, *Carom*H), 129.7 (1 C, *Carom*CH<sub>3</sub>), 126.6 (1 C, *Carom*Cl), 126.5 (1 C, *Carom*H), 113.3 (1 C, *Carom*H), 72.8 (1 C, CH), 18.6 (1 C, CH<sub>3</sub>), 16.3 (1 C, CH<sub>3</sub>) ppm. HRMS (ESI)  $m/z$  [M–H]<sup>-</sup> calcd for C<sub>10</sub>H<sub>10</sub>ClO<sub>3</sub> 213.0332, found 213.0324.

<sup>49</sup> The absolute configuration was determined to be *S* by comparison of the specific optical rotation with reported data (Vakarov, S. A.; Chulakov, E. N.; Sadretdinova, L. S.; Kodess, M. I.; Ezhikova, M. A.; Pervova, M. G.; Ganebnykh, I. N.; Levit, G. L.; Krasnov, V. P. *ChemistrySelect* **2020**, *5*, 4069-4073.).

<sup>50</sup> The absolute configuration was determined to be *S* by comparison of the specific optical rotation with reported data (Salz, U.; Ruechardt, C. *Chem. Ber.* **1984**, *117*, 3457-3462.).

### 3.5.7 Determination of the enantiomeric ratio and absolute configuration of the hydroformylation products

The absolute configurations of the hydroformylation products were assigned by comparison of the elution orders in GC or HPLC analysis on chiral stationary phases, or by comparison of the specific optical rotation obtained for the derivatization products, with reported data.<sup>51</sup>

GC analysis conditions for the hydroformylation products of **9a**: Enantiomeric ratio was determined by GC analysis with a Supelco  $\beta$ -Dex<sup>TM</sup> 225 column (30 m x 0.25 mm x 0.25  $\mu$ m). Flow rate: 1 mL/min. Temperature program: 100 °C for 5 min, then 4 °C/min to 200 °C, then 20 °C/min to 220 °C. Retention times: 3.4 min for **9a**, 11.0 (*S*)-**10a**, 11.8 (*R*)-**10a** min for the enantiomers of the branched product and 17.4 min for the linear isomer **11a**.

GC analysis conditions for the hydroformylation products of **9c**: Enantiomeric ratio was determined by GC analysis with a Supelco  $\beta$ -Dex<sup>TM</sup> 225 column (30 m x 0.25 mm x 0.25  $\mu$ m). Flow rate: 1 mL/min. Temperature program: 100 °C for 5 min, then 4 °C/min to 200 °C, then 20 °C/min to 220 °C. Retention times: 5.2 min for **9c**, 13.2 (*S*)-**10c**, 13.9 (*R*)-**10c** min for the enantiomers of the branched product and 19.5 min for the linear isomer **11c**.

GC analysis conditions for the hydroformylation products of **9d**: Enantiomeric ratio was determined by GC analysis with a Supelco  $\beta$ -Dex<sup>TM</sup> 225 column (30 m x 0.25 mm x 0.25  $\mu$ m). Flow rate: 1 mL/min. Temperature program: 100 °C for 5 min, then 4 °C/min to 200 °C, then 20 °C/min to 220 °C. Retention times: 5.6 min for **9d**, 13.8 (*S*)-**10d**, 14.8 (*R*)-**10d** min for the enantiomers of the branched product and 19.9 min for the linear isomer **11d**.

GC analysis conditions for the hydroformylation products of **9e**: Enantiomeric ratio was determined by GC analysis with a Supelco  $\beta$ -Dex<sup>TM</sup> 225 column (30 m x 0.25 mm x 0.25  $\mu$ m). Flow rate: 1 mL/min. Temperature program: 100 °C for 5 min, then 4 °C/min to 200 °C, then 20 °C/min to 220 °C. Retention times: 11.3 min for **9e**, 19.2 (*S*)-**10e**, 19.5 (*R*)-**10e** min for the enantiomers of the branched product and 24.4 min for the linear isomer **11e**.

---

<sup>51</sup> The racemic carboxylic acids have been synthesized following a reported procedure in a two steps synthesis from the corresponding phenol to the methyl ester (Wang, X.; Zhao, T.; Yang, B.; Li, Z.; Cui, J.; Dai, Y.; Qiu, Q.; Qiang, H.; Huang, W.; Qian, H. *Bioorg. Med. Chem.* **2015**, *23*, 132-140) and subsequent hydrolysis to the corresponding carboxylic acid (Li, H.; Thota, S.; Carroll, D.; Argade, A.; Tso, K.; Sran, A.; Clough, J.; Keim, H.; Bhamidipati, S.; Taylor, V.; Cooper, R.; Singh, R.; Wong, B., WO2006133426A2, **2006**).

GC analysis conditions for the hydroformylation products of **9h**: Enantiomeric ratio was determined by GC analysis with a Supelco  $\beta$ -Dex<sup>TM</sup> 225 column (30 m x 0.25 mm x 0.25  $\mu$ m). Flow rate: 1.5 mL/min. Temperature program: 130 °C for 92 min, then 20 °C/min to 220 °C, then 220 °C for 5 min. Retention times: 11.8 min for **9h**, 48.3 (*S*)-**10h**, 49.7 (*R*)-**10h** min for the enantiomers of the branched product and 96.5 min for the linear isomer **11h**.

GC analysis conditions for the hydroformylation products of **9i**: Enantiomeric ratio was determined by GC analysis with a Supelco  $\beta$ -Dex<sup>TM</sup> 225 column (30 m x 0.25 mm x 0.25  $\mu$ m). Flow rate: 1 mL/min. Temperature program: 120 °C for 90 min, then 1 °C/min to 220 °C, then 220 °C for 5 min. Retention times: 28.0 min for **9i**, 111.8 (*S*)-**10i**, 115.9 (*R*)-**10i** min for the enantiomers of the branched product and 155.8 min for the linear isomer **11i**.

GC analysis conditions for the hydroformylation products of **9k**: Enantiomeric ratio was determined by GC analysis with a Supelco  $\beta$ -Dex<sup>TM</sup> 225 column (30 m x 0.25 mm x 0.25  $\mu$ m). Flow rate: 1 mL/min. Temperature program: 120 °C for 80 min, then 4 °C/min to 200 °C, then 200 °C for 30 min. Retention times: 5.3 min for **9k**, 58.6 (*S*)-**10k**, 61.7 (*R*)-**10k** min for the enantiomers of the branched product and 95.5 min for the linear isomer **11k**.

HPLC analysis conditions for the derivatization product of **9b**: Enantiomeric ratio was determined by HPLC analysis, Daicel Chiracel<sup>®</sup> AD-H (25 x 0.46 cm), 98/2/0.1 hexane/2-propanol/trifluoroacetic acid, 0.75 mL/min, 254 nm,  $t_{R(R)}$ -**14b** = 21.7 min,  $t_{R(S)}$ -**14b** = 17.0 min.<sup>52</sup>

HPLC analysis conditions for the derivatization product of **9f**: Enantiomeric ratio was determined by HPLC analysis, Daicel Chiracel<sup>®</sup> AD-H (25 x 0.46 cm), 90/10/0.1 hexane/2-propanol/trifluoroacetic acid, 1 mL/min, 254 nm,  $t_{R(R)}$ -**14f** = 7.4 min,  $t_{R(S)}$ -**14f** = 5.8 min.

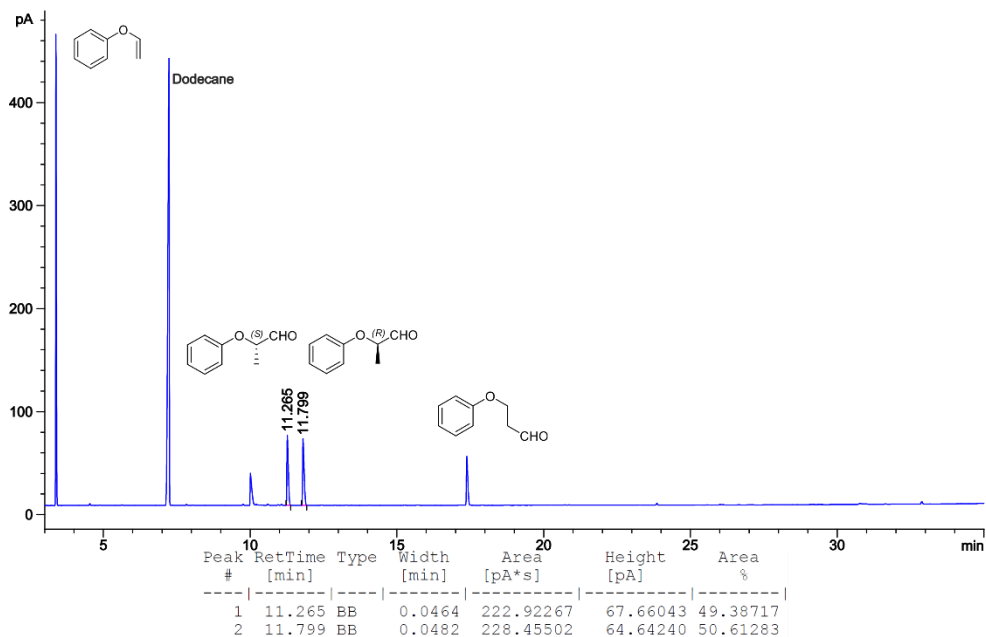
HPLC analysis conditions for the derivatization product of **9g**: Enantiomeric ratio was determined by HPLC analysis, Daicel Chiracel<sup>®</sup> ID (25 x 0.46 cm), 90/10/0.1 hexane/2-propanol/trifluoroacetic acid, 1 mL/min, 254 nm,  $t_{R(R)}$ -**14g** = 8.1 min,  $t_{R(S)}$ -**14g** = 9.6 min.

HPLC analysis conditions for the derivatization product of **9j**: Enantiomeric ratio was determined by HPLC analysis, Daicel Chiracel<sup>®</sup> IC (25 x 0.46 cm), 98/2/0.1 hexane/2-propanol/trifluoroacetic acid, 1 mL/min, 254 nm,  $t_{R(R)}$ -**14j** = 5.8 min,  $t_{R(S)}$ -**14j** = 6.9 min.<sup>52</sup>

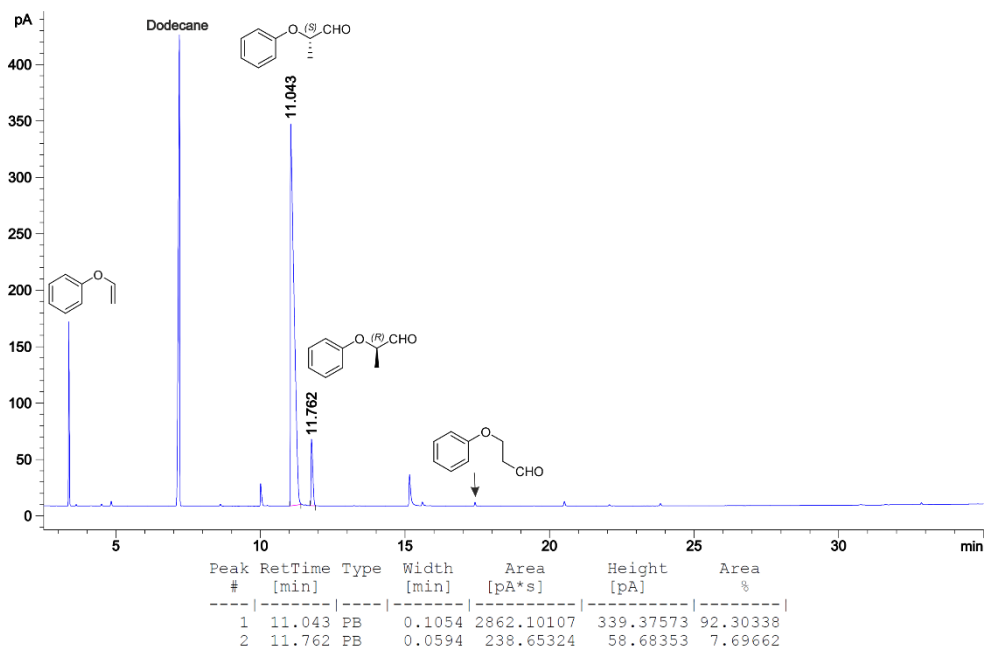
<sup>52</sup> Tengeiji, A.; Nakata, K.; Ono, K.; Shiina, I. *Heterocycles* **2012**, *86*, 1227-1252.

### 3.5.8 Selected GC and HPLC chromatograms

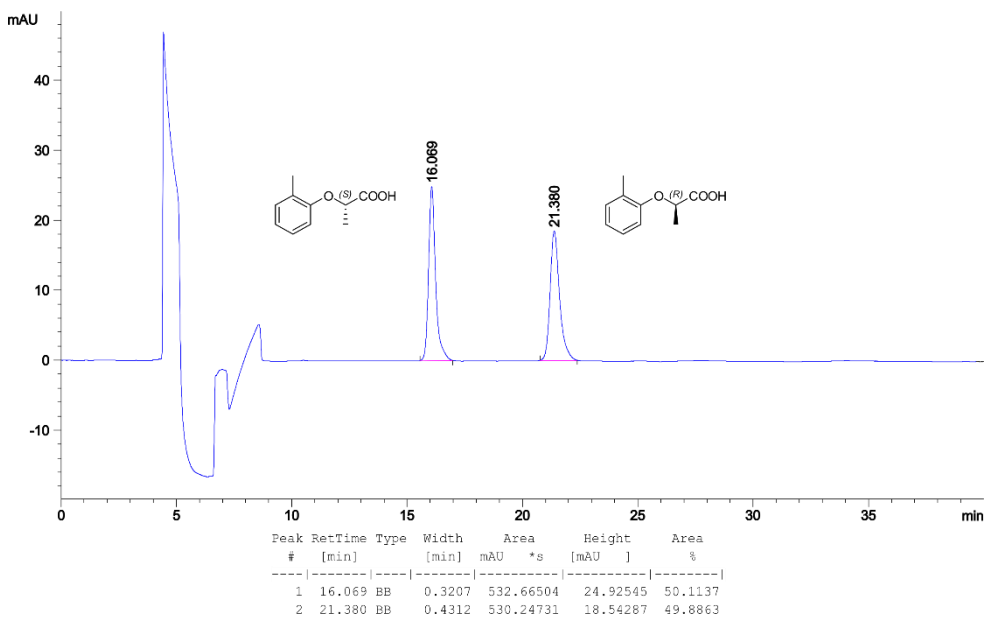
GC chromatogram of the racemic hydroformylation reaction mixture derived from **9a**



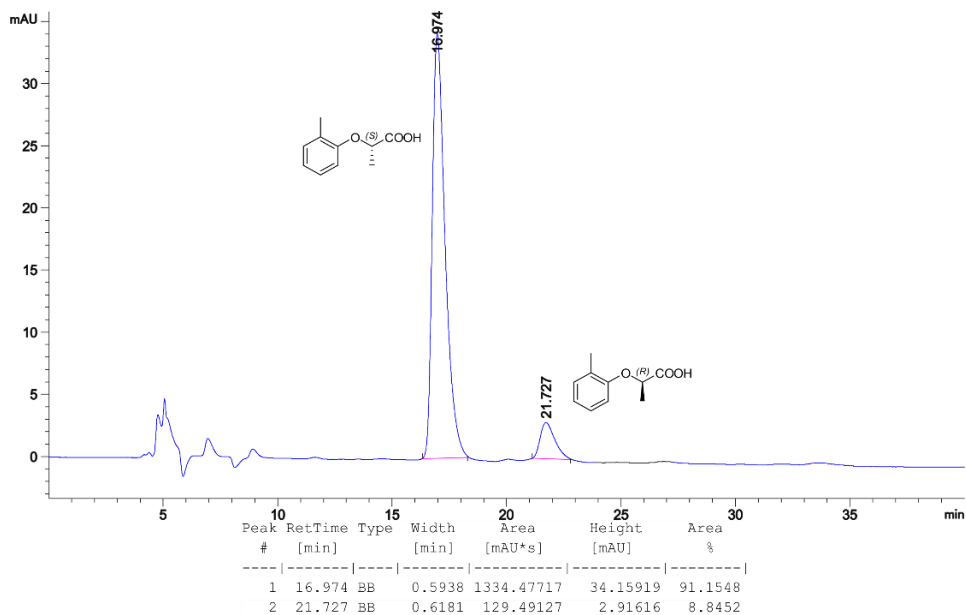
GC chromatogram of the enantioselective hydroformylation reaction mixture derived from **9a** (Table 33, entry 8)



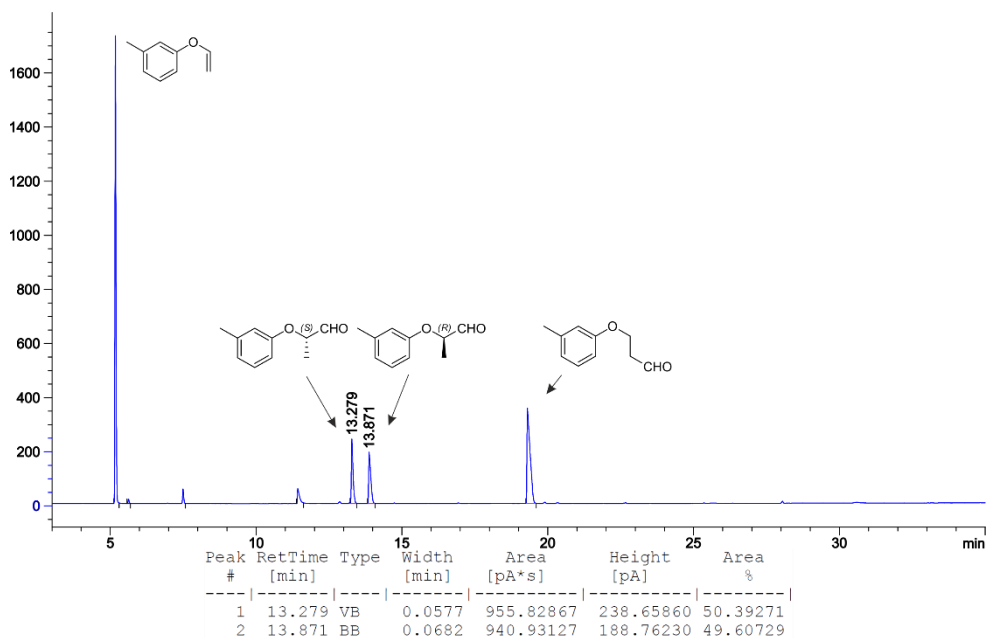
HPLC chromatogram of the racemic carboxylic acid **14b**



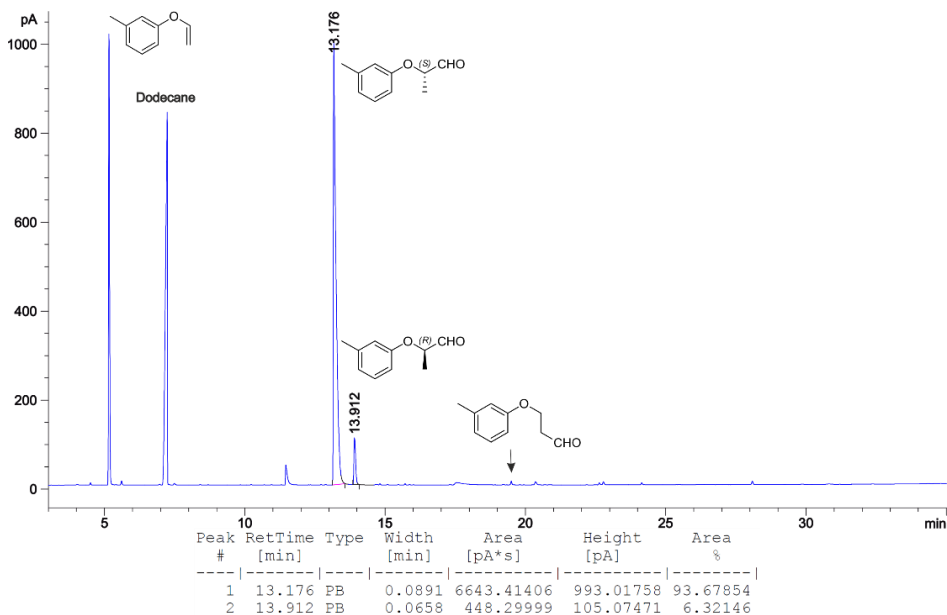
HPLC chromatogram of the enantioselective hydroformylation and subsequent derivatization to the carboxylic acid **14b** (Table 34, entry 2)



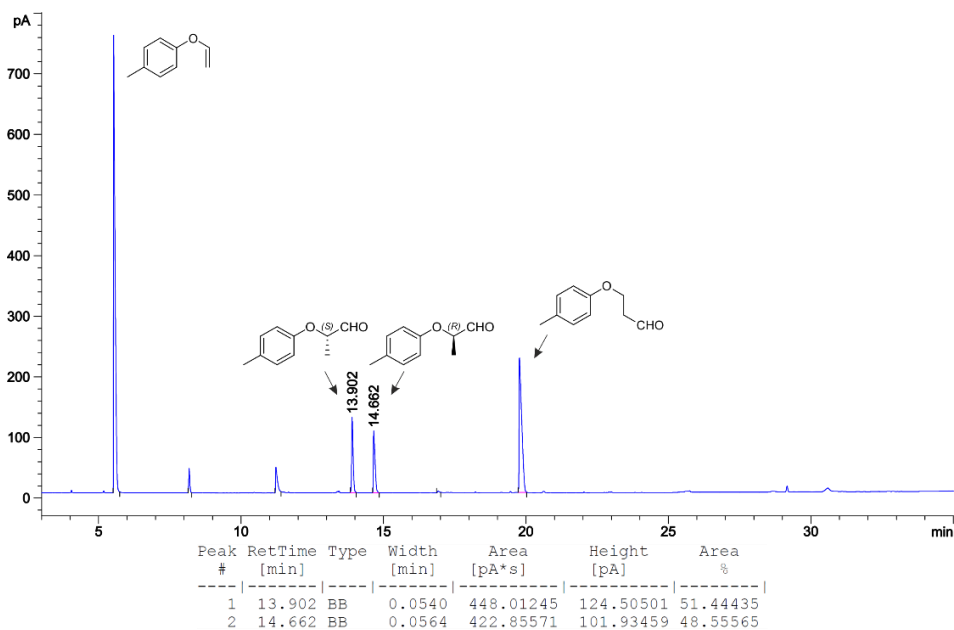
GC chromatogram of the racemic hydroformylation reaction mixture derived from **9c**



GC chromatogram of the enantioselective hydroformylation reaction mixture derived from **9c** (Table 34, entry 9)

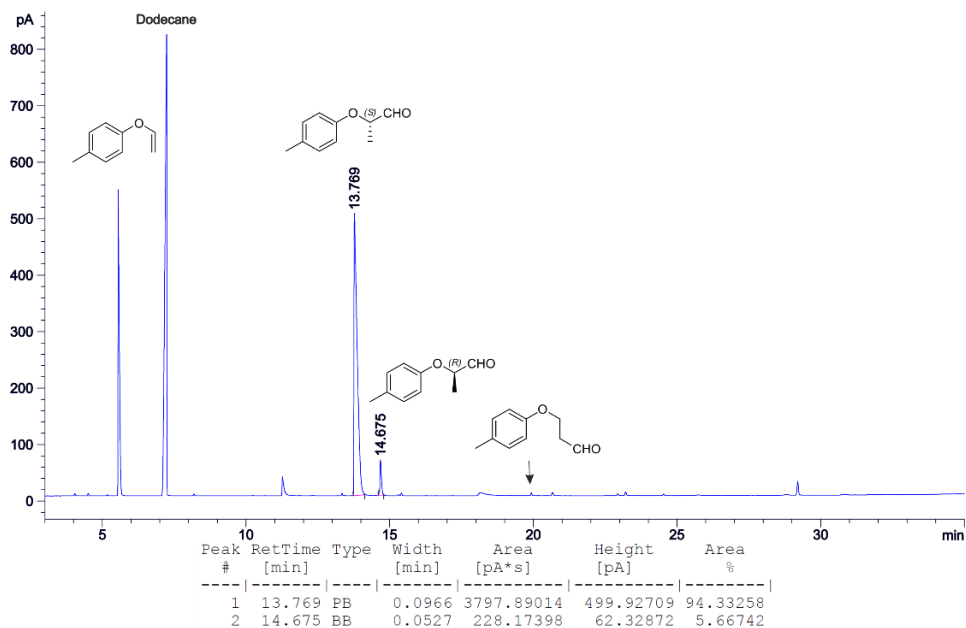


GC chromatogram of the racemic hydroformylation reaction mixture derived from **9d**

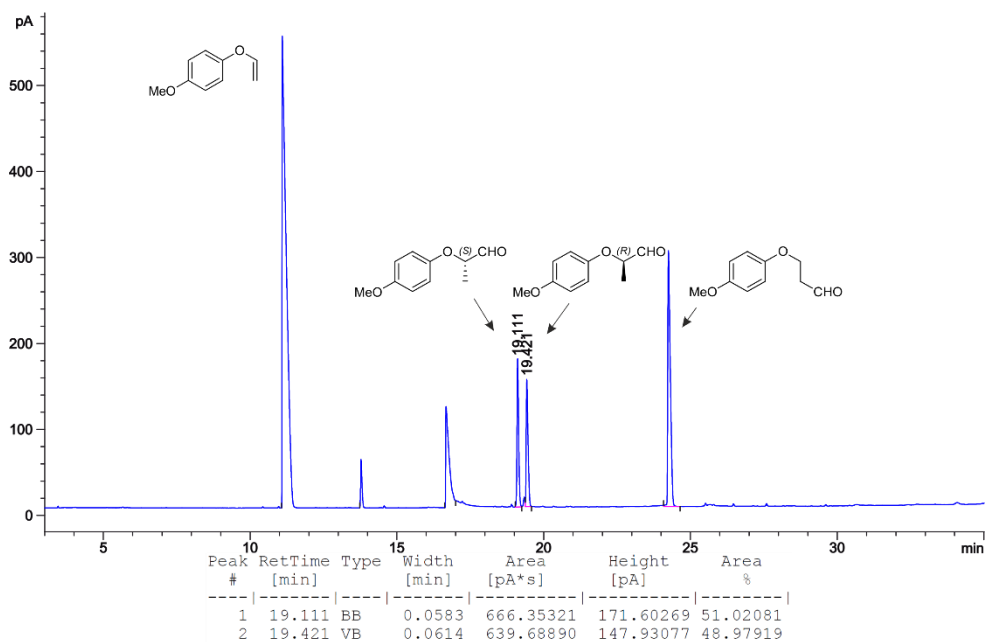




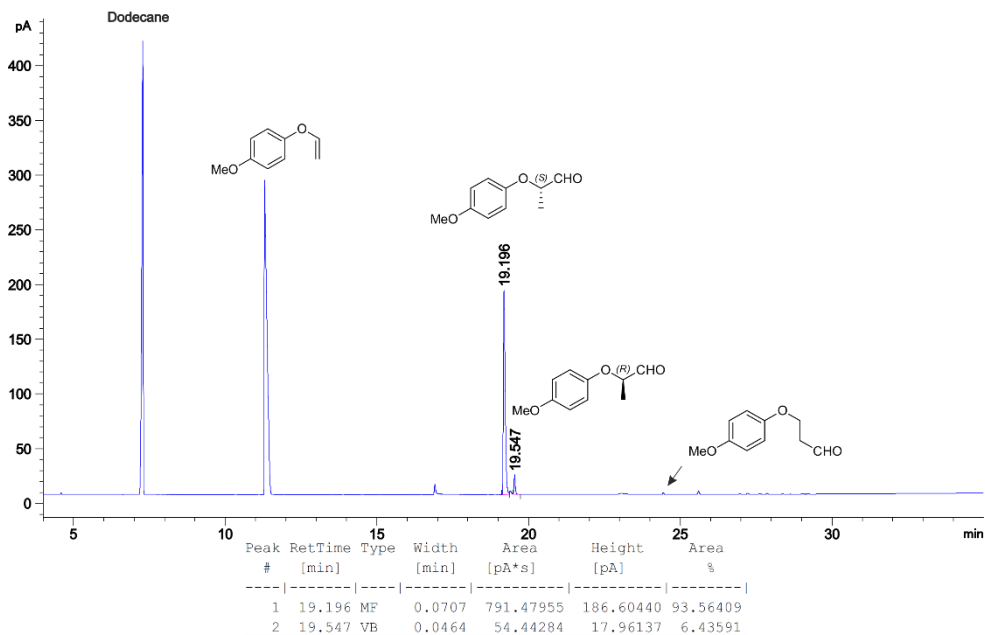
GC chromatogram of the enantioselective hydroformylation reaction mixture derived from **9d** (Table 34, entry 15)



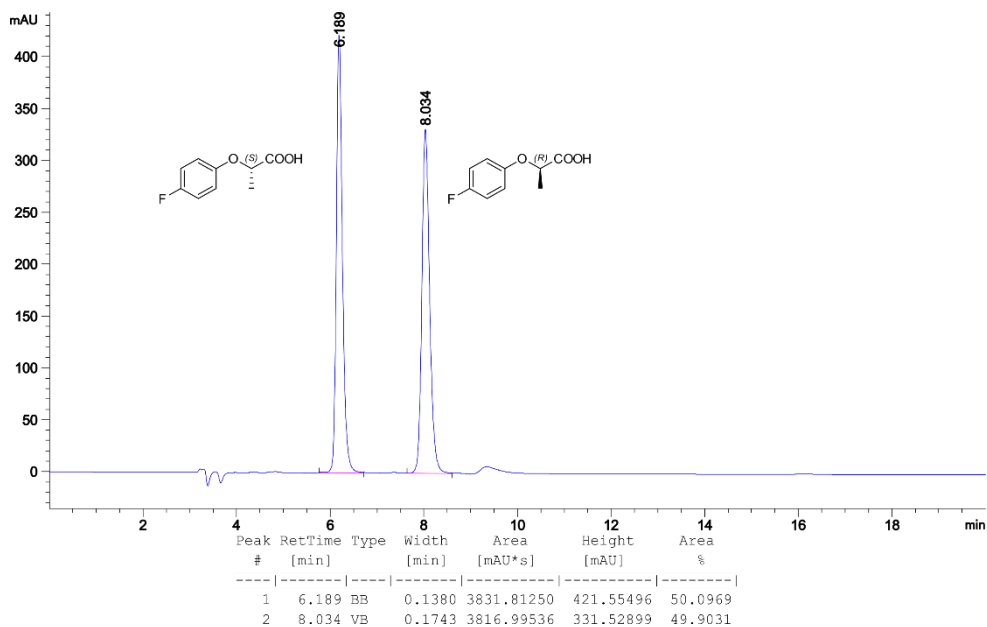
GC chromatogram of the racemic hydroformylation reaction mixture derived from **9e**



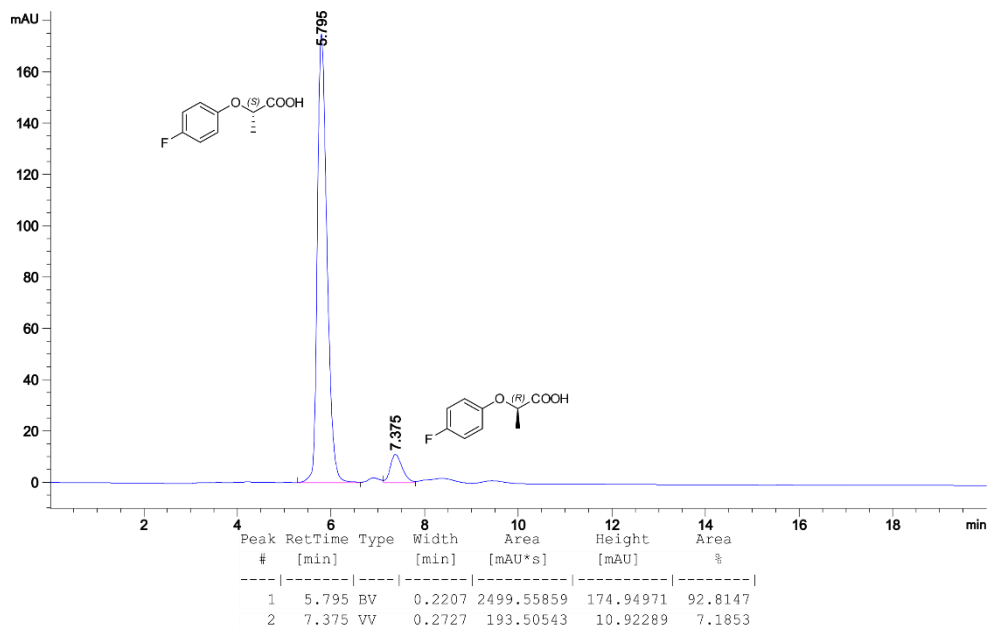
GC chromatogram of the enantioselective hydroformylation reaction mixture derived from **9e** (Table 34, entry 21)



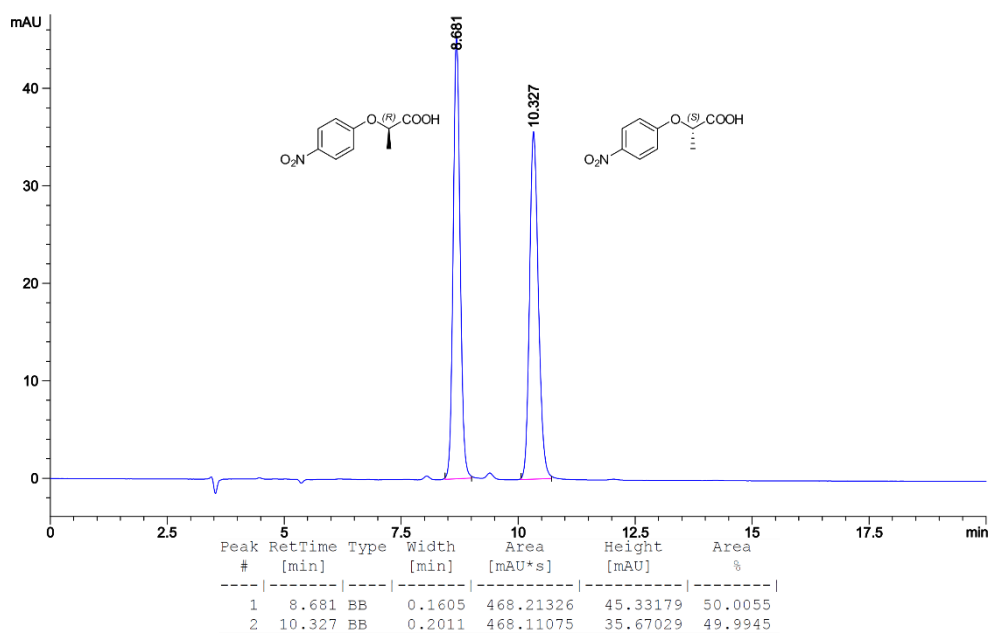
HPLC chromatogram of the racemic carboxylic acid **14f**



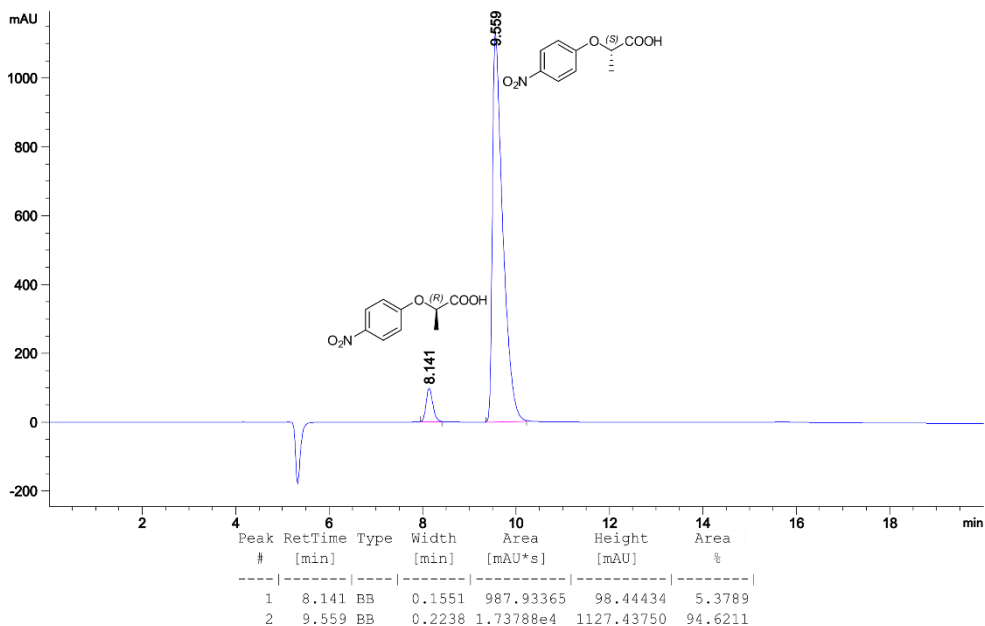
HPLC chromatogram of the enantioselective hydroformylation and subsequent derivatization to the carboxylic **14f** (Table 34, entry 28)



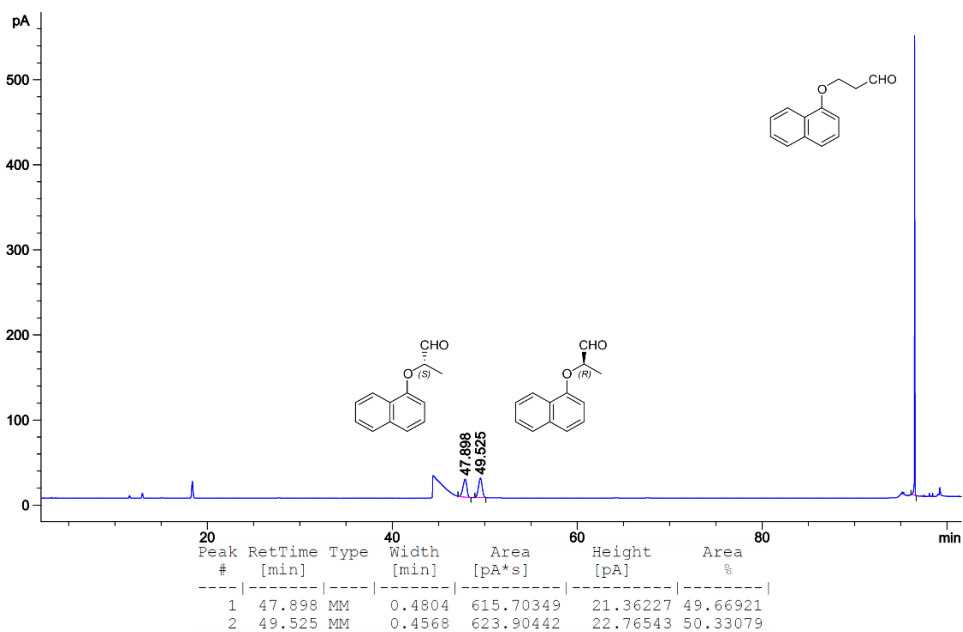
HPLC chromatogram of the racemic carboxylic acid **14g**



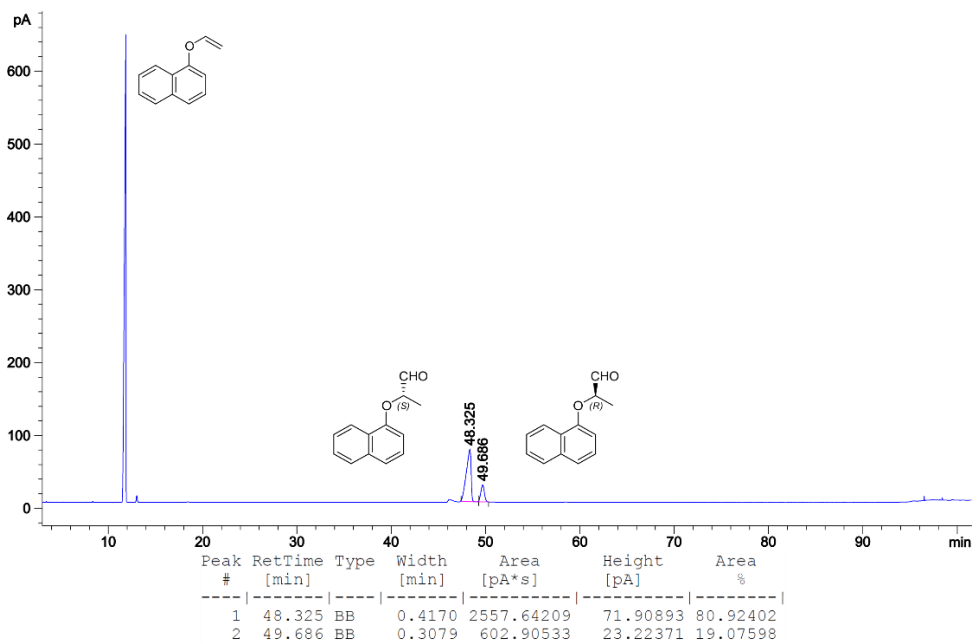
HPLC chromatogram of the hydroformylation and subsequent derivatization to the carboxylic acid derivatization products of **14g** (Table 34, entry 35)



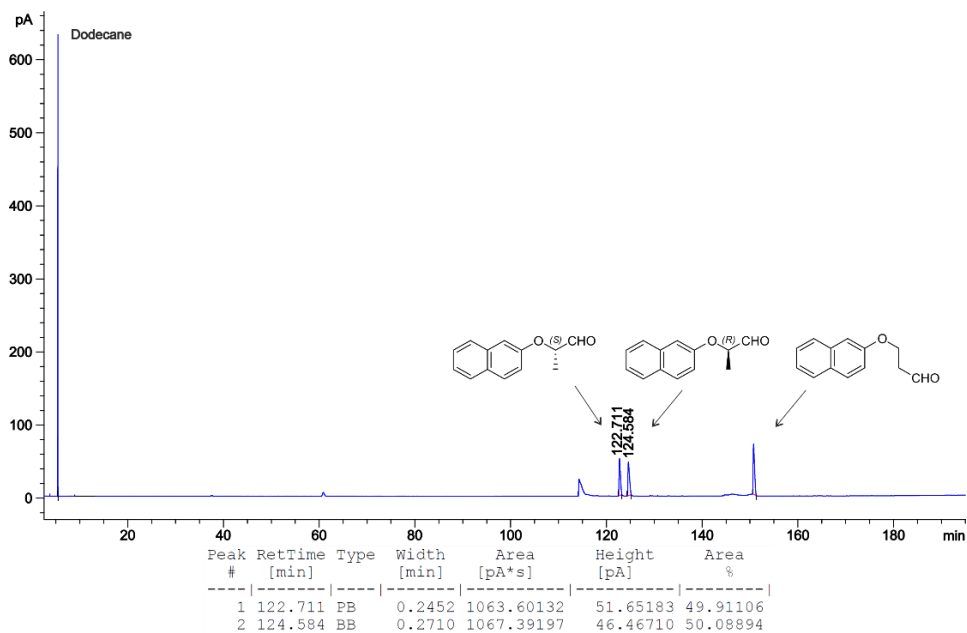
GC chromatogram of the racemic hydroformylation reaction mixture derived from **9h**



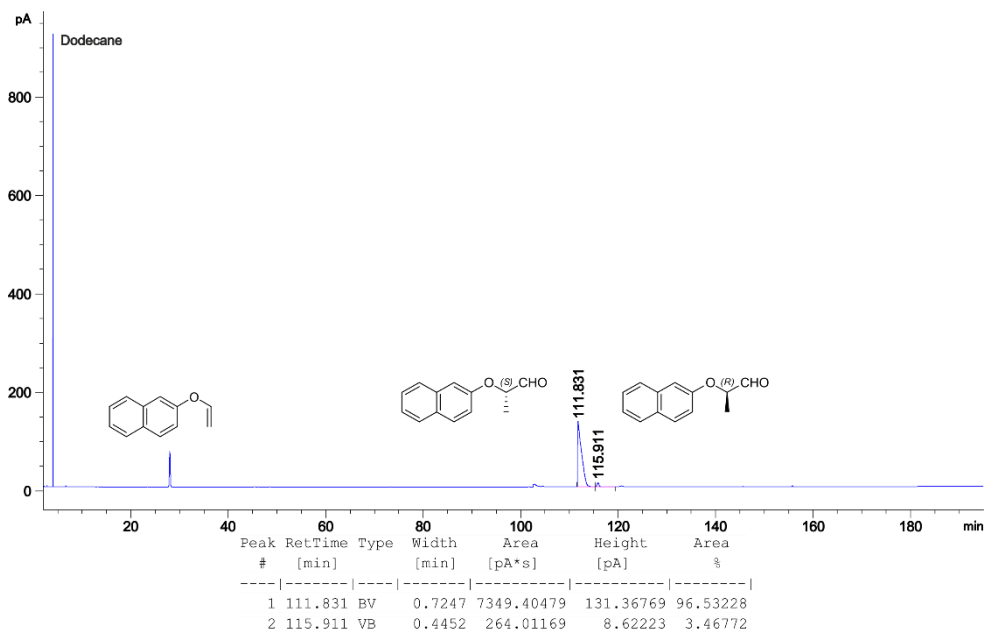
GC chromatogram of the enantioselective hydroformylation reaction mixture derived from **9h** (Table 34, entry 41)



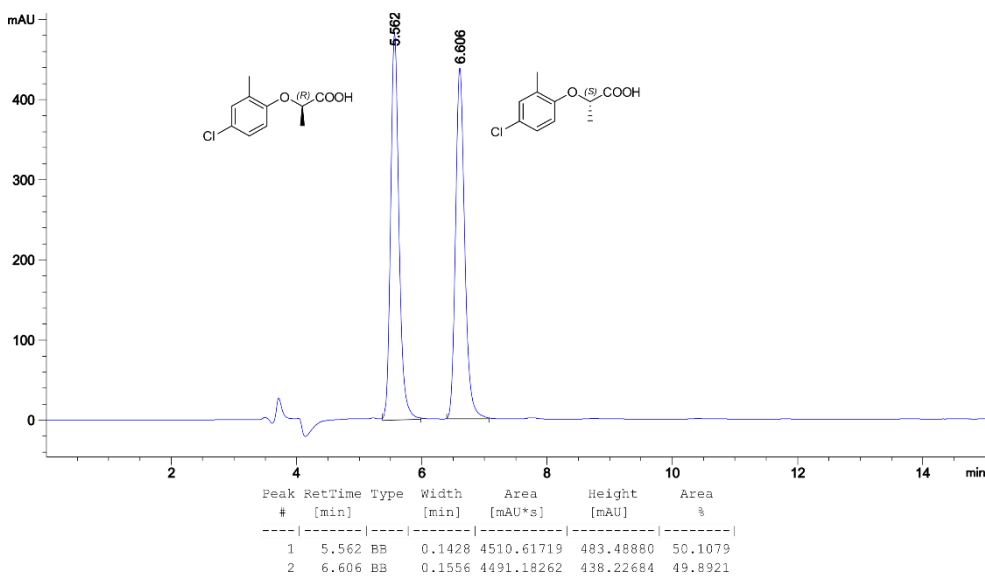
GC chromatogram of the racemic hydroformylation reaction mixture derived from **9i**



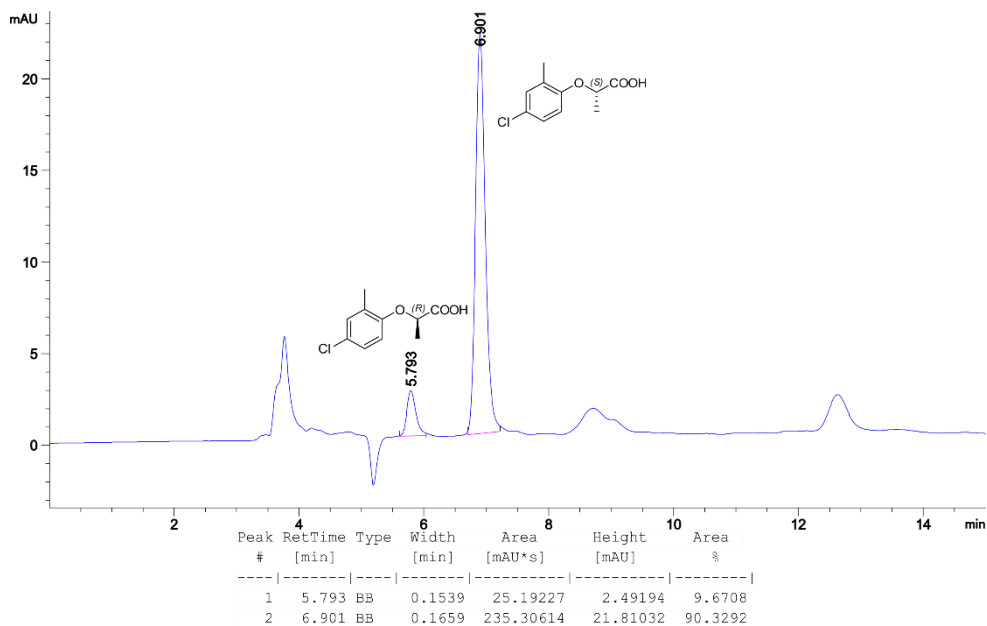
GC chromatogram of the enantioselective hydroformylation reaction mixture derived from **9i** (Table 34, entry 48)



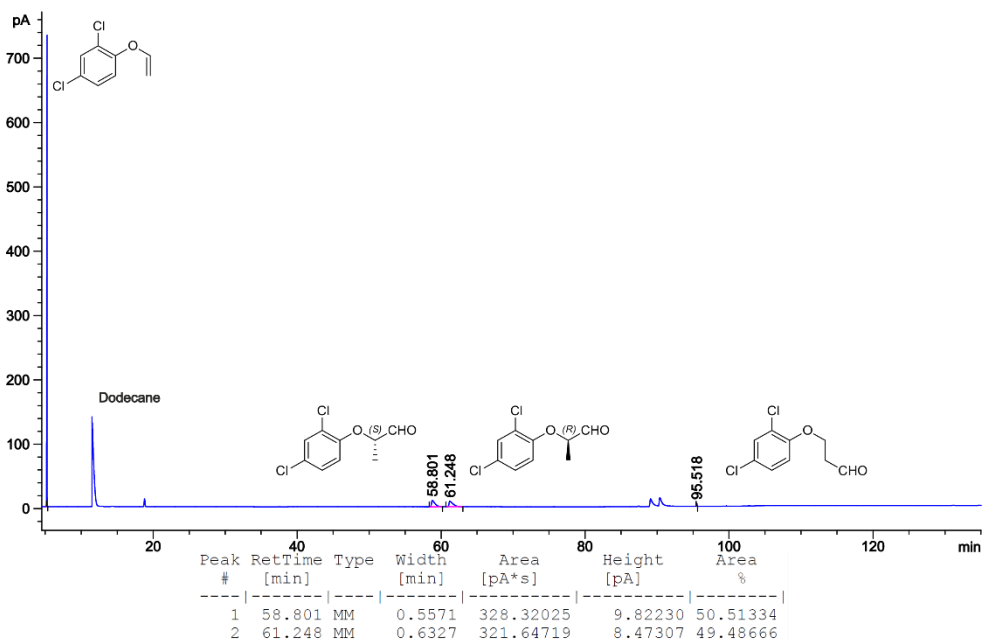
HPLC chromatogram of the racemic carboxylic acid **14j**



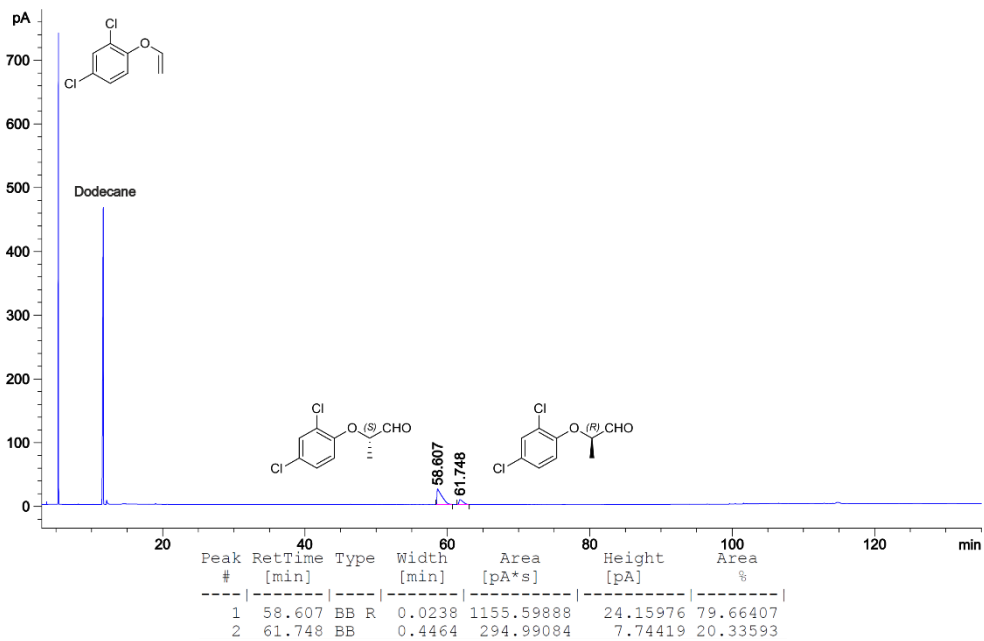
HPLC chromatogram of the enantioselective hydroformylation and subsequent derivatization to the carboxylic acid **14j** (Table 34, entry 54)



GC chromatogram of the racemic hydroformylation reaction mixture derived from **9k**



GC chromatogram of the enantioselective hydroformylation reaction mixture derived from **9k** (Table 34, entry 61)

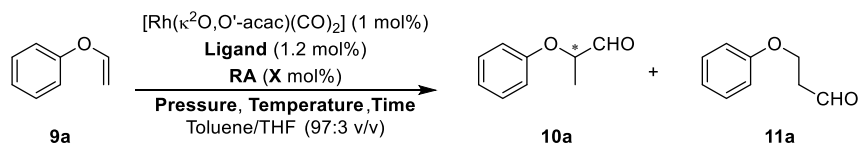




### 3.5.9 Complete set of results for the Rh-catalyzed enantioselective hydroformylation of aryl vinyl ethers

#### 3.5.9.1 Study of the influence of the ligand, RA, rhodium to RA ratio and reaction conditions

**Table 33.** Influence of the ligand, RA, rhodium to RA ratio and reaction conditions in the Rh-catalyzed enantioselective hydroformylation of (vinyl)benzene **9a**

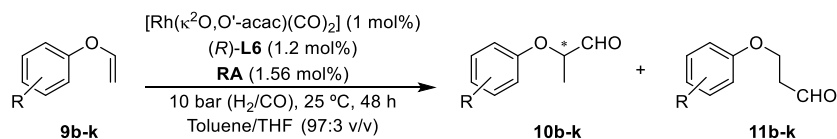


Entry	Ligand	RA	Pressure (H <sub>2</sub> /CO) (bar)	T (°C)	Time (h)	Rh/RA ratio	Conv. (%) <sup>[a]</sup>	b/l ratio <sup>[b]</sup>	<i>er</i> ( <i>S</i> : <i>R</i> ) <sup>[b]</sup>
1	( <i>R</i> )- <b>L1</b>	NaBArF	10 (1:1)	40	18	1:1.56	25	91:9	84:16
2	( <i>R</i> )- <b>L2</b>	NaBArF	10 (1:1)	40	18	1:1.56	70	89:11	61:39
3	( <i>S</i> )- <b>L3</b>	NaBArF	10 (1:1)	40	18	1:1.56	57	89:11	81:19
4	( <i>R,S</i> )- <b>L4</b>	NaBArF	10 (1:1)	40	18	1:1.56	36	> 99:1	76:24
5	( <i>R</i> )- <b>L5</b>	NaBArF	10 (1:1)	40	18	1:1.56	20	76:24	<i>rac</i>
6	( <i>R</i> )- <b>L6</b>	NaBArF	10 (1:1)	40	18	1:1.56	96	99:1	88:12
7	( <i>R</i> )- <b>L6</b>	None	10 (1:1)	40	18	1:1.56	25	92:8	78:22
8	( <i>R</i> )- <b>L6</b>	LiBArF	10 (1:1)	40	18	1:1.56	95	>99:1	92:8
9	( <i>R</i> )- <b>L6</b>	NaBArF	10 (1:1)	40	18	1:1.56	96	99:1	88:12
10	( <i>R</i> )- <b>L6</b>	KBArF	10 (1:1)	40	18	1:1.56	>99	98:2	85:15
11	( <i>R</i> )- <b>L6</b>	RbBArF	10 (1:1)	40	18	1:1.56	88	98:2	84:16
12	( <i>R</i> )- <b>L6</b>	CsBArF	10 (1:1)	40	18	1:1.56	99	98:2	79:21
13	( <i>R</i> )- <b>L6</b>	LiBArF	10 (1:1)	40	18	1:0.78	58	>99:1	91:9
14	( <i>R</i> )- <b>L6</b>	LiBArF	10 (1:1)	40	18	1:1	95	>99:1	91:9
15	( <i>R</i> )- <b>L6</b>	LiBArF	10 (1:1)	40	18	1:2	95	>99:1	92:8
16	( <i>R</i> )- <b>L6</b>	LiBArF	10 (1:1)	40	18	1:3	92	>99:1	92:8
17	( <i>R</i> )- <b>L6</b>	LiBArF	10 (1:1)	40	18	1:5	82	>99:1	92:8
18	( <i>R</i> )- <b>L6</b>	LiBArF	5 (1:1)	40	18	1:1.56	90	>99:1	92:8
19	(( <i>R</i> )- <b>L6</b>	LiBArF	10 (1:1)	25	18	1:1.56	16	>99:1	94:6
20	( <i>R</i> )- <b>L6</b>	LiBArF	10 (1:1)	25	48	1:1.56	73	>99:1	94:6
21 <sup>[c]</sup>	( <i>R</i> )- <b>L6</b>	LiBArF	10 (9:1)	25	48	1:1.56	98	>99:1	93:7
22	( <i>R</i> )- <b>L6</b>	LiBArF	10 (1:9)	25	48	1:1.56	22	>99:1	93:7
23 <sup>[d]</sup>	-	-	10 (1:1)	25	48	1:0	30	90:10	<i>rac</i>
24 <sup>[d]</sup>	-	LiBArF	10 (1:1)	25	48	0:1.56	0	-	-

The enantioselective hydroformylations were performed in a parallel autoclave. Reaction conditions: [alkene] = 0.26 M; stirring rate = 800 rpm; H<sub>2</sub>/CO in a 1:1 ratio, unless otherwise cited. [a] Conversion was determined by using <sup>1</sup>H NMR spectroscopy. [b] b/l ratio and *er* values were determined by GC analysis on a chiral stationary phase (β-Dex™ 225). [c] 4% hydrogenated product was observed [d] Background experiment employing only 1 mol% of [Rh(κ<sup>2</sup>O,O'-acac)(CO)<sub>2</sub>]. [d] Background experiment employing only 1.56 mol% LiBArF.

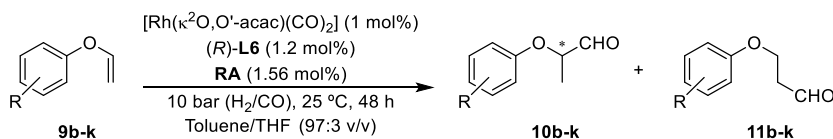
### 3.5.9.2 Substrate scope

**Table 34.** Rh-catalyzed enantioselective hydroformylation of aryl vinyl ethers **9b-k** with supramolecular ligand (*R*)-**L6**



Entry	Substrate	RA	Conversion (%) <sup>[a]</sup>	b/l ratio <sup>[b]</sup>	<i>er</i> ( <i>S</i> : <i>R</i> ) <sup>[b]</sup>
1		None	3	>99:1	-
2		LiBArF	26	>99:1	91:9
3		NaBArF	34	94:6	84:16
4	<b>9b</b>	KBArF	35	97:3	77:23
5		RbBArF	36	95:5	69:31
6		CsBArF	31	97:3	61:39
7		LiBArF <sup>[c]</sup>	57	>99:1	90:10
8		None	3	95:5	83:17
9		LiBArF	69	>99:1	94:6
10	<b>9c</b>	NaBArF	74	98:2	90:10
11		KBArF	80	98:2	88:12
12		RbBArF	78	98:2	86:14
13		CsBArF	73	99:1	80:20
14		None	5	94:6	85:15
15	<b>9d</b>	LiBArF	66	>99:1	94:6
16		NaBArF	67	97:3	89:19
17		KBArF	75	98:2	89:11
18		RbBArF	75	98:2	86:14
19		CsBArF	68	98:2	83:17
20		None	3	95:5	83:17
21	<b>9e</b>	LiBArF	34	>99:1	92:8
22		NaBArF	58	96:4	87:3
23		KBArF	65	97:3	86:14
24		RbBArF	63	98:2	83:17
25		CsBArF	61	98:2	79:21
26		LiBArF <sup>[c]</sup>	70	99:1	90:10
27		None	10	89:11	-
28	<b>9f</b>	LiBArF	63	>99:1	94:6
29		NaBArF	69	99:1	80:20
30		KBArF	75	98:2	75:25
31		RbBArF	72	99:1	70:30
32		CsBArF	69	99:1	64:36
33		LiBArF <sup>[c]</sup>	91	>99:1	94:6

Table 34. cont.



Entry	Substrate	RA	Conversion (%) <sup>[a]</sup>	b/l ratio <sup>[b]</sup>	er (S:R) <sup>[b]</sup>
34		None	7	>99:1	-
35		LiBArF	70	>99:1	95:5
36	<b>9g</b> <sup>[d]</sup>	NaBArF	94	>99:1	92:8
37		KBArF	86	>99:1	89:11
38		RbBArF	70	>99:1	86:14
39		CsBArF	76	>99:1	76:24
40		None	3	93:7	57:43
41		LiBArF	27	>99:1	82:18
42	<b>9h</b>	NaBArF	33	98:2	74:26
43		KBArF	40	98:2	66:34
44		RbBArF	41	98:2	54:46
45		CsBArF	40	99:1	47:53
46		LiBArF <sup>[c]</sup>	62	>99:1	80:20
47		None	24	98:2	85:15
48		LiBArF	88	>99:1	97:3
49	<b>9i</b>	NaBArF	96	>99:1	94:6
50		KBArF	98	>99:1	92:8
51		RbBArF	97	>99:1	89:11
52		CsBArF	95	>99:1	86:14
53		None	6	>99:1	-
54		LiBArF	25	>99:1	89:11
55		NaBArF	33	96:4	85:15
56	<b>9j</b>	KBArF	34	>99:1	79:21
57		RbBArF	30	97:3	73:27
58		CsBArF	30	>99:1	66:34
59		LiBArF <sup>[c]</sup>	60	>99:1	90:10
60		None	18	>99:1	68:32
61		LiBArF	33	>99:1	80:20
62		NaBArF	61	>99:1	73:27
63	<b>9k</b>	KBArF	54	>99:1	62:38
64		RbBArF	58	>99:1	55:45
65		CsBArF	69	>99:1	50:50
66		LiBArF <sup>[c]</sup>	65	>99:1	80:20

The enantioselective hydroformylations were performed in a parallel autoclave. Reaction conditions: [alkene] = 0.26 M; stirring rate = 800 rpm;  $\text{H}_2/\text{CO}$  in a 1:1 ratio, unless otherwise cited. [a] Conversion was determined by using  $^1\text{H}$  NMR spectroscopy. [b] b/l ratio and *er* values were determined by GC analysis on a chiral stationary phase ( $\beta\text{-Dex}^{\text{TM}}$  225) or HPLC analysis of the corresponding carboxylic acids. [c] Reaction carried out using a 3 mol% of catalyst. [d] 24 h reaction time.

### 3.5.10 Coordination studies

#### 3.5.10.1 Experimental procedure for the complexation experiments

##### 3.5.10.1.1 General procedure for the complexation experiments under inert atmosphere

In a glove box filled with nitrogen, a 0.05 M solution of  $[\text{Rh}(\kappa^2\text{O},\text{O}'\text{-acac})(\text{CO}_2)]$  (*ca.* 32.40  $\mu\text{mol}$ ), (*R*)-**L6** (*ca.* 32.40  $\mu\text{mol}$ ) and RA if required (*ca.* 42.20  $\mu\text{mol}$ ) in toluene- $d_8$ /THF- $d_8$  (97:3 v/v) was stirred for 5 h in a 2 mL vial equipped with a magnetic stirrer. The reaction mixture was transferred into a NMR Young tube and spectra were collected at 25 °C. MS measurements on these samples were rapidly recorded under  $\text{N}_2$  atmosphere. Attempts to isolate any of these complexes in analytical pure form failed.

##### Direct formation of $[\text{Rh}(\kappa^2\text{O},\text{O}'\text{-acac})(\text{CO})(\kappa^1\text{P}\text{-}(\text{R})\text{-L6})]$

The synthesis was performed following the general procedure indicated above for the complexation experiments under inert atmosphere. IR (toluene/THF (97:3 v/v),  $\text{cm}^{-1}$ ): 2932, 2005 ( $\bar{\nu}_{\text{CO}}$ ), 1581, 1521, 1443, 1413, 1224, 1133, 1045, 945.  $^1\text{H}$  NMR (400 MHz, toluene- $d_8$ /THF- $d_8$  (97:3 v/v)):  $\delta$  7.73–7.65 (m, 8H), 7.28–7.08 (m, 20H), 6.91–6.84 (m, 2H), 6.76–6.69 (m, 2H), 5.11 (s, 2H, acac), 4.16 (bs, 1H), 3.77 (bs, 4H), 3.37 (bs, 4H), 3.17–2.85 (m, 12H), 2.66 (bs, 12H), 2.37–2.28 (m, 4H), 1.60–1.41 (m, 15H), 1.41–1.33 (m, 4H) ppm.  $^{31}\text{P}\{^1\text{H}\}$  NMR (162 MHz, toluene- $d_8$ /THF- $d_8$  (97:3 v/v)):  $\delta$  146.2 (d,  $^1J_{\text{Rh-P}} = 290.0$  Hz), 142.1 (s) ppm. MS (ESI):  $m/z$   $[\text{M-Li}-(\text{acac})]^+$  calcd for  $\text{C}_{89}\text{H}_{88}\text{O}_{13}\text{P}_2\text{Rh}$  1526.5, found 1526.3.

##### Direct formation of $[\text{Rh}(\kappa^2\text{O},\text{O}'\text{-acac})(\kappa^2\text{P},\text{P}'\text{-}(\text{R})\text{-L6})]$

The synthesis was performed following the general procedure indicated above for the complexation experiments under inert atmosphere. IR (toluene/THF (97:3 v/v),  $\text{cm}^{-1}$ ): 1354, 1278, 1163, 1128, 945.  $^1\text{H}$  NMR (500 MHz, toluene- $d_8$ /THF- $d_8$  (97:3 v/v)):  $\delta$  7.49–7.46 (m, 2H), 7.40–7.08 (m, 22H), 6.94–6.49 (m, 8H), 3.71–3.61 (m, 4H), 3.14–3.06 (m, 4H), 2.97–2.49 (m, 25H), 2.33–2.17 (m, 3H), 1.70–1.59 (m, 16H), 1.45–1.32 (m, 4H) ppm.  $^{31}\text{P}\{^1\text{H}\}$  NMR (202 MHz, toluene- $d_8$ /THF- $d_8$  (97:3 v/v)):  $\delta$  127.2 (d,  $^1J_{\text{Rh-P}} = 179.6$  Hz) ppm. MS (ESI):  $m/z$   $[\text{M-Li}-(\text{acac})]^+$  calcd for  $\text{C}_{88}\text{H}_{88}\text{O}_{13}\text{P}_2\text{Rh}$  1526.5, found 1526.3.

### 3.5.10.1.2 General procedure for the complexation experiments under syngas (H<sub>2</sub>/CO) atmosphere

In a glove box filled with nitrogen, a solution 0.05 M of [Rh( $\kappa^2$ O,O'-acac)(CO)<sub>2</sub>] (*ca.* 32.40  $\mu$ mol), (R)-**L6** (*ca.* 32.40  $\mu$ mol) and RA if required (*ca.* 42.20  $\mu$ mol) in toluene-*d*<sub>8</sub>/THF-*d*<sub>8</sub> (97:3 v/v) was placed in a 2 mL vial equipped with a magnetic stirrer. This vial was transferred into an autoclave and taken out of the glove box. The autoclave was purged three times with syngas (1:1 H<sub>2</sub>/CO at a pressure not higher than 10 bar) without stirring and, finally, the autoclave was pressurized with syngas 10 bar. The reaction mixture was stirred at 40 °C (metallic block) for 16 h. The reaction was cooled down to room temperature, the pressure was carefully released in a well-ventilated hood and the reaction mixture was transferred into a 5 mm HP NMR sapphire tube. The tube was pressurized with 10 bar syngas (H<sub>2</sub>/CO 1:1 ratio) and HP NMR spectra were collected at 25 °C. MS measurements on these samples were rapidly recorded under N<sub>2</sub> atmosphere. Attempts to isolate any of these complexes in analytical pure form failed.

#### Direct formation of [Rh(H)(CO)<sub>2</sub>( $\kappa^2$ P,P'-{((R)-L6)•LiBArF})]

The synthesis was performed following the general procedure for the complexation experiments indicated above under syngas (H<sub>2</sub>/CO) atmosphere. <sup>1</sup>H NMR (500 MHz, toluene-*d*<sub>8</sub>/THF-*d*<sub>8</sub> (97:3 v/v))  $\delta$  7.63–7.47 (m, 3H), 7.40–7.34 (m, 2H), 7.28–7.08 (m, 12H), 7.02–6.99 (m, 4H), 6.90–6.58 (m, 7H), 3.83–3.30 (m, 4H), 3.12–2.19 (m, 27H), 1.69–1.32 (m, 20H), –11.13 (bs, 0.1H), –11.21 (bs, 0.1H) ppm. <sup>31</sup>P {<sup>1</sup>H} NMR (202 MHz, toluene-*d*<sub>8</sub>/THF-*d*<sub>8</sub> (97:3 v/v))  $\delta$  160.5 (d, <sup>1</sup>J<sub>Rh-P</sub> = 239.1 Hz), 159.1 (d, <sup>1</sup>J<sub>Rh-P</sub> = 240.6 Hz), 127.6 (d, <sup>1</sup>J<sub>Rh-P</sub> = 173.0 Hz) ppm. <sup>7</sup>Li NMR (194 MHz, toluene-*d*<sub>8</sub>/THF-*d*<sub>8</sub> (97:3 v/v))  $\delta$  0.60 (bs), –1.47 (bs) ppm. HRMS (ESI): *m/z* [M–BArF–Li–CO–H]<sup>+</sup> calcd for C<sub>89</sub>H<sub>88</sub>O<sub>13</sub>P<sub>2</sub>Rh 1529.4750, found 1529.4736.

#### Direct formation of [Rh(H)(CO)<sub>2</sub>( $\kappa^2$ P,P'-{((R)-L6)•NaBArF})]

The synthesis was performed following the general procedure for the complexation experiments indicated above under syngas (H<sub>2</sub>/CO) atmosphere. <sup>1</sup>H NMR (500 MHz, toluene-*d*<sub>8</sub>/THF-*d*<sub>8</sub> (97:3 v/v))  $\delta$  7.64–7.58 (m, 6H), 7.25–6.94 (m, 24H), 6.63–6.60 (m, 2H), 3.83–3.30 (m, 4H), 3.40 (bs, 3H), 3.13–2.39 (m, 34H), 2.26–2.22 (m, 2H), 1.64–1.32 (m, 23H), –11.13 (t, <sup>2</sup>J<sub>H-P</sub> = 7.1 Hz, 0.2H), –11.21 (t, <sup>2</sup>J<sub>H-P</sub> = 7.5 Hz, 0.5H) ppm. <sup>31</sup>P {<sup>1</sup>H} NMR (202 MHz, toluene-*d*<sub>8</sub>/THF-*d*<sub>8</sub> (97:3 v/v))  $\delta$  159.4 (d, <sup>1</sup>J<sub>Rh-P</sub> = 240.3 Hz), 159.1 (d, <sup>1</sup>J<sub>Rh-P</sub> = 240.4 Hz) ppm. HRMS (ESI): *m/z* [M–BArF–Na–CO–H]<sup>+</sup> calcd for C<sub>89</sub>H<sub>88</sub>O<sub>13</sub>P<sub>2</sub>Rh 1529.4750 found 1529.4771.

**Direct formation of [Rh(H)(CO)<sub>2</sub>(κ<sup>2</sup>P,P'-{((R)-L6)•KBArF})]**

The synthesis was performed following the general procedure for the complexation experiments indicated above under syngas (H<sub>2</sub>/CO) atmosphere. <sup>1</sup>H NMR (500 MHz, toluene-*d*<sub>8</sub>/THF-*d*<sub>8</sub> (97:3 v/v)) δ 7.64–7.50 (m, 6H), 7.40–6.96 (m, 22H), 6.91–6.88 (m, 2H), 6.62–6.56 (m, 2H), 3.82–3.22 (m, 6H), 2.92–2.65 (m, 26H), 2.38–2.23 (m, 4H), 1.61–1.35 (m, 20H), –11.13 (t, <sup>2</sup>J<sub>H-P</sub> = 13.8 Hz, 0.7H), –11.21 (bs) ppm. <sup>31</sup>P{<sup>1</sup>H} NMR (202 MHz, toluene-*d*<sub>8</sub>/THF-*d*<sub>8</sub> (97:3 v/v)) δ 157.4 (d, <sup>1</sup>J<sub>Rh-P</sub> = 238.0 Hz), 152.4 (d, <sup>1</sup>J<sub>Rh-P</sub> = 241.2 Hz) ppm. HRMS (ESI): *m/z* [M–BArF–K–H]<sup>+</sup> calcd for C<sub>90</sub>H<sub>88</sub>O<sub>14</sub>P<sub>2</sub>Rh, 1557.4699 found 1557.4670.

**Direct formation of [Rh(H)(CO)<sub>2</sub>(κ<sup>2</sup>P,P'-{((R)-L6)•RbBArF})]**

The synthesis was performed following the general procedure for the complexation experiments indicated above under syngas (H<sub>2</sub>/CO) atmosphere. <sup>1</sup>H NMR (500 MHz, toluene-*d*<sub>8</sub>/THF-*d*<sub>8</sub> (97:3 v/v)) δ 7.61–4.78 (m, 6H), 7.21–7.01 (m, 20H), 6.85–6.63 (m, 4H), 3.44–3.37 (m, 4H), 3.12–2.58 (m, 26H), 2.38–2.25 (m, 4H), 1.62–0.91 (m, 22H), –11.12 (t, <sup>2</sup>J<sub>H-P</sub> = 19.8 Hz, 0.7H) ppm. <sup>31</sup>P{<sup>1</sup>H} NMR (202 MHz, toluene-*d*<sub>8</sub>/THF-*d*<sub>8</sub> (97:3 v/v)) δ 155.6 (d, <sup>1</sup>J<sub>Rh-P</sub> = 236.7 Hz), 153.0 (d, <sup>1</sup>J<sub>Rh-P</sub> = 232.1 Hz) ppm.

**Direct formation of [Rh(H)(CO)<sub>2</sub>(κ<sup>2</sup>P,P'-{((R)-L6)•CsBArF})]**

The synthesis was performed following the general procedure for the complexation experiments indicated above under syngas (H<sub>2</sub>/CO) atmosphere. <sup>1</sup>H NMR (500 MHz, toluene-*d*<sub>8</sub>/THF-*d*<sub>8</sub> (97:3 v/v)) δ 7.60–7.52 (m, 6H), 7.27–6.98 (m, 21H), 6.83–6.58 (m, 4H), 7.21–7.01 (m, 20H), 3.54–3.43 (m, 4H), 3.14–2.27 (m, 32H), 1.62–1.41 (m, 20H), –11.13 (t, <sup>2</sup>J<sub>H-P</sub> = 20.1 Hz, 0.7H) ppm. <sup>31</sup>P{<sup>1</sup>H} NMR (202 MHz, toluene-*d*<sub>8</sub>/THF-*d*<sub>8</sub> (97:3 v/v)) δ 152.5 (d, <sup>1</sup>J<sub>Rh-P</sub> = 239.0 Hz) ppm.

### 3.5.10.2 NMR spectral data for the complexes obtained in the complexation experiments

**Table 35.** NMR spectral data for the rhodium complexes derived from alkali metal BArF salts in the presence of  $[\text{Rh}(\kappa^2\text{O},\text{O}'\text{-acac})(\text{CO})_2]$  and  $(R)\text{-L6}$  under  $\text{H}_2/\text{CO}$  atmosphere

Entry	RA	Complex	$\delta^{31\text{P}}$ (ppm)	$^1J_{\text{Rh-P}}$ (Hz)	$\delta^1\text{H}$ (ppm)	$^2J_{\text{P-H}}$ (Hz)
1		$[\text{Rh}(\kappa^2\text{O},\text{O}'\text{-acac})(\text{CO})(\kappa^1\text{P}\text{-}\{(R)\text{-L6}\})]$	146.4 142.2	289.7	-	-
2	None	$[\text{Rh}(\text{H})(\text{CO})_2(\kappa^2\text{P},\text{P}'\text{-}\{(R)\text{-L6}\})]$	165.4	237.8	-11.11	$\approx 8.9$
3		$[\text{Rh}(\text{H})(\text{CO})_2(\kappa^2\text{P},\text{P}'\text{-}\{(R)\text{-L6}\})]^*$	160.9	235.7	-11.23	7.8
4		$[\text{Rh}(\kappa^2\text{O},\text{O}'\text{-acac})(\kappa^2\text{P},\text{P}'\text{-}\{(R)\text{-L6}\})\cdot\text{LiBArF}]$	127.7	181.9	-	-
5	LiBArF	$[\text{Rh}(\text{H})(\text{CO})_2(\kappa^2\text{P},\text{P}'\text{-}\{(R)\text{-L6}\})\cdot\text{LiBArF}]$	160.6	234.1	-11.21	$\approx 19.3^{[b]}$
6		$[\text{Rh}(\text{H})(\text{CO})_2(\kappa^2\text{P},\text{P}'\text{-}\{(R)\text{-L6}\})\cdot\text{LiBArF}]^*$	159.2	241.5	-11.13	$\approx 20.3^{[b]}$
7	NaBArF	$[\text{Rh}(\text{H})(\text{CO})_2(\kappa^2\text{P},\text{P}'\text{-}\{(R)\text{-L6}\})\cdot\text{NaBArF}]$	159.6	240.2	-11.13	7.1
8		$[\text{Rh}(\text{H})(\text{CO})_2(\kappa^2\text{P},\text{P}'\text{-}\{(R)\text{-L6}\})\cdot\text{NaBArF}]^*$	159.2	238.6	-11.21	7.5
9	KBArF	$[\text{Rh}(\text{H})(\text{CO})_2(\kappa^2\text{P},\text{P}'\text{-}\{(R)\text{-L6}\})\cdot\text{KBArF}]$	157.6	234.3	-11.14	13.8
10		$[\text{Rh}(\text{H})(\text{CO})_2(\kappa^2\text{P},\text{P}'\text{-}\{(R)\text{-L6}\})\cdot\text{KBArF}]^*$	152.6	243.1	-11.21	n.m.
11	RbBArF	$[\text{Rh}(\text{H})(\text{CO})_2(\kappa^2\text{P},\text{P}'\text{-}\{(R)\text{-L6}\})\cdot\text{RbBArF}]$	155.7	241.3	-11.12	19.8
12		$[\text{Rh}(\text{H})(\text{CO})_2(\kappa^2\text{P},\text{P}'\text{-}\{(R)\text{-L6}\})\cdot\text{RbBArF}]^*$	153.2	239.5		
13	CsBArF	$[\text{Rh}(\text{H})(\text{CO})_2(\kappa^2\text{P},\text{P}'\text{-}\{(R)\text{-L6}\})\cdot\text{CsBArF}]$	152.7	244.2	-11.14	20.1

[a] NMR data was acquired under 10 bar syngas ( $\text{H}_2/\text{CO}$  in a 1:1 ratio) at 25 °C in 5 mm sapphire NMR tube in toluene- $d_8$ /THF- $d_8$  (97:3 v/v). [b] The width was measured at half height. The assignment of the signals of these complexes is tentative due to the small intensity of the cross-peak between the hydrido and the phosphite signals in the  $^1\text{H}\text{-}^{31}\text{P}$  HMBC spectrum.

### 3.5.10.3 Spectra of the complexation experiments

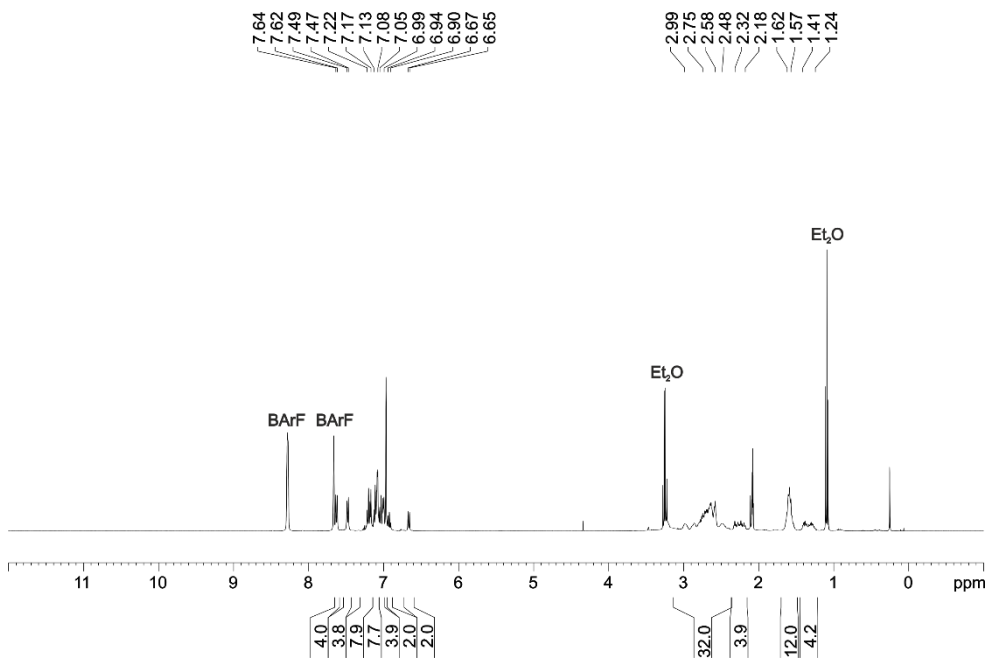


Figure 65. <sup>1</sup>H NMR spectrum of Li•BArF(R)-L6 (400 MHz, 25 °C, toluene-*d*<sub>8</sub>/THF-*d*<sub>8</sub> (97:3 v/v))

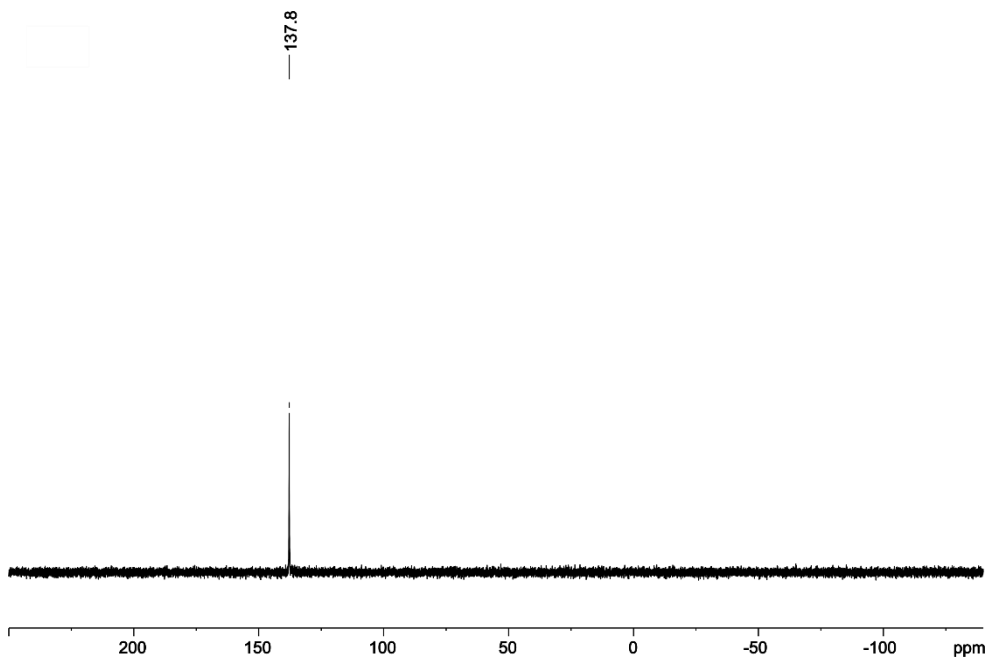
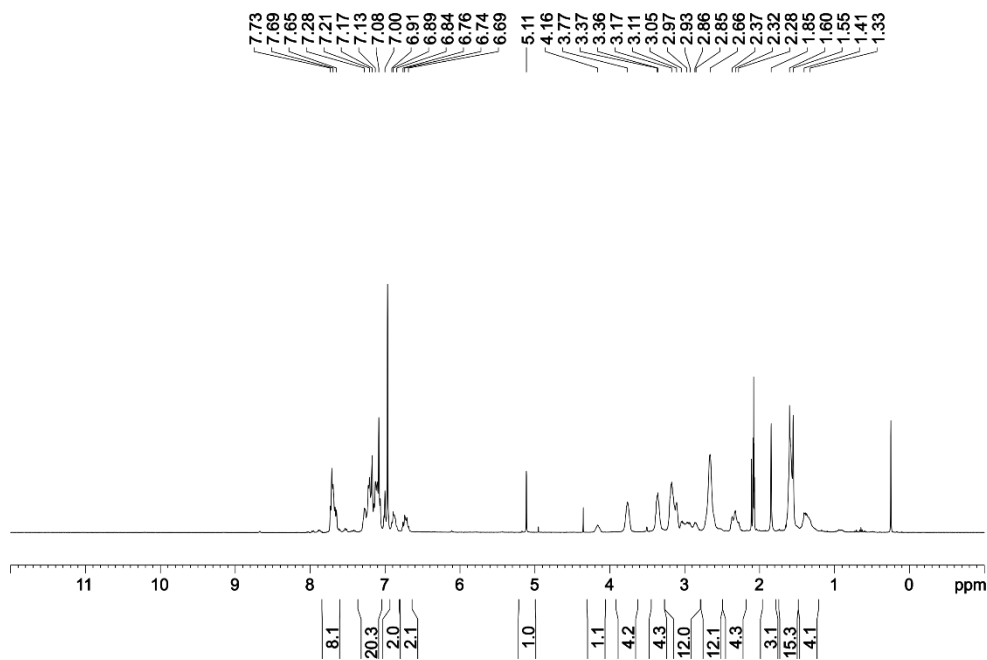
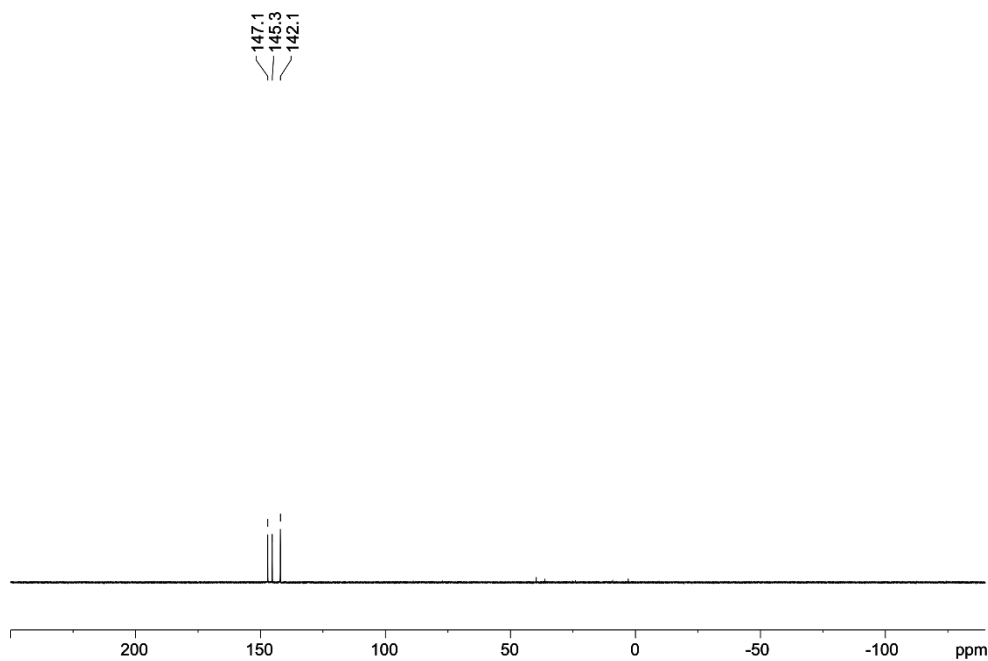


Figure 66. <sup>31</sup>P{<sup>1</sup>H} NMR spectrum of LiBArRF•(R)-L6 (162 MHz, 25 °C, toluene-*d*<sub>8</sub>/THF-*d*<sub>8</sub> (97:3 v/v))





**Figure 67.**  $^1\text{H}$  NMR spectrum of  $[\text{Rh}(\kappa^2\text{O},\text{O}'\text{-acac})(\text{CO})(\kappa^1\text{P}-\{(R)\text{-L6}\})]$  (400 MHz, 25 °C, toluene- $d_8$ /THF- $d_8$  (97:3 v/v))



**Figure 68.**  $^{31}\text{P}\{^1\text{H}\}$  NMR spectrum of  $[\text{Rh}(\kappa^2\text{O},\text{O}'\text{-acac})(\text{CO})(\kappa^1\text{P}-\{(R)\text{-L6}\})]$  (162 MHz, 25 °C, toluene- $d_8$ /THF- $d_8$  (97:3 v/v))

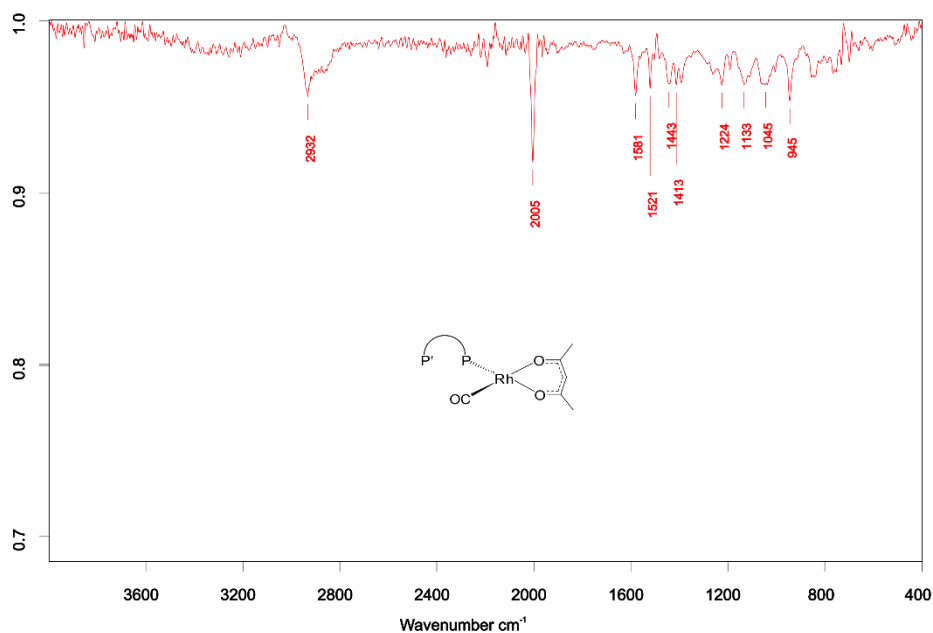


Figure 69. IR spectrum of  $[\text{Rh}(\kappa^2\text{O},\text{O}^1\text{-acac})(\text{CO})(\kappa^1\text{P}-\{(R)\text{-L6}\})]$  (25 °C, toluene- $d_8$ /THF- $d_8$  (97:3 v/v))

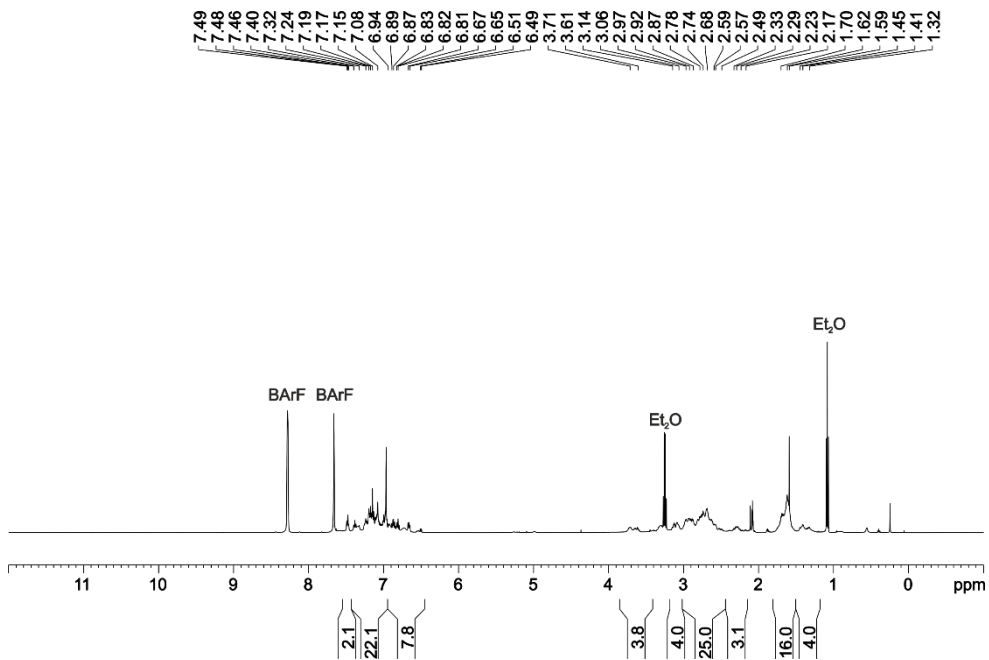
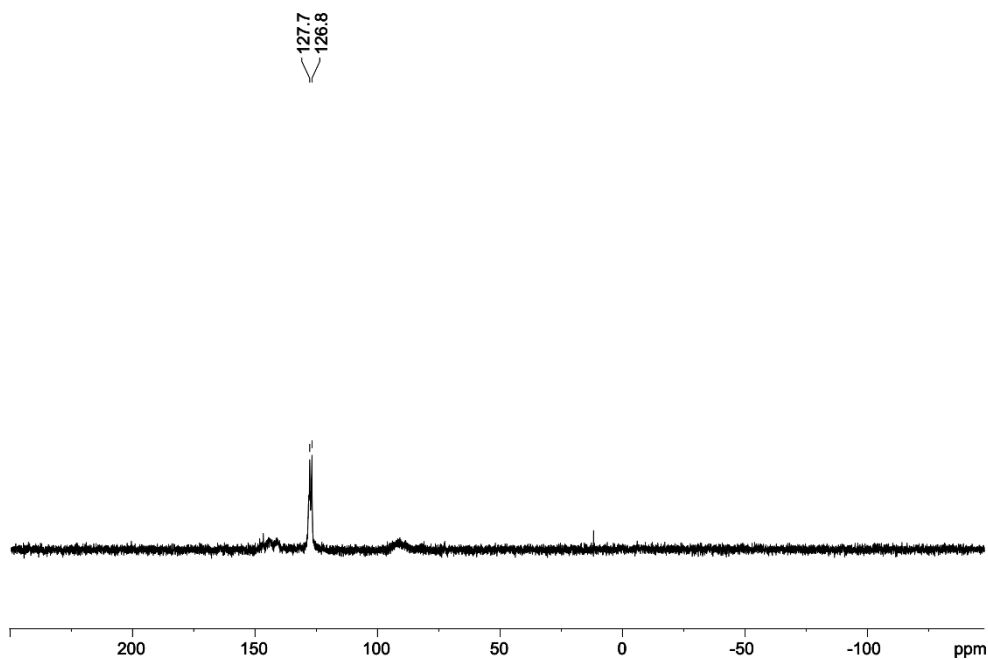
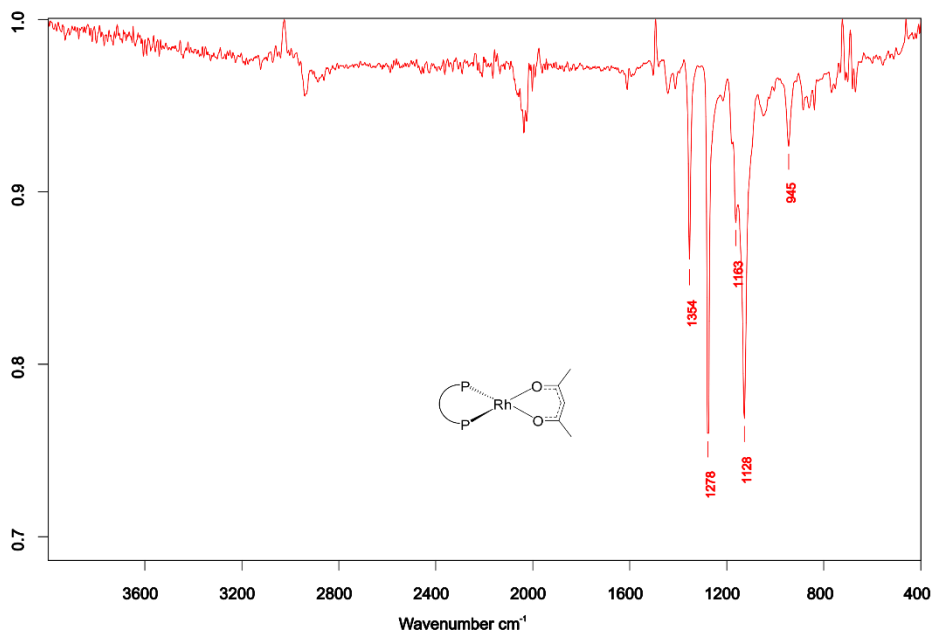


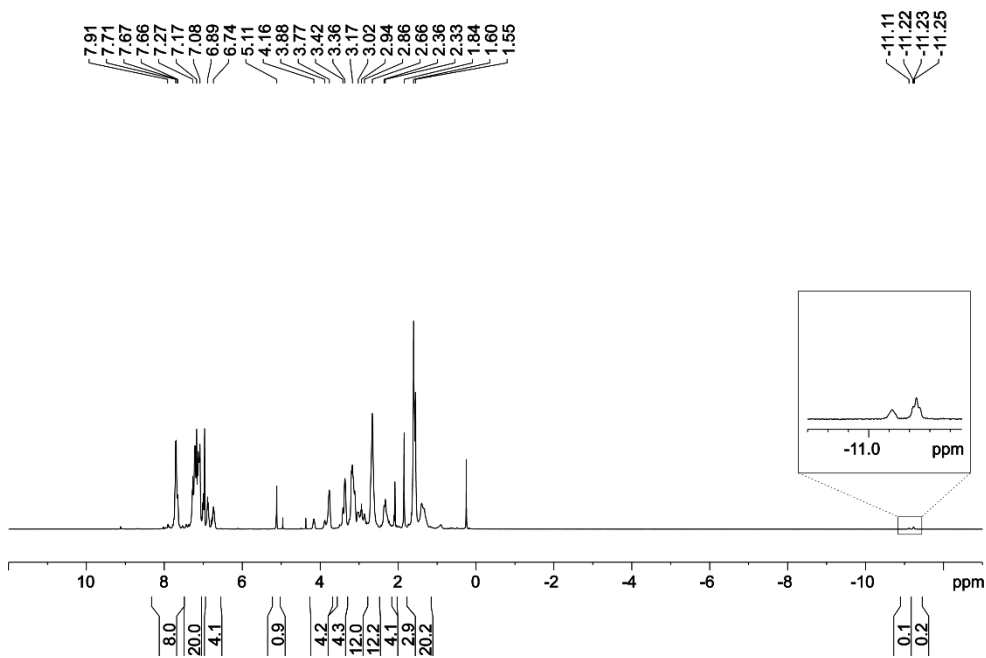
Figure 70.  $^1\text{H}$  NMR spectrum of  $[\text{Rh}(\kappa^2\text{O},\text{O}^1\text{-acac})(\kappa^2\text{P},\text{P}^1-\{(R)\text{-L6}\}\cdot\text{LiBArF})]$  (500 MHz, 25 °C, toluene- $d_8$ /THF- $d_8$  (97:3 v/v))



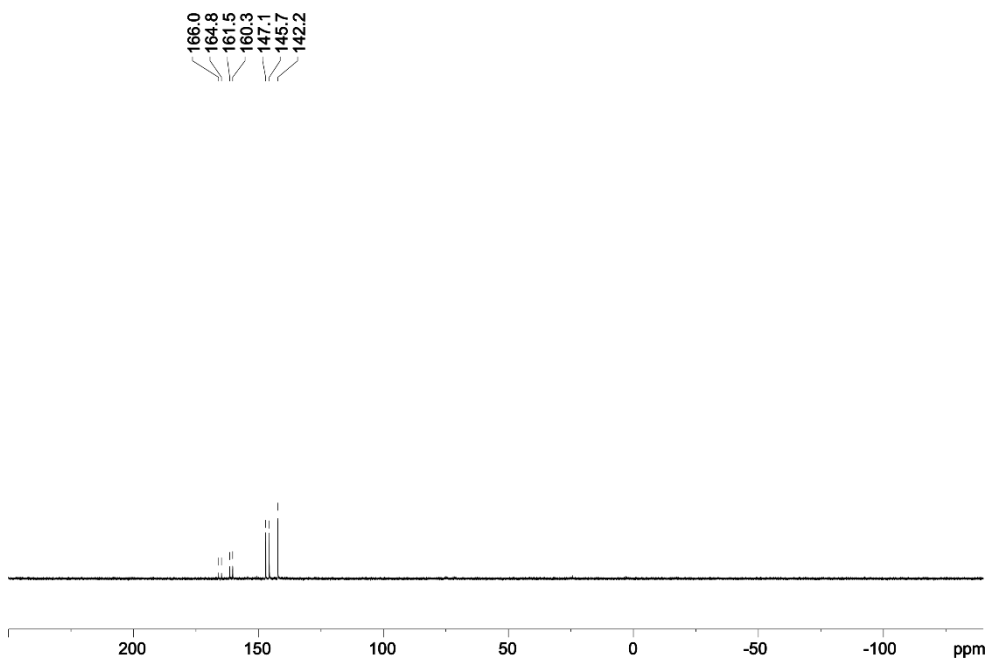
**Figure 71.**  $^{31}\text{P}\{^1\text{H}\}$  NMR spectrum of  $[\text{Rh}(\kappa^2\text{O},\text{O}'\text{-acac})(\kappa^2\text{P},\text{P}'\text{-}\{((\text{R})\text{-L6})\cdot\text{LiBArF}\})]$  (202 MHz, 25 °C, toluene- $d_8$ /THF- $d_8$  (97:3 v/v))



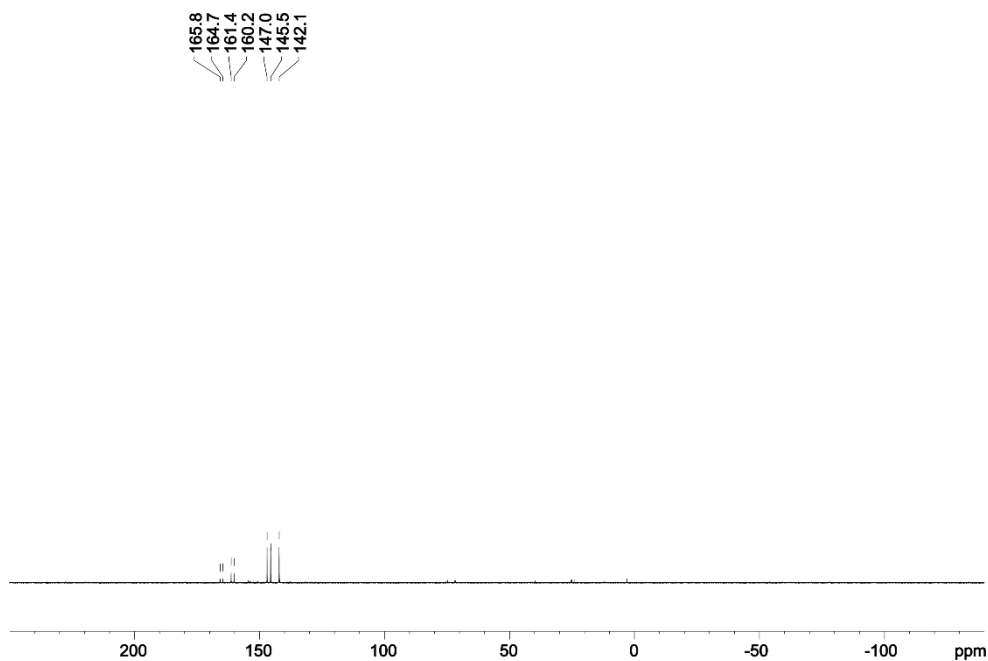
**Figure 72.** IR spectrum of  $[\text{Rh}(\kappa^2\text{O},\text{O}'\text{-acac})(\kappa^2\text{P},\text{P}'\text{-}\{((\text{R})\text{-L6})\cdot\text{LiBArF}\})]$  (25 °C, toluene- $d_8$ /THF- $d_8$  (97:3 v/v))



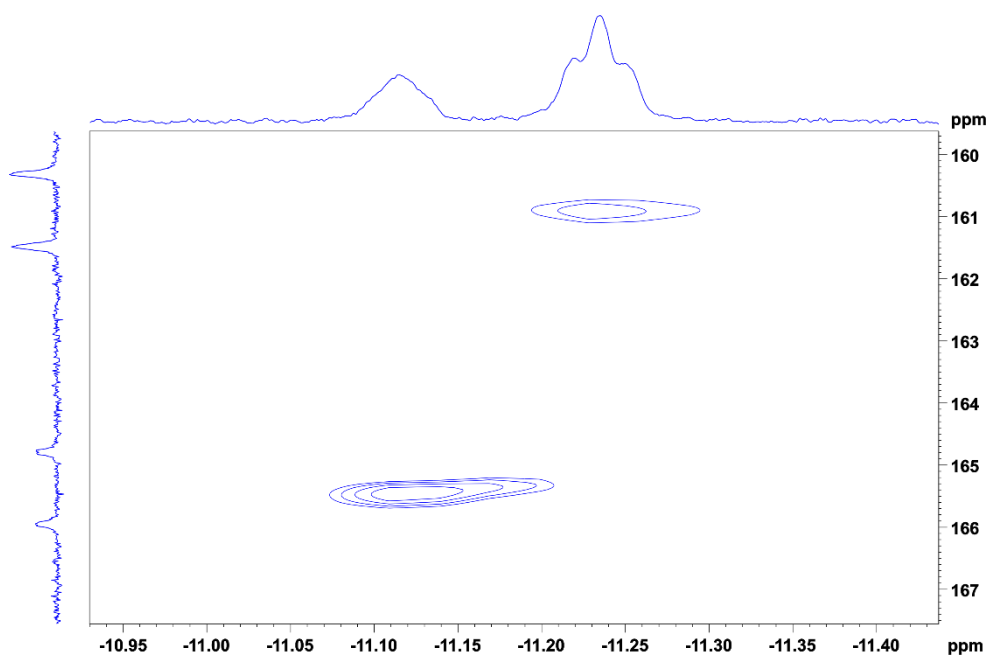
**Figure 73.** High-pressure  $^1\text{H}$  NMR spectrum of  $[\text{Rh}(\kappa^2\text{O},\text{O}^1\text{-acac})(\text{CO})_2]$  and  $(R)\text{-L6}$  (500 MHz, 10 bar  $\text{H}_2/\text{CO}$ , 25 °C, toluene- $d_8$ /THF- $d_8$  (97:3 v/v))



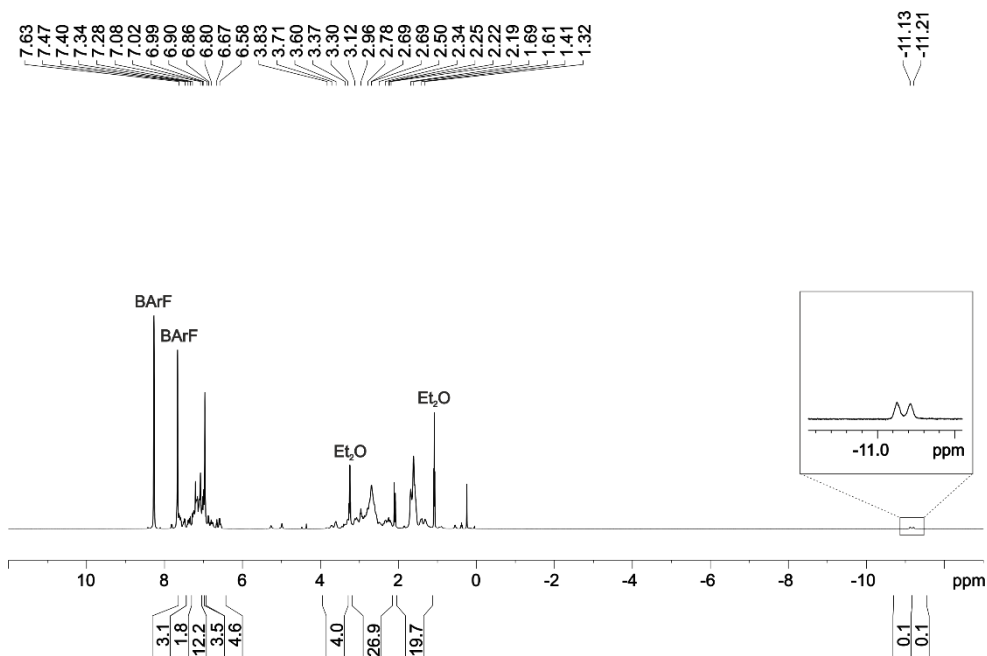
**Figure 74.** High-pressure  $^{31}\text{P}$  NMR spectrum of  $[\text{Rh}(\kappa^2\text{O},\text{O}^1\text{-acac})(\text{CO})_2]$  and  $(R)\text{-L6}$  (202 MHz, 10 bar  $\text{H}_2/\text{CO}$ , 25 °C, toluene- $d_8$ /THF- $d_8$  (97:3 v/v))



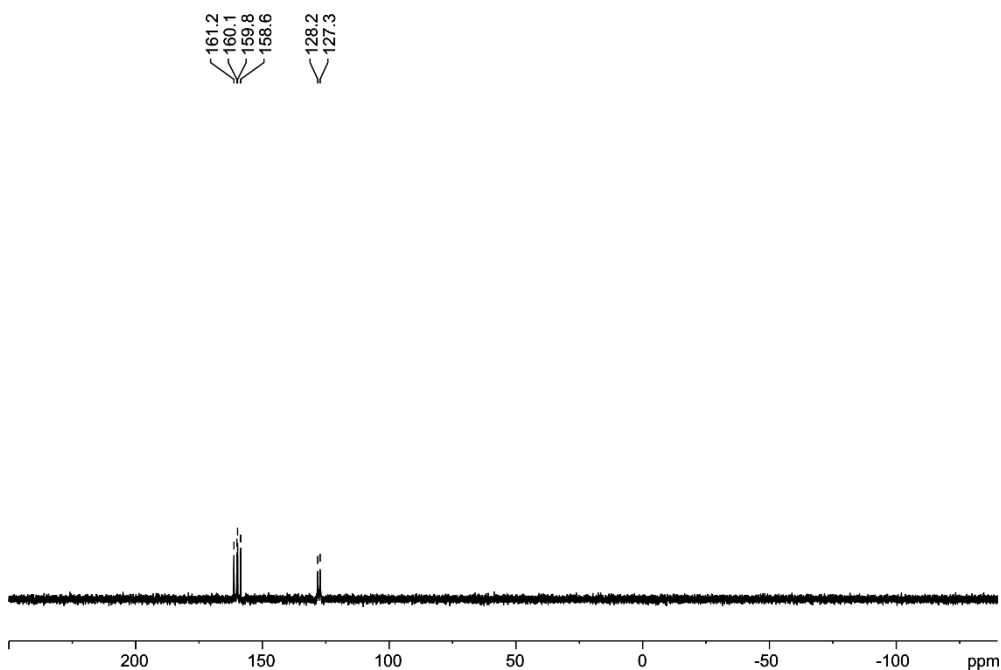
**Figure 75.** High-pressure  $^{31}\text{P}\{^1\text{H}\}$  NMR spectrum of  $[\text{Rh}(\kappa^2\text{O},\text{O}'\text{-acac})(\text{CO})_2]$  and  $(R)\text{-L6}$  (202 MHz, 10 bar  $\text{H}_2/\text{CO}$ , 25 °C, toluene- $d_8$ /THF- $d_8$  (97:3 v/v))



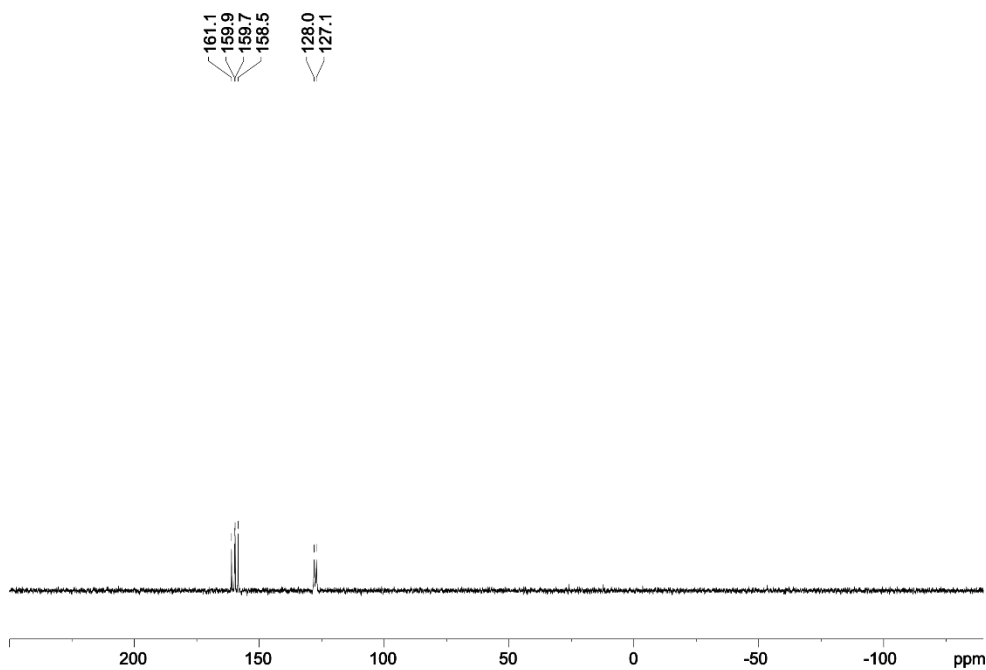
**Figure 76.** High-pressure  $^1\text{H}\text{-}^{31}\text{P}$  HMBC spectrum of  $[\text{Rh}(\text{H})(\text{CO})_2(\kappa^2\text{P},\text{P}'\text{-}\{(R)\text{-L6}\})]$  complexes (10 bar  $\text{H}_2/\text{CO}$ , 25 °C, toluene- $d_8$ /THF- $d_8$  (97:3 v/v))



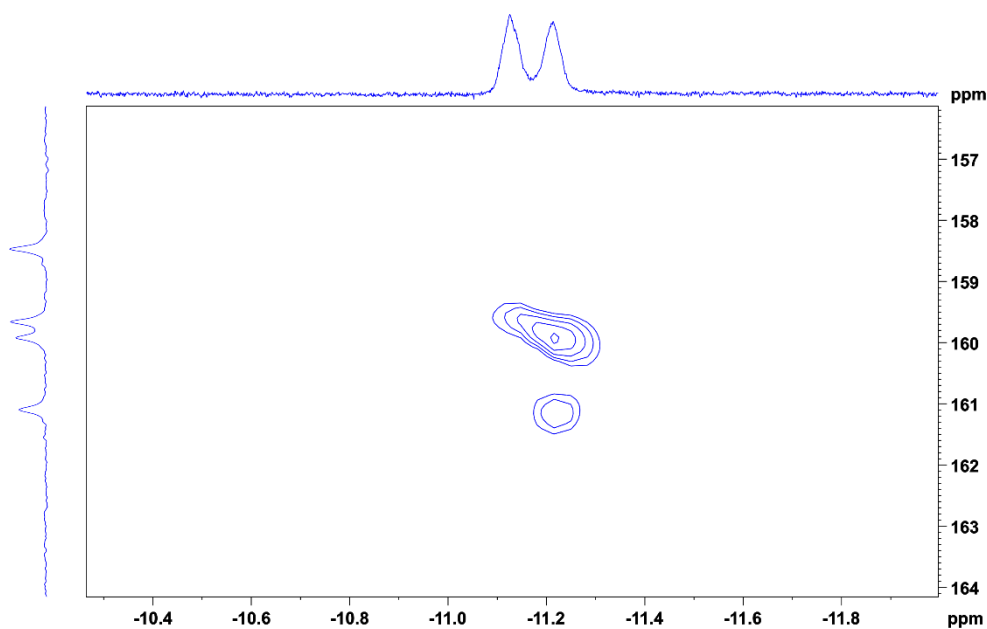
**Figure 77.** High-pressure  $^1\text{H}$  NMR spectrum of  $[\text{Rh}(\kappa^2\text{O},\text{O}'\text{-acac})(\text{CO})_2]$ , (*R*)-**L6** and LiBArF (500 MHz, 10 bar  $\text{H}_2/\text{CO}$ , 25 °C, toluene- $d_8$ /THF- $d_8$  (97:3 v/v))



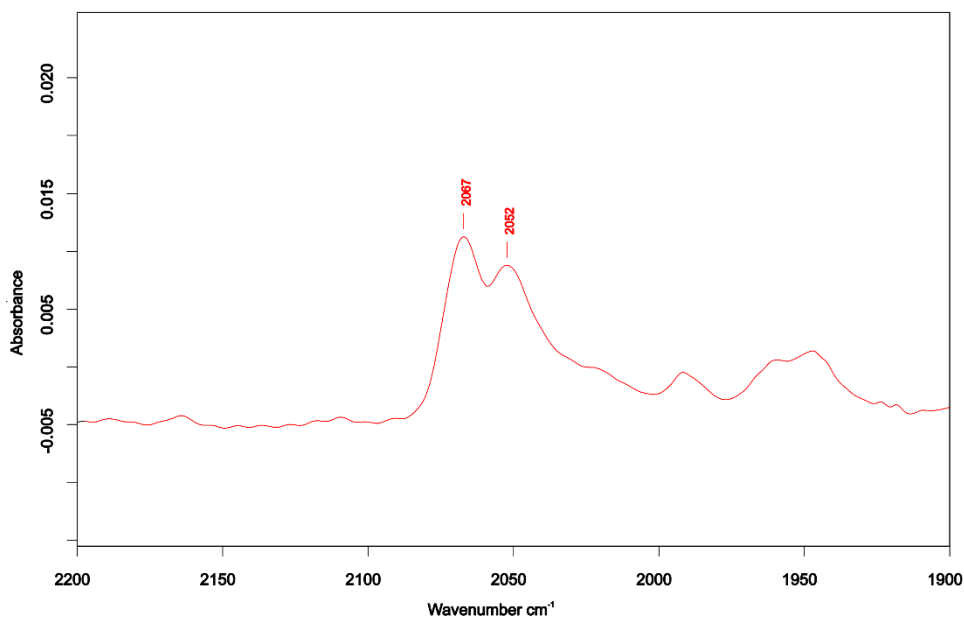
**Figure 78.** High-pressure  $^{31}\text{P}$  NMR spectrum of  $[\text{Rh}(\kappa^2\text{O},\text{O}'\text{-acac})(\text{CO})_2]$ , (*R*)-**L6** and LiBArF (202 MHz, 10 bar  $\text{H}_2/\text{CO}$ , 25 °C, toluene- $d_8$ /THF- $d_8$  (97:3 v/v))



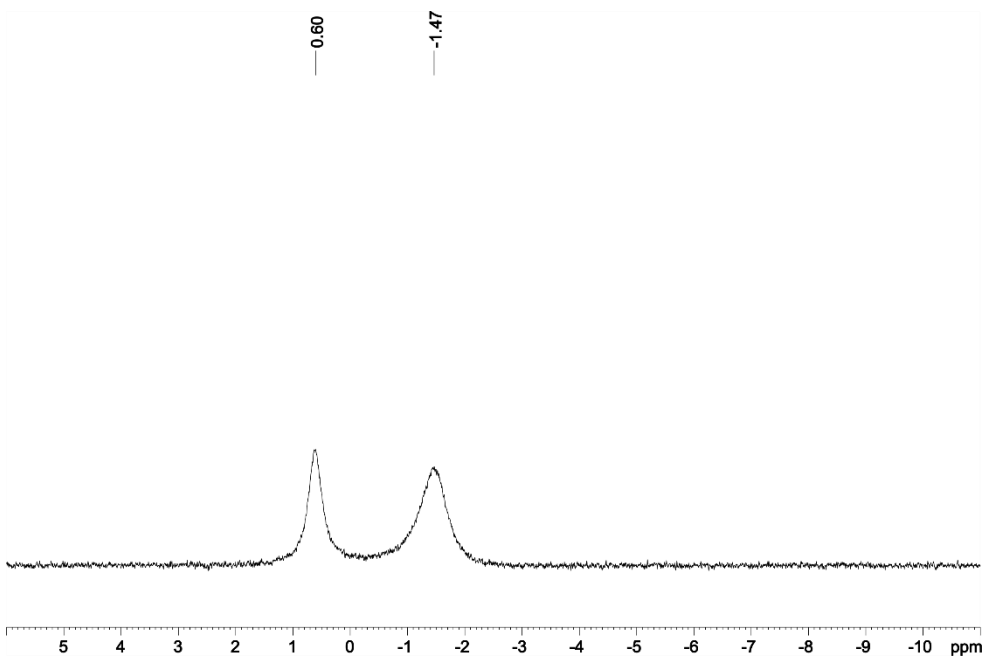
**Figure 79.** High-pressure  $^{31}\text{P}\{^1\text{H}\}$  NMR spectrum of  $[\text{Rh}(\kappa^2\text{O},\text{O}'\text{-acac})(\text{CO})_2]$ , (*R*)-**L6** and LiBARF (202 MHz, 10 bar  $\text{H}_2/\text{CO}$ , 25 °C, toluene- $d_8$ /THF- $d_8$  (97:3 v/v))



**Figure 80.** High-pressure  $^1\text{H}\text{-}^{31}\text{P}$  HMBC spectrum of  $[\text{Rh}(\text{H})(\text{CO})_2(\kappa^2\text{P},\text{P}'\text{-}\{((\text{R})\text{-L6})\cdot\text{LiBARF}\})]$  complexes (10 bar  $\text{H}_2/\text{CO}$ , 25 °C, toluene- $d_8$ /THF- $d_8$  (97:3 v/v))

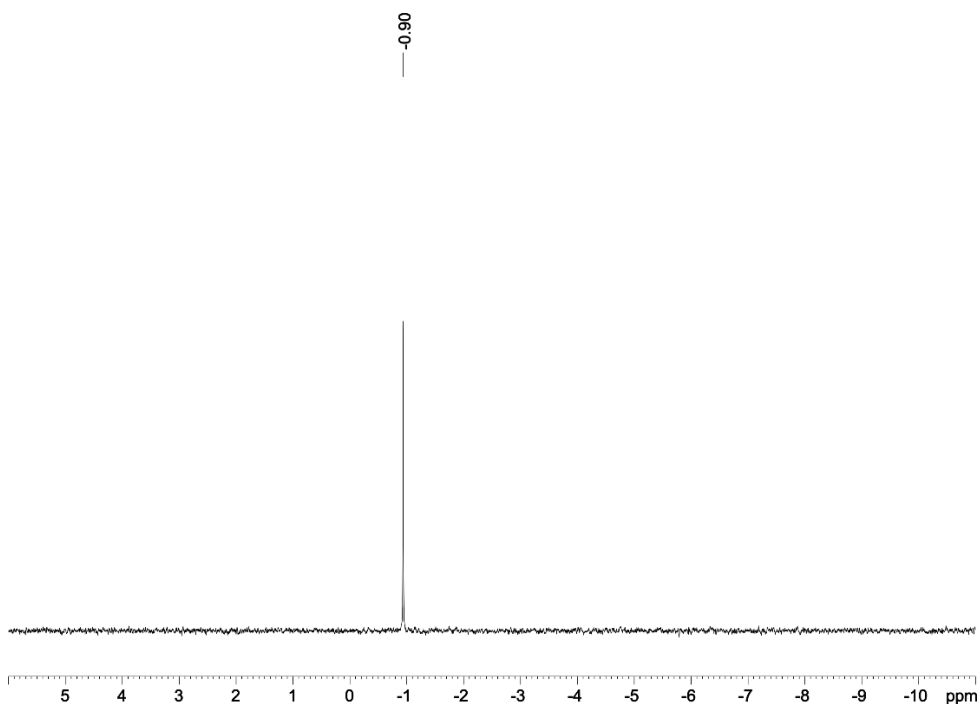


**Figure 81.** High-pressure IR spectrum of  $[\text{Rh}(\kappa^2\text{O},\text{O}^1\text{-acac})(\text{CO})_2]$ , (*R*)-**L6** and LiBARF (10 bar  $\text{H}_2/\text{CO}$ , 40 °C, toluene- $d_8$ /THF- $d_8$  (97:3 v/v))

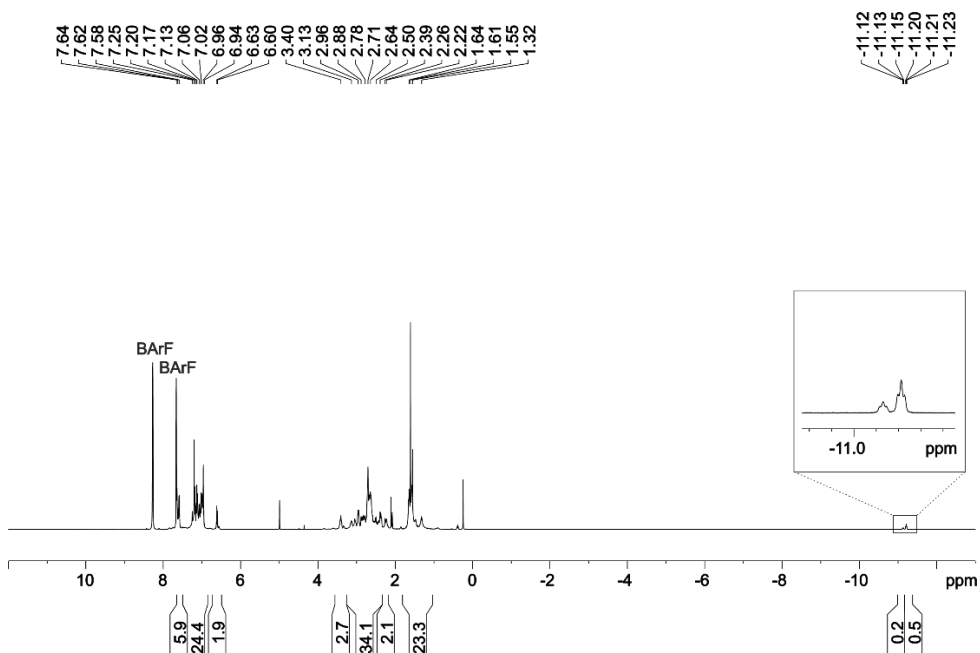


**Figure 82.** High-pressure  $^7\text{Li}$  NMR spectrum of  $[\text{Rh}(\kappa^2\text{O},\text{O}^1\text{-acac})(\text{CO})_2]$ , (*R*)-**L6** and LiBARF (194 MHz, 10 bar  $\text{H}_2/\text{CO}$ , 25 °C, toluene- $d_8$ /THF- $d_8$  (97:3 v/v))

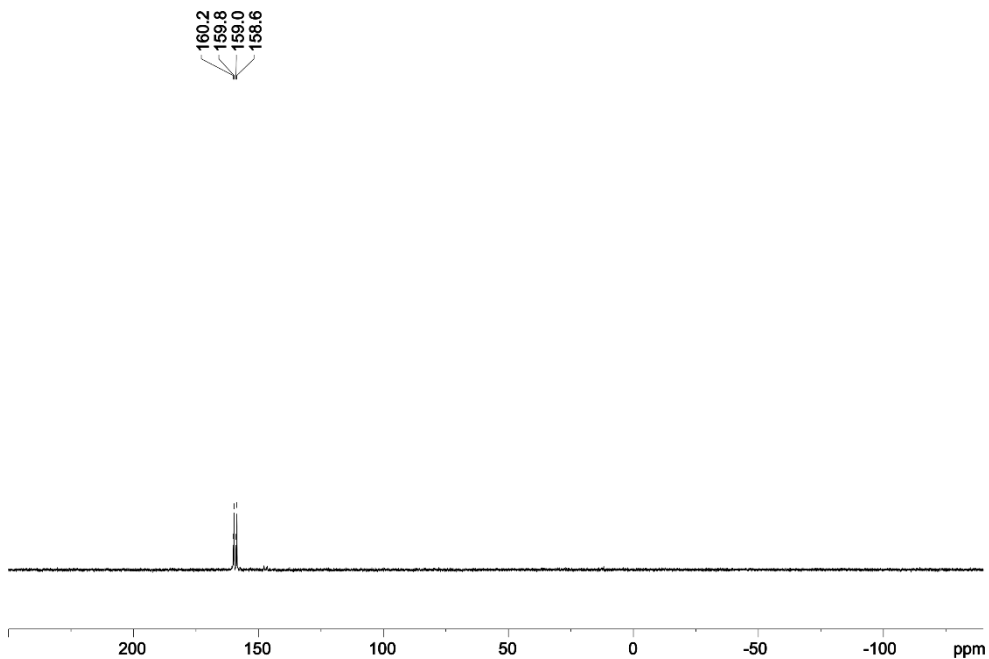




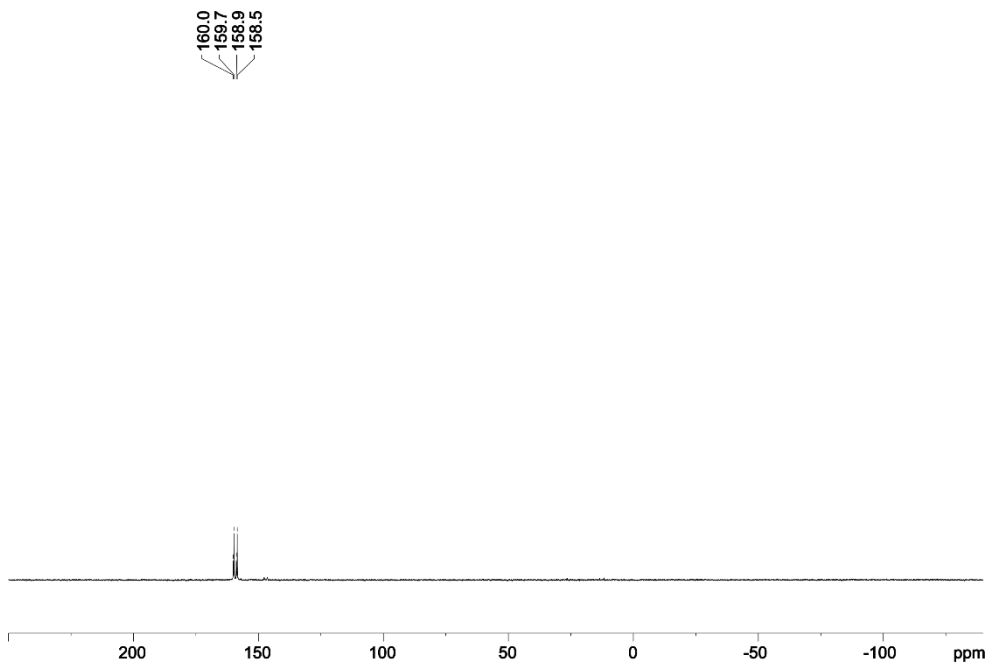
**Figure 83.**  ${}^7\text{Li}$  NMR spectrum of LiBArF (194 MHz, 10 bar  $\text{H}_2/\text{CO}$ , 25 °C, toluene- $d_8$ /THF- $d_8$  (97:3 v/v))



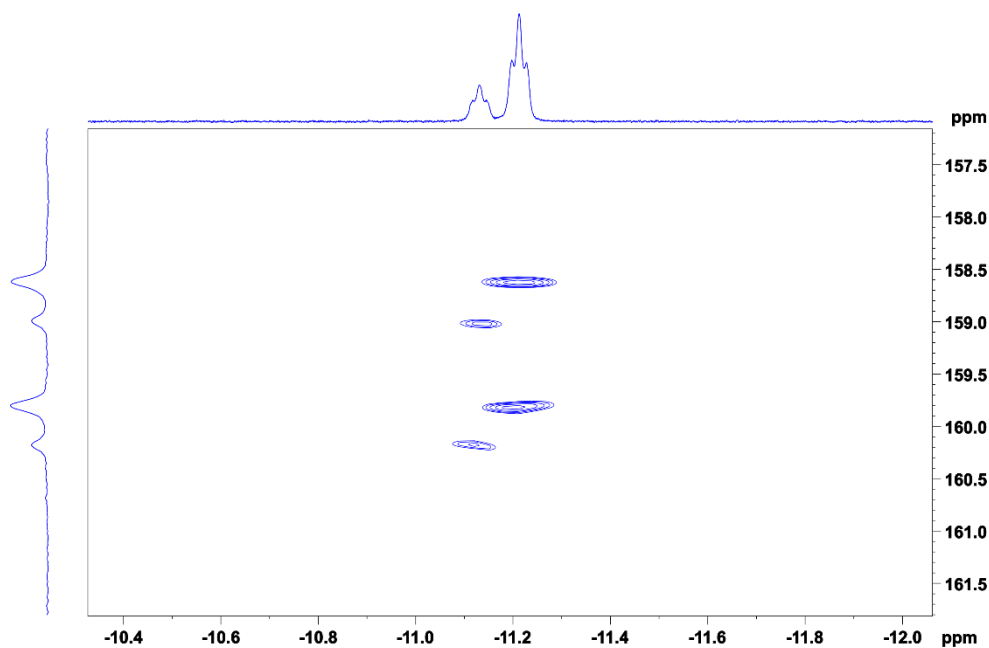
**Figure 84.** High-pressure  ${}^1\text{H}$  NMR spectrum of  $[\text{Rh}(\kappa^2\text{O},\text{O}'\text{-acac})(\text{CO})_2]$ , (R)-L6 and NaBArF (500 MHz, 10 bar  $\text{H}_2/\text{CO}$ , 25 °C, toluene- $d_8$ /THF- $d_8$  (97:3 v/v))



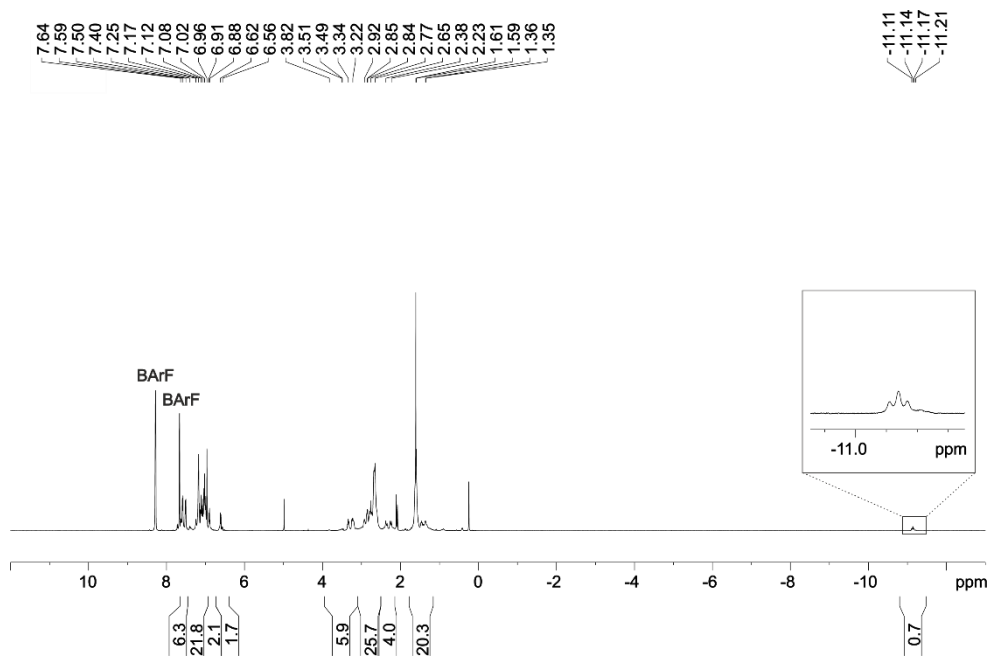
**Figure 85.** High-pressure  $^{31}\text{P}$  NMR spectrum of  $[\text{Rh}(\kappa^2\text{O},\text{O}'\text{-acac})(\text{CO})_2]$ , (R)-**L6** and NaBARF (202 MHz, 10 bar  $\text{H}_2/\text{CO}$ , 25 °C, toluene- $d_8$ /THF- $d_8$  (97:3 v/v))



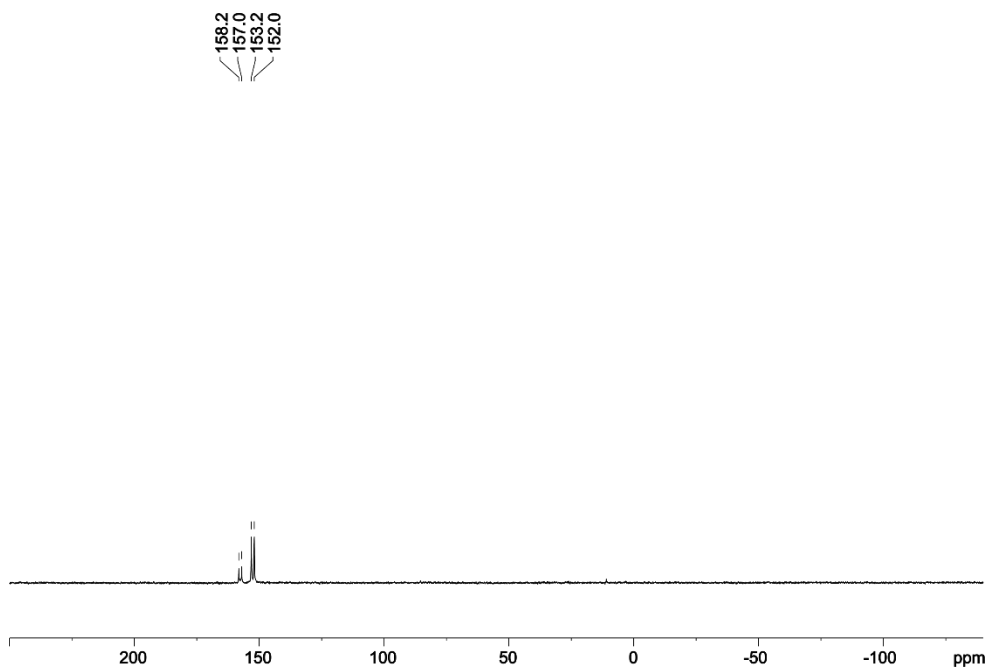
**Figure 86.** High-pressure  $^{31}\text{P}\{^1\text{H}\}$  NMR spectrum of  $[\text{Rh}(\kappa^2\text{O},\text{O}'\text{-acac})(\text{CO})_2]$ , (R)-**L6** and NaBARF (202 MHz, 10 bar  $\text{H}_2/\text{CO}$ , 25 °C, toluene- $d_8$ /THF- $d_8$  (97:3 v/v))



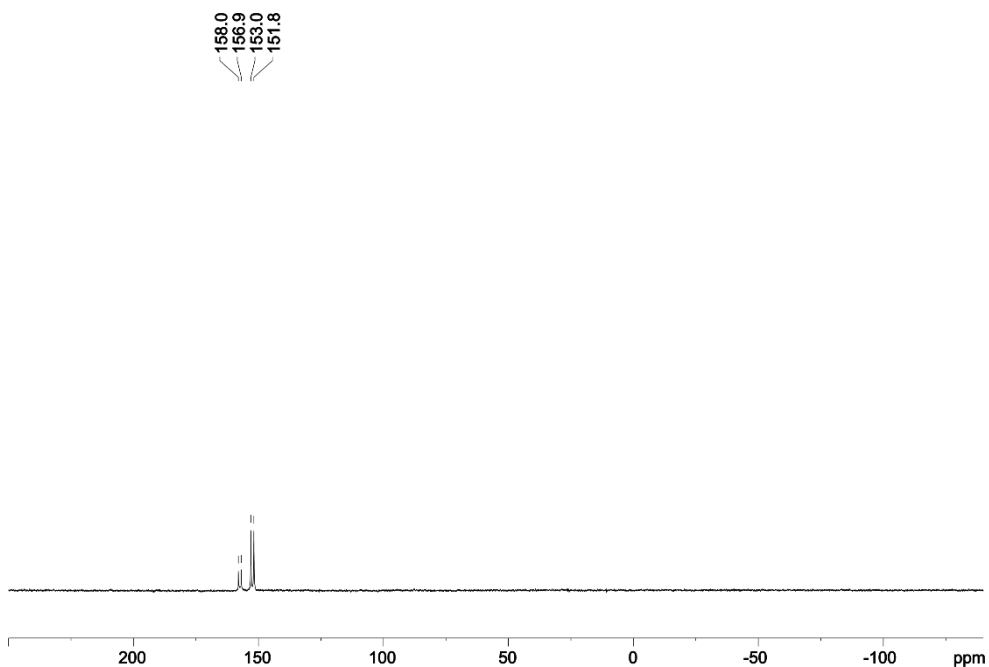
**Figure 87.** High-pressure  $^1\text{H}$ - $^{31}\text{P}$  HMBC spectrum of  $[\text{Rh}(\text{H})(\text{CO})_2(\kappa^2\text{P},\text{P}'\text{-}\{((\text{R})\text{-L6})\cdot\text{NaBArF}\})]$  complexes (10 bar  $\text{H}_2/\text{CO}$ , 25 °C, toluene- $d_8$ /THF- $d_8$  (97:3 v/v))



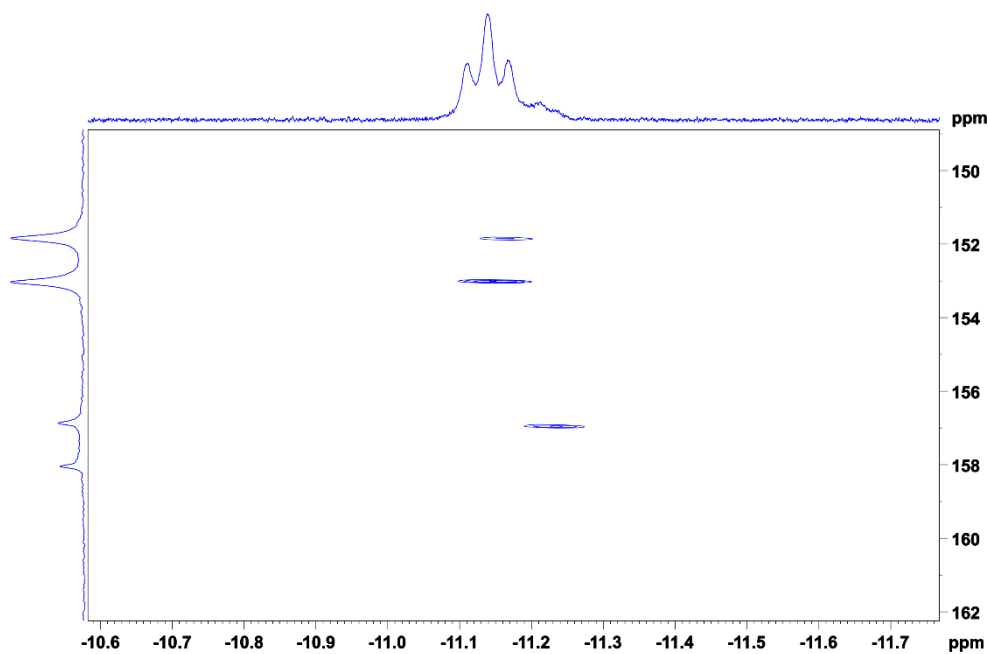
**Figure 88.** High-pressure  $^1\text{H}$  NMR spectrum of  $[\text{Rh}(\kappa^2\text{O},\text{O}'\text{-acac})(\text{CO})_2]$ , (R)-L6 and KBArF (500 MHz, 10 bar  $\text{H}_2/\text{CO}$ , 25 °C, toluene- $d_8$ /THF- $d_8$  (97:3 v/v))



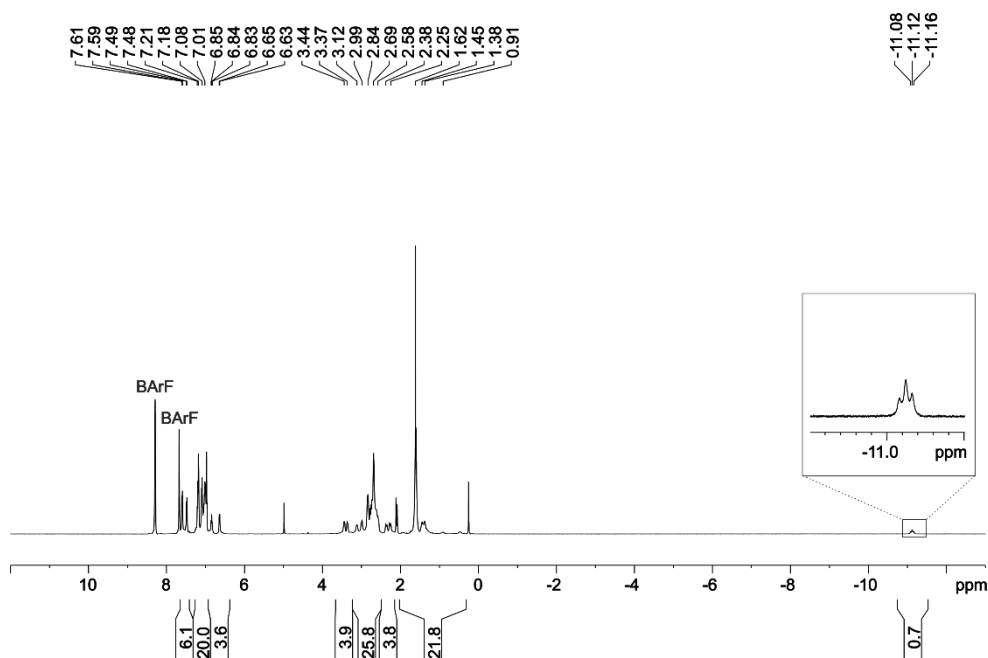
**Figure 89.** High-pressure  $^{31}\text{P}$  NMR spectrum of  $[\text{Rh}(\kappa^2\text{O},\text{O}'\text{-acac})(\text{CO})_2]$ , (*R*)-**L6** and  $\text{KBarF}$  (202 MHz, 10 bar  $\text{H}_2/\text{CO}$ , 25 °C, toluene- $d_8$ /THF- $d_8$  (97:3 v/v))



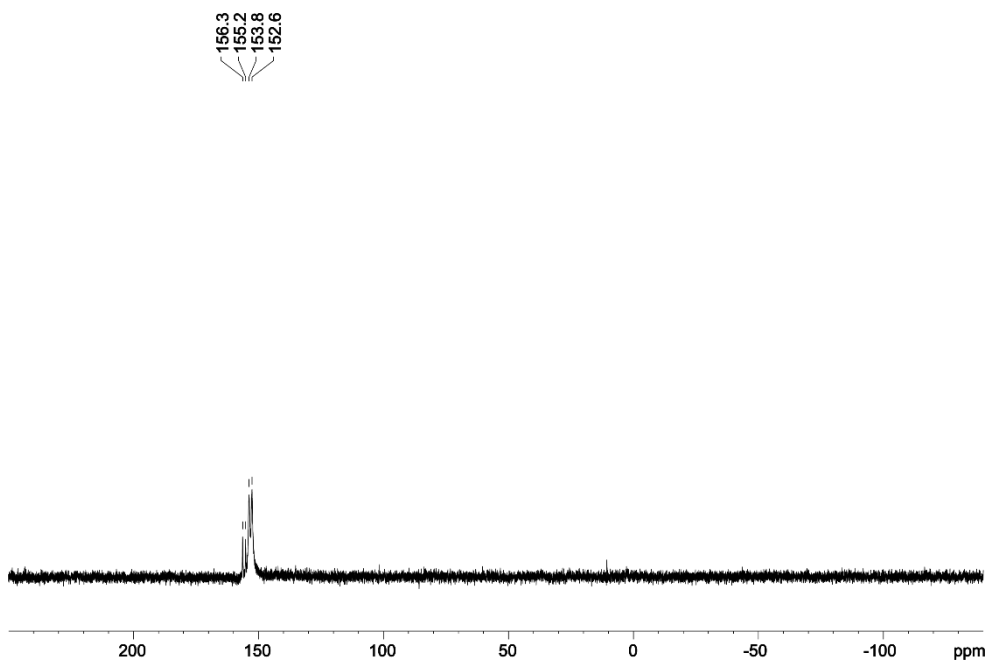
**Figure 90.** High-pressure  $^{31}\text{P}\{^1\text{H}\}$  NMR spectrum of  $[\text{Rh}(\kappa^2\text{O},\text{O}'\text{-acac})(\text{CO})_2]$ , (*R*)-**L6** and  $\text{KBarF}$  (202 MHz, 10 bar  $\text{H}_2/\text{CO}$ , 25 °C, toluene- $d_8$ /THF- $d_8$  (97:3 v/v))



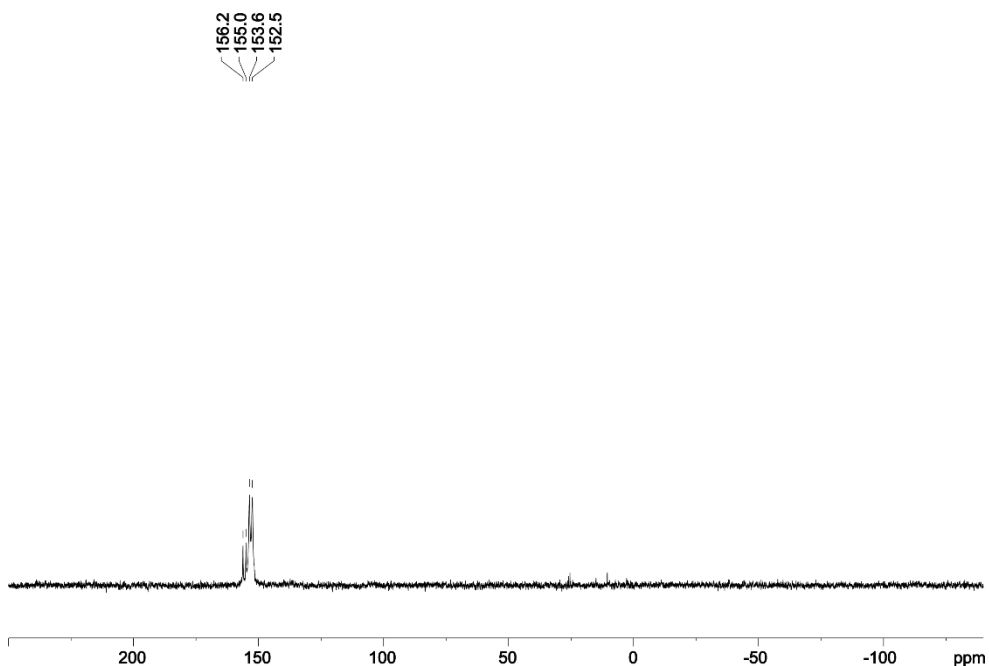
**Figure 91.** High-pressure  $^1\text{H}$ - $^{31}\text{P}$  HMBC spectrum of  $[\text{Rh}(\text{H})(\text{CO})_2(\kappa^2\text{P},\text{P}'\text{-}\{(R)\text{-L6}\}\cdot\text{KBArF})]$  complexes (10 bar  $\text{H}_2/\text{CO}$ , 25  $^\circ\text{C}$ , toluene- $d_8$ /THF- $d_8$  (97:3 v/v))



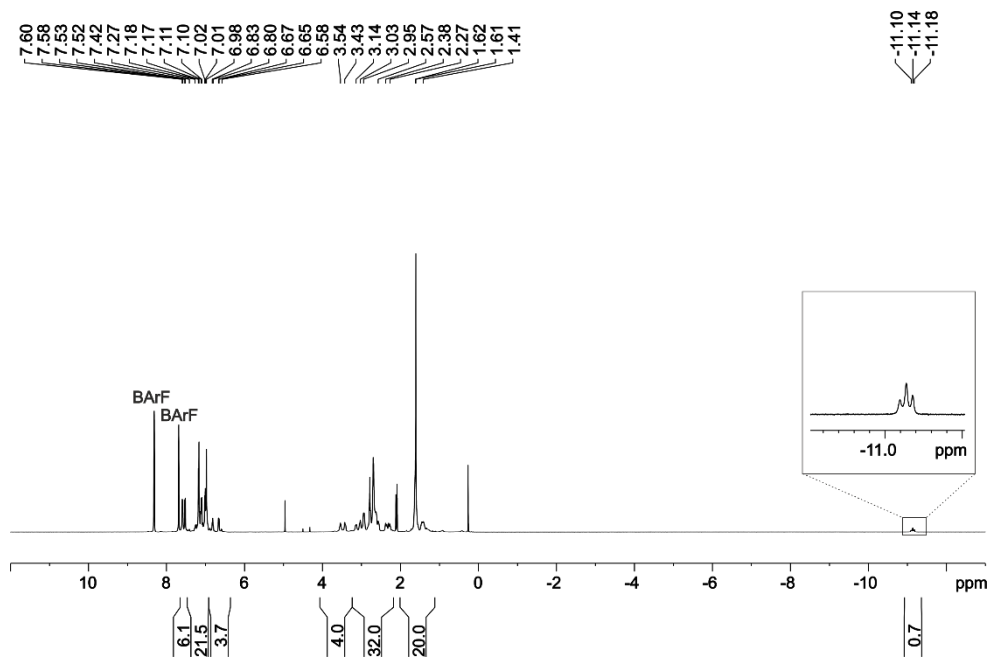
**Figure 92.** High-pressure  $^1\text{H}$  NMR spectrum of  $[\text{Rh}(\kappa^2\text{O},\text{O}'\text{-acac})(\text{CO})_2]$ ,  $(R)\text{-L6}$  and  $\text{RbBArF}$  (500 MHz, 10 bar  $\text{H}_2/\text{CO}$ , 25  $^\circ\text{C}$ , toluene- $d_8$ /THF- $d_8$  (97:3 v/v))



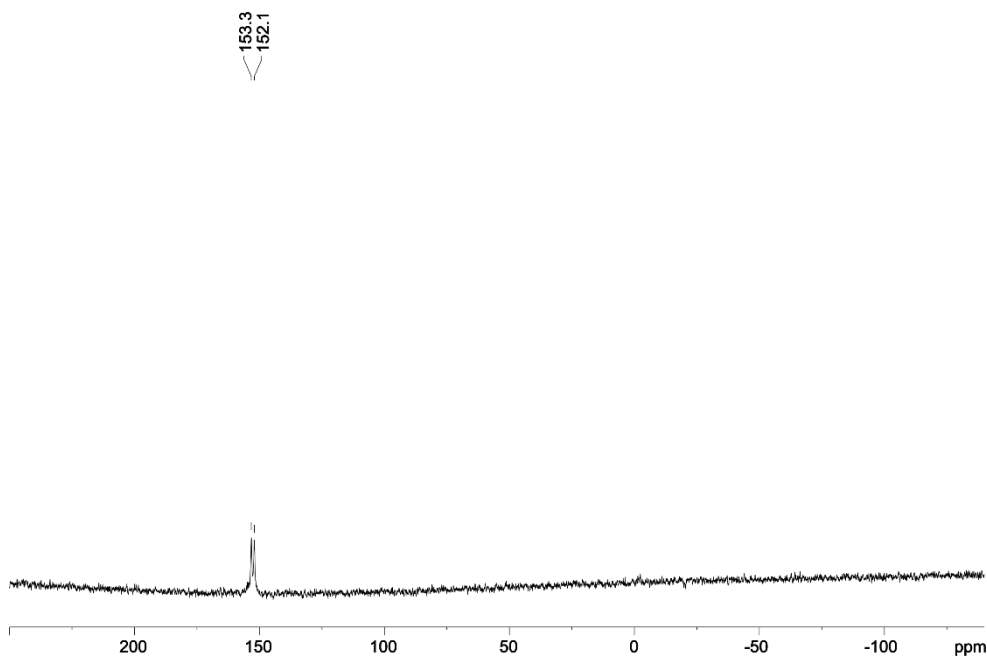
**Figure 93.** High-pressure  $^{31}\text{P}$  NMR spectrum of  $[\text{Rh}(\kappa^2\text{O},\text{O}'\text{-acac})(\text{CO})_2]$ , (R)-L6 and RbBARf (202 MHz, 10 bar  $\text{H}_2/\text{CO}$ , 25 °C, toluene- $d_8$ /THF- $d_8$  (97:3 v/v))



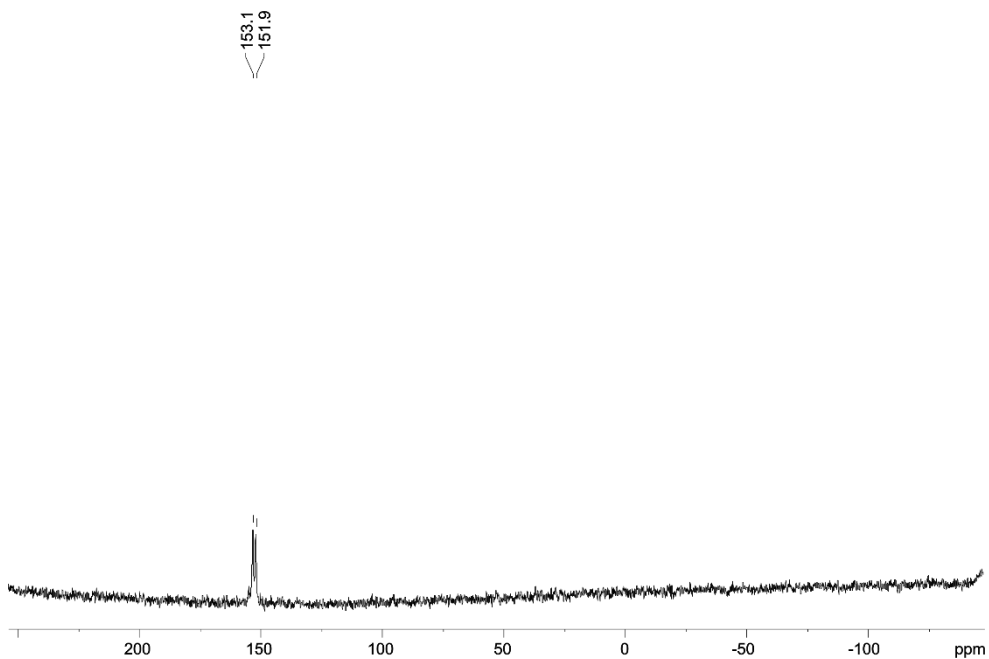
**Figure 94.** High-pressure  $^{31}\text{P}\{^1\text{H}\}$  NMR spectrum of  $[\text{Rh}(\kappa^2\text{O},\text{O}'\text{-acac})(\text{CO})_2]$ , (R)-L6 and RbBARf (202 MHz, 10 bar  $\text{H}_2/\text{CO}$ , 25 °C, toluene- $d_8$ /THF- $d_8$  (97:3 v/v))



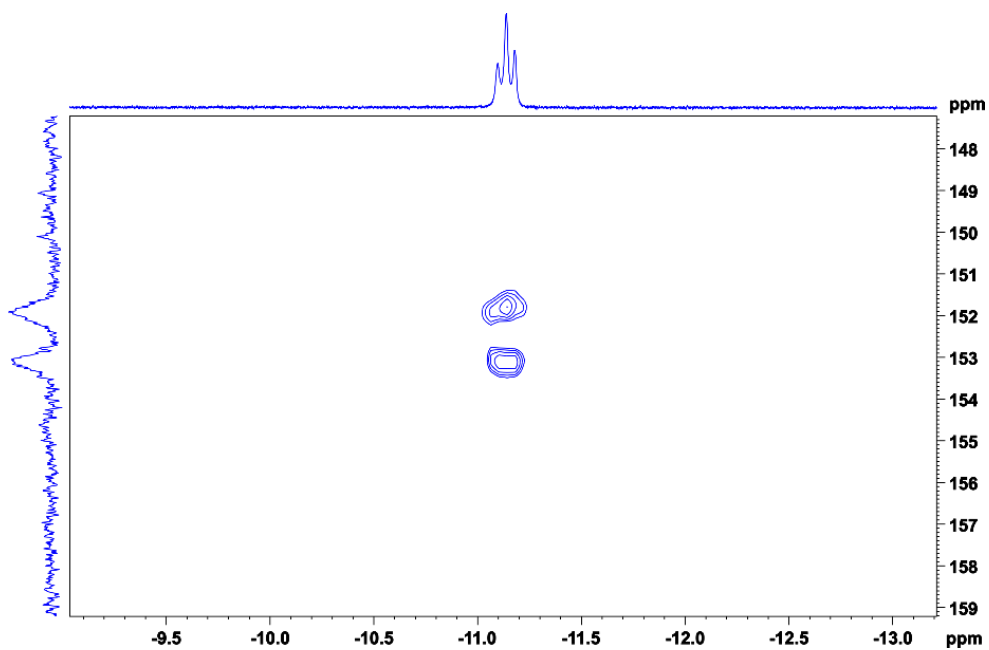
**Figure 95.** High-pressure  $^1\text{H}$  NMR spectrum of  $[\text{Rh}(\kappa^2\text{O},\text{O}'\text{-acac})(\text{CO})_2]$ , (*R*)-**L6** and CsBArF (500 MHz, 10 bar  $\text{H}_2/\text{CO}$ , 25 °C, toluene- $d_8$ /THF- $d_8$  (97:3 v/v))



**Figure 96.** High-pressure  $^{31}\text{P}$  NMR spectrum of  $[\text{Rh}(\kappa^2\text{O},\text{O}'\text{-acac})(\text{CO})_2]$ , (*R*)-**L6** and CsBArF (202 MHz, 10 bar  $\text{H}_2/\text{CO}$ , 25 °C, toluene- $d_8$ /THF- $d_8$  (97:3 v/v))



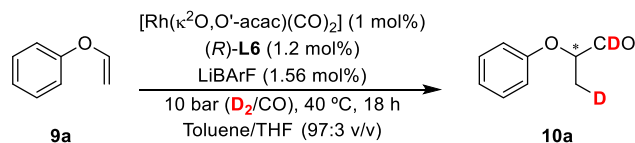
**Figure 97.** High-pressure  $^{31}\text{P}\{^1\text{H}\}$  NMR spectrum of  $[\text{Rh}(\kappa^2\text{O},\text{O}'\text{-acac})(\text{CO})_2]$ , (R)-L6 and CsBARf (202 MHz, 10 bar  $\text{H}_2/\text{CO}$ , 25 °C, toluene- $d_8$ /THF- $d_8$  (97:3 v/v))



**Figure 98.** High-pressure  $^1\text{H}-^{31}\text{P}$  HMBC spectrum of  $[\text{Rh}(\text{H})(\text{CO})_2(\kappa^2\text{P},\text{P}'\text{-}\{(R)\text{-L6}\}\cdot\text{CsBARf})]$  complexes (10 bar  $\text{H}_2/\text{CO}$ , 25 °C, toluene- $d_8$ /THF- $d_8$  (97:3 v/v))

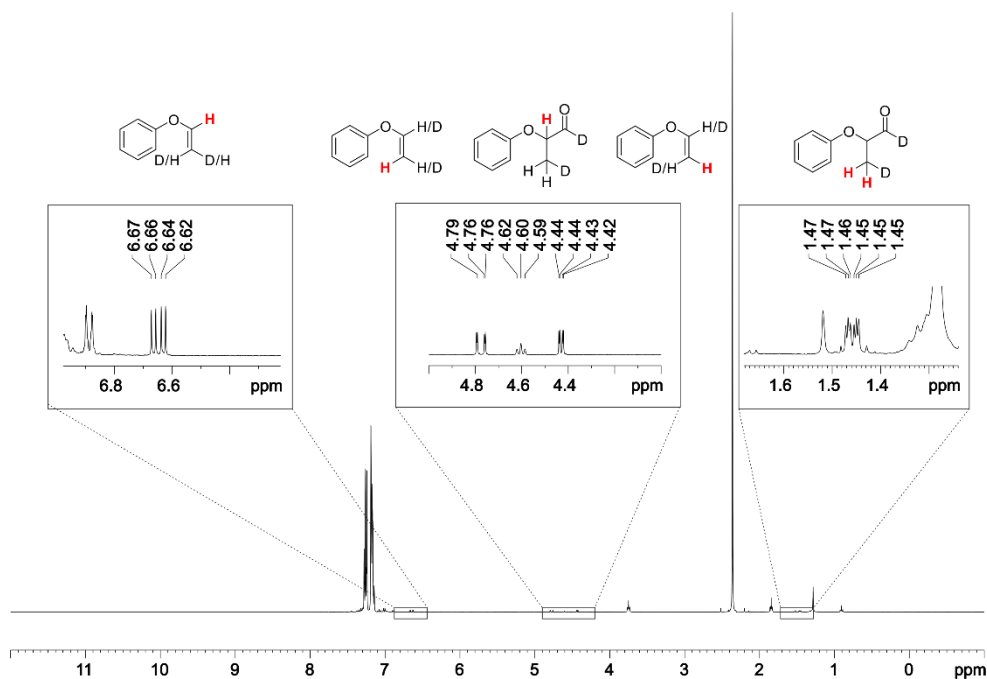


## 3.5.11 Deuteroformylation results

**Table 36.** Deuterioformylation of **9a** with supramolecular ligand (*R*)-**L6** in the presence of LiBARF

Entry	Conversion (%) <sup>[a]</sup>	b/1 ratio <sup>[a]</sup>	<i>er</i> ( <i>S</i> : <i>R</i> ) <sup>[a]</sup>
1	16	>99:1	94:6

The enantioselective hydroformylations were performed in a parallel autoclave. Reaction conditions: [alkene] = 0.26 M; stirring rate = 800 rpm; D<sub>2</sub>/CO in a 1:1 ratio, unless otherwise cited. [a] Conversion, b/1 ratio and *er* values were determined by GC analysis on a chiral stationary phase (β-Dex™ 225).

**Figure 99.** <sup>1</sup>H NMR spectrum of crude deuteroformylation reaction mixture

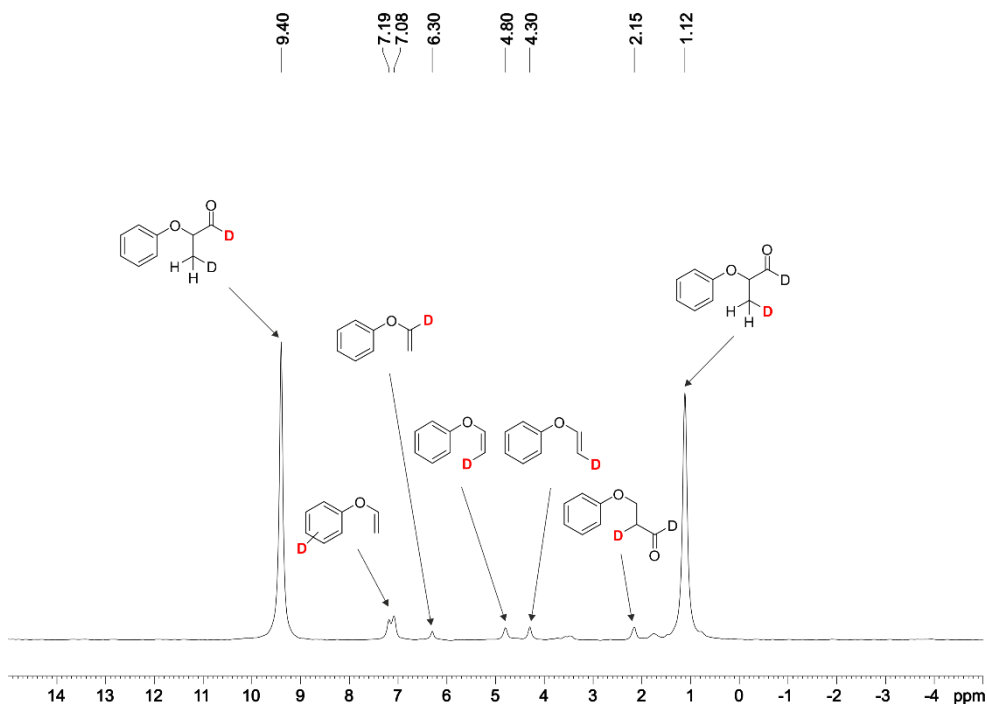


Figure 100.  $^2\text{H}$  NMR spectrum of crude deuterioformylation reaction mixture

### 3.5.12 Computational methods

Geometry optimization of compounds **B-Li (S)**, **S1**, **S2**, **S3**, **S4**, **S2-BArF** and **S4-BArF** were carried out the M06-2X<sup>53</sup>-D3 level with the def2-SVP<sup>54</sup> basis set. The geometry optimization was carried out as implemented in Gaussian 09, revision D.01.<sup>55</sup> For the calculations, we have used the above mentioned functional with the latest available correction for dispersion (D3).<sup>56</sup> Solvent effects (toluene) were incorporated employing the Polarizable Continuum Model (PCM) with the integral equation formalism (IEFPCM calculations)<sup>57</sup> with radii and non-electrostatic terms<sup>58</sup> as implemented in Gaussian 09, Revision D.01.

<sup>53</sup> Zhao, Y.; Truhlar, D. G. *Theor Chem Acc.* **2006**, *120*, 215-241.

<sup>54</sup> Schäfer, A.; Horn, H.; Ahlrichs, R. *J. Chem. Phys.* **1992**, *97*, 2571-2577.

<sup>55</sup> Gaussian 09, Revision D.01, Frisch, M. J. *et al.* Gaussian, Inc., Wallingford CT, **2016**.

<sup>56</sup> (a) Grimme, S.; Antony, J.; Ehrlich, S.; Krieg, H. *J. Chem. Phys.* **2010**, *132*, 154104/1-154104/19.

(b) Grimme, S.; Ehrlich, S.; Goerigk, L. *J. Comput. Chem.* **2011**, *32*, 1456-1465.

<sup>57</sup> Scalmani, G.; Frisch, M. J. *J. Chem. Phys.* **2010**, *132*, 114110/1-114110/15.

<sup>58</sup> Marenich, A. V.; Cramer, C. J.; Truhlar, D. G. *J. Phys. Chem.* **2009**, *113*, 6378-6396.

Cartesian coordinates**B-Li (S)**

O	3.26482700	-0.29248400	-1.44493700	H	1.61714100	-3.02484700	1.90990600
O	1.11458500	1.14857900	0.05514100	H	3.25976200	-3.72895500	1.83763300
O	-0.89565900	-2.31861700	-0.40090800	H	3.28894500	-1.60059600	3.09341900
O	2.60388200	-2.89838500	0.07624100	H	2.57056700	-0.73378700	1.69793200
O	4.47798200	-1.47144900	1.39450500	H	5.48503800	-0.36909400	2.84111300
O	6.11066700	-0.72958300	-0.39339400	H	4.65679300	0.58413500	1.59487300
O	5.58415400	-3.56365200	-0.52892100	H	7.18839700	-1.14287700	1.33405600
O	4.30820000	-2.47555800	-2.48183600	H	7.00308300	0.59487200	0.94108100
C	0.45054100	-1.89601100	-0.47684000	H	5.70021400	-5.33582300	-1.61332800
C	1.32306000	-3.14708200	-0.47299600	H	6.52400200	-3.91512000	-2.34293800
C	2.62908700	-2.89209500	1.49635300	H	4.42600900	-4.25177500	-3.55773500
C	3.20739100	-1.58997000	1.99335900	H	3.49316600	-4.31639500	-2.02120600
C	5.23339000	-0.34091200	1.76735600	H	3.39585800	-2.00977400	-4.28968000
C	6.49901800	-0.38456700	0.93592800	H	2.28546700	-2.30392500	-2.91779300
C	7.12377300	-0.96062600	-1.29718700	H	4.24628100	0.03648000	-3.23039000
C	6.70335900	-3.71738000	0.25963300	H	2.45282100	0.10659600	-3.32249700
C	5.63911300	-4.24801900	-1.77612000	H	3.92505200	1.65933400	-1.62793700
C	4.37750400	-3.88151400	-2.51974900	H	3.59118700	1.08038500	0.02581500
C	3.26074700	-1.87214500	-3.20287200	H	1.93019100	2.75476400	-1.01643800
C	3.30653000	-0.40766400	-2.85374400	H	1.32325600	1.38799000	-1.98263400
C	3.23439600	1.05550200	-1.01222900	H	9.66174900	-3.07677100	-2.05697800
C	1.84872700	1.66044300	-1.05428200	H	5.68399400	-5.09016300	1.54444500
C	7.98564100	-2.06439700	-1.17258700	H	7.67864100	-5.44325000	3.02224600
C	8.98527200	-2.22381600	-2.14293000	H	9.89366400	-1.49430000	-3.95514100
C	6.62662500	-4.57596200	1.35322800	H	9.81847900	-4.27717500	2.49045600
C	7.74162200	-4.77269300	2.16454700	H	9.93425000	-2.73094900	0.55122000
C	9.11198200	-1.33925800	-3.21111800	H	8.33070600	0.44107300	-4.15381100
C	8.93795200	-4.12151900	1.86658000	H	6.56604500	0.77984500	-2.40422800
C	9.00608800	-3.26165900	0.77285800	P	-0.22719400	1.77175300	0.75095000
C	7.88970900	-3.02978800	-0.04270600	Rh	-1.54579300	0.24694300	1.77282600
C	8.23733900	-0.25964500	-3.32336500	C	-2.85712300	0.86656300	3.09911800
C	7.25000400	-0.06896300	-2.36039000	O	-3.67863100	1.28467900	3.76048100
H	0.60472200	-1.28182900	-1.38183000	C	-4.60655300	-2.71986500	-1.24140300
H	0.71369200	-1.26082000	0.38477500	C	-5.08934700	-3.75238100	-2.07461800
H	1.46608700	-3.54776800	-1.48571900	C	-4.58233200	-3.85808400	-3.38073800
H	0.80286600	-3.92396300	0.11066700	C	-3.57019300	-2.99058300	-3.80305300
				C	-2.99990000	-2.02844200	-2.96706700
				C	-3.55705000	-1.91275400	-1.68570400
				C	-5.10811100	-2.53008000	0.15373100

C	-6.45132700	-2.21952700	0.44479900	C	4.83818200	2.45019900	4.47496000
C	-6.86119100	-2.16995700	1.79028500	C	4.14434900	1.33554100	4.94464100
C	-5.92249700	-2.36424800	2.80608600	C	2.97643200	0.94459000	4.29455400
C	-4.56608500	-2.58075100	2.55001500	C	2.50881900	1.64596000	3.18278200
C	-4.18718800	-2.66253800	1.20297700	C	-3.67171600	2.92279700	-2.65923000
H	-3.20598700	-3.08165100	-4.82934500	C	-4.51761800	1.93678000	-3.16712600
H	-6.26028600	-2.33718500	3.84509200	C	-5.19652700	1.07988800	-2.29957900
O	-2.85703700	-2.83399400	0.87486400	C	-5.04828200	1.23361200	-0.92134100
O	-3.03460600	-0.99459300	-0.80470100	C	-4.22054400	2.23504300	-0.41498500
P	-2.03703400	-1.47657500	0.40337100	C	-1.86079000	-1.18857300	-3.42380700
C	0.99954700	4.76207300	0.23619700	C	3.18697800	2.77757500	2.70022000
C	1.97731900	5.48393400	-0.48127200	C	-5.06912300	-4.92339500	-4.34421500
C	3.33312800	5.23076200	-0.20861800	C	-6.32535900	-5.64171800	-3.86529300
C	3.67200200	4.33173100	0.80356400	H	-4.26132400	-5.66325100	-4.47949200
C	2.73027500	3.60952300	1.54714400	H	-6.51498100	-6.52434300	-4.49213100
C	1.38586300	3.79520400	1.17451200	C	-6.08123400	-4.76833700	-1.53943900
C	-0.45407100	4.98014200	-0.00648300	C	-6.16410300	-6.02627500	-2.39922700
C	-1.01076300	6.25046700	0.12441400	H	-5.80583500	-5.01728300	-0.50352200
C	-2.35083100	6.51270500	-0.16223800	H	-5.24530000	-6.62473900	-2.27926900
C	-3.16976100	5.46461100	-0.61398400	C	-7.41847600	-1.81963400	-0.65361300
C	-2.63545800	4.16468100	-0.74282500	C	-8.87802600	-2.03281000	-0.26704400
C	-1.29615900	3.93267400	-0.40875000	H	-7.26716200	-0.74150800	-0.84579400
H	4.73331500	4.17747200	1.00991500	H	-9.53449500	-1.64197800	-1.05738800
H	-0.37255800	7.06863400	0.46639500	C	-8.31486600	-1.96467600	2.17152700
O	-0.76017400	2.66166200	-0.54381100	C	-9.16110400	-1.34453200	1.06429000
O	0.40057300	2.98931800	1.69839200	H	-8.36990000	-1.36081600	3.08922200
C	-3.50283900	3.07121400	-1.27711300	H	-8.92362700	-0.27167800	0.96895600
C	-3.57779200	-2.68548000	3.65558600	C	-4.61817300	5.71432600	-0.98841200
C	-0.93497300	-1.70901000	-4.34361100	C	-5.16178400	7.04278600	-0.47053400
C	0.07500600	-0.91144500	-4.87965600	H	-5.23739800	4.87827500	-0.63334400
C	0.18575600	0.42758800	-4.50054800	H	-5.33565800	6.97399700	0.61649700
C	-0.69739700	0.94451300	-3.55169700	C	-2.88527600	7.91720600	0.02861100
C	-1.70164200	0.14513800	-3.00900700	C	-4.17417200	8.17072500	-0.74486900
C	-3.69036900	-1.84719200	4.77335300	H	-3.07476000	8.07451600	1.10465600
C	-2.76551800	-1.91271400	5.81418900	H	-4.59713400	9.14483100	-0.46172900
C	-1.71649900	-2.82892900	5.76108400	C	1.58248900	6.47330300	-1.56119000
C	-1.60502500	-3.68209500	4.66247600	C	2.70907400	6.75739900	-2.55006300
C	-2.52311400	-3.61116000	3.61762200	H	0.68320700	6.11017100	-2.07901300
C	4.35895300	3.16289500	3.37949900	H	2.88497100	5.87098600	-3.18374900

C 4.45008900 5.89372100 -0.99233700  
C 3.98888700 7.10226500 -1.79836500  
H 4.87910800 5.14561500 -1.68234400  
H 4.78421900 7.41987800 -2.48712000  
H -1.01612700 -2.75250500 -4.65295400  
H 0.76192900 -1.33343800 -5.61652400  
H 0.94797900 1.06702100 -4.95159900  
H -0.63025500 1.98701400 -3.23193200  
H -2.38671400 0.57897200 -2.28354600  
H -4.49686900 -1.11293700 4.81419100  
H -2.86630500 -1.24233400 6.66908700  
H -0.99300000 -2.88326700 6.57585100  
H -0.79814100 -4.41611800 4.62227400  
H -2.43160400 -4.28270700 2.76443200  
H 4.88553300 4.06741400 3.07495600  
H 5.74170800 2.79001300 4.98342000  
H 2.40650400 0.08816900 4.65879600  
H 1.59763400 1.30752200 2.70014700  
H 4.50002100 0.79065100 5.82032600  
H -3.13310900 3.58713500 -3.33904300  
H -4.63274900 1.82534800 -4.24638700  
H -5.83851000 0.29168600 -2.69820000  
H -5.56375200 0.56259400 -0.22975400  
H -4.13290700 2.37943600 0.66290900  
H -5.23076200 -4.46578600 -5.33218800  
H -7.20102400 -4.97915200 -3.97175100  
H -7.08703800 -4.32032500 -1.47678100  
H -7.00006700 -6.65219800 -2.05698600  
H -7.17388400 -2.31620600 -1.59976900  
H -9.08798000 -3.11289000 -0.17764500  
H -8.73442900 -2.95195200 2.43242000  
H -10.22621100 -1.41232200 1.32701200  
H -4.69844100 5.68662200 -2.08938600  
H -6.13655700 7.24696300 -0.93521200  
H -2.10623400 8.64151300 -0.25277300  
H -3.95930900 8.21475900 -1.82601100  
H 1.28648500 7.42384800 -1.08683400  
H 2.41135400 7.57454700 -3.22177600  
H 5.26109400 6.16936100 -0.30171300

H 3.79360900 7.95073800 -1.12169600  
C -0.24911800 -0.65537800 2.96803900  
O 0.51673400 -1.19866400 3.61052600  
H -2.57471200 0.88659400 0.80829800  
Li 4.37290000 -1.85813700 -0.56409200

## S1

O -0.41227200 -1.60492100 2.97885600  
O 0.06873100 -1.75763300 0.02609700  
O 0.43201300 2.29027200 0.14376600  
O 1.46077800 0.80874500 3.17997300  
O 2.87168100 -1.39521000 3.70922600  
O 1.37896300 -2.73826900 5.27785100  
O 1.72638200 0.00003400 6.14921300  
O -0.65300700 -0.22477500 5.22290200  
C 0.32637700 1.20459100 1.05135400  
C 0.68172100 1.73133600 2.44134000  
C 2.81954500 0.74963500 2.77608200  
C 3.20393100 -0.68972100 2.53576100  
C 3.11970000 -2.78183600 3.67816700  
C 2.65018300 -3.32969500 5.00674000  
C 0.84665900 -2.97373000 6.52499700  
C 2.79124800 -0.46008100 6.88906500  
C 0.69906000 0.63301200 6.90854200  
C -0.40564100 0.96476900 5.93738800  
C -1.75018000 -0.21278600 4.34026900  
C -1.68829300 -1.51096100 3.58198300  
C -0.28802000 -2.74920100 2.15669800  
C -0.85795200 -2.54813900 0.77012900  
C 1.43056800 -2.44420100 7.68991300  
C 0.81209700 -2.72730400 8.91641900  
C 3.98032800 0.26506000 6.85322100  
C 5.07911100 -0.15836500 7.59633900  
C -0.35339300 -3.48634100 8.98761600  
C 4.97885000 -1.29992200 8.39059200  
C 3.78700000 -2.02031900 8.42220500  
C 2.67545400 -1.62537100 7.66414200  
C -0.92096000 -3.99406300 7.81992700

C	-0.31366800	-3.74283000	6.59260400	C	-2.54742800	3.54337400	-0.69692100
H	-0.69110900	0.77830700	1.01805700	C	-1.52393300	3.60516100	-1.65608600
H	1.01751700	0.39223900	0.77583400	C	0.00574100	4.78291100	-3.23563000
H	-0.21580400	1.94797100	3.03501000	C	-0.14458500	5.32639500	-4.52837500
H	1.23050100	2.68032200	2.32322000	C	0.98710000	5.42297800	-5.35684300
H	2.98713400	1.33145900	1.85566500	C	2.21415800	4.93140200	-4.90655600
H	3.44871000	1.18143700	3.57164600	C	2.37462900	4.28605300	-3.67622400
H	4.28407800	-0.76752700	2.32147000	C	1.23533000	4.22130200	-2.85557000
H	2.64088400	-1.10422700	1.67814100	H	-3.99146800	4.75488300	0.33812500
H	4.19565300	-2.99132800	3.54966800	H	3.08391200	5.04527800	-5.55729300
H	2.58927100	-3.24977300	2.83064400	O	1.29810100	3.60266100	-1.62947900
H	3.36520400	-3.06304000	5.79799200	O	-0.88584000	2.45095900	-2.03941600
H	2.55786900	-4.42653700	4.96403200	P	0.61520600	2.09666700	-1.46460700
H	1.08632700	1.54358700	7.39261700	C	-0.75185800	-4.74002200	-2.04170300
H	0.32755500	-0.05847500	7.68181200	C	-1.34205400	-5.88170500	-1.45868300
H	-1.30335500	1.29618000	6.48609400	C	-0.65485900	-6.54478100	-0.42580200
H	-0.09291500	1.76677200	5.24480600	C	0.61190000	-6.09448500	-0.04773100
H	-2.70194000	-0.14169200	4.89506900	C	1.21816200	-4.95998200	-0.59783000
H	-1.68591300	0.64239300	3.64540600	C	0.46549100	-4.25222600	-1.55059600
H	-1.83319800	-2.35755400	4.27798300	C	-1.39638800	-4.02755100	-3.18040200
H	-2.49013900	-1.53513000	2.82702200	C	-1.70769200	-4.70830600	-4.35553500
H	-0.77995600	-3.61216500	2.63908800	C	-2.36050100	-4.09124100	-5.42407700
H	0.78244100	-2.97631200	2.06365900	C	-2.76350300	-2.75145900	-5.29572000
H	-1.02145800	-3.52619700	0.29782600	C	-2.46454600	-2.04109300	-4.11286900
H	-1.82224800	-2.01880500	0.80972800	C	-1.73291700	-2.66796500	-3.09835900
H	1.25356100	-2.31963400	9.82858500	H	1.14845600	-6.64808800	0.72696400
H	4.01876200	1.16893200	6.24369800	H	-1.42111000	-5.75900600	-4.44349100
H	6.00954400	0.41011100	7.56285100	O	-1.38644500	-1.96735100	-1.95842600
H	-0.81839000	-3.67860100	9.95528700	O	0.92094400	-3.05155400	-2.03913800
H	5.83145700	-1.63376500	8.98323100	C	-2.99444700	-0.65297100	-3.95127700
H	3.71380000	-2.92718200	9.02616200	C	3.69421400	3.71154400	-3.29238100
H	-1.83156300	-4.59327900	7.86276600	C	-3.45855900	2.30790000	1.27464800
H	-0.72082700	-4.14542800	5.66409300	C	-3.96535000	1.16377100	1.88791800
P	0.20080600	-1.61387200	-1.59131000	C	-3.97832900	-0.05132100	1.20127800
Rh	1.40317300	0.19592400	-2.25198800	C	-3.44985600	-0.11104900	-0.08800800
C	-1.09873900	4.80769700	-2.22704900	C	-2.94509700	1.03336300	-0.70437900
C	-1.64408500	6.02807900	-1.76879100	C	4.55398000	3.22208800	-4.28966600
C	-2.70792500	5.98854400	-0.85281000	C	5.80608700	2.70250600	-3.97040000
C	-3.14954500	4.75748800	-0.35822200	C	6.22836100	2.65309700	-2.64198700

C	5.38913600	3.14188100	-1.64159200	C	-3.39773800	-7.23566900	-0.85949000
C	4.13840000	3.66810300	-1.96011400	H	-3.33383600	-5.49630300	-2.16748100
C	3.52858100	-5.68555300	-0.04066200	H	-3.68899500	-6.62036500	0.00954600
C	4.86037700	-5.45144200	0.29022200	C	-1.25103700	-7.73112800	0.30631700
C	5.32806800	-4.14477900	0.42437700	C	-2.45500900	-8.34129400	-0.40173100
C	4.44629500	-3.08256900	0.23422100	H	-1.55922500	-7.39500700	1.31200000
C	3.10812500	-3.31666100	-0.08387200	H	-2.96397800	-9.04810400	0.26902700
C	-4.30858400	-0.45963900	-3.50316000	H	-3.45049700	3.24828100	1.82830700
C	-4.85220900	0.82218400	-3.43850500	H	-4.36564600	1.22934400	2.90194900
C	-4.08752700	1.92777700	-3.81669500	H	-4.40982400	-0.94212500	1.66324600
C	-2.78065400	1.74128700	-4.26363200	H	-3.43702700	-1.05010500	-0.64536900
C	-2.24045300	0.45697000	-4.33827800	H	-2.55584200	0.95689200	-1.71848300
C	-2.97042500	2.27402700	-0.04355600	H	4.22033200	3.21027000	-5.32734700
C	2.62448000	-4.62617100	-0.23262200	H	6.45067900	2.32318700	-4.76534000
C	-3.36603000	7.25273200	-0.33526000	H	7.20695600	2.24144300	-2.38930100
C	-2.98702000	8.49733800	-1.12888000	H	5.71281300	3.12120000	-0.59920500
H	-3.06624700	7.39345300	0.71773400	H	3.50433300	4.06099300	-1.16755300
H	-3.33236100	9.39807300	-0.60120400	H	3.18691100	-6.71182400	-0.18471200
C	-1.05013200	7.35064300	-2.21590200	H	5.54053500	-6.29437700	0.42242000
C	-1.47824400	8.52436400	-1.33965400	H	4.80221500	-2.05553100	0.32722800
H	0.04625900	7.25672600	-2.23117500	H	2.43120600	-2.47313900	-0.20618800
H	-0.97441300	8.46435200	-0.35993100	H	6.37564500	-3.95504600	0.66389700
C	-1.51432500	5.68096900	-5.07448700	H	-4.90936600	-1.32520300	-3.21325000
C	-1.45875800	6.67720800	-6.22664400	H	-5.87520300	0.95953600	-3.08385000
H	-1.96686300	4.74270100	-5.44712000	H	-4.50766600	2.93361200	-3.75499700
H	-2.46506400	6.81418800	-6.64815300	H	-2.16460800	2.59904700	-4.54344300
C	0.92416500	6.08456900	-6.72022500	H	-1.22927800	0.30848100	-4.71789600
C	-0.48628400	6.18287700	-7.29153200	H	-4.45736300	7.10952000	-0.32407100
H	1.58666500	5.54599500	-7.41397800	H	-3.49114300	8.48635200	-2.11044900
H	-0.81487700	5.19042500	-7.64372400	H	-1.34238600	7.56262900	-3.25777600
C	-3.53434000	-2.06140600	-6.40439400	H	-1.15744900	9.46636000	-1.80681100
C	-3.44700400	-2.78583500	-7.74372900	H	-2.18512400	6.02638000	-4.27922500
H	-3.18116700	-1.02488000	-6.50283000	H	-1.12796600	7.66238600	-5.85359600
H	-2.44156000	-2.64240200	-8.17607300	H	1.34504000	7.10061300	-6.62290600
C	-2.61143100	-4.88216900	-6.69086900	H	-0.48746800	6.84667300	-8.16801600
C	-3.70389800	-4.27724600	-7.56468400	H	-4.59182300	-1.98295500	-6.09581700
H	-1.67109400	-4.91972400	-7.26831900	H	-4.16406000	-2.34216800	-8.44937800
H	-3.73658300	-4.79334000	-8.53510100	H	-2.84762700	-5.92406700	-6.42646700
C	-2.70967400	-6.36272500	-1.90424400	H	-4.68855400	-4.42281500	-7.08853400

H	-2.60436000	-6.94620000	-2.83413100	C	3.08171600	-0.52945800	2.00164100
H	-4.32328800	-7.65296900	-1.28117300	C	3.11181300	-2.68993100	3.02121300
H	-0.46615300	-8.48554800	0.46692600	C	2.83723600	-3.30935800	4.37343800
H	-2.12227000	-8.91747300	-1.28128900	C	1.29714000	-3.00435300	6.17255900
C	2.96351300	0.09502400	-1.06685700	C	3.37764000	-0.59431500	6.37473600
O	3.89417700	0.12273900	-0.40883700	C	1.37671100	0.59973500	6.75679100
H	0.25115100	0.46997400	-3.26500300	C	0.17561400	1.06549700	5.97337700
Li	1.04361800	-0.86567300	4.38290700	C	-1.44483800	0.13322200	4.48555900
C	-0.65681800	1.81269500	-6.97335600	C	-1.63681100	-1.12458900	3.67805100
C	-0.61006200	0.73721700	-7.86022500	C	-0.48956700	-2.57973900	2.21714800
C	0.44812100	-0.17056800	-7.78907600	C	-1.03153000	-2.32449100	0.83020900
C	1.45846600	-0.00669000	-6.84358400	C	2.07750500	-2.57926700	7.26293400
C	1.39098900	1.06474100	-5.94900700	C	1.64977800	-2.93546100	8.54976000
C	0.33661200	1.97598900	-6.00747200	C	4.57410100	0.09690600	6.19772300
O	2.39732300	1.32475700	-5.05890200	C	5.75481800	-0.40263400	6.74171500
C	2.82012200	0.40813900	-4.14005400	C	0.47867400	-3.66061000	8.75362800
C	2.39788700	-0.89762700	-4.00040700	C	5.73133800	-1.58631700	7.47863600
H	-1.48539800	2.52182200	-7.02258200	C	4.53139900	-2.27178200	7.65241500
H	-1.39210300	0.60935000	-8.61016200	C	3.33514900	-1.79931800	7.09407700
H	0.50028100	-1.00638400	-8.48891400	C	-0.29033200	-4.05568000	7.65986600
H	2.30555900	-0.69241700	-6.80658900	C	0.12672500	-3.73406500	6.37086000
H	0.31828500	2.79885900	-5.28936600	H	-0.78779900	0.63324600	1.59766200
H	3.76442900	0.74468200	-3.70754900	H	0.73230600	0.62956200	0.69364900
H	1.62135900	-1.32395300	-4.63488800	H	0.05394400	2.39516300	3.10532700
H	3.05796600	-1.60150300	-3.49456200	H	1.32841900	2.82409900	1.95473000
				H	2.97161300	1.55787600	1.52471000
				H	3.66123700	1.19595500	3.13125100
				H	4.10004200	-0.66166700	1.59789300
				H	2.35253500	-0.83673600	1.22688100
				H	4.14985300	-2.90565400	2.71486200
				H	2.44886600	-3.10035000	2.24158900
				H	3.67685200	-3.11612100	5.05626900
				H	2.69840000	-4.39839700	4.28004900
				H	1.89851200	1.45495800	7.21519000
				H	1.07056000	-0.10161900	7.55052500
				H	-0.59735500	1.45035700	6.65996500
				H	0.45954900	1.86461800	5.26595600
				H	-2.32746600	0.30805700	5.12467400
				H	-1.32435000	1.00849500	3.82500100

**S2**



H	-1.90322800	-1.96449300	4.34464000	C	-1.49419000	-3.74586400	-3.11034300
H	-2.45635200	-0.97595900	2.95446600	C	-1.80264300	-4.44244200	-4.27539800
H	-1.11638400	-3.34171000	2.71348100	C	-2.51224000	-3.85780200	-5.32506000
H	0.52646900	-2.98449000	2.13018000	C	-2.96174000	-2.53340300	-5.19067200
H	-1.22975500	-3.29261800	0.34703500	C	-2.65958400	-1.80214800	-4.01823200
H	-1.97502000	-1.75603100	0.86317300	C	-1.88954200	-2.40351600	-3.01427400
H	2.24879400	-2.61432400	9.40468600	H	1.22387300	-6.22110700	0.76623800
H	4.55703500	1.03166400	5.63547500	H	-1.47481400	-5.48067600	-4.36715500
H	6.69164200	0.13706000	6.59637100	O	-1.55793000	-1.70804900	-1.86569100
H	0.16670100	-3.91396800	9.76749600	O	0.79784700	-2.67599800	-2.05541800
H	6.65012500	-1.98170500	7.91351300	C	-3.26683900	-0.44249100	-3.86115600
H	4.51411700	-3.21034100	8.21035600	C	3.29735800	4.17795000	-1.84368600
H	-1.21044800	-4.62240700	7.80915300	C	-4.15828600	2.73496700	1.21271100
H	-0.43987400	-4.04859000	5.49306500	C	-4.53390800	1.59779200	1.92649300
P	0.01813300	-1.31245800	-1.50241700	C	-4.37769300	0.33171200	1.36075900
Rh	0.83838200	0.61648200	-2.30207200	C	-3.83160600	0.22041900	0.08076100
C	-1.58068800	5.14279300	-2.14135100	C	-3.45342400	1.35708400	-0.63060700
C	-2.23478800	6.35725600	-1.83766200	C	4.37625000	3.53585100	-2.46350200
C	-3.43470100	6.31204300	-1.10468300	C	5.48268800	3.11546300	-1.72729400
C	-3.89602200	5.09246200	-0.59781700	C	5.52920600	3.32534000	-0.35060900
C	-3.21911400	3.88643900	-0.79445100	C	4.46214600	3.96781800	0.28075400
C	-2.08753800	3.94781500	-1.62213300	C	3.35767600	4.38989300	-0.45586500
C	-0.26578600	5.10688700	-2.86177300	C	3.54204300	-5.24089000	0.08573900
C	-0.07584600	5.57266100	-4.17934400	C	4.89123700	-4.99926300	0.32957600
C	1.22871600	5.62554200	-4.70530500	C	5.42306000	-3.72514800	0.13610500
C	2.31175200	5.21289000	-3.92268500	C	4.58039200	-2.70180000	-0.29065500
C	2.14726000	4.66536800	-2.65038400	C	3.22409900	-2.93863300	-0.51463700
C	0.83569900	4.58670200	-2.16556100	C	-4.57291100	-0.33810700	-3.36295600
H	-4.81375000	5.09194000	-0.00399400	C	-5.22484300	0.89354100	-3.32771900
H	3.32000900	5.30003800	-4.33689700	C	-4.57771500	2.04241600	-3.78339000
O	0.60323800	3.91072400	-0.98735300	C	-3.27775100	1.94990000	-4.27863100
O	-1.41205500	2.79275000	-1.92677000	C	-2.63140200	0.71455000	-4.32611200
P	-0.01777000	2.37831500	-1.17539500	C	-3.62007500	2.63993900	-0.08121800
C	-0.79014500	-4.43010800	-1.98932300	C	2.67049200	-4.21895300	-0.33815400
C	-1.32921900	-5.57870100	-1.37594500	C	-4.22224600	7.56716000	-0.77941800
C	-0.59579200	-6.19064100	-0.34355200	C	-3.73792100	8.79829200	-1.53555500
C	0.66807200	-5.69744500	-0.01434300	H	-4.14477600	7.75546700	0.30522300
C	1.24482200	-4.57118200	-0.61837000	H	-4.19756300	9.70278400	-1.11193000
C	0.42847700	-3.90099800	-1.54782800	C	-1.61445000	7.68552200	-2.22715400

C	-2.21718300	8.86734100	-1.47419500	H	4.97800000	-1.70007100	-0.46243500
H	-0.52785600	7.63095300	-2.06153000	H	2.60271400	-2.11107300	-0.84166900
H	-1.89477800	8.84532500	-0.41924000	H	6.48466500	-3.53572600	0.30260900
C	-1.26451800	5.88075400	-5.06760300	H	-5.08528600	-1.23822900	-3.01475600
C	-0.91383600	6.78828300	-6.24046800	H	-6.24071400	0.95806600	-2.93412700
H	-1.62652100	4.91679500	-5.46989000	H	-5.08349200	3.00885600	-3.74876700
H	-1.78443500	6.89149500	-6.90431800	H	-2.76035600	2.84454700	-4.62969700
C	1.50985100	6.15723200	-6.09705400	H	-1.62966300	0.64235300	-4.75277400
C	0.27907900	6.21189800	-6.99607700	H	-5.28859500	7.37967500	-0.97898100
H	2.29823800	5.54152100	-6.55912500	H	-4.05449700	8.74087000	-2.59102100
H	0.02725700	5.19288000	-7.33636300	H	-1.74096800	7.85979100	-3.30861100
C	-3.80805800	-1.89235300	-6.27441000	H	-1.84198500	9.80697400	-1.90413100
C	-3.75851100	-2.63163400	-7.60806600	H	-2.10101500	6.28142300	-4.48251300
H	-3.50672900	-0.84381100	-6.40672000	H	-0.66717000	7.79923500	-5.87193800
H	-2.78575600	-2.45112700	-8.09668600	H	1.93151200	7.17261400	-5.99556200
C	-2.77838000	-4.67106300	-6.57416400	H	0.50264900	6.80177700	-7.89699900
C	-3.93849900	-4.12992000	-7.40048300	H	-4.85129000	-1.85016200	-5.91484500
H	-1.86424800	-4.66751600	-7.19311400	H	-4.53055900	-2.22815500	-8.27877900
H	-3.99307600	-4.65911700	-8.36275700	H	-2.94996900	-5.72045700	-6.29111800
C	-2.68886700	-6.11349400	-1.78070100	H	-4.89121300	-4.31490000	-6.87568600
C	-3.32484000	-6.98595200	-0.70303800	H	-2.58161300	-6.71344100	-2.70007900
H	-3.34761500	-5.27477100	-2.04884800	H	-4.24027400	-7.44815400	-1.09860400
H	-3.62601300	-6.36121300	0.15586300	H	-0.33077200	-8.09456300	0.61062800
C	-1.14151000	-7.37124100	0.43687400	H	-1.99289700	-8.62849000	-1.10552000
C	-2.33320900	-8.04310200	-0.23499000	C	2.74531200	0.52369000	-1.69329200
H	-1.44847000	-7.01256800	1.43520100	O	3.79664400	0.41936000	-1.27851700
H	-2.80368300	-8.75132100	0.46178800	H	-0.63997500	0.67915800	-2.73156200
H	-4.26992600	3.71640600	1.67736800	Li	1.23984300	-0.79821700	4.17056000
H	-4.95768400	1.70577800	2.92704100	C	1.98841100	3.04973700	-8.09272400
H	-4.69314600	-0.55967800	1.90761700	C	3.28259200	3.46972900	-8.38497900
H	-3.70488500	-0.75655900	-0.39222700	C	4.26872900	3.35528900	-7.40185400
H	-3.03718400	1.23830100	-1.62894400	C	3.96082300	2.84262700	-6.14670900
H	4.32536300	3.34844700	-3.53419900	C	2.65035100	2.44428800	-5.84724300
H	6.30772300	2.61063100	-2.23315500	C	1.66225700	2.53623400	-6.83507500
H	6.39608900	3.00042400	0.22767100	O	2.42655500	1.97906300	-4.58509000
H	4.49593900	4.15753100	1.35581100	C	1.19056200	1.38251800	-4.34343800
H	2.53833400	4.90759400	0.04336800	C	1.11638100	-0.01299000	-4.39453000
H	3.17264200	-6.26144600	0.18608700	H	1.20869500	3.11517600	-8.85420600
H	5.53469700	-5.82254100	0.64440500	H	3.52690000	3.86778200	-9.37036900

H	5.29552300	3.65622900	-7.61765600	C	-0.88910600	-4.14837900	7.81411500
H	4.73782400	2.71569200	-5.39290900	C	-0.25364500	-3.84243300	6.61374200
H	0.64480400	2.20011400	-6.64331000	H	-0.41803400	0.39366400	1.56484800
H	0.33395600	2.02353300	-4.57225400	H	1.23939100	0.53467300	0.97229600
H	2.04229100	-0.56573900	-4.56929900	H	-0.05495800	2.18032500	3.21290900
H	0.19688800	-0.52353800	-4.68449200	H	1.40374700	2.72615400	2.37113700

**S3**

O	-0.24467800	-1.54147700	3.07492600	H	3.17274300	1.51926000	2.24624300
O	0.48095200	-1.62921400	0.14847500	H	3.55053100	1.22181800	3.96613200
O	-0.04969800	2.06503900	0.42189400	H	4.38830500	-0.62743800	2.58572000
O	1.57349600	0.97353600	3.46943800	H	2.75540300	-0.90991800	1.89575700
O	2.94832400	-1.31781300	3.91347100	H	4.33593000	-2.85754100	3.74594000
O	1.45741300	-2.76218300	5.38436200	H	2.77007700	-3.14802200	2.95802700
O	1.71796700	-0.05422100	6.36226100	H	3.43299300	-3.06539700	5.95639500
O	-0.63527400	-0.23926200	5.33743000	H	2.68769200	-4.40627200	5.03489200
C	0.39008000	1.11310700	1.36936300	H	1.02564500	1.43434600	7.64373600
C	0.81490900	1.83213200	2.63792000	H	0.26536800	-0.18026600	7.84024500
C	2.94439400	0.87807900	3.11242900	H	-1.32084600	1.23659900	6.63637300
C	3.30562500	-0.55029600	2.78630800	H	-0.05799100	1.74028600	5.46093400
C	3.24906200	-2.69384600	3.84176100	H	-2.64202500	-0.04618600	4.82903400
C	2.75089500	-3.31049200	5.12987700	H	-1.48203600	0.75620700	3.73182500
C	0.89478700	-3.05243100	6.60656200	H	-1.85210000	-2.26561400	4.15124600
C	2.77258800	-0.51541300	7.11630700	H	-2.28611300	-1.31508200	2.69490200
C	0.66043100	0.54322900	7.10891100	H	-0.64320400	-3.52163900	2.63541500
C	-0.40525900	0.91718000	6.11063900	H	0.98464400	-2.92217500	2.22331200
C	-1.64595600	-0.13506000	4.36205700	H	-0.66779800	-3.37633800	0.29708000
C	-1.57496200	-1.39115800	3.53461600	H	-1.47455300	-1.86399200	0.76586300
C	-0.08223300	-2.66263400	2.22635600	H	1.19953100	-2.51148900	9.94169700
C	-0.51971500	-2.41169400	0.79969500	H	3.97809100	1.16171000	6.55994500
C	1.43605600	-2.55511700	7.80614100	H	5.95088800	0.40167500	7.90679800
C	0.79041900	-2.89377200	9.00384300	H	-0.84956800	-3.91194800	9.96156400
C	3.94479300	0.23732000	7.13815200	H	5.78124600	-1.69445800	9.25057800
C	5.03291200	-0.18757000	7.89593700	H	3.69365300	-3.03508100	9.19047900
C	-0.36201900	-3.67574300	9.01502700	H	-1.79044900	-4.76295500	7.81103500
C	4.93731900	-1.35855600	8.64678700	H	-0.63030700	-4.21454600	5.65988700
C	3.76209900	-2.10616100	8.62048200	P	0.77527300	-1.50583500	-1.45257600
C	2.66274500	-1.70987200	7.84537600	Rh	1.67887700	0.43961700	-2.04565800
				C	-1.05738400	4.87818900	-1.96909300
				C	-1.78917100	6.02415500	-1.58453600
				C	-3.02663700	5.84665700	-0.94193700

C	-3.45883100	4.55850900	-0.61055100	C	6.19486100	3.23309400	-0.36729900
C	-2.70774900	3.41194000	-0.88024400	C	5.09707200	3.70018200	0.35582100
C	-1.52058600	3.61284700	-1.60156900	C	3.95816000	4.15761300	-0.30341600
C	0.27457900	4.98927100	-2.64547900	C	4.03593900	-5.32000700	0.80392000
C	0.44433100	5.61722000	-3.89635800	C	5.32720100	-5.03151400	1.23661200
C	1.74835800	5.84087800	-4.37582400	C	5.81267400	-3.72596500	1.17250300
C	2.84380600	5.40692900	-3.62448700	C	4.98342400	-2.71839800	0.68478300
C	2.70601800	4.68815700	-2.43455400	C	3.68257300	-3.00378000	0.27037000
C	1.39614700	4.46720000	-1.98054200	C	-3.50492600	-0.64156800	-3.98352700
H	-4.42120100	4.45194700	-0.10386800	C	-4.09675300	0.61811500	-4.06370600
H	3.84909100	5.62628400	-3.99289300	C	-3.32572700	1.73291400	-4.39600200
O	1.18618400	3.69952500	-0.85971000	C	-1.96608500	1.57550000	-4.66173600
O	-0.74142800	2.53352800	-1.94269000	C	-1.37570200	0.31212800	-4.59742500
P	0.58902700	2.15322100	-1.06991100	C	-3.12189800	2.07961500	-0.35660300
C	0.00853600	-4.67802100	-1.81314400	C	3.18086800	-4.31521200	0.31348900
C	-0.61147600	-5.78835900	-1.20069700	C	-3.89650200	7.02304700	-0.54151400
C	-0.03350800	-6.32755600	-0.03721500	C	-3.43994400	8.34375300	-1.14921700
C	1.17440100	-5.80697700	0.43170800	H	-3.88227900	7.10949800	0.55872100
C	1.82146200	-4.71342300	-0.15669600	H	-3.97510700	9.17917500	-0.67543800
C	1.15334300	-4.11055800	-1.23754600	C	-1.21502700	7.41267200	-1.79581900
C	-0.54537000	-4.07132100	-3.05667300	C	-1.93238400	8.48494600	-0.98133700
C	-0.73596200	-4.84665500	-4.19798300	H	-0.14217800	7.39223100	-1.55104000
C	-1.30972100	-4.33235400	-5.36131900	H	-1.67535900	8.38133800	0.08657300
C	-1.73692400	-2.99483800	-5.37797200	C	-0.75265000	5.93318300	-4.77271700
C	-1.55952100	-2.18652400	-4.23420700	C	-0.46116500	6.98882500	-5.83323100
C	-0.92557700	-2.72201200	-3.10754400	H	-1.03370500	4.99413700	-5.28238900
H	1.62512500	-6.27157900	1.31202900	H	-1.32266300	7.08188500	-6.51001400
H	-0.42014500	-5.89265200	-4.18119400	C	2.00176800	6.59244500	-5.66833500
O	-0.73609600	-1.94296700	-1.97914800	C	0.79891800	6.61358200	-6.60472600
O	1.60950300	-2.92141600	-1.75548700	H	2.88123900	6.16333500	-6.17071000
C	-2.13707400	-0.80639200	-4.23979400	H	0.65999400	5.61697100	-7.05687400
C	3.89767200	4.17124900	-1.70695300	C	-2.41097000	-2.40785900	-6.60276100
C	-3.80323400	2.01194200	0.87071100	C	-2.23112800	-3.24920500	-7.86166000
C	-4.23379200	0.79392000	1.39343800	H	-2.04098100	-1.38493400	-6.76443700
C	-3.98439800	-0.39183800	0.70105900	H	-1.19978000	-3.13590700	-8.23628600
C	-3.28522300	-0.34304800	-0.50556700	C	-1.45492400	-5.23010900	-6.57117200
C	-2.85113100	0.87472200	-1.02772500	C	-2.49093900	-4.72133300	-7.56633900
C	5.01618200	3.71265100	-2.42098000	H	-0.47287900	-5.29195600	-7.07251900
C	6.14995900	3.24284400	-1.75981100	H	-2.45556700	-5.32177800	-8.48677600

C	-1.90346000	-6.36096100	-1.75091700	H	-3.50420100	-4.83724900	-7.14507100
C	-2.69297000	-7.15352700	-0.71424500	H	-1.67057200	-7.02752800	-2.59813600
H	-2.51430000	-5.55019000	-2.17246600	H	-3.54468700	-7.64839800	-1.20246300
H	-3.11162000	-6.46734500	0.04241800	H	0.07660200	-8.15021300	1.09200300
C	-0.69438800	-7.44512700	0.74656500	H	-1.33374600	-8.82226300	-0.79531900
C	-1.78705100	-8.16987200	-0.03021300	C	3.34014600	0.42320200	-0.94501400
H	-1.13520800	-7.00715600	1.65986100	O	4.23302600	0.40821700	-0.24001000
H	-2.35848500	-8.82104500	0.64661300	H	0.36391500	0.45400400	-2.85102900
H	-3.99284100	2.92915700	1.43104300	Li	1.12027800	-0.85165800	4.56554500
H	-4.77407300	0.77477800	2.34239400	C	1.67889800	-3.25432300	-7.20229800
H	-4.33880500	-1.34672800	1.09620600	C	2.23146800	-4.23642500	-6.37483000
H	-3.06821900	-1.25662300	-1.06367300	C	2.67082100	-3.88703100	-5.10109700
H	-2.31237800	0.87863700	-1.97444400	C	2.57984200	-2.56883100	-4.64846900
H	4.99624100	3.71272600	-3.51291100	C	2.03062300	-1.59778300	-5.48602200
H	7.00288300	2.88658900	-2.34000300	C	1.56847400	-1.94008500	-6.76233100
H	7.08341500	2.86980300	0.15164300	O	1.91304300	-0.28499400	-5.13696400
H	5.13066000	3.71856700	1.44710100	C	2.68354900	0.23890000	-4.13298200
H	3.11099900	4.53147300	0.27089300	C	2.52142900	1.57322100	-3.80859400
H	3.69801000	-6.35704000	0.81139100	H	1.33870300	-3.51428000	-8.20681900
H	5.96598900	-5.83876400	1.59881400	H	2.31761100	-5.26624900	-6.72495000
H	5.35069100	-1.69320900	0.61586700	H	3.09237600	-4.64376500	-4.43626200
H	3.05453900	-2.19151800	-0.08388000	H	2.91492800	-2.31307700	-3.64555000
H	6.83277700	-3.49845800	1.48612100	H	1.14776400	-1.15819900	-7.39655800
H	-4.11022900	-1.51312300	-3.72258300	H	3.62904600	-0.28219500	-3.95799700
H	-5.16157700	0.73129400	-3.85284400	H	1.75354900	2.15768300	-4.32012500
H	-3.78375800	2.72245500	-4.44774600	H	3.36580700	2.11181100	-3.38733200
H	-1.35412400	2.44135300	-4.92084600				
H	-0.31928000	0.18423900	-4.84049700				
H	-4.94030600	6.80422700	-0.81496900				
H	-3.68828800	8.36951400	-2.22408300				
H	-1.26959200	7.68706100	-2.86236900				
H	-1.58667700	9.47902100	-1.29917600				
H	-1.62687500	6.20351800	-4.16902200				
H	-0.31940600	7.97322400	-5.35378200				
H	2.27337600	7.63123700	-5.41100300				
H	0.98172500	7.31706700	-7.42965300				
H	-3.48772300	-2.29407800	-6.38675800				
H	-2.90100900	-2.87756700	-8.65025000				
H	-1.69367400	-6.25152300	-6.23790200				
				<b>S4</b>			
				O	-0.32440200	-1.37672500	3.07012800
				O	0.26879300	-1.52897200	0.12879000
				O	-0.29092900	2.25419700	0.37596100
				O	1.51703500	1.11177000	3.28173300
				O	2.90916600	-1.17786900	3.63570700
				O	1.57241600	-2.57533900	5.28760400
				O	1.87042800	0.12946700	6.21046700
				O	-0.54863900	-0.04841800	5.33955400
				C	0.10065600	1.28184800	1.32389000
				C	0.68268900	1.98300700	2.54259500

C	2.82617600	0.98407000	2.74596700	H	-1.50877700	0.94373400	3.79631400
C	3.12743900	-0.46201700	2.44035200	H	-1.86647200	-2.07428300	4.25299100
C	3.22429900	-2.55121200	3.59563100	H	-2.38345000	-1.12760200	2.82229200
C	2.85143600	-3.11413300	4.94852600	H	-0.79527900	-3.35300800	2.68747600
C	1.09846200	-2.86990600	6.54642300	H	0.82708900	-2.80762100	2.19356300
C	2.97520100	-0.30888200	6.90376700	H	-0.90550800	-3.24947600	0.34703800
C	0.86541000	0.74339700	7.01412300	H	-1.66724500	-1.71159900	0.82370500
C	-0.25542100	1.11639300	6.07868500	H	1.60987700	-2.30020100	9.85119500
C	-1.62629300	0.05434700	4.43874500	H	4.13038700	1.37058600	6.25018000
C	-1.61972100	-1.20641700	3.61451400	H	6.18279100	0.65435400	7.49628700
C	-0.23051000	-2.51728500	2.23778400	H	-0.39161600	-3.75639000	10.01467100
C	-0.72308900	-2.27934900	0.82793000	H	6.11444300	-1.41850400	8.88210700
C	1.70639700	-2.35245400	7.70456000	H	4.04263300	-2.78332100	8.96280500
C	1.15020500	-2.69891400	8.94419900	H	-1.44680700	-4.65213800	7.93480700
C	4.13809500	0.45578800	6.84435800	H	-0.45032700	-4.08329800	5.70955100
C	5.27231800	0.05557400	7.54629100	P	0.47882600	-1.36423100	-1.47998500
C	0.02373500	-3.51243300	9.03619700	Rh	1.40095000	0.56766600	-2.09268200
C	5.23368800	-1.10290700	8.32139800	C	-1.26229100	5.05273300	-2.05425400
C	4.06806900	-1.86358600	8.37459800	C	-1.97034600	6.21913100	-1.68669000
C	2.92139700	-1.49161400	7.65841200	C	-3.19961200	6.07710600	-1.01961900
C	-0.56702400	-4.00983900	7.87575500	C	-3.63883400	4.80587900	-0.63556400
C	-0.02328900	-3.69236800	6.63415300	C	-2.90853800	3.64199900	-0.88712800
H	-0.77492200	0.66424800	1.57766700	C	-1.74122700	3.80445500	-1.64971800
H	0.85668600	0.60369400	0.89952700	C	0.06848200	5.12374600	-2.73966800
H	-0.10335300	2.35600200	3.21409200	C	0.25021400	5.72594100	-4.00153000
H	1.25572000	2.86267800	2.20371000	C	1.55773300	5.91453300	-4.48697700
H	2.93518300	1.57985400	1.82511200	C	2.64598900	5.46752500	-3.73239000
H	3.54740200	1.36607700	3.48676700	C	2.49391900	4.77248400	-2.53046300
H	4.17406000	-0.56646500	2.10716100	C	1.18139200	4.58970800	-2.06885000
H	2.46133500	-0.84676600	1.64304700	H	-4.58766400	4.72871300	-0.09883300
H	4.30146400	-2.70588000	3.41232500	H	3.65542800	5.65336000	-4.10817900
H	2.67769300	-3.05202900	2.77819800	O	0.96275500	3.84379500	-0.93519700
H	3.59650100	-2.81486800	5.69976100	O	-0.99194200	2.70424200	-1.99050100
H	2.80297700	-4.21402200	4.91170000	P	0.33710800	2.30665700	-1.12139400
H	1.26963200	1.63637700	7.51663900	C	-0.39394600	-4.51488500	-1.80468400
H	0.50828400	0.03016900	7.77473300	C	-0.98850900	-5.61386200	-1.15060400
H	-1.13266500	1.45633900	6.65448800	C	-0.32592600	-6.17442400	-0.04352500
H	0.06277200	1.92404100	5.39569300	C	0.92617200	-5.67984600	0.33016900
H	-2.58610000	0.14479100	4.97615600	C	1.54644600	-4.59342700	-0.29974800

C	0.80364900	-3.97485500	-1.32074200	C	-1.37787100	7.59317700	-1.93797800
C	-1.01222000	-3.89505700	-3.00981200	C	-2.06923000	8.69611100	-1.14207100
C	-1.29360800	-4.67551800	-4.12930900	H	-0.30305200	7.56156300	-1.70354900
C	-1.91695900	-4.15679300	-5.26468800	H	-1.80103900	8.61507200	-0.07496800
C	-2.30077900	-2.80583400	-5.27259200	C	-0.94132600	6.05030600	-4.88226100
C	-2.02771600	-1.99120800	-4.15071000	C	-0.63257000	7.08753200	-5.95569000
C	-1.34961500	-2.53248400	-3.05055300	H	-1.23683200	5.10996100	-5.38146600
H	1.43671900	-6.16249800	1.16713100	H	-1.49317600	7.18867200	-6.63249500
H	-1.01237200	-5.73133400	-4.11560700	C	1.82300300	6.64422900	-5.78975900
O	-1.07505600	-1.74586500	-1.94689400	C	0.61895600	6.67941900	-6.72439500
O	1.23566100	-2.79580100	-1.87855500	H	2.69244200	6.19151200	-6.28888600
C	-2.56706900	-0.59573500	-4.13995600	H	0.45994900	5.68111700	-7.16616000
C	3.66996600	4.22744900	-1.79801300	C	-3.03097800	-2.21290400	-6.46224700
C	-3.94259300	2.32207800	0.96112200	C	-2.95299400	-3.07507000	-7.71846100
C	-4.34845900	1.12858600	1.55589400	H	-2.64334500	-1.20358100	-6.66225200
C	-4.12589200	-0.08715800	0.90775100	H	-1.94386200	-3.00098300	-8.15840800
C	-3.47793700	-0.09176300	-0.32797100	C	-2.17060200	-5.06767100	-6.44838800
C	-3.06788800	1.10113300	-0.92092800	C	-3.24577100	-4.53314200	-7.38699900
C	4.75874100	3.69426600	-2.50452800	H	-1.22764400	-5.18431900	-7.01028100
C	5.87486500	3.19445300	-1.83534400	H	-3.28645400	-5.14634700	-8.29857000
C	5.93004100	3.22679200	-0.44386800	C	-2.33673200	-6.14854800	-1.59341800
C	4.86058100	3.76636000	0.27190100	C	-3.04906500	-6.93752400	-0.49924500
C	3.74022500	4.25653100	-0.39493500	H	-2.96149200	-5.31676700	-1.94992100
C	3.82306900	-5.24541400	0.46285500	H	-3.38080800	-6.25456100	0.30215600
C	5.15511700	-4.98451300	0.77516200	C	-0.93580100	-7.29670800	0.77450300
C	5.65847400	-3.68868100	0.66999000	C	-2.10756900	-7.98408200	0.08370200
C	4.80945800	-2.66282000	0.25950500	H	-1.28282900	-6.87424600	1.73409800
C	3.47181000	-2.92081500	-0.03685400	H	-2.62980600	-8.63841900	0.79609000
C	-3.91413700	-0.39496300	-3.80934700	H	-4.10836300	3.26342100	1.48814000
C	-4.47922700	0.87775800	-3.86875700	H	-4.84900300	1.15273200	2.52615300
C	-3.70187200	1.97063200	-4.25433600	H	-4.46524500	-1.02305600	1.35754000
C	-2.36416000	1.77866500	-4.59682700	H	-3.28676200	-1.02899000	-0.85524300
C	-1.80346500	0.50154700	-4.55239800	H	-2.56929500	1.06140000	-1.88796400
C	-3.31138600	2.33519700	-0.29427500	H	4.73051000	3.65745900	-3.59568400
C	2.94854400	-4.22177400	0.05435800	H	6.70386000	2.77658600	-2.40904700
C	-4.04874300	7.27588000	-0.64144700	H	6.80409000	2.83659600	0.08021700
C	-3.58050600	8.57342300	-1.28869700	H	4.90240200	3.81549700	1.36202200
H	-4.02235300	7.39097500	0.45583200	H	2.91559600	4.68943800	0.17099500
H	-4.09775600	9.42868800	-0.83070100	H	3.46506100	-6.27515900	0.50109300

H	5.80685400	-5.80604000	1.07739100
H	5.19230300	-1.64690200	0.14820900
H	2.84031700	-2.09516600	-0.35086600
H	6.70756300	-3.48259400	0.88915100
H	-4.52395300	-1.24975300	-3.50743400
H	-5.52743900	1.01872400	-3.59988700
H	-4.13757100	2.97093200	-4.28797100
H	-1.74837100	2.62807500	-4.89727500
H	-0.76695200	0.34747600	-4.85701200
H	-5.09817400	7.06456100	-0.89893500
H	-3.84133800	8.57517900	-2.36093800
H	-1.43999900	7.84275200	-3.01006000
H	-1.71236200	9.67658800	-1.48850700
H	-1.81163800	6.34071200	-4.28216400
H	-0.47190800	8.07461400	-5.48792200
H	2.11618300	7.68027500	-5.54546800
H	0.81453300	7.37023100	-7.55711300
H	-4.08866200	-2.06558400	-6.18254400
H	-3.65664400	-2.68978700	-8.47007800
H	-2.43133400	-6.07116600	-6.07956900
H	-4.23489400	-4.60720000	-6.90373000
H	-2.19665000	-6.81003300	-2.46461400
H	-3.95296900	-7.40519900	-0.91462300
H	-0.15018900	-8.02320200	1.03074200
H	-1.73699800	-8.62908300	-0.73056300
C	3.11779600	0.56456200	-1.06323400
O	4.07651100	0.54189900	-0.45537200
H	0.08439100	0.55426300	-2.89625000
Li	1.14679000	-0.70179100	4.47072100
C	4.17303800	-3.56427900	-3.36613000
C	5.53195300	-3.67753200	-3.09001200
C	6.32042800	-2.52293500	-3.05573000
C	5.75554500	-1.27644600	-3.29752200
C	4.38831500	-1.17578000	-3.58516900
C	3.59167700	-2.31940000	-3.61805400
O	3.92209200	0.08225500	-3.81639800
C	2.58654300	0.31934800	-4.04018100
C	2.16105400	1.63220000	-3.93211500
H	3.53973600	-4.45387500	-3.38342300

H	5.97599000	-4.65440200	-2.89319300
H	7.38732900	-2.59446900	-2.83601500
H	6.35109900	-0.36267200	-3.27428300
H	2.52361900	-2.25559100	-3.80825800
H	2.06918200	-0.41231500	-4.66625100
H	2.89117700	2.39411000	-3.66658700
H	1.27403900	1.96099900	-4.47326300

**S2-BArF**

O	-1.70968300	-1.19553700	3.05718500
O	-1.53519100	-1.65841700	0.19963900
O	-1.93700800	1.32752100	0.99498400
O	-0.40346500	1.98521800	3.73061700
O	1.19545100	0.35456000	5.10801800
O	-0.19544500	-1.63968200	5.75342900
O	-0.89324500	1.01858000	7.07539100
O	-2.65635300	0.30384600	5.10103000
C	-0.56306400	1.20176800	1.42205300
C	-0.12691800	2.32028500	2.35016500
C	0.53001700	2.56241600	4.65146200
C	1.73833400	1.64297300	4.84157800
C	2.00187600	-0.57850200	5.81309600
C	1.22618500	-1.90562900	5.80724600
C	-1.04110000	-2.15764700	6.71564100
C	-0.02450000	0.60834000	8.06048100
C	-2.30254300	1.04897300	7.32720600
C	-2.95852700	1.36440200	5.99893100
C	-3.29084800	0.42954200	3.81969500
C	-3.10720700	-0.87471400	3.08034400
C	-1.40502400	-2.45953200	2.45619400
C	-2.01296700	-2.68940300	1.07870200
C	-0.96046700	-1.75803400	8.07233300
C	-1.86636700	-2.34244300	8.98653600
C	0.91556500	1.55245800	8.51174200
C	1.90689800	1.18590700	9.43415600
C	-2.85075300	-3.24801100	8.56378700
C	1.94677700	-0.12848500	9.92981400
C	1.00021800	-1.06591500	9.48874700



C	0.01051000	-0.72879700	8.53894800	C	-6.23253600	4.53102500	1.05418300
C	-2.94772300	-3.58773900	7.20345900	C	-6.37395400	3.14904900	1.26435300
C	-2.03792700	-3.04746700	6.28391200	C	-5.51463300	2.18213100	0.70001900
H	-0.45789600	0.21334800	1.90057500	C	-4.53896100	2.68833000	-0.19971600
H	0.10462100	1.19949600	0.53800700	C	-3.43156000	4.54372400	-1.53935500
H	-0.64720600	3.26256900	2.07402700	C	-3.81093300	5.34410400	-2.65578000
H	0.96270900	2.47521100	2.21605300	C	-2.80140400	6.01828400	-3.38440400
H	0.85094000	3.57640400	4.32545900	C	-1.45673000	5.89377900	-2.99123700
H	-0.00425900	2.64924000	5.61759400	C	-1.03525400	5.04174800	-1.95206400
H	2.35245400	2.00318700	5.69894000	C	-2.05628800	4.32460300	-1.28426900
H	2.38634500	1.60070500	3.93636400	H	-7.19520000	2.81585700	1.91660200
H	2.18313800	-0.21749700	6.84924100	H	-0.69089700	6.43663300	-3.56593800
H	2.98996100	-0.72560200	5.32056900	O	-1.72882900	3.41880300	-0.28317800
H	1.47711600	-2.51046200	6.70118000	O	-3.67940200	1.80231800	-0.82453600
H	1.46326700	-2.49498100	4.89726300	P	-2.03800800	1.77570700	-0.60144600
H	-2.54766200	1.83548000	8.07688600	C	-2.30485400	-4.72599900	-2.16578300
H	-2.66317900	0.06739300	7.70383300	C	-2.76970300	-5.99139800	-1.70430800
H	-4.06121600	1.45445900	6.14292600	C	-1.96990400	-6.72338600	-0.79499200
H	-2.58085400	2.33314800	5.59392800	C	-0.72591700	-6.20024500	-0.39809800
H	-4.38063900	0.61698800	3.93398600	C	-0.25315500	-4.93658800	-0.80516200
H	-2.84883800	1.27431700	3.24545700	C	-1.10033300	-4.19100400	-1.66023700
H	-3.67445400	-1.69215900	3.58274600	C	-3.06986200	-3.95331300	-3.18357000
H	-3.50052400	-0.74160100	2.05322100	C	-3.37601900	-4.51877700	-4.43194800
H	-1.74970300	-3.29172900	3.11836300	C	-4.14787600	-3.84651200	-5.39321000
H	-0.30220300	-2.50141100	2.38449000	C	-4.65362800	-2.55835400	-5.09060800
H	-1.69907800	-3.69642400	0.73753700	C	-4.34373500	-1.95165500	-3.84092800
H	-3.12205300	-2.66761600	1.10048100	C	-3.52801800	-2.64306700	-2.91599600
H	-1.80744300	-2.04172700	10.04387100	H	-0.07915300	-6.81033100	0.25175300
H	0.85231000	2.57578400	8.11419500	H	-2.99088200	-5.52411900	-4.66233400
H	2.64449000	1.92993400	9.77009500	O	-3.19448600	-2.07683600	-1.68360800
H	-3.55069300	-3.67846900	9.29516000	O	-0.74096400	-2.88836700	-2.01216100
H	2.71809600	-0.42606200	10.65524700	C	-4.95581600	-0.62802400	-3.50985900
H	1.03451900	-2.10185900	9.86008800	C	0.39939900	4.97985300	-1.55939600
H	-3.72520800	-4.28593800	6.85854100	C	-6.35590400	0.36891300	2.23835000
H	-2.07513000	-3.30329200	5.21627000	C	-6.59235800	-0.97311300	2.57004000
P	-1.58965200	-1.55129500	-1.43971700	C	-6.16289000	-2.00234500	1.71385300
Rh	-1.05508200	0.50508700	-2.20881400	C	-5.47267100	-1.66128200	0.54037400
C	-4.43210500	4.05732500	-0.53111300	C	-5.21459300	-0.31857500	0.22166500
C	-5.22849300	5.00479900	0.17626200	C	1.16773200	6.16844400	-1.53456100

C	2.53673600	6.13764800	-1.22488200	H	-5.72439500	-4.37054600	-8.47114100
C	3.17258500	4.91896100	-0.92709500	C	-4.11651000	-6.53705800	-2.15707600
C	2.42021800	3.73198000	-0.94186000	C	-4.67934200	-7.61089100	-1.21665900
C	1.05367800	3.76649000	-1.25019000	H	-4.83316500	-5.69954800	-2.28338400
C	1.49877500	-4.72472600	0.98056500	H	-4.99035500	-7.14501300	-0.25423600
C	2.82482500	-4.49237900	1.37258300	C	-2.42125300	-8.05559300	-0.21345300
C	3.75362700	-4.00225000	0.44207300	C	-3.61573800	-8.68093800	-0.94433000
C	3.34379800	-3.69590100	-0.86513900	H	-2.69590500	-7.88928000	0.85395400
C	2.01609800	-3.92085500	-1.25830100	H	-4.03018500	-9.52059700	-0.34888200
C	-6.14759600	-0.56819400	-2.76153400	H	-6.69944300	1.14788800	2.93434700
C	-6.73992600	0.66814700	-2.45325200	H	-7.11929000	-1.21479000	3.50618000
C	-6.14540000	1.86226500	-2.88839600	H	-6.35872500	-3.05622000	1.96471000
C	-4.97526000	1.81263100	-3.66304300	H	-5.11273300	-2.43551100	-0.15349800
C	-4.39562500	0.57741800	-3.98494200	H	-4.65833600	-0.10483400	-0.69260200
C	-5.67545500	0.73926400	1.04697500	H	0.68213100	7.13085300	-1.75759900
C	1.08308100	-4.47454100	-0.34978200	H	3.11428600	7.07500900	-1.21570800
C	-7.14397800	5.48012300	1.81972200	H	4.24588200	4.89121800	-0.69003700
C	-7.06495300	6.93393900	1.34061300	H	2.90695900	2.76478800	-0.74736800
H	-6.86265100	5.43840300	2.89705800	H	0.49328900	2.83139600	-1.32465300
H	-7.57859500	7.60178000	2.06268700	H	0.77318400	-5.12695300	1.70587000
C	-4.96940100	6.49696000	0.02884700	H	3.15211100	-4.70234300	2.40205200
C	-5.59781400	7.33420100	1.14987400	H	4.07511700	-3.29903300	-1.58588000
H	-3.87479000	6.66640100	-0.03479200	H	1.70485400	-3.70752600	-2.29049300
H	-5.04405400	7.17323100	2.10202000	H	4.79717500	-3.84841800	0.74185800
C	-5.25763500	5.42349100	-3.12033400	H	-6.59735200	-1.50261200	-2.39406800
C	-5.55896700	6.66914300	-3.96184900	H	-7.65276000	0.69728800	-1.83970400
H	-5.45728100	4.53121400	-3.75407300	H	-6.58555500	2.83058300	-2.61071200
H	-6.59729500	6.61953400	-4.35073500	H	-4.48947600	2.74160100	-3.99805700
C	-3.12565900	6.94107600	-4.54916100	H	-3.50304400	0.53809600	-4.62388600
C	-4.54375500	6.77467300	-5.10659500	H	-8.18821000	5.10276100	1.77203200
H	-2.36714500	6.79453100	-5.34580300	H	-7.60055300	7.04280900	0.37118300
H	-4.59834700	5.84829900	-5.72107100	H	-5.36991000	6.85764300	-0.94315400
C	-5.57543800	-1.83707800	-6.06312400	H	-5.50309900	8.41290300	0.90855000
C	-5.56813600	-2.41987600	-7.48253500	H	-5.95799800	5.32691000	-2.26861600
H	-5.32820400	-0.75718300	-6.08969100	H	-5.49987300	7.58143100	-3.32560300
H	-4.63108900	-2.12011700	-8.00327200	H	-2.99287000	7.99006700	-4.19660800
C	-4.41922900	-4.51523600	-6.73045700	H	-4.78765500	7.61762400	-5.78559300
C	-5.65059700	-3.94950400	-7.44707700	H	-6.60737900	-1.87555700	-5.64408700
H	-3.52495400	-4.37575600	-7.38052500	H	-6.40468800	-1.98610700	-8.06820900

H	-4.51241400	-5.61199700	-6.58388800	C	6.78905600	-4.88462500	-1.37298700
H	-6.57438500	-4.25834500	-6.90783400	C	6.94383100	-3.65493300	-0.71398400
H	-4.01187900	-6.98007300	-3.17236700	H	6.50114100	-1.56038800	-3.35548000
H	-5.59217800	-8.05736100	-1.66208300	C	5.94076800	-3.68971900	-4.87434700
H	-1.56034200	-8.75726700	-0.19000400	H	6.31711500	-5.88140300	-3.25402900
H	-3.28025900	-9.11407000	-1.91275700	C	6.96634100	-6.15478000	-0.57763300
C	0.85587800	0.46962100	-1.79987500	H	7.18690700	-3.67656400	0.35906400
O	1.98004800	0.39055600	-1.53427000	F	6.16805000	-4.87303600	-5.49982900
H	-2.58767600	0.44184300	-2.61577300	F	4.60413200	-3.43656900	-4.98253400
Li	-0.69576800	-0.07610500	4.54657100	F	6.57832800	-2.72368000	-5.58146800
C	1.26746700	5.77726500	-5.51506600	F	6.64635400	-7.26444800	-1.28861700
C	0.29380900	6.00779900	-6.50718500	F	8.24769400	-6.30292400	-0.14980200
C	-0.75078900	5.08345400	-6.66727800	F	6.18684800	-6.15436200	0.54084800
C	-0.84554900	3.95037600	-5.83940400	C	8.50269300	-0.85275500	-0.04201100
C	0.11852300	3.74657100	-4.82998400	C	9.55876600	-1.43825000	-0.77449100
C	1.19065800	4.65434700	-4.68366200	C	10.90546800	-1.26809300	-0.40795100
O	0.09313600	2.70612200	-3.94036900	C	11.24951900	-0.48939100	0.70835200
C	-0.97190400	1.80273700	-3.95932400	C	10.21877100	0.10760400	1.44904900
C	-0.72832700	0.46066400	-4.37358600	C	8.87419300	-0.08025200	1.08100400
H	2.10162700	6.48319600	-5.38350400	H	9.32798300	-2.04794500	-1.66122700
H	0.35943800	6.89213000	-7.15825200	C	11.97864700	-1.98671000	-1.19072300
H	-1.50614900	5.23526800	-7.45411800	H	12.30028200	-0.34490400	0.99097000
H	-1.65915300	3.22847400	-5.99048900	C	10.52691000	0.92527600	2.67788800
H	1.93591100	4.46413600	-3.90191400	H	8.09162500	0.39880600	1.69115100
H	-1.95941300	2.28240800	-4.08608900	F	13.20407600	-1.42465700	-1.02158100
H	0.29917500	0.19527100	-4.66557000	F	12.08486100	-3.28799500	-0.80602100
H	-1.52677500	-0.13146700	-4.84501000	F	11.71573900	-1.99394700	-2.52243400
F	6.99220500	5.03510100	-2.31600000	F	10.23227800	0.24102600	3.81924600
F	8.49418600	4.01125100	-1.09741600	F	11.83371800	1.28156700	2.75558200
F	6.59091900	4.60720600	-0.21247500	F	9.79100000	2.06867400	2.71448100
C	7.16755700	4.09844900	-1.34938100	C	4.59549800	-0.84656400	0.78803700
B	6.93714000	-1.01139100	-0.49870400	C	3.71535600	-1.17287100	1.83488200
C	6.79043500	-2.41159900	-1.36882400	C	4.15565400	-1.88122200	2.95549800
C	5.34039300	0.31646000	-2.21043100	C	5.51094900	-2.23762100	3.02471600
C	5.95658400	-1.21342000	0.81801500	C	6.39186900	-1.89450600	1.98572600
C	6.43899000	0.33280500	-1.31269200	H	4.19019600	-0.31412900	-0.08486200
C	6.55167300	-2.48199500	-2.75915000	C	2.28195500	-0.77286700	1.69866300
C	6.36639300	-3.70800700	-3.42726500	H	3.45769700	-2.18128200	3.74592700
C	6.47087800	-4.92488700	-2.73865500	C	5.94996500	-3.07941400	4.19396500

H	7.45019700	-2.17860200	2.08546400	C	-0.21067100	2.12516400	2.01361800
F	1.53178900	-1.08202800	2.80979600	C	1.88187500	2.23404800	3.19389600
F	2.18109900	0.58560900	1.53792500	C	3.01936300	1.22068200	3.32266500
F	1.64777200	-1.34131900	0.65381400	C	3.39277800	-0.71480800	4.74120600
F	7.28904500	-3.16317900	4.31781500	C	2.56549100	-1.85345200	5.35262500
F	5.45593500	-2.59273600	5.37400500	C	0.64148000	-1.58592400	6.81928400
F	5.46871200	-4.35339300	4.08438700	C	1.97796600	1.31529400	6.83510500
C	4.90467800	1.46765300	-2.88652500	C	-0.36788000	1.82293900	6.68034800
C	5.50053500	2.71399400	-2.63354000	C	-1.46572800	1.74135100	5.64053900
C	6.55945200	2.76762500	-1.71689400	C	-2.84379900	0.04310700	4.69496800
C	7.03236800	1.59598300	-1.09500900	C	-2.86667400	-1.40245200	4.24246600
H	4.80170800	-0.62098300	-2.40631600	C	-2.13618500	-2.70005900	2.35651000
C	3.82346400	1.40130700	-3.93576400	C	-3.21113400	-2.44304300	1.30535800
H	5.15271600	3.62061400	-3.14701800	C	1.08249100	-0.79964900	7.91140500
H	7.89705100	1.68388500	-0.42102000	C	0.47708800	-1.01873400	9.16880600
F	3.30242900	0.15683700	-4.08860100	C	2.99159600	2.27284700	6.67003600
F	2.78616400	2.23151600	-3.63586600	C	4.19690100	2.15492300	7.37642000
F	4.28748700	1.79423600	-5.15082800	C	-0.55498700	-1.95744800	9.32609300
C	6.55945200	2.76762500	-1.71689400	C	4.37689100	1.09178400	8.27591800
C	7.03236800	1.59598300	-1.09500900	C	3.35106500	0.15349200	8.46094300
H	4.80170800	-0.62098300	-2.40631600	C	2.14004100	0.23426700	7.73783000
C	3.82346400	1.40130700	-3.93576400	C	-0.99939200	-2.70312100	8.22016100
H	5.15271600	3.62061400	-3.14701800	C	-0.39379600	-2.52168300	6.96755400
H	7.89705100	1.68388500	-0.42102000	H	-1.73928100	0.63047400	2.46526400
F	3.30242900	0.15683700	-4.08860100	H	-0.81954700	0.28555900	0.99358000
F	2.78616400	2.23151600	-3.63586600	H	-0.71895300	3.02700800	2.43094100
F	4.28748700	1.79423600	-5.15082800	H	0.37105800	2.44895600	1.12366600
				H	2.09429500	2.92182900	2.35279800
				H	1.77768200	2.83960800	4.11899800
				H	3.85855200	1.66550800	3.89894900
				H	3.41711200	0.92001100	2.32996000
				H	3.88800300	-0.09776600	5.52029100
				H	4.18823000	-1.14282600	4.08818700
				H	3.01304400	-2.18527100	6.31013700
				H	2.52135900	-2.72236700	4.67419800
				H	-0.27772700	2.86503600	7.06347400
				H	-0.60068900	1.14415000	7.53054100
				H	-2.42672100	2.04465300	6.11529800
				H	-1.26326400	2.43961700	4.79444400

**S4-BArF**

O	-1.90800900	-1.58370500	3.21778800
O	-2.79242400	-1.37721300	0.43291700
O	-2.27954000	1.77552900	0.85755800
O	0.65624400	1.52815400	2.97211400
O	2.48506600	0.08173200	3.99186500
O	1.19295000	-1.42194000	5.56384000
O	0.84834200	1.42061600	6.03765200
O	-1.53663400	0.39641100	5.16320900
C	-1.26017800	1.10472400	1.59413500

H	-3.58726200	0.17441600	5.51671600	C	-2.77789700	-4.19858400	-1.69413000
H	-3.15712400	0.70440200	3.85334200	C	-3.98378300	-3.03179900	-3.58579800
H	-2.65607400	-2.08169800	5.10434600	C	-3.90903400	-3.06668400	-4.98756100
H	-3.90518000	-1.60772500	3.89050700	C	-4.38547500	-2.01805300	-5.78858400
H	-2.41055400	-3.60975500	2.94116100	C	-5.01801100	-0.90533700	-5.17362600
H	-1.17568100	-2.91052200	1.84931300	C	-5.05229200	-0.81322000	-3.75129700
H	-4.16694900	-2.12573500	1.77072300	C	-4.46233600	-1.84687100	-2.98318400
H	0.81294100	-0.41453700	10.02562000	H	-2.96475800	-7.43809700	-0.64913100
H	2.82491500	3.09980800	5.96559900	H	-3.45008200	-3.94401700	-5.46637700
H	5.00404900	2.88201500	7.21298900	O	-4.28931400	-1.70387300	-1.60435900
H	-1.01701800	-2.10263300	10.31392400	O	-2.06501300	-3.04804400	-1.40329200
H	5.32889200	0.98191400	8.81431000	C	-5.81876200	0.28471400	-3.08566000
H	3.49273600	-0.69233300	9.15149100	C	1.11681000	3.54842600	-2.35756900
H	-1.81007900	-3.43829700	8.33587200	C	-5.52782100	2.33805200	2.60682400
H	-0.69400900	-3.10303600	6.08392000	C	-5.87753200	1.15246700	3.27234300
P	-2.63997300	-1.46894600	-1.19772800	C	-6.01956000	-0.04812000	2.55326600
Rh	-1.58491100	0.25691100	-2.20477800	C	-5.79467200	-0.04578200	1.16627600
C	-3.56712100	4.89964800	-1.10499500	C	-5.44272700	1.13698500	0.50453600
C	-3.99997300	6.13623600	-0.55075100	C	1.87165600	2.89074400	-3.35686000
C	-4.97301000	6.11365300	0.48032600	C	3.06553000	2.22703100	-3.04582200
C	-5.42165600	4.88151300	0.99407300	C	3.54143700	2.20605100	-1.72598600
C	-4.94646800	3.63703200	0.53390400	C	2.82036500	2.87590800	-0.72402200
C	-4.04565500	3.69474900	-0.55582200	C	1.62501600	3.54146000	-1.03494400
C	-2.50921100	4.83430300	-2.16741500	C	-1.72652900	-5.97254800	1.38798200
C	-2.67691500	5.39553000	-3.45939500	C	-0.71498500	-6.14189000	2.34597700
C	-1.56493300	5.44139200	-4.33867400	C	0.60313100	-5.75416000	2.05230400
C	-0.33277600	4.89746300	-3.93208500	C	0.89221700	-5.16792800	0.80685000
C	-0.16070000	4.22538900	-2.70527200	C	-0.12343200	-4.96667500	-0.13741100
C	-1.28667500	4.19017400	-1.84851300	C	-7.00633800	-0.04143400	-2.39253300
H	-6.17091900	4.89497500	1.80213700	C	-7.81329400	0.96243200	-1.83473200
H	0.53024600	4.97973000	-4.61203200	C	-7.44778900	2.31299200	-1.96377200
O	-1.24009500	3.44249300	-0.67925100	C	-6.26550100	2.64983600	-2.64201000
O	-3.58334000	2.52362100	-1.12630300	C	-5.45483000	1.64487100	-3.19218500
P	-2.06658700	1.94577600	-0.77197500	C	-5.31509700	2.35988700	1.20578300
C	-3.70120200	-4.24054700	-2.76223900	C	-1.44380400	-5.39222000	0.12949300
C	-4.42720300	-5.44403300	-3.02162400	C	-5.50374300	7.39806000	1.10210300
C	-4.16623600	-6.59604500	-2.24214700	C	-5.13159100	8.66218200	0.31825300
C	-3.19813700	-6.52897700	-1.22643600	H	-5.09705800	7.48007100	2.13632600
C	-2.48920000	-5.35324200	-0.92572200	H	-5.36822000	9.56566500	0.91754500

C	-3.38806600	7.44649200	-1.02067300	H	-0.95346300	-6.59630600	3.32018500
C	-3.64805000	8.61741700	-0.06417200	H	1.92429500	-4.87502000	0.56645400
H	-2.30080800	7.29780000	-1.18652500	H	0.11037100	-4.50186700	-1.10530000
H	-3.03471800	8.49824200	0.85676300	H	1.41104400	-5.92385300	2.77947600
C	-4.05646800	5.80947200	-3.94673000	H	-7.29232800	-1.09990900	-2.29753100
C	-4.02026700	6.79443800	-5.12023600	H	-8.72674900	0.68697500	-1.28636500
H	-4.57280500	4.87815200	-4.27865400	H	-8.06954700	3.10192900	-1.51527700
H	-5.04643200	6.95929000	-5.50927600	H	-5.94955200	3.70073200	-2.71207400
C	-1.65867500	6.12759300	-5.69397200	H	-4.50951800	1.91645800	-3.68351900
C	-3.09301100	6.26510900	-6.22160900	H	-6.60548700	7.31860100	1.22292500
H	-1.02010700	5.59323700	-6.42833300	H	-5.74477100	8.72601300	-0.60847700
H	-3.46411700	5.27191900	-6.55991000	H	-3.79535200	7.71020600	-2.02237200
C	-5.70960600	0.14339700	-6.03275700	H	-3.32484700	9.56737400	-0.53744200
C	-5.23432400	0.16669300	-7.49097800	H	-4.67638200	6.19486500	-3.11418700
H	-5.60375800	1.14809600	-5.58377400	H	-3.65041400	7.78330000	-4.76674400
H	-4.21129500	0.60380800	-7.53833100	H	-1.21101500	7.14358500	-5.59447000
C	-4.20696600	-2.10633400	-7.29382700	H	-3.10861100	6.92784300	-7.11161200
C	-5.20293000	-1.24740400	-8.07963400	H	-6.80418700	-0.06497600	-5.99842000
H	-3.17063300	-1.77332500	-7.52973800	H	-5.89064000	0.83512300	-8.08584800
H	-4.92721900	-1.22791000	-9.15436600	H	-4.25186200	-3.16902500	-7.61183400
C	-5.49726900	-5.49141400	-4.10510500	H	-6.21989900	-1.69584500	-8.01864100
C	-6.48280200	-6.65576800	-3.94553600	H	-5.00600600	-5.58231800	-5.09875800
H	-6.03454100	-4.52201700	-4.13920000	H	-7.14429400	-6.70767600	-4.83498600
H	-7.14397900	-6.47451500	-3.06856000	H	-4.21036400	-8.75224000	-2.36451100
C	-4.92224400	-7.90239300	-2.43784300	H	-5.02809400	-8.12382600	-4.60244400
C	-5.71952900	-7.96846700	-3.74439500	C	0.32505900	-0.09219500	-2.02467000
H	-5.62242900	-8.02774900	-1.57993900	O	1.46002000	-0.31500700	-2.02357400
H	-6.40642300	-8.83993900	-3.72923300	H	-3.11490800	0.53324300	-2.52855500
H	-5.39651700	3.26312000	3.18869700	Li	0.47634400	-0.02681700	4.25733000
H	-6.04229100	1.16798000	4.36141800	C	-0.50804700	-3.02616500	-4.04872600
H	-6.31315400	-0.97519200	3.07149500	C	-0.64972100	-4.40337900	-4.27703600
H	-5.88954600	-0.96584400	0.57002800	C	-0.81209600	-4.89564400	-5.58462700
H	-5.26181600	1.10009500	-0.57272500	C	-0.82331600	-4.00084300	-6.66949700
H	1.50502300	2.87286700	-4.39449400	C	-0.69201600	-2.61958000	-6.44843100
H	3.61006100	1.69073600	-3.83258400	C	-0.54942500	-2.13834700	-5.13606100
H	4.46953900	1.66753100	-1.48923100	H	-0.32778800	1.71899600	-4.25628900
H	3.20055600	2.88999000	0.30803400	C	-1.32731300	1.28411000	-4.11978700
H	1.07974600	4.08265000	-0.24984700	C	-1.49653300	-0.09365200	-4.41679800
H	-2.75640800	-6.29405900	1.60920900	H	-0.38704200	-2.62861600	-3.03537800

H	-0.63818000	-5.09814300	-3.42374700	H	6.30761400	3.35174400	4.47027900
H	-0.92160400	-5.97688100	-5.75747200	C	5.38835800	4.16983100	2.04443400
H	-0.93762300	-4.37850000	-7.69724500	H	5.72794800	2.05802600	0.37600600
H	-2.16528800	1.98026500	-4.27055600	F	7.18635400	1.99920700	6.27648400
O	-0.40182700	-0.77459500	-4.94641800	F	6.30061400	0.01576000	5.99887300
H	-2.46989900	-0.50590000	-4.73305500	F	8.39852900	0.34648000	5.51535600
F	7.57746400	2.56484500	-4.63020800	F	5.98578100	5.17082100	2.73429600
F	9.06743900	2.17598400	-3.07521600	F	5.46600200	4.46253000	0.73138800
F	7.36444300	3.46883200	-2.64845400	F	4.04906500	4.22652600	2.37946500
C	7.73816700	2.33517000	-3.30278000	C	3.94753800	-1.20527100	0.94087000
B	6.51701800	-0.74567300	0.63950900	C	2.83280400	-1.87040100	1.47004100
C	7.94408800	-1.54611300	0.65425000	C	2.99079300	-3.03565800	2.23364000
C	5.44500100	-0.97370800	-1.81072300	C	4.28965900	-3.51320800	2.46546500
C	5.26557300	-1.66328700	1.16597500	C	5.40683900	-2.83271000	1.94463500
C	6.30914100	-0.29203300	-0.92079100	H	3.78640000	-0.29853000	0.33752200
C	9.14513800	-0.99842100	1.15542500	C	1.45329800	-1.34240000	1.21317100
C	10.36944300	-1.68555100	1.06390200	H	2.11279900	-3.55051300	2.64394600
C	10.43203900	-2.95658700	0.47101700	C	4.44634600	-4.77844000	3.27078200
C	9.25210600	-3.51480900	-0.04401800	H	6.41190100	-3.22960400	2.14994800
C	8.03711500	-2.81403200	0.03908600	F	0.66666900	-1.41428300	2.34193500
H	9.13729700	-0.00774900	1.63419800	F	1.47077200	-0.04915600	0.81698200
C	11.64565600	-1.03277700	1.54068100	F	0.77644500	-2.04351200	0.26569500
H	11.38398100	-3.49998500	0.40557900	F	5.73161100	-5.10362400	3.50579300
C	9.26060200	-4.89707400	-0.65085200	F	3.82609500	-4.67607600	4.49085400
H	7.13613800	-3.26657800	-0.40486500	F	3.85952200	-5.83995600	2.64599000
F	12.52085800	-1.94098600	2.04806300	C	5.32112000	-0.60694900	-3.16015400
F	12.28860700	-0.39671300	0.52503400	C	6.06964200	0.46515900	-3.67633300
F	11.42016100	-0.10529300	2.50557100	C	6.94400100	1.14604800	-2.81812400
F	10.50511000	-5.29691500	-1.01505200	C	7.07076600	0.76022100	-1.47058800
F	8.78564700	-5.82478300	0.22663400	H	4.83596900	-1.81308600	-1.44672800
F	8.47132700	-4.96564000	-1.75340000	C	4.38976500	-1.35780100	-4.08535300
C	6.49095200	0.50752400	1.70493300	H	5.97184400	0.76970200	-4.72707300
C	6.84561900	0.26639800	3.05247000	H	7.78886800	1.30059100	-0.83333200
C	6.78187500	1.26771600	4.03739600	F	3.62292300	-2.26144800	-3.43246300
C	6.34389300	2.56019000	3.71033200	F	3.54479500	-0.51046200	-4.74323000
C	5.95848200	2.81652200	2.38388400	F	5.07796100	-2.02771100	-5.04738100
C	6.02928400	1.80869800	1.40403800	H	-0.69162700	-1.89827400	-7.27835500
H	7.19203400	-0.73916700	3.34142700	H	-3.39916700	-3.38079100	0.74295000
C	7.17524600	0.91733200	5.45048900				

### 3.5.13 Collection of spectra

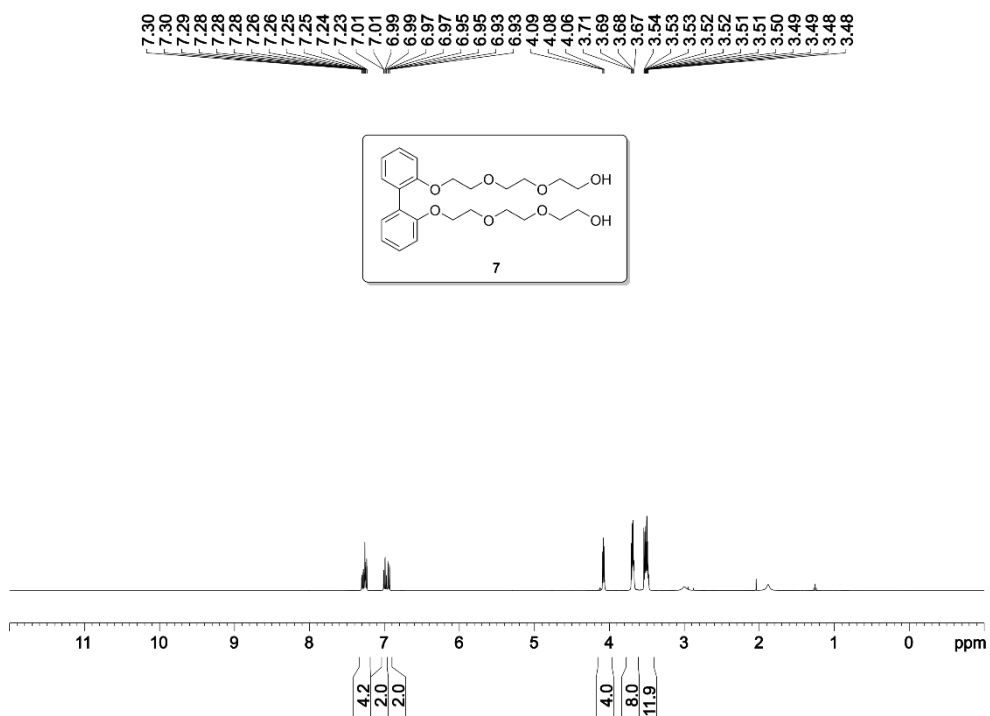


Figure 101. <sup>1</sup>H NMR spectrum (400 MHz, CDCl<sub>3</sub>) of 7



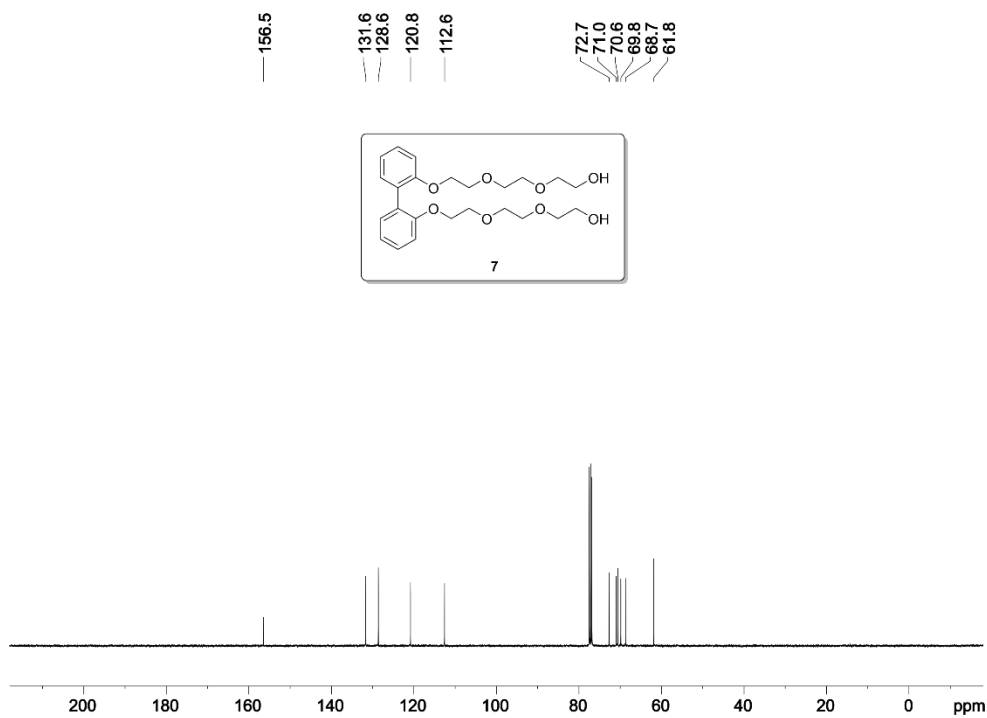


Figure 102.  $^{13}\text{C}\{^1\text{H}\}$  NMR spectrum (101 MHz,  $\text{CDCl}_3$ ) of **7**

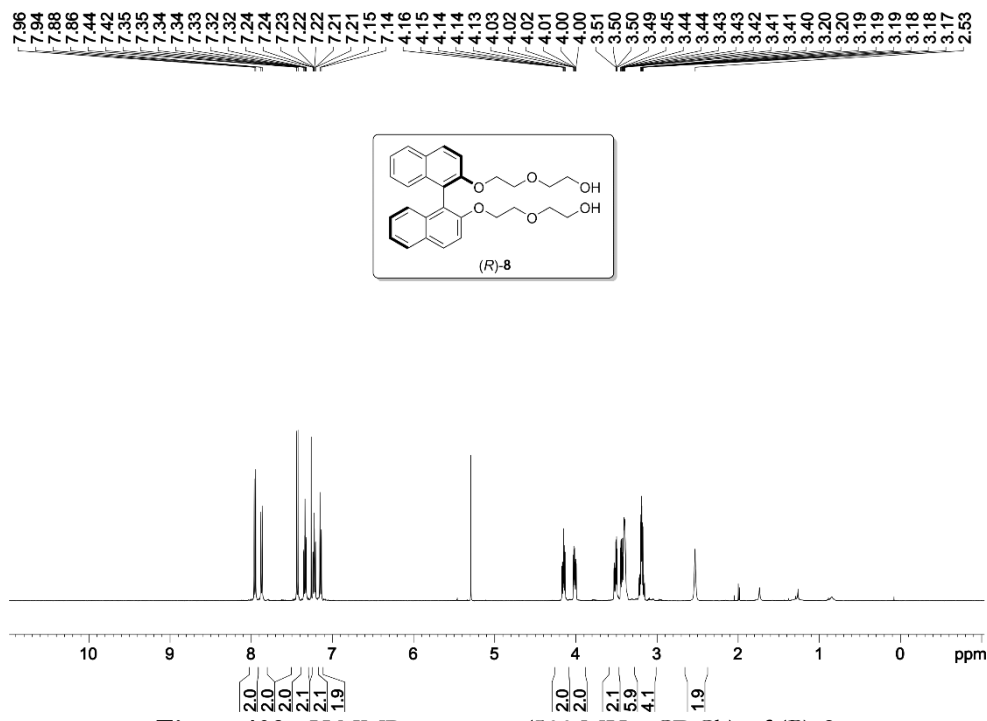
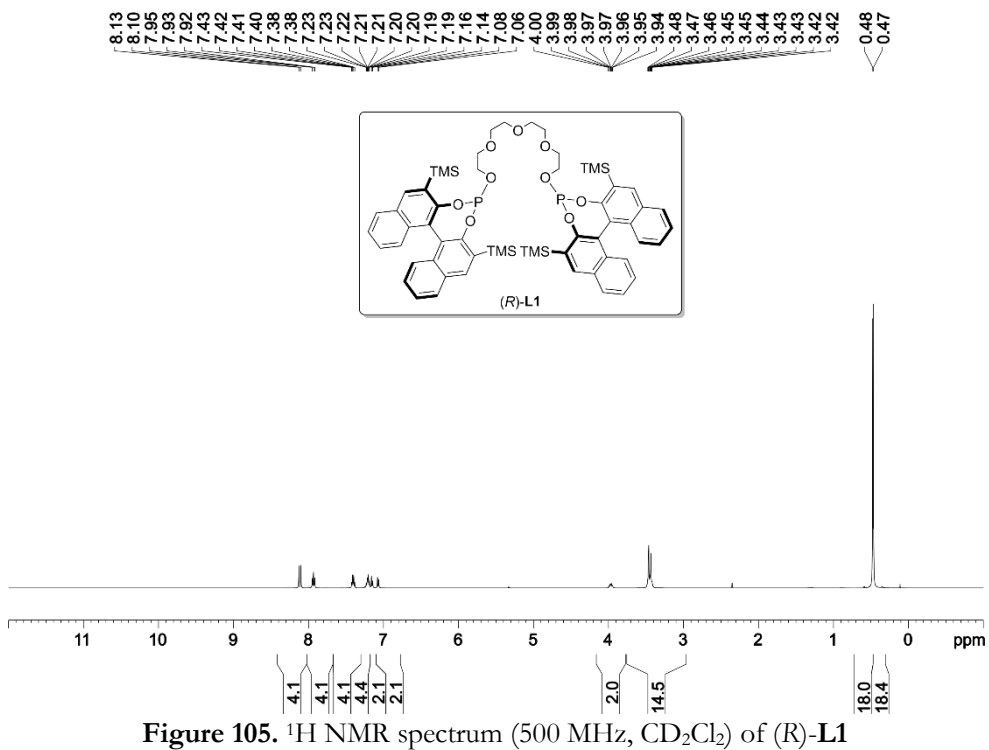
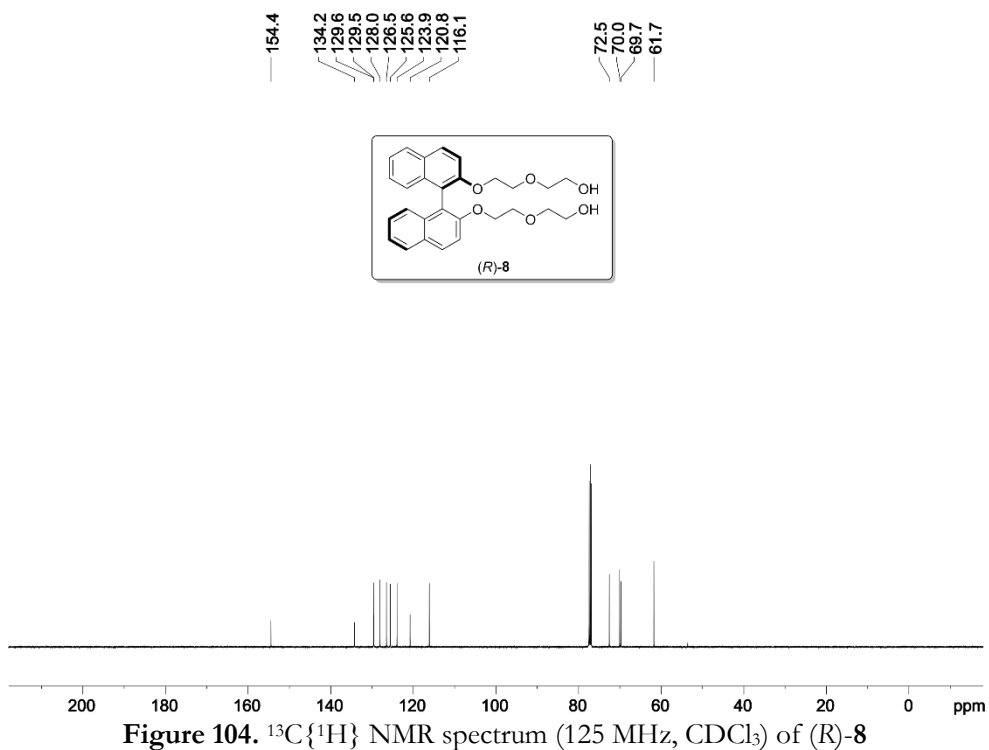


Figure 103.  $^1\text{H}$  NMR spectrum (500 MHz,  $\text{CDCl}_3$ ) of **(R)-8**



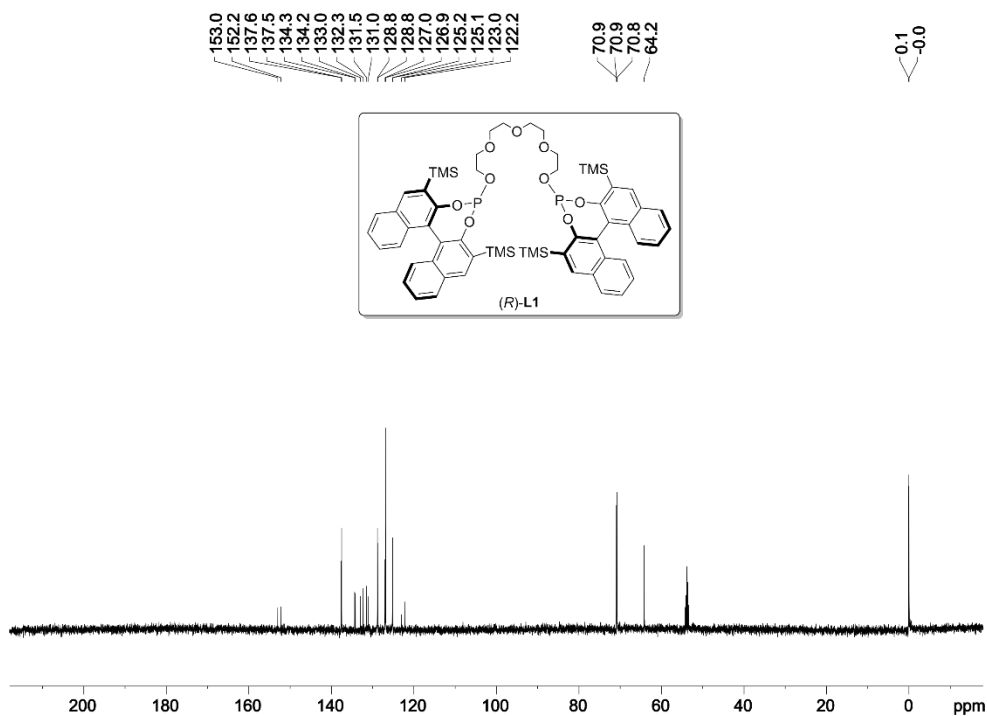


Figure 106.  $^{13}\text{C}\{^1\text{H},^{31}\text{P}\}$  NMR spectrum (126 MHz,  $\text{CD}_2\text{Cl}_2$ ) of (R)-L1

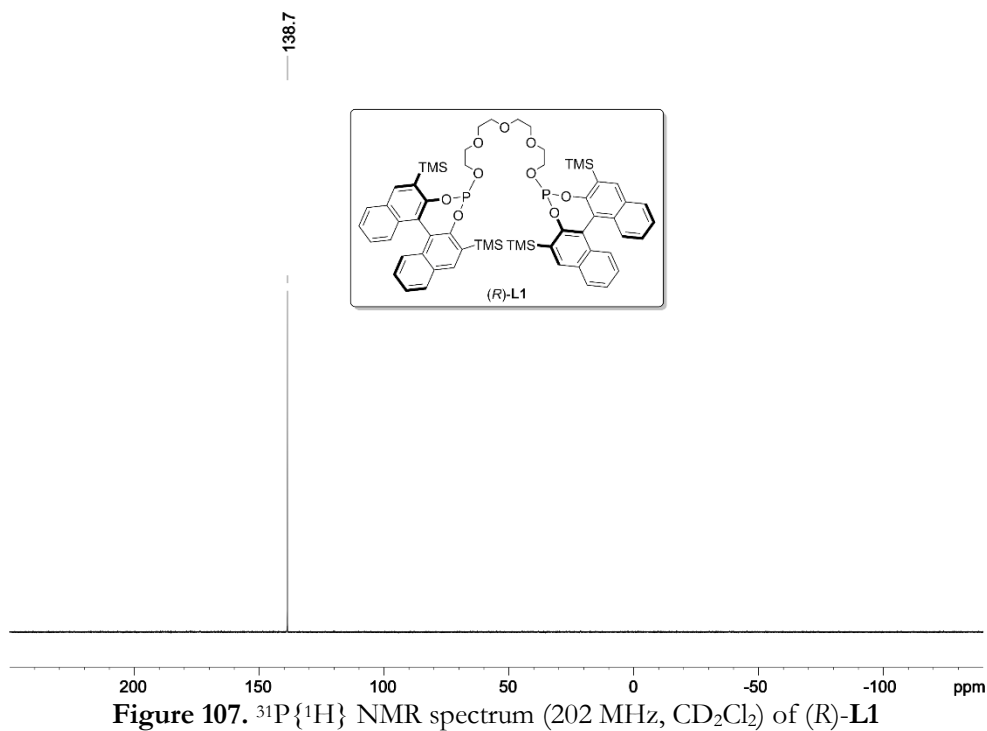


Figure 107.  $^{31}\text{P}\{^1\text{H}\}$  NMR spectrum (202 MHz,  $\text{CD}_2\text{Cl}_2$ ) of (R)-L1

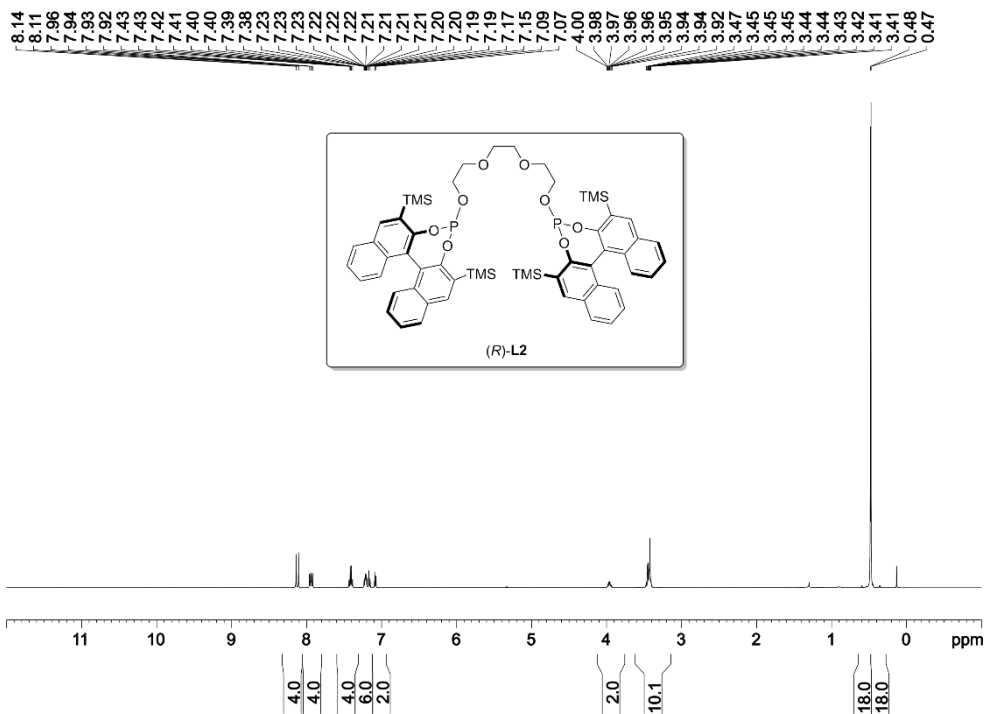


Figure 108. <sup>1</sup>H NMR spectrum (500 MHz, CD<sub>2</sub>Cl<sub>2</sub>) of (R)-L2

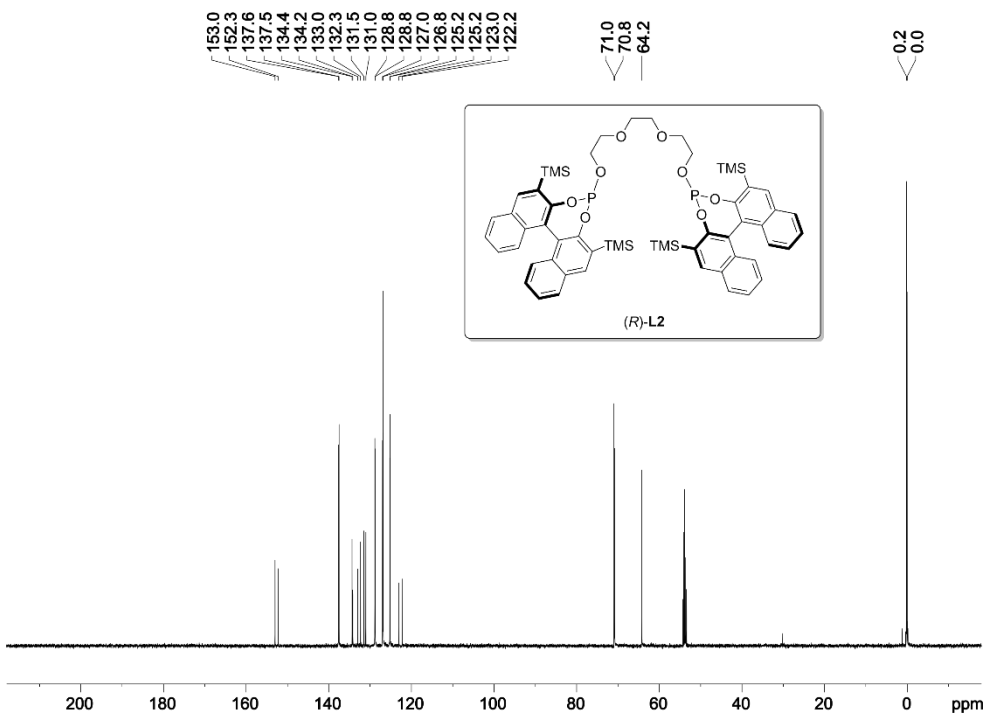
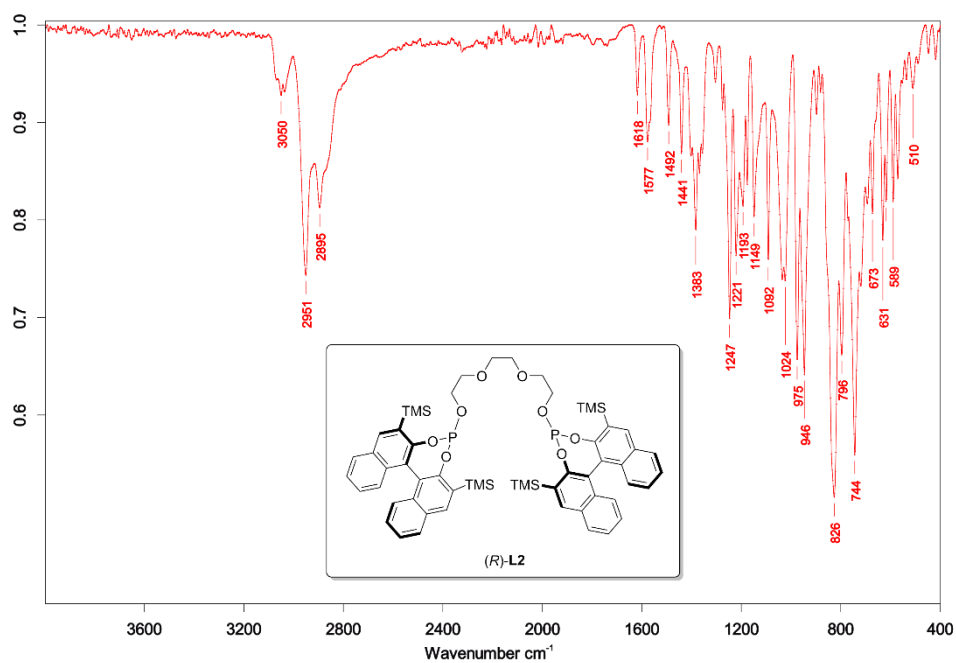
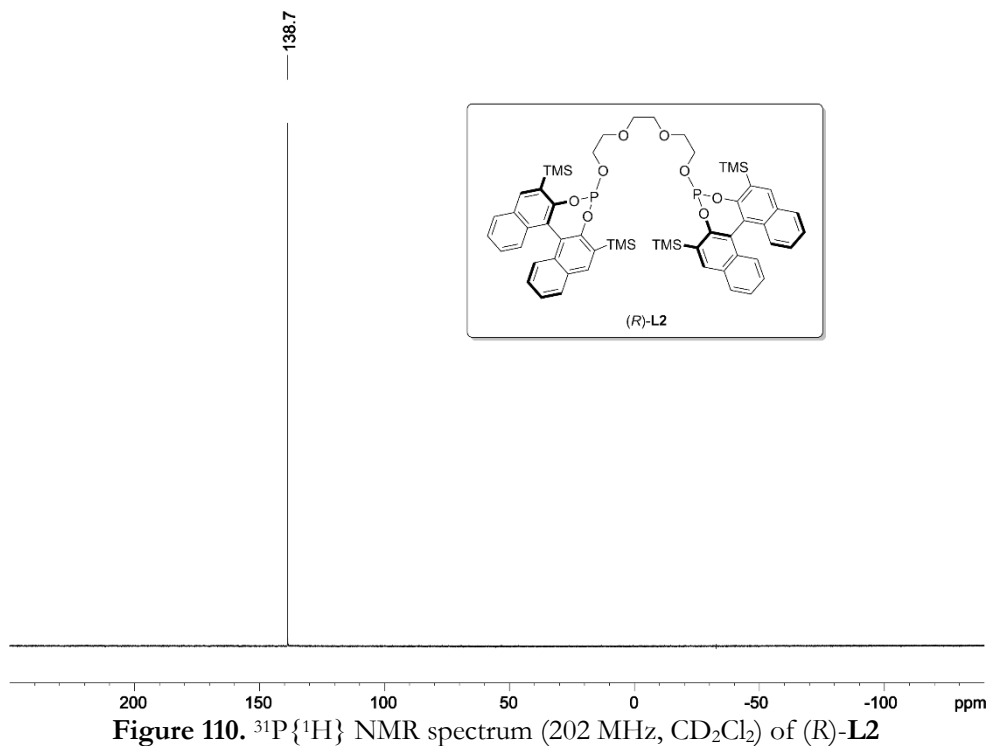


Figure 109. <sup>13</sup>C{<sup>1</sup>H,<sup>31</sup>P} NMR spectrum (126 MHz, CD<sub>2</sub>Cl<sub>2</sub>) of (R)-L2



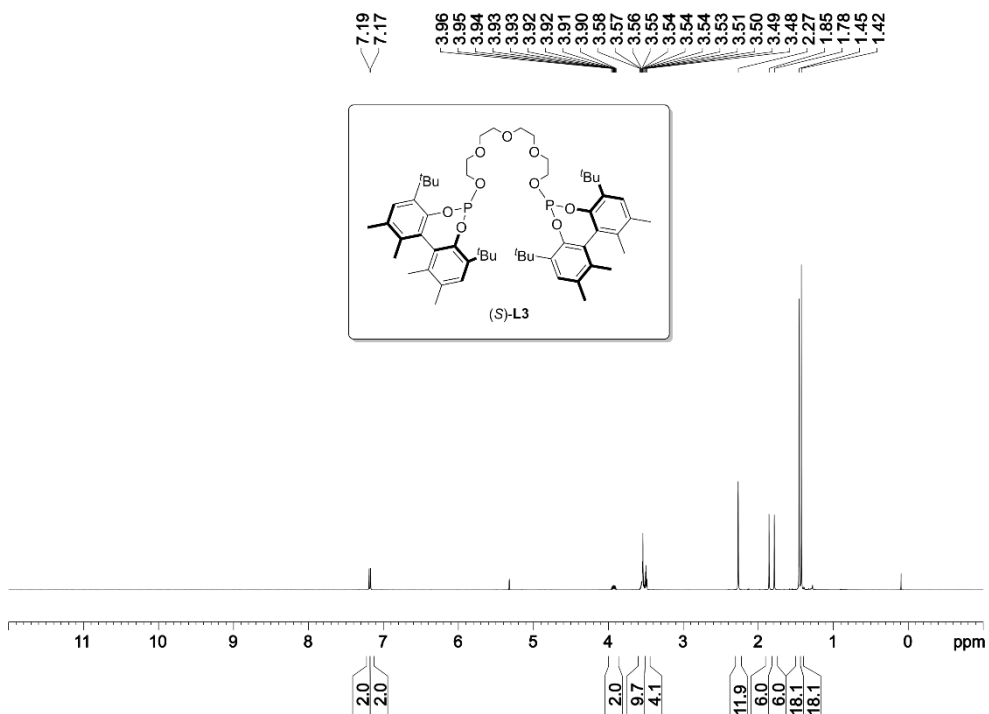


Figure 112.  $^1\text{H}$  NMR spectrum (500 MHz,  $\text{CD}_2\text{Cl}_2$ ) of (S)-L3

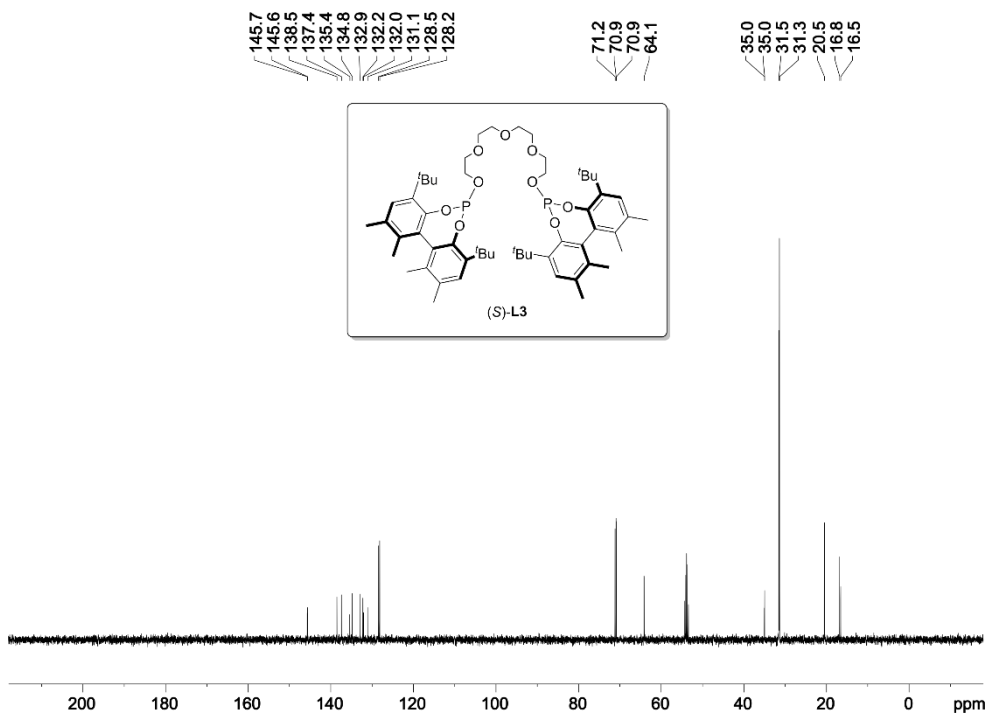


Figure 113.  $^{13}\text{C}\{^1\text{H},^{31}\text{P}\}$  NMR spectrum (126 MHz,  $\text{CD}_2\text{Cl}_2$ ) of (S)-L3

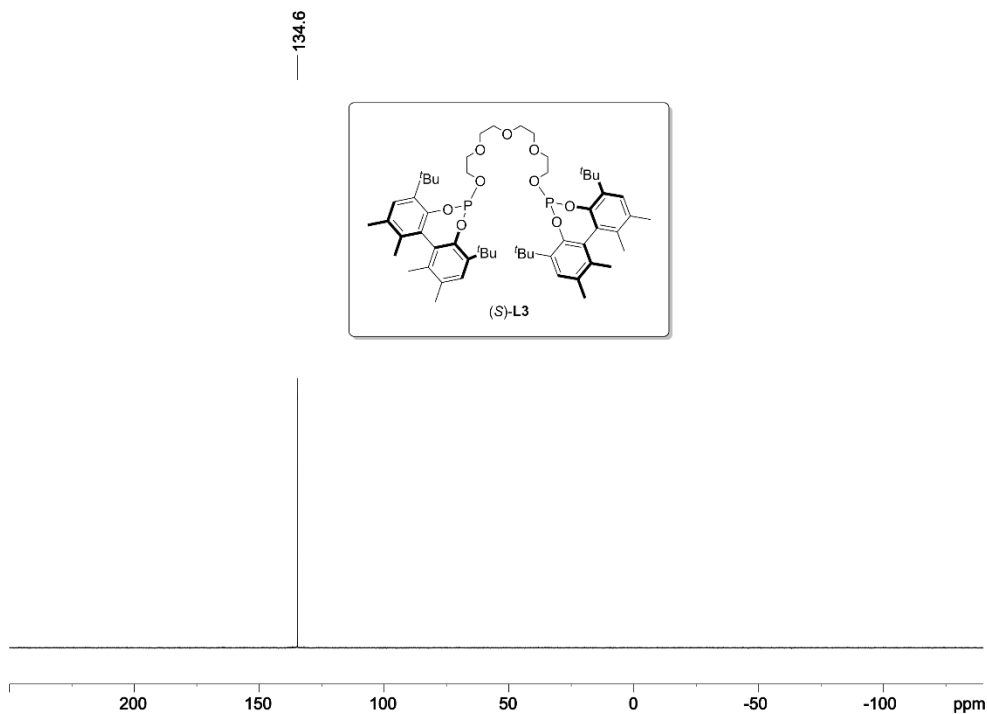


Figure 114.  $^{31}\text{P}\{^1\text{H}\}$  NMR spectrum (202 MHz,  $\text{CD}_2\text{Cl}_2$ ) of (S)-L3

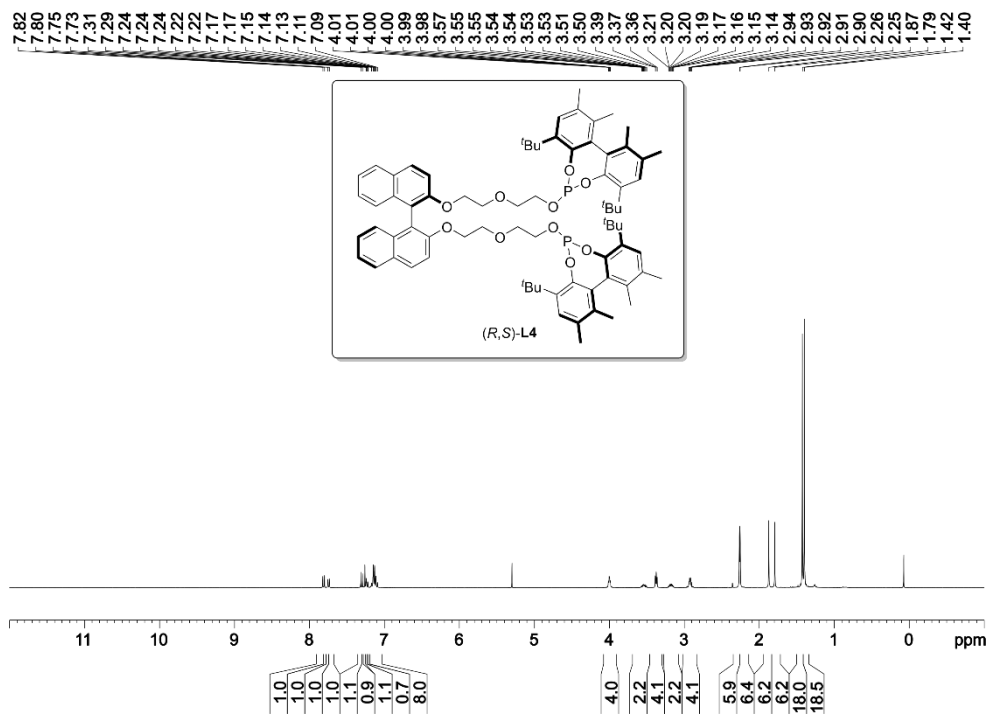
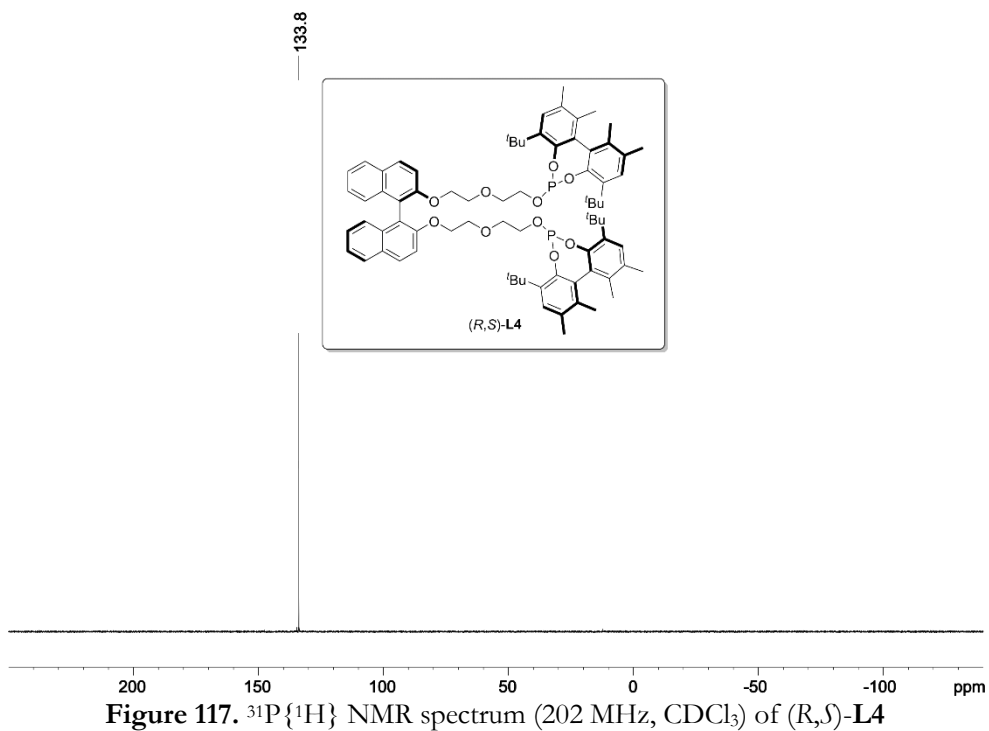
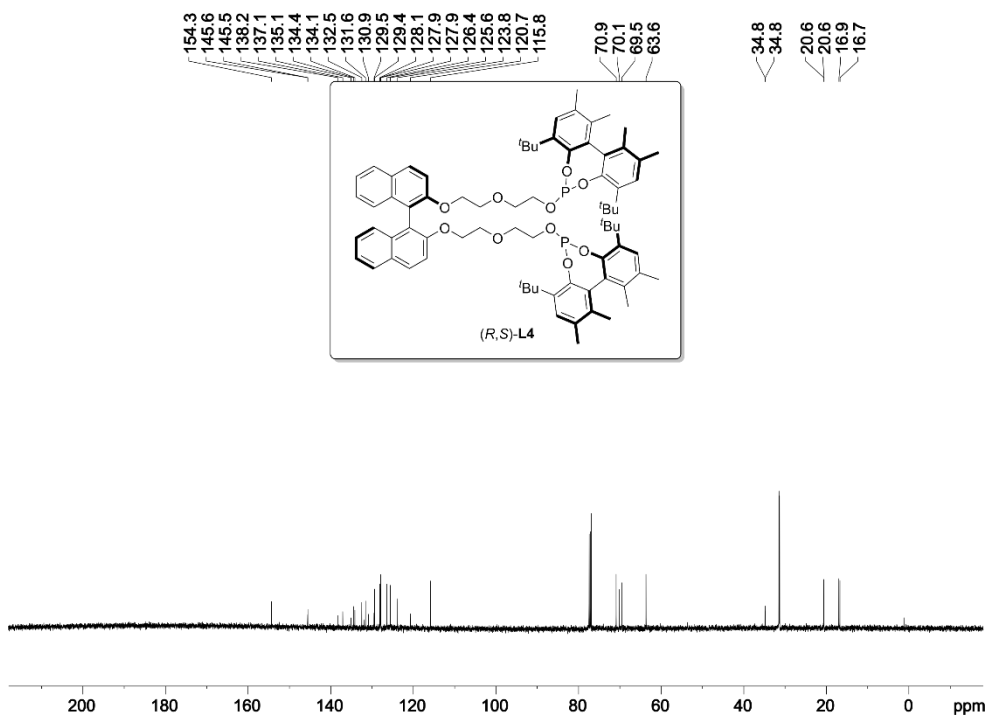
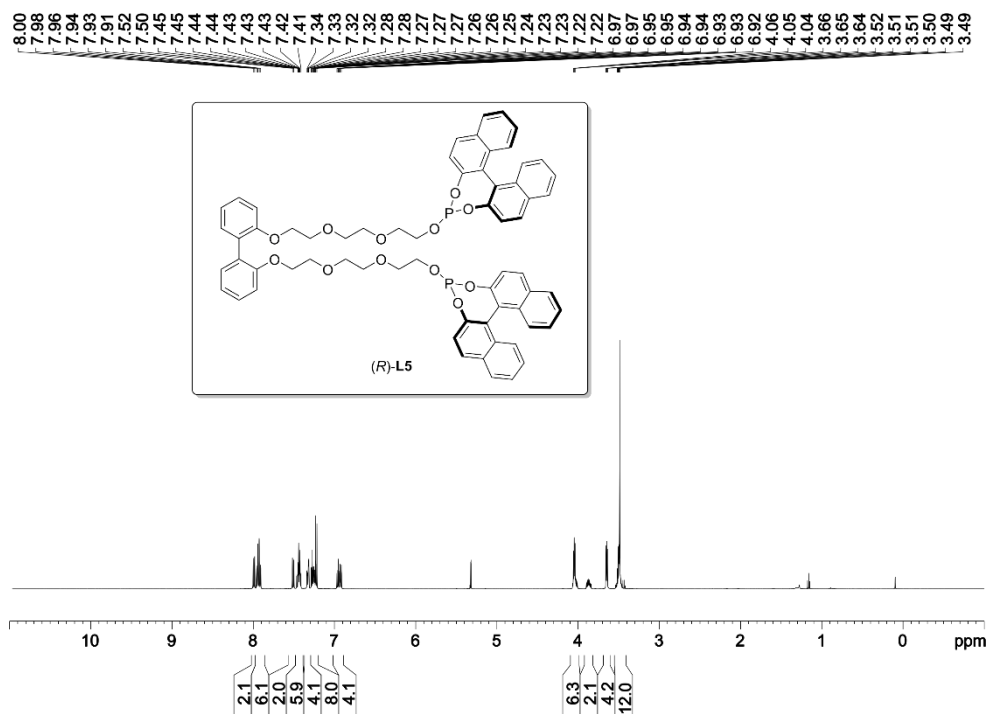
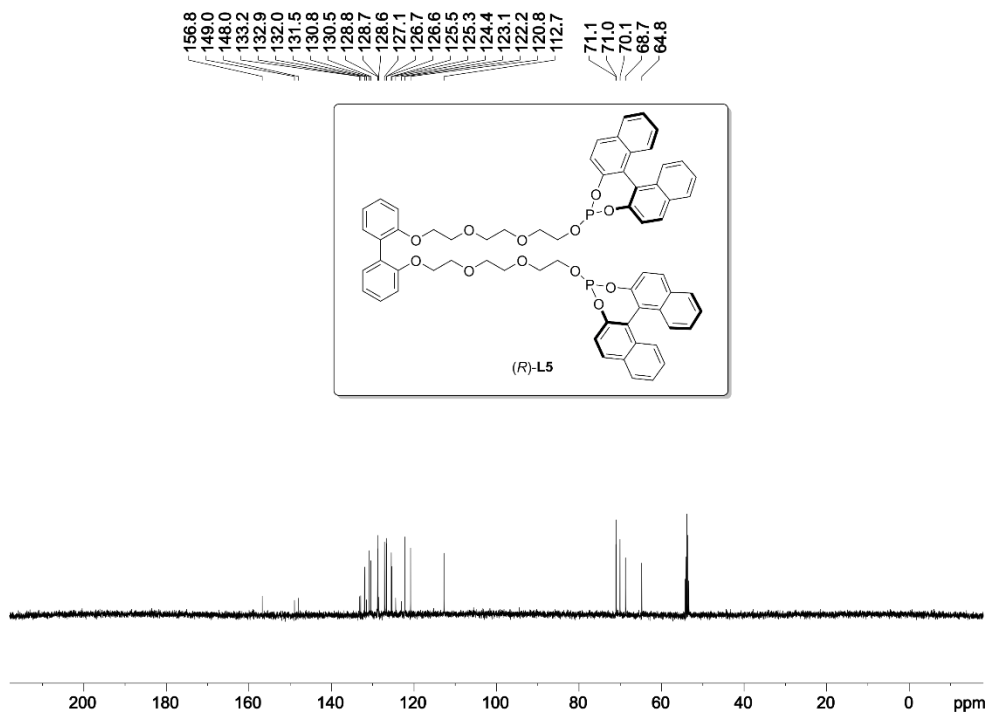
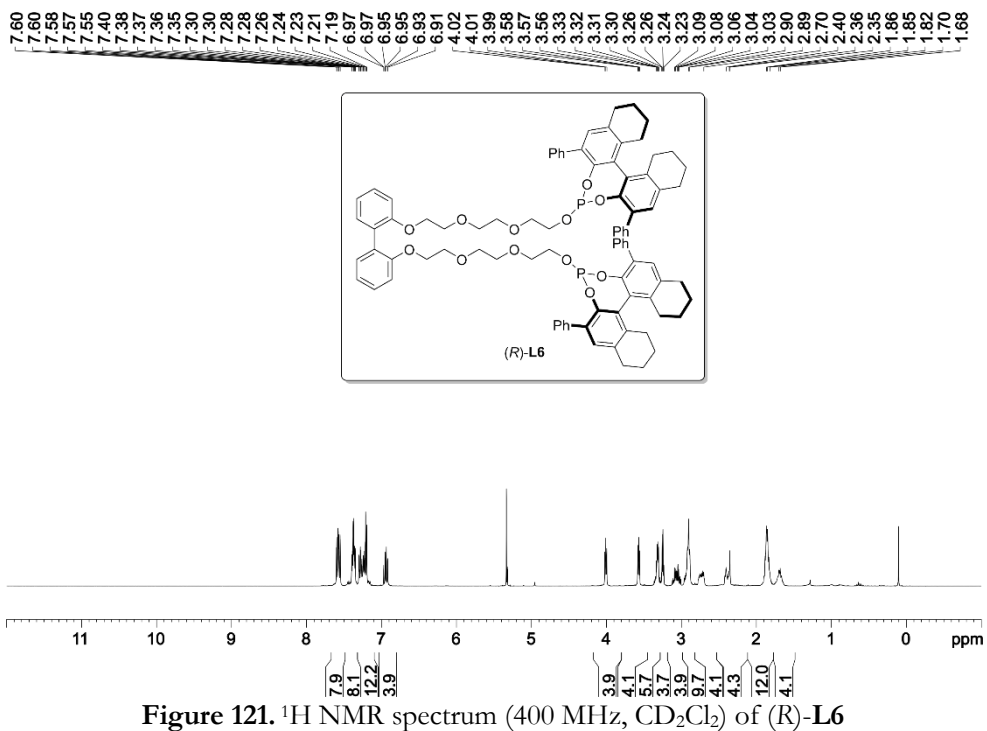
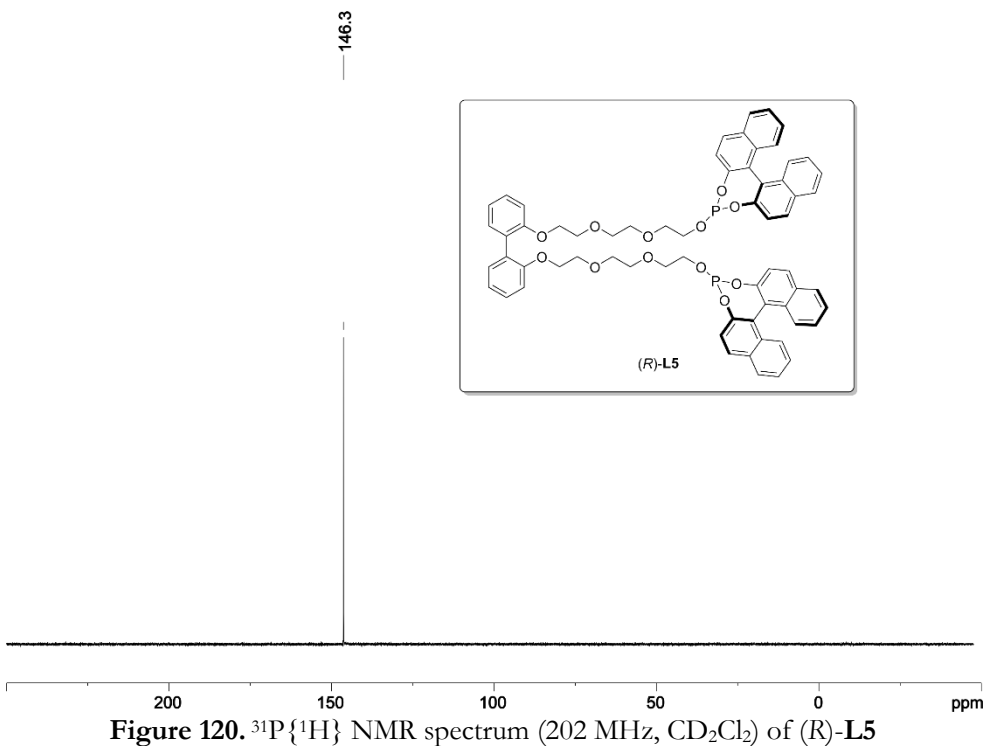


Figure 115.  $^1\text{H}$  NMR spectrum (400 MHz,  $\text{CDCl}_3$ ) of (R,S)-L4





Figure 118. <sup>1</sup>H NMR spectrum (500 MHz, CD<sub>2</sub>Cl<sub>2</sub>) of (R)-L5Figure 119. <sup>13</sup>C {<sup>1</sup>H, <sup>31</sup>P} NMR spectrum (126 MHz, CD<sub>2</sub>Cl<sub>2</sub>) of (R)-L5



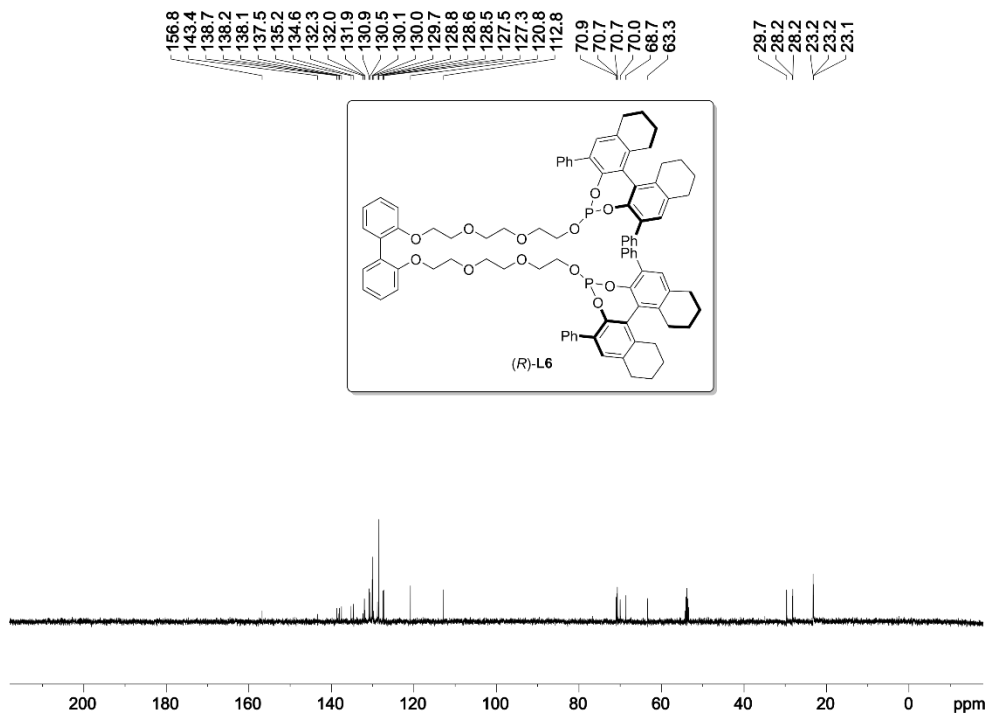


Figure 122.  $^{13}\text{C}\{^1\text{H},^{31}\text{P}\}$  NMR spectrum (126 MHz,  $\text{CD}_2\text{Cl}_2$ ) of (R)-L6

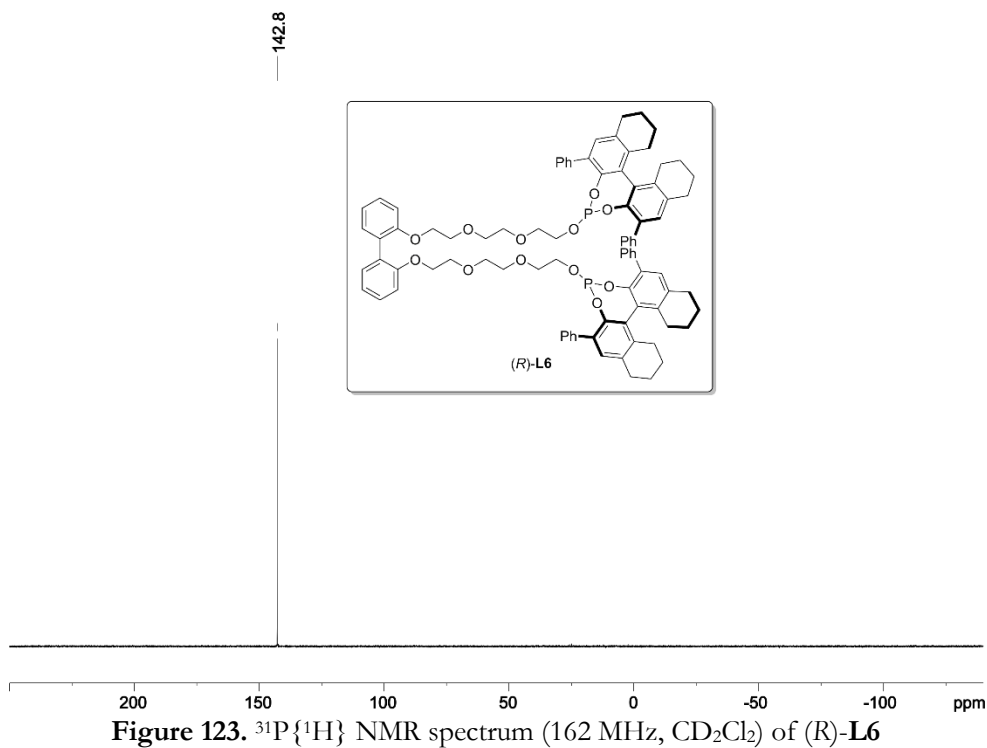
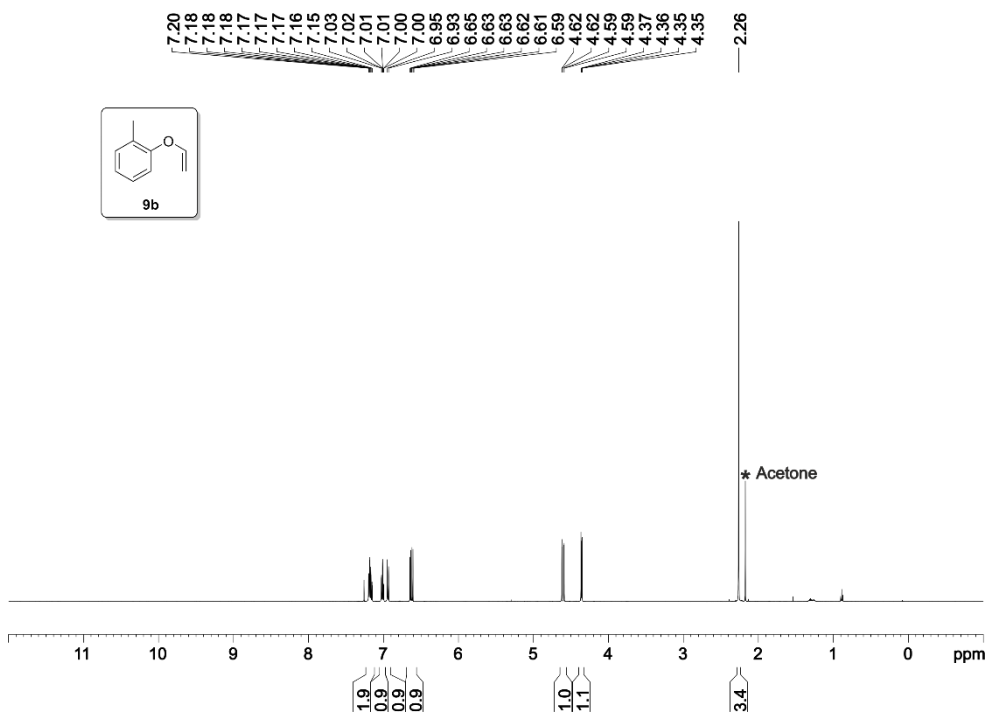
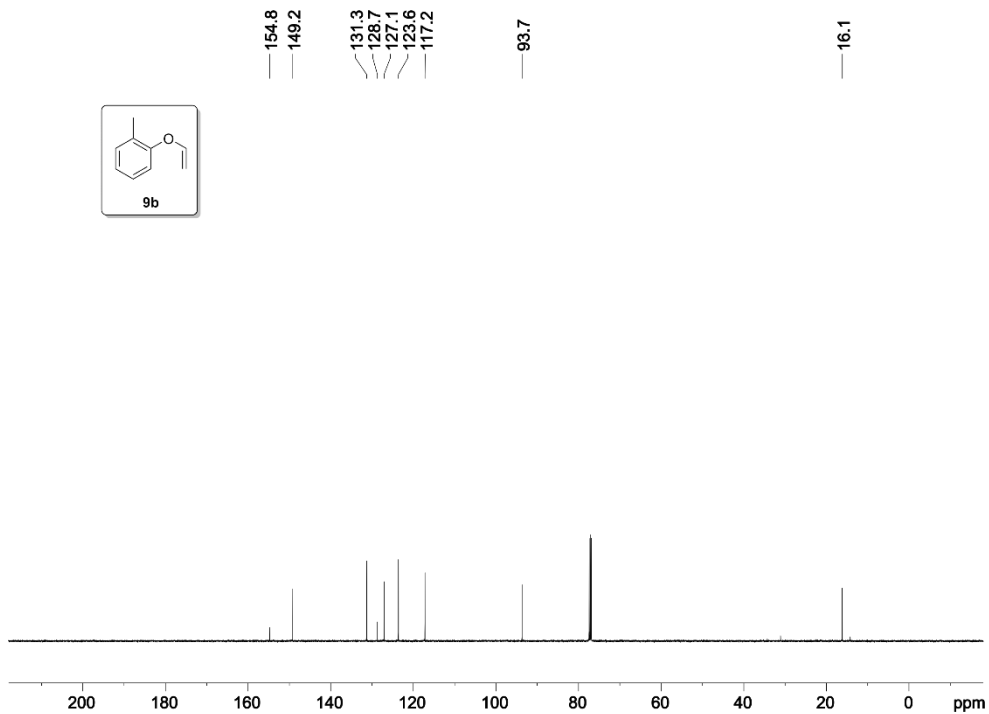
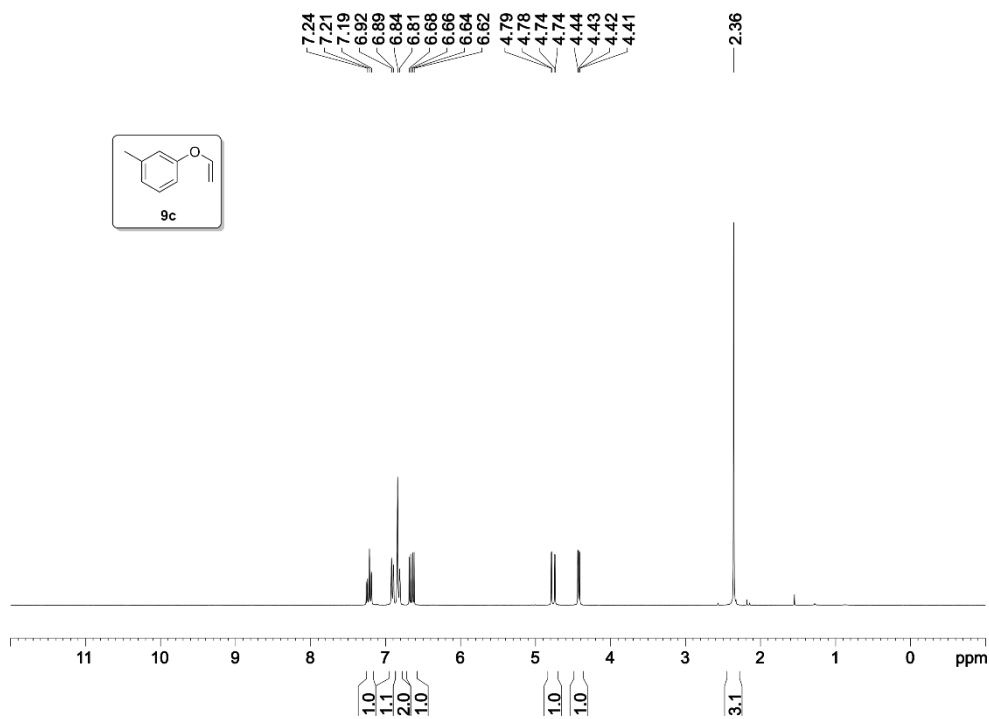
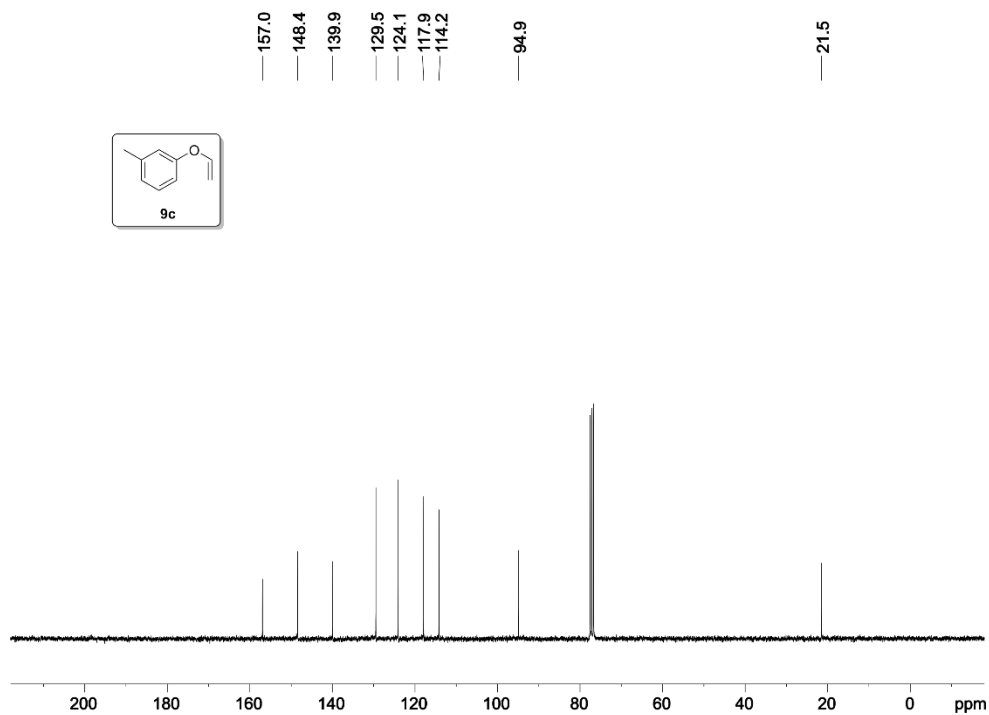


Figure 123.  $^{31}\text{P}\{^1\text{H}\}$  NMR spectrum (162 MHz,  $\text{CD}_2\text{Cl}_2$ ) of (R)-L6

Figure 124. <sup>1</sup>H NMR spectrum (500 MHz, CDCl<sub>3</sub>) of **9b**Figure 125. <sup>13</sup>C{<sup>1</sup>H} NMR spectrum (126 MHz, CDCl<sub>3</sub>) of **9b**

Figure 126.  $^1\text{H}$  NMR spectrum (300 MHz,  $\text{CDCl}_3$ ) of 9cFigure 127.  $^{13}\text{C}\{^1\text{H}\}$  NMR spectrum (75 MHz,  $\text{CDCl}_3$ ) of 9c

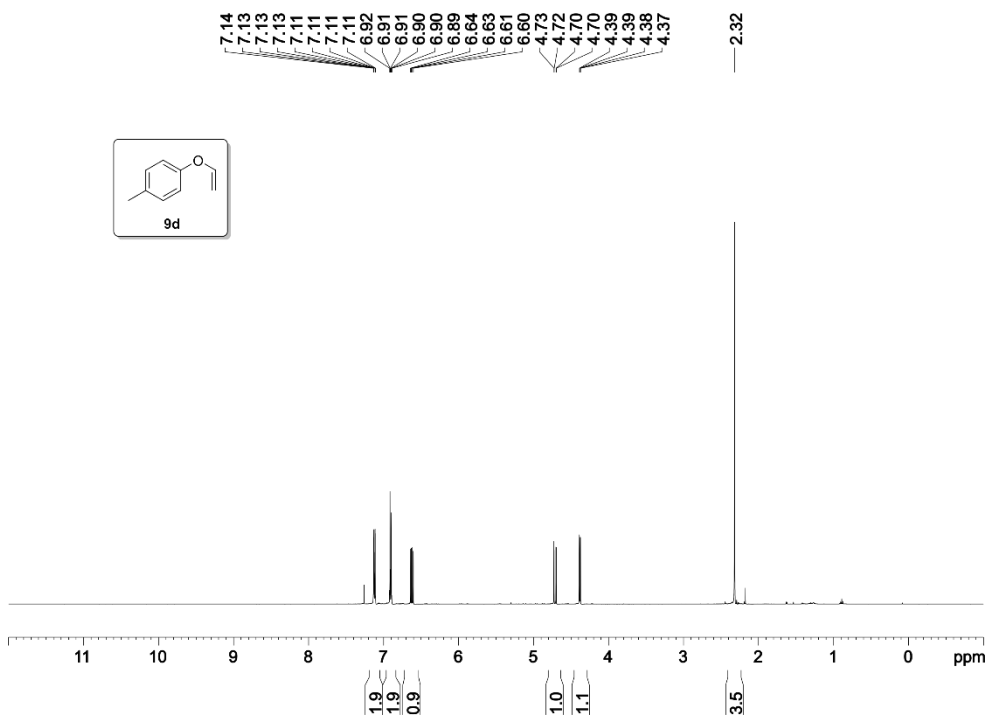


Figure 128.  $^1\text{H}$  NMR spectrum (500 MHz,  $\text{CDCl}_3$ ) of **9d**

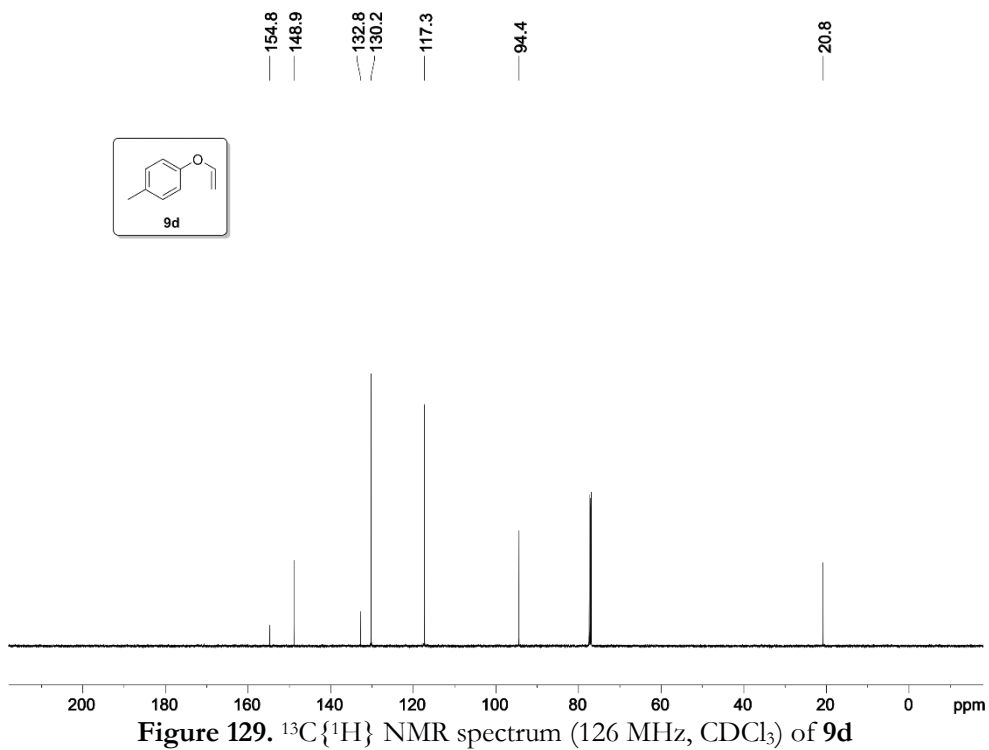


Figure 129.  $^{13}\text{C}\{^1\text{H}\}$  NMR spectrum (126 MHz,  $\text{CDCl}_3$ ) of **9d**

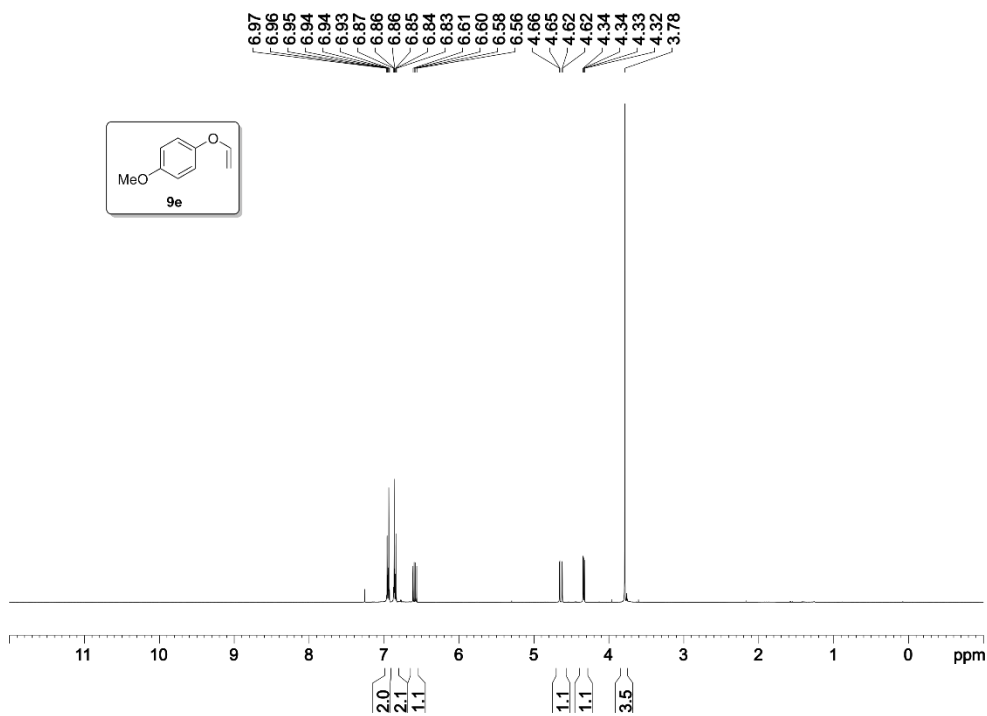


Figure 130.  $^1\text{H}$  NMR spectrum (400 MHz,  $\text{CDCl}_3$ ) of **9e**

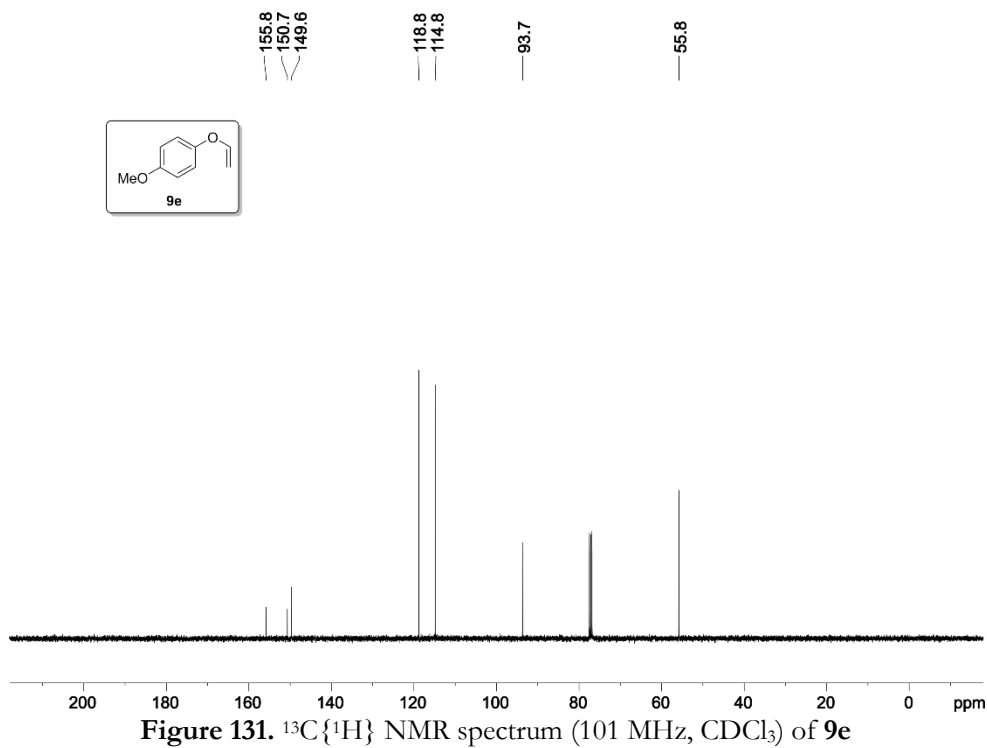


Figure 131.  $^{13}\text{C}\{^1\text{H}\}$  NMR spectrum (101 MHz,  $\text{CDCl}_3$ ) of **9e**

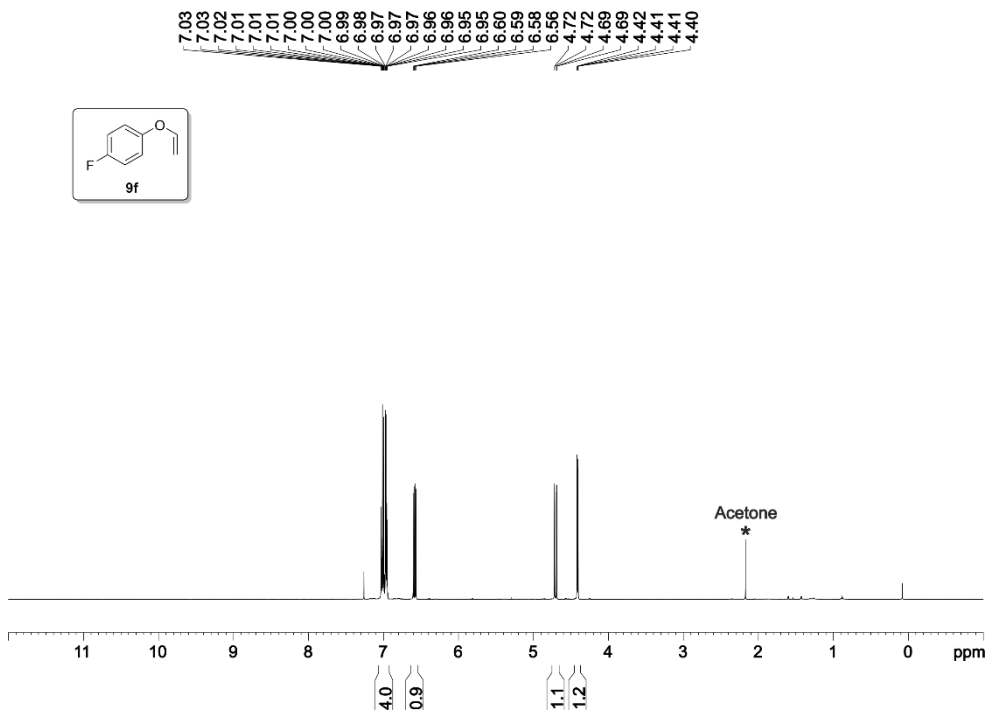


Figure 132. <sup>1</sup>H NMR spectrum (500 MHz, CDCl<sub>3</sub>) of 9f

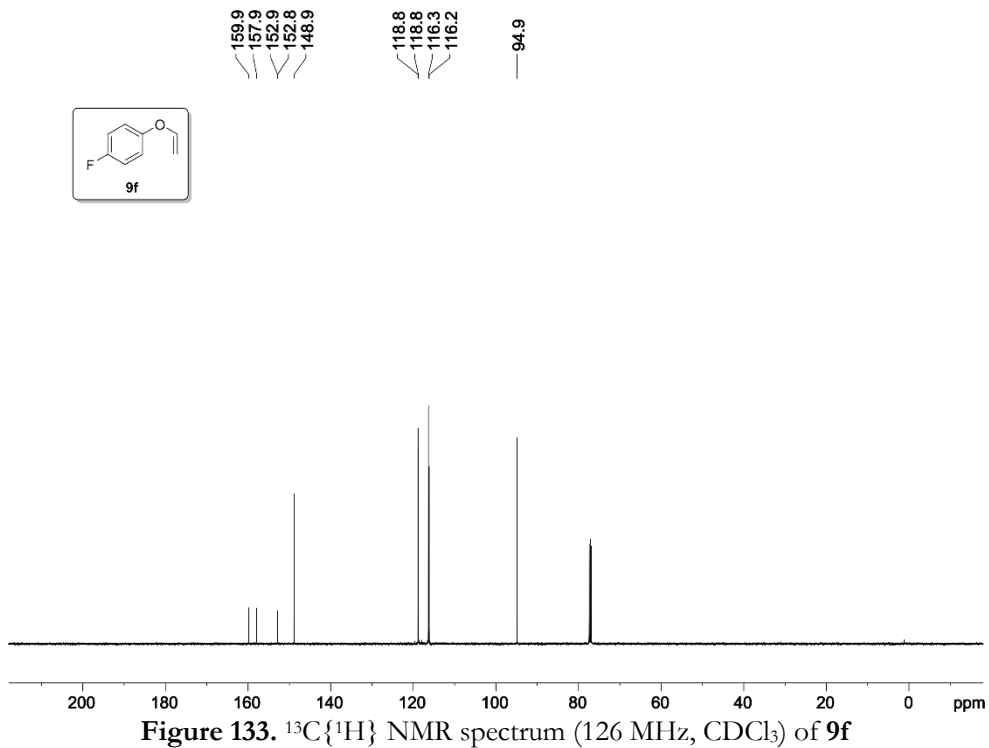


Figure 133. <sup>13</sup>C{<sup>1</sup>H} NMR spectrum (126 MHz, CDCl<sub>3</sub>) of 9f



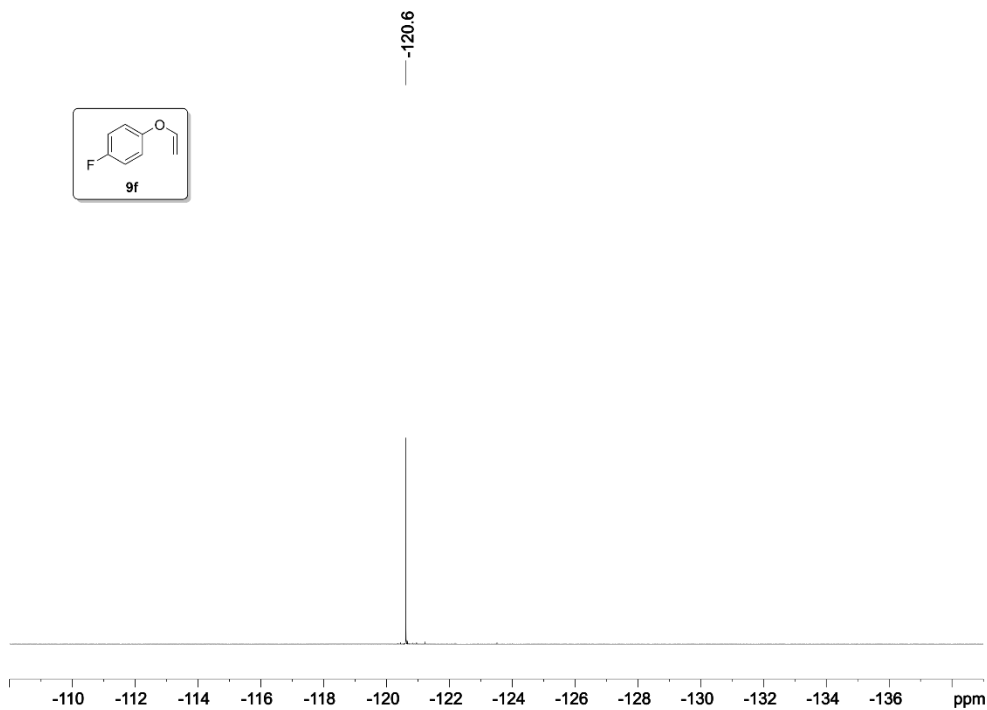


Figure 134.  $^{19}\text{F}\{^1\text{H}\}$  NMR spectrum (471 MHz,  $\text{CDCl}_3$ ) of 9f

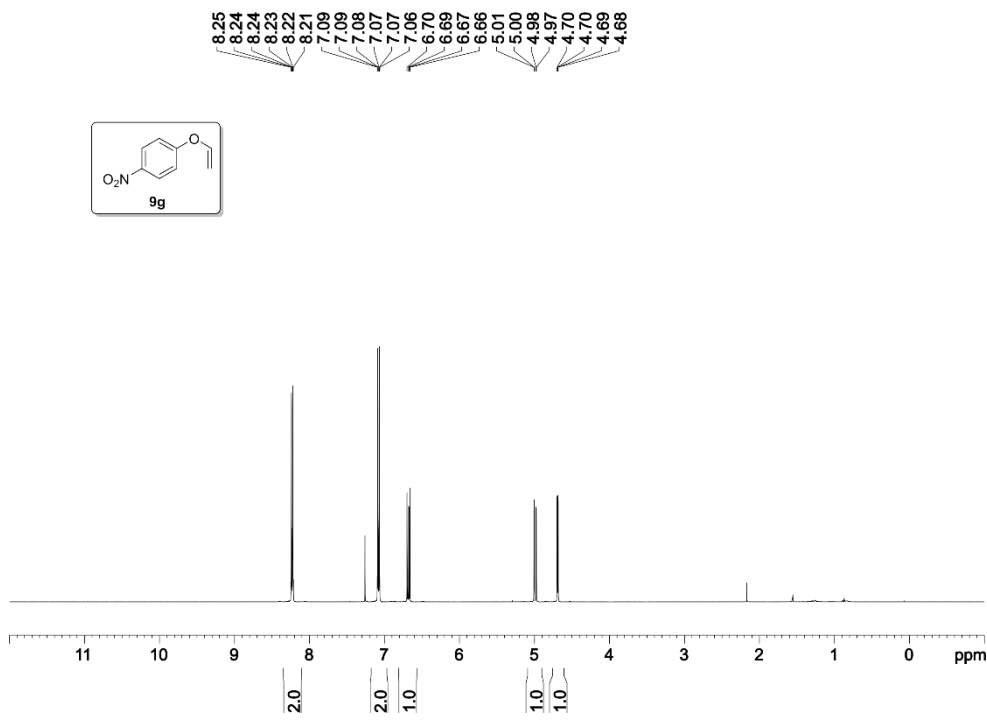
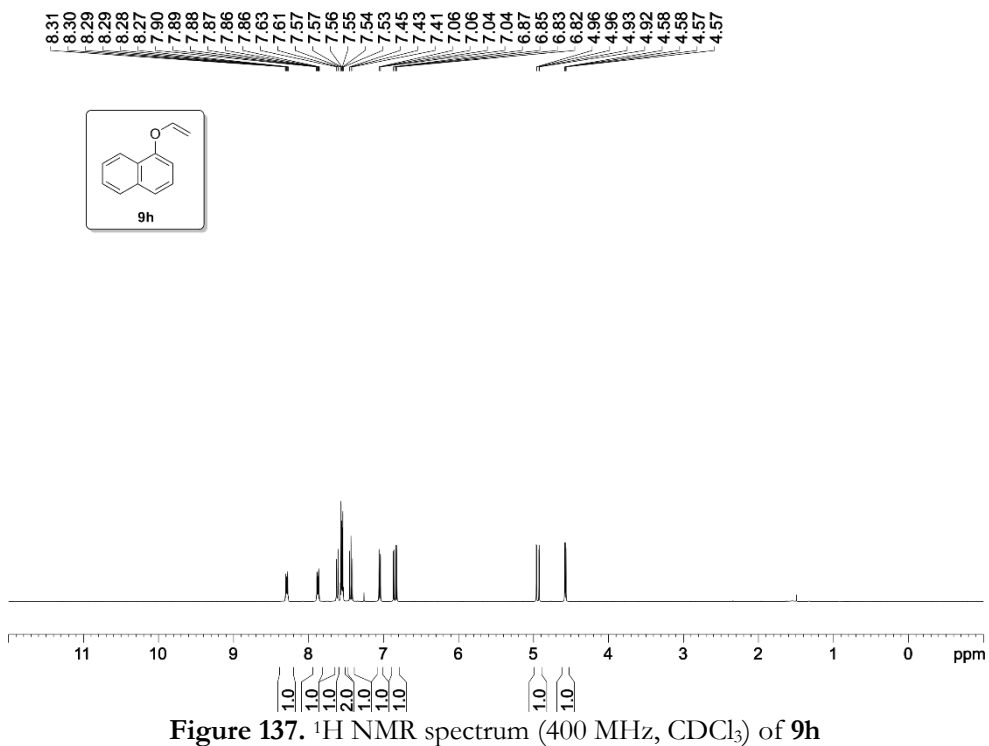
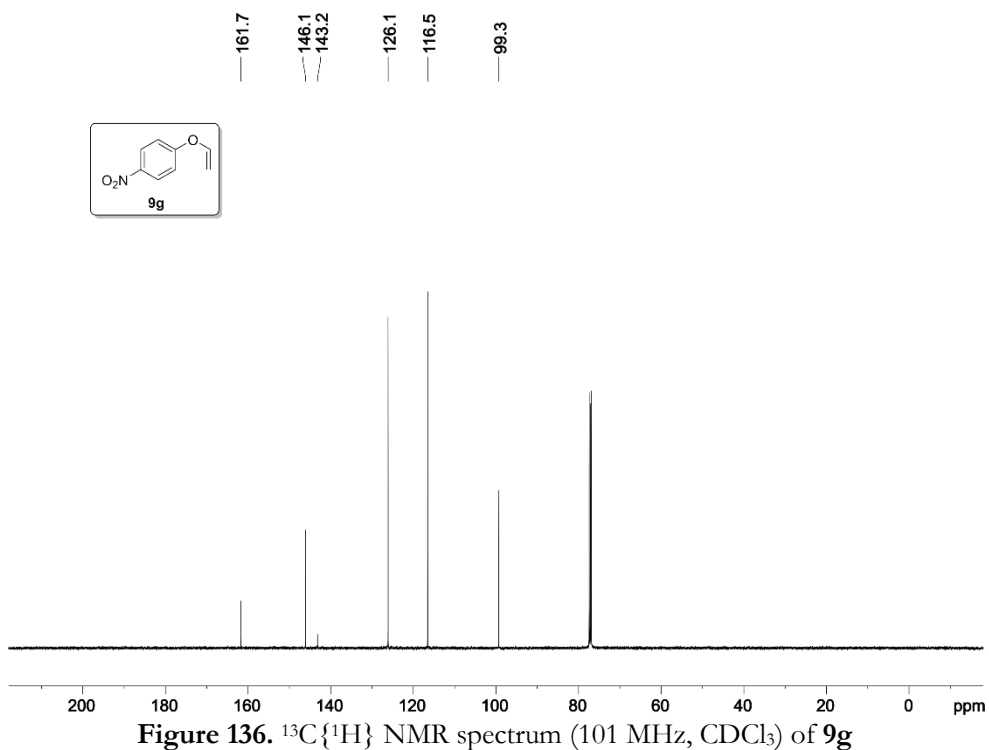
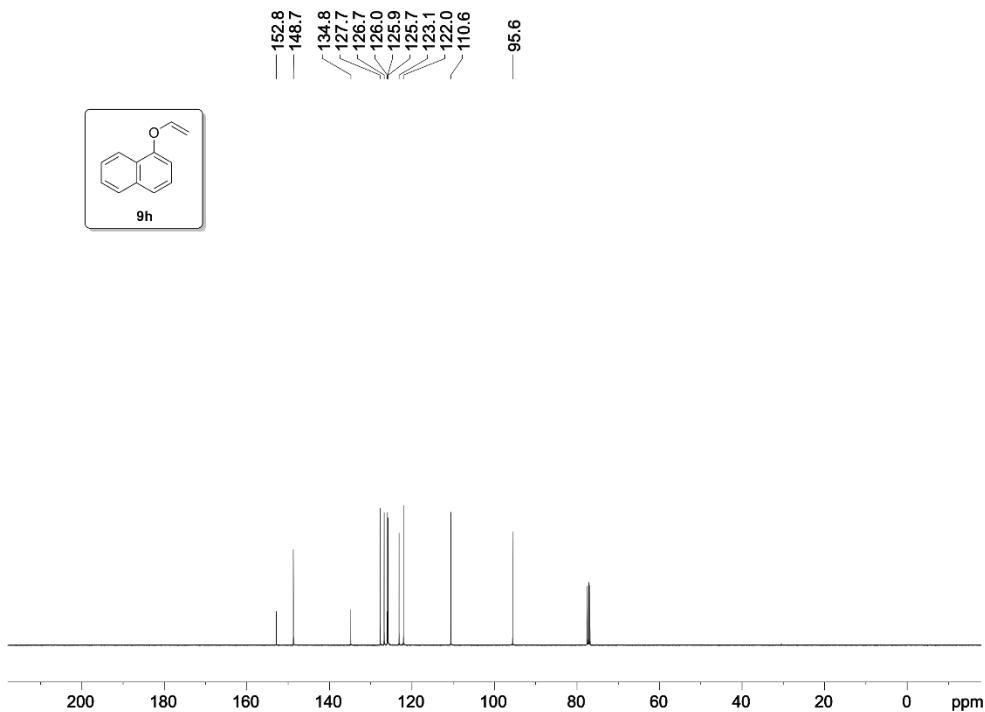
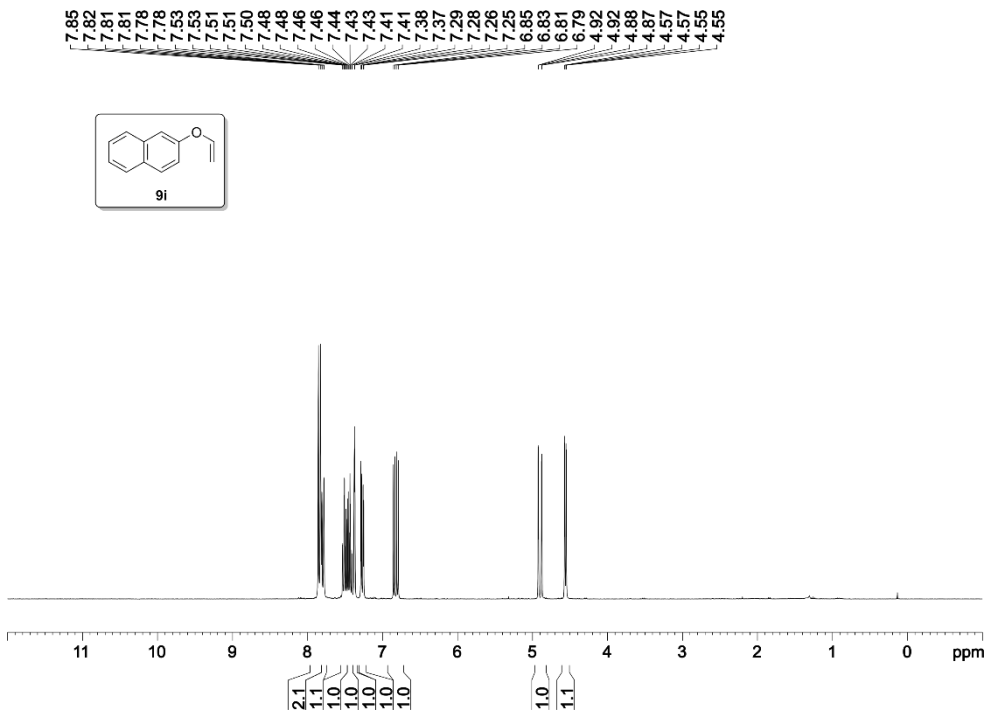


Figure 135.  $^1\text{H}$  NMR spectrum (500 MHz,  $\text{CDCl}_3$ ) of 9g



Figure 138.  $^{13}\text{C}\{^1\text{H}\}$  NMR spectrum (101 MHz,  $\text{CDCl}_3$ ) of **9h**Figure 139.  $^1\text{H}$  NMR spectrum (300 MHz,  $\text{CDCl}_3$ ) of **9i**

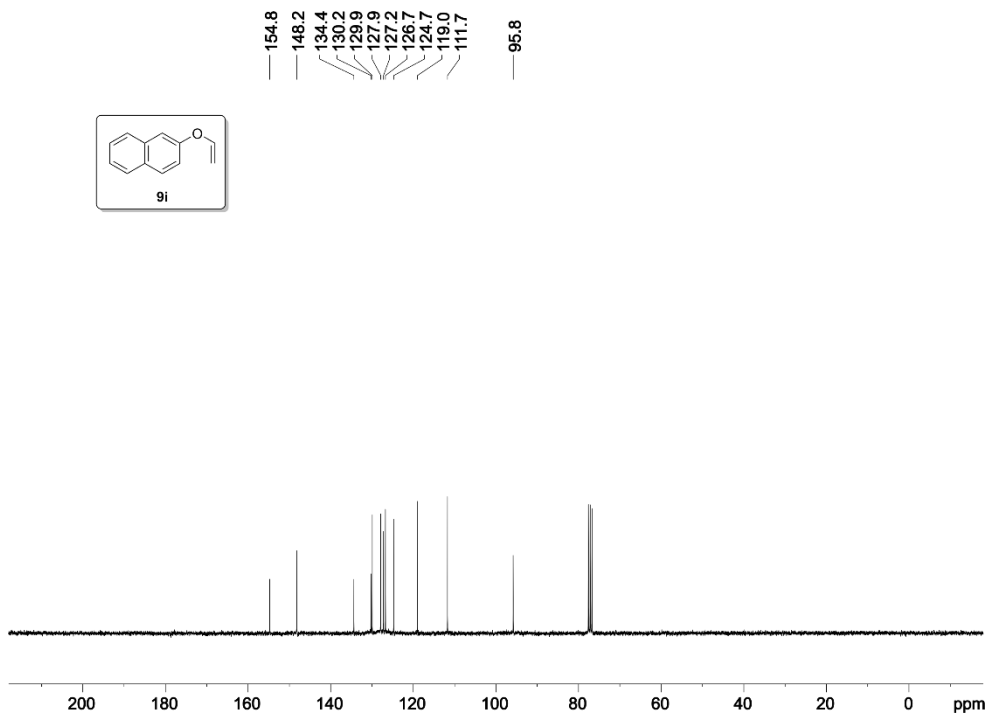


Figure 140.  $^{13}\text{C}\{^1\text{H}\}$  NMR spectrum (75 MHz,  $\text{CDCl}_3$ ) of **9i**

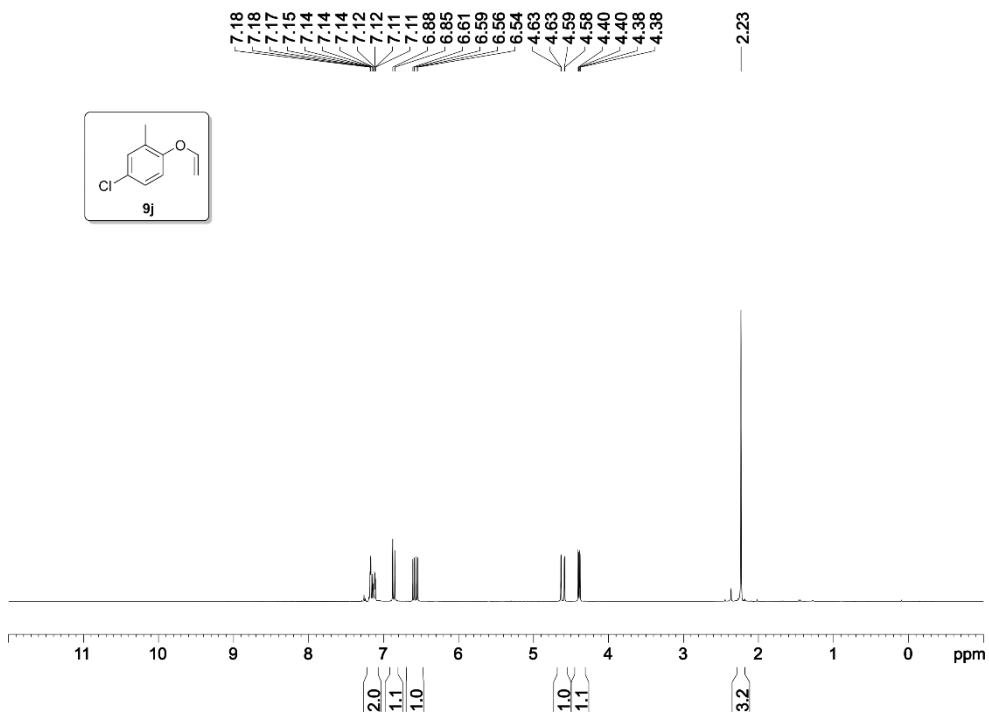


Figure 141.  $^1\text{H}$  NMR spectrum (300 MHz,  $\text{CDCl}_3$ ) of **9j**

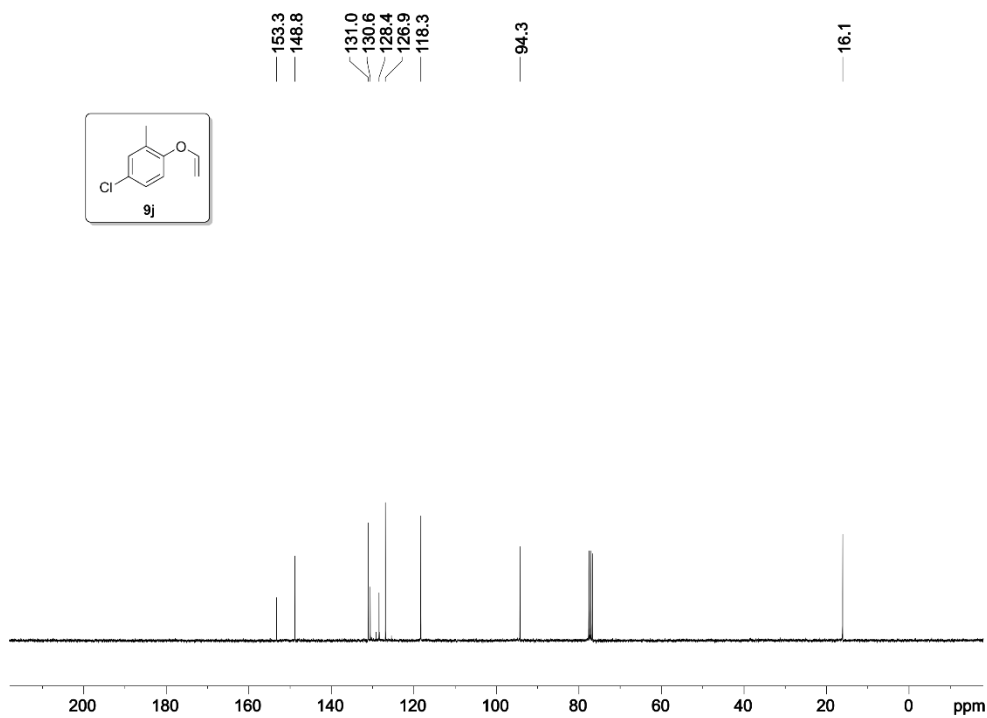


Figure 142.  $^{13}\text{C}\{^1\text{H}\}$  NMR spectrum (75 MHz,  $\text{CDCl}_3$ ) of 9j

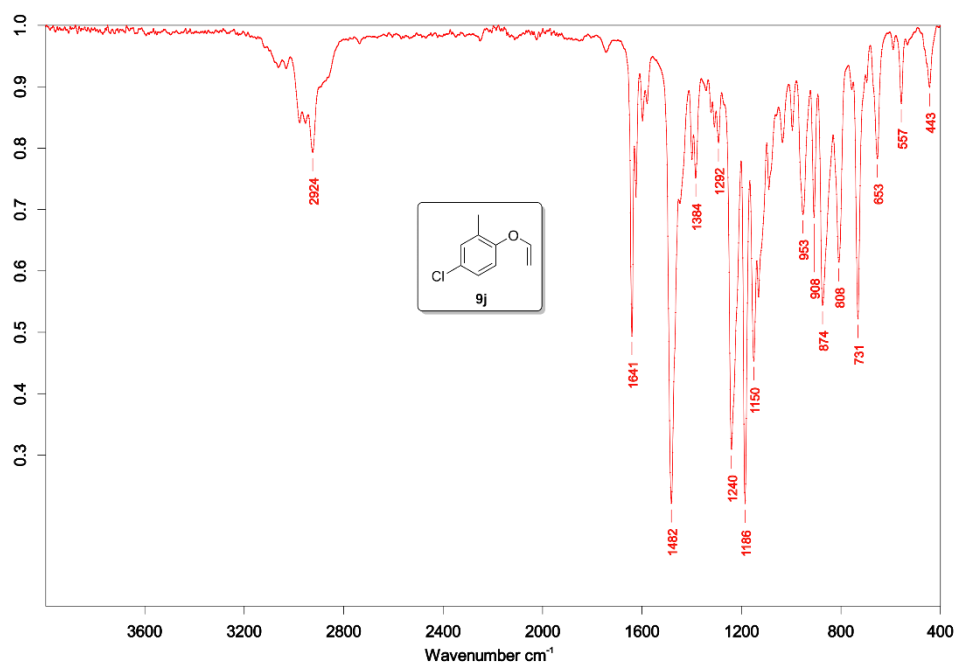


Figure 143. IR spectrum of 9j

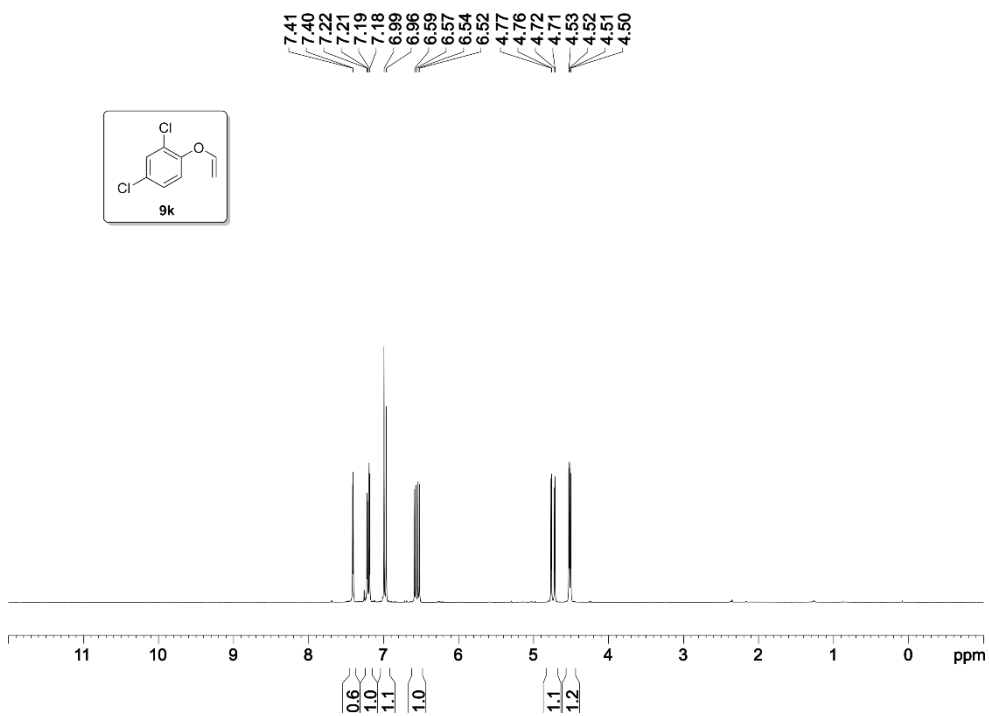


Figure 144.  $^1\text{H}$  NMR spectrum (300 MHz,  $\text{CDCl}_3$ ) of 9k

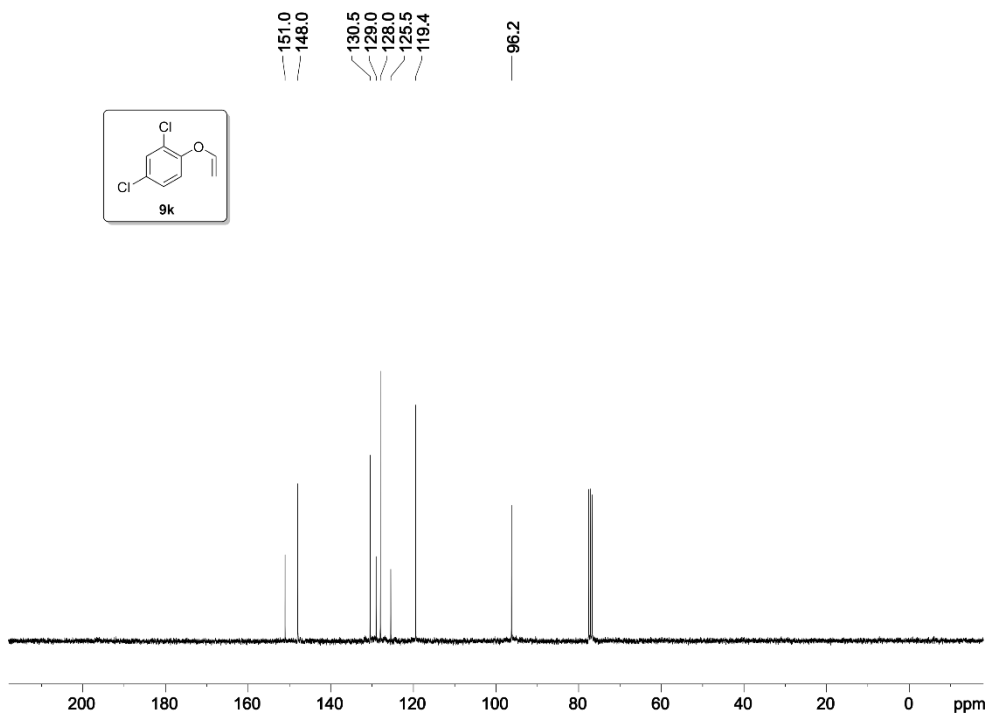
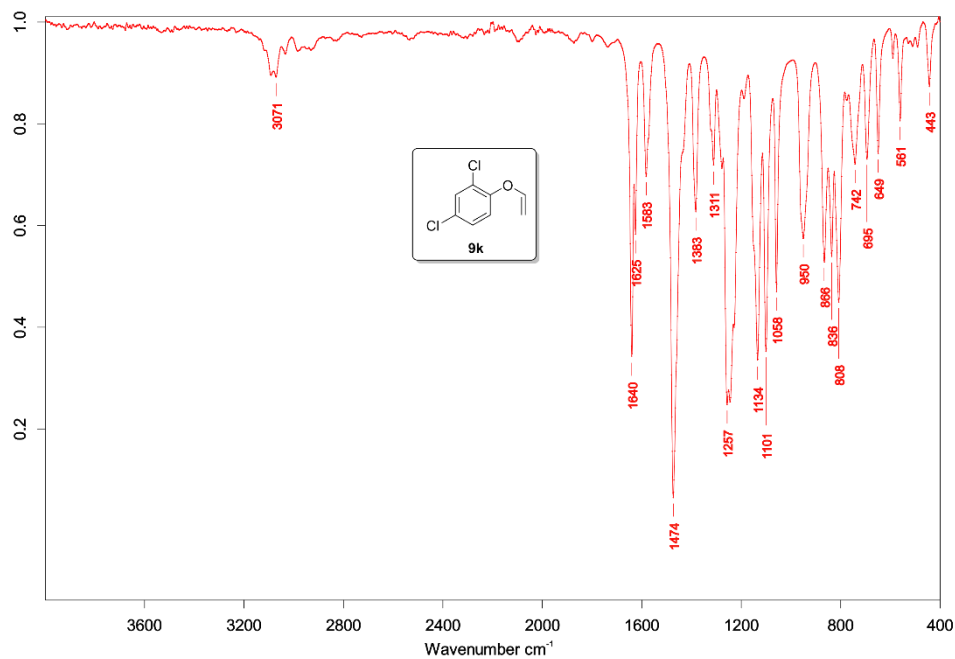
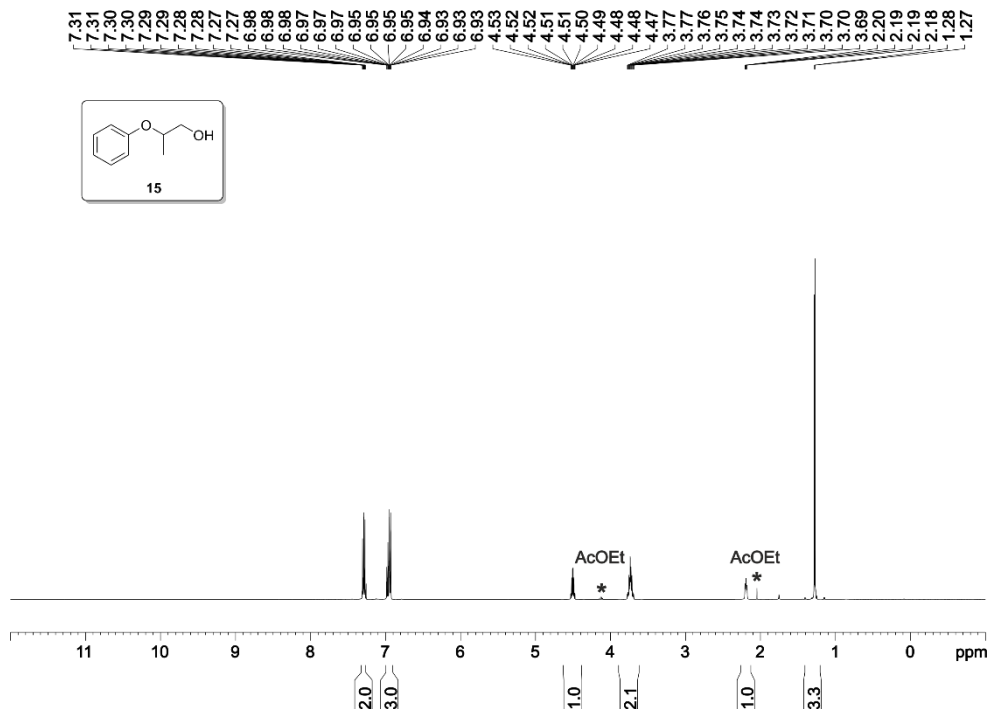


Figure 145.  $^{13}\text{C}\{^1\text{H}\}$  NMR spectrum (101 MHz,  $\text{CDCl}_3$ ) of 9k

Figure 146. IR spectrum of **9k**Figure 147.  $^1\text{H}$  NMR spectrum (500 MHz,  $\text{CDCl}_3$ ) of **15**

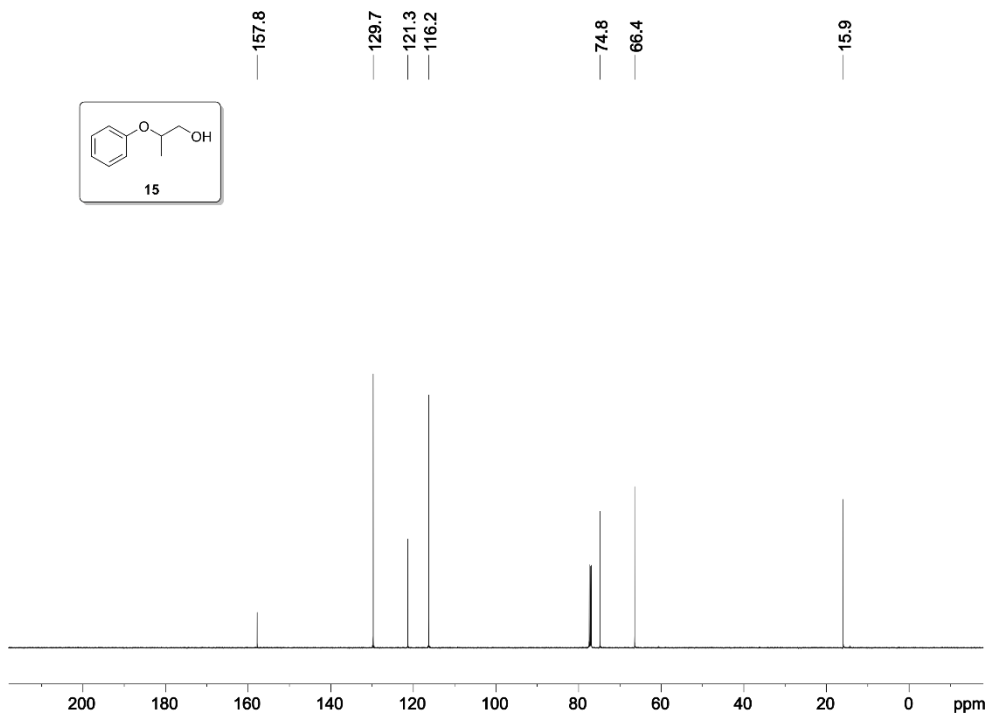


Figure 148.  $^{13}\text{C}\{^1\text{H}\}$  NMR spectrum (101 MHz,  $\text{CDCl}_3$ ) of **15**

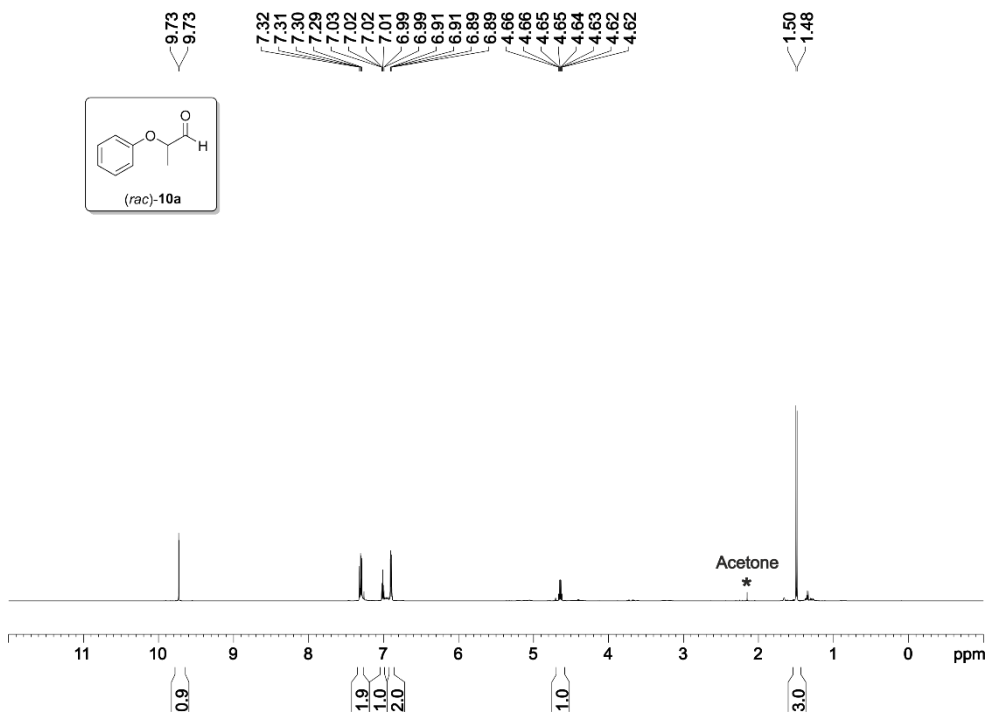


Figure 149.  $^1\text{H}$  NMR spectrum (500 MHz,  $\text{CDCl}_3$ ) of **(rac)-10a**



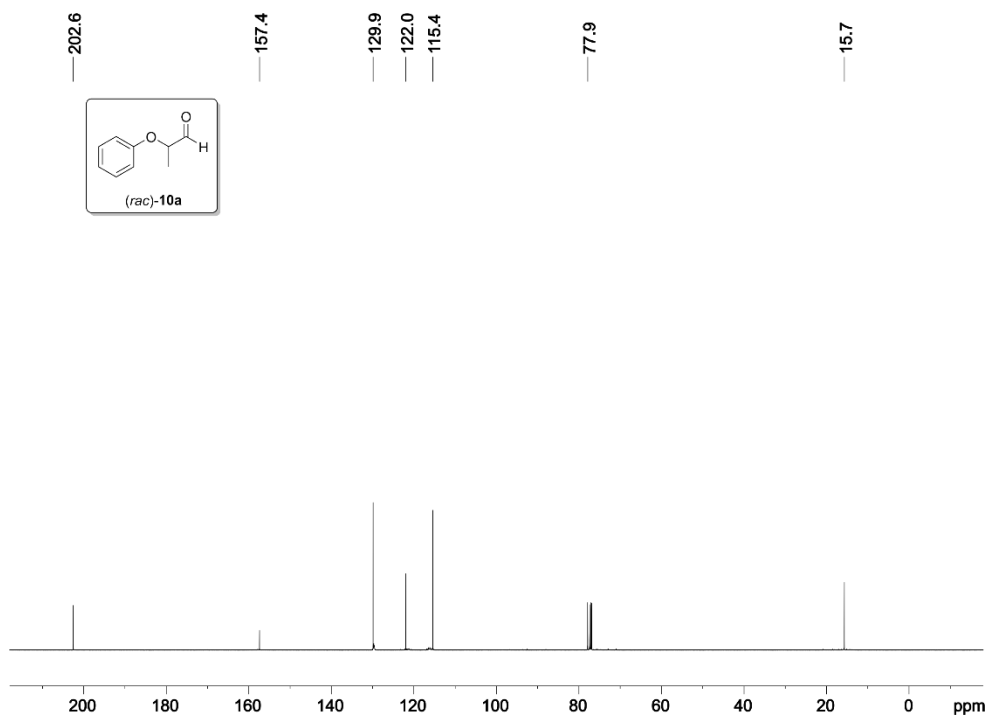


Figure 150.  $^{13}\text{C}\{^1\text{H}\}$  NMR spectrum (126 MHz,  $\text{CDCl}_3$ ) of (rac)-10a

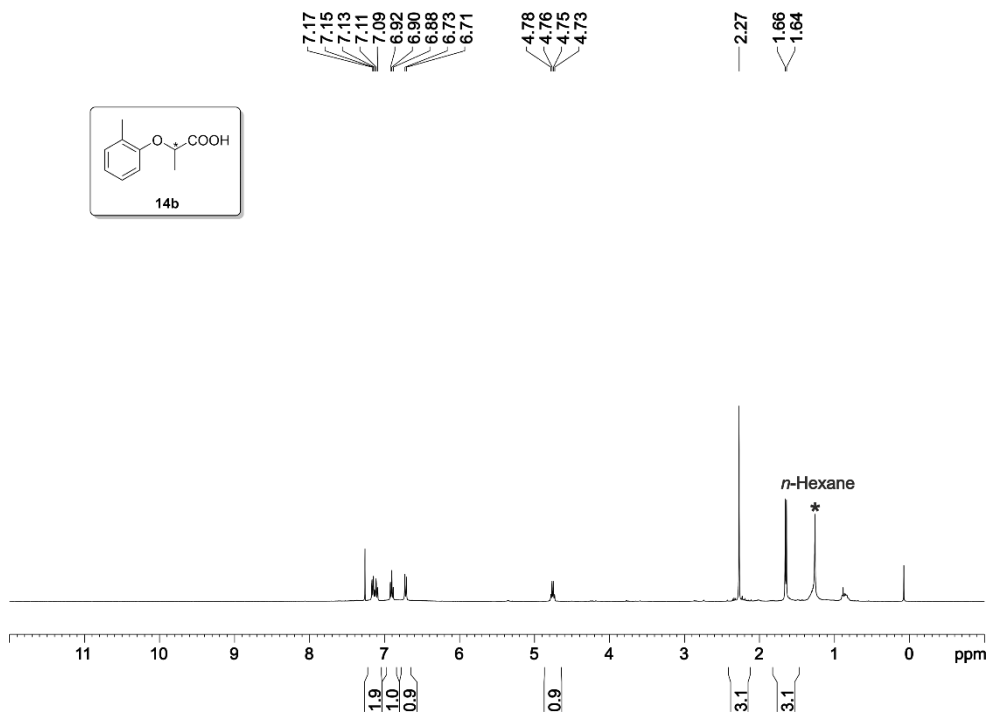


Figure 151.  $^1\text{H}$  NMR spectrum (400 MHz,  $\text{CDCl}_3$ ) of 14b

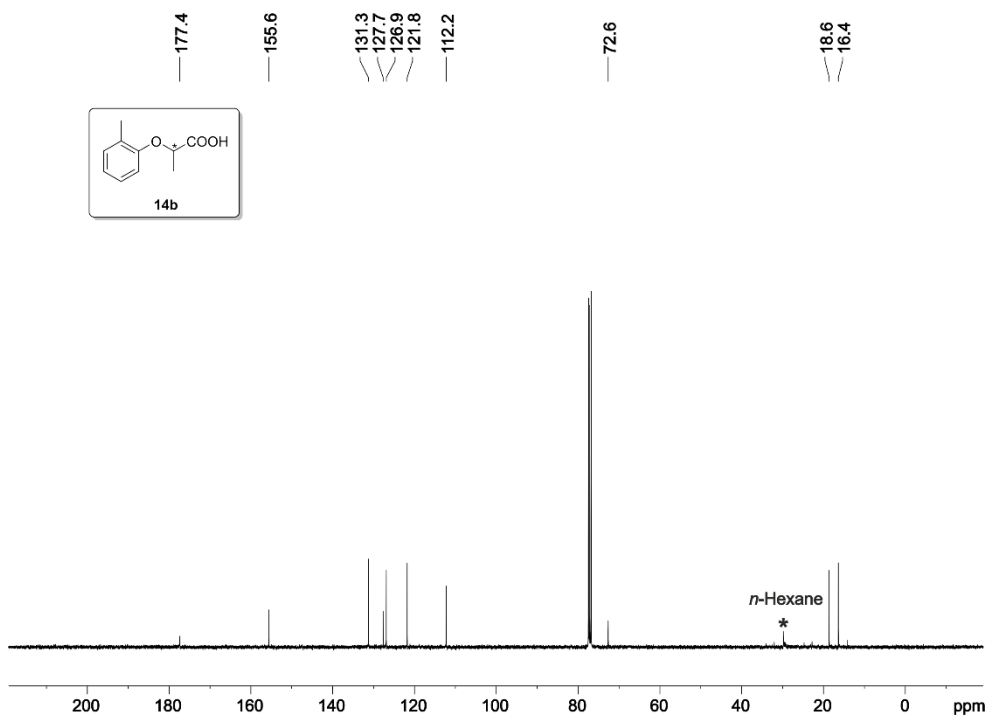


Figure 152.  $^{13}\text{C}\{^1\text{H}\}$  NMR spectrum (101 MHz,  $\text{CDCl}_3$ ) of **14b**

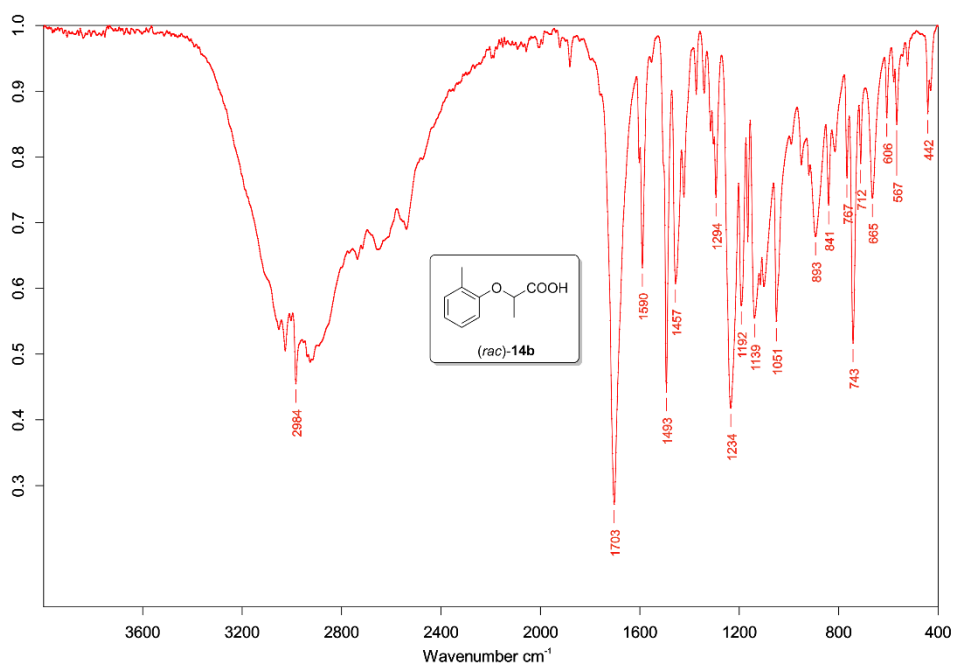


Figure 153. IR spectrum of **14b**

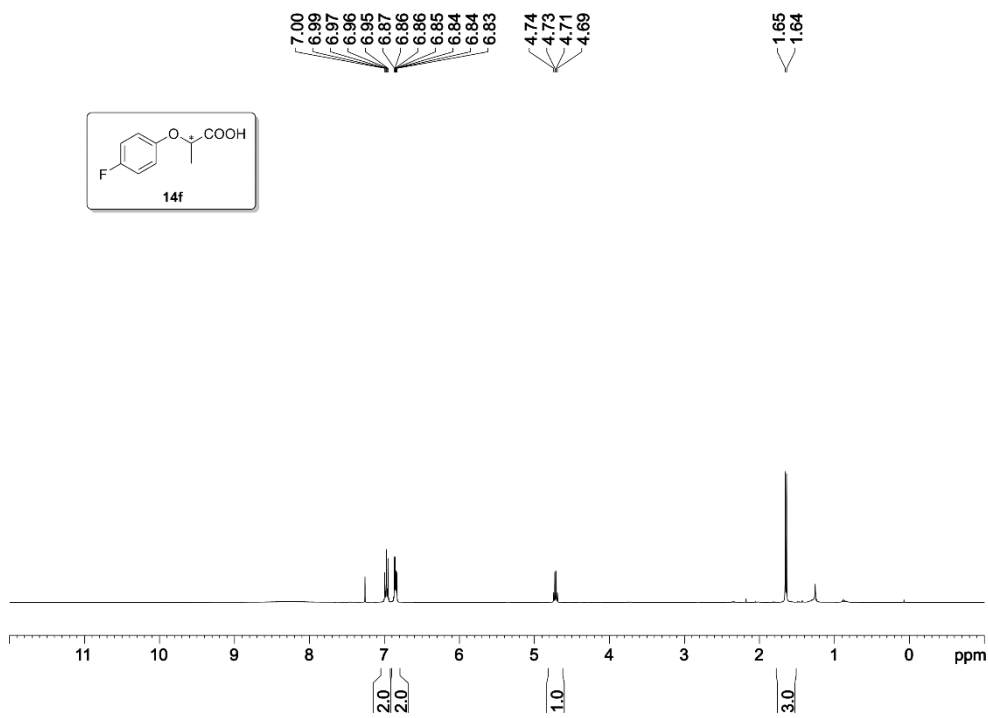


Figure 154.  $^1\text{H}$  NMR spectrum (400 MHz,  $\text{CDCl}_3$ ) of **14f**

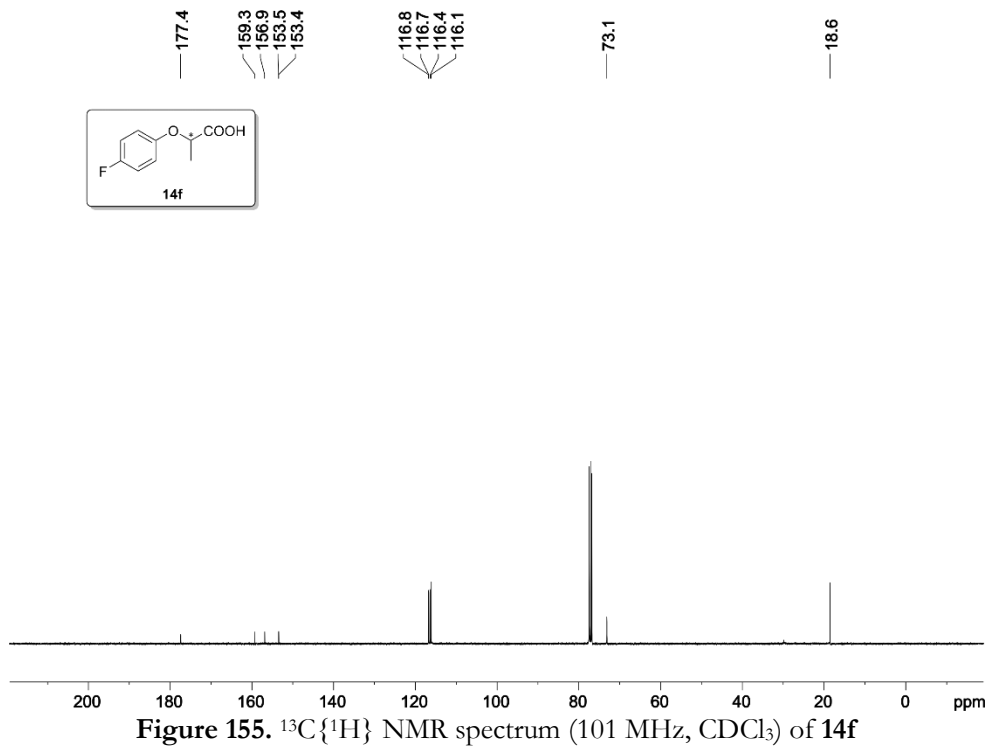


Figure 155.  $^{13}\text{C}\{^1\text{H}\}$  NMR spectrum (101 MHz,  $\text{CDCl}_3$ ) of **14f**

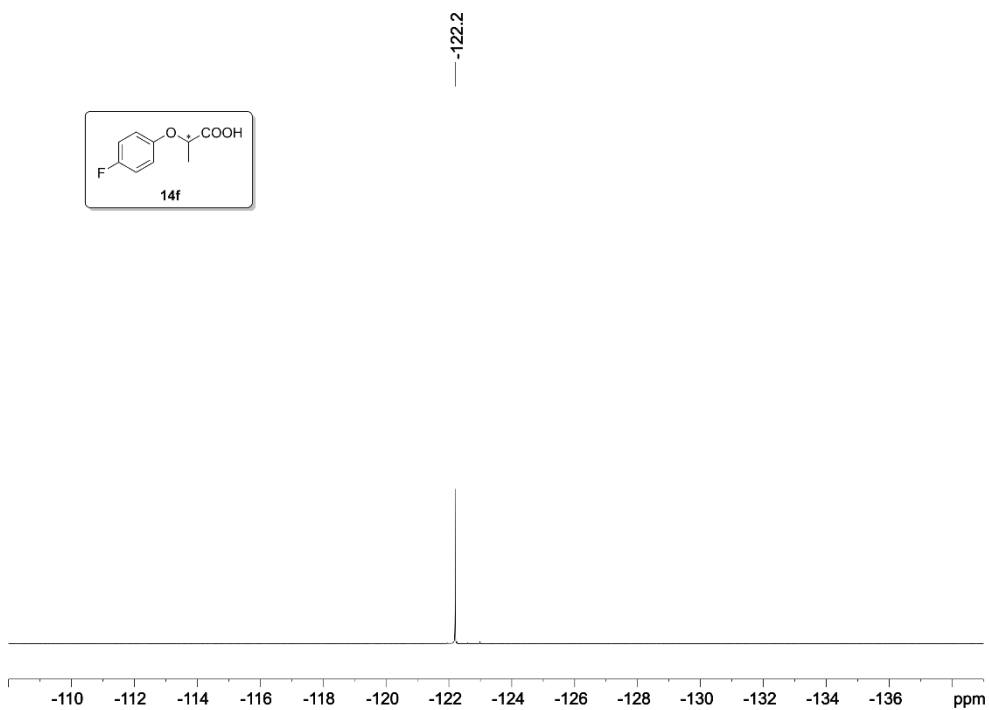


Figure 156.  $^{19}\text{F}\{^1\text{H}\}$  NMR spectrum (376 MHz,  $\text{CDCl}_3$ ) of **14f**

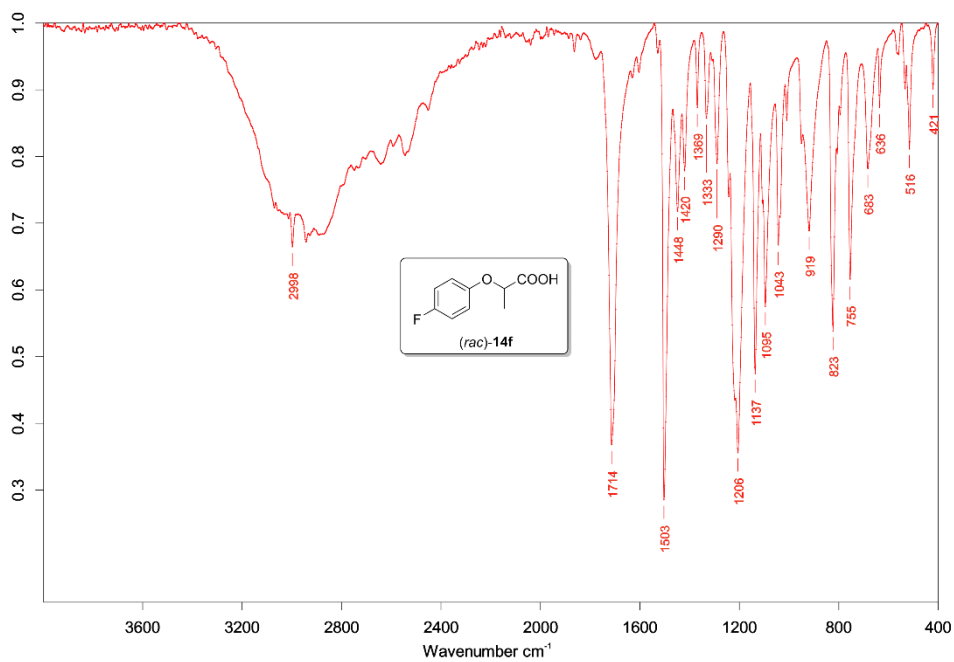
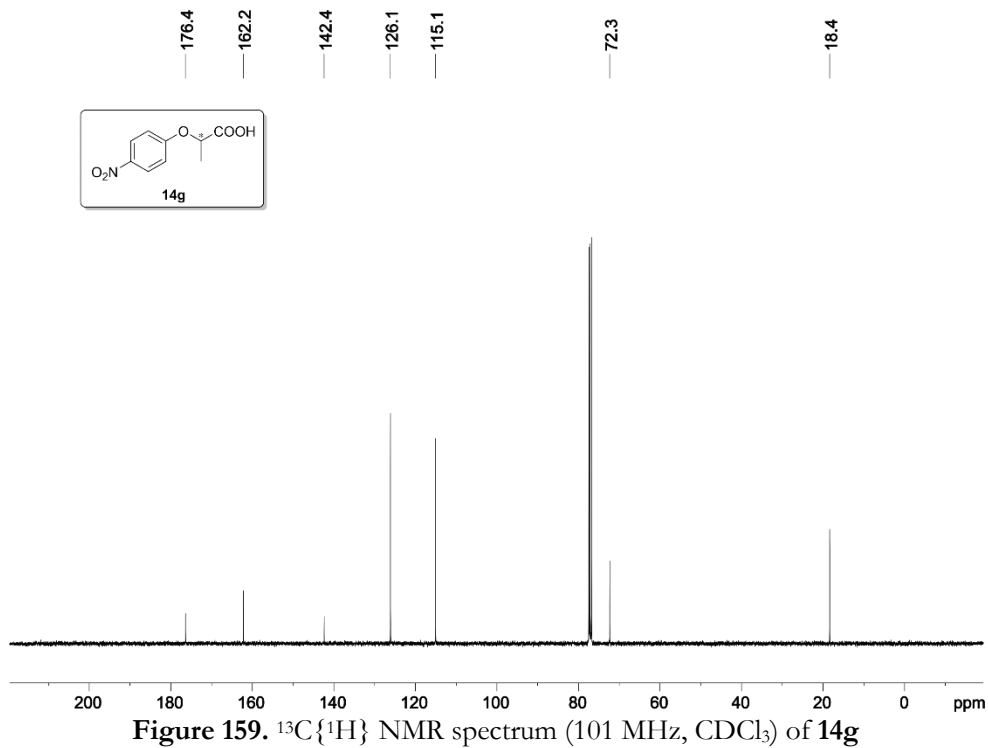
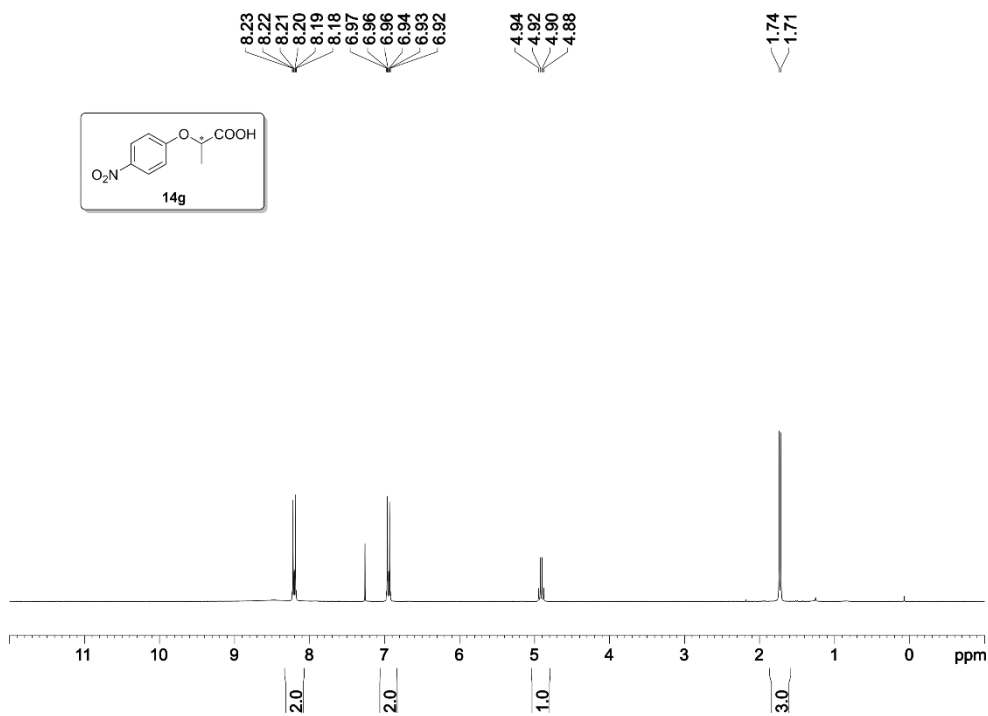
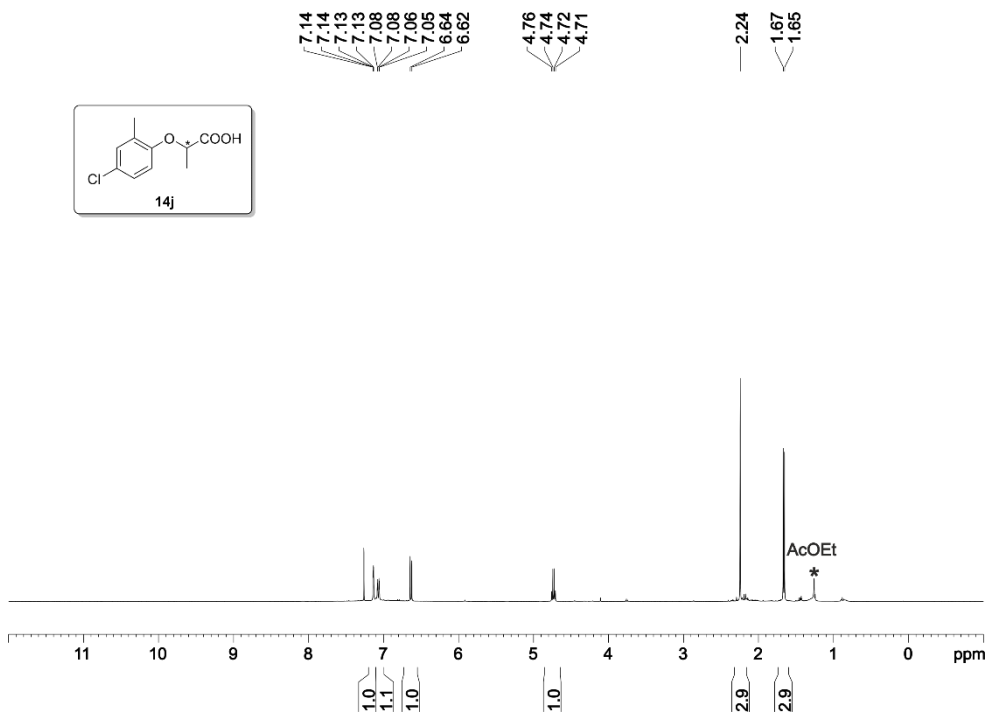
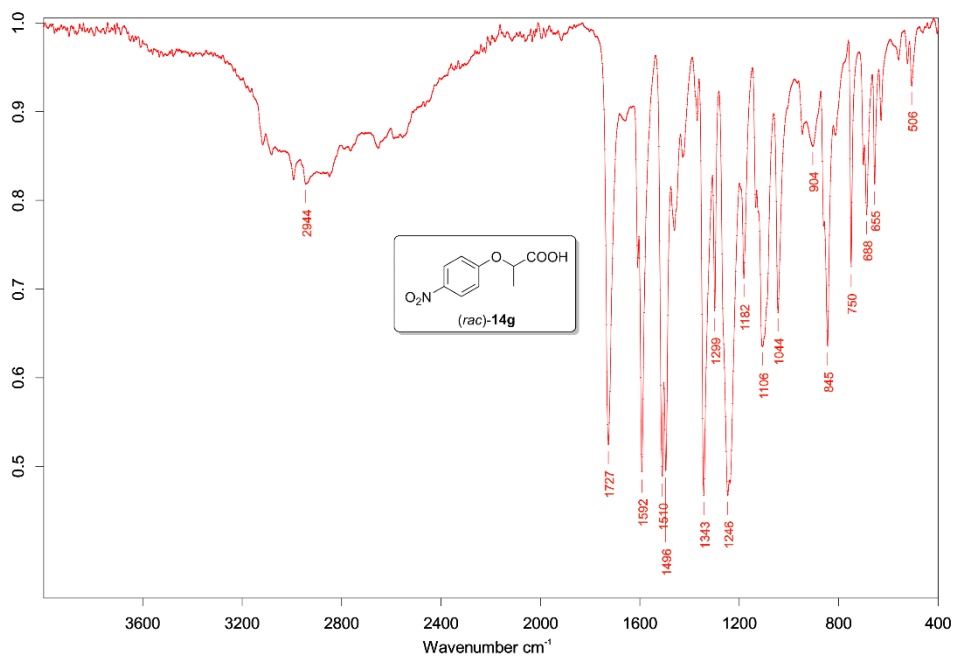
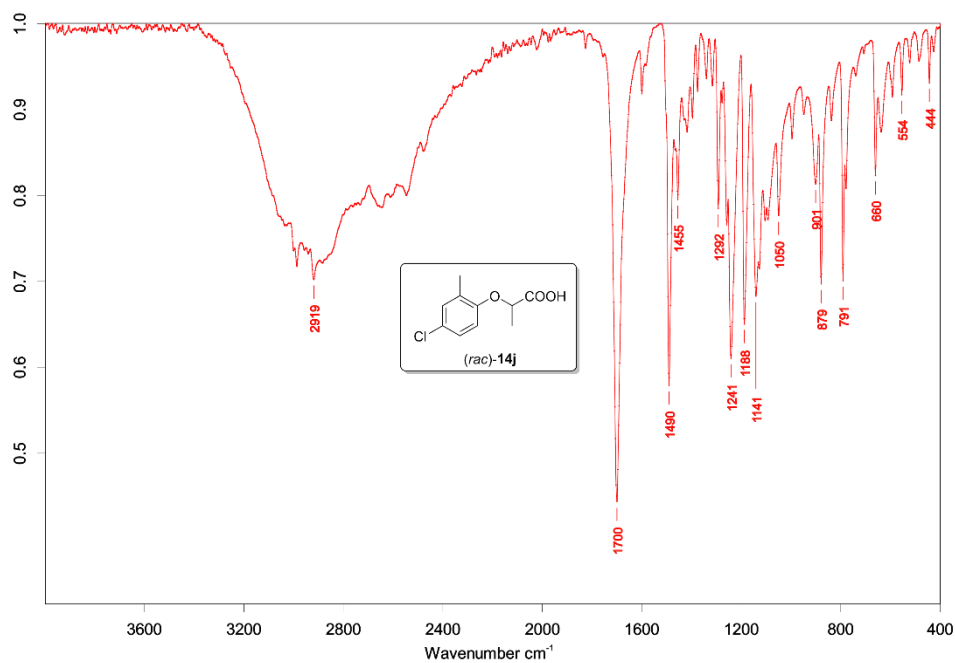
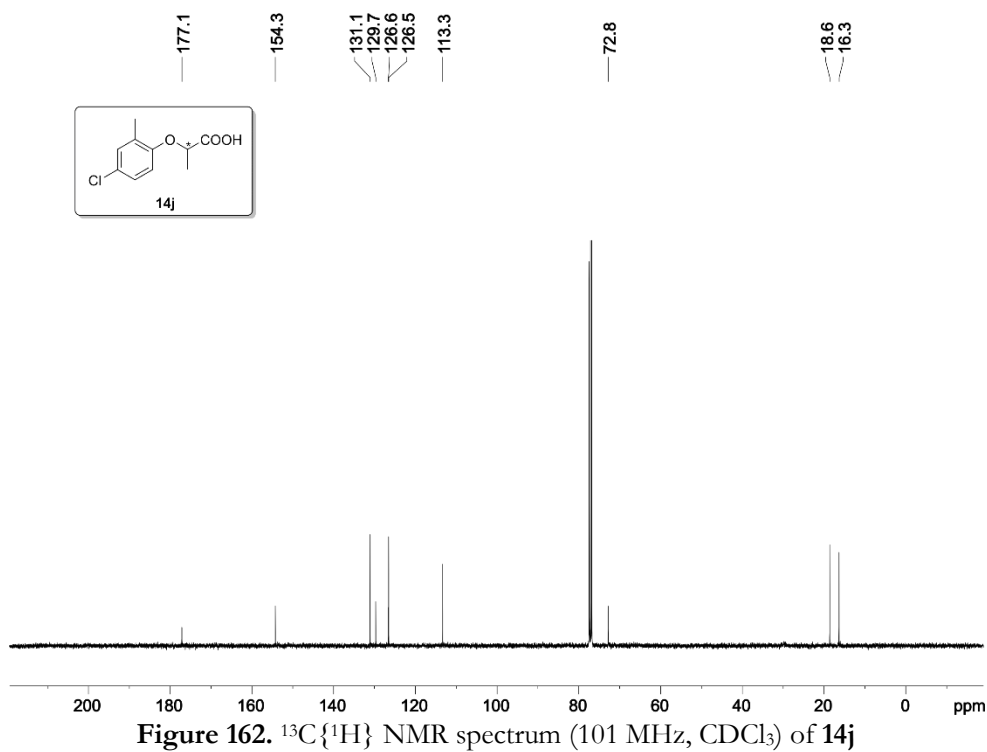
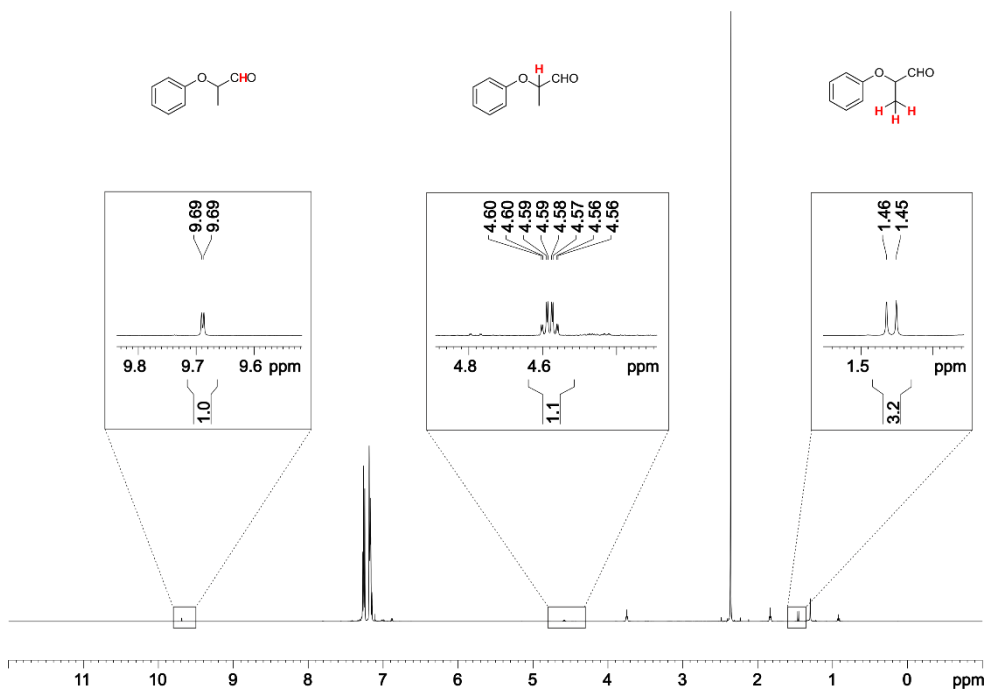


Figure 157. IR spectrum of **14f**

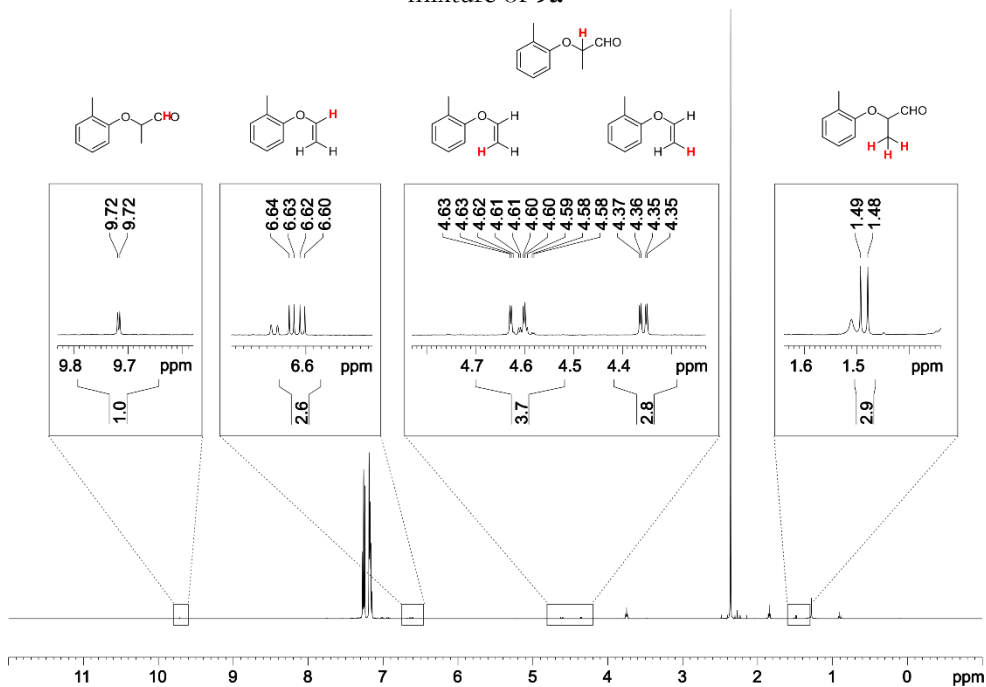






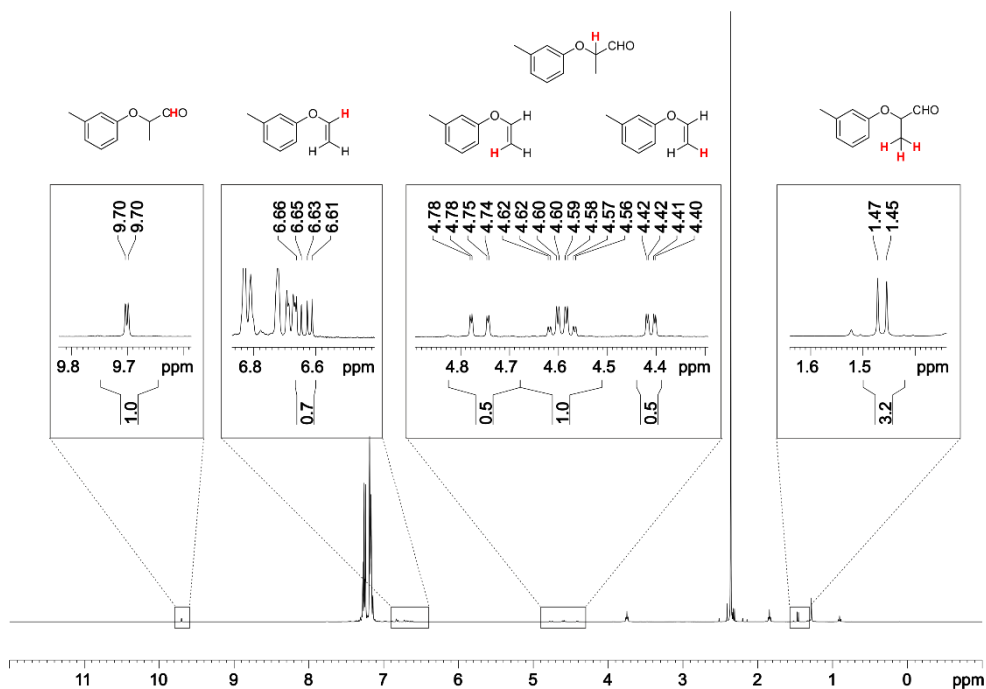


**Figure 164.**  $^1\text{H}$  NMR spectrum (500 MHz,  $\text{CDCl}_3$ ) of the hydroformylation reaction mixture of **9a**

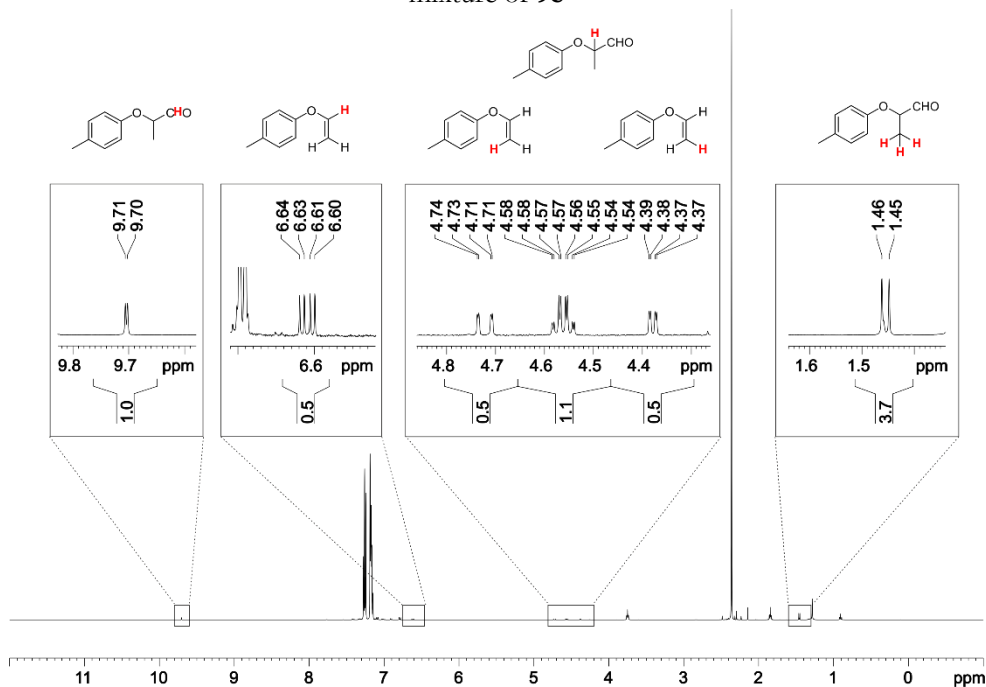


**Figure 165.**  $^1\text{H}$  NMR spectrum (500 MHz,  $\text{CDCl}_3$ ) of the hydroformylation reaction mixture of **9b**

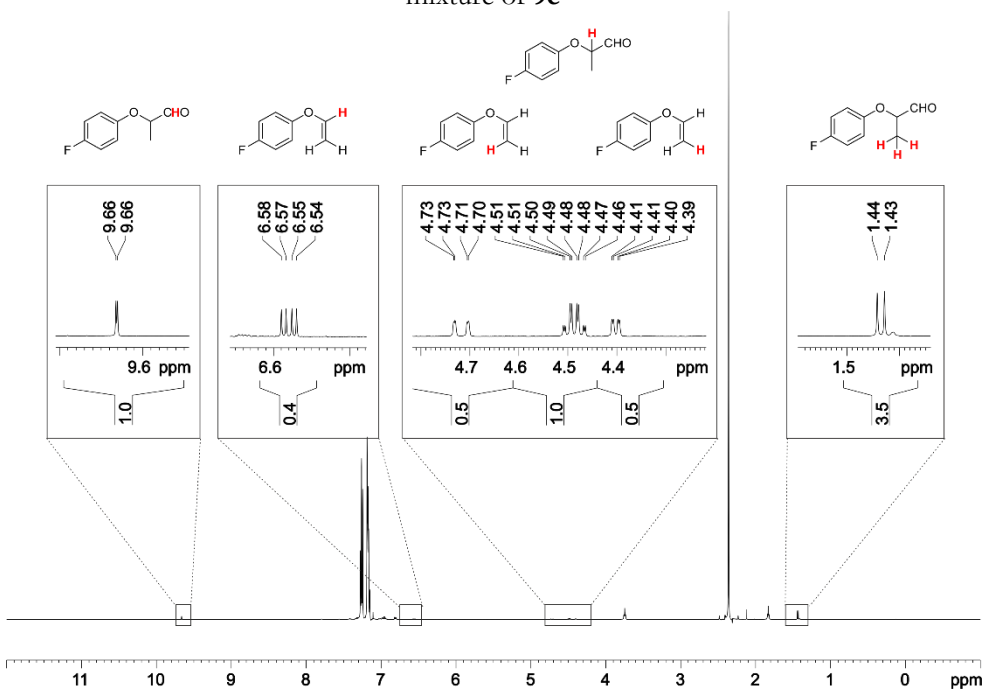
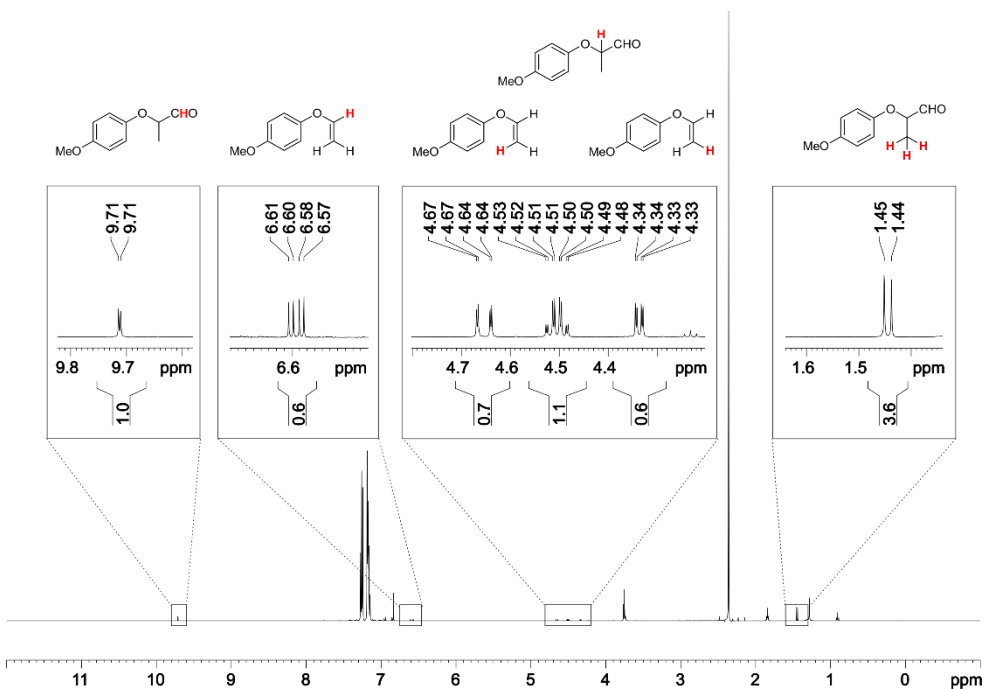




**Figure 166.**  $^1\text{H}$  NMR spectrum (400 MHz,  $\text{CDCl}_3$ ) of the hydroformylation reaction mixture of **9c**



**Figure 167.**  $^1\text{H}$  NMR spectrum (500 MHz,  $\text{CDCl}_3$ ) of the hydroformylation reaction mixture of **9d**



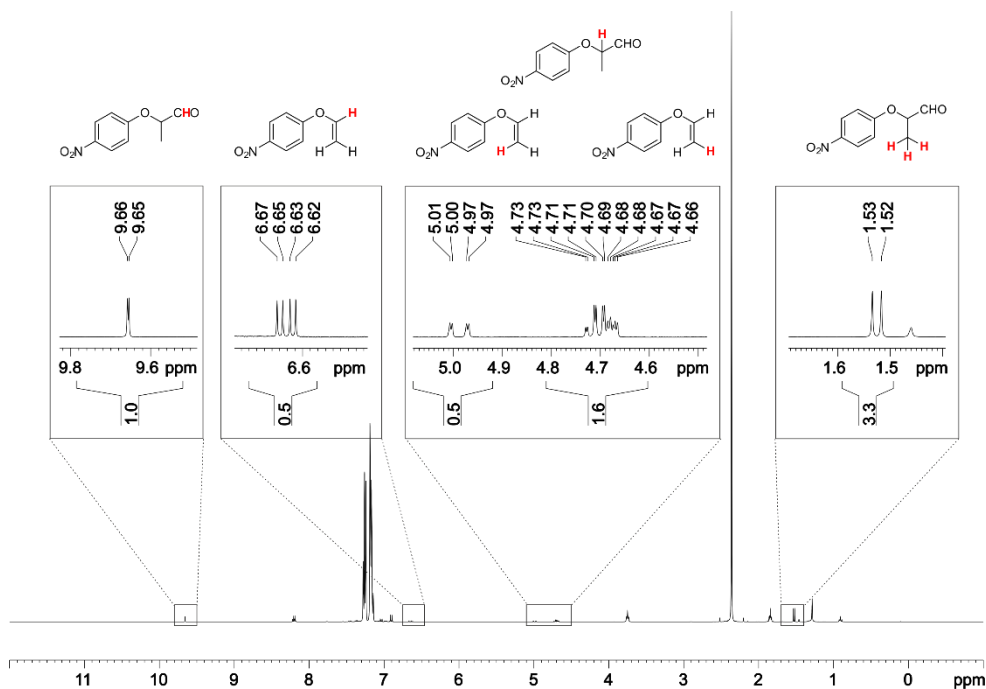


**Figure 170.**  $^1\text{H}$  NMR spectrum (400 MHz,  $\text{CDCl}_3$ ) of the hydroformylation reaction mixture of **9g**

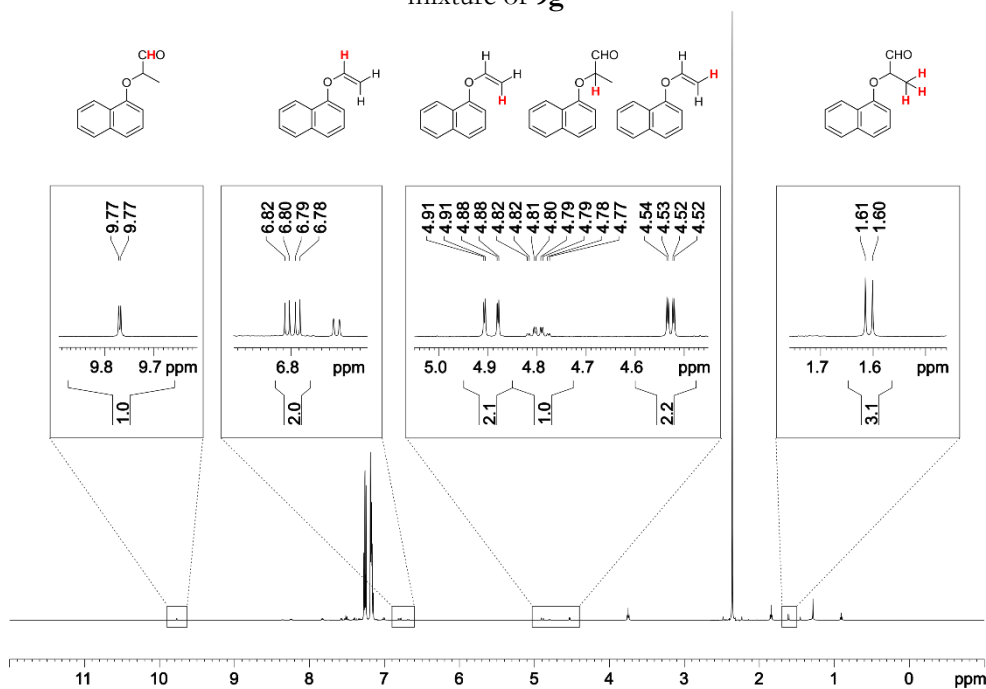


**Figure 171.**  $^1\text{H}$  NMR spectrum (500 MHz,  $\text{CDCl}_3$ ) of the hydroformylation reaction mixture of **9h**

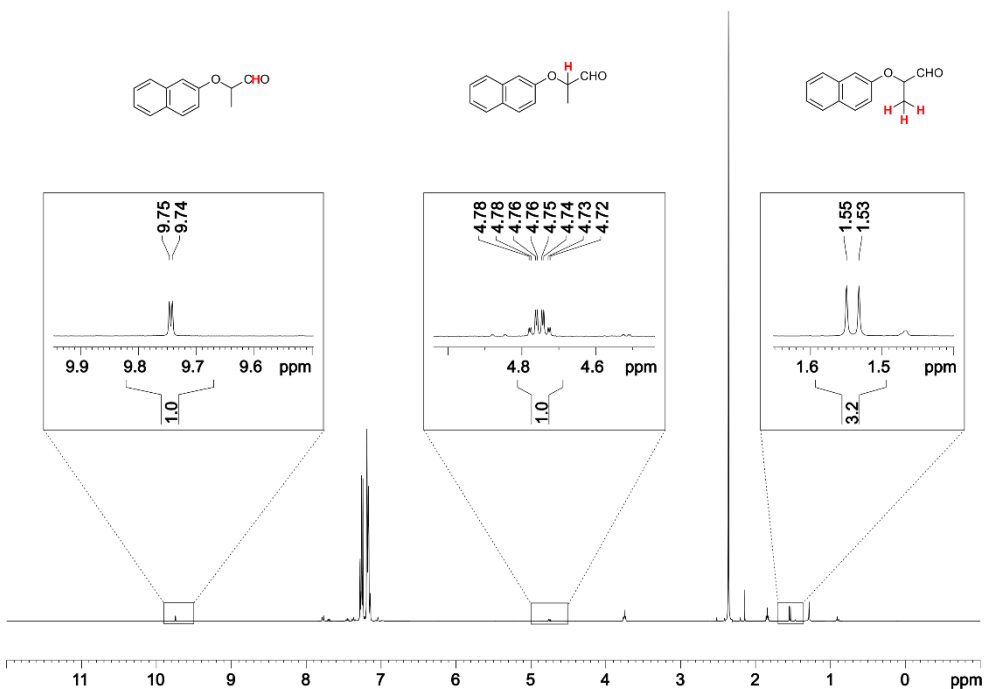


Figure 172. <sup>1</sup>H NMR spectrum (400 MHz, CDCl<sub>3</sub>) of the hydroformylation reaction mixture of 9i

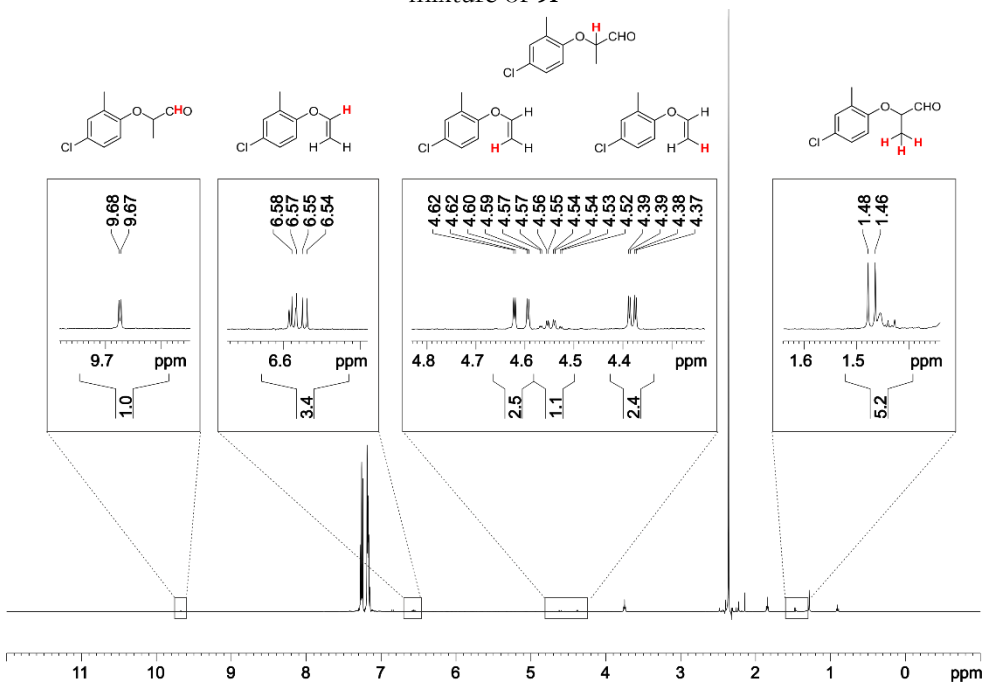
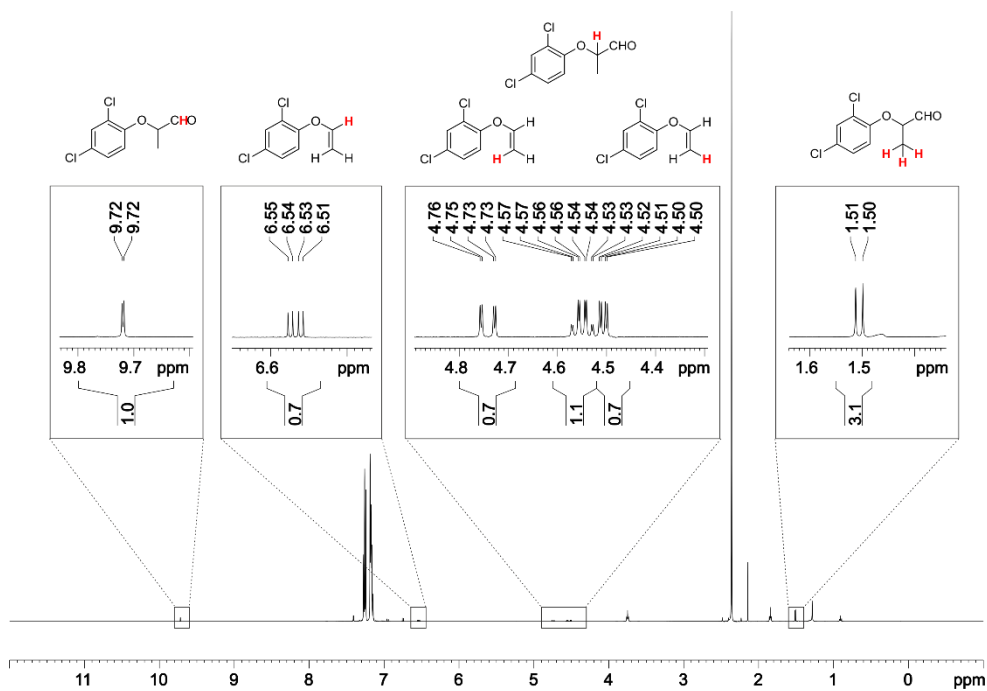


Figure 173. <sup>1</sup>H NMR spectrum (500 MHz, CDCl<sub>3</sub>) of the hydroformylation reaction mixture of 9j



**Figure 174.**  $^1\text{H}$  NMR spectrum (500 MHz,  $\text{CDCl}_3$ ) of the hydroformylation reaction mixture of **9k**

# Chapter IV

## Kinetic Treatments for Catalyst Activation Processes based on Variable Time Normalization Analysis

UNIVERSITAT ROVIRA I VIRGILI

THE HYDROFORMYLATION REACTION: FROM COVALENT TO SUPRAMOLECULAR APPROACHES AND OPERANDO KINETIC STUDIES

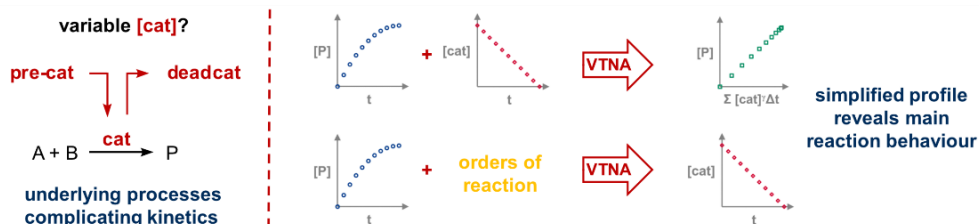
Alicia Martínez Carrión

# Kinetic Treatments for Catalyst Activation Processes based on Variable Time Normalization Analysis

*Angew. Chem. Int. Ed.* **2019**, *58*, 10189-10193

Alicia Martínez-Carrión,<sup>a,b</sup> Michael G. Howlett,<sup>c</sup> Carla Alamillo-Ferrer,<sup>c</sup> Adam D. Clayton,<sup>d</sup> Richard A. Bourne,<sup>d</sup> Anna Codina,<sup>e</sup> Anton Vidal-Ferran,<sup>b,f\*</sup> Ralph W. Adams,<sup>c\*</sup> and Jordi Burés<sup>c\*</sup>

- a Universitat Rovira i Virgili, Departament de Química Analítica i Química Orgànica, C. Marcel·lí Domingo 1, 43007, Tarragona, Spain.
- b Institut Català d'Investigació Química (ICIQ) & Barcelona Institute of Science and Technology (BIST), Av. Països Catalans 16, 43007, Tarragona, Spain.
- c School of Chemistry, The University of Manchester, Oxford Road, M13 9PL, Manchester, United Kingdom.
- d Institute of Process Research and Development, School of Chemistry & School of Chemical and Process Engineering, University of Leeds, LS2 9JT, Leeds, United Kingdom.
- e Bruker (UK) Ltd, Banner Lane, CV4 9GH, Coventry, United Kingdom.
- f Institució Catalana de Recerca i Estudis Avançats (ICREA), Pg. Lluís Companys 23, 08010, Barcelona, Spain.





## 4.1 ABSTRACT

Reaction progress analysis is a useful tool for mechanistic and kinetic elucidations. In high-pressure reactions, there are few examples of HP-NMR setups that allow for reaction monitoring. We have designed and developed a high-pressure flow NMR setup based on a commercially available probe for the continuous analysis of a reaction mixture under pressure. Progress reaction profiles are affected by catalyst activation processes occurring alongside the main reaction. These processes complicate the kinetic analysis of reactions, often directing researchers toward incorrect conclusions. We report the application of two kinetic treatments, based on variable time normalization analysis, to reactions involving catalyst activation. The first kinetic treatment allows the removal of induction periods from kinetic profiles when the quantity of active catalyst can be measured. The second treatment allows the estimation of the activation (or deactivation) profile of the catalyst when the order of the reactants for the main reaction is known. Both treatments facilitate the kinetic analysis of these reactions and allow for the calculation of the percentages of hydrido-containing supramolecular rhodium complexes during the reaction with respect to the total amount of rhodium complexes.

## 4.2 INTRODUCTION

In homogeneous catalysis, the elucidation of the structure and/or monitoring of the concentration of active species are key for the understanding of the reaction under study. The development of instrumentation for the monitoring of the progress of a reaction is crucial for transformations carried out under non-standard conditions, such as reactions under pressure. The development of *online* high-pressure infrared (HP-IR) cells has enabled a better understanding of catalytic systems, due to the *online* monitoring of IR-active species under the specific reaction conditions involving gas-liquid mixtures. Meanwhile, analogous *online* high-pressure NMR (HP-NMR) instrumentation are underdeveloped, and the available designs suffer from gas bubbles in solution,<sup>1</sup> affecting the NMR lineshape due to the inhomogeneity of the solution under study or requiring sophisticated instrumentation setups.<sup>2</sup> Flow NMR techniques have emerged as a

---

<sup>1</sup> (a) Iggo, J. A.; Shirley, D.; Tong, N. C. *New J. Chem.* **1998**, 22, 1043-1045. (b) Selent, D.; Baumann, W.; Börner, A. DE10333143A1, **2005**.

<sup>2</sup> Beach, N. J.; Knapp, S. M. M.; Landis, C. R. *Rev. Sci. Instrum.* **2015**, 86, 104101-104109.

useful approach for monitoring diverse reaction mixtures.<sup>3</sup> During the writing of this thesis, Hintermair *et al.* have applied flow NMR techniques for the kinetic studies of the rhodium-catalyzed hydroformylation of hex-1-ene with PPh<sub>3</sub> as ligand, showing the potential of flow NMR for the elucidation of catalytic intermediates in high-pressure reactions.<sup>3d</sup> Herein we describe an experimental setup for the monitoring of hydroformylation reaction mixtures under high-pressure employing a commercially available NMR Flow Probe.

Processes of catalyst activation and deactivation occur at the same time as the main reaction.<sup>4</sup> As a consequence, the concentration of active catalyst<sup>5</sup> varies throughout the course of the reaction, affecting the reaction's intrinsic kinetic profile. This perturbation of the kinetic profile adds a layer of complexity to its analysis. Often, this complication limits the quantitative kinetic analysis to those sections of the reaction with no significant variation of catalyst concentration. Herein, we describe two treatments that facilitate a quantitative analysis of reactions involving catalyst activation. One or other of these treatments can be used, depending on the available information. We show the feasibility of both methods in the kinetic analysis of a real reaction with changes of active catalyst concentration during the course of a hydroformylation reaction catalyzed by a supramolecular rhodium complex.<sup>6</sup>

The two kinetic treatments presented herein are based on the recently described Variable Time Normalization Analysis (VTNA).<sup>7</sup> This analysis allows for the removal of the kinetic effects of any component of a reaction from the temporal concentration profiles. Therefore, if both the concentration of active catalyst and the progress of the reaction can be measured simultaneously by any appropriate method, then the intrinsic profile of the main reaction can be obtained (Scheme 44a). The resulting reaction profile of this first kinetic treatment is much simpler

---

<sup>3</sup> (a) Hall, A. M. R.; Broomfield-Tagg, R.; Camilleri, M.; Carbery, D. R.; Codina, A.; Whittaker, D. T. E.; Coombes, S.; Lowe, J. P.; Hintermair, U. *Chem. Commun.* **2018**, *54*, 30-33. (b) Buser, J. Y.; McFarland, A. D. *Chem. Commun.* **2014**, *50*, 4234-4237. (c) Buser, J. Y.; Luciani, C. V. *React. Chem. Eng.* **2018**, *3*, 442-446. (d) Bara-Estaun, A.; Lyall, C.; Lowe, J. P.; Pringle, P. G.; Kamer, P.; Franke, R.; Hintermair, U. *Faraday Discuss.* **2020**, 10.1039/c9fd00145j.

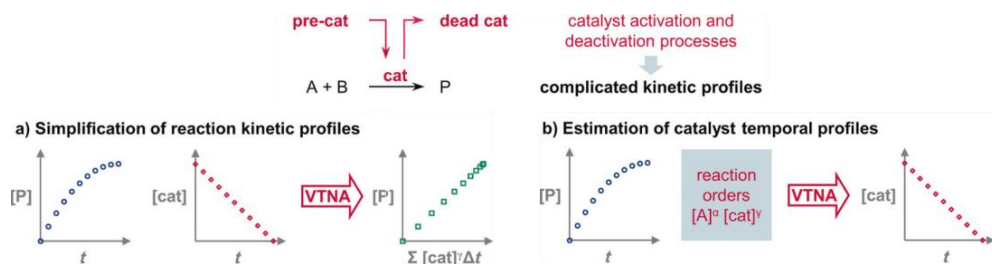
<sup>4</sup> Crabtree, R. H. *Chem. Rev.* **2015**, *115*, 127-150.

<sup>5</sup> Active catalyst refers only to on-cycle catalytic species. Therefore, the presented methods are applicable to catalytic systems regardless of the reversible or irreversible nature of the off-cycle processes.

<sup>6</sup> Vidal-Ferran, A.; Mon, I.; Bauzá, A.; Frontera, A.; Rovira, L. *Chem. - Eur. J.* **2015**, *21*, 11417-11426.

<sup>7</sup> (a) Burés, J. *Angew. Chem., Int. Ed.* **2016**, *55*, 2028-2031. (b) Burés, J. *Angew. Chem., Int. Ed.* **2016**, *55*, 16084-16087. (c) Nielsen, C. D. T.; Burés, J. *Chem. Sci.* **2019**, *10*, 348-353.

to analyze than the original profile and facilitates the extraction of mechanistic information, such as the orders of reaction or the reaction rate constant ( $k_{\text{obs}}$ ). The second kinetic treatment presented herein uses the reaction progress profile and the orders of reaction to extract the catalyst activation profile (Scheme 44b). This profile is informative of the pathways of catalyst activation (or deactivation), and their kinetics. This knowledge can help to rationally modify reaction conditions to maximize the outcome of the reaction.



**Scheme 44.** Variable Time Normalization Analysis (VTNA) as useful tool for kinetic analysis with catalyst activation (or deactivation) processes

### 4.3 RESULT AND DISCUSSION

As the hydroformylation reaction is performed in a pressurized vessel with a constant supply of syngas (if the hydroformylation is performed at constant pressure), continuous monitoring by NMR spectroscopy of the evolution of the reaction components and catalyst was challenging.<sup>8</sup> To overcome this challenge, we designed and developed a high-pressure flow NMR system. The experimental setup is shown in Figure 175. A high-pressure reactor was modified to place inlet and outlet sample transfer lines (blue lines), which permit the continuous sample circulation to the spectrometer in absence of gas bubbles. A pressurization system was designed (black lines), allowing for the reactor pressurization with inert gas ( $\text{N}_2$ ) or syngas ( $\text{H}_2/\text{CO}$  in a 1:1 ratio) and with an exhaust for reaction depressurization. To circulate the reaction mixture inside the NMR spectrometer, a Bruker InsightMR flow probe with a flow interface apparatus was used.<sup>9</sup> This device allowed for temperature control and for continuously recirculating a small volume of the liquid reaction mixture through the reaction vessel and a modified

<sup>8</sup> Brezny, A. C.; Landis, C. R. *J. Am. Chem. Soc.* **2017**, *139*, 2778-2785.

<sup>9</sup> (a) Foley, D. A.; Bez, E.; Codina, A.; Colson, K. L.; Fey, M.; Krull, R.; Piroli, D.; Zell, M. T.; Márquez, B. L. *Anal. Chem.* **2014**, *86*, 12008-12013. (b) <https://www.bruker.com/products/mr/nmr/software/insightmr.html>, accessed May, 27<sup>th</sup>, 2020.

NMR tube, enabling the *online* monitoring of the reaction mixture by NMR spectroscopy under these challenging reaction conditions.

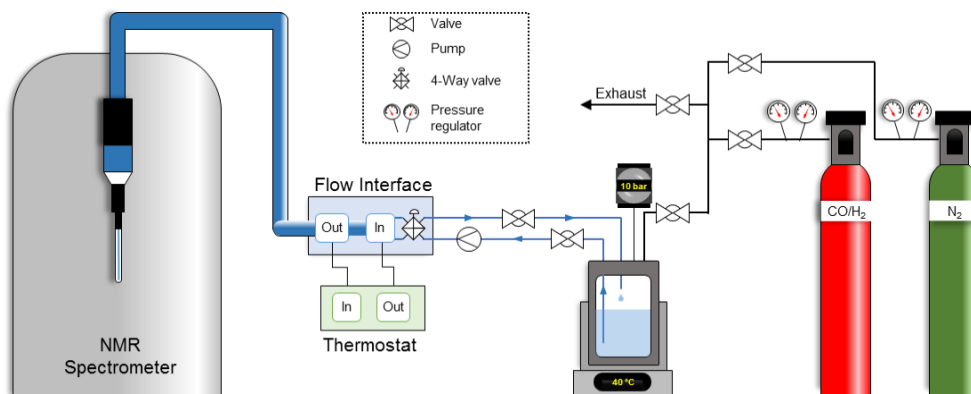
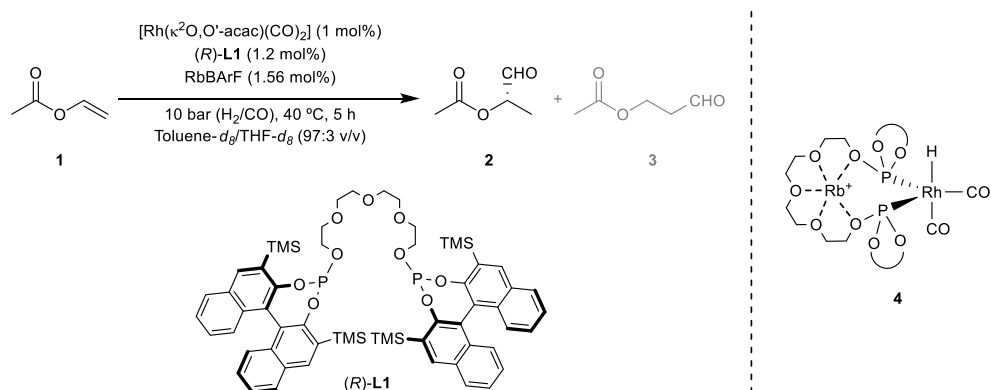


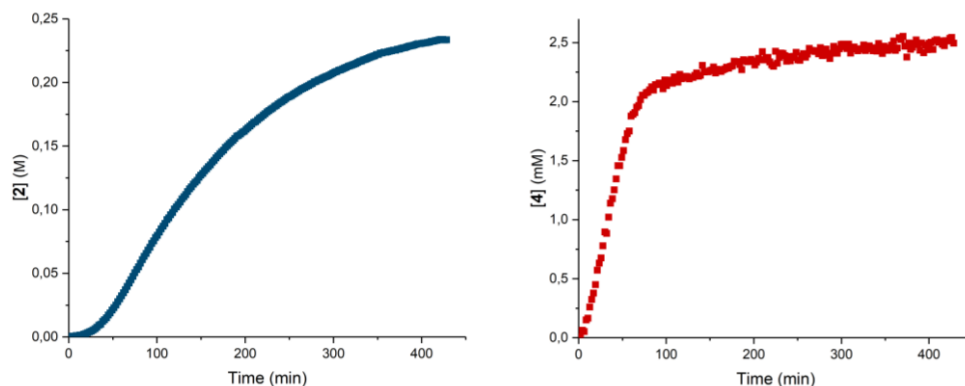
**Figure 175.** Experimental setup for *online* monitoring of high-pressure reactions.

The first data treatment allows for the intrinsic reaction profile of a reaction altered by catalyst activation processes to be uncovered. To demonstrate its potential, we chose to study the enantioselective hydroformylation catalyzed by a supramolecular rhodium complex with an induction period, as changes in the catalyst concentration are large in this case.

The enantioselective hydroformylation of vinyl acetate **1** is catalyzed by a supramolecular rhodium complex, which requires three different units to come together to form the active catalyst:  $[\text{Rh}(\kappa^2\text{O},\text{O}'\text{-acac})(\text{CO})_2]$  as active metal center, the enantiopure bisphosphite (*R*)-**L1** as ligand, and  $\text{RbBARF}$  to regulate the geometry of the catalyst (Scheme 45).<sup>6</sup> The reaction is regioselective, with a >99:1 b/l ratio and highly enantioselective, with a 99% *ee* for the (*S*)-**2** enantiomer, when the reaction is performed under batch conditions. As the formation of hydrido-containing rhodium complexes is not immediate, the concentration of these species increases over the course of the reaction and the overall reaction profile shows a clear induction period in the formation of the product (Scheme 45).



In this case, we were able to simultaneously monitor both the concentration of product **2** (Graph 5a) and the amount of hydrido-containing rhodium complexes (Graph 5b). It should be noted at this point that complex **4** is considered a resting state of the catalytic species.

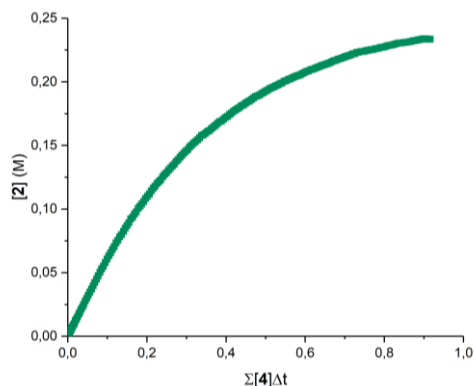


**Graph 5.** Original reaction profile of a) hydroformylation product **2** and b) supramolecular catalyst **4** activation profile.

The catalyst activation profile (Graph 5b) was used to normalize the time scale of the original progress reaction profile using VTNA. For the normalization process, equation 1 (Eq. 1) was used.

$$\text{normalized time} = \sum_{i=1}^n \left( \frac{[\mathbf{4}]_i + [\mathbf{4}]_{i-1}}{2} \right)^1 (t_i - t_{i-1}) \quad \text{Eq. 1}$$

The resulting reaction profile (Graph 6) was much simpler than the original profile with no trace of any induction period, which revealed the real first-order<sup>10</sup> profile of the original reaction in catalytic species.

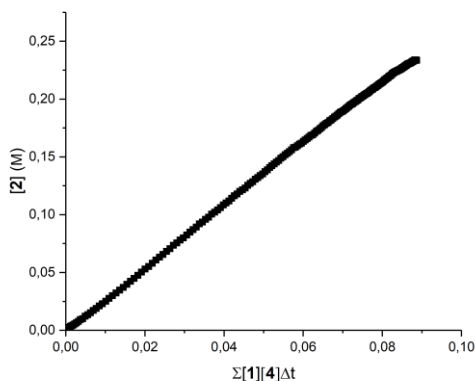


**Graph 6.** Time normalization using VTNA of the reaction profile of **2** by the removal of the kinetic effects due to the formation of the complex **4**

When the time scale is normalized by all the kinetically relevant components of the reaction, whose concentrations change with time, the reaction profile becomes a straight line. Thus, when the data from Graph 6 was subjected to VTNA analysis including the effects of the substrate as expressed in Eq. 2, the reaction profile simplified to a straight line (Graph 7). This analysis also revealed a real first-order profile in substrate **1**, as the only value for the exponent of the substrate concentration term in Eq. 2 that provided a straight line was the exponent one.

$$\text{normalized time} = \sum_{i,j=1}^n \left( \frac{[\mathbf{1}]_j + [\mathbf{1}]_{j-1}}{2} \right)^1 \left( \frac{[\mathbf{4}]_i + [\mathbf{4}]_{i-1}}{2} \right)^1 (t_i - t_{i-1}) \quad \text{Eq. 2}$$

<sup>10</sup> The exponent in equation 1 of the VTNA mathematical treatment that simplifies the original reaction profile (*i.e.*, exponent  $x = 1$ ,  $y = 0$ ) by removing the induction period corresponds to the order of the catalyst in the rate law  $r = k [\text{catalyst}]^x [\text{substrate}]^y$ .



**Graph 7.** Time normalization using VTNA of the reaction profile of **2** extracting the kinetic effects of substrate **1** and complex **4**

The slope of the straight line in Graph 7 corresponds to the rate constant (*i.e.*,  $k_{\text{obs}}$ ) for the rate equation (Eq. 3) of the hydroformylation process catalyzed by complexes derived from **4**.

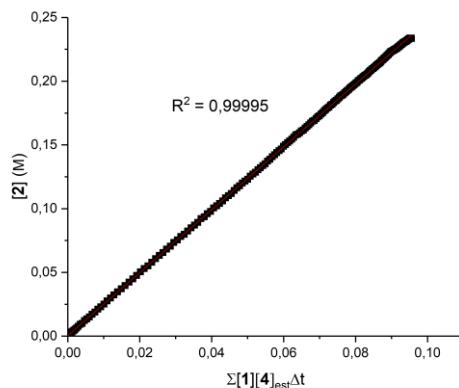
$$\text{rate} = k_{\text{obs}} \cdot [\mathbf{1}]^1 \cdot [\mathbf{4}]^1 \quad \text{with } k_{\text{obs}} = 2.68 \text{ M}^{-1} \text{ min}^{-1} \quad \text{Eq. 3}$$

The second kinetic treatment for reactions with activation (or deactivation) processes serves to estimate the concentration profile of active catalyst when it cannot be measured during the reaction. The amount of active catalyst is estimated by deconvolving its effect on the shape of the reaction profile using VTNA. The VTNA subtracts the kinetic effect of a component from the reaction profile when its concentration to the power of the correct order of the reaction is used to normalize the time scale.<sup>7</sup> When the time scale is normalized by all the kinetically relevant components of the reaction, whose concentrations change during the reaction, the reaction profile becomes a straight line. Therefore, the amount of catalyst can be estimated by maximizing the linearity of the resulting VTNA profile. This process can be easily performed by many algorithms accessible to all chemists. For the sake of generality, we have used the universally available Microsoft Excel add-in Solver.<sup>11</sup> To check the viability of this method, we took the data of the hydroformylation reaction, as it was possible to compare

<sup>11</sup> Walsh, S.; Diamond, D. *Talanta* **1995**, *42*, 561-572.

the estimated profiles of hydrido-containing rhodium complexes with the measured profiles.

In the case of the hydroformylation reaction of **1** with the supramolecular rhodium complex, there is a clear induction period in the original reaction profile (Graph 5a). This phenomenon is indicative of the amount of active catalyst building up, so the only constraint imposed on Solver was that the amount of active catalyst could not decrease with time.<sup>12</sup> To avoid any bias in the solution, the search started from values of 0% of active catalyst at all time points. The solution automatically found by Solver provided a straight line with  $R^2=0.99995$  for the progress reaction profile (Graph 8) when the time was normalized against the concentration of starting material **1** and that of variable active catalyst (Graph 7).

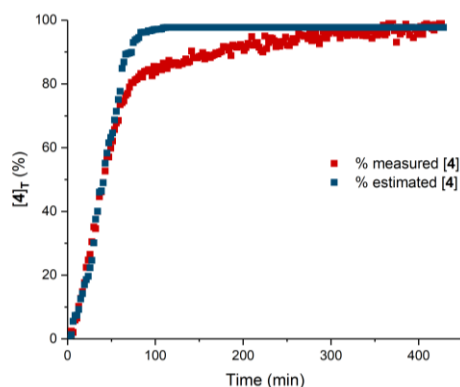


**Graph 8.** Time-normalized profile of **2** employing VTNA with the estimated catalyst profile

As the only evaluation parameter is the straightness of the VTNA plot, the profile of estimated active catalyst has the correct shape but not necessarily the correct magnitude. Therefore, the obtained profile is better presented as a percentage of active catalyst (Graph 9). The estimated profile for the activation of the catalyst (blue curve in Graph 9) is in reasonable agreement with the measured profile (red curve in Graph 9). The small discrepancy after the induction period could be a consequence of measuring hydrido-containing rhodium complexes only instead of the total amount of catalytic complexes.

<sup>12</sup> See section 4.5.9 in the experimental section.





**Graph 9.** Estimated profile of catalyst **4** activation (blue points) overlays with the measured catalyst **4** activation profile (red points)

There are some caveats to keep in mind when using VTNA to estimate the temporal profile of active catalyst. The first is that the values of the resulting catalyst profile are relative because the evaluation of the best profiles is based only on the  $R^2$  value of the resulting VTNA plot. This means that there is an infinite number of profiles with the same shape but different magnitudes that would yield a straight line with an identical  $R^2$  value. Therefore, the solution found by Solver should be treated as a percentage of the maximum amount of active catalyst at each time, and if a concentration profile is desired, the concentration of active catalyst at one time point must be known. Another caveat is that, if the order of the substances whose concentration is changing during the reaction is not accurate, the VTNA plot, and therefore the estimated profile of active catalyst, will be affected. To minimize this effect, the order of kinetically relevant reactants and catalyst should be known before applying the method.

Regarding the mechanistic insights learnt from this analysis, it should be considered that the mechanism of the rhodium-catalyzed hydroformylation reaction is complex and contains multiple potentially reversible elementary steps (see introduction, page 13).<sup>13</sup> Numerous mechanistic studies have established that the reaction proceeds by alkene coordination to the  $[\text{Rh}(\text{H})(\text{CO})_2(\text{Ligand})]$  complex, followed by alkene insertion into the Rh–H bond, migratory insertion

<sup>13</sup> (a) van Leeuwen, P. W. N. M.; Claver, C., Eds.; *Rhodium Catalyzed Hydroformylation*; Kluwer Academic Publishers, Dordrecht, **2002**. (b) Kubis, C.; Selent, D.; Sawall, M.; Ludwig, R.; Neymeyr, K.; Baumann, W.; Franke, R.; Börner, A. *Chem. - Eur. J.* **2012**, *18*, 8780-8794. (c) Gueven, S.; Nieuwenhuizen, M. M. L.; Hamers, B.; Franke, R.; Priske, M.; Becker, M.; Vogt, D. *ChemCatChem* **2014**, *6*, 603-610. (d) Börner, A.; Franke, R.; *Hydroformylation: Fundamentals, Processes and Applications in Organic Synthesis*; Wiley-VCH, Weinheim, **2016**. (e) Brezny, A. C.; Landis, C. R. *ACS Catal.* **2019**, *9*, 2501-2513.

of CO into a Rh–alkyl bond and hydrogenolysis of the corresponding Rh–CO–alkyl complex, which finally renders the product and a rhodium species that reenters the catalytic cycle. The relative magnitudes of the rate constants of the elementary steps and their reversibility (or irreversibility) depend on the nature of the catalytic system and experimental conditions. Within this complex mechanistic scenario, and despite the already published methods for the analysis of kinetic data,<sup>3d,13</sup> identification of the rate- and stereo-determining step(s), as well as the rationalization of the effects of reagent concentration, for a particular catalytic system under specific reaction conditions is not a trivial task. Interestingly, the first order rate dependence observed for substrate and catalyst in the hydroformylation of vinyl acetate **1** establishes that our system follows the so-called *type I* kinetics (Eq. 4).<sup>14</sup>

$$\text{Type I kinetics} \quad \text{rate} = k \frac{[\text{cat}] \cdot [\text{alkene}]}{[\text{CO}]} \quad \text{Eq. 4}$$

This hydroformylation regime is associated with alkene coordination/insertion as the rate-determining step and insertion as the step that establishes the stereochemical outcome of the reaction. It should also be noted that the low CO pressures employed (*i.e.*, 5 bar) could favor reversibility during the coordination/insertion steps, which contributes to achieving high regio- and enantioselectivities.<sup>13c</sup>

With the aim of gaining further mechanistic insight of the supramolecularly regulated rhodium-catalyzed enantioselective hydroformylation of vinyl acetate **1** employing (R)-**L1** as ligand, we studied the effects of changing the relative molar amounts of H<sub>2</sub> and CO in the catalytic activity and stereoselectivity. For practical reasons, these reactions were performed employing batch conditions. To correctly assess the effects of H<sub>2</sub> and CO in the catalytic activity and selectivity, the catalyst was formed *prior* to the addition of the substrate and the reactions were stopped before completion (*i.e.*, one hour reaction time). Complex **4** was prepared *in situ* by mixing 1 mol% of [Rh(κ<sup>2</sup>O,O'-acac)(CO)<sub>2</sub>] as metal precursor, an excess of ligand (R)-**L1** (1.2 mol%) to ensure full complexation of rhodium and an excess of RbBARf with respect to ligand (1.3 mol%) to ensure quantitative

---

<sup>14</sup> For further details on *type I* kinetics, see reference 13a and the introduction section, page 13. As opposed to this reaction regime, it should be noted that hydroformylation type II kinetics are characterized by the hydrogenolysis of the intermediate acyl–Rh complex as the rate-determining step and by the independence of the rate law with the concentration of alkene.

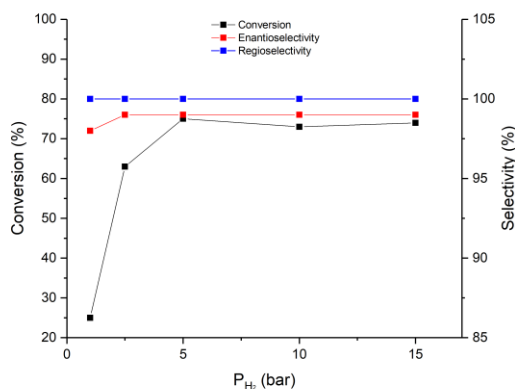
formation of the supramolecular complex **4**, at 10 bar syngas ( $H_2/CO$  in a 1:1 ratio), 40 °C for 2 h. After the addition of substrate **1**, the reactor was pressurized with the selected partial pressures of  $H_2$  and CO (maintaining in each reaction one reagent gas with a constant pressure of 5 bar) at 40 °C for 1 h (Table 37).

**Table 37.** Effect of the partial pressure of  $H_2$  and CO under catalytic conditions in the Rh-catalyzed enantioselective hydroformylation of vinyl acetate

Entry	$H_2$ pressure (bar)	CO pressure (bar)	Conversion (%) <sup>[a]</sup>	b/l ratio <sup>[a]</sup>	ee (%) <sup>[a]</sup> (config.) <sup>[b]</sup>
1	1	5	25	>99:1	98 ( <i>S</i> )
2	2.5	5	63	>99:1	99 ( <i>S</i> )
3	5	5	75	>99:1	99 ( <i>S</i> )
4	10	5	73	>99:1	99 ( <i>S</i> )
5	15	5	74	>99:1	99 ( <i>S</i> )
6	5	1	36	>99:1	95 ( <i>S</i> )
7	5	2.5	82	>99:1	97 ( <i>S</i> )
8	5	10	42	>99:1	99 ( <i>S</i> )

The enantioselective hydroformylations were performed in a parallel autoclave. Reaction conditions: [alkene] = 0.26 M; stirring rate = 800 rpm. [a] Conversion, b/l ratio and ee values were determined by GC analysis on a chiral stationary phase ( $\beta$ -Dex™ 225). [b] The configuration of the branched product was assigned by comparison with reported elution-order data (see ref.6)

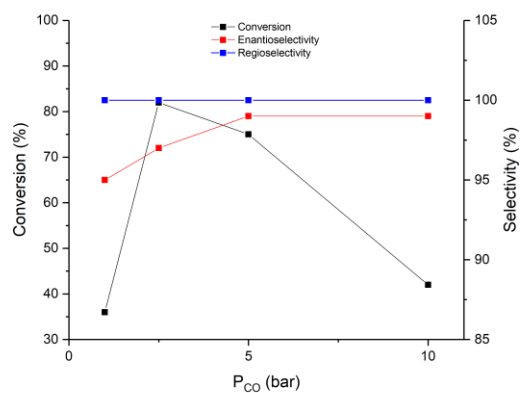
The effect of the partial pressure of  $H_2$  in the catalytic outcome was first studied with a constant partial pressure of CO at 5 bar (Graph 10). The use of 1 bar and 2.5 bar of  $H_2$  (Table 37, entries 1 and 2, respectively) had a negative effect in the catalytic activity (25% and 63% conv., respectively). It has been proposed that, in case of low pressure of  $H_2$ , dimeric rhodium complexes are formed, leading to a reduced amount of the active catalyst.<sup>13a</sup> The use of equimolar or higher molar amounts of  $H_2$  (Table 37, entries 3, 4 and 5) did not have a great influence on the catalytic activity, as conversion remained similar. The regioselectivity and the enantioselectivity were not affected throughout the whole study. These results are in agreement with a *type I* kinetics.



**Graph 10.** Effects of the partial pressure of  $H_2$  in the Rh-catalyzed enantioselective hydroformylation of **1**

The effects of changing the relative molar amounts of CO and  $H_2$  in the hydroformylation reaction was also studied with a constant partial pressure of  $H_2$  of 5 bar (Graph 11). The use of 1 bar of CO (Table 37, entry 6) led to a decrease in the conversion down to 36%. The best catalytic activity was observed when 2.5 bar of CO were used, with a 82% conversion (Table 37, entry 7). When 5 bar of CO were used, a slight drop in the catalytic activity was observed, achieving a 75% conv. (Table 37, entry 3). Partial pressures of 10 bar of CO led to a dramatic decrease of the conversion down to 42% (Table 37, entry 8). At high-pressures of CO, the equilibria in the catalytic cycle are shifted towards the formation of the CO saturated off-cycle species, preventing alkene coordination. These results are in agreement with a *type I* kinetics, in which high concentrations of CO are detrimental for the reaction rate.

Although the use of the VTNA method has not been able to unveil the overall mechanism, this kinetic analysis method has revealed very relevant mechanistic features. VTNA kinetic analyses, in combination with the study of the effects produced by changing the relative molar amounts of  $H_2$  and CO in the catalytic transformation, have brought the mechanistic understanding of the supramolecularly regulated hydroformylation one step forward.



**Graph 11.** Effects of the partial pressure of CO in the Rh-catalyzed enantioselective hydroformylation of **1**

## 4.4 CONCLUSIONS

A high-pressure setup for the continuous flow NMR analysis of the hydroformylation reaction mixture was designed and developed from a commercially available high-pressure reactor and a Bruker flow NMR probe. The reaction profiles with the concentrations of (pre-)catalytic species, substrate and product against time in the supramolecularly regulated enantioselective hydroformylation of vinyl acetate were measured under catalytic conditions.

Variable Time Normalization Analysis (VTNA) was used for analyzing the kinetic data (*i.e.*, the concentration profile of substrate, product and catalytically relevant intermediates as a function of time) in order to determine the reaction orders of the olefin and rhodium species and calculate the value of the observed rate constant of the hydroformylation process. The generation of catalytically active supramolecular complexes for hydroformylation reactions required an induction period, in which the concentration of the catalyst was not constant due to its building-up. The use of VTNA enabled the simplification of the concentration profiles of the hydroformylation by mathematically eliminating the induction period and unravelling the kinetic data of the reaction as if the catalytic species would have been present from the beginning. Analysis of the kinetic data revealed that the coordination of the alkene to the metal center followed by the insertion of the terminal alkene carbon into the Rh–H bond were the rate- and stereo-determining steps. Moreover, VTNA analysis also provided a satisfactory estimation of the percentages of hydrido-containing supramolecular rhodium complexes during the reaction with respect to the total amount of rhodium complexes by identifying the best linearization of the variable time normalized reaction profile.

VTNA kinetic analyses, in combination with the study of the effects produced by changing the relative molar amounts of H<sub>2</sub> and CO in the catalytic transformation, have revealed that the supramolecularly regulated rhodium-catalyzed hydroformylation of vinyl acetate with bisphosphite ligand (*R*)-**L1** and RbBARF follows the so-called *type I* kinetics.

## 4.5 EXPERIMENTAL SECTION

### 4.5.1 General considerations

All syntheses were carried out using chemicals purchased from commercial sources unless otherwise cited. Air- and moisture-sensitive manipulations and hydroformylation reactions were performed under inert atmosphere, either in a N<sub>2</sub>-filled glove box or with standard Schlenk techniques. Glassware was dried *in vacuo* before use with a hot air gun. All solvents were dried and deoxygenated by using a Solvent Purification system (SPS). Silica gel 60 (230-400 mesh) or C18-SiO<sub>2</sub> (200-400 mesh) was used for column chromatography. NMR spectra were recorded at room temperature in a 400 MHz or 500 MHz spectrometers in CDCl<sub>3</sub>, unless otherwise cited. <sup>1</sup>H NMR, <sup>13</sup>C{<sup>1</sup>H} NMR chemical shifts were quoted in ppm relative to the residual solvent peaks. <sup>31</sup>P{<sup>1</sup>H} NMR chemical shifts were quoted in ppm relative to 85% phosphoric acid in water. <sup>11</sup>B{<sup>1</sup>H} NMR chemical shifts are quoted in ppm relative to BF<sub>3</sub>·(CH<sub>3</sub>)<sub>2</sub>O in CDCl<sub>3</sub>. <sup>19</sup>F{<sup>1</sup>H} NMR chemical shifts are quoted in ppm relative to CFCl<sub>3</sub> in CDCl<sub>3</sub>. GC analyses were performed on an Agilent 6890N chromatograph equipped with a FID detector.

### 4.5.2 Experimental setup

Hydroformylation reactions were carried out in a 25 mL 316SS autoclave from Berghof equipped with inlet and outlet sample lines. Sample circulation was carried out using a HPLC pump (JASCO-PU-1580). The temperature of the reaction mixture was stabilized and kept constant with a Cole-Parmer Polystat Refrigerated Circulating Bath. The hydroformylation mixture was circulated into the spectrometer using an InsightMR flow tube (4 meters) from Bruker. The syngas cylinder (CO/H<sub>2</sub> 1:1 ratio) and the pressure regulator was purchased from BOC Group. Fluorinated ethylene propylene (FEP) tubing was used ((IDEX-Upchurch Product #1692: FEP Capillary 1/32" OD (0.80 mm) x 0.016" ID (0.405 mm))) and the length of tubing connecting the reactor and pump to the spectrometer was minimized. The FEP tubing is a non-reactive material and offers chemical and mechanical stability (up to 50 °C, up to 120 bar) along with low gas permeability and good flexibility. Fittings used in the system were stainless steel from Swagelok or Upchurch PEEK (polyether ether ketone) from Teknokroma Analítica S.A.

All the equipment was positioned 0.5 m outside the 5 Gauss line of the spectrometer's magnet.

The high-pressure flow system configuration used for hydroformylation reactions is shown in section 4.3, Figure 175.

A 25 mL Berghof autoclave equipped with inlet and outlet sample lines (blue lines) was used. The reaction mixture was circulated from the reactor to the HPLC pump, then to the InsightMR flow tube and back to the reactor employing FEP tubing as sample lines (total volume of the system *ca.* 3.4 mL, circulation time for the sample *ca.* 41 s). The temperature was kept constant throughout the whole system (*i.e.*, reactor, spectrometer and InsightMR flow tube). The reactor was connected to the high-pressure cylinder using stainless tubing (black lines), Swagelok fittings and valves. The design of the system allowed both the pressurization with different gases (N<sub>2</sub> and syngas) and depressurization by connecting the system to an exhaust. Due to the toxicity and flammability of syngas, CO and H<sub>2</sub> detectors were placed in the vicinity of the reactor, syngas cylinder and exhaust.

#### 4.5.3 Preparation of the catalyst precursors in flow experiments

Bisphosphite ligand (R)-**L1** and RbBArF were synthesized following the procedures described in the literature and their spectroscopic data were in agreement with those reported.<sup>6,15</sup>

General procedure for the *online* monitoring of Rh-catalyzed hydroformylation of vinyl acetate **1**.

In an argon-filled glove box, the following solutions were prepared:

Solution A: ligand (R)-**L1** (52 mg, 46.8 μmol), RbBArF (58 mg, 60.8 μmol) in 450 μL of THF-*d*<sub>8</sub>, [Rh(κ<sup>2</sup>O,O'-acac)(CO)<sub>2</sub>] (10 mg, 39.0 μmol) and toluene-*d*<sub>8</sub> were mixed until a total volume of 10 mL.

Solution B: vinyl acetate **1** (336 mg, 3.9 mmol), dodecane (199 mg, 1.17 mmol) and toluene-*d*<sub>8</sub> were mixed until a total volume of 5 mL.

For the hydroformylation reactions, the corresponding temperature value (40 °C) was set in the thermostat, NMR spectrometer and heating plate. The system

---

<sup>15</sup> Carreras, L.; Rovira, L.; Vaquero, M.; Mon, I.; Martin, E.; Benet-Buchholz, J.; Vidal-Ferran, A. *RSC Adv.* **2017**, 7, 32833-32841.



was purged three times with 2 bar of N<sub>2</sub>. With a positive flow of N<sub>2</sub> (1 bar) in the reactor, the sample inlet valve was opened and solution A was injected followed by solution B. The stirring rate was set at 800 rpm. The reaction mixture was circulated under nitrogen at 5 mL/min for 5 min. NMR spectra were recorded while flowing under nitrogen atmosphere. The system was purged three times with 10 bar of syngas (H<sub>2</sub>/CO in a 1:1 ratio) and the syngas cylinder was left open during the reaction monitoring. Once the experiment was finished, the syngas cylinder was closed and the reactor was depressurized. The thermostat, NMR spectrometer and heating plate were switched off, the crude mixture was removed from the reactor and the sample lines were cleaned. For cleaning the sample lines, acetone was injected at 5 mL/min followed by air flushing until complete dryness. Conversion, branched to linear ratio and enantioselectivity for the products derived from the hydroformylations of **1** were determined by GC analyses with a Supelco β-Dex<sup>TM</sup> 225 column by using the dodecane present in the reaction mixture as internal standard.

#### 4.5.4 General procedure for the Rh-catalyzed enantioselective hydroformylation of vinyl acetate **1** with variable partial pressures

In a glove box filled with nitrogen, the ligand (*R*)-**L1** (*ca.* 2.7 μmol in 360 μL of toluene), RbBArF salt (*ca.* 3.6 μmol in 27 μL of THF) and [Rh(κ<sup>2</sup>O,O'-acac)(CO)<sub>2</sub>] (*ca.* 2.3 μmol in 65 μL of toluene) were placed into a 2 mL vial equipped with a magnetic stirrer. Dodecane (*ca.* 69 μmol) and additional toluene were charged to provide the desired final concentration of catalyst (2.6 mM) in toluene/THF (97:3 v/v). The vial was transferred into an autoclave and taken out of the glove box. The autoclave was purged three times with syngas (1:1 H<sub>2</sub>/CO at 5 bar) and, finally, the autoclave was pressurized with 10 bar syngas. The reaction mixture was stirred at 40 °C (metallic block) for 2 h in order to generate the catalytically active rhodium species. The reaction was cooled and the pressure was carefully released in a well-ventilated hood. In a glove box filled with nitrogen substrate **1** (*ca.* 230 μmol) was added. The vial was transferred into an autoclave and taken out of the glove box. The autoclave was purged three times with the reactive gas in higher proportion (at a pressure not higher than that planned for the hydroformylation reaction and without stirring) and finally, the autoclave was pressurized with the reactive gas in lower proportion at the required pressure. The reaction mixture was stirred at 40 °C (metallic block) for 1 h. The reaction was cooled and the pressure was carefully released in a well-ventilated hood. Conversion, branched to linear ratio and enantioselectivity for

the products derived from the hydroformylations of **1** were determined by GC analyses with a Supelco  $\beta$ -Dex<sup>TM</sup> 225 column by using the dodecane present in the reaction mixture as internal standard.

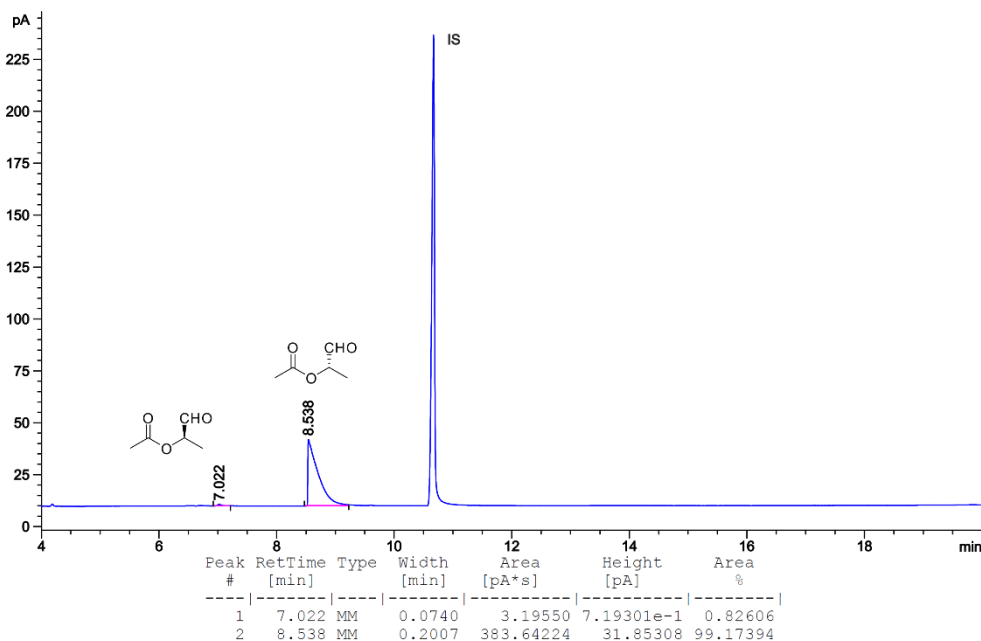
#### 4.5.5 Determination of regioselectivity and enantiomeric excess of **2**

The regioselectivity and enantioselectivity was determined by GC analysis, performed using chiral stationary phases. GC analysis of the crude mixture confirmed the already reported regio- and enantioselectivity.<sup>6</sup>

GC analysis conditions for the hydroformylation products derived from **1**: Enantiomeric ratio was determined by GC analysis with a Supelco  $\beta$ -Dex<sup>TM</sup> 225 column (30 m x 0.25 mm x 0.25  $\mu$ m). Flow rate: 1 mL/min. Temperature program: 100 °C for 5 min, then 4 °C/min to 160 °C. Retention times: 2.4 min for **1**, 7.0 (R)-**2**, 8.5 (S)-**2** min for the enantiomers of the branched regioisomer and 11.7 min for the linear isomer **3**.

#### 4.5.6 Selected GC chromatograms

GC chromatogram of the hydroformylation products of **1**



#### 4.5.7 Complete set of results for the Rh-catalyzed enantioselective hydroformylation of vinyl acetate 1

**Table 38.** Rh-catalyzed enantioselective hydroformylation of vinyl acetate **1** in flow and batch conditions

Entry	H <sub>2</sub> pressure (bar)	CO pressure (bar)	Conversion (%)	b/l ratio	ee (%) (config.)
1 <sup>[b]</sup>	5	5	99	>99:1	98 ( <i>S</i> )
2	1	5	25	>99:1	98 ( <i>S</i> )
3	2.5	5	63	>99:1	99 ( <i>S</i> )
4	5	5	75	>99:1	99 ( <i>S</i> )
5	10	5	73	>99:1	99 ( <i>S</i> )
6	15	5	74	>99:1	99 ( <i>S</i> )
7	5	1	36	>99:1	95 ( <i>S</i> )
8	5	2.5	82	>99:1	97 ( <i>S</i> )
9	5	10	42	>99:1	99 ( <i>S</i> )

The enantioselective hydroformylations were performed in a parallel autoclave in batch. Reaction conditions: [alkene] = 0.26 M; stirring rate = 800 rpm; total reaction volume *ca.* 900 μL; time = 1 h. Conversion, b/l ratio and *ee* values were determined by GC analysis on a chiral stationary phase (β-Dex<sup>TM</sup> 225). [b] The enantioselective hydroformylations were performed in flow system (for experimental set-up, see Figure 175). Reaction conditions: [alkene] = 0.26 M; stirring rate = 1000 rpm; total reaction volume *ca.* 15 mL; time = 12 h; flow = 5 mL/min. Conversion, b/l ratio and *ee* values were determined by GC analysis on a chiral stationary phase (β-Dex<sup>TM</sup> 225).



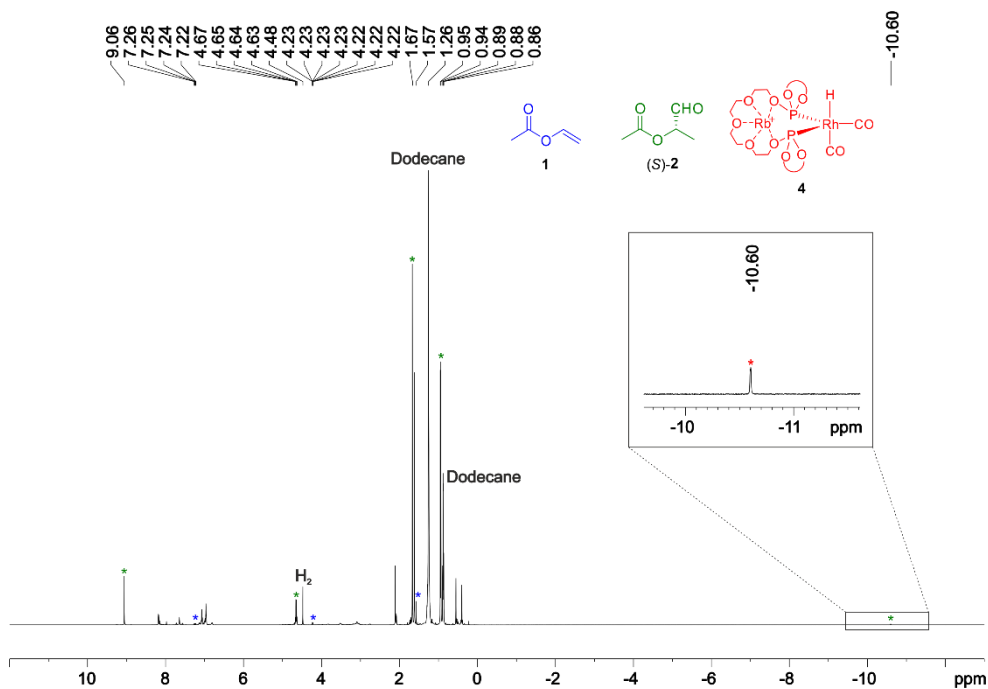


Figure 177.  $^1\text{H}$  NMR spectrum (500 MHz,  $\text{toluene-}d_8$ ) of the hydroformylation reaction mixture after 426 minutes

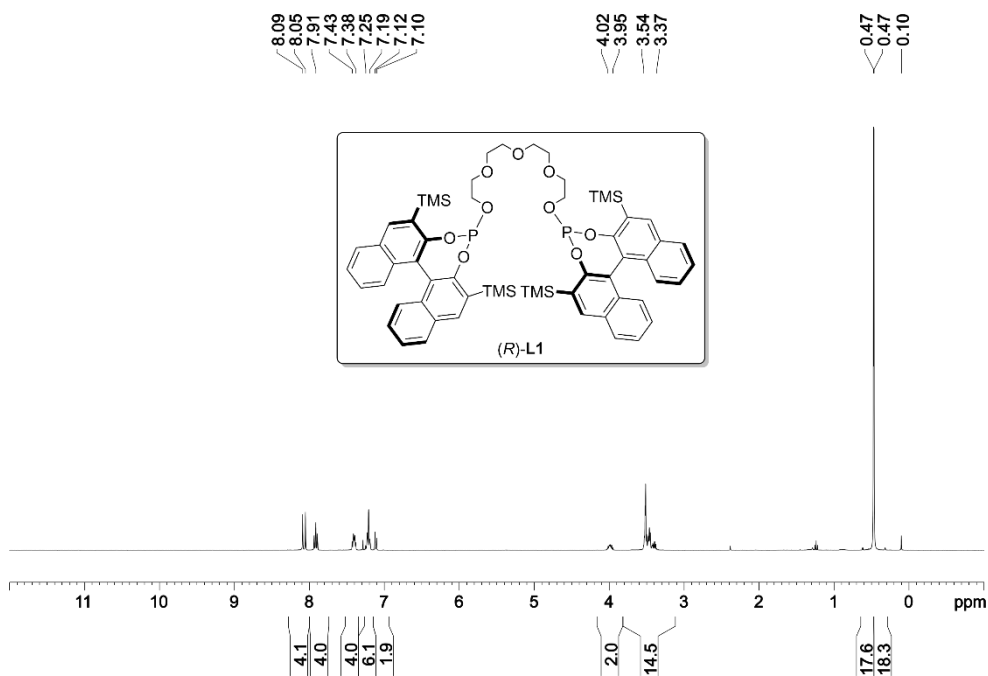


Figure 178.  $^1\text{H}$  NMR spectrum (400 MHz,  $\text{CDCl}_3$ ) of (R)-L1

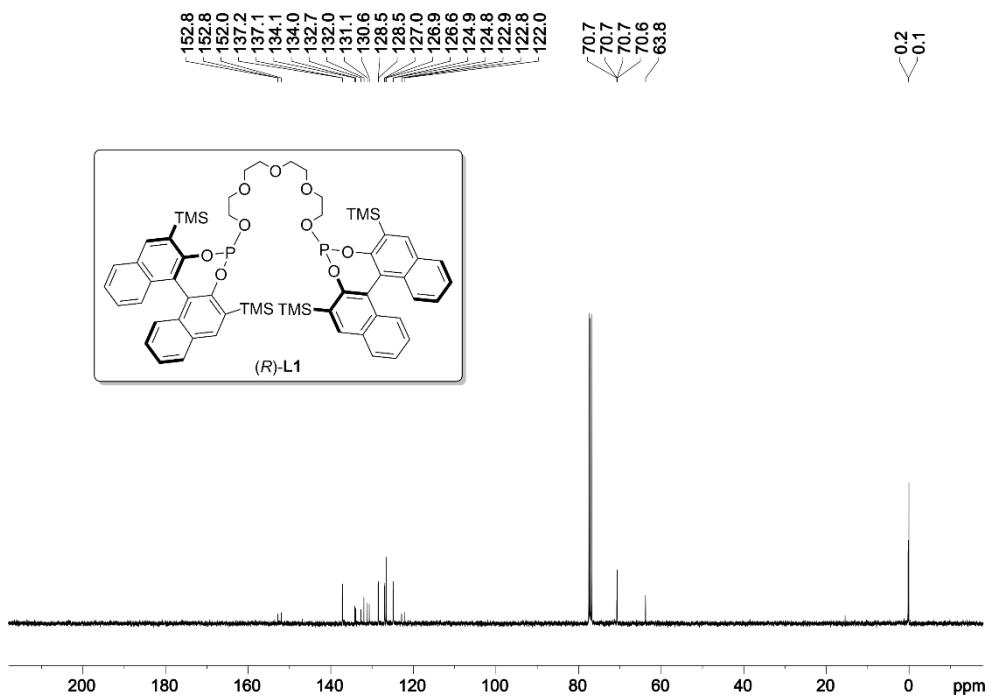


Figure 179.  $^{13}\text{C}\{^1\text{H}\}$  NMR spectrum (101 MHz,  $\text{CDCl}_3$ ) of (R)-L1

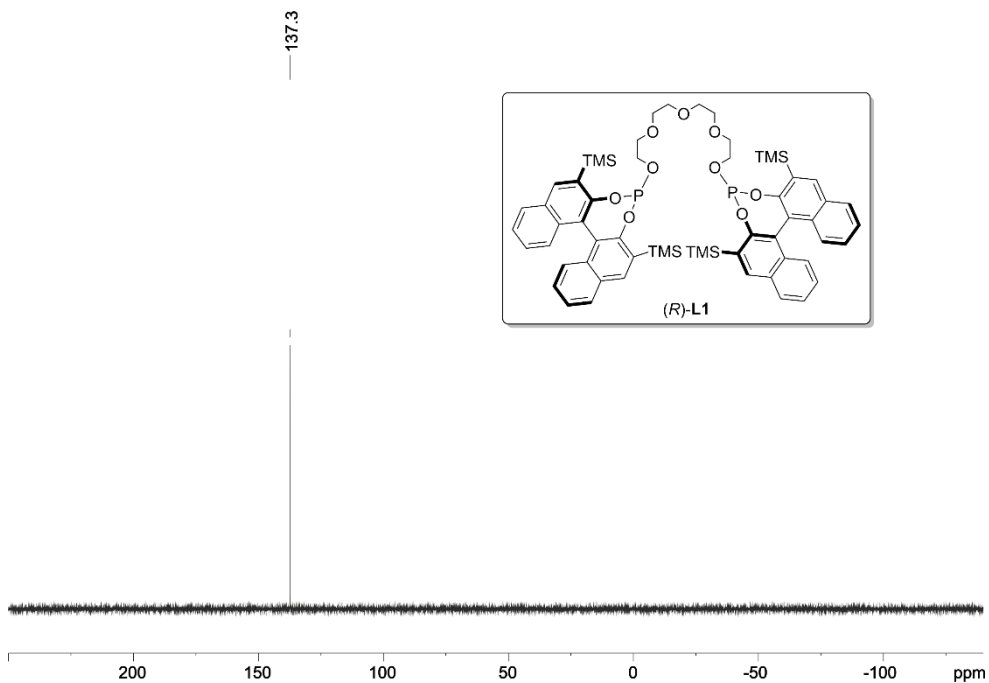


Figure 180.  $^{31}\text{P}\{^1\text{H}\}$  NMR spectrum (162 MHz,  $\text{CDCl}_3$ ) of (R)-L1

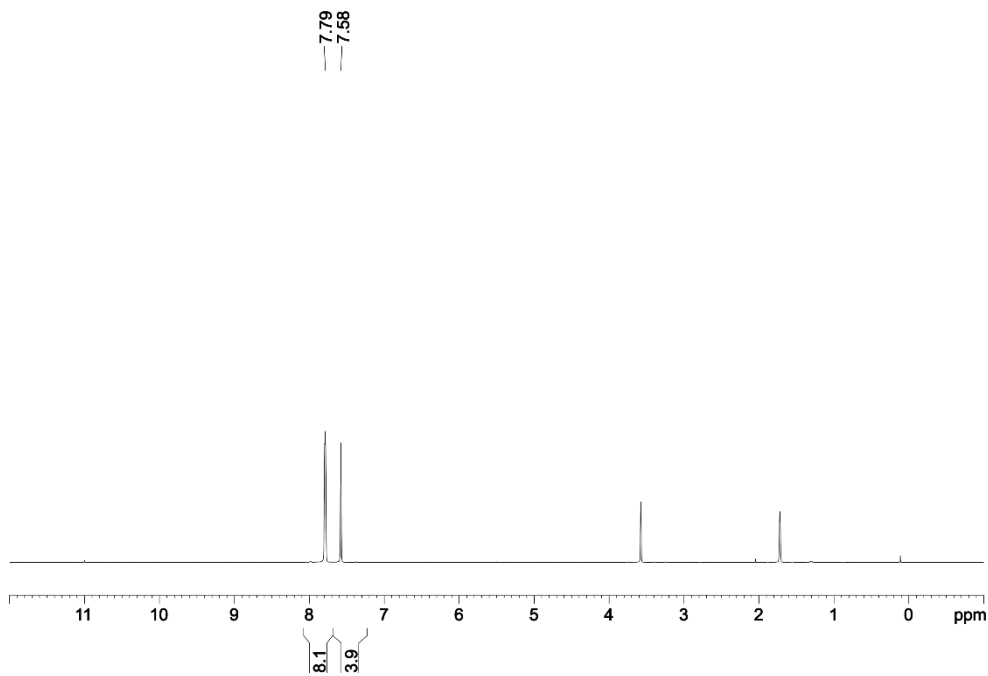


Figure 181.  $^1\text{H}$  NMR spectrum (400 MHz,  $\text{THF-}d_8$ ) of RbBArF

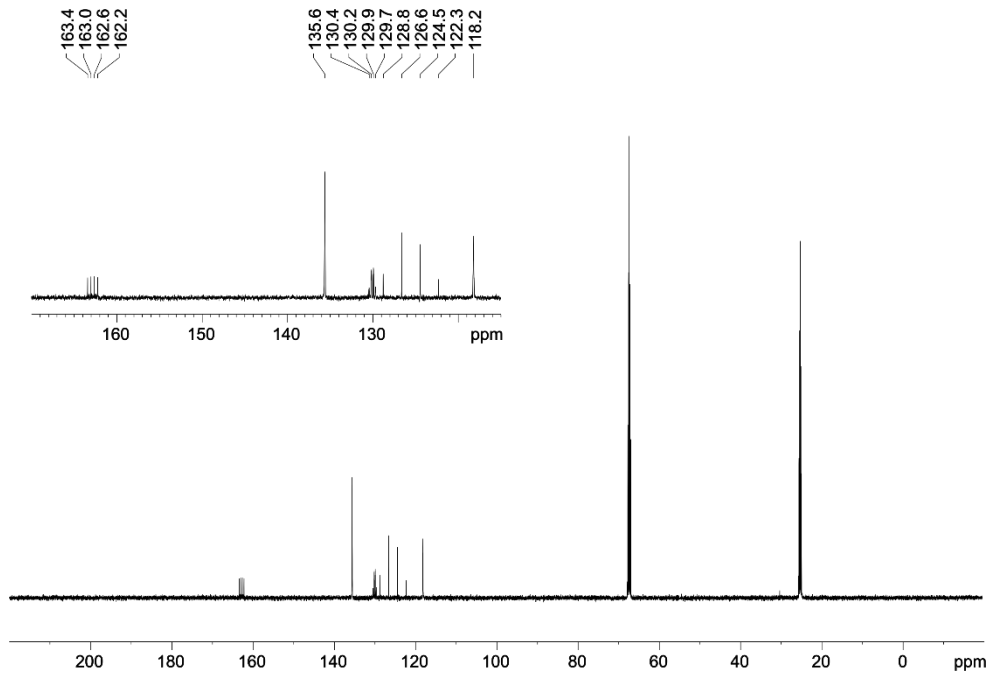


Figure 182.  $^{13}\text{C}\{^1\text{H}\}$  NMR spectrum (126 MHz,  $\text{THF-}d_8$ ) of RbBArF

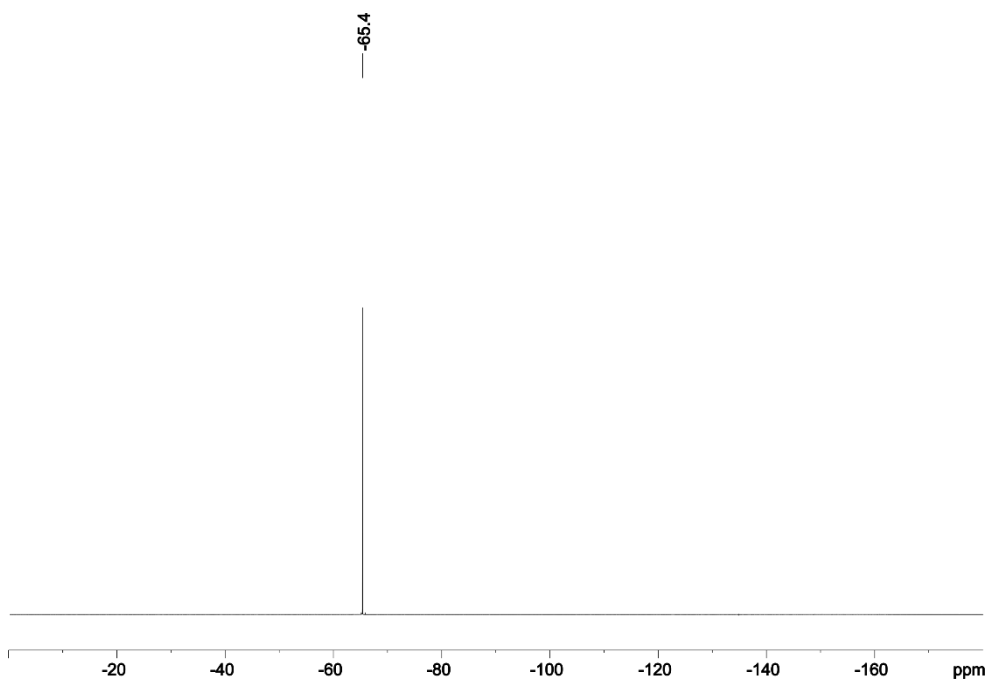


Figure 183.  $^{19}\text{F}\{^1\text{H}\}$  NMR spectrum (376 Mz,  $\text{THF-}d_8$ ) of RbBArF

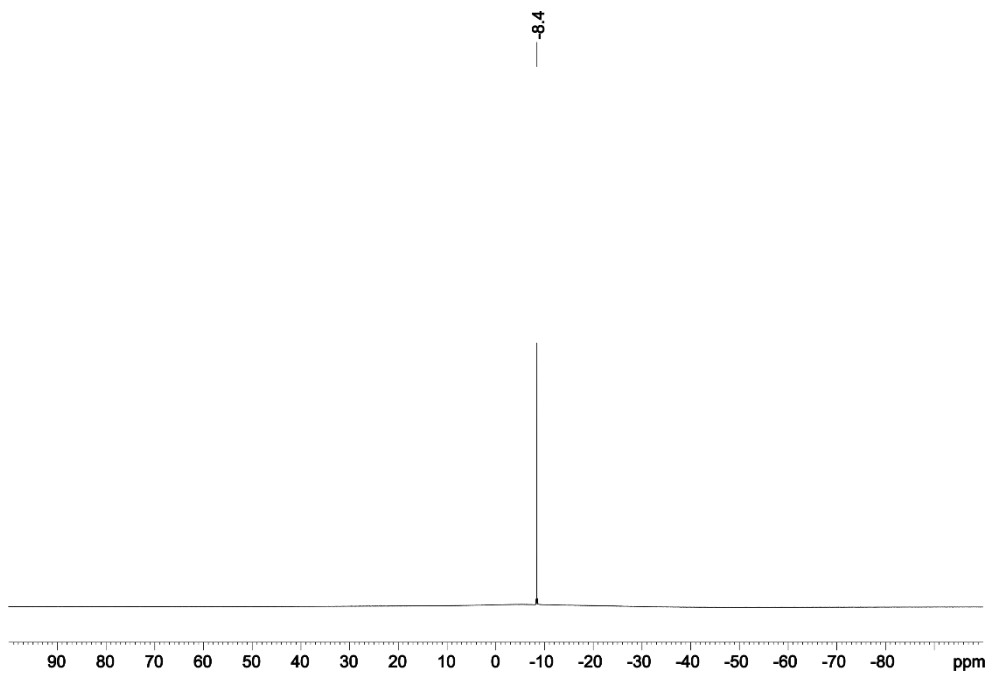


Figure 184.  $^{11}\text{B}\{^1\text{H}\}$  NMR spectrum (128 Mz,  $\text{THF-}d_8$ ) of RbBArF



### 4.5.9 Kinetic data

Graph 5 shows the concentrations of product **2** and hydrido-containing supramolecular rhodium complex **4** that were obtained from the integration of consecutive  $^1\text{H-NMR}$  spectra. The numerical values for both figures are shown in Table 39.

Graph 6 shows the reaction profile corrected by the amount of hydrido-containing supramolecular rhodium complex **4** at each time point. The time values shown in Table 39 have been calculated using the VTNA formula (Eq. 1):

$$\text{normalized time} = \sum_{i=1}^n \left( \frac{[\mathbf{4}]_i + [\mathbf{4}]_{i-1}}{2} \right)^1 (t_i - t_{i-1}) \quad \text{Eq. 1}$$

Graph 7 shows the reaction profile corrected by the amount of hydrido-containing supramolecular rhodium complexes and starting material **1** (vinyl acetate) at each time point. The time values shown in Table 39 have been calculated using the VTNA formula (Eq. 2):

$$\text{normalized time} = \sum_{i,j=1}^n \left( \frac{[\mathbf{1}]_j + [\mathbf{1}]_{j-1}}{2} \right)^1 \left( \frac{[\mathbf{4}]_i + [\mathbf{4}]_{i-1}}{2} \right)^1 (t_i - t_{i-1}) \quad \text{Eq. 2}$$

**Table 39.** Data for Graph 5, Graph 6 and Graph 7

time (min)	[2] (M)	[4] (mM)	[1]=[1] <sub>0</sub> -[2] (M)	VTNA using 4	VTNA using 1 and 4
2.150	0.000357	0.006481	0.259643	0.000014	0.000004
4.283	0.000568	0.062713	0.259432	0.000088	0.000023
6.417	0.000298	0.051924	0.259702	0.000210	0.000055
8.567	0.000985	0.150575	0.259015	0.000428	0.000111
10.700	0.001087	0.166071	0.258913	0.000765	0.000198
12.850	0.001456	0.260574	0.258544	0.001224	0.000317
14.983	0.001521	0.324562	0.258479	0.001848	0.000478
17.133	0.002191	0.377941	0.257809	0.002603	0.000673
19.267	0.002524	0.449942	0.257476	0.003487	0.000901
21.400	0.003352	0.572287	0.256648	0.004577	0.001181
23.550	0.003955	0.631517	0.256045	0.005871	0.001513
25.683	0.004546	0.676197	0.255454	0.007266	0.001870
27.833	0.005455	0.777741	0.254545	0.008829	0.002268
29.967	0.006412	0.896483	0.253588	0.010615	0.002722
32.100	0.007683	0.884364	0.252317	0.012514	0.003202
34.250	0.009242	1.021546	0.250758	0.014563	0.003718
36.383	0.010007	1.138909	0.249993	0.016868	0.004295
38.533	0.012146	1.177914	0.247854	0.019358	0.004915
40.667	0.013443	1.251882	0.246557	0.021950	0.005555
42.817	0.015104	1.344928	0.244896	0.024742	0.006241
44.950	0.017124	1.457053	0.242876	0.027730	0.006970
47.100	0.018905	1.457003	0.241095	0.030863	0.007728
49.233	0.021093	1.527969	0.238907	0.034047	0.008493
51.367	0.022968	1.584891	0.237032	0.037367	0.009283
53.517	0.025094	1.676899	0.234906	0.040874	0.010110
55.650	0.027647	1.729469	0.232353	0.044507	0.010959
57.800	0.029931	1.749759	0.230069	0.048247	0.011824
59.933	0.032300	1.877047	0.227700	0.052116	0.012709
62.083	0.034772	1.892712	0.225228	0.056168	0.013627
64.217	0.037141	1.906997	0.222859	0.060221	0.014535
66.367	0.039678	1.952342	0.220322	0.064370	0.015454
68.500	0.042305	1.966563	0.217695	0.068550	0.016370

Table 39. cont.

time (min)	[2] (M)	[4] (mM)	[1]=[1] <sub>0</sub> -[2] (M)	VTNA using 4	VTNA using 1 and 4
70.633	0.044899	2.017056	0.215101	0.072800	0.017289
72.783	0.047556	2.054739	0.212444	0.077177	0.018225
74.917	0.050393	2.052759	0.209607	0.081558	0.019150
77.067	0.052960	2.075148	0.207040	0.085996	0.020074
79.200	0.055157	2.081308	0.204843	0.090429	0.020987
81.333	0.057943	2.099322	0.202057	0.094888	0.021894
83.483	0.060690	2.125603	0.199310	0.099430	0.022806
85.617	0.063263	2.098041	0.196737	0.103936	0.023698
87.767	0.065631	2.143164	0.194369	0.108495	0.024590
89.900	0.068296	2.145193	0.191704	0.113069	0.025473
92.050	0.070555	2.156997	0.189445	0.117694	0.026354
94.183	0.073456	2.153356	0.186544	0.122292	0.027218
96.333	0.075474	2.108371	0.184526	0.126873	0.028068
98.467	0.078088	2.183690	0.181912	0.131451	0.028907
100.600	0.079923	2.135618	0.180077	0.136058	0.029741
102.750	0.082403	2.181242	0.177597	0.140699	0.030571
104.883	0.084941	2.168216	0.175059	0.145338	0.031389
107.033	0.087076	2.155352	0.172924	0.149986	0.032198
109.167	0.089235	2.209565	0.170765	0.154642	0.032998
111.317	0.092106	2.176811	0.167894	0.159358	0.033796
113.450	0.093527	2.165135	0.166473	0.163989	0.034571
115.583	0.095973	2.230476	0.164027	0.168678	0.035345
117.733	0.097846	2.194052	0.162154	0.173434	0.036121
119.867	0.100485	2.202985	0.159515	0.178124	0.036875
122.017	0.102237	2.213808	0.157763	0.182872	0.037629
124.150	0.103985	2.212425	0.156015	0.187594	0.038369
126.300	0.106077	2.191602	0.153923	0.192328	0.039103
128.433	0.108398	2.204654	0.151602	0.197017	0.039819
130.583	0.110128	2.204077	0.149872	0.201757	0.040534
132.717	0.111861	2.220534	0.148139	0.206476	0.041237
134.850	0.114196	2.242340	0.145804	0.211237	0.041937
137.000	0.116354	2.215293	0.143646	0.216029	0.042630

Table 39. cont.

time (min)	[2] (M)	[4] (mM)	[1]=[1] <sub>0</sub> -[2] (M)	VTNA using 4	VTNA using 1 and 4
139.133	0.117874	2.222584	0.142126	0.220762	0.043307
141.283	0.120037	2.306519	0.139963	0.225631	0.043993
143.417	0.121543	2.250504	0.138457	0.230492	0.044670
145.550	0.123050	2.252581	0.136950	0.235295	0.045331
147.700	0.125374	2.251389	0.134626	0.240137	0.045989
149.833	0.127127	2.260964	0.132873	0.244950	0.046633
151.983	0.128497	2.267592	0.131503	0.249818	0.047276
154.117	0.130581	2.292608	0.129419	0.254683	0.047911
156.267	0.132050	2.242682	0.127950	0.259558	0.048538
158.400	0.133727	2.273747	0.126273	0.264375	0.049150
160.550	0.135180	2.266756	0.124820	0.269257	0.049763
162.683	0.137242	2.254386	0.122758	0.274079	0.050360
164.817	0.138715	2.269060	0.121285	0.278904	0.050949
166.967	0.140692	2.276345	0.119308	0.283790	0.051537
169.100	0.142299	2.291865	0.117701	0.288663	0.052114
171.250	0.143960	2.282368	0.116040	0.293580	0.052689
173.383	0.145503	2.297578	0.114497	0.298466	0.053252
175.533	0.146776	2.302777	0.113224	0.303411	0.053815
177.667	0.148873	2.342390	0.111127	0.308366	0.054371
179.800	0.150139	2.336172	0.109861	0.313356	0.054922
181.950	0.151782	2.338902	0.108218	0.318382	0.055470
184.083	0.153003	2.313500	0.106997	0.323345	0.056004
186.233	0.154432	2.270176	0.105568	0.328272	0.056528
188.367	0.156017	2.353802	0.103983	0.333204	0.057045
190.517	0.157841	2.345430	0.102159	0.338256	0.057566
192.650	0.158346	2.337109	0.101654	0.343251	0.058075
194.783	0.159595	2.339901	0.100405	0.348240	0.058579
196.933	0.160933	2.357443	0.099067	0.353289	0.059082
199.067	0.161709	2.343412	0.098291	0.358303	0.059577
201.217	0.163275	2.309745	0.096725	0.363306	0.060065
203.350	0.164548	2.333950	0.095452	0.368259	0.060541
205.500	0.165805	2.366876	0.094195	0.373312	0.061020

Table 39. cont.

time (min)	[2] (M)	[4] (mM)	[1]=[1] <sub>0</sub> -[2] (M)	VTNA using 4	VTNA using 1 and 4
207.633	0.167151	2.354671	0.092849	0.378349	0.061491
209.767	0.168543	2.422389	0.091457	0.383444	0.061960
211.917	0.169119	2.352762	0.090881	0.388577	0.062428
214.050	0.170561	2.366078	0.089439	0.393611	0.062882
216.200	0.171992	2.373630	0.088008	0.398706	0.063334
218.333	0.172892	2.335911	0.087108	0.403730	0.063774
220.483	0.174221	2.311668	0.085779	0.408726	0.064206
222.617	0.175369	2.298956	0.084631	0.413644	0.064625
224.750	0.176829	2.426153	0.083171	0.418684	0.065048
226.900	0.177750	2.324879	0.082250	0.423791	0.065470
229.033	0.178858	2.373821	0.081142	0.428803	0.065880
231.183	0.179752	2.411065	0.080248	0.433947	0.066295
233.317	0.181182	2.407153	0.078818	0.439086	0.066704
235.467	0.181935	2.388840	0.078065	0.444242	0.067108
237.600	0.183135	2.341245	0.076865	0.449287	0.067499
239.750	0.184299	2.381038	0.075701	0.454364	0.067886
241.883	0.185060	2.345446	0.074940	0.459405	0.068266
244.017	0.186140	2.372371	0.073860	0.464438	0.068640
246.167	0.187256	2.383025	0.072744	0.469550	0.069015
248.300	0.188415	2.416708	0.071585	0.474670	0.069384
250.450	0.188978	2.352474	0.071022	0.479796	0.069750
252.583	0.189702	2.349117	0.070298	0.484811	0.070104
254.717	0.190784	2.386360	0.069216	0.489863	0.070457
256.867	0.191679	2.405502	0.068321	0.495014	0.070811
259.000	0.192614	2.376003	0.067386	0.500114	0.071157
261.150	0.193541	2.400904	0.066459	0.505249	0.071501
263.283	0.194629	2.451125	0.065371	0.510425	0.071842
265.433	0.195387	2.434252	0.064613	0.515677	0.072183
267.600	0.196083	2.431846	0.063917	0.520948	0.072522
269.733	0.196910	2.423850	0.063090	0.526128	0.072851
271.883	0.197671	2.431066	0.062329	0.531347	0.073178
274.017	0.198591	2.404978	0.061409	0.536505	0.073497

Table 39. cont.

time (min)	[2] (M)	[4] (mM)	[1]=[1] <sub>0</sub> -[2] (M)	VTNA using 4	VTNA using 1 and 4
276.150	0.199222	2.456083	0.060778	0.541690	0.073814
278.300	0.200447	2.388598	0.059553	0.546898	0.074127
280.433	0.200859	2.423224	0.059141	0.552031	0.074432
282.583	0.201801	2.443747	0.058199	0.557263	0.074739
284.717	0.202213	2.392027	0.057787	0.562421	0.075038
286.867	0.203172	2.364342	0.056828	0.567534	0.075331
289.000	0.203882	2.409773	0.056118	0.572627	0.075619
291.150	0.204548	2.466708	0.055452	0.577869	0.075911
293.283	0.204977	2.417643	0.055023	0.583079	0.076199
295.433	0.205658	2.408473	0.054342	0.588267	0.076483
297.567	0.206498	2.447222	0.053502	0.593446	0.076762
299.717	0.207362	2.484563	0.052638	0.598748	0.077043
301.850	0.208179	2.487277	0.051821	0.604051	0.077320
304.000	0.208613	2.463801	0.051387	0.609374	0.077595
306.133	0.209628	2.448693	0.050372	0.614614	0.077862
308.283	0.209960	2.487182	0.050040	0.619920	0.078128
310.417	0.210577	2.410350	0.049423	0.625144	0.078388
312.550	0.211308	2.452700	0.048692	0.630331	0.078642
314.700	0.211829	2.462045	0.048171	0.635614	0.078898
316.833	0.212710	2.446185	0.047290	0.640850	0.079148
318.983	0.213131	2.429901	0.046869	0.646092	0.079395
321.117	0.213754	2.443023	0.046246	0.651289	0.079637
323.250	0.214297	2.446746	0.045703	0.656505	0.079877
325.400	0.214922	2.480027	0.045078	0.661801	0.080117
327.533	0.215684	2.432884	0.044316	0.667042	0.080351
329.683	0.216625	2.471916	0.043375	0.672314	0.080582
331.817	0.216868	2.472383	0.043132	0.677588	0.080811
333.967	0.217630	2.447244	0.042370	0.682877	0.081037
336.100	0.218103	2.429895	0.041897	0.688079	0.081256
338.233	0.218636	2.457033	0.041364	0.693292	0.081473
340.383	0.219466	2.427080	0.040534	0.698542	0.081688
342.517	0.219929	2.491924	0.040071	0.703789	0.081899

Table 39. cont.

time (min)	[2] (M)	[4] (mM)	[1]=[1] <sub>0</sub> -[2] (M)	VTNA using 4	VTNA using 1 and 4
344.667	0.220535	2.464392	0.039465	0.709117	0.082111
346.800	0.220942	2.407909	0.039058	0.714314	0.082315
348.933	0.221967	2.468146	0.038033	0.719516	0.082516
351.083	0.222135	2.457182	0.037865	0.724810	0.082717
353.217	0.223008	2.433621	0.036992	0.730027	0.082912
355.367	0.223170	2.443044	0.036830	0.735270	0.083105
357.500	0.223722	2.477595	0.036278	0.740518	0.083297
359.650	0.223767	2.512934	0.036233	0.745883	0.083492
361.783	0.224226	2.434309	0.035774	0.751160	0.083682
363.917	0.224596	2.454163	0.035404	0.756375	0.083867
366.067	0.224852	2.540064	0.035148	0.761743	0.084057
368.200	0.225271	2.524973	0.034729	0.767146	0.084245
370.350	0.225361	2.553587	0.034639	0.772605	0.084435
372.483	0.226064	2.468867	0.033936	0.777963	0.084618
374.633	0.226124	2.377353	0.033876	0.783172	0.084795
376.767	0.226746	2.496774	0.033254	0.788372	0.084970
378.917	0.227128	2.442120	0.032872	0.793681	0.085145
381.050	0.227325	2.459780	0.032675	0.798910	0.085317
383.200	0.227922	2.493495	0.032078	0.804234	0.085489
385.333	0.228451	2.521839	0.031549	0.809584	0.085659
387.467	0.228700	2.482888	0.031300	0.814922	0.085827
389.617	0.229053	2.434806	0.030947	0.820209	0.085991
391.750	0.229429	2.496186	0.030571	0.825469	0.086153
393.900	0.229940	2.413707	0.030060	0.830747	0.086313
396.033	0.230397	2.478858	0.029603	0.835965	0.086469
398.183	0.230478	2.440024	0.029522	0.841253	0.086625
400.317	0.230754	2.495482	0.029246	0.846518	0.086780
402.450	0.230974	2.502520	0.029026	0.851849	0.086935
404.600	0.231158	2.440775	0.028842	0.857163	0.087089
406.733	0.231378	2.514522	0.028622	0.862449	0.087241
408.883	0.231777	2.523651	0.028223	0.867865	0.087395
411.033	0.232300	2.502749	0.027700	0.873268	0.087546

**Table 39. cont.**

time (min)	[2] (M)	[4] (mM)	[1]=[1] <sub>0</sub> -[2] (M)	VTNA using 4	VTNA using 1 and 4
413.167	0.232485	2.515137	0.027515	0.878621	0.087694
415.300	0.232825	2.486234	0.027175	0.883955	0.087840
417.450	0.233121	2.473302	0.026879	0.889287	0.087984
419.583	0.233611	2.516704	0.026389	0.894609	0.088125
421.733	0.233848	2.513270	0.026152	0.900017	0.088267
423.867	0.233809	2.535449	0.026191	0.905402	0.088408
426.000	0.233458	2.543003	0.026542	0.910819	0.088551
428.150	0.233575	2.494818	0.026425	0.916235	0.088695

Graph 8 shows the linearized VTNA profile resulting from the normalization of the time scale by the concentration of starting material **1** (vinyl acetate) and the concentration of estimated active catalyst. Numerical data are shown in Table 40 and have been calculated using the VTNA formula (Eq. 5).

$$normalized\ time = \sum_{i,j=1}^n \left( \frac{[4]_{est(i)} + [4]_{est(i-1)}}{2} \right)^1 \left( \frac{[1]_j + [1]_{j-1}}{2} \right)^1 (t_i - t_{i-1}) \quad \text{Eq. 5}$$

Graph 9 shows the comparison of the estimated percentage of catalyst and that measured from the <sup>1</sup>H-NMR spectra over time. The values for the estimated concentration profile were found using Solver. In this case, the condition that the concentration of catalyst could not decrease during the reaction was imposed. To do so in Excel, the concentration of catalyst at a given time was defined as the concentration in the previous time plus the corresponding increment. Specifically, these increments represented the Variable Cells, which were changed by Solver in order to maximize the R<sup>2</sup> (SQR function: square of the Pearson product moment correlation coefficient through data points (concentration of product, normalized time)) of the resulting VTNA profile shown in Graph 8.



**Table 40.** Data for Graph 8 and Graph 9

time (min)	[2] (M)	estimated [active cat] (mM)	% estimated active catalyst	% measured 4	VTNA using estimated [active catalyst]
2.150	0.000357	0.001256	0.05	0.25	0.000000
4.283	0.000568	0.033431	1.31	2.46	0.000010
6.417	0.000298	0.141336	5.53	2.03	0.000058
8.567	0.000985	0.186178	7.29	5.90	0.000149
10.700	0.001087	0.189802	7.43	6.50	0.000253
12.850	0.001456	0.236077	9.24	10.20	0.000372
14.983	0.001521	0.320082	12.53	12.71	0.000525
17.133	0.002191	0.362538	14.20	14.80	0.000714
19.267	0.002524	0.434342	17.01	17.62	0.000933
21.400	0.003352	0.474824	18.59	22.41	0.001183
23.550	0.003955	0.502241	19.67	24.73	0.001452
25.683	0.004546	0.569087	22.29	26.48	0.001744
27.833	0.005455	0.629314	24.64	30.46	0.002073
29.967	0.006412	0.769377	30.13	35.11	0.002452
32.100	0.007683	0.958992	37.55	34.63	0.002918
34.250	0.009242	1.021600	40.01	40.00	0.003454
36.383	0.010007	1.175246	46.02	44.60	0.004040
38.533	0.012146	1.185522	46.43	46.13	0.004672
40.667	0.013443	1.251378	49.00	49.02	0.005315
42.817	0.015104	1.406698	55.09	52.67	0.006017
44.950	0.017124	1.489075	58.31	57.06	0.006770
47.100	0.018905	1.569862	61.48	57.06	0.007566
49.233	0.021093	1.613991	63.20	59.84	0.008381
51.367	0.022968	1.649038	64.58	62.07	0.009209
53.517	0.025094	1.753467	68.67	65.67	0.010072
55.650	0.027647	1.822837	71.38	67.73	0.010964
57.800	0.029931	1.916824	75.06	68.52	0.011893
59.933	0.032300	1.983209	77.66	73.51	0.012845
62.083	0.034772	2.167532	84.88	74.12	0.013856
64.217	0.037141	2.218107	86.86	74.68	0.014904

Table 40. cont.

time (min)	[2] (M)	estimated [active cat] (mM)	% estimated active catalyst	% measured 4	VTNA using estimated [active catalyst]
66.367	0.039678	2.280643	89.31	76.45	0.015975
68.500	0.042305	2.286054	89.52	77.01	0.017042
70.633	0.044899	2.290337	89.69	78.99	0.018099
72.783	0.047556	2.296412	89.93	80.46	0.019153
74.917	0.050393	2.374631	92.99	80.39	0.020204
77.067	0.052960	2.394171	93.76	81.26	0.021272
79.200	0.055157	2.403436	94.12	81.51	0.022326
81.333	0.057943	2.414251	94.54	82.21	0.023371
83.483	0.060690	2.454987	96.14	83.24	0.024422
85.617	0.063263	2.456780	96.21	82.16	0.025459
87.767	0.065631	2.457195	96.23	83.93	0.026492
89.900	0.068296	2.457389	96.23	84.01	0.027504
92.050	0.070555	2.467363	96.62	84.47	0.028513
94.183	0.073456	2.467605	96.63	84.33	0.029503
96.333	0.075474	2.472968	96.84	82.57	0.030488
98.467	0.078088	2.477392	97.02	85.51	0.031456
100.600	0.079923	2.480014	97.12	83.63	0.032413
102.750	0.082403	2.481087	97.16	85.42	0.033367
104.883	0.084941	2.481106	97.16	84.91	0.034300
107.033	0.087076	2.482383	97.21	84.40	0.035228
109.167	0.089235	2.493052	97.63	86.53	0.036140
111.317	0.092106	2.494176	97.67	85.25	0.037048
113.450	0.093527	2.494818	97.70	84.79	0.037938
115.583	0.095973	2.494818	97.70	87.35	0.038817
117.733	0.097846	2.494818	97.70	85.92	0.039692
119.867	0.100485	2.494818	97.70	86.27	0.040548
122.017	0.102237	2.494818	97.70	86.69	0.041399
124.150	0.103985	2.494818	97.70	86.64	0.042234
126.300	0.106077	2.494818	97.70	85.82	0.043065
128.433	0.108398	2.494818	97.70	86.34	0.043878

Table 40. cont.

time (min)	[2] (M)	estimated [active cat] (mM)	% estimated active catalyst	% measured 4	VTNA using estimated [active catalyst]
130.583	0.110128	2.494818	97.70	86.31	0.044687
132.717	0.111861	2.494818	97.70	86.96	0.045480
134.850	0.114196	2.494818	97.70	87.81	0.046262
137.000	0.116354	2.494818	97.70	86.75	0.047038
139.133	0.117874	2.494818	97.70	87.04	0.047799
141.283	0.120037	2.494818	97.70	90.32	0.048555
143.417	0.121543	2.494818	97.70	88.13	0.049296
145.550	0.123050	2.494818	97.70	88.21	0.050029
147.700	0.125374	2.494818	97.70	88.17	0.050758
149.833	0.127127	2.494818	97.70	88.54	0.051469
151.983	0.128497	2.494818	97.70	88.80	0.052178
154.117	0.130581	2.494818	97.70	89.78	0.052873
156.267	0.132050	2.494818	97.70	87.82	0.053563
158.400	0.133727	2.494818	97.70	89.04	0.054240
160.550	0.135180	2.494818	97.70	88.77	0.054913
162.683	0.137242	2.494818	97.70	88.28	0.055572
164.817	0.138715	2.494818	97.70	88.86	0.056221
166.967	0.140692	2.494818	97.70	89.14	0.056866
169.100	0.142299	2.494818	97.70	89.75	0.057497
171.250	0.143960	2.494818	97.70	89.38	0.058124
173.383	0.145503	2.494818	97.70	89.97	0.058738
175.533	0.146776	2.494818	97.70	90.18	0.059348
177.667	0.148873	2.494818	97.70	91.73	0.059945
179.800	0.150139	2.494818	97.70	91.49	0.060533
181.950	0.151782	2.494818	97.70	91.59	0.061118
184.083	0.153003	2.494818	97.70	90.60	0.061691
186.233	0.154432	2.494818	97.70	88.90	0.062261
188.367	0.156017	2.494818	97.70	92.18	0.062819
190.517	0.157841	2.494818	97.70	91.85	0.063372
192.650	0.158346	2.494818	97.70	91.52	0.063914

Table 40. cont.

time (min)	[2] (M)	estimated [active cat] (mM)	% estimated active catalyst	% measured 4	VTNA using estimated [active catalyst]
194.783	0.159595	2.494818	97.70	91.63	0.064452
196.933	0.160933	2.494818	97.70	92.32	0.064987
199.067	0.161709	2.494818	97.70	91.77	0.065512
201.217	0.163275	2.494818	97.70	90.45	0.066035
203.350	0.164548	2.494818	97.70	91.40	0.066546
205.500	0.165805	2.494818	97.70	92.69	0.067055
207.633	0.167151	2.494818	97.70	92.21	0.067553
209.767	0.168543	2.494818	97.70	94.86	0.068043
211.917	0.169119	2.494818	97.70	92.14	0.068532
214.050	0.170561	2.494818	97.70	92.66	0.069012
216.200	0.171992	2.494818	97.70	92.95	0.069488
218.333	0.172892	2.494818	97.70	91.48	0.069954
220.483	0.174221	2.494818	97.70	90.53	0.070418
222.617	0.175369	2.494818	97.70	90.03	0.070871
224.750	0.176829	2.494818	97.70	95.01	0.071318
226.900	0.177750	2.494818	97.70	91.04	0.071761
229.033	0.178858	2.494818	97.70	92.96	0.072196
231.183	0.179752	2.494818	97.70	94.42	0.072629
233.317	0.181182	2.494818	97.70	94.27	0.073052
235.467	0.181935	2.494818	97.70	93.55	0.073473
237.600	0.183135	2.494818	97.70	91.68	0.073885
239.750	0.184299	2.494818	97.70	93.24	0.074294
241.883	0.185060	2.494818	97.70	91.85	0.074695
244.017	0.186140	2.494818	97.70	92.90	0.075091
246.167	0.187256	2.494818	97.70	93.32	0.075484
248.300	0.188415	2.494818	97.70	94.64	0.075868
250.450	0.188978	2.494818	97.70	92.12	0.076251
252.583	0.189702	2.494818	97.70	91.99	0.076627
254.717	0.190784	2.494818	97.70	93.45	0.076998
256.867	0.191679	2.494818	97.70	94.20	0.077367

Table 40. cont.

time (min)	[2] (M)	estimated [active cat] (mM)	% estimated active catalyst	% measured 4	VTNA using estimated [active catalyst]
259.000	0.192614	2.494818	97.70	93.05	0.077728
261.150	0.193541	2.494818	97.70	94.02	0.078087
263.283	0.194629	2.494818	97.70	95.99	0.078438
265.433	0.195387	2.494818	97.70	95.33	0.078787
267.600	0.196083	2.494818	97.70	95.23	0.079134
269.733	0.196910	2.494818	97.70	94.92	0.079472
271.883	0.197671	2.494818	97.70	95.20	0.079808
274.017	0.198591	2.494818	97.70	94.18	0.080138
276.150	0.199222	2.494818	97.70	96.18	0.080463
278.300	0.200447	2.494818	97.70	93.54	0.080786
280.433	0.200859	2.494818	97.70	94.89	0.081101
282.583	0.201801	2.494818	97.70	95.70	0.081416
284.717	0.202213	2.494818	97.70	93.67	0.081725
286.867	0.203172	2.494818	97.70	92.59	0.082032
289.000	0.203882	2.494818	97.70	94.37	0.082333
291.150	0.204548	2.494818	97.70	96.60	0.082632
293.283	0.204977	2.494818	97.70	94.68	0.082926
295.433	0.205658	2.494818	97.70	94.32	0.083219
297.567	0.206498	2.494818	97.70	95.83	0.083506
299.717	0.207362	2.494818	97.70	97.30	0.083791
301.850	0.208179	2.494818	97.70	97.40	0.084069
304.000	0.208613	2.494818	97.70	96.48	0.084346
306.133	0.209628	2.494818	97.70	95.89	0.084616
308.283	0.209960	2.494818	97.70	97.40	0.084886
310.417	0.210577	2.494818	97.70	94.39	0.085150
312.550	0.211308	2.494818	97.70	96.05	0.085412
314.700	0.211829	2.494818	97.70	96.42	0.085671
316.833	0.212710	2.494818	97.70	95.79	0.085925
318.983	0.213131	2.494818	97.70	95.16	0.086178
321.117	0.213754	2.494818	97.70	95.67	0.086426

Table 40. cont.

time (min)	[2] (M)	estimated [active cat] (mM)	% estimated active catalyst	% measured 4	VTNA using estimated [active catalyst]
323.250	0.214297	2.494818	97.70	95.82	0.086670
325.400	0.214922	2.494818	97.70	97.12	0.086914
327.533	0.215684	2.494818	97.70	95.27	0.087152
329.683	0.216625	2.494818	97.70	96.80	0.087387
331.817	0.216868	2.494818	97.70	96.82	0.087617
333.967	0.217630	2.494818	97.70	95.84	0.087846
336.100	0.218103	2.494818	97.70	95.16	0.088071
338.233	0.218636	2.494818	97.70	96.22	0.088292
340.383	0.219466	2.494818	97.70	95.05	0.088512
342.517	0.219929	2.494818	97.70	97.59	0.088726
344.667	0.220535	2.494818	97.70	96.51	0.088940
346.800	0.220942	2.494818	97.70	94.30	0.089149
348.933	0.221967	2.494818	97.70	96.65	0.089354
351.083	0.222135	2.494818	97.70	96.22	0.089557
353.217	0.223008	2.494818	97.70	95.30	0.089757
355.367	0.223170	2.494818	97.70	95.67	0.089955
357.500	0.223722	2.494818	97.70	97.02	0.090149
359.650	0.223767	2.494818	97.70	98.41	0.090344
361.783	0.224226	2.494818	97.70	95.33	0.090535
363.917	0.224596	2.494818	97.70	96.11	0.090725
366.067	0.224852	2.494818	97.70	99.47	0.090914
368.200	0.225271	2.494818	97.70	98.88	0.091100
370.350	0.225361	2.494818	97.70	100.00	0.091286
372.483	0.226064	2.494818	97.70	96.68	0.091468
374.633	0.226124	2.494818	97.70	93.10	0.091650
376.767	0.226746	2.494818	97.70	97.78	0.091829
378.917	0.227128	2.494818	97.70	95.63	0.092006
381.050	0.227325	2.494818	97.70	96.33	0.092181
383.200	0.227922	2.494818	97.70	97.65	0.092354
385.333	0.228451	2.494818	97.70	98.76	0.092524

Table 40. cont.

time (min)	[2] (M)	estimated [active cat] (mM)	% estimated active catalyst	% measured 4	VTNA using estimated [active catalyst]
387.467	0.228700	2.494818	97.70	97.23	0.092691
389.617	0.229053	2.494818	97.70	95.35	0.092858
391.750	0.229429	2.494818	97.70	97.75	0.093021
393.900	0.229940	2.494818	97.70	94.52	0.093184
396.033	0.230397	2.494818	97.70	97.07	0.093343
398.183	0.230478	2.494818	97.70	95.55	0.093501
400.317	0.230754	2.494818	97.70	97.72	0.093658
402.450	0.230974	2.494818	97.70	98.00	0.093813
404.600	0.231158	2.494818	97.70	95.58	0.093968
406.733	0.231378	2.494818	97.70	98.47	0.094121
408.883	0.231777	2.494818	97.70	98.83	0.094273
411.033	0.232300	2.494818	97.70	98.01	0.094423
413.167	0.232485	2.494818	97.70	98.49	0.094570
415.300	0.232825	2.494818	97.70	97.36	0.094716
417.450	0.233121	2.494818	97.70	96.86	0.094861
419.583	0.233611	2.494818	97.70	98.56	0.095003
421.733	0.233848	2.494818	97.70	98.42	0.095144
423.867	0.233809	2.494818	97.70	99.29	0.095283
426.000	0.233458	2.494818	97.70	99.59	0.095423
428.150	0.233575	2.494818	97.70	97.70	0.095565

## CONCLUSIONS

- An array of phosphine- and phosphite-containing supramolecular ligands incorporating a polyethyleneoxy chain as regulation site has been synthesized. Supramolecular ligands have been successfully used in the Rh-catalyzed hydroformylation of a representative example of a 1,1'-disubstituted allene. The use of a ligand with phosphine moieties as coordinating groups was not active in the hydroformylation reaction, but led to the formation of the  $\beta,\gamma$ -unsaturated aldehyde in 22% in the presence of an external regulation agent (21% increase in the yield with NaBArF as the regulation agent). The use of 3,3'-disubstituted [1,1'-biphenyl]-2,2'-diol phosphite motifs in the supramolecular ligands improved the catalytic activity with respect to that observed for the bisphosphine ligands. For the supramolecularly regulated bisphosphite ligand **L4**, the use of an external regulation agent provided a remarkable enhancement in the yield of the corresponding  $\beta,\gamma$ -unsaturated aldehyde (up to 60% increase). The benefits of our regulation approach have been demonstrated, as the presence of alkali metal BArF salts increase the catalytic activity. These studies have demonstrated that the modular design of the supramolecular ligands and the right combination of coordinating group, binding site and regulation agent is crucial for the catalytic outcome in the hydroformylation of allenes, with the formation of side-products being suppressed.
- The complex  $[\text{Co}(\text{H})(\text{CO})_2(\text{Xantphos})]$  has been efficiently synthesized and characterized for its application in the hydroformylation of styrene, oct-1-ene and a set of octene isomers. Comparative studies employing preformed catalyst  $[\text{Co}(\text{H})(\text{CO})_2(\text{Xantphos})]$  or the catalyst formed *in situ* from Xantphos and  $[\text{Co}_2(\text{CO})_8]$  indicated that higher selectivities towards the desired aldehydes were obtained with the *in situ* prepared catalyst. For styrene, the cobalt-catalyzed hydroformylation took place with poor selectivities towards the formation of aldehydes, with the corresponding hydrogenated product being the major product being formed. Moderate linear to branched product ratios were observed (up to 59:41), taking into consideration the inherent preference of styrene to yield branched aldehydes. The regioselectivity was majorly influenced by the temperature, observing higher ratios of the linear aldehyde by increasing the temperature. The cobalt-catalyzed hydroformylation of oct-1-ene employing Xantphos as



ligand was highly selective towards aldehydes under the optimized catalytic reaction conditions (140 °C, 40 bar H<sub>2</sub>/CO in 1:1 ratio, 1/1 ratio Xantphos/[Co<sub>2</sub>(CO)<sub>8</sub>], 0.26 M), with formation of side-reaction products such as hydrogenated products, unreacted isomerized starting material, and alcohol derivatives being minimized. Hydroformylation of internal octene isomers have been successfully carried out. High aldehyde selectivities were observed in all the cases, independently of the position or geometry of the C=C double bond in the starting material. Linear to branched ratios for all studied octene isomers also remained practically constant, independently of the substrate being hydroformylated. These results led us to hypothesize that under the effects of our Xantphos-cobalt based catalyst, a tandem isomerization-hydroformylation process could be taking place. Cobalt-catalyzed hydroformylation of a mixture of octenes with Xantphos as ligand, has proven to be an interesting strategy in the valorization of petroleum feedstocks with potential application at the industrial scale.

- The rhodium-catalyzed enantioselective hydroformylation of challenging aryl vinyl ethers has been described employing supramolecularly regulated rhodium complexes derived from polyether-containing bisphosphite ligands. The presence of regulation agents had an important influence in the catalytic activity and enantioselectivity, probably by inducing subtle changes in the geometry of the catalytic site. By choosing the matched regulation agent for a given substrate, the catalytic activity (up to 66%) and enantioselectivity (up to 97:3 *er*) were enhanced. The enantioselectivities attained with our supramolecularly regulated catalyst are among the highest reported in the hydroformylation of aryl vinyl ethers. Steric effects induced by *ortho* substituents to the vinyloxy group in the aromatic ring of the substrates, as well as electronic effects induced by strong electron-donating groups to the aryl group of the substrate, decreased the conversion of the hydroformylation reaction. Our synthetic methodology was applied to the preparation of advanced synthetic intermediates of relevant agrochemicals such as Napropamide, Mecoprop and Dichlorprop. Complexation studies demonstrated that the formation of catalytic species under syngas atmosphere in the presence of regulation agents led to the formation of two isomeric hydrido dicarbonyl rhodium complexes, with their ratio depending on the RA used. It was demonstrated that the bisphosphite ligand was coordinated to the equatorial positions of a trigonal bipyramidal rhodium

center with the hydrido ligand being coordinated at the apical position. Mechanistic studies revealed the reversibility of the alkene insertion under catalytic conditions and the irreversibility of the hydrogenolysis step. A tentative rationalization of the stereochemical outcome of the reaction from the alkene complexes with catalytic species derived from  $[\text{Rh}(\kappa^2\text{O},\text{O}'\text{-acac})(\text{CO})_2]$ , (*R*)-**L6** and LiBArF as the regulation agent has been made.

- A high-pressure setup for the continuous flow NMR analysis of the hydroformylation reaction mixture was designed and developed from a commercially available high-pressure reactor and a Bruker flow NMR probe. The reaction profiles with the concentrations of (pre-)catalytic species, substrate and product against time in the supramolecularly regulated enantioselective hydroformylation of vinyl acetate were measured under catalytic conditions. Variable Time Normalization Analysis (VTNA) was used for analyzing the kinetic data (*i.e.*, the concentration profile of substrate, product and catalytically relevant intermediates as a function of time) in order to determine the reaction orders of the olefin and rhodium species and calculate the value of the observed rate constant of the hydroformylation process. The generation of catalytically active supramolecular complexes for hydroformylation reactions required an induction period, in which the concentration of the catalyst was not constant due to its building-up. The use of VTNA enabled the simplification of the concentration profiles of the hydroformylation by mathematically eliminating the induction period and unravelling the kinetic data of the reaction as if the catalytic species would have been present from the beginning. Analysis of the kinetic data revealed that the coordination of the alkene to the metal center followed by the insertion of the terminal alkene carbon into the Rh–H bond were the rate- and stereo-determining steps. Moreover, VTNA analysis also provided a satisfactory estimation of the percentages of hydrido-containing supramolecular rhodium complexes during the reaction with respect to the total amount of rhodium complexes by identifying the best linearization of the variable time normalized reaction profile. VTNA kinetic analyses, in combination with the study of the effects produced by changing the relative molar amounts of  $\text{H}_2$  and CO in the catalytic transformation, have revealed that the supramolecularly regulated rhodium-catalyzed hydroformylation of vinyl acetate with bisphosphite ligand (*R*)-**L1** and RbBArF follows the so-called *type I* kinetics.

UNIVERSITAT ROVIRA I VIRGILI

THE HYDROFORMYLATION REACTION: FROM COVALENT TO SUPRAMOLECULAR APPROACHES AND OPERANDO KINETIC STUDIES

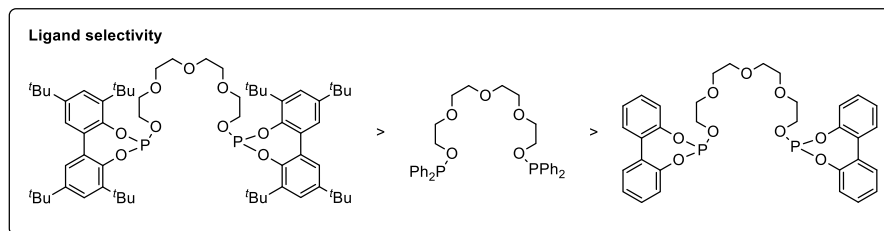
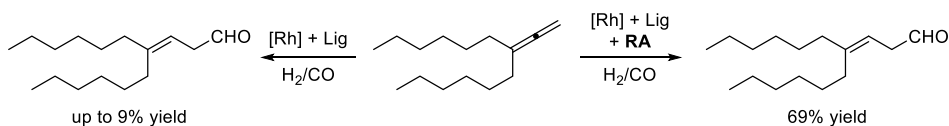
Alicia Martínez Carrión

## SUMMARY

The hydroformylation reaction is one of the most important examples of homogeneous catalysis applied at the industrial scale. The potential of this transformation is recognized as it enables the transformation of inexpensive and easily available alkenes into functionalized organic molecules, which are relevant intermediates in the production of commodities and fine-chemistry products.

The aim of the present doctoral thesis comprises the study of the hydroformylation reaction from different perspectives (*i.e.*, from the methodological and mechanistic points of view) and the use of rhodium- and cobalt-based catalysts. This work encompasses the hydroformylation of alkenes employing phosphine-based cobalt-catalysts, the design and synthesis of new supramolecularly regulated bisphosphine and bisphosphite ligands for the rhodium-catalyzed hydroformylation of diverse substrates, and kinetic studies on the supramolecularly regulated rhodium-catalyzed hydroformylation of vinyl acetate.

Initial efforts focused on the study of efficient supramolecular catalytic systems for hydroformylation reactions. Therefore, bisphosphine and bisphosphite ligands incorporating a polyether-chain as regulation site were designed and synthesized (Chapter I) (Scheme 46). The application in the hydroformylation of 1,1'-disubstituted allenes highlighted the high catalytic activity of the supramolecular catalysts based on phosphite ligands. The incorporation of 3,3',5,5'-tetra-*tert*-butyl-(1,1'-biphenyl)-2,2'-diol-based phosphite groups in the supramolecular ligands enhanced the selectivity to form the corresponding  $\beta,\gamma$ -unsaturated aldehyde in a 64% yield. The regulation strategy was demonstrated when alkali metal BArF salts were used as regulation agents. Under optimized catalytic conditions, the presence of KBarF as regulation agent improved the selectivity by 60% in favor of the  $\beta,\gamma$ -unsaturated aldehyde.

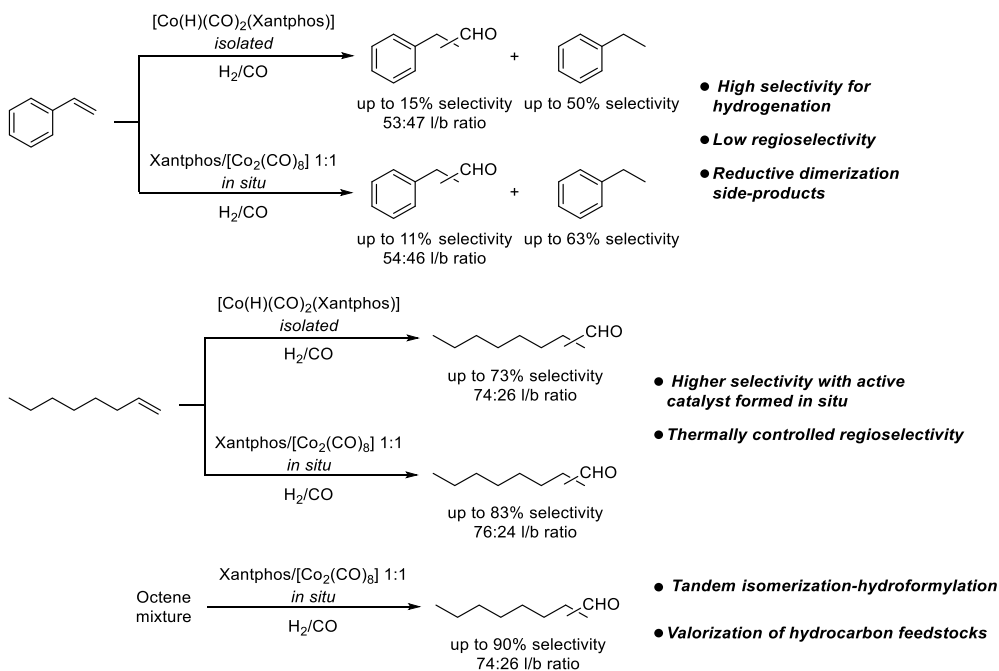


- Higher selectivity for bisphosphite ligands with bulky substituents in ortho position
- Enhancement in the formation of the  $\beta,\gamma$ -unsaturated aldehyde upon RA addition

**Scheme 46.** Rhodium-catalyzed supramolecularly regulated hydroformylation of 1,1'-disubstituted allenes

Coinciding with the main aim of this Thesis, cobalt-catalyzed hydroformylations employing Xantphos as ligand (Chapter II) were studied. We envisaged that the combination of a cobalt precursor and a bisphosphine ligand with a wide bite angle, would provide high selectivity towards linear aldehydes. A comparative study of the performance of the catalytically active  $[\text{Co}(\text{H})(\text{CO})_2(\text{Xantphos})]$  complex was performed, comparing the catalytic behavior of the complex generated *in situ* with that previously synthesized (Scheme 47). The catalytic activity of the Xantphos-based cobalt complexes was evaluated in the hydroformylation of styrene: low chemoselectivity was observed for the formation of aldehydes (11% selectivity), being the hydrogenated product the major product (63% selectivity) under the best catalytic conditions. Moderate regioselectivities that were only affected by the reaction temperature were observed. The hydroformylation of 1-octene revealed a different scenario: high selectivity yielding aldehydes as major products (83% selectivity) and minimal formation of side-reaction products, such as hydrogenation products, alcohols derived from the hydrogenation of aldehydes and unreacted or isomerized substrates. The transformation was extended to internal alkenes, which are less reactive than the analogous terminal counterpart. High selectivity towards the aldehydes was observed for all octene isomers, with a constant regioselectivity, independently of the position or geometry of the double bond. The similar outcome of the reaction, independently from the starting material, led us to hypothesize that a tandem isomerization-hydroformylation transformation was taking place. For all the substrates, a better catalytic performance was observed

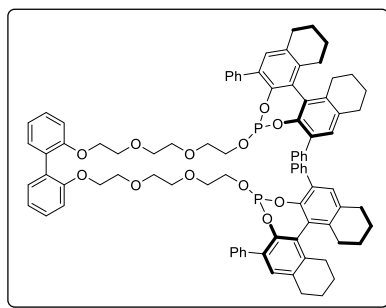
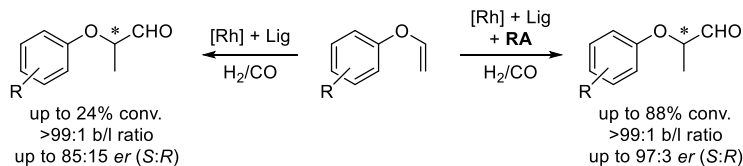
when the catalyst was formed *in situ* with a 1:1 Xantphos/[Co<sub>2</sub>(CO)<sub>8</sub>] ratio than with pre-formed catalyst.



**Scheme 47.** Cobalt-catalyzed hydroformylation of aryl- and alkyl-substituted alkenes employing Xantphos as ligand

In the hydroformylation of alkenes with predominant formation of the branched aldehydes, a stereogenic center is formed in the transformation. In this context, the enantioselective hydroformylation is a valuable approach for the synthesis of optically enriched (or even enantiopure) molecules for the pharmaceutical, biological or agrochemical sectors. Following our efforts in developing highly efficient supramolecular catalytic systems incorporating a distal regulation site, we focused our interest on the enantioselective hydroformylation of aryl vinyl ethers (Chapter III) (Scheme 48). After ligand screening, we observed that a ligand incorporating 3,3'-diphenyl substituted H<sub>8</sub>-BINOL-based phosphite moieties (as coordinating groups) and a linear poly-ether chain containing a conformationally labile biphenyl motif (as regulation site) provided high catalytic activity, regioselectivity and from moderate to high enantiomeric ratios. The selection of LiBArF as regulation agent enhanced the catalytic activity and enantiomeric ratio (up to 70% increase in conv. and enantiomeric ratios from 78:22 to 92:8 *S*:*R*-configured aldehydes). Aiming to broaden the applicability of this transformation, the enantioselective hydroformylation was expanded to aryl

vinyl ethers with electronically diverse substituents at different positions in the aromatic ring, observing a lower conversion with substituents in *ortho* position or when electron-donating groups were present in the aromatic ring. The preparation of advanced synthetic intermediates of agrochemicals was performed using this methodology.



- 11 examples

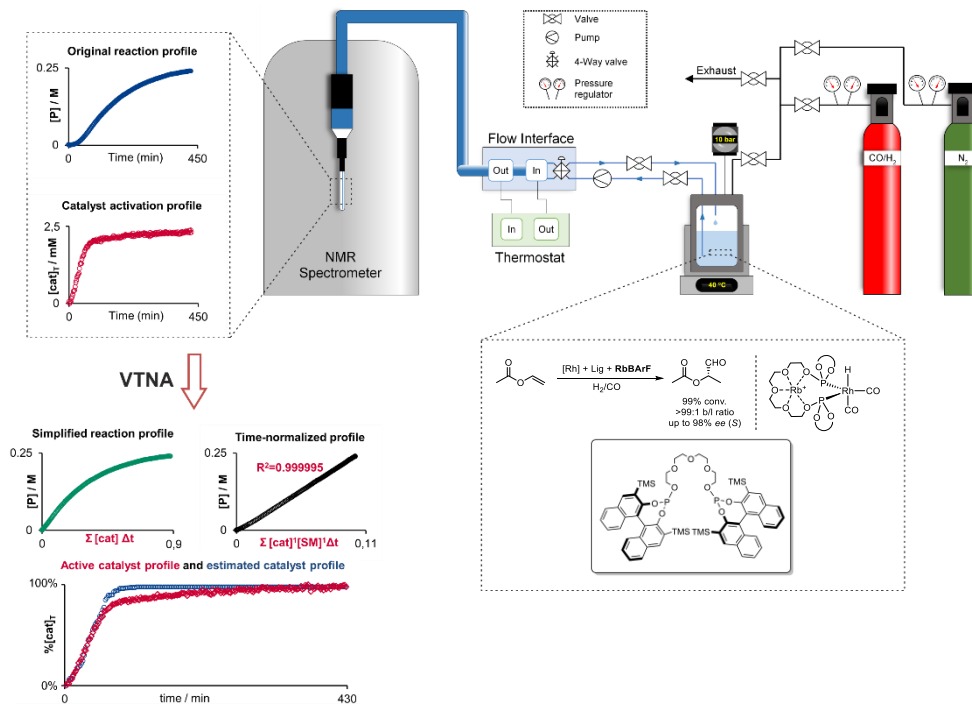
- Preparation of intermediates of relevant agrochemicals as Napropamide, Mecoprop and Dichlorprop

- Positive regulation effects with impact in the catalyst speciation

**Scheme 48.** Rhodium-catalyzed supramolecularly regulated enantioselective hydroformylation of aryl vinyl ethers

Research efforts were also directed towards the mechanistic understanding of the supramolecularly regulated enantioselective hydroformylation of vinyl acetate. For this purpose, an experimental setup was designed and developed for the *online* reaction monitoring of the reaction under catalytic conditions (Chapter IV). The experimental setup is based on a NMR flow probe assembled with a high-pressure reactor and a pressurization system, allowing the reaction mixture to flow between the spectrometer and the reactor (Scheme 49). The effectiveness of this experimental setup enabled the monitoring of the hydroformylation under reaction conditions (*i.e.*, 40 °C and 10 bar H<sub>2</sub>/CO 1:1). Concentration reaction profiles revealed an induction period in the catalyst formation. Variable Time Normalization Analysis (VTNA) was used as a visual kinetic analysis method to extract the relevant kinetic information. The VTNA allowed for the removal of the induction period observed in the product formation, revealing a simple profile and a real first-order dependence on substrate and catalyst concentrations in the hydroformylation reaction. A second kinetic treatment served to estimate the concentration percentage of active catalyst (Scheme 49). The kinetic studies allowed for the determination of the rate-determining step in the early stages of

the catalytic cycle, particularly in the olefin coordination or insertion into the Rh–H bond steps. Although the hydroformylation mechanism could not be fully demonstrated, the kinetic analysis unveiled relevant mechanistic information of the supramolecularly regulated hydroformylation.



**Scheme 49.** Kinetic studies of the rhodium-catalyzed supramolecularly regulated enantioselective hydroformylation of vinyl acetate



UNIVERSITAT ROVIRA I VIRGILI

THE HYDROFORMYLATION REACTION: FROM COVALENT TO SUPRAMOLECULAR APPROACHES AND OPERANDO KINETIC STUDIES

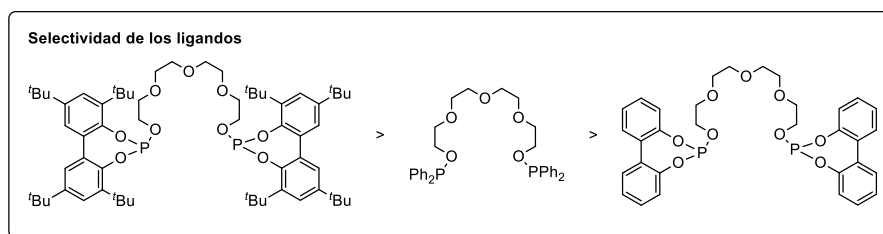
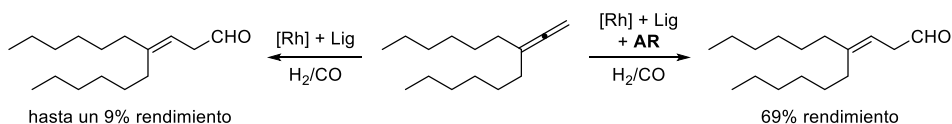
Alicia Martínez Carrión

## RESUMEN

La reacción de hidroformilación es uno de los ejemplos más importantes de catálisis homogénea aplicados a nivel industrial. El potencial de esta transformación está ampliamente reconocido, debido a que permite la transformación de alquenos que son abundantes y económicamente asequibles en moléculas orgánicas funcionalizadas, las cuales son importantes intermedios en la producción de productos básicos y de química fina.

El objetivo de la presente tesis doctoral comprende el estudio de la reacción de hidroformilación desde diferentes perspectivas (esto es, desde el punto de vista metodológico y mecanístico) y el uso de catalizadores basados en rodio y cobalto. Este trabajo abarca la hidroformilación de diversos alquenos empleando catalizadores de cobalto modificados con ligandos de tipo fosfina; el diseño y síntesis de nuevos ligandos modulares de tipo bisfosfina y bisfosfito regulados mediante interacciones supramoleculares para su aplicación en la hidroformilación de diversos alquenos empleando catalizadores de rodio; y los estudios cinéticos de la hidroformilación de acetato de vinilo catalizada mediante sistemas supramoleculares de rodio.

Las actividades de investigación se centraron en el estudio de sistemas catalíticos supramoleculares eficientes en reacciones de hidroformilación. Para ello, se diseñaron y sintetizaron ligandos modulares con grupos coordinantes de tipo bisfosfina y bisfosfito que incorporan una cadena de polietilenglicol como centro de regulación (Capítulo I) (Esquema 50). Estos ligandos fueron empleados para la hidroformilación de alenos 1,1'-disustituidos, demostrando una mayor actividad catalítica mediante el empleo de los catalizadores supramoleculares con grupos fosfito. La incorporación de grupos fosfito del tipo 3,3',5,5'-tetra-*tert*-butilo-[1,1'-bifenilo]-2,2'-diol en los ligandos supramoleculares permitió la formación del aldehído  $\beta,\gamma$ -insaturado de manera más selectiva (hasta un 64% de rendimiento). La eficacia de la estrategia de regulación fue demostrada mediante el uso de sales de BArF de metales alcalinos como agentes de regulación (AR). Con las condiciones optimizadas de reacción, el uso de KBarF como agente de regulación mejoró la formación del aldehído  $\beta,\gamma$ -insaturado de manera selectiva, hasta en un 60%.

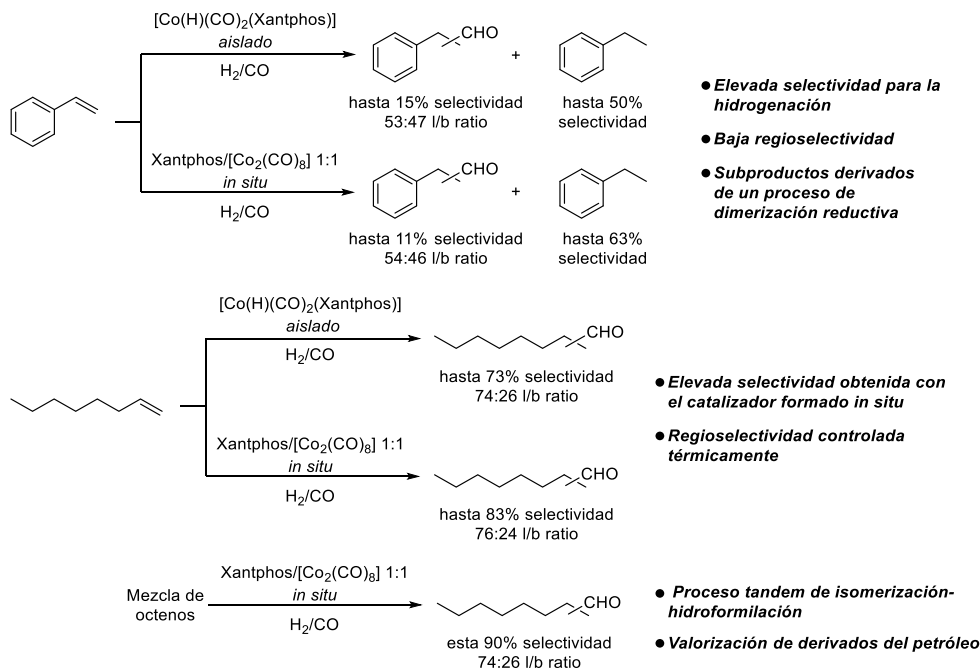


- **Mayor selectividad observada en ligandos bisfosfito con sustituyentes voluminosos en la posición orto**
- **Aumento de la formación del aldehído  $\beta,\gamma$ -insaturado debido a la presencia de AR**

**Esquema 50.** Hidroformilación de alenos 1,1'-disustituídos mediante el empleo de catalizadores de rodio supramoleculares

Otras actividades de investigación se centraron en el estudio de la transformación de hidroformilación catalizada por cobalto en presencia del ligando Xantphos (Capítulo II). Nuestra hipótesis de partida concebía que el uso combinado de un precursor de cobalto y un ligando de tipo bisfosfina con un amplio “bite angle” daría lugar a la formación de aldehídos lineales de manera más selectiva. Para ello, se llevó a cabo un estudio del comportamiento y eficiencia del complejo catalíticamente activo  $[\text{Co}(\text{H})(\text{CO})_2(\text{Xantphos})]$ , comparando el complejo generado *in situ* y el sintetizado de manera previa (Esquema 51). La actividad catalítica del complejo de cobalto modificado con Xantphos fue evaluada en la hidroformilación de estireno: tras la optimización de las condiciones de reacción, se observó una baja quimioselectividad hacia la formación de aldehídos (11% selectividad), siendo el producto derivado de la hidrogenación de estireno el obtenido en mayor proporción (63% selectividad). La regioselectividad obtenida para los aldehídos fue moderada y solo se vio afectada por variaciones en la temperatura de reacción. En el caso de la hidroformilación de 1-octeno, los resultados mostraron una situación distinta: se observó una mayor selectividad en la formación de aldehídos, siendo éstos los productos mayoritarios (83% selectividad) y se vio reducida la formación de subproductos de reacción, como los derivados de la hidrogenación de alquenos, los alcoholes provenientes de la hidrogenación de aldehídos y los alquenos de partida isomerizados. La utilidad de esta transformación se amplió a alquenos internos, sustratos análogos a los alquenos terminales pero que presentan una menor reactividad química. La formación de aldehídos como productos de reacción fue altamente selectiva para todos los isómeros del octeno, sin importar

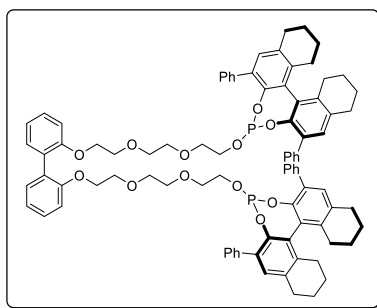
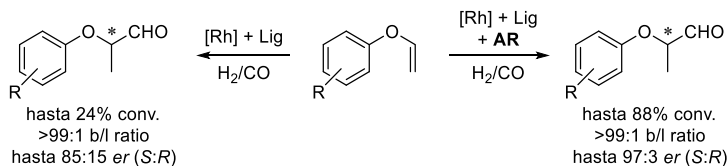
la posición o geometría del doble enlace. La obtención de resultados catalíticos similares, independientemente del octeno utilizado como sustrato de partida, nos llevó a postular que la transformación tiene lugar en una secuencia tándem de hidrogenación y posterior hidroformilación. Para todos los sustratos sometidos a dicha transformación, el catalizador formado *in situ* con una relación 1:1 entre el ligando Xantphos y el precursor  $[\text{Co}_2(\text{CO})_8]$  dio mejores resultados que el sintetizado previamente.



**Esquema 51.** Hidroformilación de alquenos sustituidos con grupos arilo y alquilo catalizada por cobalto en presencia de Xantphos como ligando

Cuando la reacción de hidroformilación transcurre de manera selectiva hacia la formación de aldehídos ramificados, tiene lugar la formación de un centro estereogénico. Es por ello, que la reacción de hidroformilación en su versión enantioselectiva es una estrategia eficiente para llevar a cabo la síntesis de productos ópticamente enriquecidos (o incluso ópticamente puros) en el ámbito farmacéutico, biológico o con importancia en el sector de la agroquímica. Con el objetivo de continuar con el desarrollo de sistemas catalíticos eficientes regulados supramolecularmente mediante la incorporación de un centro de regulación distal, nuestra investigación se centró en la aplicación de dichos sistemas catalíticos en la hidroformilación enantioselectiva de aril vinil éteres (Capítulo III) (Esquema 52). La evaluación de diferentes tipos de ligandos supramoleculares

demonstró que la combinación de grupos coordinantes de tipo fosfito basados en fragmentos de H<sub>8</sub>-BINOL con sustituyentes fenilo en las posiciones 3 y 3' y de una cadena lineal de tipo poliéter que contiene un esqueleto de bifenilo sin restricciones conformacionales, como centro de regulación, da lugar a sistemas con elevada actividad catalítica, regioselectividad y enantioselectividades que oscilan entre moderadas y altas. El empleo de LiBARF como agente de regulación dio lugar al aumento de la actividad catalítica y el ratio enantiomérico (hasta un 70% de incremento en la conversión y un aumento del ratio enantiomérico del 78:22 al 92:8 de aldehídos con configuración *S*:*R*). Con el objetivo de ampliar la aplicabilidad de esta transformación, se expandió la hidroformilación enantioselectiva a aril vinil éteres con sustituyentes con diversos efectos electrónicos y estéricos. Se observó que la actividad catalítica disminuía con la presencia de sustituyentes en la posición *orto* o de grupos electrodonadores en el anillo aromático. Esta aproximación catalítica permitió la síntesis de intermedios sintéticos avanzados de compuestos agroquímicos.



- 11 ejemplos

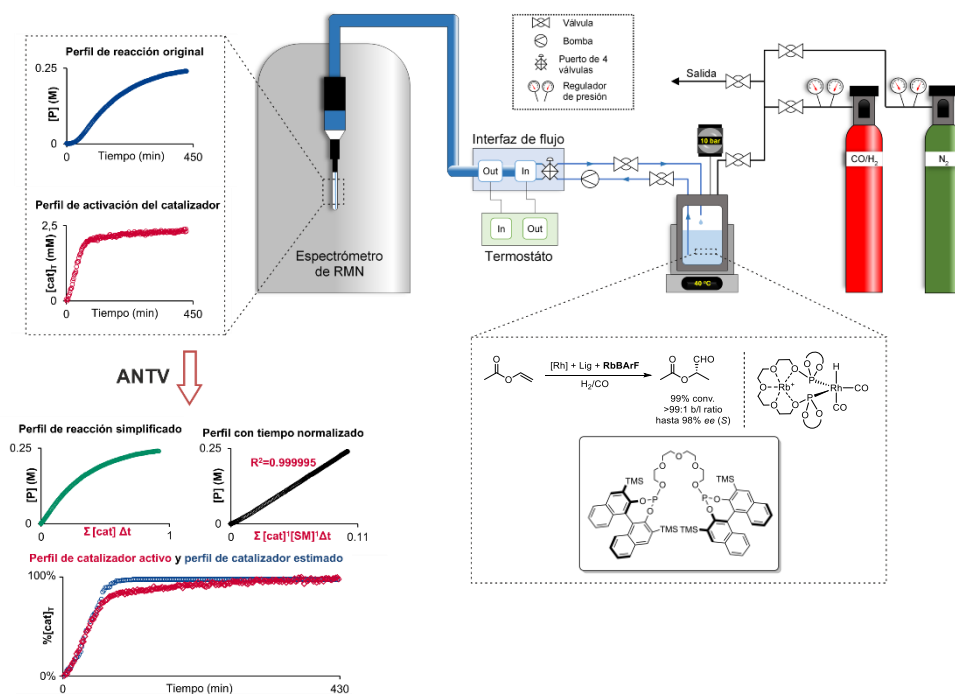
- Preparación de intermedios con importancia en el sector agroquímico como Napropamida, Mecoprop y Diclorprop

- Efectos positivos de regulación supramolecular con impacto en la especiación del catalizador

**Esquema 52.** Hidroformilación enantioselectiva de aril vinil éteres catalizada por sistemas supramoleculares de rodio

Las actividades investigadoras también se enfocaron hacia la comprensión mecanístico de la reacción de hidroformilación enantioselectiva del acetato de vinilo catalizada mediante sistemas supramoleculares de rodio. Para ello, se llevó a cabo el diseño y desarrollo de un montaje experimental para la monitorización *online* de reacciones en condiciones catalíticas de reacción (Capítulo IV). El montaje experimental se componía de una sonda en flujo de RMN ensamblada con un reactor de alta presión y un sistema de presurización, que permitía el flujo de la mezcla de reacción entre el espectrómetro y el reactor a alta presión

(Esquema 53). La eficacia de esta instalación ha permitido la monitorización de la reacción de hidroformilación en condiciones catalíticas (*i.e.*, 40 °C y 10 bar H<sub>2</sub>/CO en una proporción 1:1). Los perfiles de concentración de la reacción revelaron la presencia de un periodo de inducción en la formación del catalizador supramolecular. Se empleó el Análisis de Normalización de Tiempo Variable (ANTV) como un método de análisis cinético visual y sencillo para extraer la información cinética relevante de la transformación. El ANTV permitió la eliminación del periodo de inducción observado en la formación del producto de reacción, mostrando un perfil de reacción simplificado y el verdadero primer orden de reacción en concentración de sustrato y catalizador para la reacción de hidroformilación. El empleo de un segundo tratamiento cinético permitió la estimación del porcentaje de concentración de catalizador activo (Esquema 53). Los estudios cinéticos permitieron determinar que el paso limitante de la velocidad de la reacción tiene lugar en las primeras etapas del ciclo catalítico, particularmente en la reacción de coordinación o inserción del carbono terminal de la olefina al enlace Rh–H. Aunque no ha sido posible la elucidación del mecanismo en su totalidad, el uso de estudios cinéticos *in situ* y técnicas *operando* ha permitido obtener información mecanística relevante de los sistemas catalíticos supramoleculares aplicados a la reacción de hidroformilación.



**Esquema 53.** Estudios cinéticos de la reacción de hidroformilación enantioselectiva de acetato de vinilo catalizada mediante sistemas supramoleculares de rodio

UNIVERSITAT ROVIRA I VIRGILI

THE HYDROFORMYLATION REACTION: FROM COVALENT TO SUPRAMOLECULAR APPROACHES AND OPERANDO KINETIC STUDIES

Alicia Martínez Carrión

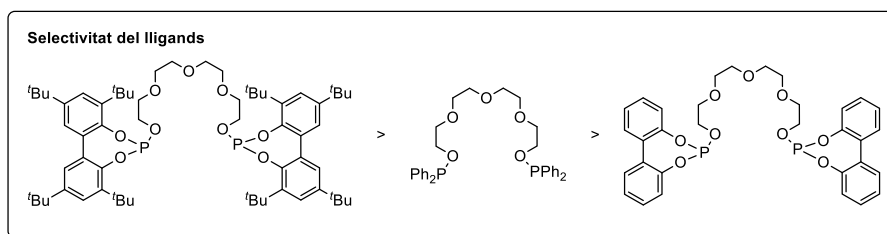
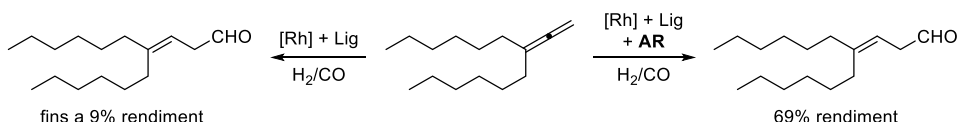
## RESUM

La reacció d'hydroformilació és un dels exemples més importants de catalisi homogènia aplicats a nivell industrial. El potencial d'aquesta transformació està àmpliament reconegut, pel fet que permet la transformació d'alquens que són abundants i econòmicament assequibles en molècules orgàniques funcionalitzades, que són importants intermedis en la producció de productes bàsics i de química fina.

L'objectiu de la present tesi doctoral comprèn l'estudi de la reacció d'hydroformilació des de diferents perspectives (això és, des del punt de vista metodològic i mecanístic) i l'ús de catalitzadors basats en rodi i cobalt. Aquest treball abasta la hydroformilació de diversos alquens emprant catalitzadors de cobalt modificats amb lligands de tipus fosfina; el disseny i síntesi de nous lligands modulars de tipus bisfosfina i bisfosfit regulats mitjançant interaccions supramoleculares per a l'aplicació en la hydroformilació de diversos alquens emprant catalitzadors de rodi; i els estudis cinètics de la hydroformilació d'acetat de vinil catalitzada mitjançant sistemes supramoleculares de rodi.

Les activitats de recerca es van centrar en l'estudi de sistemes catalítics supramoleculares eficients en reaccions d'hydroformilació. Amb aquesta finalitat, es van dissenyar i sintetitzar lligands modulars amb grups coordinants de tipus bisfosfina i bisfosfit que incorporen una cadena de polietilenglicol com a centre de regulació (Capítol I) (Esquema 54). Aquests lligands van ser emprats per a la hydroformilació d'al·lens 1,1'-disubstituïts, mostrant una major activitat catalítica mitjançant l'ús dels catalitzadors supramoleculares amb grups fosfit. La incorporació de grups fosfits del tipus 3,3',5,5'-tetra-*tert*-butil-(1,1'-bifenil)-2,2'-diol en els lligands supramoleculares va permetre la formació de l'aldehid  $\beta,\gamma$ -insaturat de manera més selectiva (fins a un 64% de rendiment). L'eficàcia de l'estratègia de regulació va ser demostrada mitjançant l'ús de sals de BArF alcalines com a agents de regulació (AR). Amb les condicions optimitzades de reacció, l'ús de KBarF com a agent de regulació va millorar la formació de l'aldehid  $\beta,\gamma$ -insaturat de manera selectiva, fins a un 60%.



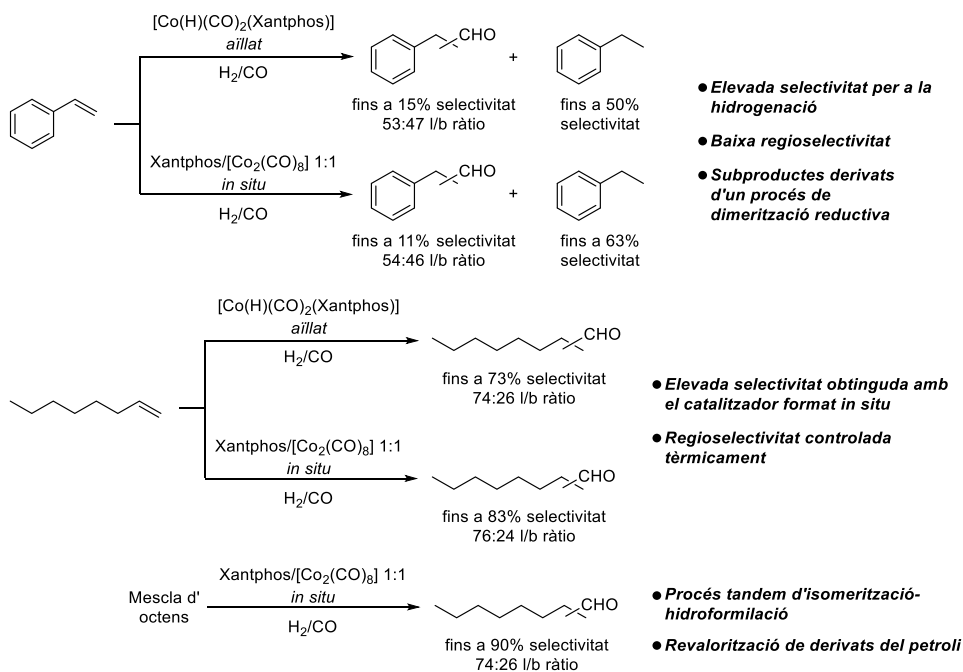


- Major selectivitat observada en lligands bisfosfit amb substituents voluminosos en la posició orto
- Augment de la formació de l'aldehid  $\beta,\gamma$ -insaturat a causa de la presència d'AR

**Esquema 54.** Hidroformilació d'al·lens 1,1'-disubstituïts mitjançant l'ús de catalitzadors de rodi supramoleculars

Altres activitats de recerca es van enfocar a l'estudi de la transformació d'hidroformilació catalitzada amb cobalt en presència del lligand Xantphos (Capítol II). La nostra hipòtesi de partida concebia que l'ús combinat d'un precursor de cobalt i un lligand de tipus bisfosfina amb un ampli "bite angle" donaria lloc a la formació d'aldehids lineals de manera més selectiva. Amb aquesta finalitat, es va dur a terme l'estudi del comportament i eficiència del complex catalíticament actiu  $[\text{Co}(\text{H})(\text{CO})_2(\text{Xantphos})]$ , comparant el complex generat *in situ* i el sintetitzat de manera prèvia (Esquema 55). L'activitat catalítica del complex de cobalt modificat amb Xantphos va ser avaluada en la hidroformilació d'estirè: després de l'optimització de les condicions de reacció, es va observar una baixa quimioselectivitat cap a la formació d'aldehids (11% selectivitat), sent el producte derivat de la hidrogenació d'estirè l'obtingut en major proporció (63% selectivitat). La regioselectivitat obtinguda dels aldehids va ser moderada i només es va veure afectada per variacions en la temperatura de reacció. En el cas de la hidroformilació del 1-octè, els resultats van mostrar una situació diferent: es va observar una major selectivitat en la formació d'aldehids, sent aquest el producte majoritari (83% selectivitat) i es va veure reduïda la formació de subproductes de reacció, com els derivats de la hidrogenació d'alquens, els alcohols provinents de la hidrogenació d'aldehids i els alquens de partida isomeritzats. La utilitat d'aquesta transformació es va ampliar a alquens interns, substrats anàlegs als alquens terminals però que presenten una menor reactivitat química. La formació d'aldehids com a productes de reacció va ser altament selectiva per a tots els isòmers de l'octè, sense importar la posició o geometria del doble enllaç. L'obtenció de resultats catalítics similars independentment de l'octè

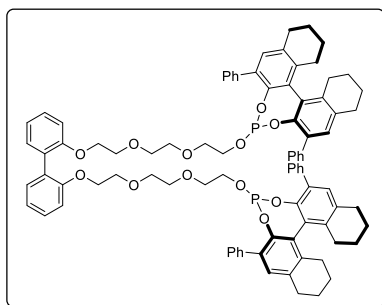
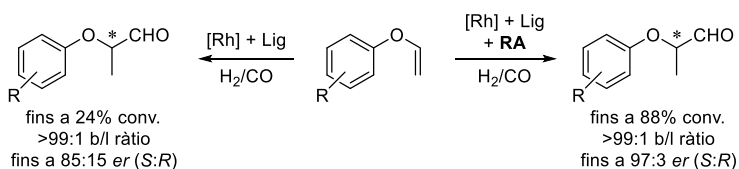
utilitzat com a substrat de partida ens va portar a postular que la transformació té lloc en una seqüència tàndem d'hidrogenació i posterior hidroformilació. Per a tots els substrats sotmesos a aquesta transformació, el catalitzador format *in situ* amb una relació 1:1 entre el lligand Xantphos i el precursor  $[\text{Co}_2(\text{CO})_8]$  va donar millors resultats que el sintetitzat prèviament.



**Esquema 55.** Hidroformilació d'alcens substituïts amb grups aril i alquil catalitzada per cobalt en presència de Xantphos com a lligand

Quan la reacció d'hidroformilació transcorre de manera selectiva cap a la formació d'aldehids ramificats, es crea un centre estereogènic. És per això que la reacció d'hidroformilació en la seva versió enantioselectiva és una estratègia eficient per a dur a terme la síntesi de productes en forma òpticament enriquida (o fins i tot òpticament pura) amb rellevància en l'àmbit farmacèutic, biològic o amb importància en el sector de l'agroquímica. Amb l'objectiu de continuar amb el desenvolupament de sistemes catalítics eficients regulats supramolecularment mitjançant la incorporació d'un centre de regulació distal, la nostra recerca es va centrar en l'aplicació d'aquests sistemes catalítics en la hidroformilació enantioselectiva d'aril vinil èters (Capítol III) (Esquema 56). L'avaluació de diferents tipus de lligands supramoleculars va demostrar que la combinació de grups coordinants de tipus fosfit basats en fragments d' $\text{H}_8$ -BINOL amb substituents fenil en les posicions 3 i 3' i d'una cadenes lineal de tipus polièter

que contenia un grup bifenil sense restriccions conformacionals, com a centre de regulació, va donar lloc a sistemes amb elevada activitat catalítica, regioselectivitat i enantioselectivitats que oscil·laven entre moderades i altes. L'ús de LiBArF com a agent de regulació va donar lloc a l'augment de l'activitat catalítica i el ràtio enantiomèric (fins a un 70% d'increment en la conversió i un augment del ràtio enantiomèric del 78:22 al 92:8 d'aldehids amb configuració *S*:*R*). Amb l'objectiu d'ampliar l'aplicabilitat d'aquesta transformació, es va expandir la hidroformilació enantioselectiva a aril vinil èters amb substituents amb diverses propietats electròniques i estèriques. Es va observar que l'activitat catalítica disminuïa amb la presència de substituents en la posició *orto* o de grups electroattractors a l'anell aromàtic. Aquesta aproximació catalítica va permetre la síntesi d'intermedis sintètics avançats de compostos agroquímics.

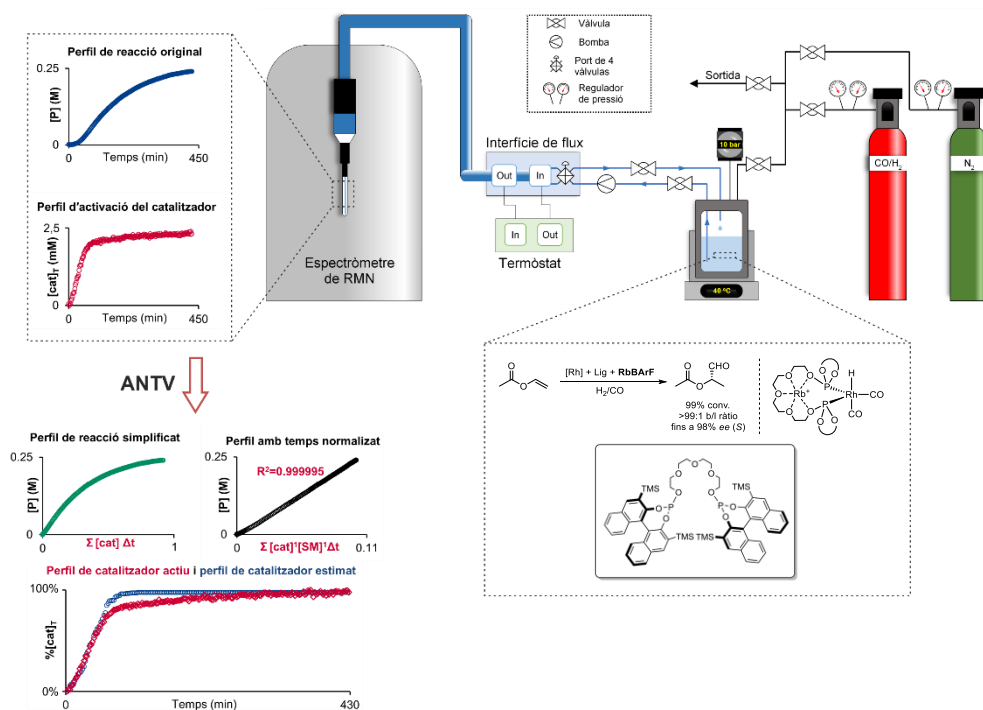


- 11 exemples
- Preparació d'intermedis amb importància en el sector agroquímic com Napropamida, Mecoprop i Diclorprop
- Efectes positius de regulació supramolecular amb impacte en l'especiació del catalitzador

**Esquema 56.** Hidroformilació enantioselectiva d'aril vinil èters catalitzada per sistemes supramolculars de rodi

Les activitats de recerca també es van centrar en la comprensió mecanística de la reacció d'hydroformilació enantioselectiva d'acetat de vinil catalitzada mitjançant sistemes supramolculars de rodi. Per aquest motiu, es va dur a terme el disseny i desenvolupament d'un muntatge experimental per al monitoratge *online* de reaccions en condicions catalítiques de reacció (Capítol IV). El muntatge experimental estava format per un sonda en flux de RMN assemblat amb un reactor d'alta pressió i un sistema de pressurització, que permetia el flux de la mescla de reacció entre l'espectròmetre i el reactor a alta pressió (Esquema 57). L'eficàcia d'aquest muntatge va permetre el monitoratge de la reacció d'hydroformilació en condicions catalítiques (això és, 40 °C i 10 bar H<sub>2</sub>/CO en

una proporció 1:1). Els perfils de concentració de la reacció van revelar la presència d'un període d'inducció en la formació del catalitzador supramolecular. Es va emprar l'Anàlisi de Normalització de Temps Variable (ANTV) com un mètode d'anàlisi cinètic visual i senzill per a extreure la informació cinètica rellevant de la transformació. El ANTV va permetre l'eliminació del període d'inducció observat en la formació del producte de reacció, mostrant un perfil de reacció simplificat i el veritable primer ordre de reacció en concentració de substrat i catalitzador per a la reacció d'hydroformilació. L'ús d'un segon tractament cinètic va permetre l'estimació del percentatge de concentració de catalitzador actiu (Esquema 57). Els estudis cinètics van permetre determinar que el pas limitant de la velocitat de la reacció té lloc en les primeres etapes del cicle catalític, particularment en la reacció de coordinació o inserció del carboni terminal de l'olefina a l'enllaç Rh–H. Encara que no ha estat possible l'elucidació del mecanisme en forma íntegra, la combinació d'estudis cinètics *in situ* i tècniques *operando* ha permès obtenir informació mecànica rellevant dels sistemes catalítics supramoleculars aplicats a la reacció d'hydroformilació.



**Esquema 57.** Estudis cinètics de la reacció d'hydroformilació enantioselectiva d'acetat de vinil catalitzada mitjançant sistemes supramoleculars de rodi

UNIVERSITAT ROVIRA I VIRGILI

THE HYDROFORMYLATION REACTION: FROM COVALENT TO SUPRAMOLECULAR APPROACHES AND OPERANDO KINETIC STUDIES

Alicia Martínez Carrión

UNIVERSITAT ROVIRA I VIRGILI

THE HYDROFORMYLATION REACTION: FROM COVALENT TO SUPRAMOLECULAR APPROACHES AND OPERANDO KINETIC STUDIES

Alicia Martínez Carrión

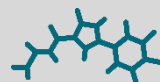
UNIVERSITAT ROVIRA I VIRGILI

THE HYDROFORMYLATION REACTION: FROM COVALENT TO SUPRAMOLECULAR APPROACHES AND OPERANDO KINETIC STUDIES

Alicia Martínez Carrión



UNIVERSITAT  
ROVIRA i VIRGILI



ICIQ<sup>R</sup>

Institut  
Català  
d'Investigació  
Química